Partners in UK offshore wind

MONA OFFSHORE WIND PROJECT

Environmental Statement

Volume 6, Annex 1.1: Physical processes technical report

Document Number: MOCNS-J3303-RPS-10068

Document Reference: F6.1.1

APFP Regulations: 5(2)(a)

February 2024

F01

Image of an offshore wind farm

www.morganandmona.com/en

Document status

Version	Purpose of document	Authored by	Reviewed by	Approved by	Review date
F01	Application	RPS	Mona Offshore Wind Ltd	Mona Offshore Wind Ltd	Feb 2024

Prepared by:

RPS

Prepared for:

Mona Offshore Wind Limited.

Contents

1 PHYSICAL PROCESSES TECHNICAL REPORT 1
1.1 Introduction 1
1.2 Study area 2
1.3 Modelling in support of the PEIR 4
1.3.1 Overview 4
1.3.2 Methodology 4
1.3.3 Desktop study 9
1.3.4 Site-specific surveys 10
1.3.5 Baseline environment 12
1.3.6 Potential environmental changes (as presented in the PEIR) 67
1.3.7 Potential changes during construction (as presented in the PEIR) 101
1.4 Modelling to support the Environmental Statement 186
1.4.1 Overview 186
1.4.2 Suction bucket foundations 188
1.4.3 Conical gravity base foundations 209
1.4.4 Rectangular gravity base foundations 229
1.5 Summary 250
1.6 References 252

Tables

Table 1.1: MIKE suite of models. 5
Table 1.2: Summary of Modelled Environmental Variation Scenarios for PEIR. 5
Table 1.3: Summary of Key Resources. 9
Table 1.4: Summary of survey undertaken to inform physical processes. 10
Table 1.5: Tidal Levels at Standard Ports. 16
Table 1.6: Summary of Modelled Environmental Variation Scenarios for the Environmental Statement. 187

Figures

Figure 1.1: Physical processes study area. 3
Figure 1.2: Physical processes model domain (blue outline). 8
Figure 1.3: MEDIN bathymetric data coverage 13
Figure 1.4: Mona and Morgan Generation Assets Array Areas bathymetric survey data coverage – Source: Gardline (2022) and XOcean (2022). 14
Figure 1.5: Model bathymetry within the east Irish Sea. 15
Figure 1.6: Model mesh with section of Mona PEIR Array Area inset. 16
Figure 1.7: Extent and bathymetry of Irish Seas tidal and storm surge model. 18
Figure 1.8: Availability of metocean datasets across the east Irish Sea. 19
Figure 1.9: Location of calibration data presented. 20
Figure 1.10: Comparison of model and admiralty harmonic tide data for Llandudno. 22
Figure 1.11: Comparison of model and recorded Mona Array Area metocean site – current speed and direction spring. 23
Figure 1.12: Comparison of model and recorded Mona Array Area metocean site – current speed and direction neap. 23
Figure 1.13: Comparison of model and recorded at the Morgan Generation Assets metocean site – current speed and direction spring. 24
Figure 1.14: Comparison of model and recorded Morgan at the Generation Assets metocean site – current speed and direction neap. 24
Figure 1.15: Comparison of modelled metocean and recorded DA ASG and SIG – current speed and direction spring. 25

Figure 1.16: Comparison of modelled Morgan Generation Assets metocean site and recorded ASG – spring surface elevation. 25
Figure 1.17: Comparison of modelled metocean and recorded DA ASG and SIG depth averaged– current speed and direction neap. 26
Figure 1.18: Comparison of modelled Morgan Generation Assets metocean site and recorded ASG – neap surface elevation. 26
Figure 1.19: Comparison of model and recorded data BODC Location A – current speed and direction spring. 27
Figure 1.20: Comparison of model and recorded data BODC Location A – current speed and direction neap.27
Figure 1.21: Comparison of model and recorded data BODC Location B – current speed and direction spring. 28
Figure 1.22: Comparison of model and recorded data BODC Location B – current speed and direction neap.28
Figure 1.23: Comparison of model and recorded data BODC Location C – current speed and direction spring. 29
Figure 1.24: Comparison of model and recorded data BODC Location C – current speed and direction neap.29
Figure 1.25: Comparison of model and recorded data BODC Location D – current speed and direction spring. 30
Figure 1.26: Comparison of model and recorded data BODC Location D – current speed and direction neap.30
Figure 1.27: Comparison of model and recorded data BODC Location E – current speed and direction spring. 31
Figure 1.28: Comparison of model and recorded data BODC Location E – current speed and direction neap.31
Figure 1.29: Tidal flow patterns – neap tide flood. 32
Figure 1.30: Tidal flow patterns – neap tide ebb. 33
Figure 1.31: Tidal flow patterns – spring tide flood. 34
Figure 1.32: Tidal flow patterns – spring tide ebb. 35
Figure 1.33: Wave rose for the Mona PEIR Array Area. 37
Figure 1.34: Wind rose for the Mona PEIR Array Area. 38
Figure 1.35: Location of wave calibration data presented. 39
Figure 1.36: Validation of modelled mean wave direction with measured data at CIV. 40
Figure 1.37: Validation of modelled significant wave height with measured data at CIV. 40
Figure 1.38: Validation of Modelled Peak Wave Period with Measured Data at CIV 41
Figure 1.39: Validation of modelled mean wave direction with measured data at GyM. 41
Figure 1.40: Validation of modelled significant wave height with measured data at GyM. 41
Figure 1.41: Validation of modelled peak wave period with measured data at GyM. 42
Figure 1.42: Validation of modelled mean wave direction with measured data at RhF. 42
Figure 1.43: Validation of modelled significant wave height with measured data at RhF. 42
Figure 1.44: Validation of modelled peak wave period with measured data at RhF. 43
Figure 1.45: Wave roses for model boundaries - 22 year ECMWF Dataset and wind rose for 40 year NOAA dataset. 45
Figure 1.46: Wave climate 1 in 1 year storm from 000° MHW. 46
Figure 1.47: Wave climate 1 in 1 year storm from 090° MHW. 47
Figure 1.48: Wave climate 1 in 1 year storm from 240° MHW. 48
Figure 1.49: Wave climate 1 in 1 year storm from 270° MHW. 49
Figure 1.50: Wave climate 1 in 20 year storm from 000° MHW. 50
Figure 1.51: Wave climate 1 in 20 year storm from 090° MHW. 51
Figure 1.52: Wave climate 1 in 20 year storm from 240° MHW. 52
Figure 1.53: Wave climate 1 in 20 year storm from 270° MHW. 53
Figure 1.54: Littoral current 1 in 1 year storm from 270° - Flood Tide. 54
Figure 1.55: Littoral current 1 in 1 year storm from 270° - Ebb Tide. 55
Figure 1.56: Seabed sample data Folk classification - BGS. 57
Figure 1.57: Seabed substrate geology - EMODnet. 58
Figure 1.58: Residual current spring tide. 60
Figure 1.59: Potential sediment transport over the course of 1 day (two tide cycles). 61
Figure 1.60: Sediment transport – flood tide. 62
Figure 1.61: Sediment transport – ebb tide. 63
Figure 1.62: Residual current spring tide with 1 in 1 year storm from 270°. 64

Figure 1.63: Turbidity levels from the Morgan Generation Assets metocean site. 65
Figure 1.64: Distribution of average non-algal suspended particulate matter (CEFAS, 2016). 66
Figure 1.65: Modelled array and trenching route indicative layout for PEIR. 68
Figure 1.66: Post-construction tidal flow pattern – flood tide. 70
Figure 1.67: Change in tidal flow (post-construction minus baseline) – flood tide. 71
Figure 1.68: Change in tidal flow (post-construction minus baseline) PEIR Mona Array Area – flood tide detail view. 72
Figure 1.69: Post-construction tidal flow pattern – ebb tide. 73
Figure 1.70: Change in tidal flow (post-construction minus baseline) – ebb tide. 74
Figure 1.71: Change in tidal flow (post-construction minus baseline) PEIR Mona Array Area – ebb tide detailed view. 75
Figure 1.72: Post-construction wave climate 1 in 1 year storm 000° MHW. 77
Figure 1.73: Change in wave climate 1 in 1 year storm 000° MHW (post-construction minus baseline). 78
Figure 1.74: Post-construction wave climate 1 in 20 year storm 000° MHW. 79
Figure 1.75: Change in wave climate 1 in 20 year storm 000° MHW (post-construction minus baseline). 80
Figure 1.76: Post-construction wave climate 1 in 20 year storm 090° MHW. 81
Figure 1.77: Change in wave climate 1 in 20 year storm 090° MHW (post-construction minus baseline). 82
Figure 1.78: Post-construction wave climate 1 in 20 year storm 240° MHW. 83
Figure 1.79: Change in wave climate 1 in 20 year storm 240° MHW (post-construction minus baseline). 84
Figure 1.80: Post-construction wave climate 1 in 20 year storm 270° MHW. 85
Figure 1.81: Change in wave climate 1 in 20 year storm 270° MHW (post-construction minus baseline). 86
Figure 1.82: Post-construction littoral current 1 in 1 year storm from 270° - Flood Tide. 87
Figure 1.83: Change in littoral current 1 in 1 year storm from 270° - flood tide (post-construction minus baseline). 88
Figure 1.84: Change in littoral current 1 in 1 year storm from 270° - flood tide (post-construction minus baseline) detailed view. 89
Figure 1.85: Post-construction littoral current 1 in 1 year storm from 270° - ebb tide. 90
Figure 1.86: Change in littoral current 1 in 1 year storm from 270° - ebb tide (post-construction minus baseline). 91
Figure 1.87: Change in littoral current 1 in 1 year storm from 270° - ebb tide (post-construction minus baseline) detailed view. 92
Figure 1.88: Post-construction residual current spring tide. 94
Figure 1.89: Change in residual current spring tide (post-construction minus baseline). 95
Figure 1.90: Change in residual current spring tide (post-construction minus baseline) Mona Offshore Wind Project PEIR detailed view. 96
Figure 1.91: Post-construction potential sediment over the course of 1 day (two tide cycles). 97
Figure 1.92: Difference in potential sediment transport over the course of 1 day (post-construction minus baseline). 98
Figure 1.93: Post-construction residual current 1 in 1 year storm from 270° spring tide. 99
Figure 1.94: Change in residual current 1 in 1 year storm from 270° spring tide (post-construction minus baseline). 100
Figure 1.95: Change in residual current 1 in 1 year storm from 270° spring tide (post-construction minus baseline) Mona Offshore Wind Project PEIR detailed view. 101
Figure 1.96: Sand wave clearance paths modelled for PEIR. 103
Figure 1.97: Location of Constable Bank in relation to the Mona Offshore Cable Corridor. 105
Figure 1.98: Suspended sediment concentration during dredging phase – offshore export cable path. 106
Figure 1.99: Suspended sediment concentration during dumping phase – offshore export cable path. 107
Figure 1.100: Suspended sediment concentration with sediment re-mobilisation – offshore export cable path. 108
Figure 1.101: Average suspended sediment concentration during operation – offshore export cable path. 109
Figure 1.102: Average sedimentation during operation – offshore export cable path. 110
Figure 1.103: Average sedimentation during operation – offshore export cable path detailed view. 111
Figure 1.104: Sedimentation 1 day following cessation of operation – offshore export cable path. 112
Figure 1.105: Sedimentation 1 day following cessation of operation – offshore export cable path detailed view. 113
Figure 1.106: Suspended sediment concentration during dredging phase – inter-array cable path. 114

Figure 1.107: Suspended sediment concentration during dumping phase – inter-array cable path. 115
Figure 1.108: Suspended sediment concentration with sediment re-mobilisation – inter-array cable path. . 116
Figure 1.109: Average suspended sediment concentration during operation – inter-array cable path. 117
Figure 1.110: Average sedimentation during operation – inter-array cable path..... 118
Figure 1.111: Average sedimentation during operation – inter-array cable path detailed view..... 119
Figure 1.112: Sedimentation 1 day following cessation of operation – inter-array cable path. 120
Figure 1.113: Sedimentation 1 day following cessation of operation – inter-array cable path detail view. ... 121
Figure 1.114: Location of modelled piled installation for piling – PEIR scenario A..... 124
Figure 1.115: Average suspended sediment concentration – pile installation scenario A..... 125
Figure 1.116: Suspended sediment concentration day 1 flood – pile installation scenario A..... 126
Figure 1.117: Suspended sediment concentration day 1 ebb – pile installation scenario A. 127
Figure 1.118: Suspended sediment concentration day 3 flood – pile installation scenario A..... 128
Figure 1.119: Suspended sediment concentration day 3 ebb – pile installation scenario A. 129
Figure 1.120: Average sedimentation during pile installation – scenario A. 130
Figure 1.121: Average sedimentation during pile installation – scenario A detail view. 131
Figure 1.122: Sedimentation 1 day following cessation of pile installation – Pile scenario A..... 132
Figure 1.123: Sedimentation 1 day following cessation of pile installation – Pile scenario A detail view..... 133
Figure 1.124: Location of modelled piled installation for piling – PEIR scenario B..... 135
Figure 1.125: Average suspended sediment concentration – pile installation scenario B..... 136
Figure 1.126: Suspended sediment concentration day 1 flood – pile installation scenario B..... 137
Figure 1.127: Suspended sediment concentration day 1 ebb – pile installation scenario B. 138
Figure 1.128: Suspended sediment concentration day 3 flood – pile installation scenario B..... 139
Figure 1.129: Suspended sediment concentration day 3 ebb – pile installation scenario B. 140
Figure 1.130: Average sedimentation during pile installation – scenario B. 141
Figure 1.131: Average sedimentation during pile installation – scenario B detail view. 142
Figure 1.132: Sedimentation 1 day following cessation of pile installation – Pile scenario B..... 143
Figure 1.133: Sedimentation 1 day following cessation of pile installation – Pile scenario B detail view..... 144
Figure 1.134: Location of modelled piled installation for piling – PEIR scenario C. 146
Figure 1.135: Average suspended sediment concentration – pile installation scenario C. 147
Figure 1.136: Suspended sediment concentration day 1 flood – Pile Installation scenario C..... 148
Figure 1.137: Suspended sediment concentration day 1 ebb – pile installation scenario C. 149
Figure 1.138: Suspended sediment concentration day 3 flood – pile installation scenario C. 150
Figure 1.139: Suspended sediment concentration day 3 ebb – pile installation scenario C. 151
Figure 1.140: Average sedimentation during pile installation – scenario C..... 152
Figure 1.141: Average sedimentation during pile installation – scenario C detail view..... 153
Figure 1.142: Sedimentation 1 day following cessation of pile installation – Pile scenario C. 154
Figure 1.143: Sedimentation 1 day following cessation of pile installation – Pile scenario C detail view..... 155
Figure 1.144: Modelled inter-array cable route for PEIR. 157
Figure 1.145: Average suspended sediment concentration during inter-array cable trenching. 158
Figure 1.146: Suspended sediment concentration day 2 flood – inter-array cable installation. 159
Figure 1.147: Suspended sediment concentration day 2 ebb – inter-array cable installation. 160
Figure 1.148: Suspended sediment concentration day 3 flood – inter-array cable installation. 161
Figure 1.149: Suspended sediment concentration day 3 ebb – inter-array cable installation. 162
Figure 1.150: Suspended sediment concentration day 4 flood – inter-array cable installation. 163
Figure 1.151: Suspended sediment concentration day 4 ebb – inter-array cable installation. 164
Figure 1.152: Average sedimentation during inter-array cable installation..... 165
Figure 1.153: Sedimentation 1 day following cessation of inter-array cable installation. 166
Figure 1.154: Modelled export cable route for PEIR..... 168
Figure 1.155: Average suspended sediment concentration during offshore export cable trenching..... 169
Figure 1.156: Suspended sediment concentration day 2 peak flood – offshore export cable installation..... 170
Figure 1.157: Suspended sediment concentration day 2 peak ebb – offshore export cable installation..... 171
Figure 1.158: Suspended sediment concentration day 3 peak flood – offshore export cable installation..... 172
Figure 1.159: Suspended sediment concentration day 3 peak ebb – offshore export cable installation..... 173
Figure 1.160: Suspended sediment concentration day 4 peak flood – offshore export cable installation..... 174
Figure 1.161: Suspended sediment concentration day 4 peak ebb – offshore export cable installation..... 175
Figure 1.162: Average sedimentation during offshore export cable installation. 176

Figure 1.163: Sedimentation 1 day following cessation of offshore export cable installation. 177
Figure 1.164: Modelled offshore export cables in the intertidal area for PEIR. 178
Figure 1.165: Average suspended sediment concentration during offshore export cables in the intertidal area trenching (SSSI – light blue, SAC – pink). 179
Figure 1.166: Average suspended sediment concentration during offshore export cables in the intertidal area trenching detailed view (SSSI – light blue, SAC – pink). 180
Figure 1.167: Suspended sediment concentration flood – offshore export cables in the intertidal area installation (SSSI – light blue, SAC – pink). 181
Figure 1.168: Suspended sediment concentration ebb – offshore export cables in the intertidal area installation (SSSI – light blue, SAC – pink). 182
Figure 1.169: Average sedimentation during offshore export cables in the intertidal area installation (SSSI – light blue, SAC – pink). 183
Figure 1.170: Average sedimentation during offshore export cables in the intertidal area installation detail view (SSSI – light blue, SAC – pink). 184
Figure 1.171: Sedimentation 1 day following cessation of offshore export cables in the intertidal area installation (SSSI – light blue, SAC – pink). 185
Figure 1.172: Sedimentation 1 day following cessation of offshore export cables in the intertidal area installation detail view (SSSI – light blue, SAC – pink). 186
Figure 1.173: Location of foundation used for sensitivity modelling within the Mona Offshore Wind Project Environmental Statement Boundary. 188
Figure 1.174: Baseline tidal flow pattern – flood tide. 190
Figure 1.175: Change in tidal flow (post-construction minus baseline) suction bucket foundation – flood tide. 191
Figure 1.176: Baseline tidal flow pattern – ebb tide. 192
Figure 1.177: Change in tidal flow (post-construction minus baseline) suction bucket foundation – ebb tide. 193
Figure 1.178: Baseline wave climate 1 in 1 year storm 000° MHW. 194
Figure 1.179: Change in wave climate 1 in 1 year storm 000° MHW (post-construction minus baseline) – suction bucket foundation. 195
Figure 1.180: Baseline wave climate 1 in 1 year storm 090° MHW. 196
Figure 1.181: Change in wave climate 1 in 1 year storm 090° MHW (post-construction minus baseline) – suction bucket foundation. 197
Figure 1.182: Baseline wave climate 1 in 1 year storm 240° MHW. 198
Figure 1.183: Change in wave climate 1 in 1 year storm 240° MHW (post-construction minus baseline) – suction bucket foundation. 199
Figure 1.184: Baseline wave climate 1 in 1 year storm 270° MHW. 200
Figure 1.185: Change in wave climate 1 in 1 year storm 270° MHW (post-construction minus baseline) – suction bucket foundation. 201
Figure 1.186: Baseline wave climate 1 in 20 year storm 000° MHW. 202
Figure 1.187: Change in wave climate 1 in 20 year storm 000° MHW (post-construction minus baseline) – suction bucket foundation. 203
Figure 1.188: Baseline wave climate 1 in 20 year storm 090° MHW. 204
Figure 1.189: Change in wave climate 1 in 20 year storm 090° MHW (post-construction minus baseline) – suction bucket foundation. 205
Figure 1.190: Baseline wave climate 1 in 20 year storm 240° MHW. 206
Figure 1.191: Change in wave climate 1 in 20 year storm 240° MHW (post-construction minus baseline) – suction bucket foundation. 207
Figure 1.192: Baseline wave climate 1 in 20 year storm 270° MHW. 208
Figure 1.193: Change in wave climate 1 in 20 year storm 270° MHW (post-construction minus baseline) – suction bucket foundation. 209
Figure 1.194: Baseline tidal flow pattern – flood tide. 210
Figure 1.195: Change in tidal flow (post-construction minus baseline) conical gravity base foundation – flood tide. 211
Figure 1.196: Baseline tidal flow pattern – ebb tide. 212
Figure 1.197: Change in tidal flow (post-construction minus baseline) conical gravity base foundation – ebb tide. 213
Figure 1.198: Baseline wave climate 1 in 1 year storm 000° MHW. 214

Figure 1.199: Change in wave climate 1 in 1 year storm 000° MHW (post-construction minus baseline) – conical gravity base foundation. 215
Figure 1.200: Baseline wave climate 1 in 1 year storm 090° MHW. 216
Figure 1.201: Change in wave climate 1 in 1 year storm 090° MHW (post-construction minus baseline) – conical gravity base foundation. 217
Figure 1.202: Baseline wave climate 1 in 1 year storm 240° MHW. 218
Figure 1.203: Change in wave climate 1 in 1 year storm 240° MHW (post-construction minus baseline) – conical gravity base foundation. 219
Figure 1.204: Baseline wave climate 1 in 1 year storm 270° MHW. 220
Figure 1.205: Change in wave climate 1 in 1 year storm 270° MHW (post-construction minus baseline) – conical gravity base foundation. 221
Figure 1.206: Baseline wave climate 1 in 20 year storm 000° MHW. 222
Figure 1.207: Change in wave climate 1 in 20 year storm 000° MHW (post-construction minus baseline) – conical gravity base foundation. 223
Figure 1.208: Baseline wave climate 1 in 20 year storm 090° MHW. 224
Figure 1.209: Change in wave climate 1 in 20 year storm 090° MHW (post-construction minus baseline) – conical gravity base foundation. 225
Figure 1.210: Baseline wave climate 1 in 20 year storm 240° MHW. 226
Figure 1.211: Change in wave climate 1 in 20 year storm 240° MHW (post-construction minus baseline) – conical gravity base foundation. 227
Figure 1.212: Baseline wave climate 1 in 20 year storm 270° MHW. 228
Figure 1.213: Change in wave climate 1 in 20 year storm 270° MHW (post-construction minus baseline) – conical gravity base foundation. 229
Figure 1.214: Baseline tidal flow pattern – flood tide. 231
Figure 1.215: Change in tidal flow (post-construction minus baseline) rectangular gravity base foundation – flood tide. 232
Figure 1.216: Baseline tidal flow pattern – ebb tide. 233
Figure 1.217: Change in tidal flow (post-construction minus baseline) rectangular gravity base foundation – ebb tide. 234
Figure 1.218: Baseline wave climate 1 in 1 year storm 000° MHW. 235
Figure 1.219: Change in wave climate 1 in 1 year storm 000° MHW (post-construction minus baseline) - rectangular gravity base foundation. 236
Figure 1.220: Baseline wave climate 1 in 1 year storm 090° MHW. 237
Figure 1.221: Change in wave climate 1 in 1 year storm 090° MHW (post-construction minus baseline) - rectangular gravity base foundation. 238
Figure 1.222: Baseline wave climate 1 in 1 year storm 240° MHW. 239
Figure 1.223: Change in wave climate 1 in 1 year storm 240° MHW (post-construction minus baseline) - rectangular gravity base foundation. 240
Figure 1.224: Baseline wave climate 1 in 1 year storm 270° MHW. 241
Figure 1.225: Change in wave climate 1 in 1 year storm 270° MHW (post-construction minus baseline) - rectangular gravity base foundation. 242
Figure 1.226: Baseline wave climate 1 in 20 year storm 000° MHW. 243
Figure 1.227: Change in wave climate 1 in 20 year storm 000° MHW (post-construction minus baseline) - rectangular gravity base foundation. 244
Figure 1.228: Baseline wave climate 1 in 20 year storm 090° MHW. 245
Figure 1.229: Change in wave climate 1 in 20 year storm 090° MHW (post-construction minus baseline) - rectangular gravity base foundation. 246
Figure 1.230: Baseline wave climate 1 in 20 year storm 240° MHW. 247
Figure 1.231: Change in wave climate 1 in 20 year storm 240° MHW (post-construction minus baseline) - rectangular gravity base foundation. 248
Figure 1.232: Baseline wave climate 1 in 20 year storm 270° MHW. 249
Figure 1.233: Change in wave climate 1 in 20 year storm 270° MHW (post-construction minus baseline) - rectangular gravity base foundation. 250

Glossary

Term	Meaning
Bathymetry	The measurement of depth of water in oceans, seas, or lakes.
Bed resistance coefficient	Represents the roughness or friction applied to the flow by the seabed.
Ebb tide	The tidal phase during which the water level is falling.
Erosion	Depletion of sediment in the intertidal region.
Fetch	Length in the wind direction of the marine area where water waves are generated by wind.
Flood tide	The tidal phase during which the water level is rising.
Folk classification	A technical descriptive classification of sedimentary rocks devised by Robert L. Folk.
High Water Mark	The level reached by the sea at high tide.
Highest Astronomical Tide	The highest tidal height predicted to occur under average meteorological conditions and any combination of astronomical conditions.
Hydrodynamic boundary conditions	The conditions used in a model boundary which can included surface elevation and velocity which will affect the rest of the model domain. The boundary condition can vary with time and along the boundary.
Intertidal region	An area of a shoreline that is covered at high tide and uncovered at low tide.
Lee	Shelter from wind or weather given by an object.
Littoral currents	Flow derived from tide and wave climate.
Low Water Mark (LWM)	The level reached by the sea at low tide.
Lowest Astronomical Tide	The lowest tidal height predicted to occur under average meteorological conditions and any combination of astronomical conditions.
Mean High Water	The highest water level reached during and average tide.
Mean High Water Spring	The most inshore level location reached by the sea at high tide during mean high water spring tide. This is defined as the average throughout the year, of two successive high waters, during a 24-hour period in each month when the range of the tide is at its greatest.
Mean Low Water Spring	The most offshore location reached by the sea at low tide during low water spring tide. This is defined as the average throughout the year, of two successive low waters, during a 24-hour period in each month when the range of the tide is at its greatest.
Mean Sea Level	The average tidal height over a long period of time.
Metocean	Refers to the syllabic abbreviation of meteorology and (physical) oceanography.
Neap tide	Tide that occurs when the sun and moon are at right angles to each other and the gravitational pull of the sun partially cancels out the pull of the moon on the ocean.
Refraction	The change in direction of a wave passing from one medium to another caused by its change in speed.
Residual current	The net flow over the course of the tidal cycle. This is effectively the driving force of the sediment transport.
Sandwave	A lower regime sedimentary structure that forms across from tidal currents.
Scour protection	Measures to prevent loss of seabed sediment around any structure placed in or on the seabed (e.g. by use of protective aprons, mattresses, rock and gravel placement).
Sedimentation	The process of settling or being deposited as a sediment.

Term	Meaning
Significant wave height	Mean wave height (trough to crest) of the highest third of the waves.
Slack tide	Tidal phase at which the current turns from flood to ebb (high-water slack tide) or from ebb to flood (low-water slack tide).
Spectral waves	Describes the distribution of wave energy with frequency (1/ period) and direction.
Spring tide	Tide that occurs when the sun and moon are directly in line with the Earth and their gravitational pulls on the ocean reinforce each other.
Suspended Particulate Matter	Particles that are suspended in the water column.
Turbidity	The quality of being cloudy, opaque, or thick with suspended matter.
Wave height	The distance from trough to crest of a wave.
Wave period	The time it takes for two successive crests (one wavelength) to pass a specified point.

Acronyms

Acronym	Description
2D UHRS	2D Ultra High Resolution Seismic
ASG	Aanderaa Seaguard
BEIS	Department for Business, Energy and Industrial Strategy
BERR	Department for Business Enterprise and Regulatory Reform
BGS	British Geological Survey
BODC	British Oceanographic Data Centre
CCO	Coastal Channel Observatory
CD	Chart Datum (generally defined as LAT)
CEFAS	Centre for Environment, Fisheries and Aquaculture Science
ClV	Cleveleys
DA	Depth Averaged
DHI	Danish Hydraulic Institute
DSV	Digital Sound Velocity
ECMWF	European Centre for Medium Range Forecasts
EMODnet	European Marine Observation and Data Network
FM	Flexible Mesh
GEMS	Geotechnical Engineering and Marine Surveys
GSI	Geological Survey Ireland
GyM	Gwynt y Môr
HAT	Highest Astronomical Tide
HWM	High Water Mark
INFOMAR	Integrated Mapping for the Sustainable Developments of Ireland's Marine Resource

Acronym	Description
LAT	Lowest Astronomical Tide
LWM	Low Water Mark
MBES	Multi-Beam Echo Sounder
MDS	Maximum Design Scenario
MEDIN	Marine Environmental Data and Information Network
MHW	Mean High Water
MHWN	Mean High Water Neaps
MHWS	Mean High Water Springs
MLWN	Mean Low Water Neaps
MLWS	Mean Low Water Springs
MSL	Mean Sea Level
MT	Mud Transport
NOAA	National Oceanic and Atmospheric Administration
NRW	Natural Resources Wales
OSP	Offshore Substation Platform
PDE	Project Design Envelope
PEIR	Preliminary Environmental Report
PSA	Particle Size Analysis
PT	Particle Tracking
RhF	Rhyl Flats
SAC	Special Area of Conservation
SBP	Sub-Bottom Profiler
SIG	Nortek Signature
SPM	Suspended Particulate Matter
SSC	Suspended Sediment Concentration
SSS	Side Scan Sonar
SSSI	Site of Special Scientific Interest
ST	Sediment Transport
SW	Spectral Wave
TSSF	Tide and Storm Surge Forecast
UKCP	United Kingdom Climate Projections
UKCS	United Kingdom Continental Shelf
UKHO	United Kingdom Hydrographic Office

Units

Unit	Description
º	Degrees (angle from True north)
cm	Centimetre (distance)
cm/s	Centimetre per second (speed)
mm	Millimetre (distance)
m	Metre (distance)
m^3	Cubic metres (volume)
m^3/h	Cubic metres per hour (rate of change)
km	Kilometre (distance)
$m^3/d/m$	Cubic metres transported per day per metre width of transport path (i.e. perpendicular to direction of transport)
m/s	Metres per second (speed)
mg/l	Milligrams per litre (suspended sediment concentration)

1 Physical processes technical report

1.1 Introduction

1.1.1.1 This physical processes technical report provides information relating to the physical environment and processes for the Mona Offshore Wind Project. The purpose of the technical report is to provide details of the supporting studies undertaken by means of numerical modelling. It describes the current baseline conditions and quantifies the potential changes due to the installation and presence of the Mona Offshore Wind Project. Modelling was undertaken to support the Preliminary Environmental Information Report (PEIR) and was supplemented with additional work to support the Environmental Statement.

1.1.1.2 The preparation of a PEIR and subsequent Environmental Statement is a live process, with refinements being made to the project description throughout this period as information is acquired from the range of studies and assessments undertaken. For this reason, modelled scenarios based on the project description at both the PEIR and Environmental Statement stages of the application are presented within this report, and together are considered to sufficiently underpin the assessment.

1.1.1.3 The Mona Array Area has been reduced by approximately 33% since the publication of the PEIR and now lies wholly within Welsh offshore waters, (Mona Offshore Wind Limited, 2023). The changes in the Mona Array Area are accompanied by revised indicative layouts, however, given that the reductions in area are modest and lie wholly within the boundaries assessed for PEIR it was concluded that all physical processes impacts would be negligible (not significant in EIA terms). The representative/indicative layout applied within the modelling studies undertaken for the PEIR is therefore deemed to provide appropriate information to support the physical processes assessment of the Mona Offshore Wind Project for the Environmental Statement.

1.1.1.4 In some cases, the modelling of construction activities extends beyond the revised Mona Array Area boundary. These areas do however have bathymetry, tidal currents and sediment classifications consistent with those within the Mona Array Area presented at PEIR due to their close proximity to the Mona Array Area. It is considered that, given these similarities, and that the revised layout represents a modest change in terms of the physical processes assessment, the modelling undertaken for the PEIR remains valid and has therefore been used to inform the physical processes assessment presented for the Environmental Statement.

1.1.1.5 Modelling scenarios undertaken for the PEIR and presented within this technical report were informed by the project description presented at PEIR. The results will, therefore, in some instances, vary from those assessed for the DCO application. The modelled scenarios are nonetheless deemed to provide appropriate information to support the physical processes assessment of the Mona Offshore Wind Project for the Environmental Statement given the modelled layout examined for PEIR remains representative of that proposed in the Environmental Statement. Additional sensitivity testing has been included in section 1.3 to support updates made since the PEIR was published. When disparities occur, they are cited within the assessment with reference to the applicability of the modelled data presented in this report and used to support the assessment.

1.1.1.6 This report is divided into two main sections:

- Modelling in support of the PEIR

  - Baseline conditions – describing current hydrography and sedimentology
  - Environmental variations – describing changes to baseline arising from the installation and presence of the Mona PEIR Offshore Wind Project
  - Construction phase changes – describing the dispersion and fate of sediment mobilised during construction phase activities
- Modelling in support of the Environmental Statement
  - Sensitivity testing for alternative foundation types.

1.1.1.7 For the purposes of this physical processes technical report, physical processes are defined as encompassing the following elements:

- Tidal elevations and currents
- Waves
- Bathymetry
- Seabed sediments
- Suspended sediments
- Sediment transport (ST).

1.2 Study area

1.2.1.1 The Mona physical processes study area is illustrated in Figure 1.1 and defined as the:

- Mona Array Area (the area within which the wind turbines, foundations, inter-array cables, interconnector cables, offshore export cables and Offshore Substation Platforms (OSPs) forming part of the Mona Offshore Wind Project will be located)
- Mona Offshore Cable Corridor (the corridor located between the Mona Array Area and the landfall up to Mean High Water Springs (MHWS), in which the offshore export cables will be located)
- Landfall area
- Seabed and coastal areas that may be influenced by changes to physical processes due to the Mona Offshore Wind Project for PEIR defined as one spring tidal excursion from the Mona PEIR Array Area and Mona PEIR Offshore Cable Corridor - which is the distance suspended sediment is transported prior to being carried back on the returning tide.

1.2.1.2 It is however noted that the physical processes study area forms the focus for the assessment and that the numerical model extent is not limited to this region. The modelling study therefore also identifies any potential impacts beyond the physical processes study area. Figure 1.1 also demonstrates how the Mona Array Area has been reduced in size since the publication of the PEIR. However, to be conservative, the physical processes study area remains unchanged.

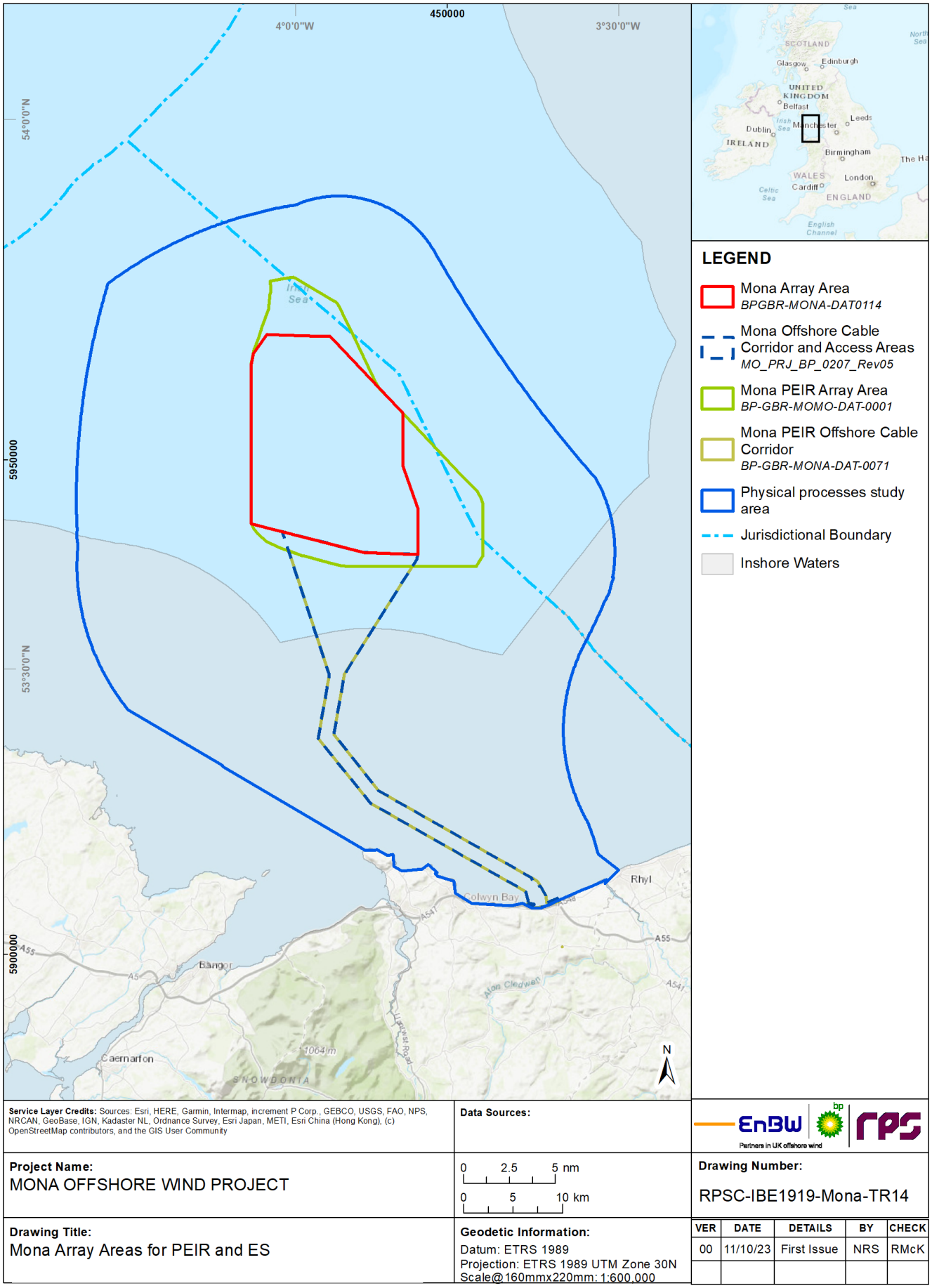

Figure 1.1: Physical processes study area.

1.3 Modelling in support of the PEIR

1.3.1 Overview

1.3.1.1 The following section outlines the modelling study undertaken for the Mona Offshore Wind Project PEIR. As noted, the application process is a live process with refinements being made to the project description throughout this period, as information is acquired from the range of studies and assessments undertaken. For this reason, the modelled scenarios presented in this section will, inevitably, vary by a small degree from those assessed in the Environmental Statement. When disparities occur, they are cited within the assessment with reference to the applicability of the modelled data presented in this report and used to support the application.

1.3.2 Methodology

1.3.2.1 The physical processes study was undertaken to provide information of potential changes to physical processes and the fate of mobilised sediment during the construction phase by means of numerical modelling. Numerical models were developed and calibrated using a combination of publicly available datasets and those collected specifically for the Mona Offshore Wind Project.

1.3.2.2 These models were then implemented in comparative studies to determine the potential impact of the infrastructure on tidal flow, wave climate and sediment transport patterns for a representative project design scenario. It is noted that this method investigates the influence on the drivers of physical processes rather than instigating detailed morphological studies. In the event that significant potential impacts were identified more detailed studies may be required, such as three-dimensional modelling where density stratified regions may be impacted.

1.3.2.3 The models were also used to undertake simulations of site preparation, cable trenching and pile installation activities to quantify potential increases in suspended sediment concentration and subsequent deposition. This information was then applied in the context of the physical processes environmental impact assessment and those of related disciplines.

Numerical modelling

1.3.2.4 Numerical modelling techniques were used to describe tide, wave and sediment transport regimes. The MIKE suite of software was employed, as a single model mesh could be used to simulate these processes both individually and in combination. The model domain is shown in Figure 1.2. The MIKE suite of models is a widely used industry standard modelling suite developed by the Danish Hydraulic Institute (DHI). It has been approved for use by industry and government bodies including Natural Resources Wales (NRW). The MIKE suite is a modular system that contains a number of different but complementary modules encompassing different physical processes: these are summarised in Table 1.1 and described in further detail within the relevant sections. A summary of the modelled environmental scenarios is provided in Table 1.2 noting that modelled scenarios are based on the project description for PEIR whilst the sensitivity testing relates to potential variations in relation to the application and Environmental Statement project descriptions.

Table 1.1: MIKE suite of models.

Simulation	Model	Description
Baseline and post-construction tidal flow	MIKE21 Flexible Mesh (FM) modelling system	The FM Module is a 2-dimensional, depth averaged (DA) hydrodynamic model which simulates the water level variations and flows in response to a variety of forcing functions in lakes, estuaries and coastal areas. The water levels and flows are resolved on a mesh covering the area of interest when provided with bathymetry, bed resistance coefficient, wind field, hydrodynamic boundary conditions, etc.
Baseline and post-construction wave climate	MIKE21 Spectral Wave (SW)	The wave modelling was undertaken using the spectral wave model, MIKE21 SW. The waves were computed on the same grid as the tidal flows. The model resolves the wave field by simulating wind generation of waves within the model domain and the propagation of externally generated swell waves through the domain. The model setup ensured that the detail of both locally generated wind waves and swell conditions from further afield were captured.
Baseline and post-construction littoral currents	MIKE21 FM and SW	The MIKE suite facilitates the coupling of models. The depth averaged hydrodynamic model, used for the tidal modelling, coupled with a spectral wave model, provides a full wave climate incorporating the impact of water levels and currents on waves and wave breaking. Using this, the littoral currents (i.e. those currents driven by tidal, wave and meteorological forces) were examined.
Baseline and post-construction sediment transport	MIKE21 Sand Transport (ST)	This module enables assessment of bed sediment transport rates and initial rates of bed level change for non-cohesive sediment resulting from currents or combined wave-current flows. The model combines inputs from both the hydrodynamic model and, if required, the wave propagation model. It uses sediment size and gradation to determine the bed level changes and sediment transport rates.
Foundation installation	MIKE21 Mud Transport (MT)	A sample of four representative pile installation scenarios were simulated to cover the range of conditions across the PEIR Mona Array Area both in terms of tidal currents and sediment type. The MIKE MT module allows the modelling of erosion, transport and deposition of cohesive and cohesive/granular sediments. This model is suited to sediment releases in the water column and allows sediment sources which may vary spatially and temporally.
Cable installation	MIKE21 Particle Tracking (PT)	The PT module was implemented for cable installation as it has the advantage that it could be used to describe the transport of material released in a specific part of the water column. In this way, the dispersion would not be over-estimated, or the corresponding sedimentation underestimated.

Table 1.2: Summary of Modelled Environmental Variation Scenarios for PEIR.

Variation/ operation	Description	Parameter modelled
Hydrography Section 1.3.6	Models updated to take account of the installation of the Mona PEIR Offshore Wind Project and associated features to quantify: • Changes to tidal currents; • Changes to wave climate; and • Changes to littoral currents.	• Wind turbines: 68 installations with four-legged suction bucket foundations, each jacket leg with a diameter of 5 m, spaced 48 m apart, and each bucket with a diameter of 16 m. Scour protection to a height of 2.5 m. Total footprint of 10,816 m^2 per wind turbine • OSPs: four installations with three-legged suction bucket foundations, each jacket leg with a diameter of 3 m,

Variation/ operation	Description	Parameter modelled
		spaced 30 m apart, and each bucket with a diameter of 14 m. Scour protection to a height of 2.5 m. Total footprint of 3,277 m^2 footprint per OSP • Inter-array cables: cable protection with a height of 3 m and 5 m width. Cable crossings, each crossing with a height of 4 m, a width of 32 m and a length of 60 m • Interconnector cables: cable protection with a height of 3 m and 10 m width. Cable crossings, each crossing with a height of 3 m, a width of 20 m and a length of 50 m • Export cables: cable protection with a height of 3 m and 10 m width. Cable crossings, each crossing with a height of 3 m, a width of 30 m and a length of 50 m.
Sedimentology Section 1.3.6	Models updated to take account of the installation of the Mona Offshore Wind Project and associated features to quantify: • Changes to sediment transport characteristics.	As above with the addition of: • Scour protection simulated using an area of fixed bed around each structure.
Seabed features clearance Section 1.3.7	Dispersion modelling relating to sandwave clearance. Dredging of sandwave crest and disposal at troughs is undertaken in a cycle along cable routes.	• Clearance is undertaken at 100 m/h along 5 km sample cable routes of a width of 104 m with dredging undertaken at 10,000 m^3/h with a spill rate of 3% • Mona Offshore Cable Corridor clearance is undertaken to an average depth of 5.1 m • Inter-array cable clearance is undertaken to an average depth of 5.1 m • With sediment released through water column.
Augured pile installation Section 1.3.7	Dispersion modelling of suspended sediment arising from augured pile installation. Under a range of tidal conditions.	Four sample scenarios are presented, in each case: • Piles are 16 m in diameter and 60 m deep • Two adjacent operations occur simultaneously • Drilling undertaken at 0.89m/h • 13,460 m^3 of material mobilised per pile • Released throughout water column.
Cable installation Section 1.3.7	Dispersion modelling of suspended sediment arising from cable installation via trenching. Relating to • Offshore export cable • Inter-array cable • Intertidal cable	For offshore and inter-array cables sample trenching operations are presented. • Trench 3 m wide at seabed and 3 m deep with triangular cross section • Trenching is undertaken at 450 m/h.

Variation/ operation	Description	Parameter modelled
		Inter-tidal trenching is undertaken for an 800 m route over an eight hour period for a trench 1 m wide and 3 m deep.

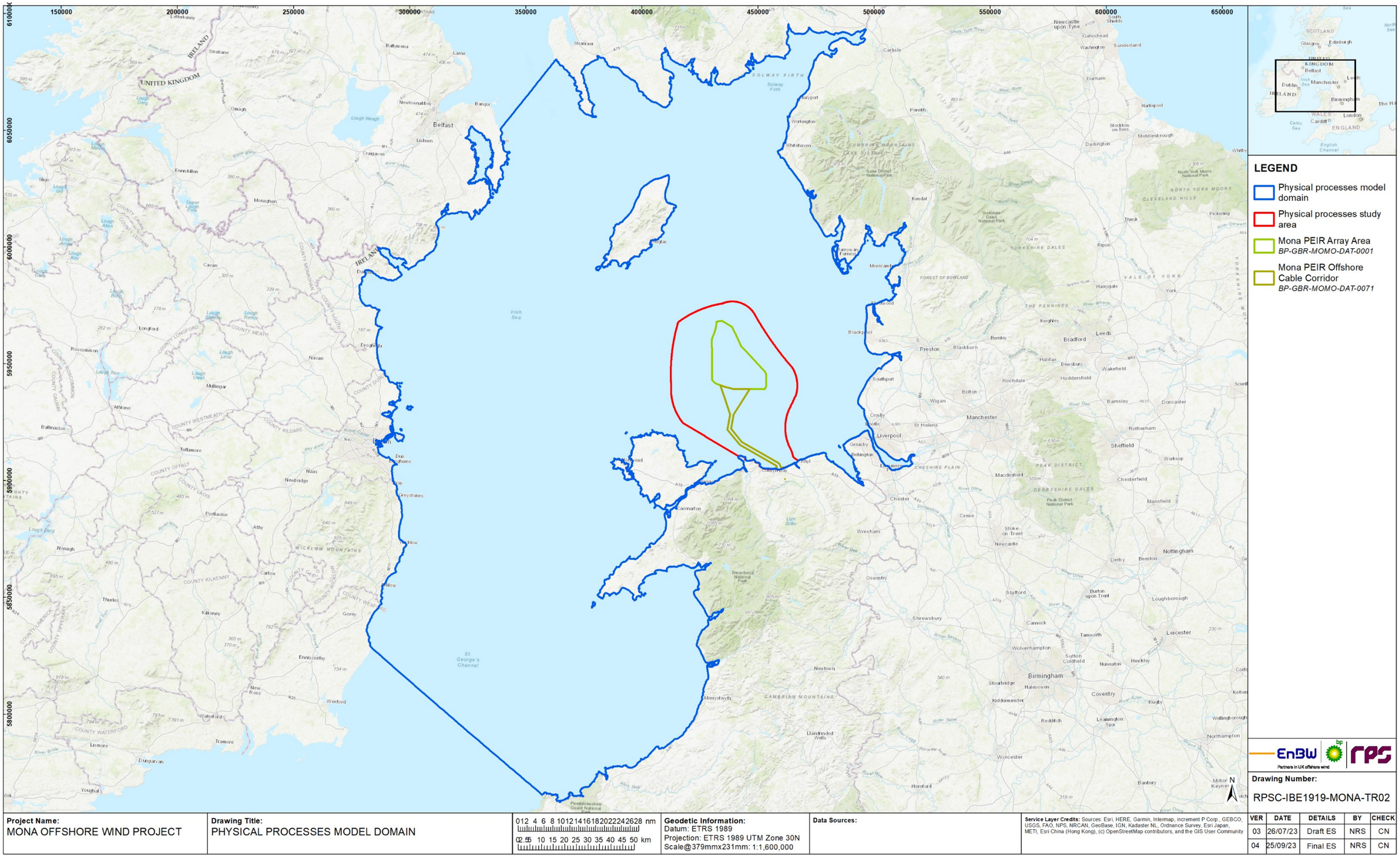

Figure 1.2: Physical processes model domain (blue outline).

1.3.3 Desktop study

1.3.3.1 Information on the physical environment within the physical processes study area and beyond to the model domain was collected through a detailed desktop review of existing studies and datasets. These are summarised in Table 1.3.

Table 1.3: Summary of Key Resources.

Title	Source	Year	Author
European Marine Observation and Data Network (EMODnet) – Seabed classification	https://www.emodnet-geology.eu/	2022	EMODnet
EMODnet – Bathymetry data	https://www.emodnet-bathymetry.eu/	2022	EMODnet
EMODnet – Metocean data	https://map.emodnet-physics.eu/	2022	EMODnet
Department for Environment Food and Rural Affairs – Bathymetry data	https://environment.data.gov.uk/DefraDataDownload	2022	DEFRA
National Oceanic and Atmospheric Administration (NOAA) –Atmospheric data	DHI Metocean Data Portal	2022	NOAA
National Network of Regional Coastal Monitoring Programmes	https://coastalmonitoring.org/cco/	2022	Coastal Channel Observatory
Centre for Environment, Fisheries and Aquaculture Science (CEFAS) – wave data	https://wavenet.cefas.co.uk/map	2022	CEFAS
ABPmer Data exporer	https://www.seastates.net/explore-data/	2022	ABPmer
Hydrography of the Irish Sea, SEA6 Technical Report	UK Government	2005	Howarth M.J.
Atlas of UK Marine Renewable Energy Resources	https://www.renewables-atlas.info/	2022	ABPmer
Manx Marine Environmental Assessment Physical Environment Hydrology, Weather and Climate, Climatology	https://www.gov.im/	2018	Isle of Man Government Kennington and Hiscott
Geology of the seabed and shallow subsurface: The Irish Sea.	British Geological Survey	2015	Mellett *et al*.
British Geological Survey – sediment sample data	https://mapapps2.bgs.ac.uk/geoindex_offshore	2022	BGS
Geological Ground Model Mona Windfarm Development Irish Sea	Mona Offshore Wind Ltd	2023	bp
Suspended Sediment Climatologies around the UK.	Department for Business, Energy & Industrial Strategy (BEIS)	2016	Cefas

Title	Source	Year	Author
Metocean Data collection for the Ormonde offshore wind project.	Marine Data Exchange	2011	Geotechnical Engineering and Marine Surveys (GEMS)
Irish Sea Zone Hydrodynamic measurment campaign	Marine Data Exchange	2010-2013	EMU Ltd (now Fugro Ltd)
Admiralty Tide Tables	United Kingdom Hydrographic Office (UKHO)	2022	UKHO
Marine Environmental Data Information Network (MEDIN) Seabed Mapping Programme	Admiralty Marine Data Portal	2022	MEDIN
Integrated Mapping for the Sustainable Developments of Ireland's Marine Resource (INFOMAR) Seabed Mapping Programme	Geological Survey Ireland (GSI) and Marine Institute	2022	INFOMAR
Long term wind and wave datasets	European Centre for Medium-range Weather Forecast (ECMWF)	2022	ECMWF
UK tide gauge network and database of current observation	British Oceanographic Data Centre (BODC)	2021	BODC
UK Climate Projections (UKCP)	Met Office	2018	Met Office
A user-friendly database of coastal flooding in the UK from 1915-2014	Scientific Data (journal)	2015	Haigh *et al.*
British Oceanographic Data Centre	National Oceanography Centre	various	National Oceanography Centre
Review of aggregate dredging off the Welsh coast	HR Wallingford	2016	HR Wallingford

1.3.4 Site-specific surveys

1.3.4.1 A summary of the surveys undertaken of relevance to physical processes and utilised within the physical processes modelling study is outlined in Table 1.4. Results from recent geophysical and benthic surveys of the Mona PEIR Offshore Cable Corridor route were made available after the model study completion. These were used to verify that the data used within the physical processes modelling was appropriate and to inform the Environmental Statement.

Table 1.4: Summary of survey undertaken to inform physical processes.

Title	Extent of survey	Overview of survey	Survey contractor	Date	Reference to further information
Environmental Baseline Surveys and Habitat Assessments	Mona and Morgan Offshore Wind Project: Generation Assets (hereafter referred to as	Geophysical survey to establish bathymetry and determine characteristics of seabed sediment, characterise benthic communities (infauna and epifauna) and identification of any environmentally	Gardline Ltd	June to September 2021	Gardline (2022)

Title	Extent of survey	Overview of survey	Survey contractor	Date	Reference to further information
	the Morgan Generation Assets) Array Areas	significant habitats (e.g., potential Habitats Directive Annex I and priority marine features). Deployment included multi-beam echo sounder (MBES), digital sound velocity (DSV) sensor, side scan sonar system (SSS), Sub-Bottom Profiler (SBP) & 2D Ultra High Resolution Seismic (2D UHRS) sensor. Additionally, seabed imagery was collected along with grab samples (with Particle Size Analysis (PSA) undertaken).			
Geophysical survey	Mona and Morgan Generation Assets Array Areas	Geophysical survey to establish bathymetry, seabed sediment and identify seabed features. Deployment included MBES with multibeam backscatter.	XOCEAN Ltd	June 2021 to March 2022	XOCEAN (2022)
Metocean survey	Mona and Morgan Generation Assets Array Areas	Metocean deployments to ascertain wind, wave, and tidal currents.	Fugro	November 2021 to November 2022	Fugro (2022)
Environmental Baseline Surveys and Habitat Assessments	Mona and Morgan Generation Assets Array Areas and Mona and Morgan Generation Assets Offshore Cable Corridors	Geophysical survey to establish bathymetry and determine characteristics of seabed sediment, characterise benthic communities (infauna and epifauna) and identification of any environmentally significant habitats (e.g., potential Habitats Directive Annex I and priority marine features). Deployment included multi-beam echo sounder (MBES), digital sound velocity (DSV) sensor, side scan sonar system (SSS), Sub-Bottom Profiler (SBP) & 2D Ultra High Resolution Seismic (2D UHRS) sensor. Additionally, seabed imagery was collected along with grab samples (with PSA undertaken).	Gardline Ltd	April 2022 – August 2022	Ocean Ecology (2023)

1.3.5 Baseline environment

Bathymetry

1.3.5.1 The model domain had full bathymetry data coverage and was populated using a combination of data sources. The site-specific geophysical survey undertaken for both the Morgan Generation Assets and Mona Scoping Array Areas and the resulting bathymetry data, as detailed in Table 1.4, was used to populate the model. The extent of this survey data is shown in Figure 1.4, Gardline (2022) and XOcean (2022). The survey data provided to Lowest Astronomical Tide (LAT) vertical datum was converted to model mean sea level datum using reference values published by Admiralty.

1.3.5.2 Where additional data was required for the model extent beyond the survey area, bathymetry data was sourced from the MEDIN Seabed Mapping Programme via the Admiralty Marine Data Portal as shown in Figure 1.3. Each of the datasets for the east Irish Sea area was combined into a single set giving priority to the most recent survey data. For areas within region which did not have coverage from the MEDIN dataset further data was sourced from the DEFRA Survey Data Download site. This was undertaken for specific bays such as Conwy Bay and the Dee Estuary.

1.3.5.3 For the remaining model domain, the EMODnet 100 m resolution tiled data was utilised. This database is available under the European Inspire Directive and provides access to data in a variety of formats, datums and resolutions based on a combination of survey datasets. All data was converted, where necessary, to mean sea level datum generally with a resolution of at least three times the mesh resolution to ensure that coastal features were represented within the numerical modelling, as illustrated in Figure 1.5.

1.3.5.4 The resolution of the model bathymetry was designed to reflect variations in water depth and bed forms for the accurate simulation of tidal currents. Additional model resolution was also included to incorporate the installation of the Mona Offshore Wind Project. This enabled the same cell arrangement to be used for the baseline and post-construction assessment, thereby avoiding the introduction of any numerical mesh effects into the assessment. Across the Mona PEIR Array Area and Mona PEIR Offshore Cable Corridor the resolution varied between circa 50 m down to 10 m in order that the influence of scour protection on the tidal flow and sediment transport for the Mona PEIR Offshore Wind Project could be quantified. With increasing distance from the physical processes study area, the cell size was increased but maintained at a level which retained model accuracy. Figure 1.3 illustrates the mesh resolution with an inset of the mesh within the Mona PEIR Array Area.

1.3.5.5 The extent of the domain, Figure 1.2, was designed to provide the basis for a model which could be utilised for tide, wave and sediment transport modelling. The focus of the study is a tidal excursion from the Mona PEIR Array Area and Mona PEIR Offshore Cable Corridor to quantify any changes due to the installation however a larger domain is required to develop wave fields and ensure that tidal currents are simulated and had the benefit of identifying any potential effects beyond the physical processes study area.

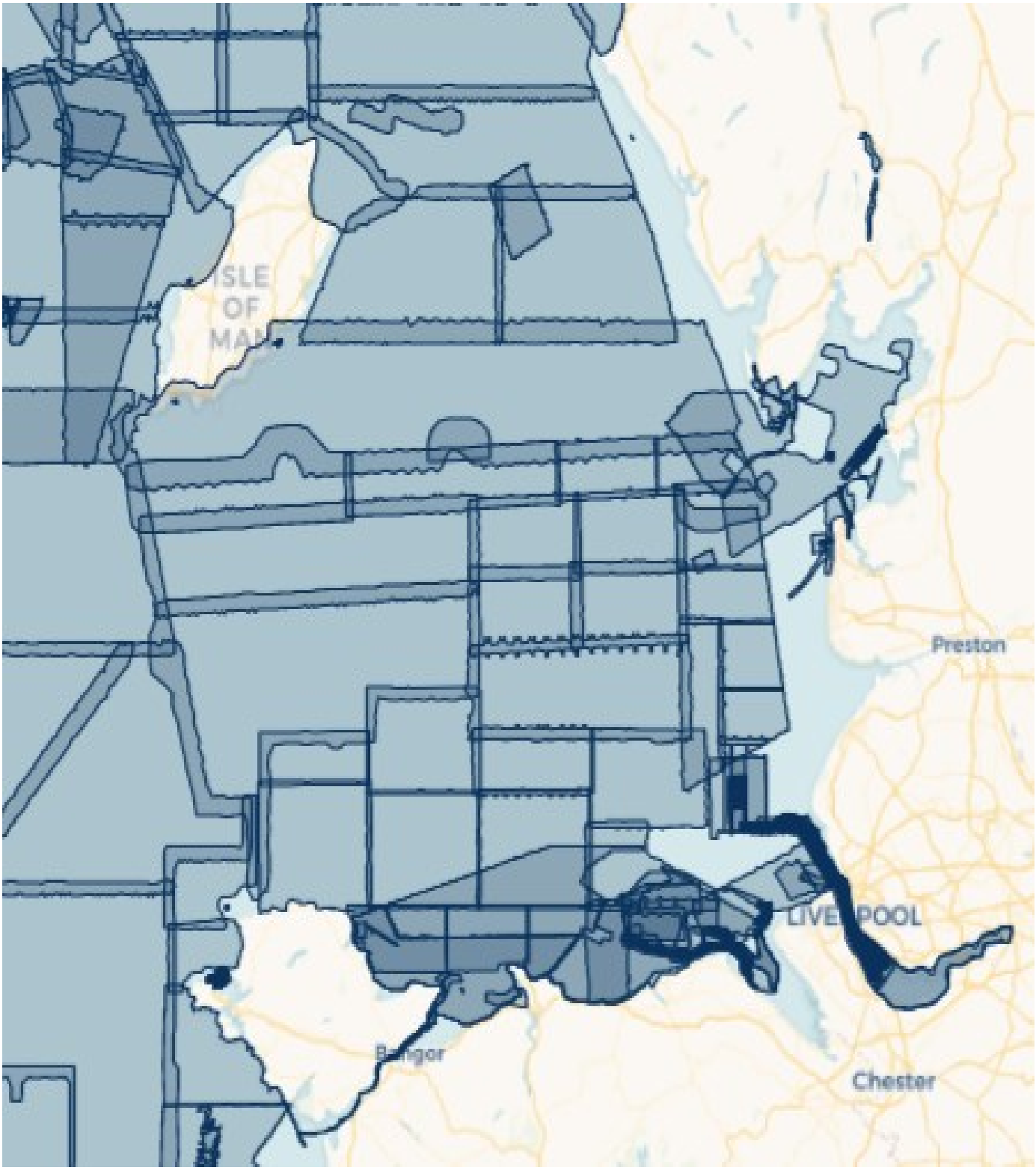

Figure 1.3: MEDIN bathymetric data coverage

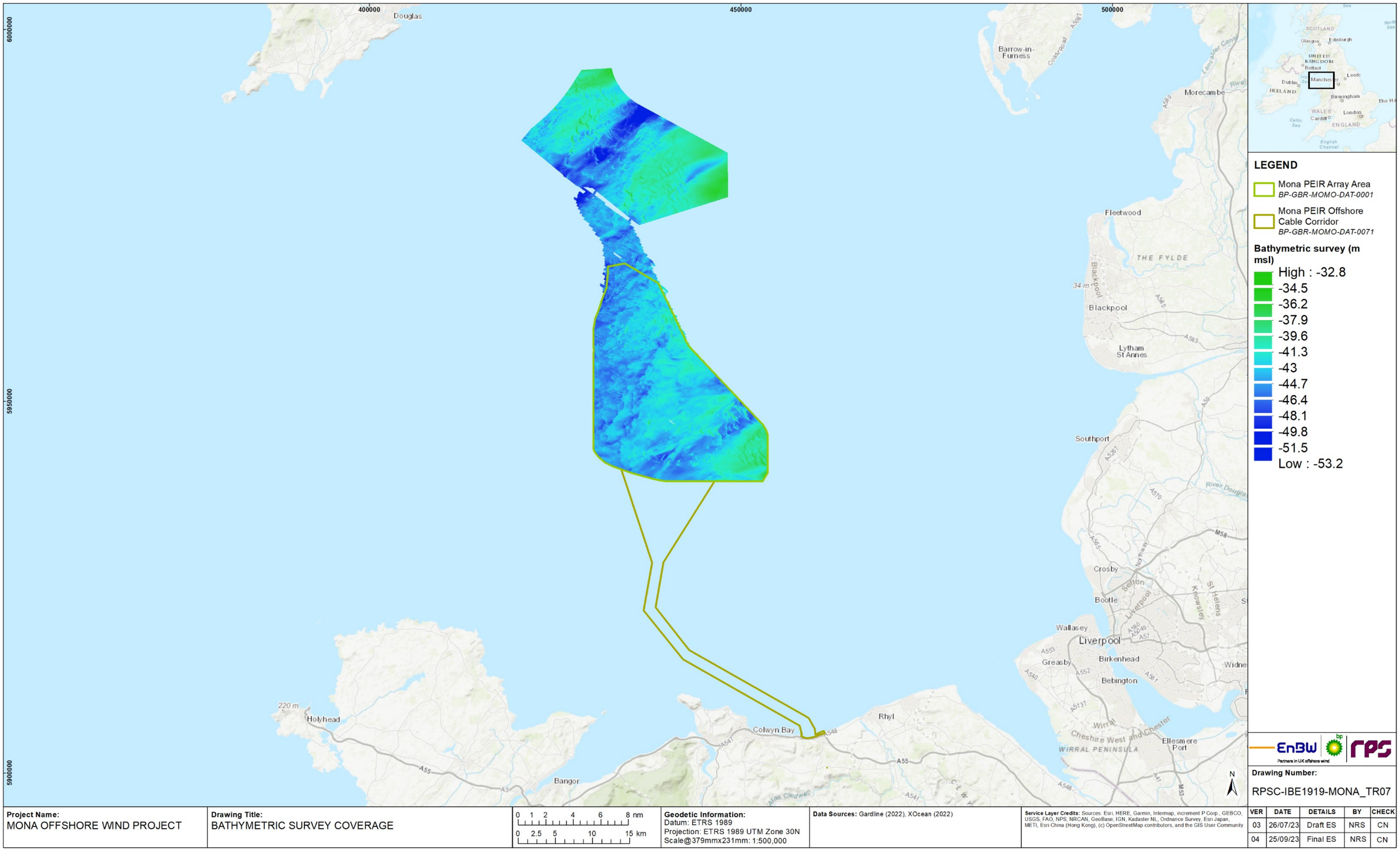

Figure 1.4: Mona and Morgan Generation Assets Array Areas bathymetric survey data coverage – Source: Gardline (2022) and XOcean (2022).

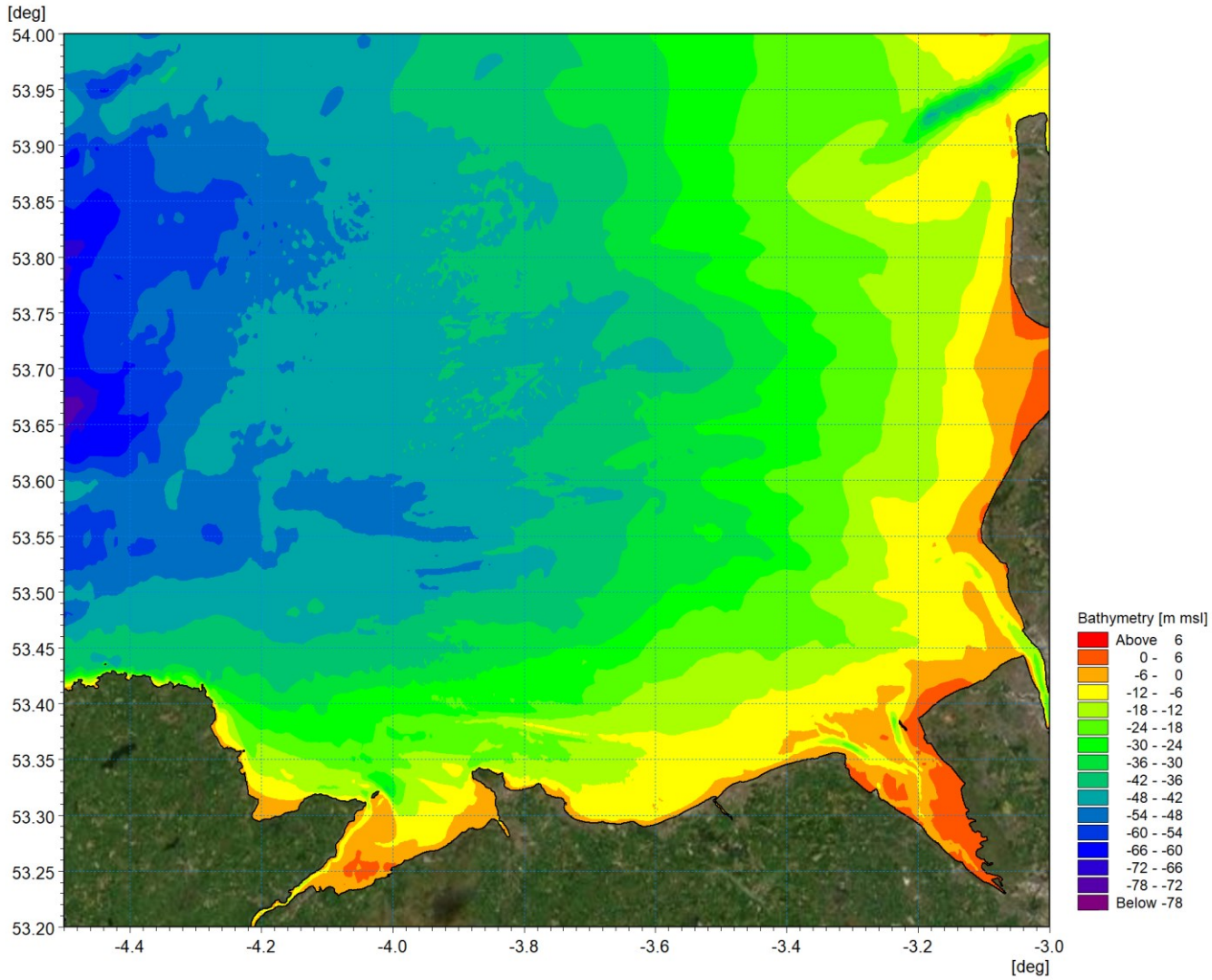

Figure 1.5: Model bathymetry within the east Irish Sea.

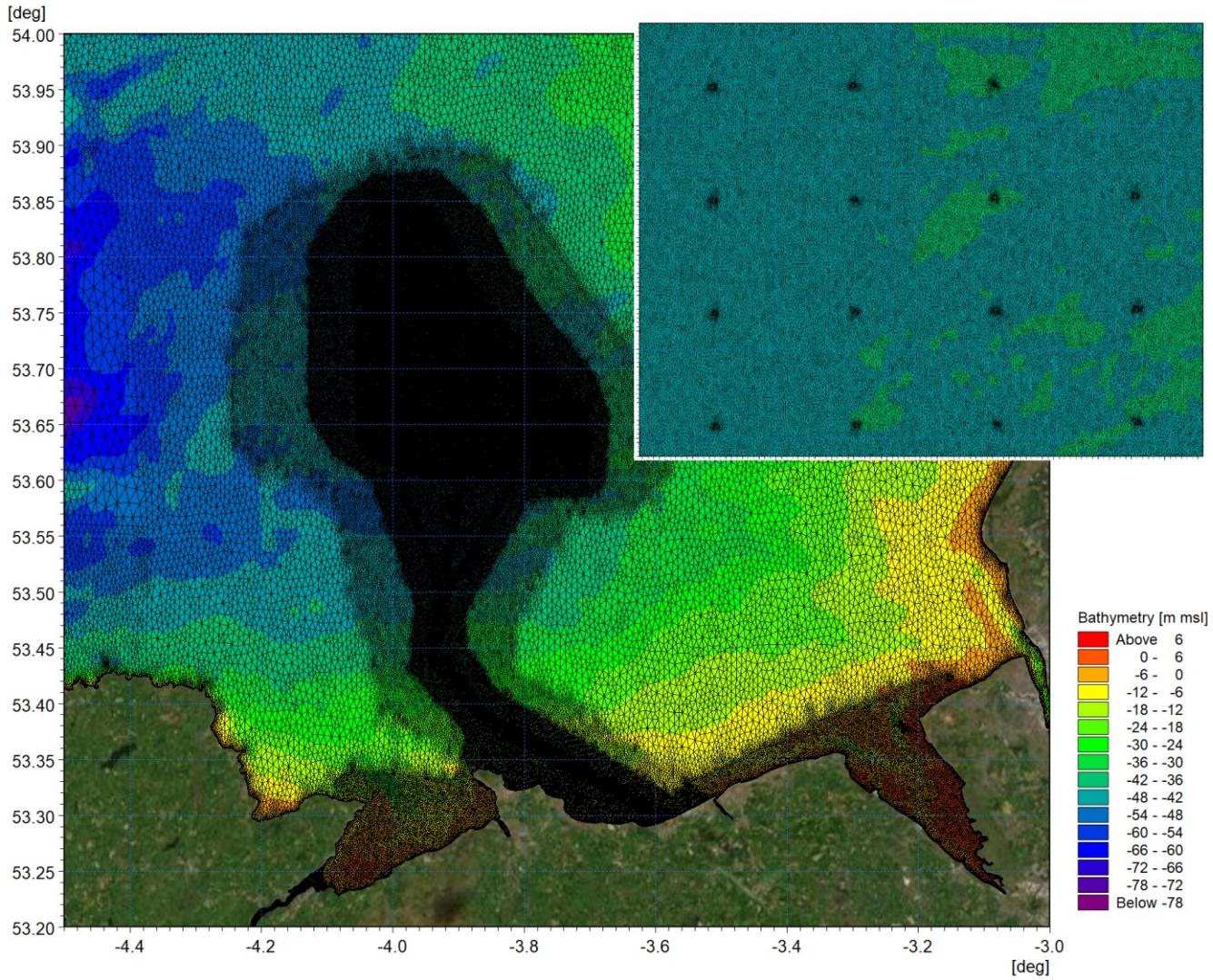

Figure 1.6: Model mesh with section of Mona PEIR Array Area inset.

Hydrography

1.3.5.6 The UKHO states that the mean tidal range at the Standard Port of Holyhead is approximately 3.65 m whilst at Douglas it is 4.55 m. The tidal characteristics shown in Table 1.5 in metres referenced to Chart Datum (CD):

Table 1.5: Tidal Levels at Standard Ports.

Tidal level (m CD)	Holyhead	Douglas
LAT	0.0	-0.3
Mean Low Water Springs (MLWS)	0.7	0.8
Mean Low Water Neaps (MLWN)	2.0	2.4
Mean Sea Level (MSL)	3.3	3.8
Mean High Water Neaps (MHWN)	4.4	5.4
MHWS	5.6	6.9

Tidal level (m CD)	Holyhead	Douglas
Highest Astronomical Tide (HAT):	6.3	7.9

1.3.5.7 The semi-diurnal tides are the dominant physical process in the Irish Sea moving into the Irish Sea from the Atlantic Ocean through both the North Channel and St. George's Channel. The tidal range in the Irish Sea is highly variable with the range in Liverpool Bay exceeding 10 m on the largest spring tides, the second largest in Britain.

1.3.5.8 The tidal flow simulations which form the basis of the study were undertaken using the MIKE21 FM flexible mesh modelling system. The FM Module is a two-dimensional, depth averaged hydrodynamic model which simulates the water level variations and flows in response to a variety of forcing functions in lakes, estuaries and coastal areas. The water levels and flows are resolved on a mesh covering the area of interest when provided with bathymetry, bed resistance coefficient, hydrodynamic boundary conditions, etc.

1.3.5.9 The tidal model was driven using boundary conditions extracted from RPS' Tide and Storm Surge Forecast (TSSF) model of Irish coastal waters (RPS, 2018), the extent and bathymetry of which is illustrated in Figure 1.7. This model was also developed using flexible mesh technology with the mesh size (model resolution) varying from circa 24 km along the offshore Atlantic boundary to circa 200 m around the Irish coastline. These boundaries were fully defined 'flather' boundaries for which both surface elevation and current vectors are specified.

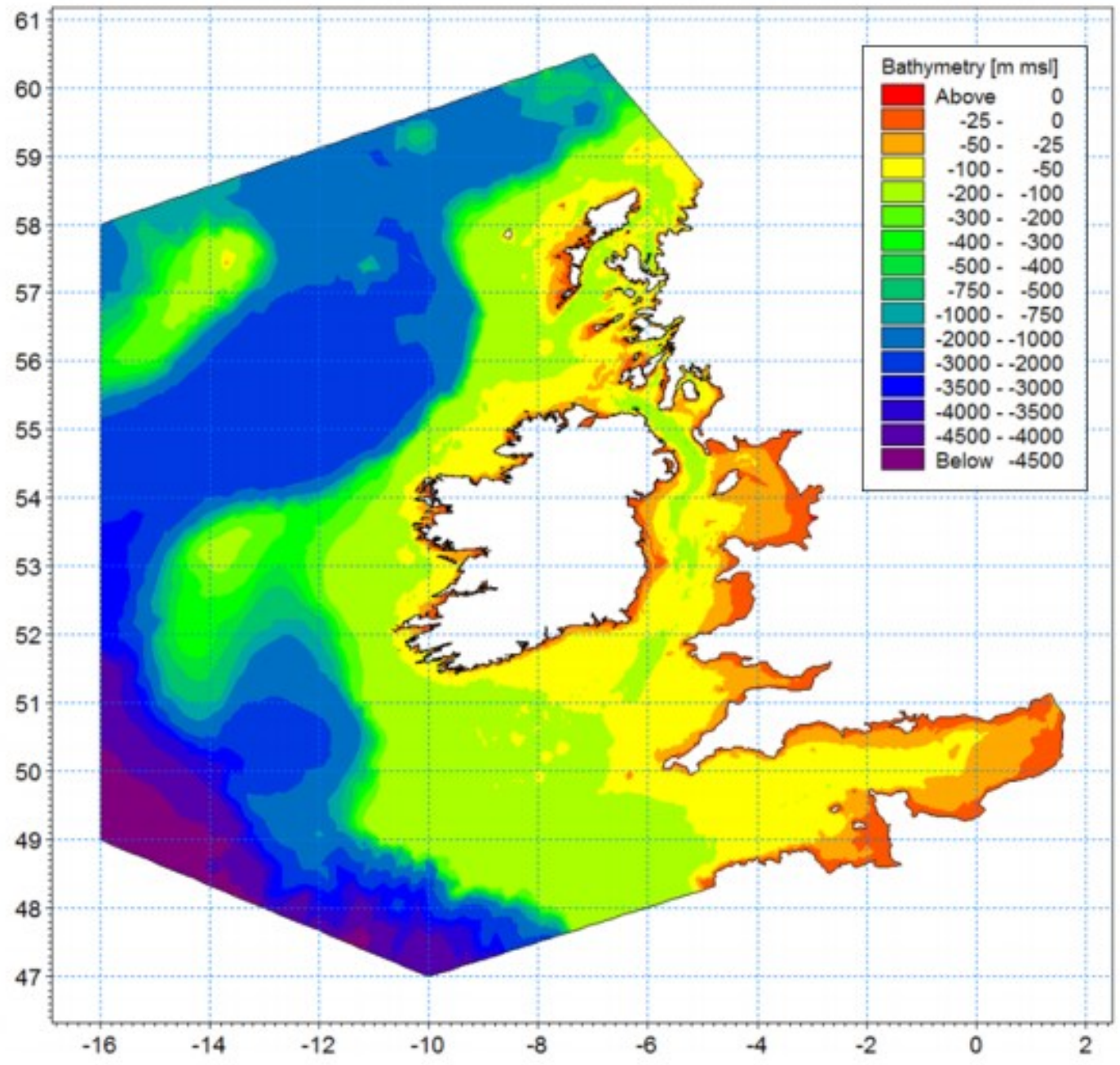

Figure 1.7: Extent and bathymetry of Irish Seas tidal and storm surge model.

1.3.5.10 A large amount of hydrometric data was available across the model domain as detailed in Table 1.3. The principal resources such as Admiralty tidal harmonics, BODC and Coastal Channel Observatory (CCO) are illustrated in Figure 1.8 with a range of these datasets being implemented during model calibration. The locations of the selection of calibration data presented in this document for tidal flow is shown in Figure 1.9.

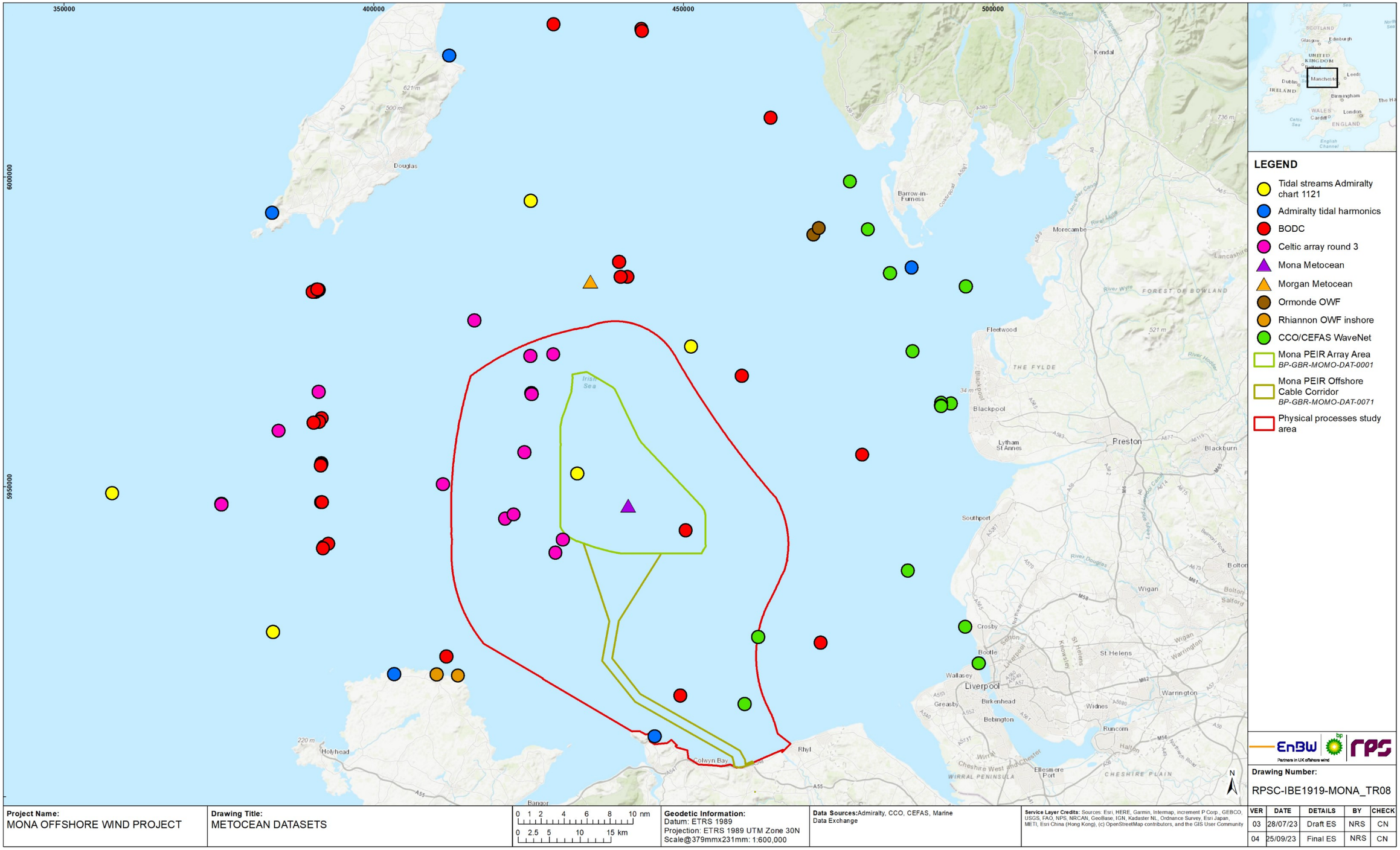

Figure 1.8: Availability of metocean datasets across the east Irish Sea.

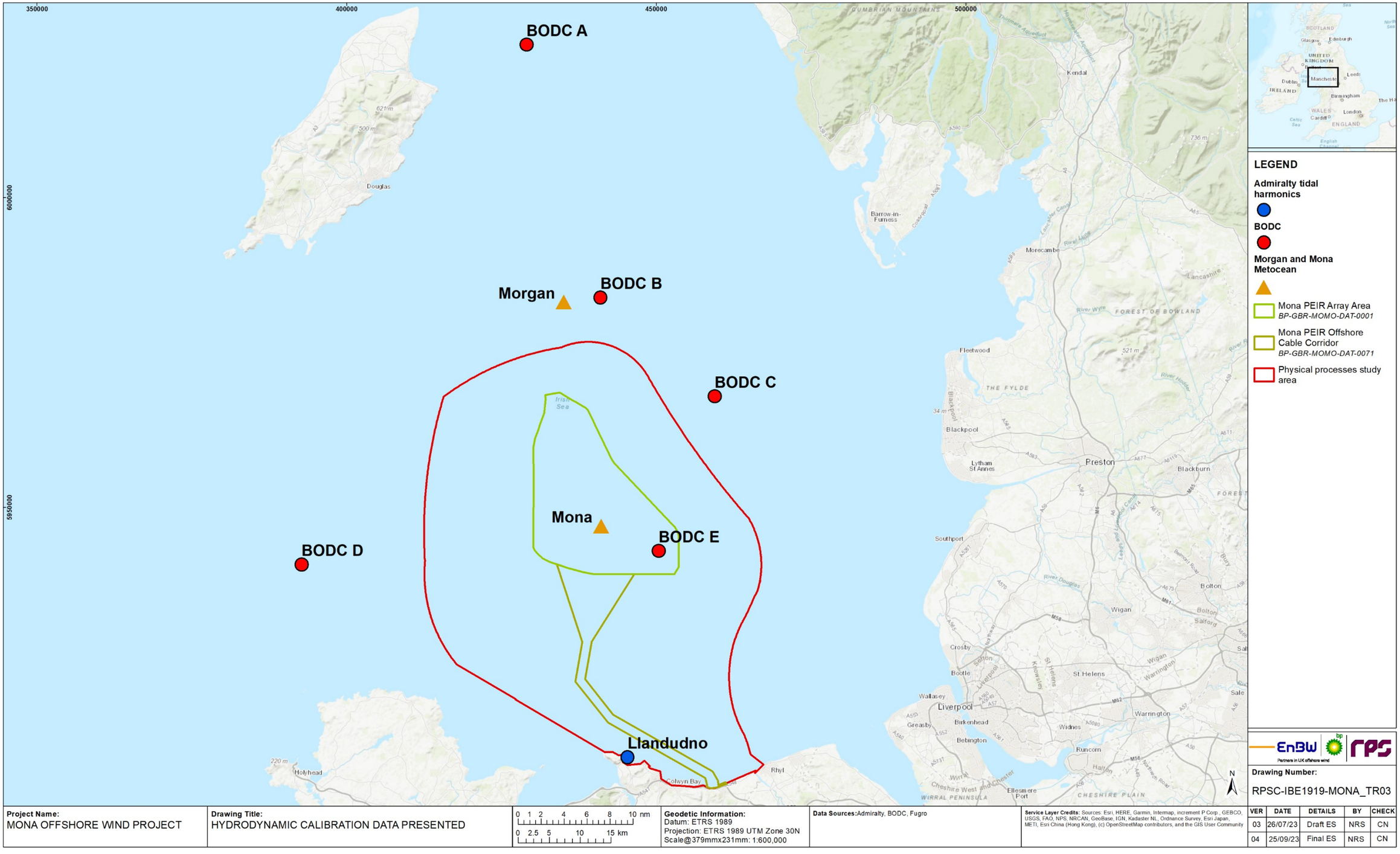

Figure 1.9: Location of calibration data presented.

1.3.5.11 Figure 1.10 shows the comparison of the modelled (red) and Admiralty tidal levels predicted from harmonic analysis (blue) at Llandudno. The model correlated well through both spring and neap tidal phases. The comparative study undertaken to quantify the potential changes in tidal currents was undertaken during both and neap spring tides to ensure a wide range of tidal conditions were applied in the modelling. The validation data presented therefore includes both tidal phases for each location.

1.3.5.12 For site specific calibration data, Mona metocean data plots are presented first illustrating spring and neap tides within the Mona Array Area. Each plot displays the current speed data on the left axis and the current direction on the right axis. The modelled depth average current speed is shown by a red trace and current direction by an orange trace. The measured data was collected at various water depths noted within the legend.

1.3.5.13 The Mona metocean buoy and Morgan Generation Assets metocean buoy tidal current data are presented in Figure 1.11 to Figure 1.14 and show similar trends in that current speeds during neap tides are half of the speed during spring tides. As well as the flood tide approaching from an easterly direction with the ebb tide being slightly weaker. The modelled data fits within the range of the Mona and Morgan Generation Assets measured data following similar tidal flow patterns.

1.3.5.14 Figure 1.15 to Figure 1.17 show the comparison between the Aanderaa Seaguard (ASG) and Nortek Signature (SIG) measuring devices against modelled metocean data during different tidal phases. The two devices were deployed at the Morgan Generation Assets site and the depth averaged (DA) current speed and direction are reported. The model current directionality correlates between both the ASG and SIG devices however current speeds between the model and ASG are more correlated than with the SIG device during the spring tide. In the neap tidal phase, the device speed and direction are within the range of the modelled data however the correlation is weaker than during the spring tidal phase. Comparisons of surface elevation between the ASG and modelled data are illustrated for both spring and neap tidal phases in Figure 1.16 and Figure 1.18.

1.3.5.15 For each location of BODC data, a pair of plots are presented firstly relating to spring tides and secondly neap tides. In each plot the current speed data is presented on the left axis whilst the current direction is presented to the right. The modelled depth average current speed is shown by a red trace and current direction by an orange trace. The measured data was collected at various water depths noted within the legend.

1.3.5.16 Sites A and B are presented in Figure 1.19 to Figure 1.22 and indicate that the flood tide which approaches the Mona PEIR Offshore Wind Project from an easterly direction is more dominant than the ebb tide. Peak neap tidal current speeds are typically half of those experienced during spring tide. The modelled data largely lie within the range of the measured data and replicates the asymmetric tidal flows patterns.

1.3.5.17 This is also the case for site C shown in Figure 1.23 and Figure 1.24 for spring and neap respectively. Current directions and the dominance of flood tides are replicated with the model domain. Tidal currents at site D are more strongly bi-directional as flow is accelerated around Anglesey as illustrated in Figure 1.25 and Figure 1.26. It is noted that there is a wide variation in the measured tidal currents with respect to depth and 70 m at this location would represent near bed conditions. The model does however correlate in terms of current directionality and the dominance of flood tide currents.

1.3.5.18 Finally, at the Mona Array Area, site E, the tidal current speeds and directions are well represented by the model. This is the case for both spring, Figure 1.27, and neap, Figure 1.28, tidal flows. The calibration data demonstrates that the numerical model simulates the tidal currents in the region. This includes the representation of the dominant flood tide.

1.3.5.19 To provide a representation of tidal flows across the domain, Figure 1.29 and Figure 1.30 illustrate tidal patterns during peak ebb and flood on a neap tide, whilst Figure 1.31 and Figure 1.32 illustrate the spring tide. These points in the tidal cycle are used as reference for the assessment of potential impacts and changes to tidal flows due to the Mona PEIR Offshore Wind Project. Also, for reference, the location of designated areas of relevance to physical processes are shown by a pink outline Figure 1.29 to Figure 1.32. The period selected for the comparative study represents a spring tide on the upper end of the range experienced in the region; this was to ensure the study included the greatest variation in tidal conditions (i.e. water depth and current speed). Residual tidal flows and how they drive sediment transport regimes are examined in section 1.6.6.

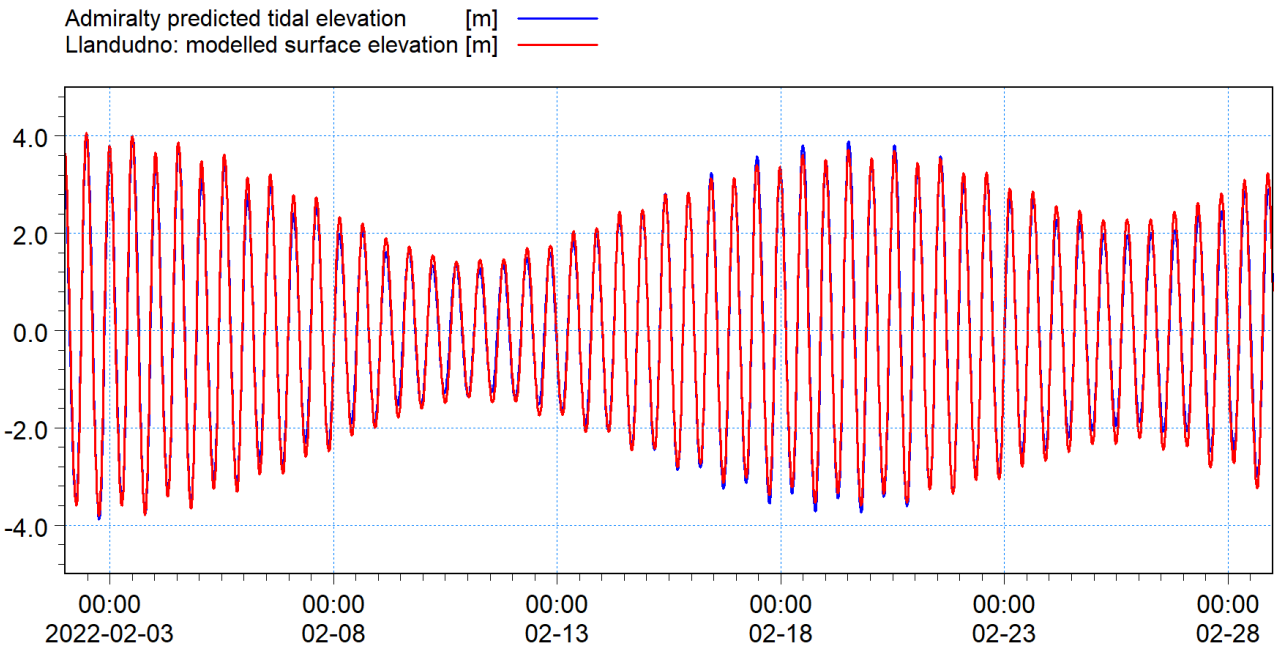

Figure 1.10: Comparison of model and admiralty harmonic tide data for Llandudno.

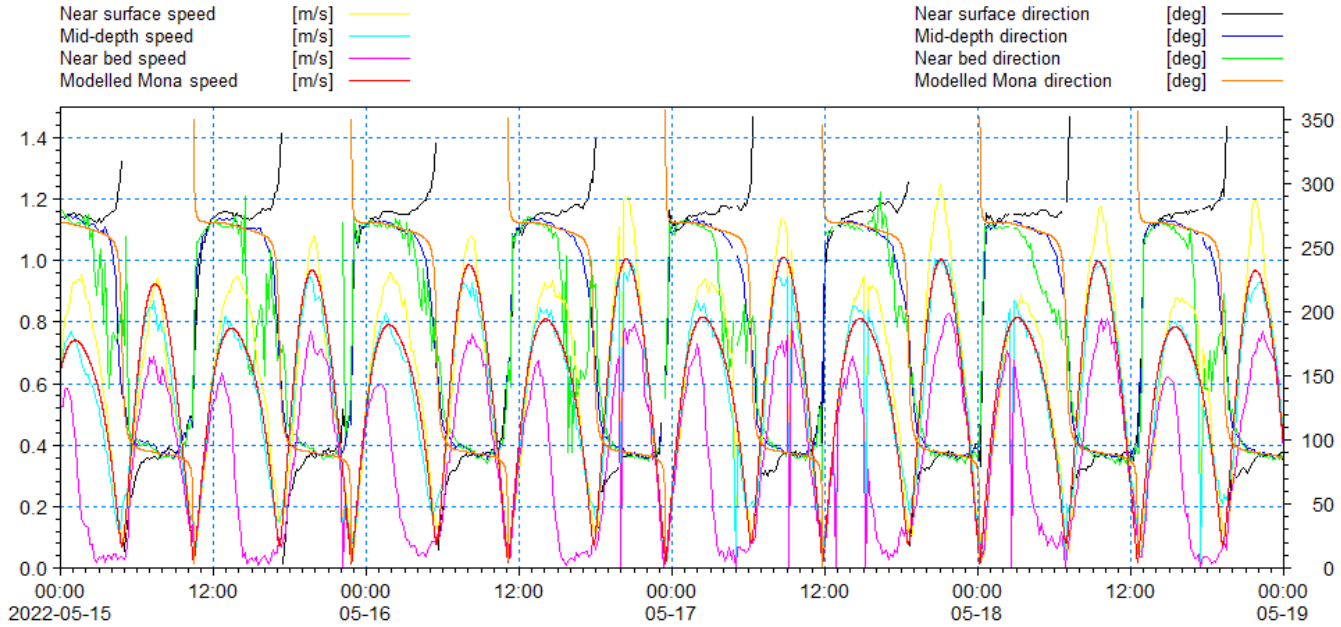

Figure 1.11: Comparison of model and recorded Mona Array Area metocean site – current speed and direction spring.

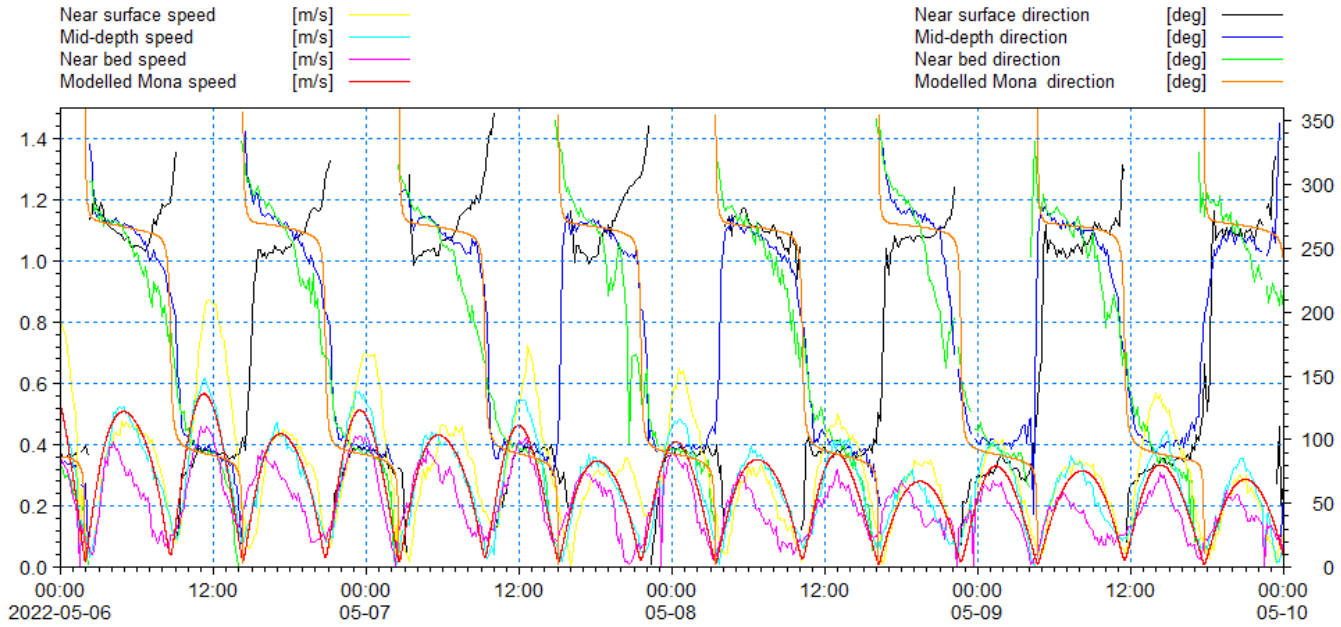

Figure 1.12: Comparison of model and recorded Mona Array Area metocean site – current speed and direction neap.

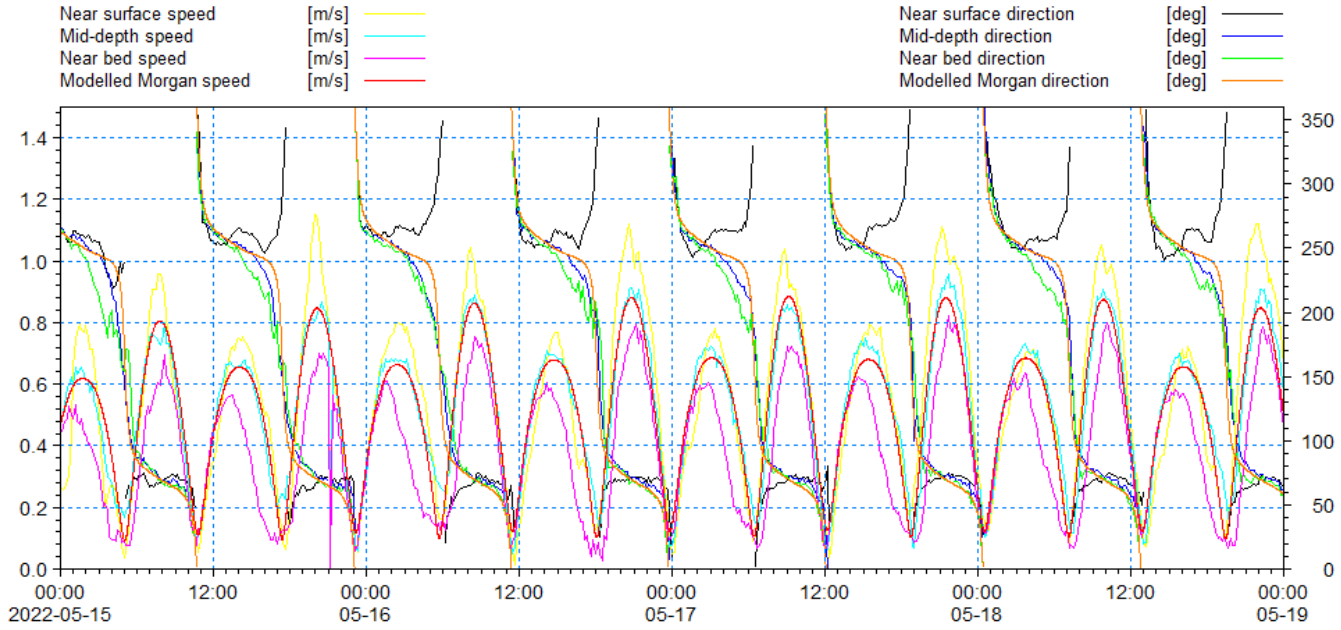

Figure 1.13: Comparison of model and recorded at the Morgan Generation Assets metocean site – current speed and direction spring.

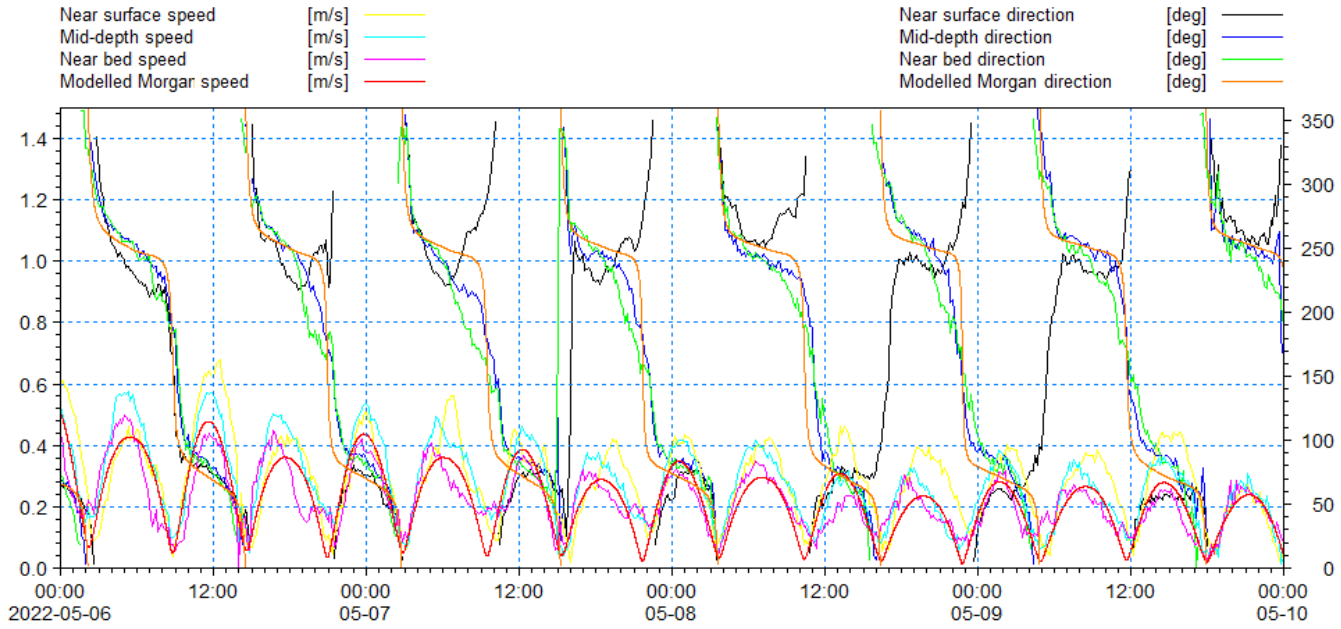

Figure 1.14: Comparison of model and recorded Morgan at the Generation Assets metocean site – current speed and direction neap.

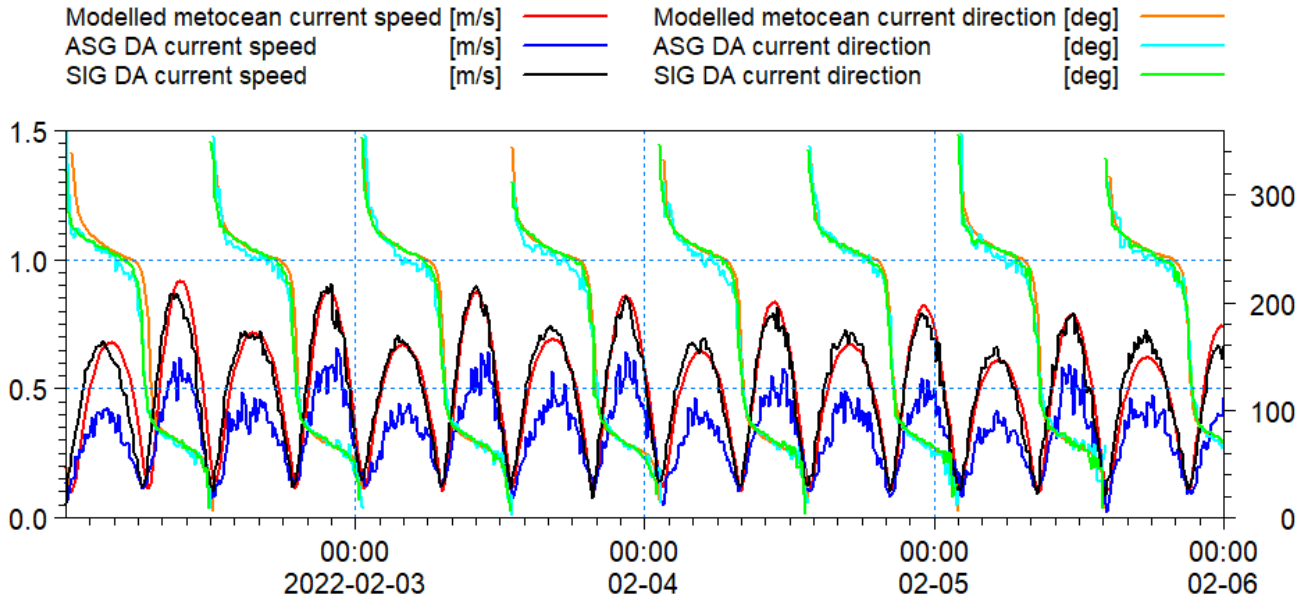

Figure 1.15: Comparison of modelled metocean and recorded DA ASG and SIG – current speed and direction spring.

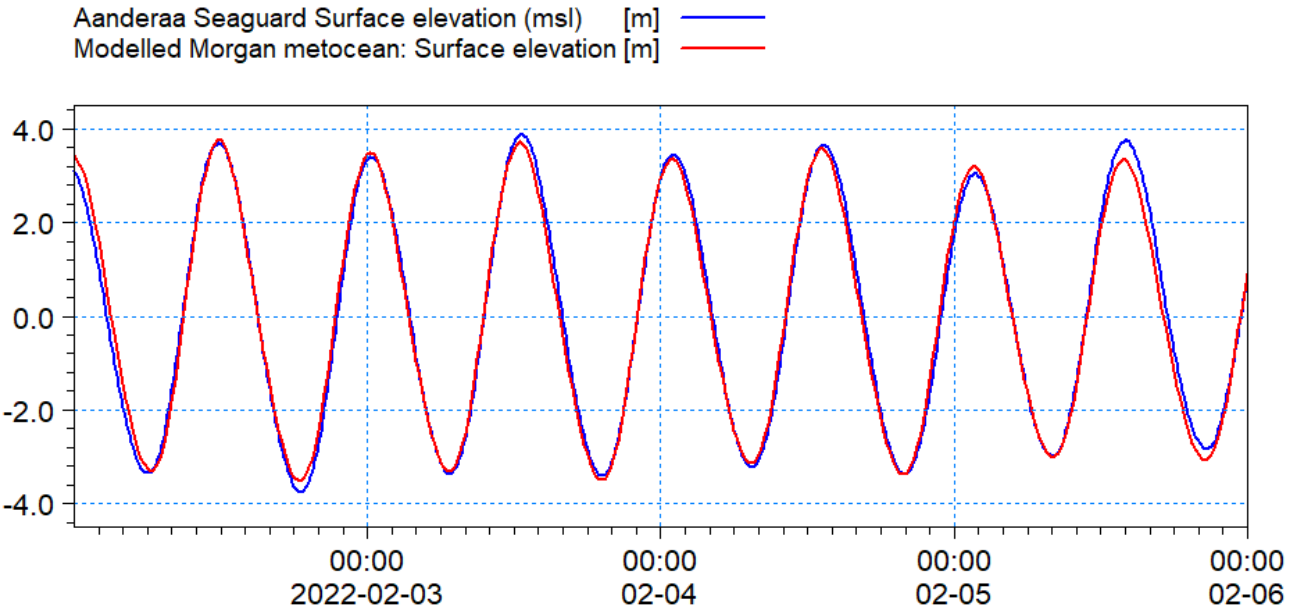

Figure 1.16: Comparison of modelled Morgan Generation Assets metocean site and recorded ASG – spring surface elevation.

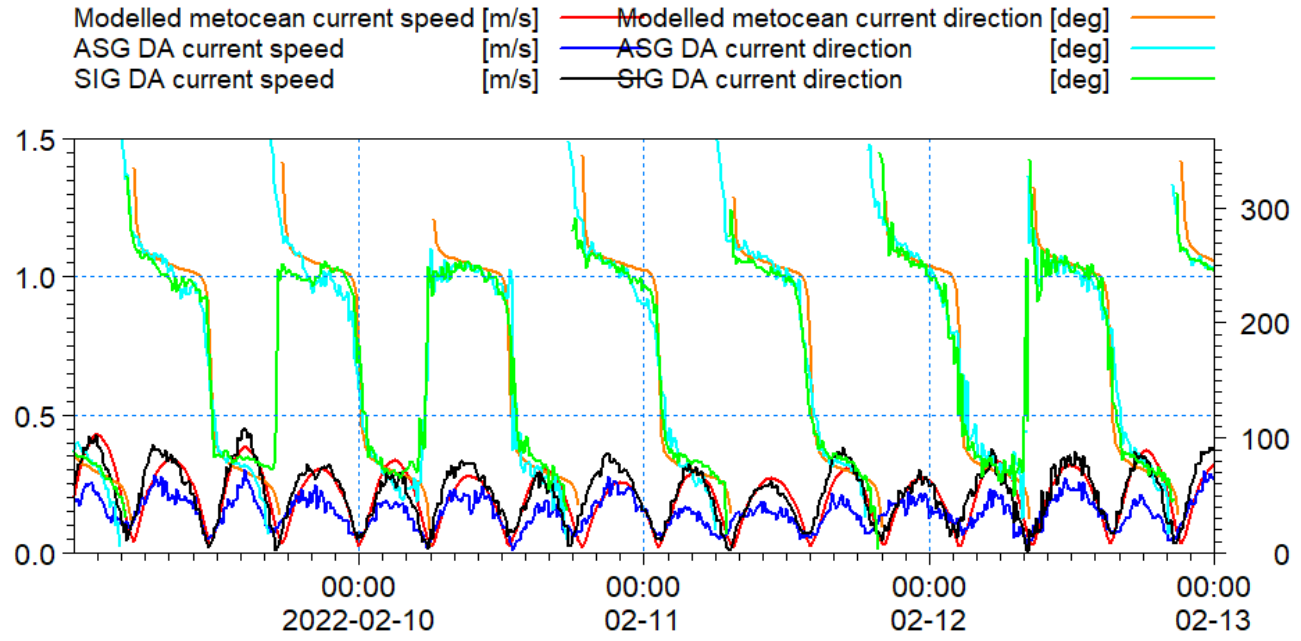

Figure 1.17: Comparison of modelled metocean and recorded DA ASG and SIG depth averaged– current speed and direction neap.

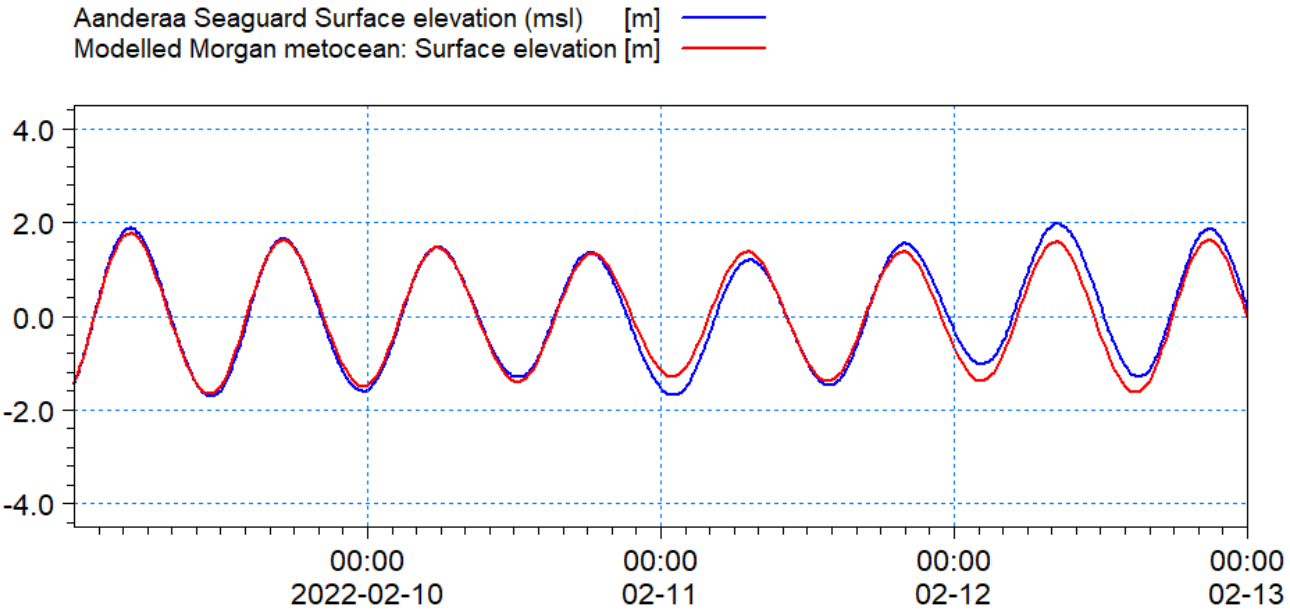

Figure 1.18: Comparison of modelled Morgan Generation Assets metocean site and recorded ASG – neap surface elevation.

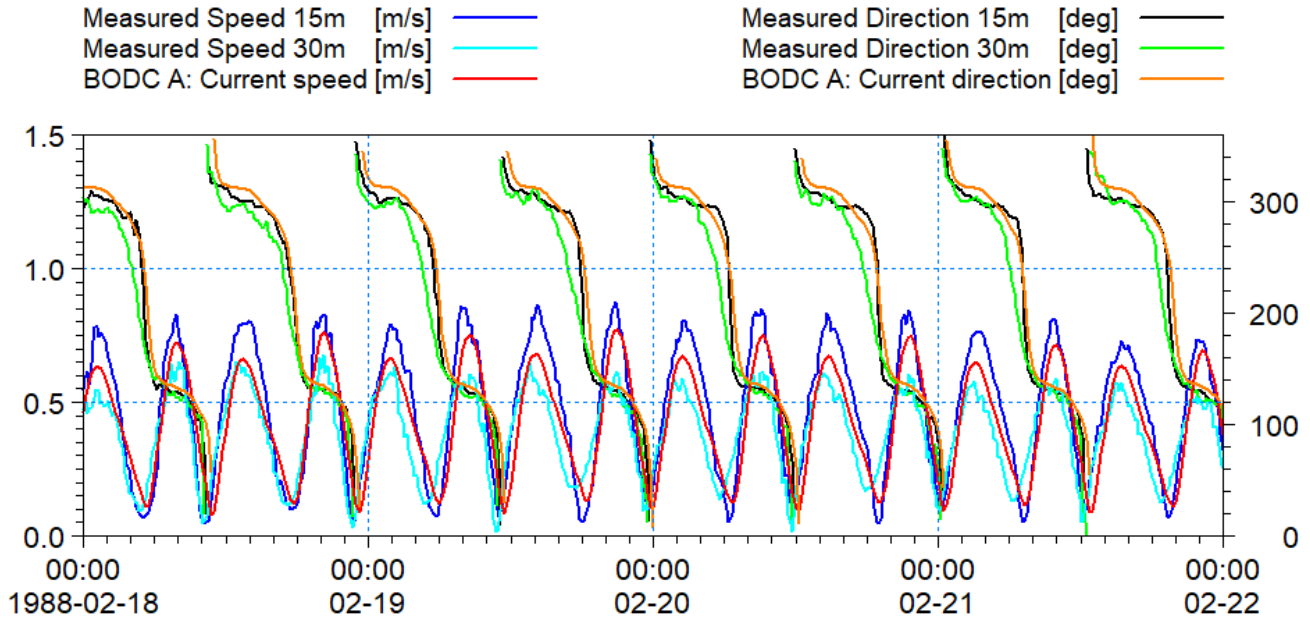

Figure 1.19: Comparison of model and recorded data BODC Location A – current speed and direction spring.

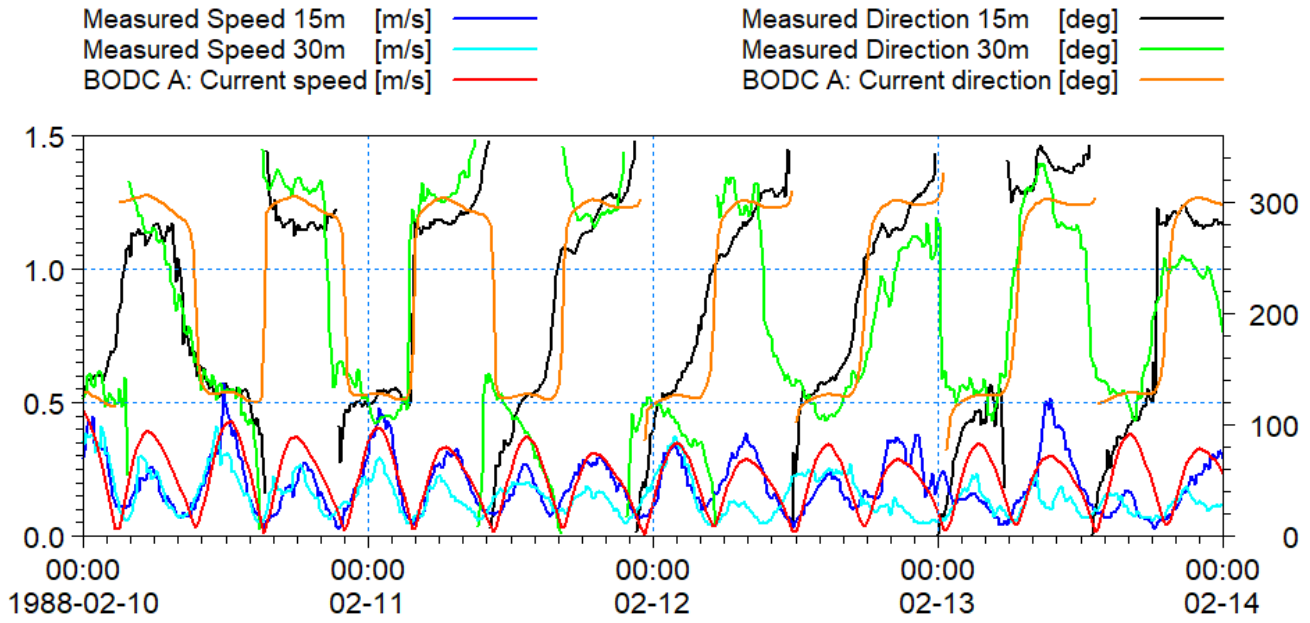

Figure 1.20: Comparison of model and recorded data BODC Location A – current speed and direction neap.

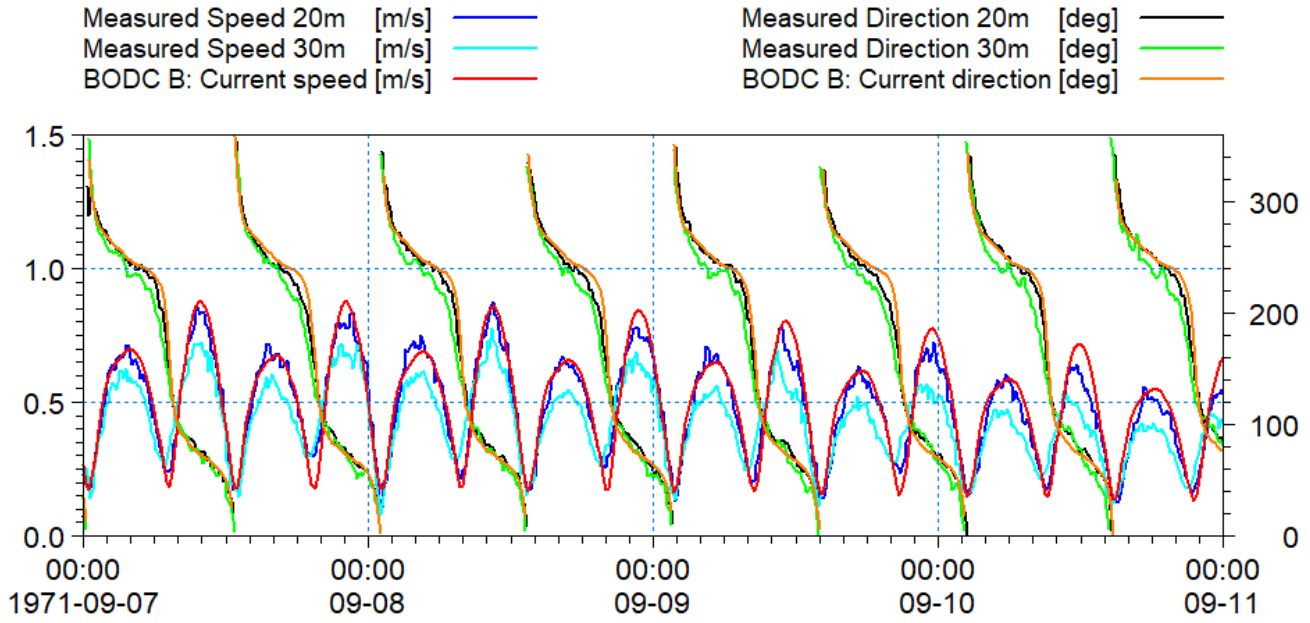

Figure 1.21: Comparison of model and recorded data BODC Location B – current speed and direction spring.

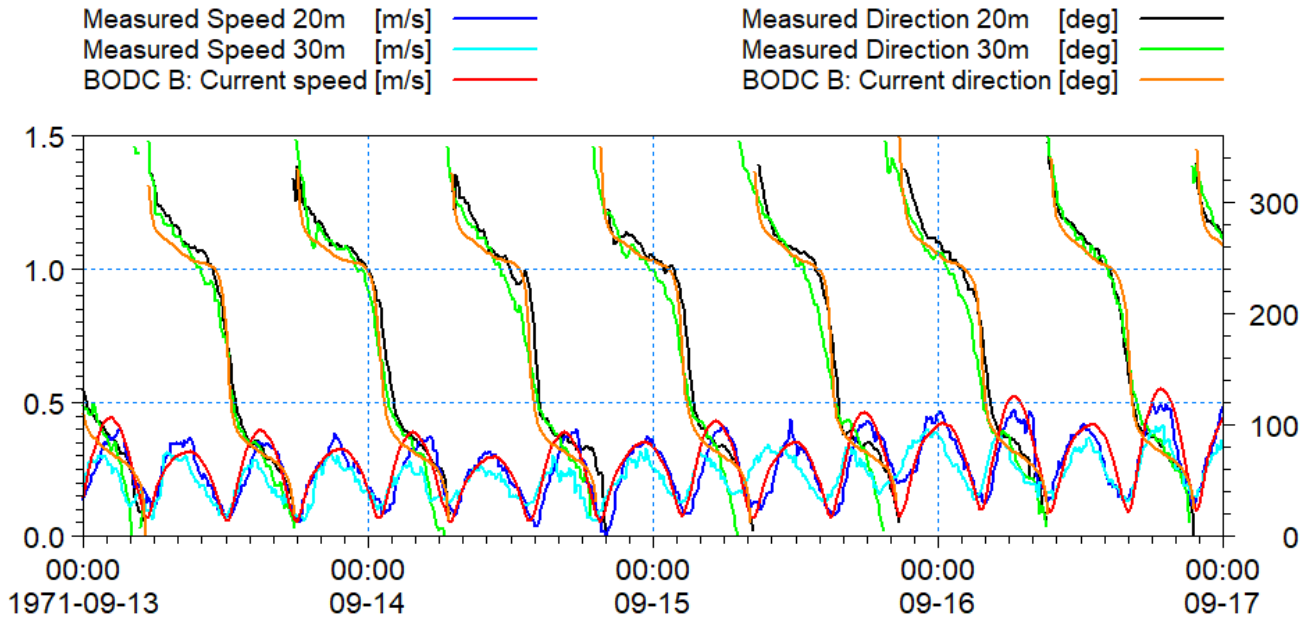

Figure 1.22: Comparison of model and recorded data BODC Location B – current speed and direction neap.

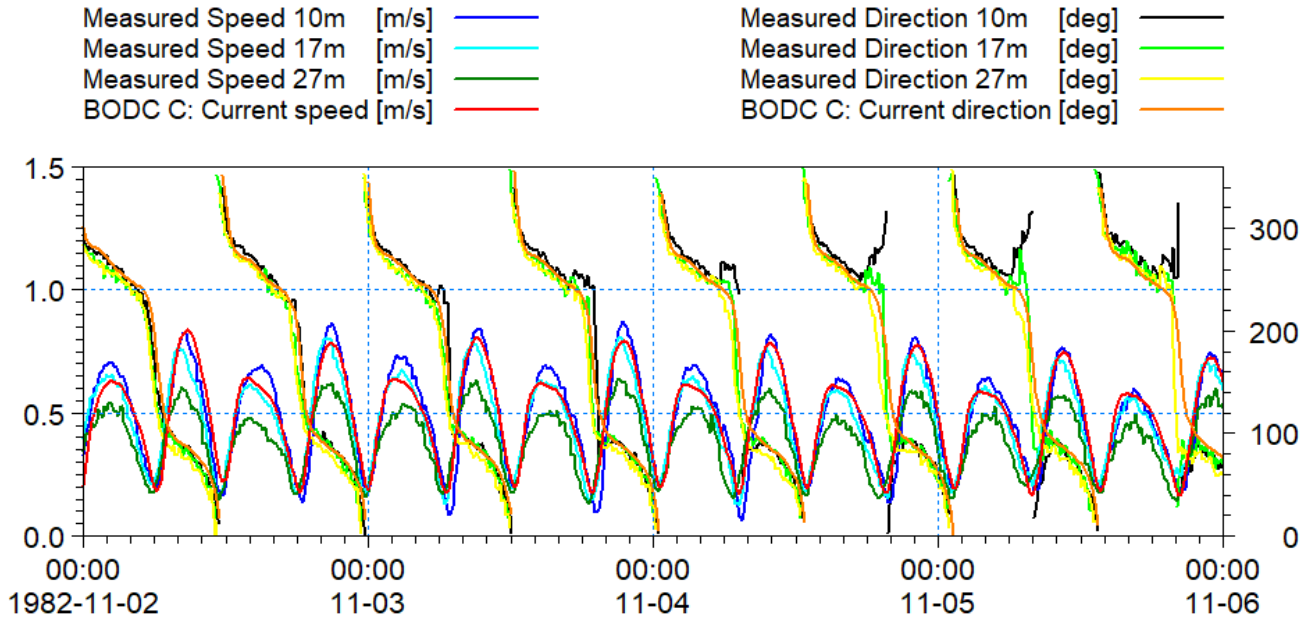

Figure 1.23: Comparison of model and recorded data BODC Location C – current speed and direction spring.

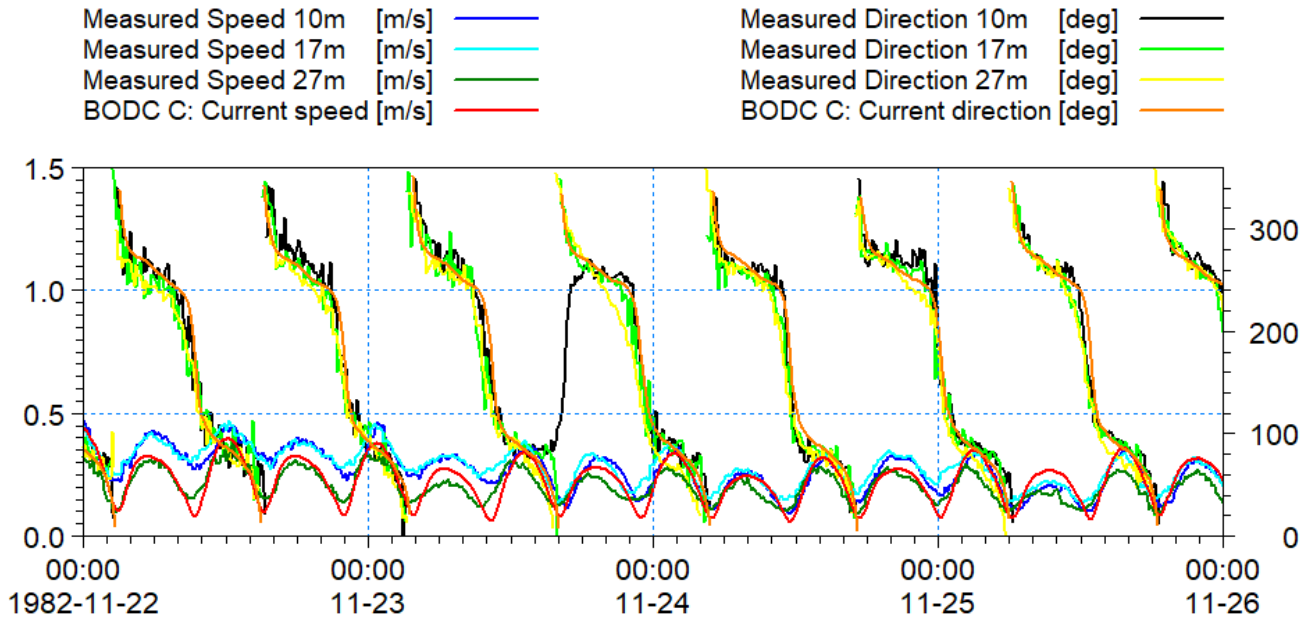

Figure 1.24: Comparison of model and recorded data BODC Location C – current speed and direction neap.

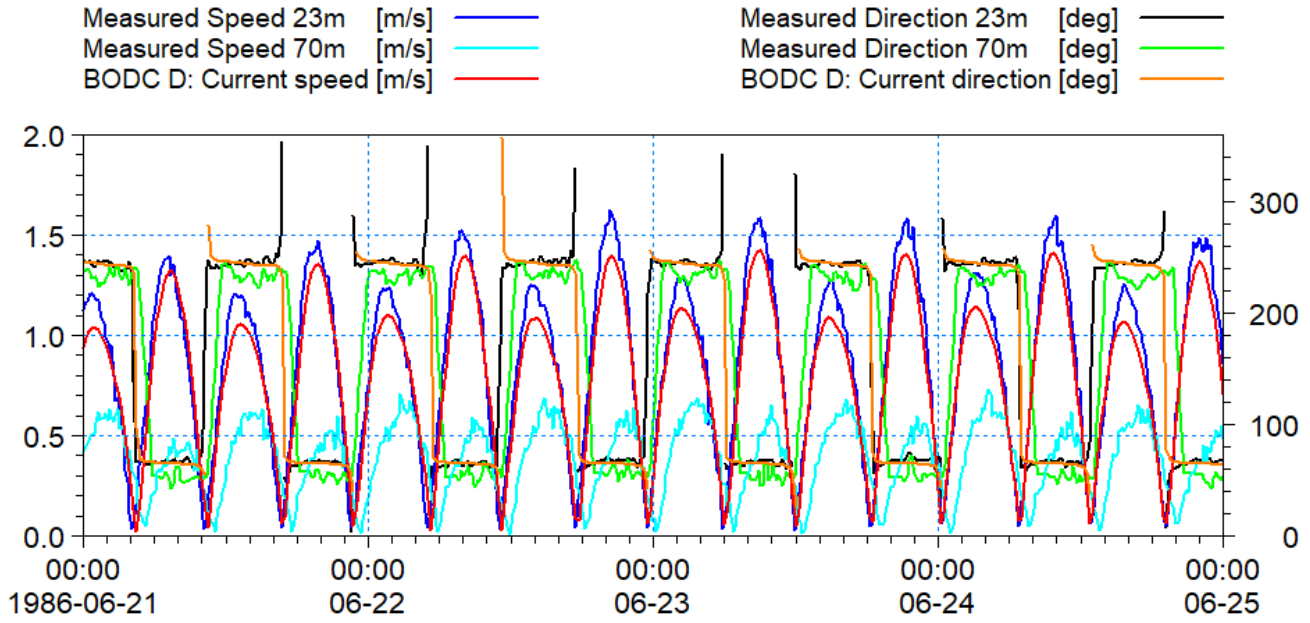

Figure 1.25: Comparison of model and recorded data BODC Location D – current speed and direction spring.

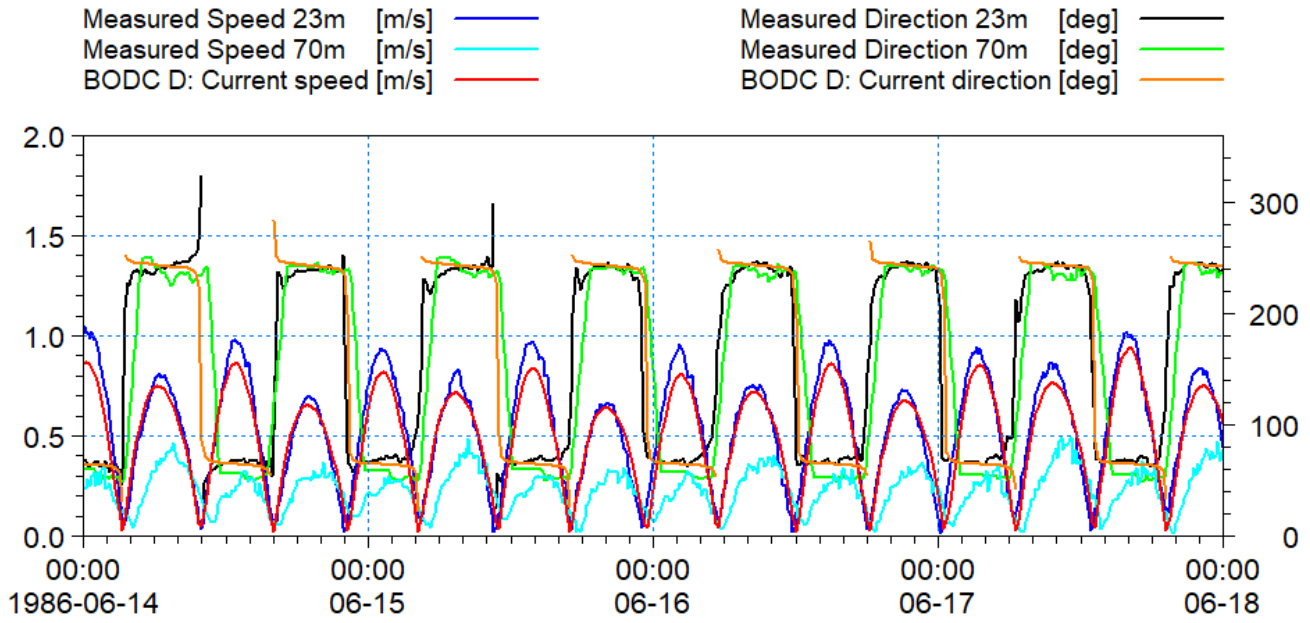

Figure 1.26: Comparison of model and recorded data BODC Location D – current speed and direction neap.

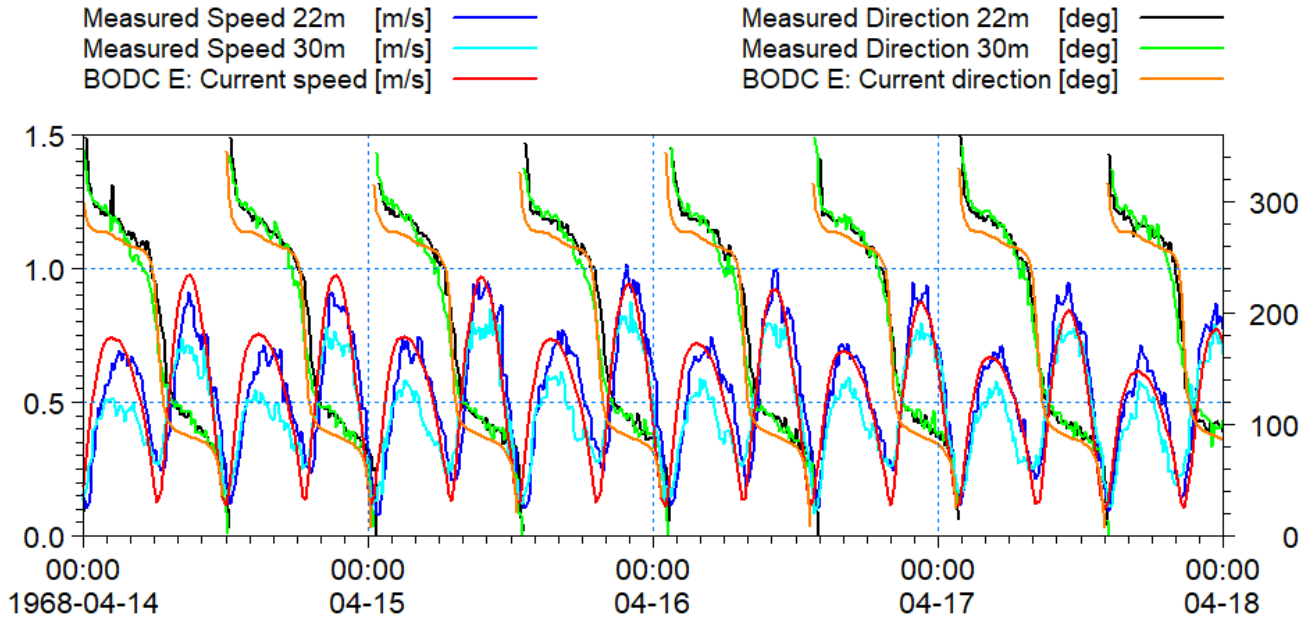

Figure 1.27: Comparison of model and recorded data BODC Location E – current speed and direction spring.

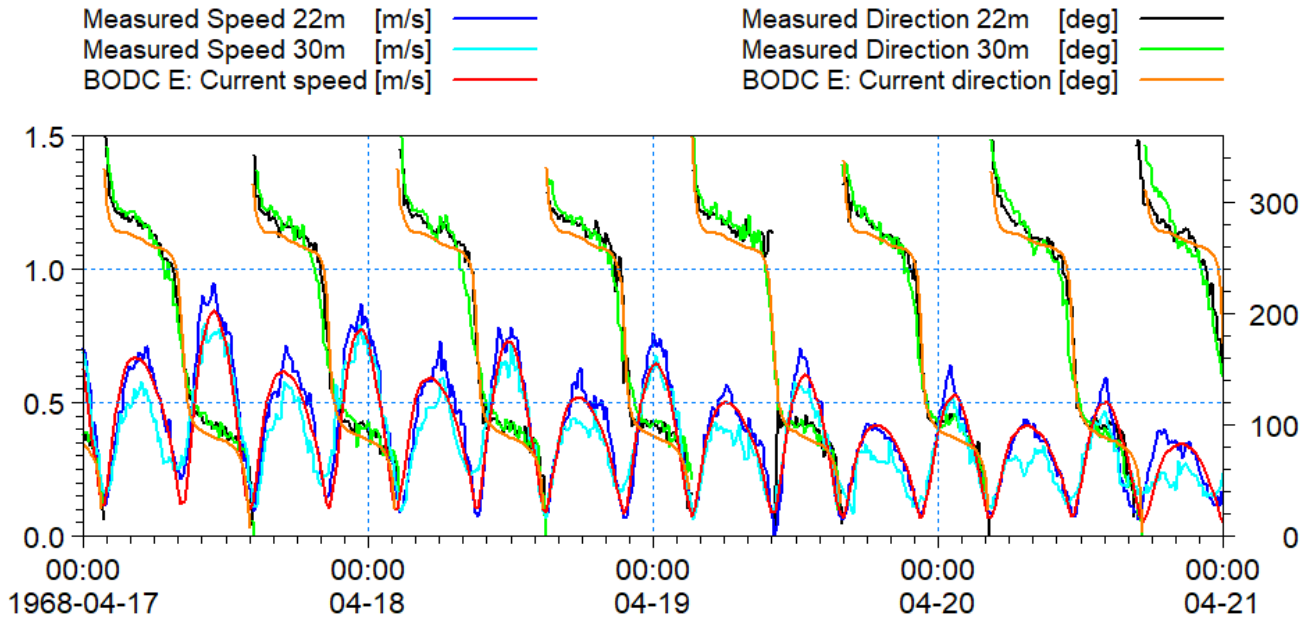

Figure 1.28: Comparison of model and recorded data BODC Location E – current speed and direction neap.

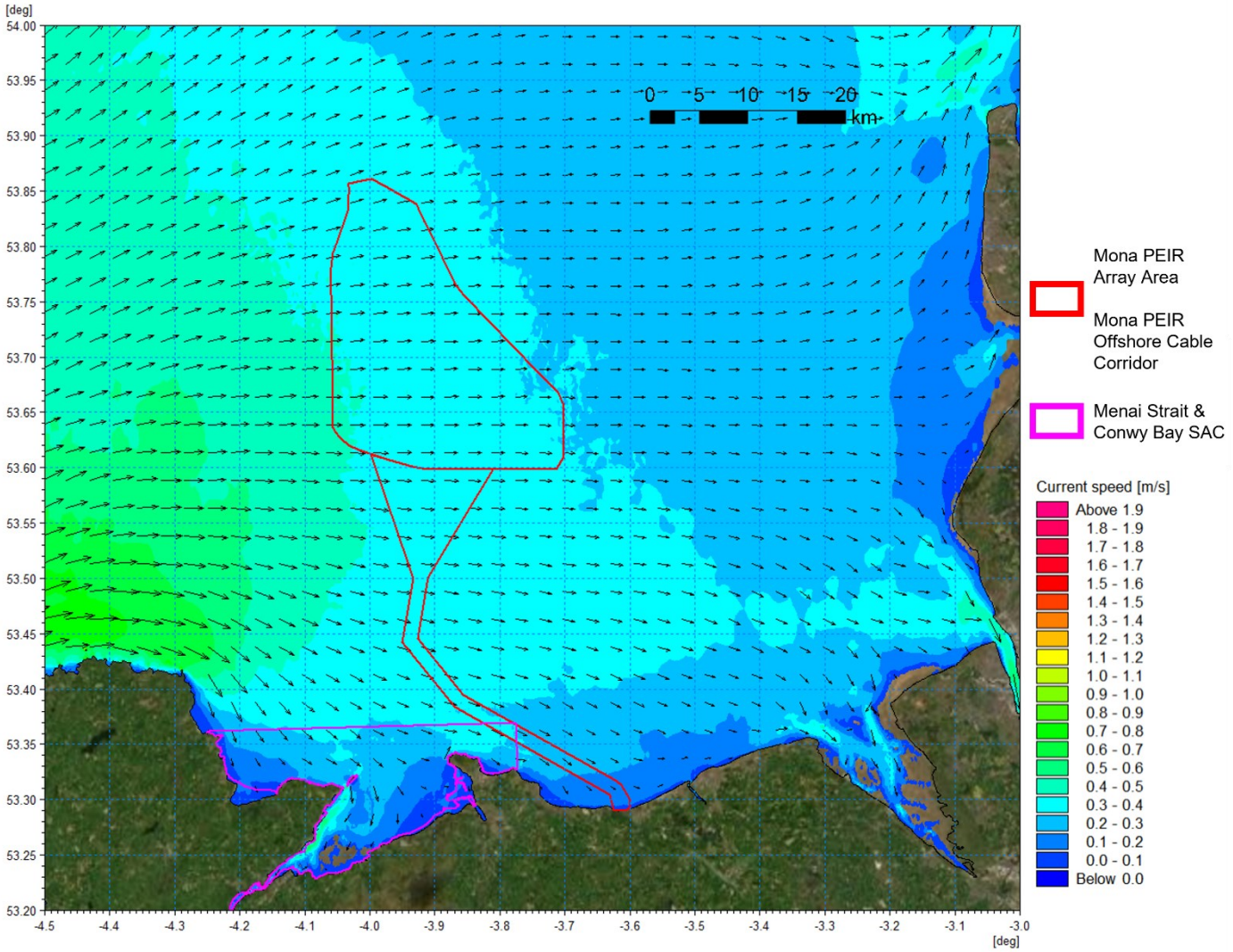

Figure 1.29: Tidal flow patterns – neap tide flood.

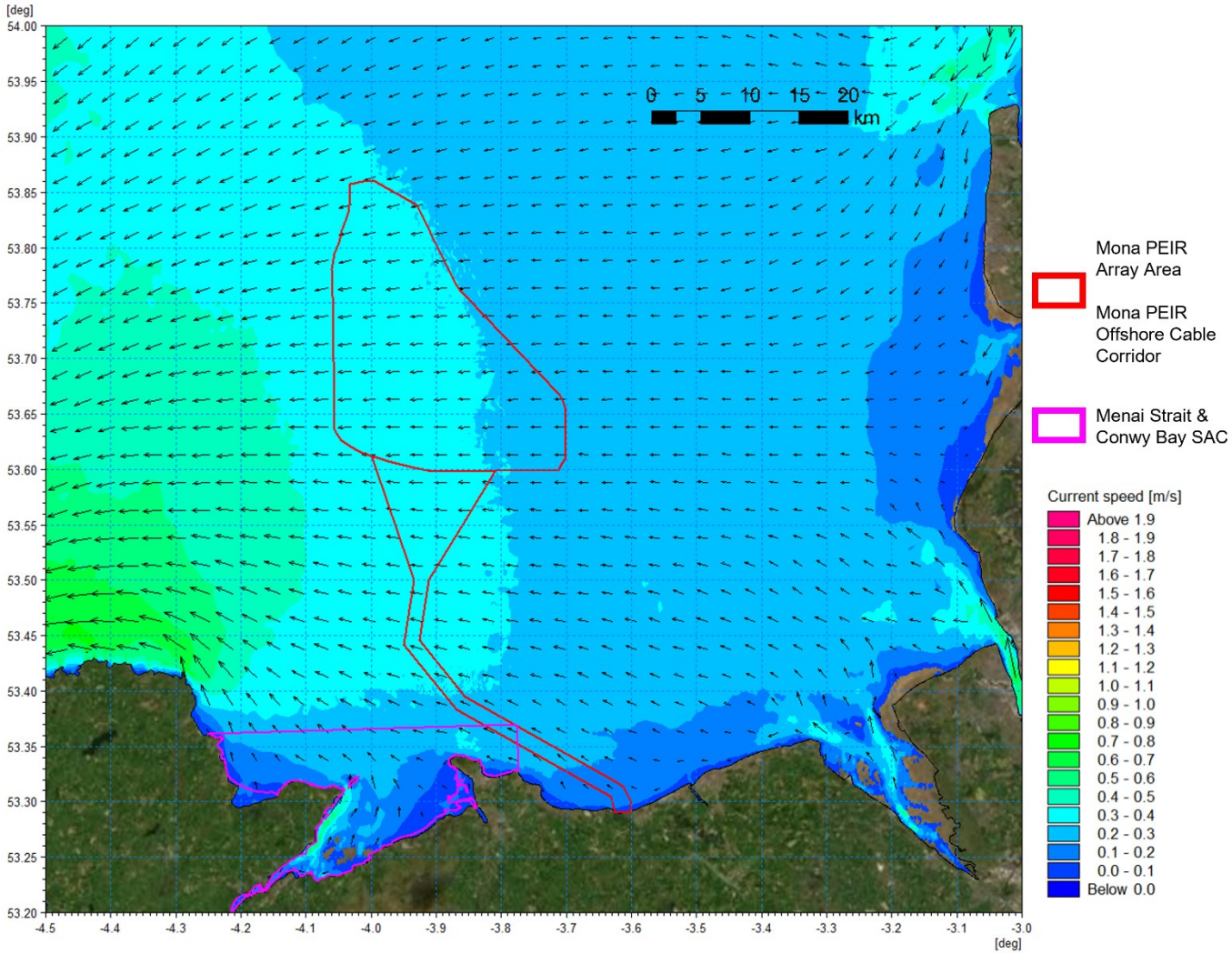

Figure 1.30: Tidal flow patterns – neap tide ebb.

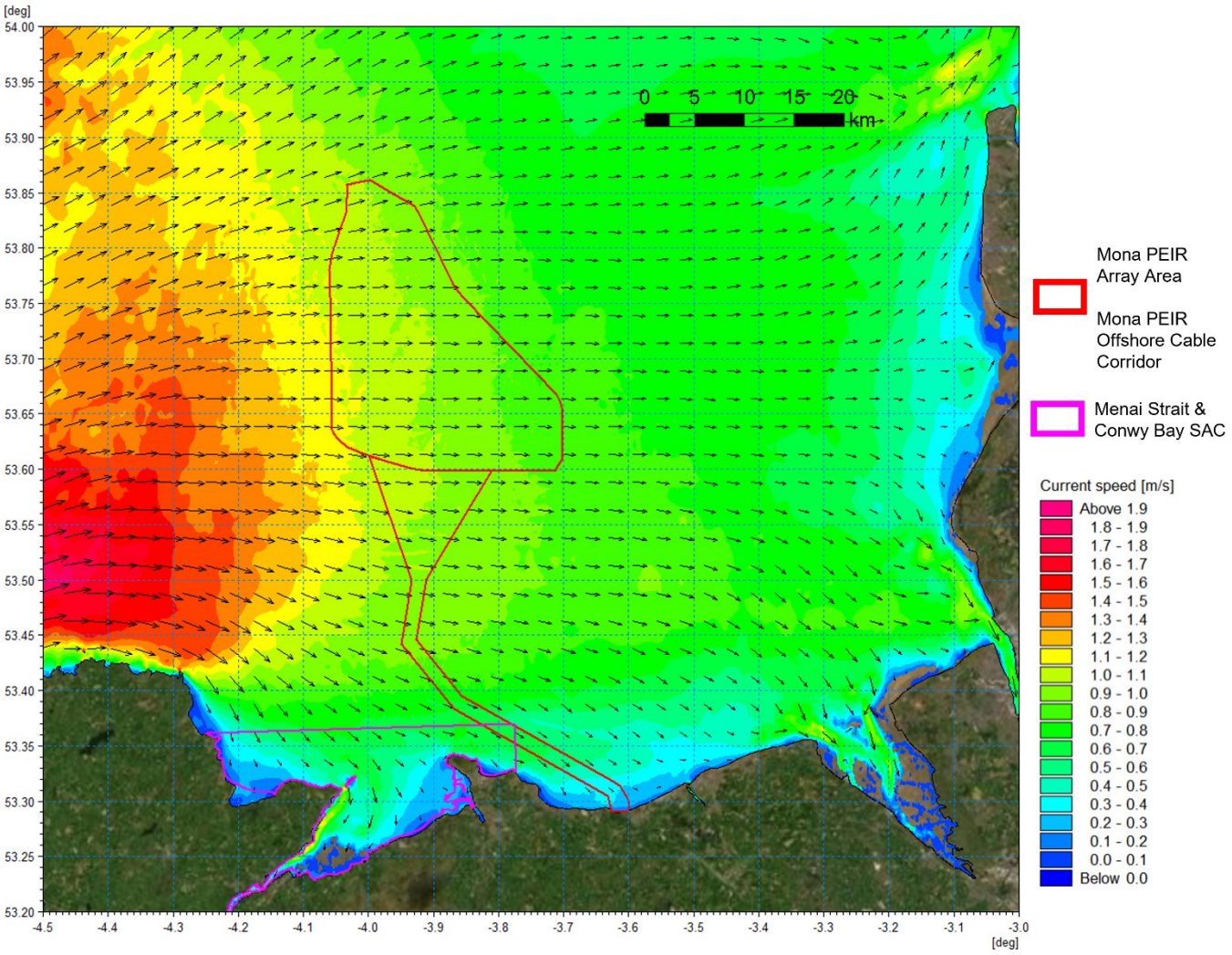

Figure 1.31: Tidal flow patterns – spring tide flood.

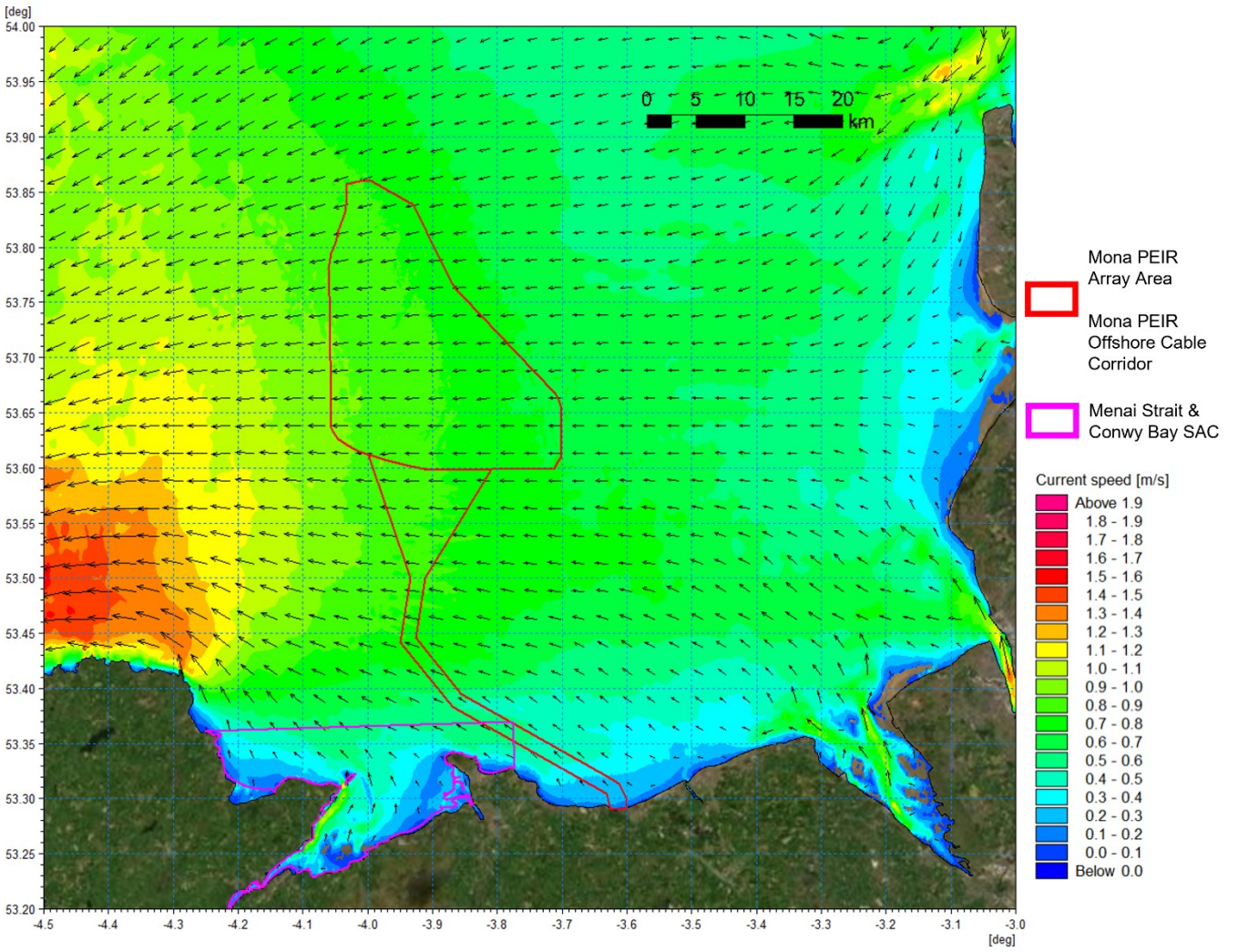

Figure 1.32: Tidal flow patterns – spring tide ebb.

Wave climate

1.3.5.20 Waves in the east Irish Sea are highest to the southwest of the Isle of Man with the highest mean annual significant wave height of 1.39 m recorded between the Isle of Man and Anglesey. Significant wave height is reduced closer to the coast with the lowest significant wave height of 0.73 m recorded to the west of the Dee Estuary (ABPmer, 2008). In the Mona physical processes study area mean annual wave height ranges from 1.1 m to 1.3 m. Over 40% of the waves arise from the southwest with all significant wave heights (>4 m) arriving from the southwest or west (ABPmer, 2018). This is illustrated in Figure 1.33 which shows the wave rose for a point located within this area. Similarly, the corresponding wind rose presented in Figure 1.33 which illustrates the predominant winds are from the southwest with the site being located in the lee of the Isle of Man.

1.3.5.21 As offshore waves transfer from the deep offshore water to shallower coastal areas, a number of important modifications may result due to interactions of offshore deep-water waves with the seabed, with the resultant modifications producing shallow water waves. These physical 'wave transformation' interactions include:

- Shoaling and refraction (due to both depth and current interactions with the wave)

- Energy loss due to breaking
- Energy loss due to bottom friction
- Momentum and mass transport effect.

1.3.5.22 The wave model developed for the assessment was calibrated using data collected during storm Christoph which occurred during January 2021. The model simulated water levels using boundary data extracted from the RPS storm surge model and applied meteorological conditions from the European Centre for Medium-range Weather Forecasting (ECMWF) operational dataset. Wave conditions at the model boundary were also provided from the ECMWF operational dataset.

1.3.5.23 The model output data was then compared with measured data obtained from the National Network of Regional Coastal Monitoring Programmes held by the CCO at the locations shown in Figure 1.35. For each of the three location three parameters are presented relating to mean wave direction, significant wave height and peak wave period.

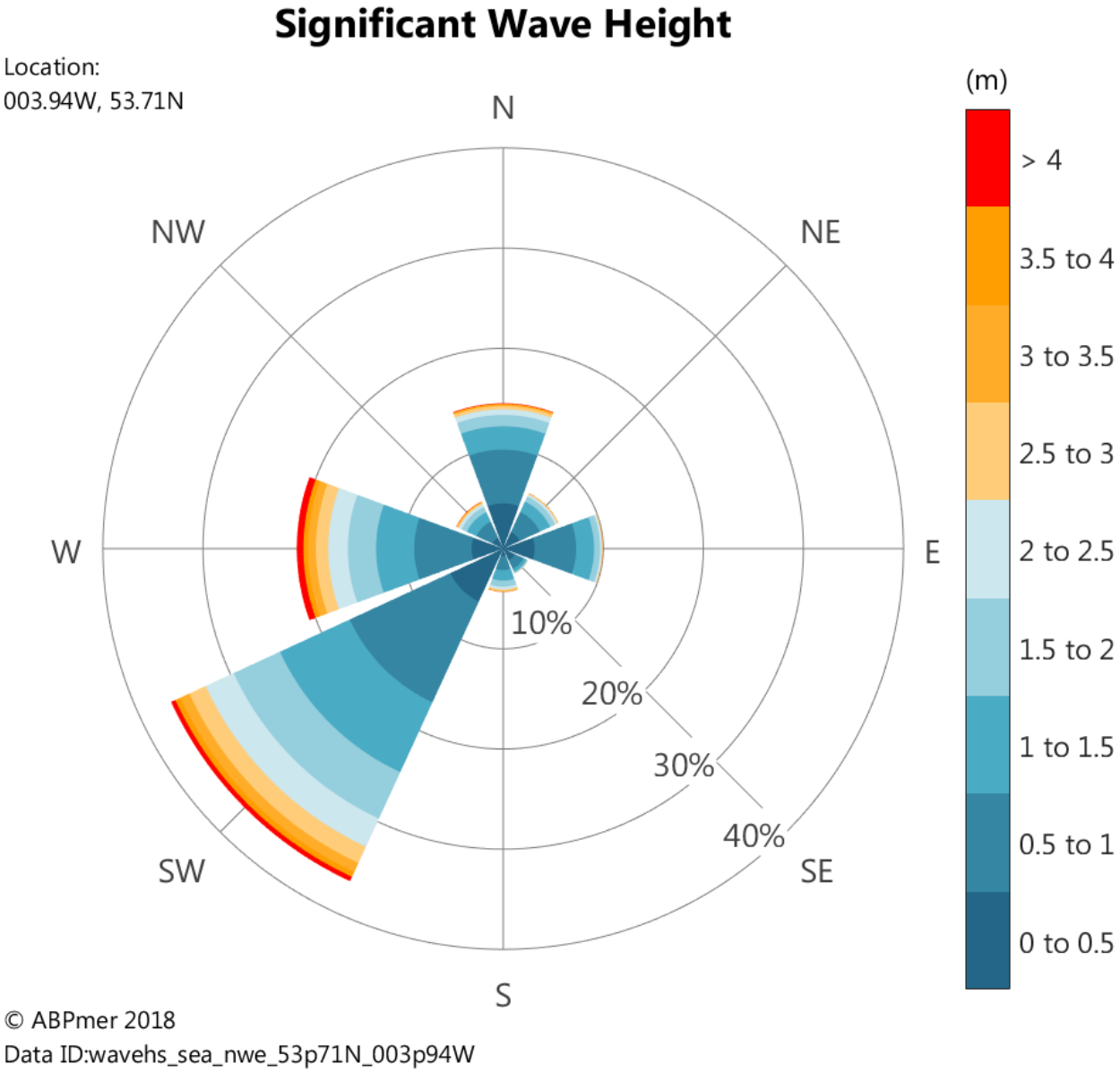

Figure 1.33: Wave rose for the Mona PEIR Array Area.

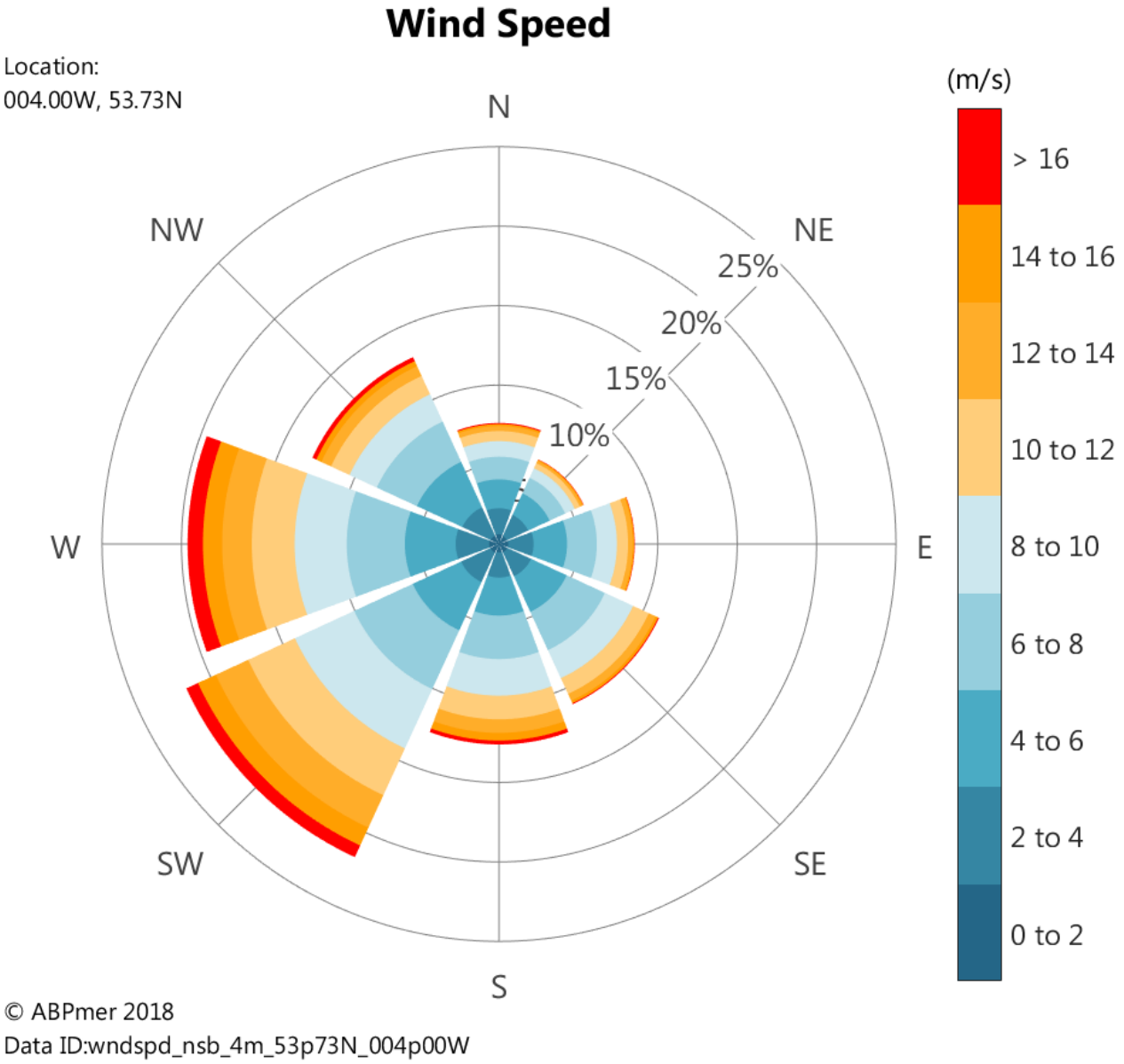

Figure 1.34: Wind rose for the Mona PEIR Array Area.

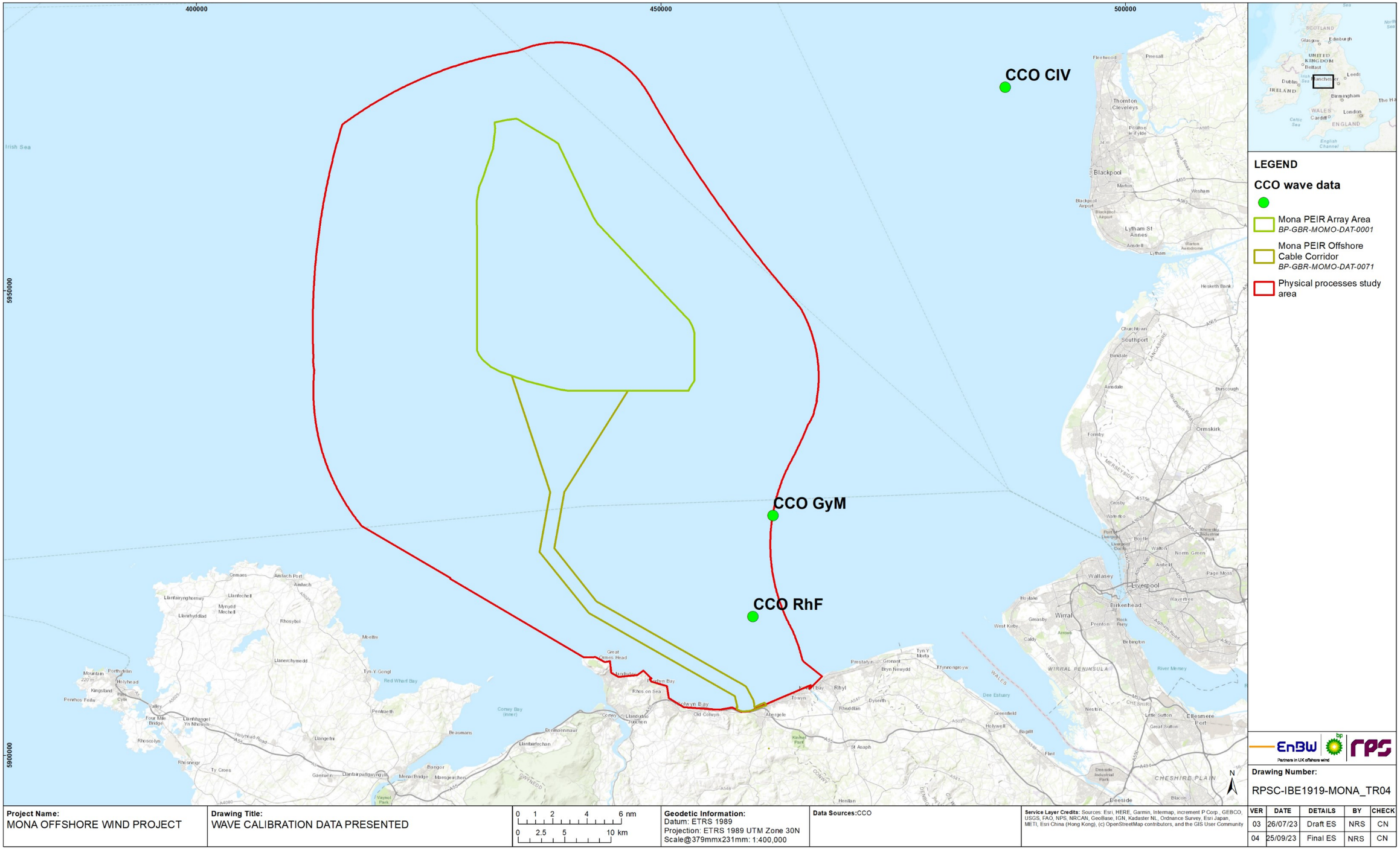

Figure 1.35: Location of wave calibration data presented.

1.3.5.24 Storm Christoph approached the east Irish Sea from and easterly direction and therefore the calibration site located to the east of the physical processes study area provide a good indicator as to how well the wave model transforms wave through the physical processes study area. Model and measured data for site Cleveleys (CIV) located at the mouth of Morecambe Bay are presented in Figure 1.36 to Figure 1.38. In each case it can be seen that the hourly interval model data tracks the progress of the storm. It is noted that the model is less 'peaky', but this is to be expected given that the ECMWF data is at three hourly intervals and linear interpolation was applied.

1.3.5.25 For the two southerly sites Gwynt y Môr (GyM) (Figure 1.39 to Figure 1.41) and Rhyl Flats (RhF) (Figure 1.42 to Figure 1.44) located on the south east extent of the physical processes study area there is also a good correlation between modelled and monitored data. This indicated that the wave model was suitable for use in the comparative study of the potential impacts of the Mona PEIR Offshore Wind Project infrastructure on wave climate.

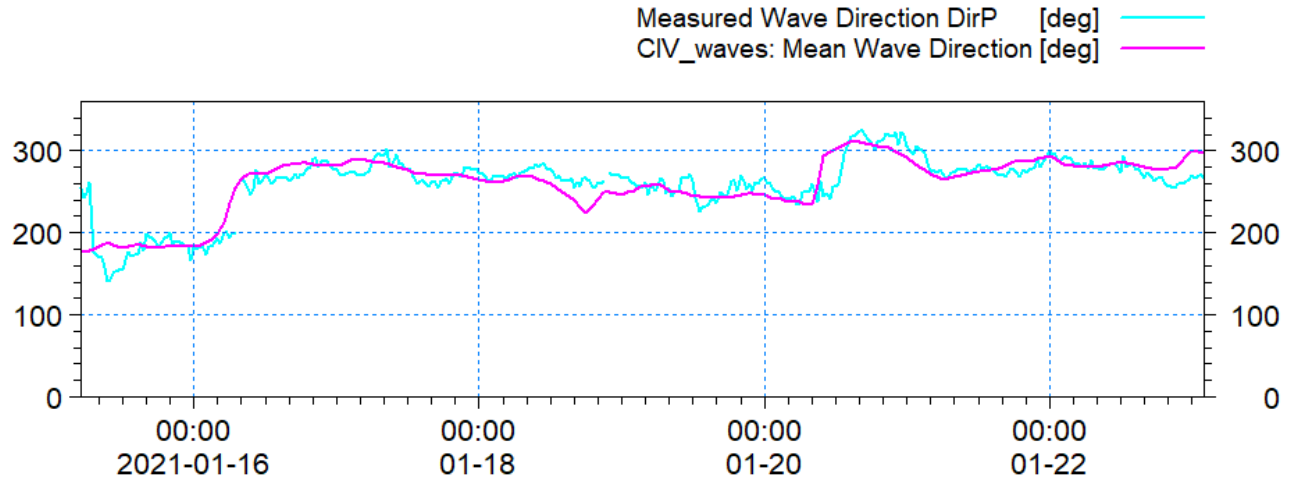

Figure 1.36: Validation of modelled mean wave direction with measured data at CIV.

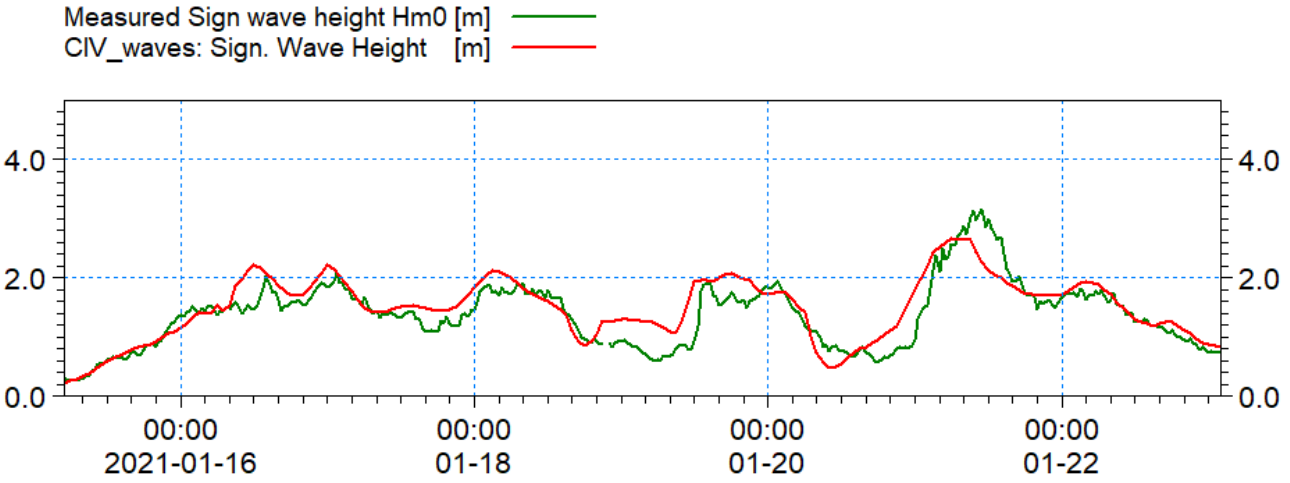

Figure 1.37: Validation of modelled significant wave height with measured data at CIV.

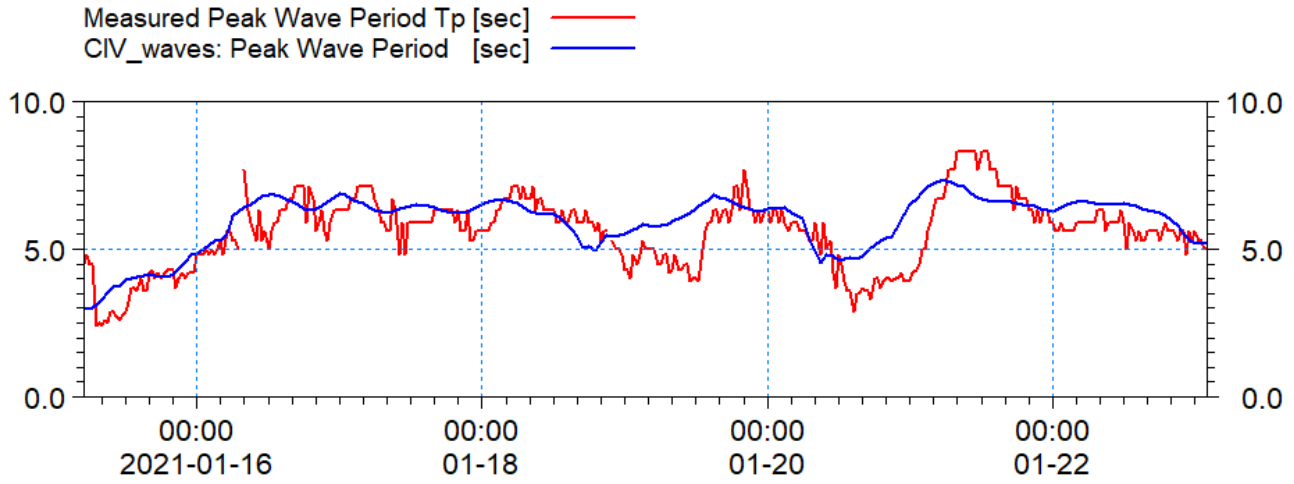

Figure 1.38: Validation of Modelled Peak Wave Period with Measured Data at CIV

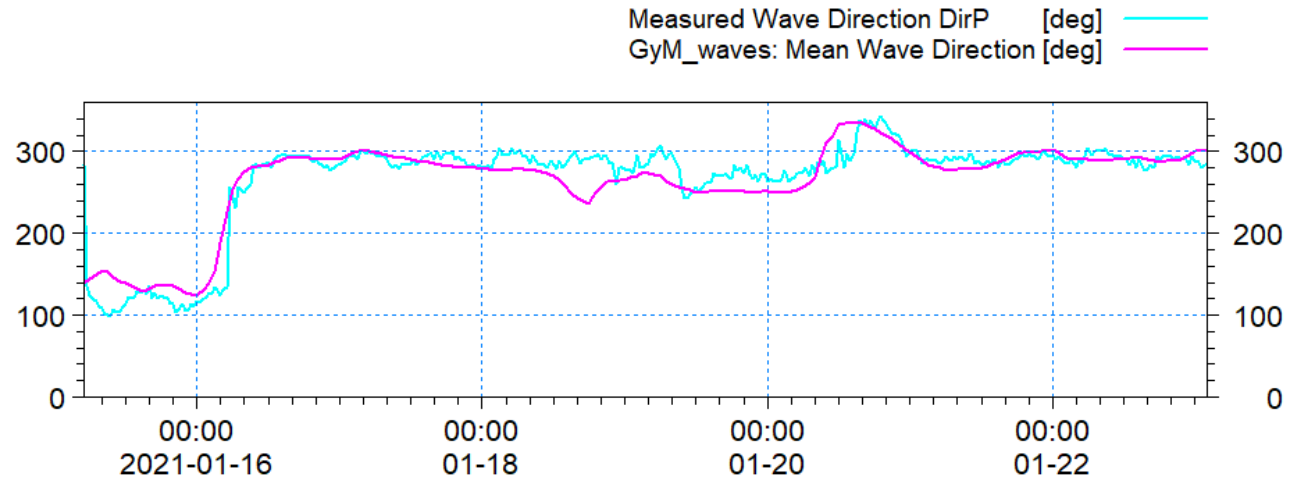

Figure 1.39: Validation of modelled mean wave direction with measured data at GyM.

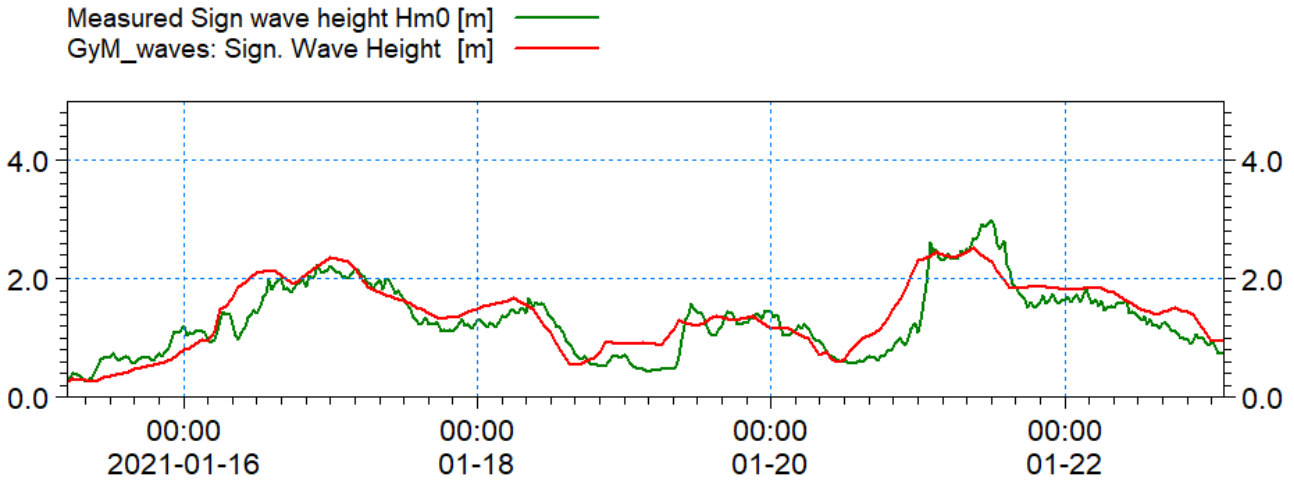

Figure 1.40: Validation of modelled significant wave height with measured data at GyM.

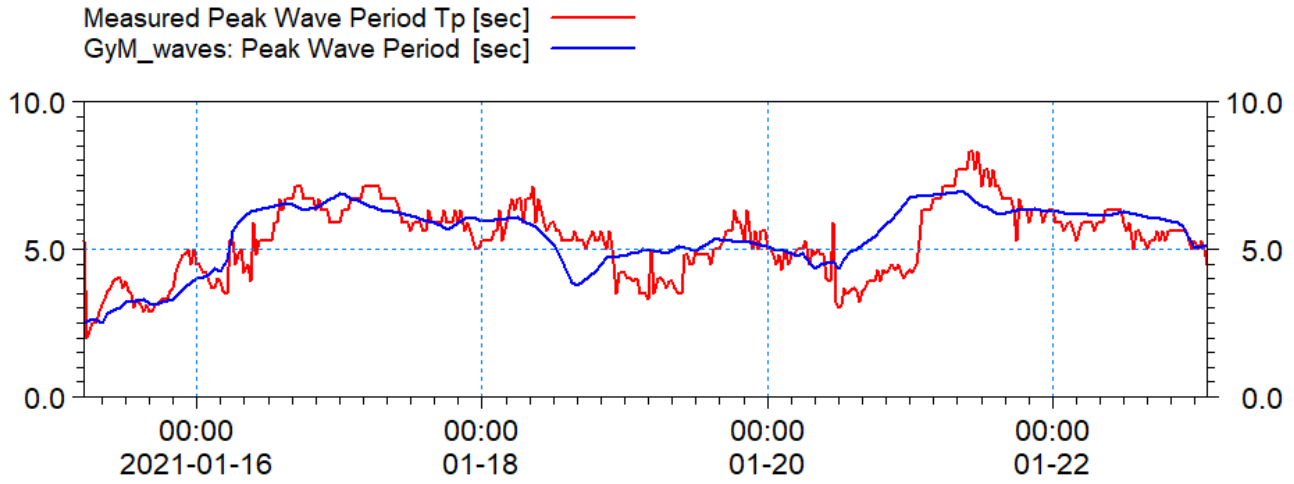

Figure 1.41: Validation of modelled peak wave period with measured data at GyM.

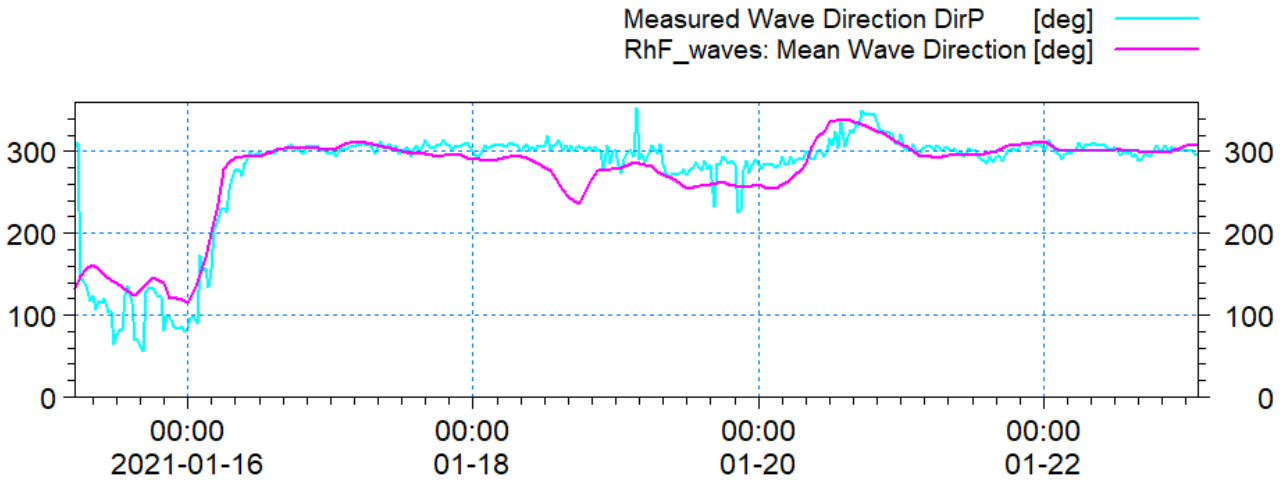

Figure 1.42: Validation of modelled mean wave direction with measured data at RhF.

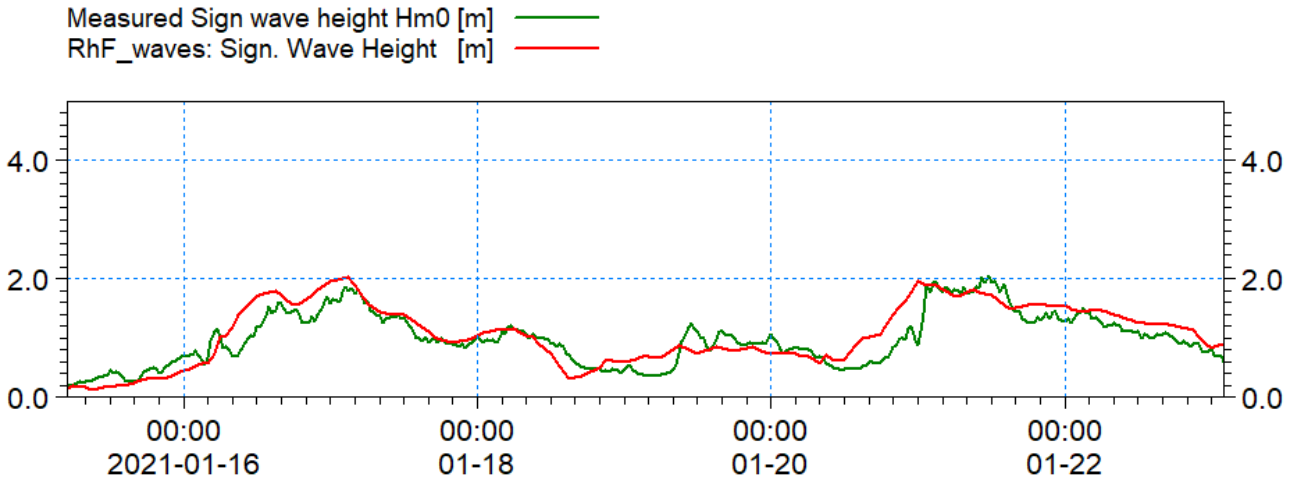

Figure 1.43: Validation of modelled significant wave height with measured data at RhF.

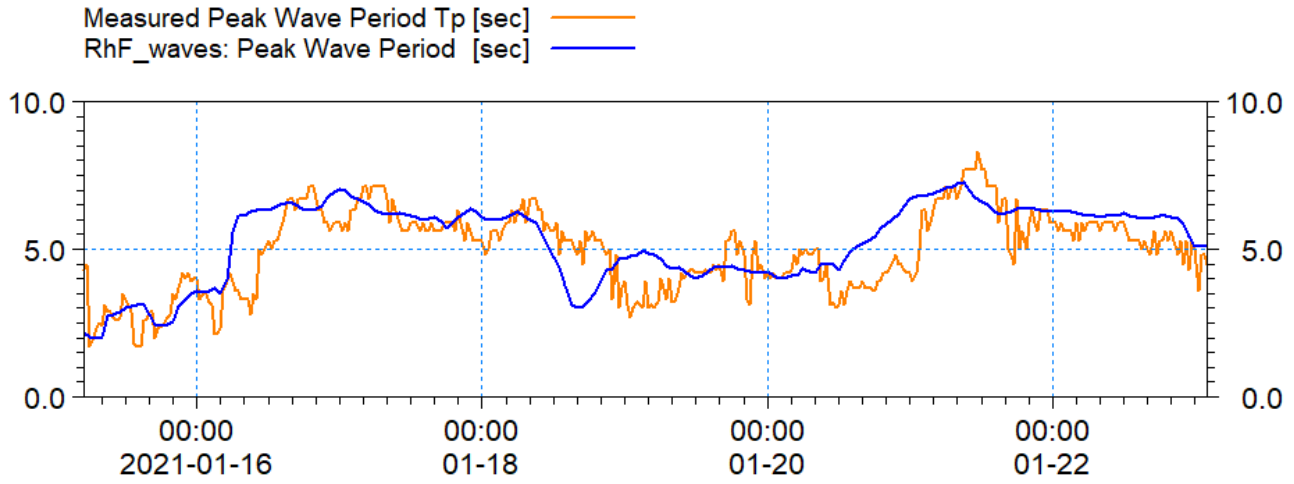

Figure 1.44: Validation of modelled peak wave period with measured data at RhF.

1.3.5.26 In order to evaluate the potential changes in wave climate due to the Mona PEIR Offshore Wind Project, a comparative study was carried out. This meant that baseline wave climate was required; due to the comparative nature of the assessment, a full metocean study was not essential however representative sea-states were required.

1.3.5.27 An analysis was undertaken to determine the offshore conditions for which waves reach the site from all directions. Twenty-two years of data were obtained from the ECMWF operational dataset for locations on the north and south boundaries of the model domain. Extreme value analysis using peak over threshold was undertaken for each 30° sector to determine the 1 in 1 and 1 in 20 year offshore wave climate. These were then used as boundary conditions within the wave modelling to determine the resultant wave climate at the site and across the physical processes study area.

1.3.5.28 In addition to boundary wave data, it was necessary to analyse the wind field to include the contribution of local wind seas. For this, for a representative point for each of the key directions, was identified and utilised from the NOAA 40 year dataset. This was analysed on the same sectoral basis as the wave data to give an indication of the return period wind speed. Figure 1.45 shows the model domain with wind and wave roses relating to the forcing data.

1.3.5.29 The wave modelling was undertaken using the spectral wave model, MIKE21 SW, to provide a full wave climate and wave breaking across the physical processes study area. The model used a quasi stationary formulation which meant that for each event the wave field fully established over a number of numerical iterations until convergence was reached. The model resolves the wave field by simulating wind generation of waves within the model domain and the propagation of externally generated swell waves through the domain. The model setup ensured that the detail of both locally generated wind waves and swell conditions from further afield were captured.

1.3.5.30 The following set of figures (Figure 1.46 to Figure 1.49) show the wave climate for four 1 in 1 year return period events from the principal directions; north (000°), northeast (030°), southwest (240º) and west (270°) direction respectively. These sectors were selected to be representative of the characteristics of the wave climate and also for sectors for which the Mona Offshore Wind Project may potentially affect marine processes along the coastline. The wave modelling was undertaken at mean high water (MHW) being the high water level on an average tide. Figure 1.49 shows the waves approaching from the west and demonstrates, as anticipated, the largest waves approach from this sector.

1.3.5.31 A second set of figures are presented relating to the 1 in 20 year return period; Figure 1.50 to Figure 1.53. These show data for the same sectors and tidal height as the 1 in 1 year return period. They have been introduced to ensure that the baseline for a more arduous conditions is established for assessment of the potential effect of the Mona PEIR Offshore Wind Project on wave climate.

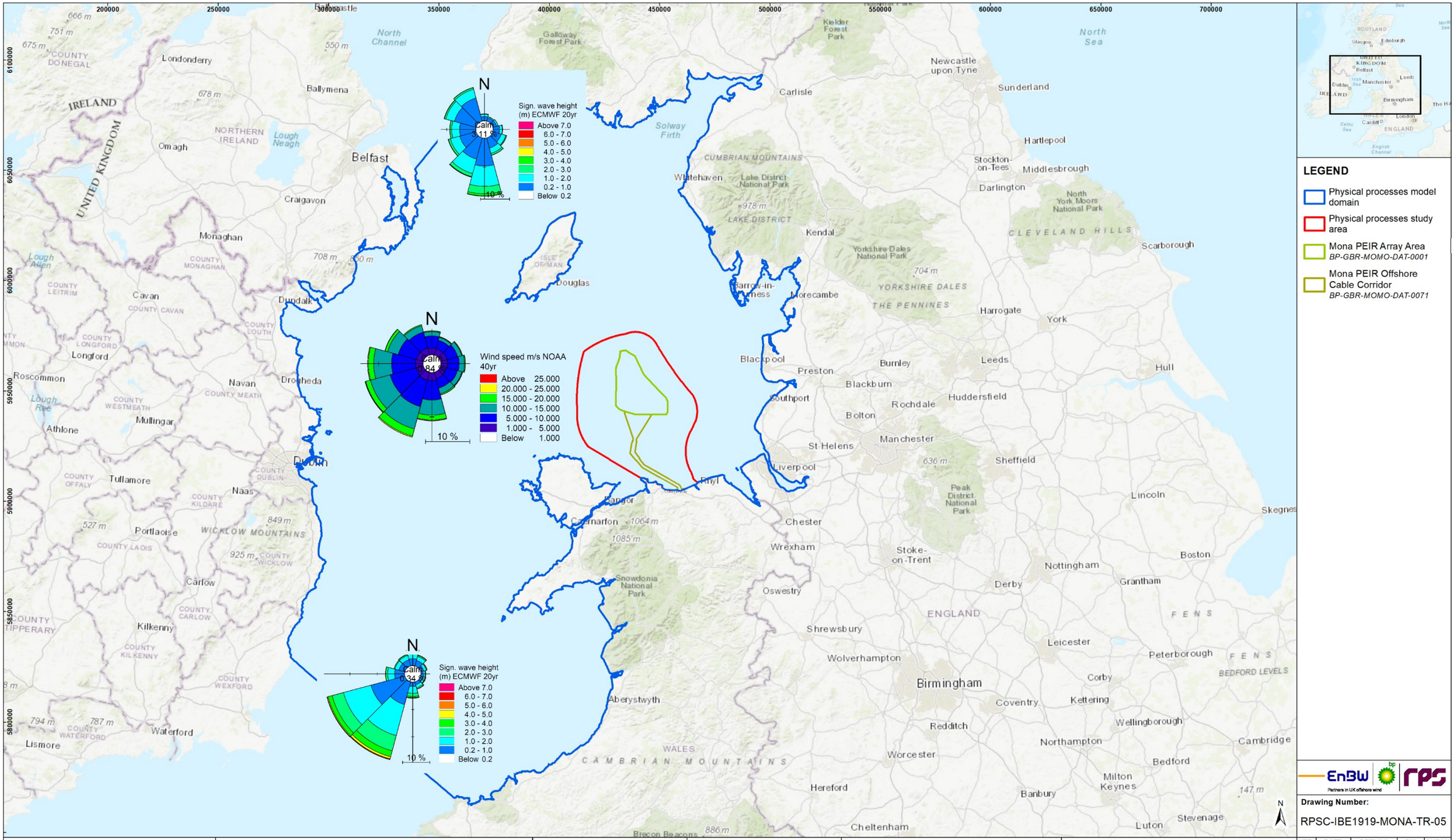

Figure 1.45: Wave roses for model boundaries - 22 year ECMWF Dataset and wind rose for 40 year NOAA dataset.

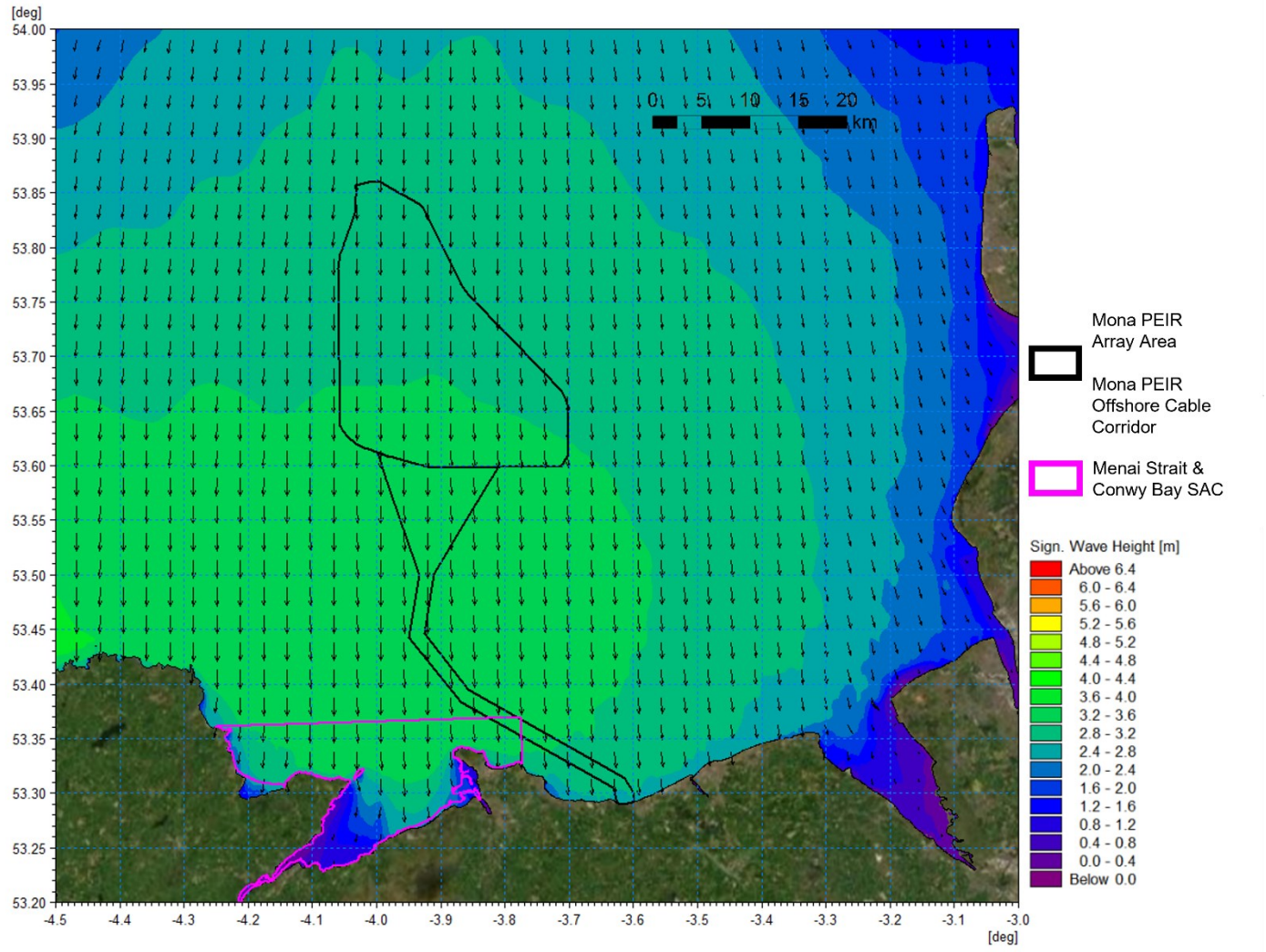

Figure 1.46: Wave climate 1 in 1 year storm from 000° MHW.

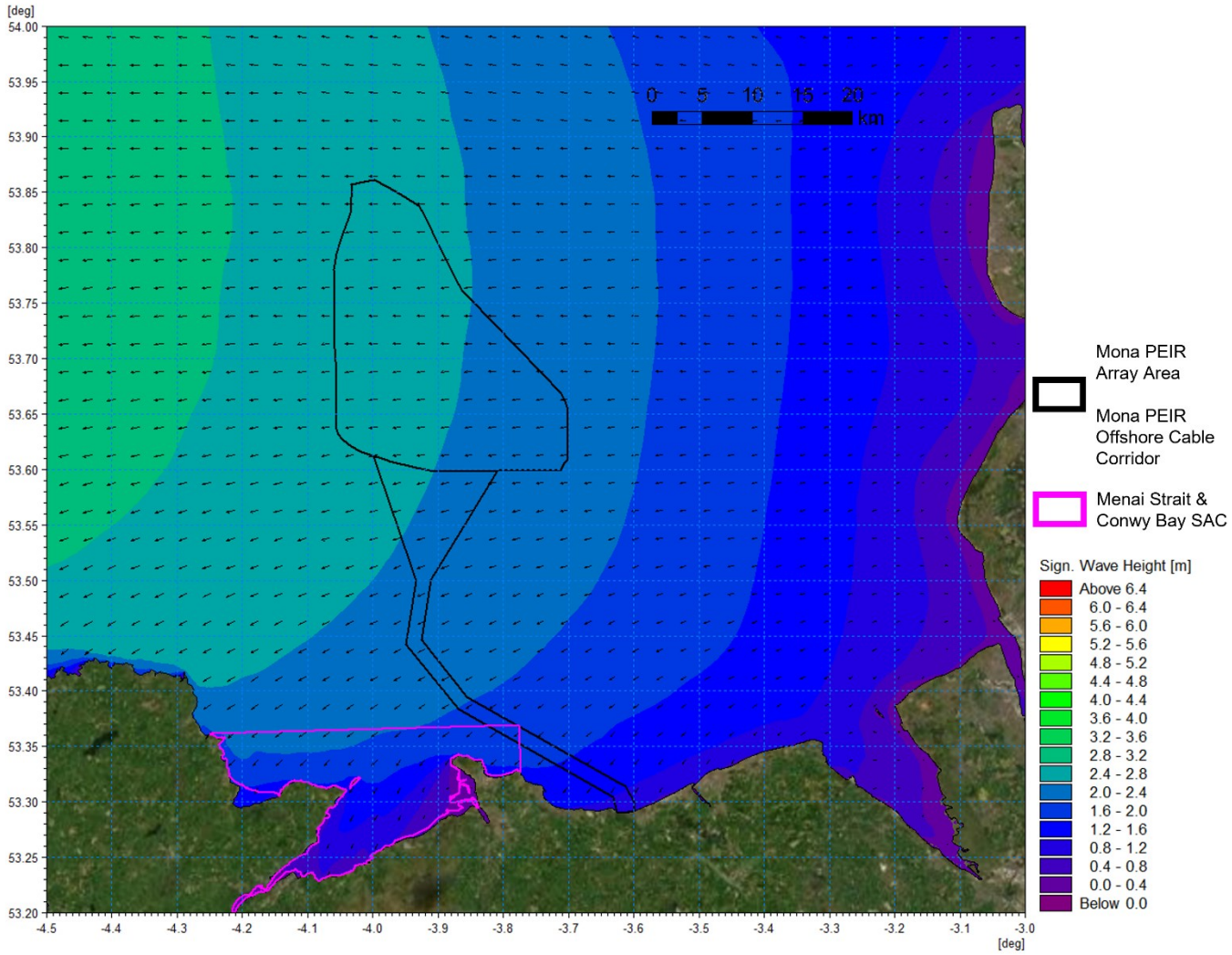

Figure 1.47: Wave climate 1 in 1 year storm from 090° MHW.

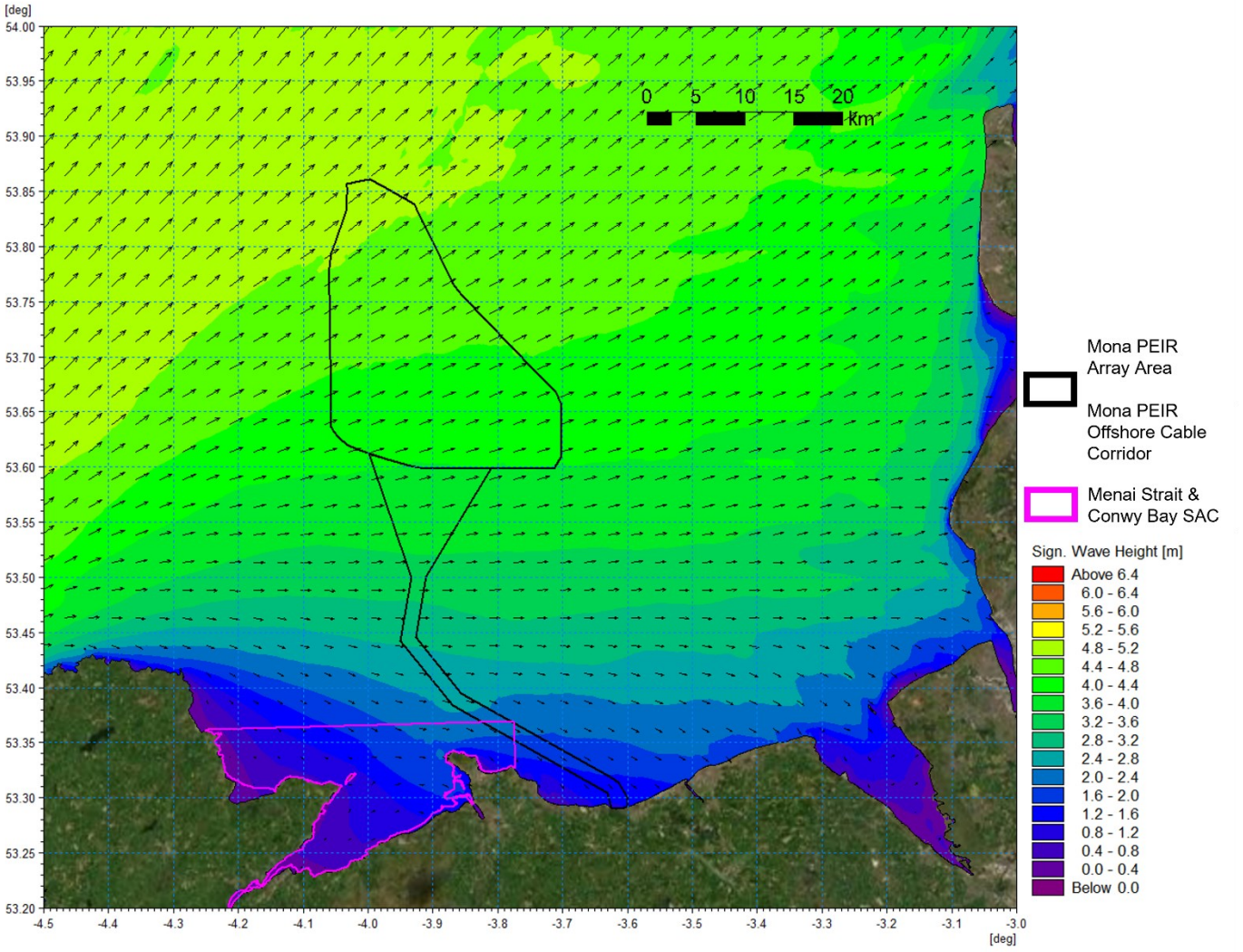

Figure 1.48: Wave climate 1 in 1 year storm from 240° MHW.

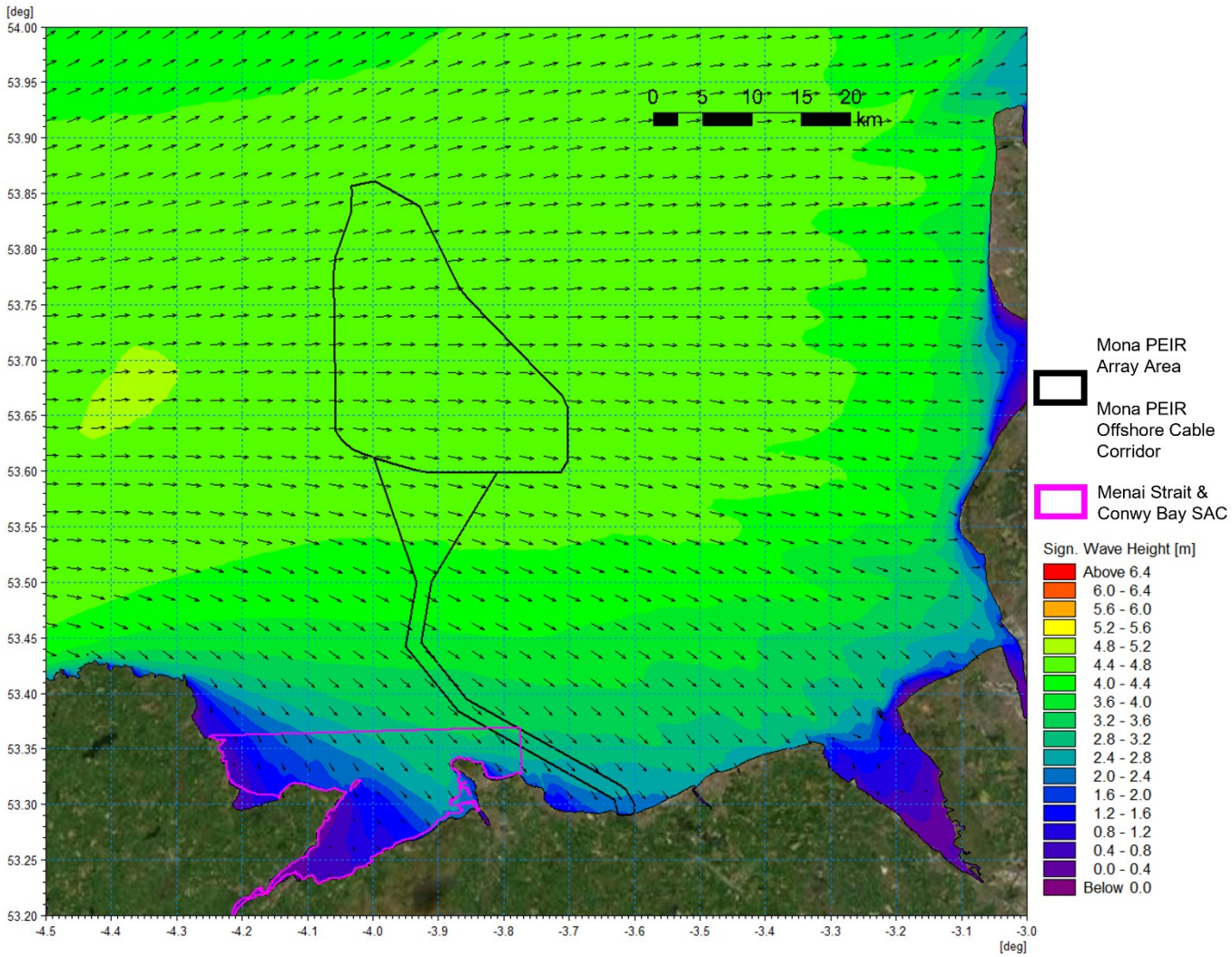

Figure 1.49: Wave climate 1 in 1 year storm from 270° MHW.

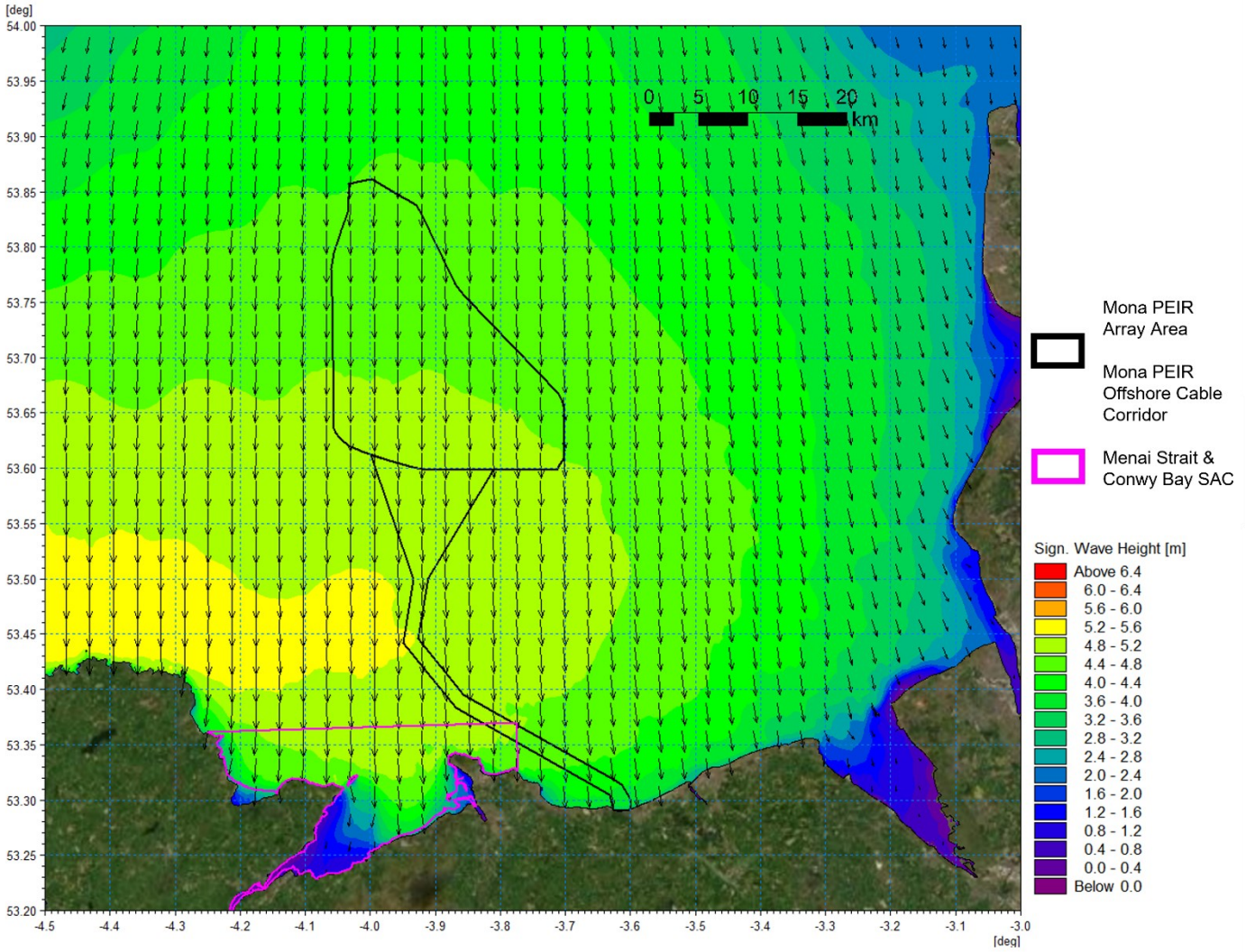

Figure 1.50: Wave climate 1 in 20 year storm from 000° MHW.

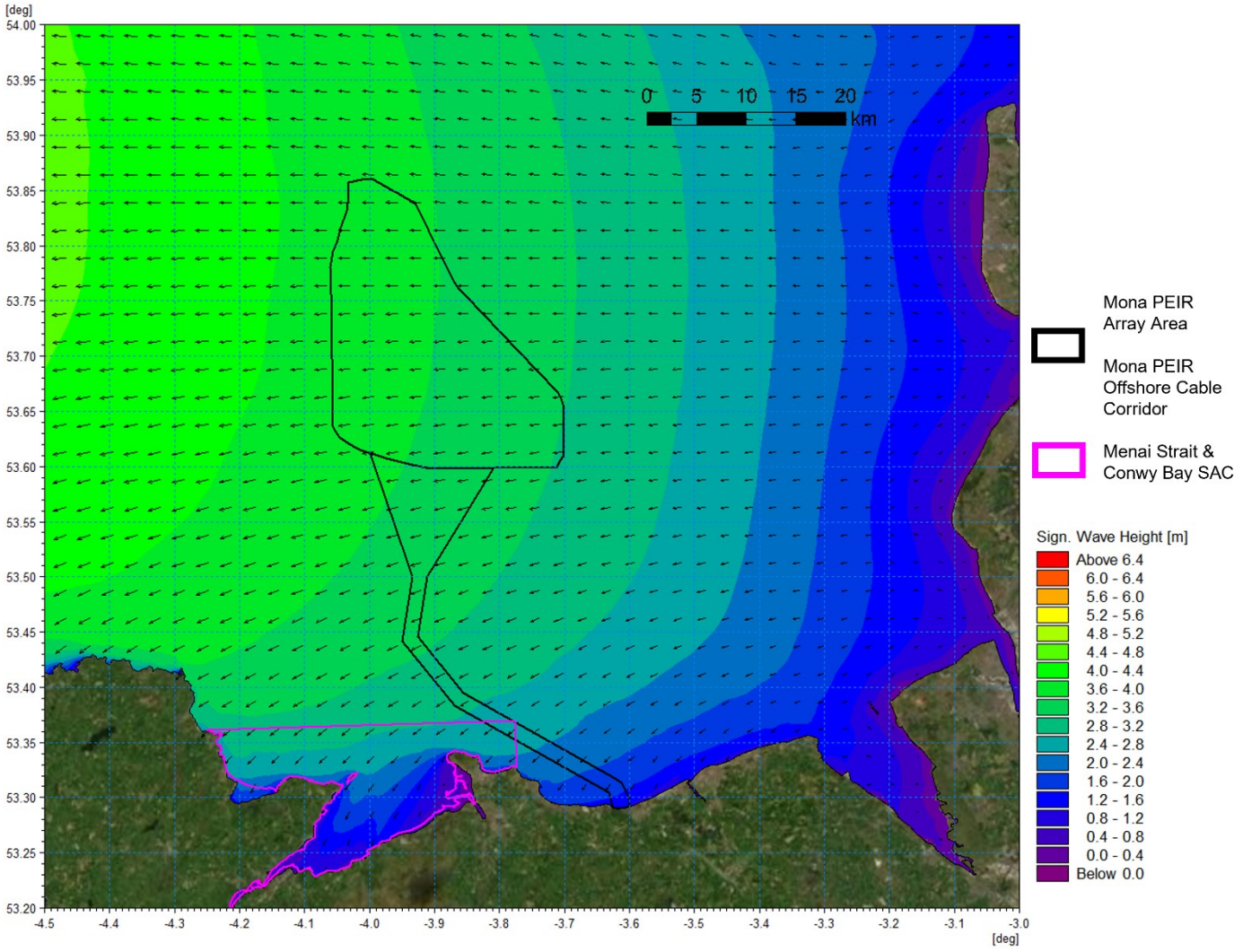

Figure 1.51: Wave climate 1 in 20 year storm from 090° MHW.

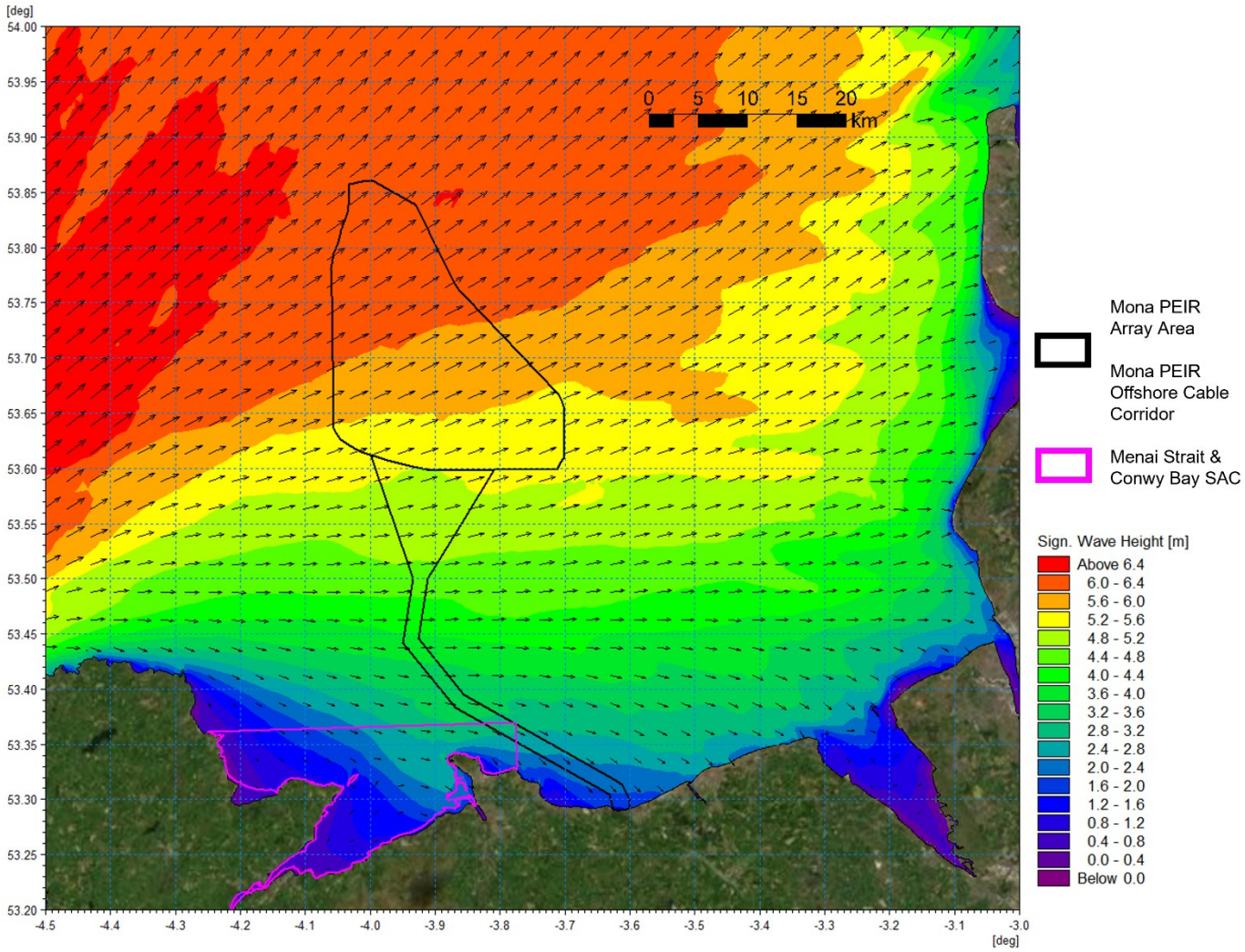

Figure 1.52: Wave climate 1 in 20 year storm from 240° MHW.

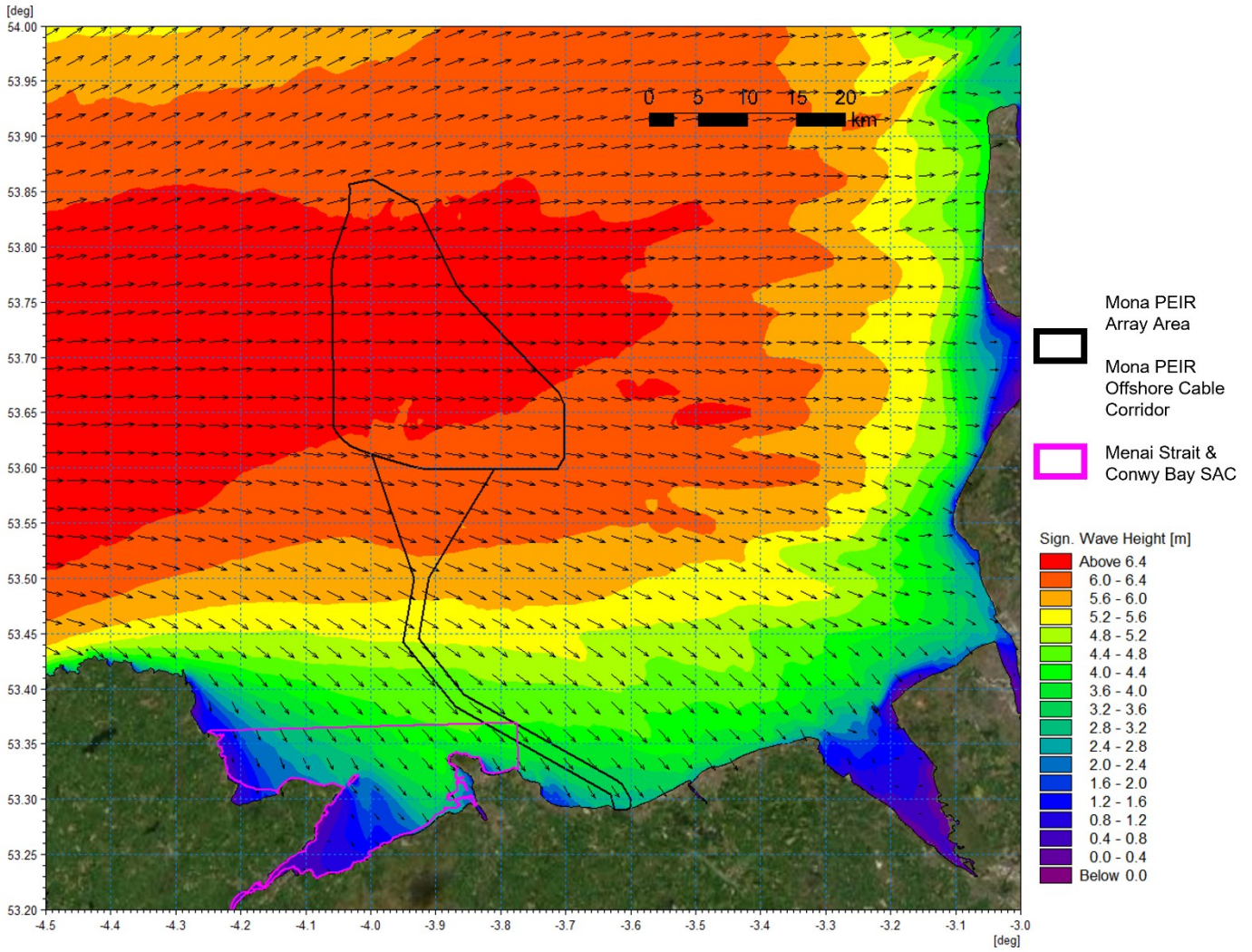

Figure 1.53: Wave climate 1 in 20 year storm from 270° MHW.

Littoral currents

1.3.5.32 The MIKE suite facilitates the coupling of models. The depth averaged hydrodynamic model, used for the tidal modelling, coupled with the spectral wave model, provides a full wave climate incorporating the impact of water levels and currents on waves and wave breaking. Using this, the littoral currents (i.e. those currents driven by tidal, wave and meteorological forces) were examined.

1.3.5.33 As previously stated, the purpose of the modelling was to provide a baseline against which the impact of the installation of the Mona PEIR Offshore Wind Project was to be examined against. It was not designed to be an exhaustive physical processes modelling study and therefore an example storm condition was used as a benchmark. The 1 in 1 year storm from 270° sector was simulated with the inclusion of spring tides to encompass a wide range of tidal conditions and the resulting flood and ebb currents are presented in Figure 1.54 and Figure 1.55 respectively. These correspond with the (calm) tidal plots presented in Figure 1.31 and Figure 1.32. As expected, the presence of the southeast going waves increase the currents on the flood tide whilst reducing them on the ebb.

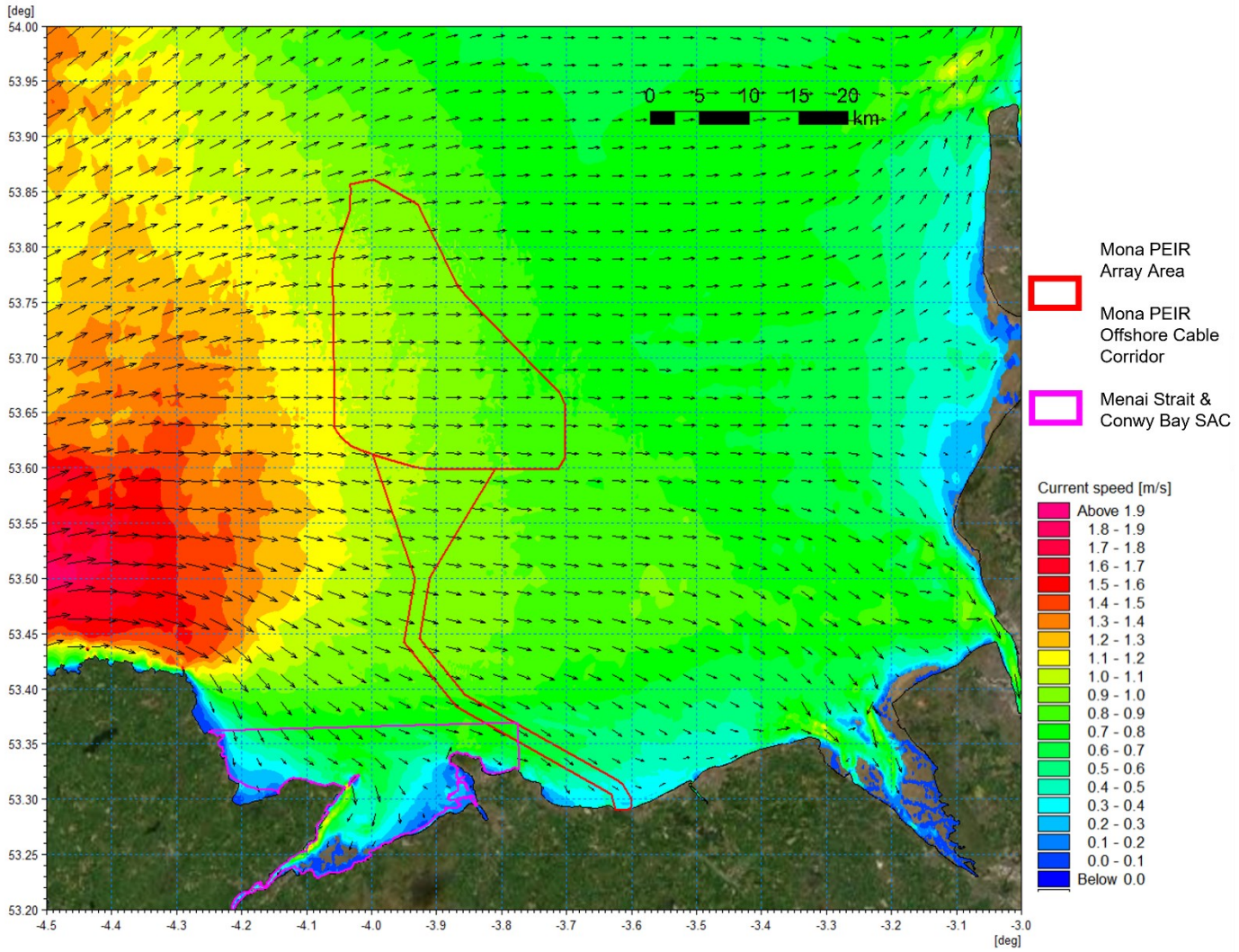

Figure 1.54: Littoral current 1 in 1 year storm from 270° - Flood Tide.

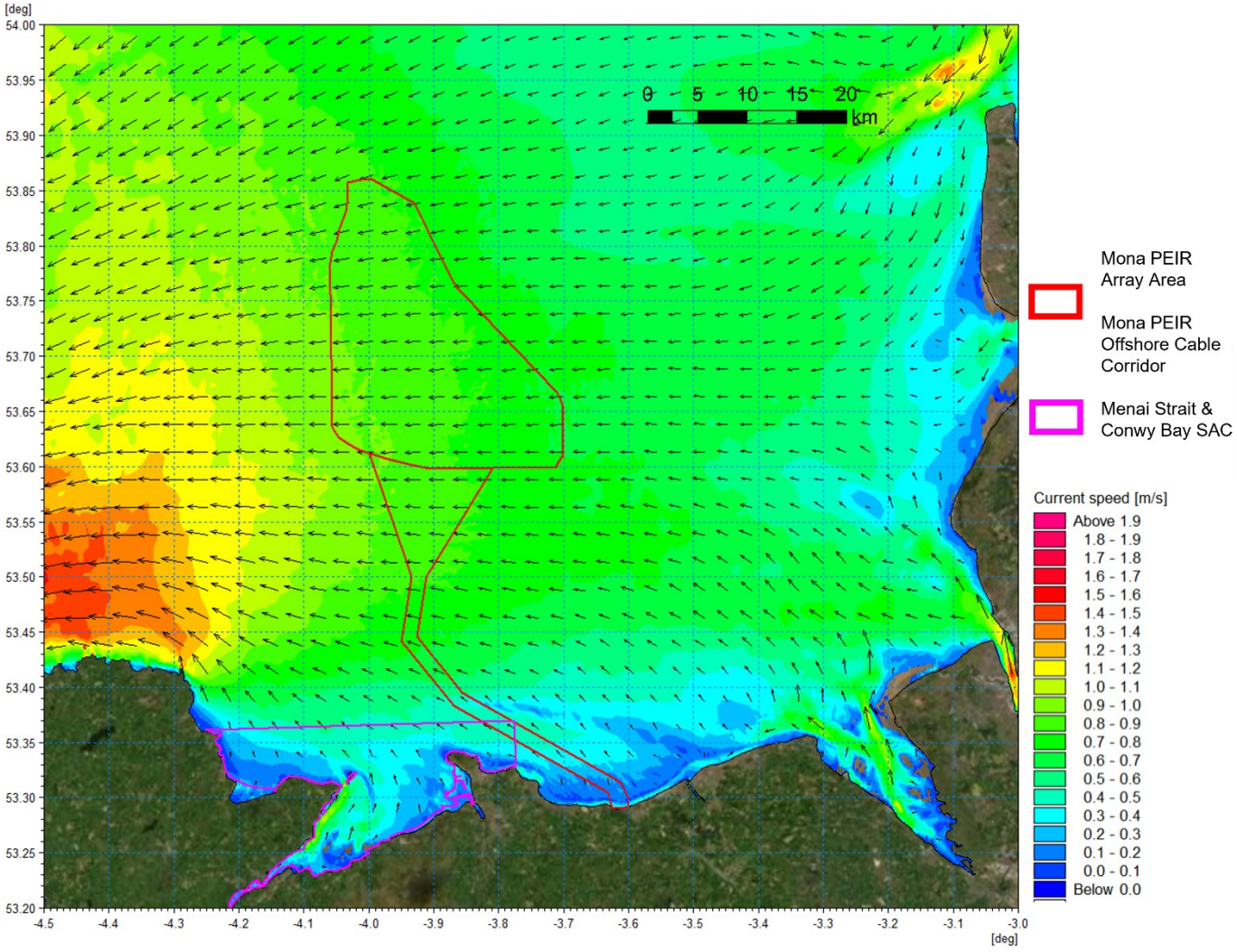

Figure 1.55: Littoral current 1 in 1 year storm from 270° - Ebb Tide.

Sedimentology and seabed substrate

1.3.5.34 An overview of surficial sediment geology and the seabed features data is presented in this section, based on a range of data sources including both publicly available datasets and interpretation undertaken of the SSS data collected during the recent geophysical surveys (Table 1.4). An understanding of seabed substrate types is required to assess the potential impacts which may arise due to the installation of wind turbines, offshore platform foundations, array cables and export cables.

1.3.5.35 The sediment grading properties applied within the modelling for both sediment transport assessment and characterisation of mobilised material during seabed preparation and installation operations was derived from British Geological Survey (BGS) datasets as illustrated in Figure 1.56. These datasets included both generalised Folk classification from borehole logs and detailed particle analysis data.

1.3.5.36 Following completion of the modelling studies for PEIR, a detailed analysis was undertaken of the geophysical and geotechnical data collected during the site-specific surveys for the project (bp, 2023). It concluded that the Mona PEIR Array Area and Mona PEIR Offshore Cable Corridor is comprised of two regions; a glacial floodplain to the north dominated by sand, and a clay dominated area to the south associated with glacial lake deposition where ribbons of mobile bedforms are present. These classifications highlight that the seabed substrate would be derived from glacial origins and some areas more generally classified as boulders, cobbles and rocky outcrops in the preliminary assessment (and indeed within the EMODnet dataset) would be more precisely termed moraines which are comprised of glacial till. This data was verified against PSA of sediment samples collected during site specific surveys the results of which were made available following completion of the modelling study.

1.3.5.37 The SSS interpretation defined a range of sediment types within the Mona PEIR Array Area comprising sand, gravelly sand and sandy gravel. Sandwaves and mega ripples are associated with these sediment types. To inform the modelling study seabed sediment information was required beyond the extent of the survey data and the EMODnet Geology database was utilised. The seabed classification shown in Figure 1.57 shows both the datasets applied within the modelling context. The sediment parameters applied within the modelling used grading properties derived directly from the BGS sampled datasets, and subsequently verified from PSA of the site-specific grab samples. The re-characterisation of this material would not impact the modelling outcomes, as dispersion characteristics are not sensitive to the origin of the material but rather to the physical characteristics of the sediment.

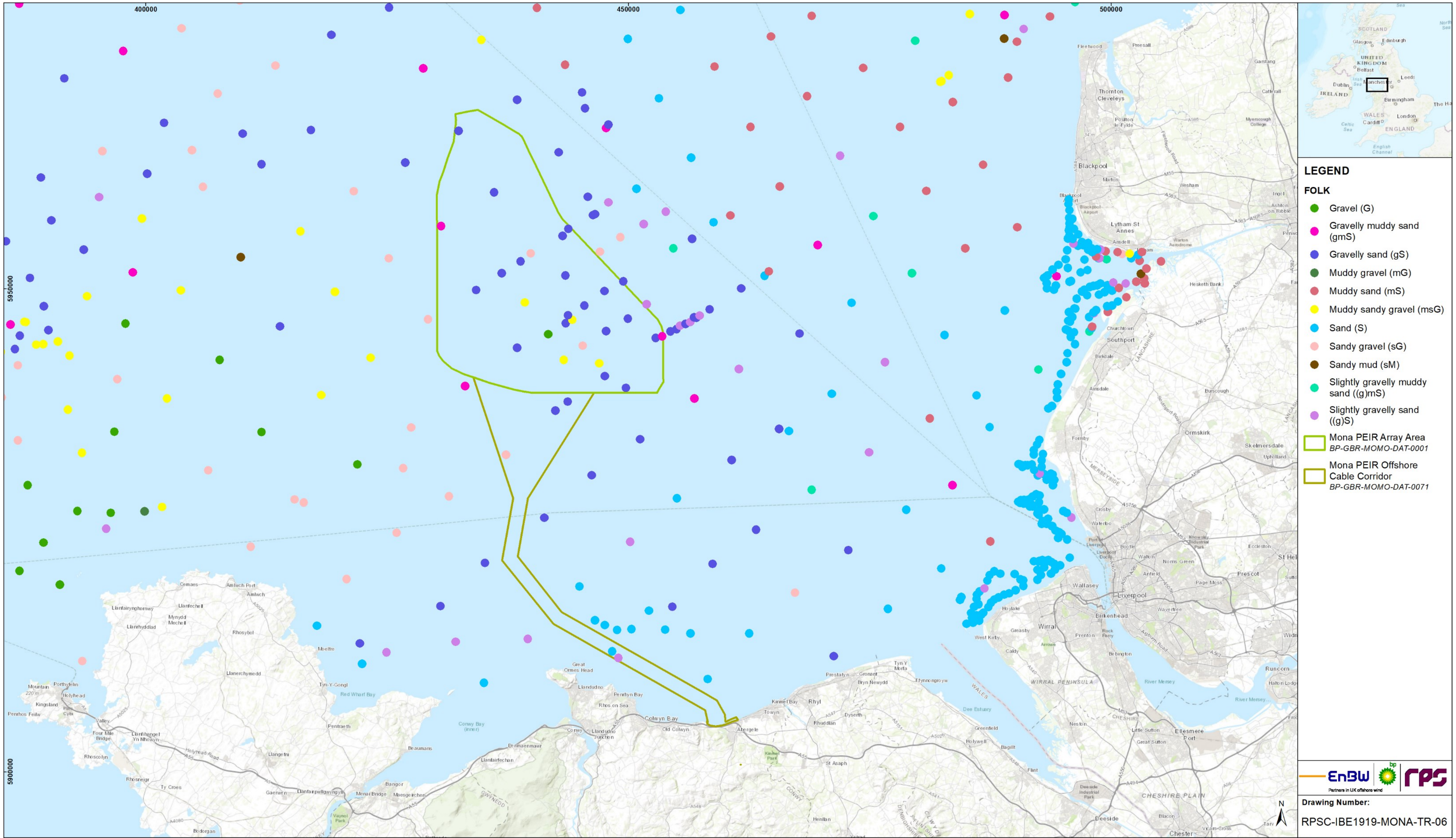

Drawing Number: RPSC-IBE1919-MONA-TR-06

Project Name:	Drawing Title:	Geodetic Information:	Data Sources:
MONA OFFSHORE WIND PROJECT	BGS SEABED SAMPLE DATA - FOLK CLASSIFICATION	Datum: ETRS 1989 Projection: ETRS 1989 UTM Zone 30N Scale@379mmx231mm: 1:400,000	British Geological Society

Scale: 0 1 2 4 6 nm; 0 2.5 5 10 km

Service Layer Credits: Sources: Esri, HERE, Garmin, Intermap, increment P Corp., GEBCO, USGS, FAO, NPS, NRCAN, GeoBase, IGN, Kadaster NL, Ordnance Survey, Esri Japan, METI, Esri China (Hong Kong), (c) OpenStreetMap contributors, and the GIS User Community

VER	DATE	DETAILS	BY	CHECK
03	26/07/23	Draft ES	NRS	CN
04	25/09/23	Final ES	NRS	CN

Figure 1.56: Seabed sample data Folk classification - BGS.

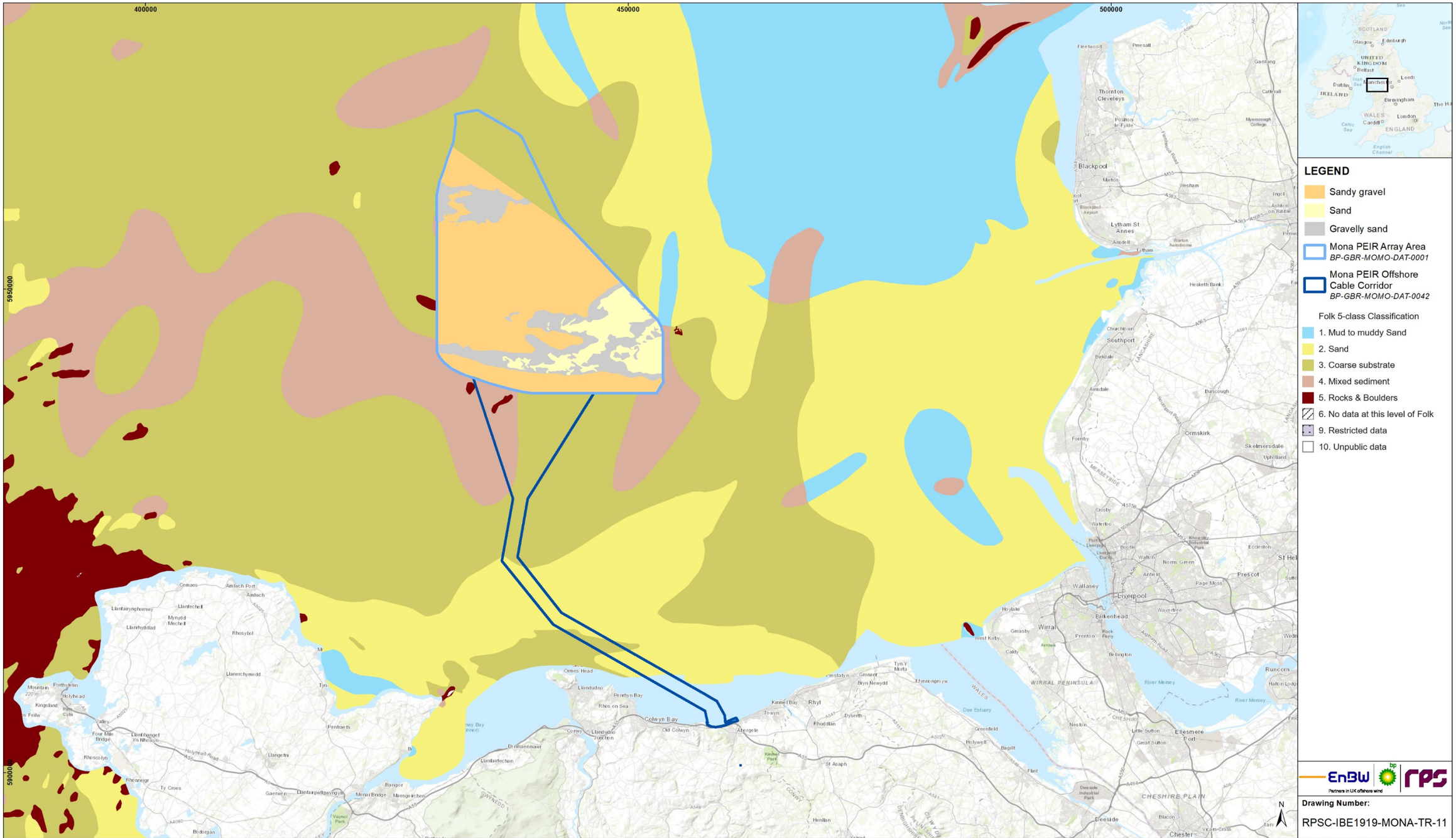

Figure 1.57: Seabed substrate geology - EMODnet.

Sediment transport

1.3.5.38 The MIKE21 ST module enables assessment of bed sediment transport rates for non-cohesive sediment resulting from currents or combined wave-current flows. It was used to determine the sediment transport pattern within the model domain. The model combines inputs from both the hydrodynamic model and, if required, the wave propagation model. It used sediment characterisation provided by the recent survey and EMODnet data as presented in the previous section to determine the sediment transport characteristics. For each region a representative sample from the BGS was used to define the bed sediment and grading.

1.3.5.39 It is noted that for a detailed sediment transport study greater detail of sediment characteristics across the model domain and along the coastline would be required. In the context of a comparative study to identify the impact of the Mona PEIR Offshore Wind Project infrastructure on sediment transport patterns the sediment characteristics identified within the survey and sampling were interpolated to those areas in the EMODnet data with similar sediment classifications.

1.3.5.40 The model domain was set up with a layer of mobile bed sediment. In areas where sediment is present an initial layer depth was set to 3 m and tapered to zero in the areas characterised as “Rocks and Boulders” in the EMODnet geology datasets where the seabed is less mobile. These areas were subsequently classified as moraines which are comprised of glacial till and associated with glacial lakes during detailed analysis of geophysical survey data. The re-characterisation of this material would not impact the modelling outcomes, as dispersion characteristics are not sensitive to the origin of the material but rather to the physical characteristics of the sediment and the parameters applied within the modelling used grading properties derived directly from the BGS sampled datasets, and subsequently verified from PSA of the site-specific grab samples. This initial depth ensured that sediment was not exhausted during the simulated events. Sediment transport was examined relating to spring tidal conditions over the course of two tidal cycles (one day) to provide a ‘snap-shot’ for comparison. The simulation included a period for the hydrodynamics to stabilise and develop across the domain prior to sediment transport being enabled (i.e. a “warm-up” period).

1.3.5.41 Three aspects were examined:

- Residual current, which is the net flow over the course of the tidal cycle. This is effectively the driving force of the sediment transport
- Potential sediment transport over this period
- Potential sediment transport during flood and ebb tides. This provides information for a ‘snap-shot’ in time to enable the process to be illustrated.

1.3.5.42 The residual current is presented in Figure 1.58 and it should be noted that a log scale has been used to cover the range of residual current speeds encountered. The current vectors indicate residual flow into the east Irish Sea from the north and west which correlates with this region being a sediment sink. There are strong circulatory currents where tidal flows interact with headlands and embayments.

1.3.5.43 An indication of transport rate is shown in Figure 1.59, again using a log scale palette as the values within the offshore regions are several orders of magnitude smaller than those along the coastline. The greatest transport rates are seen in areas where finer sand fractions are present and in estuaries and at headland where tidal currents are strongest. The mechanism is more clearly illustrated in Figure 1.60 and Figure 1.61 for

flood and ebb tides respectively. It is evident that transport rates are highest during the dominant flood tide and the region is a sediment sink.

1.3.5.44 As previously discussed, the modelling undertaken was not designed to form a detailed sediment transport modelling study but to provide an indication of potential changes as a result of the installation of the Mona PEIR Offshore Wind Project. Therefore, by way of completeness, and for use in the comparative study, residual currents relating to the 1 in 1 year return period storm approaching from 270° are also presented, Figure 1.62. As anticipated, the littoral currents and dominant flood tide significantly increase easterly residual currents particularly along the Welsh coastline. This in turn would result in increased sediment transport rates during storm conditions.

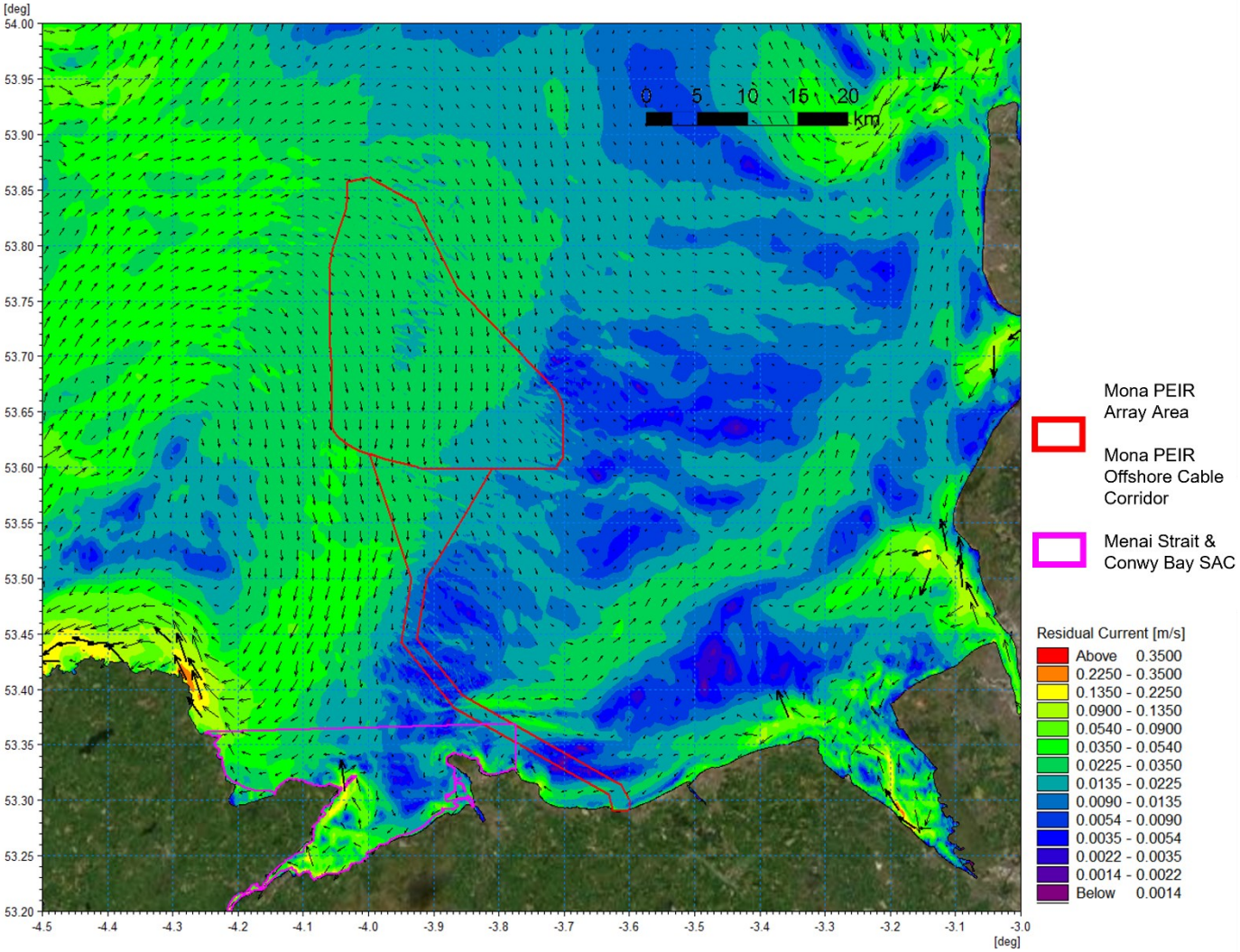

Figure 1.58: Residual current spring tide.

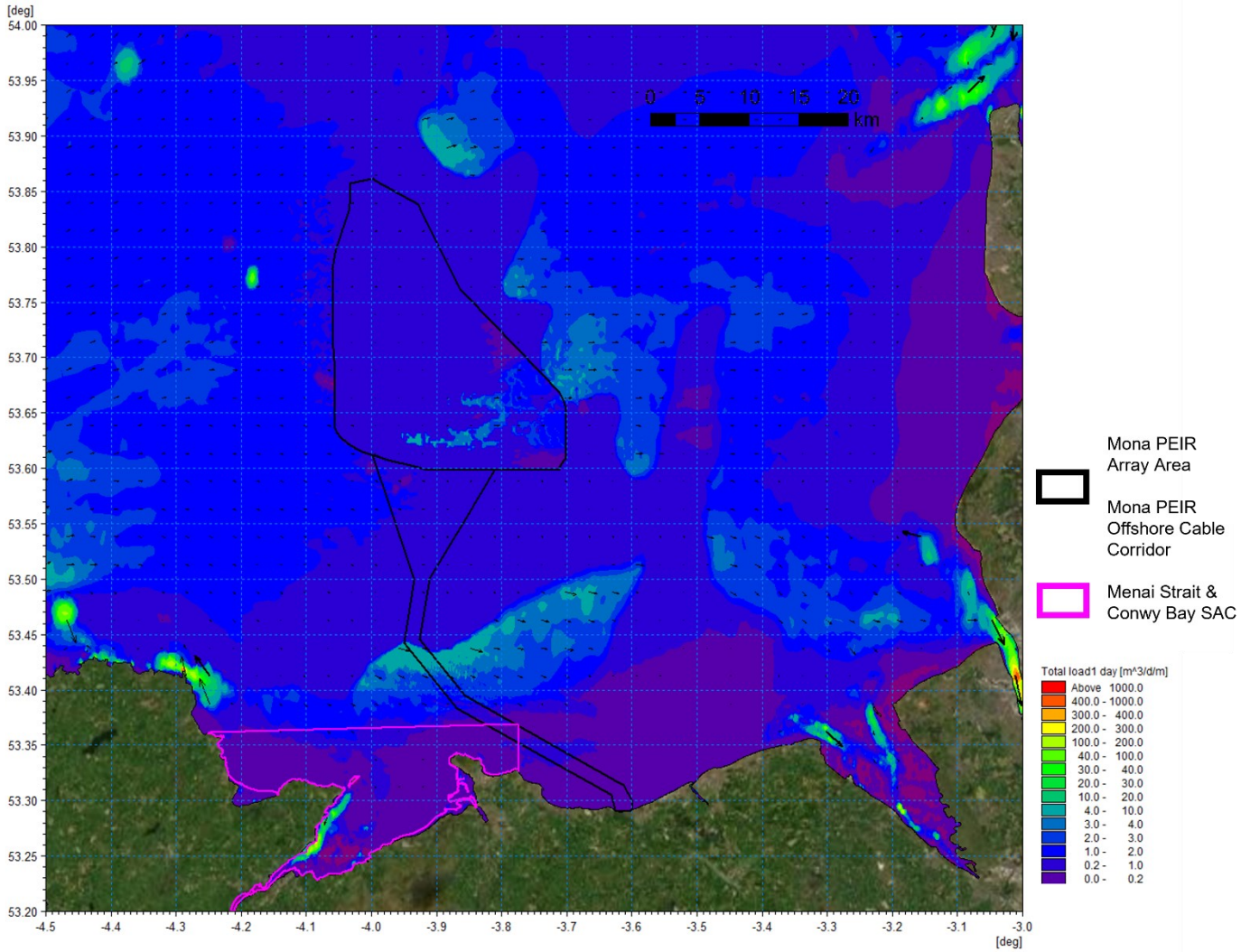

Figure 1.59: Potential sediment transport over the course of 1 day (two tide cycles).

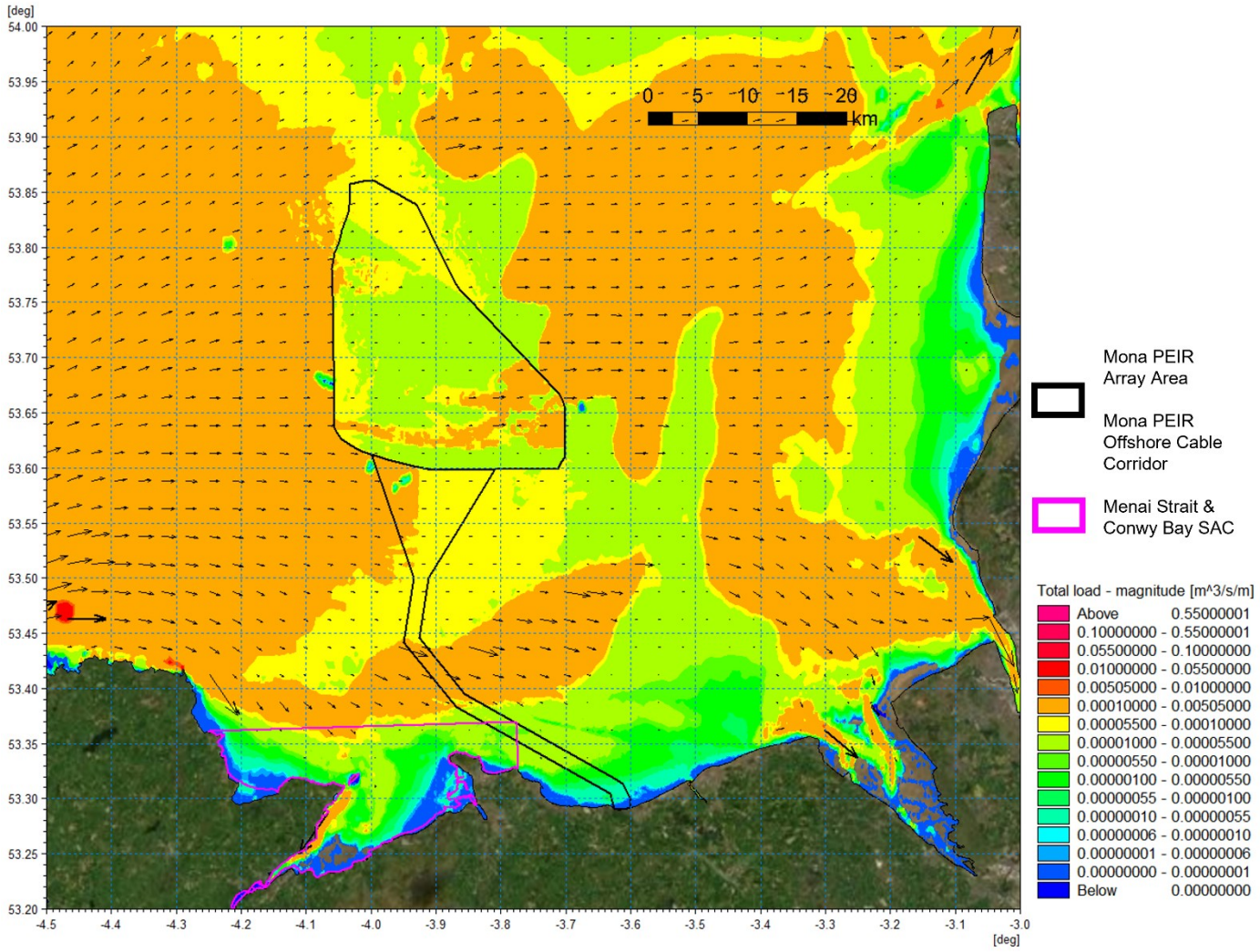

Figure 1.60: Sediment transport – flood tide.

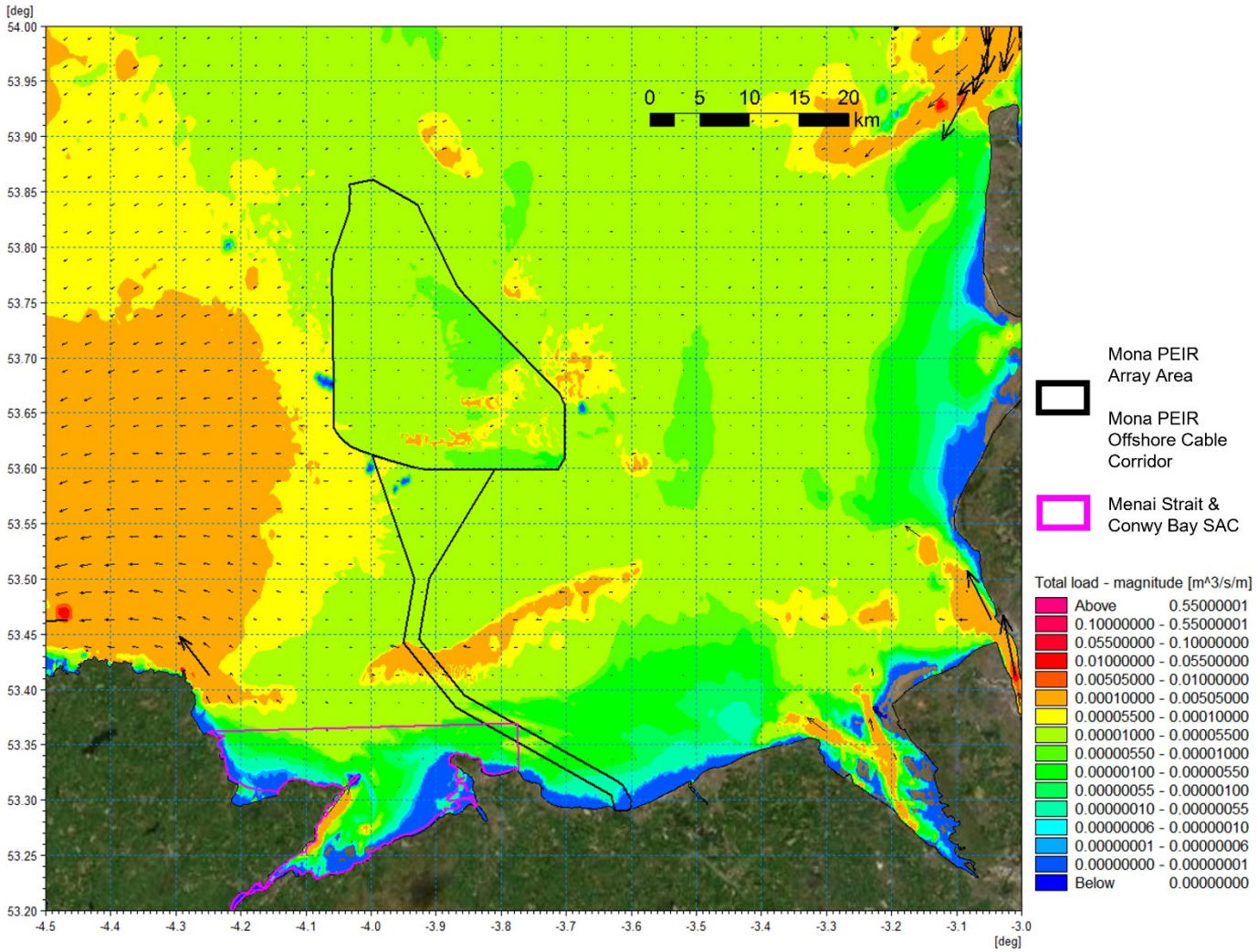

Figure 1.61: Sediment transport – ebb tide.

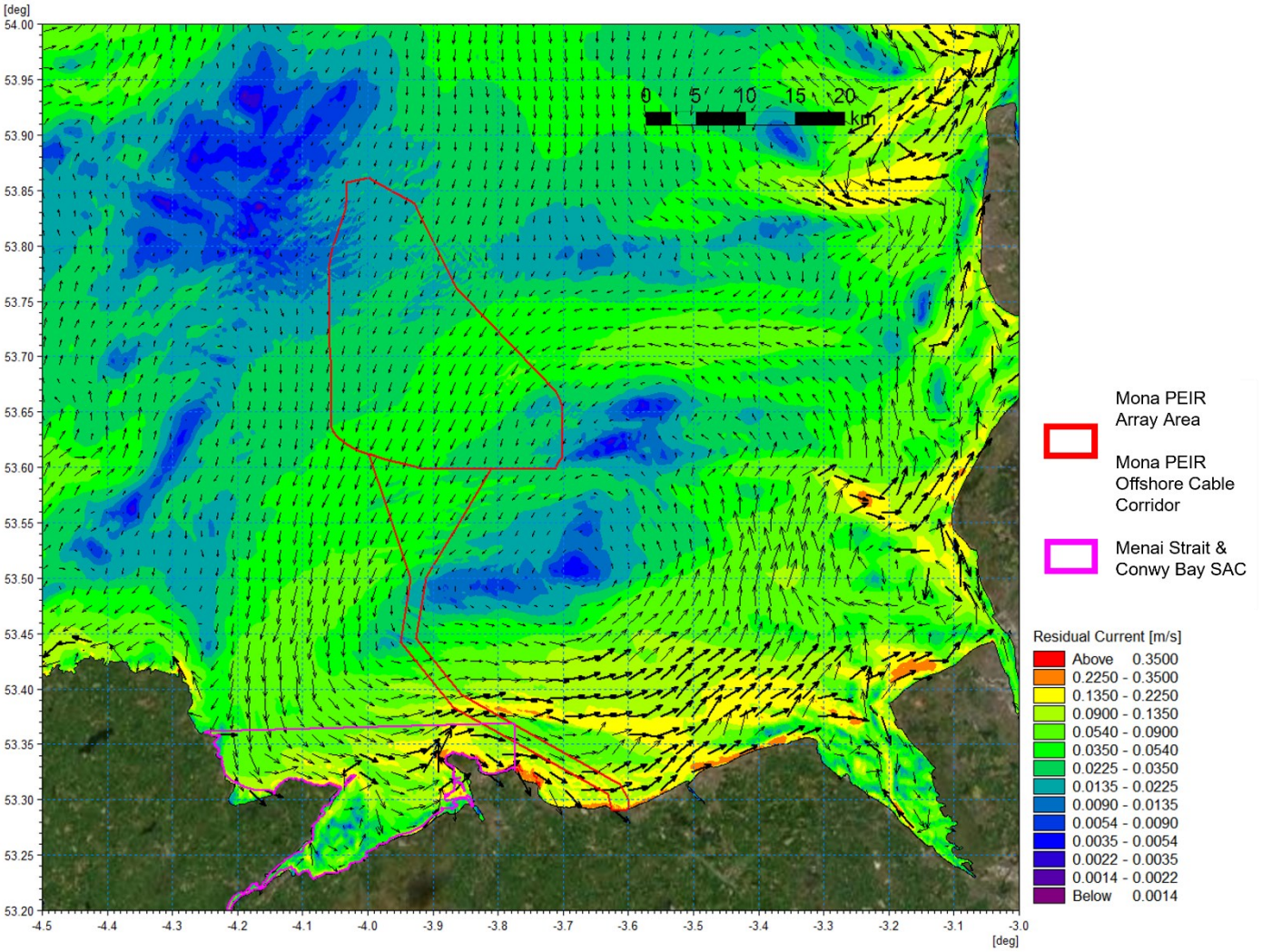

Figure 1.62: Residual current spring tide with 1 in 1 year storm from 270°.

Suspended sediments

1.3.5.45 The principal mechanisms governing Suspended Sediment Concentration (SSC) in the water column are tidal currents, with fluctuations observed across the spring-neap cycle and across the different tidal stages (high water, peak ebb, low water, peak flood) observed throughout both datasets. It is key to note that SSCs can also be temporarily elevated by wave-driven currents during storm events. During high-energy storm events, levels of SSC can rise significantly, both near bed and extending into the water column. Following storm events, SSC levels will gradually decrease to baseline conditions, regulated by the ambient regional tidal regimes. The seasonal nature and frequency of storm events supports a broadly seasonal pattern for SSC levels.

1.3.5.46 Based on the data recorded within the Morgan Generation Assets metocean study site, located in close proximity to the Mona PEIR Offshore Wind Project, the average near bed turbidity associated is circa 2 mg/l. As shown in Figure 1.63, spikes in near surface turbidity correspond with increases in the significant wave height during storm conditions. The data is presented for the November 2021 to March 2022 period with peaks reaching circa 20 mg/l.

1.3.5.47 For more generalised conditions the Cefas Climatology Report 2016 (Cefas, 2016) and associated dataset provides the spatial distribution of average non-algal

Suspended Particulate Matter (SPM) for the majority of the UK Continental Shelf (UKCS). Between 1998 and 2005, the greatest plumes are associated with large rivers such as those that discharge into the Thames Estuary, The Wash and Liverpool Bay, which show mean values of SPM above 30 mg/l. The levels of SPM reported by CEFAS between 1998 to 2005 of approximately 0.9 mg/l to 3 mg/l are similar to the values recorded at the Morgan Generation Assets site. Higher levels of SPM are experienced more commonly in the winter months; however, due to the tidal influence, even during summer months the levels may become elevated.

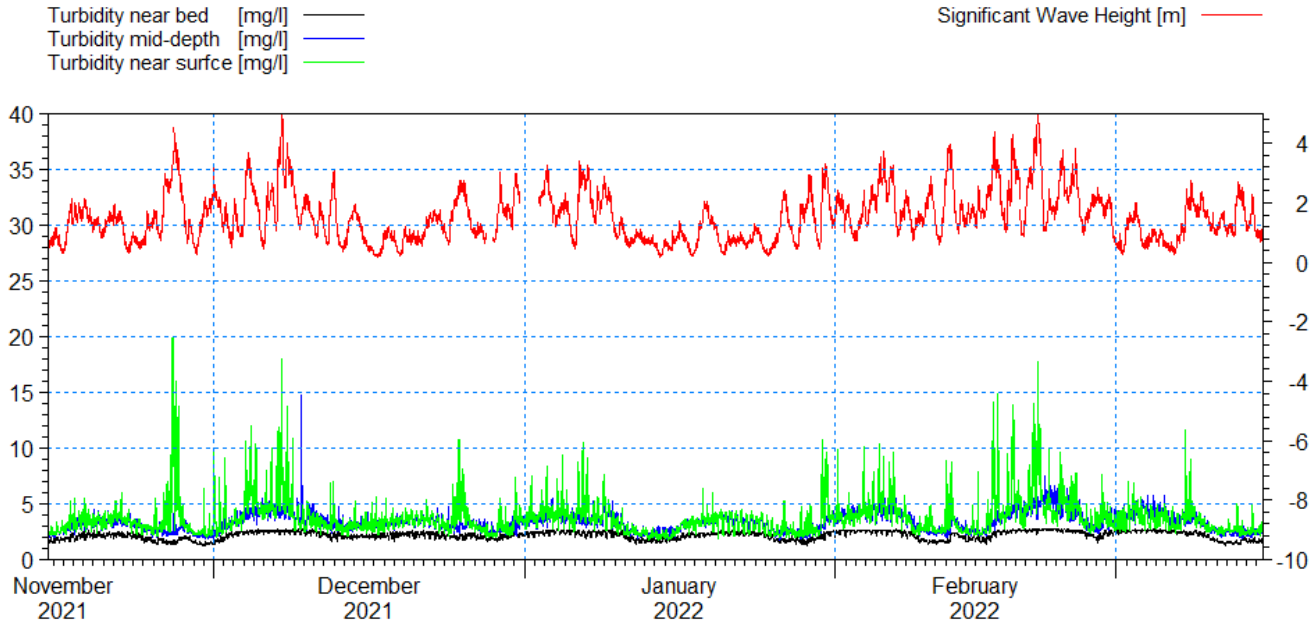

Figure 1.63: Turbidity levels from the Morgan Generation Assets metocean site.

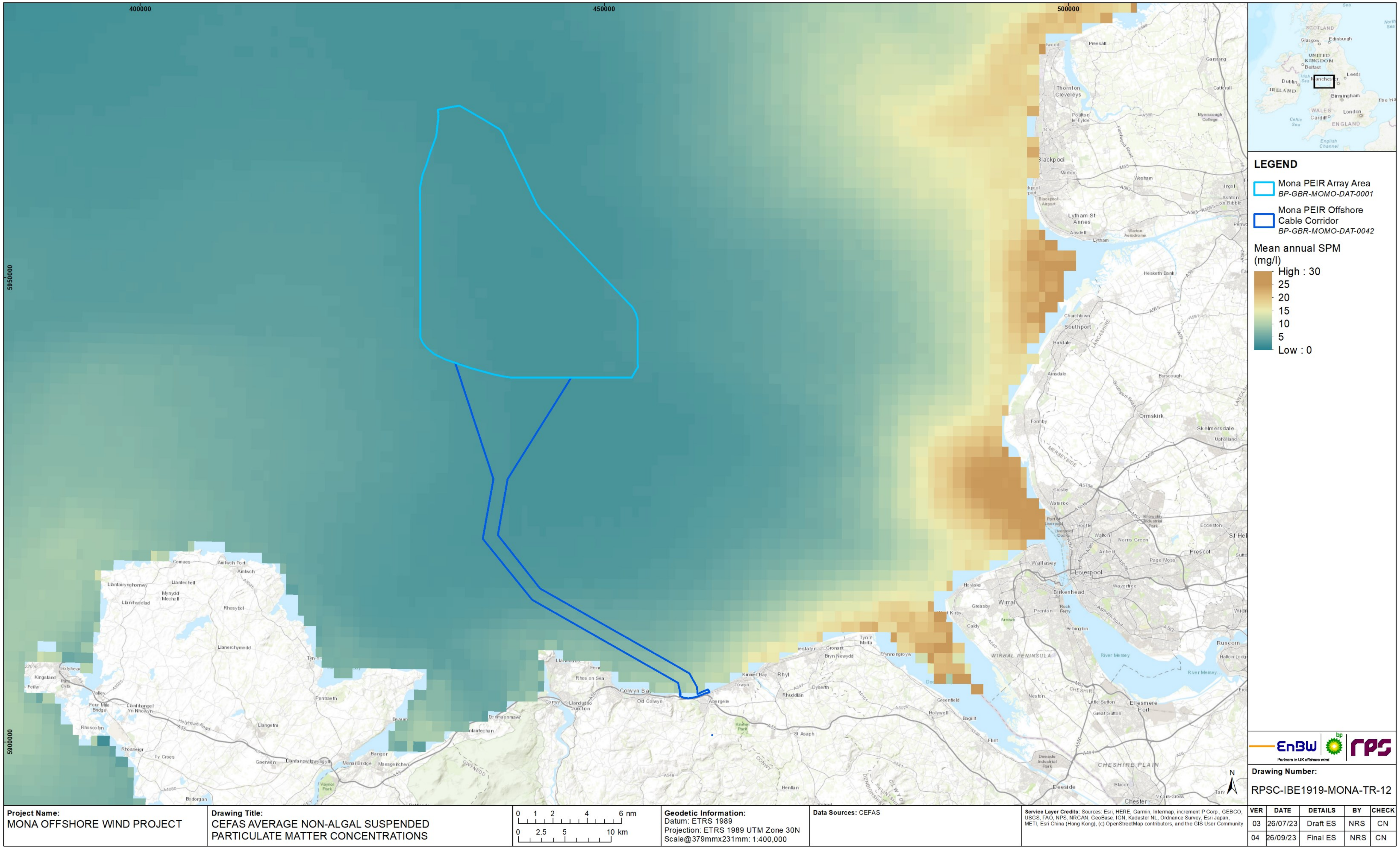

Figure 1.64: Distribution of average non-algal suspended particulate matter (CEFAS, 2016).

1.3.6 Potential environmental changes (as presented in the PEIR)

Overview

1.3.6.1 The potential changes to the baseline hydrographic conditions as a result of the installation and presence of the Mona Offshore Wind Project as defined for the PEIR are quantified in the following sections. These changes relate to the presence of the infrastructure within the water column and seabed and are therefore associated with turbine legs along with cable and scour protection. The potential changes to sea state and sediment transport regimes were established by repeating the modelling undertaken in the previous section with the inclusion of the Mona Offshore Wind Project as defined in the project description for PEIR. The modelling was undertaken using an indicative layout which included the following changes in line with the Maximum Design Scenario (MDS) for PEIR associated with physical processes parameters:

- Leg structures 5 m in diameter relating to 68 wind turbines each comprising four legs
- Scour protection 56 m diameter and 2.5 m in height associated with 16 m suction bucket foundations for each wind turbine leg
- Leg structures 3 m in diameter relating to 4 OSPs each comprising three legs
- Scour protection 49 m diameter and 2.5 m in height associated with 14 m suction bucket foundations for each OSP leg
- Inter-array cable protection to a height of 3 m and 10 m width with cable crossings 4 m in height, 32 m width and 60 m length
- Interconnector cable protection to a height of 3 m and 10 m width with cable crossings 3 m in height, 20 m width and 50 m length
- Offshore export cable protection to a height of 3 m and 10 m width with cable crossings 3 m in height, 30 m width and 50 m length.

1.3.6.2 In addition to these structures the modelling also included provision of an Offshore Booster Substation located mid-distance along the offshore export cable. The need for this infrastructure has subsequently been removed from the Mona Offshore Wind Project therefore the modelling results of potential environmental changes presented here would be conservative.

1.3.6.3 It should be noted that the scale of the model mesh meant that the general flow and sediment patterns around the structures could be observed on the wider scale. The detailed impact of secondary scour is localised, site and design specific in nature. The modelling included the provision of scour protection and a detailed assessment of the effectiveness of the scour protection proposed at each foundation location was not undertaken as this was not the purpose of the computational modelling. The scour protection does not have implications on the global scale and is restricted to reducing sediment erosion in the vicinity of the foundations; there would be larger implications if scour protection were not provided (Whitehouse *et al.*, 2006).

1.3.6.4 The methodology implemented for the modelling used parameters selected from the project description associated with the Mona PEIR Offshore Wind Project, to ascertain the most influential and likely scenario for each physical process aspect under examination. The indicative layout used within the modelling study is presented in Figure 1.65 it applied cable protection in regions where trenching to 3 m depth was

unlikely (i.e. in the vicinity of moraines comprised glacial till) and where inter-array cable connects with generating assets.

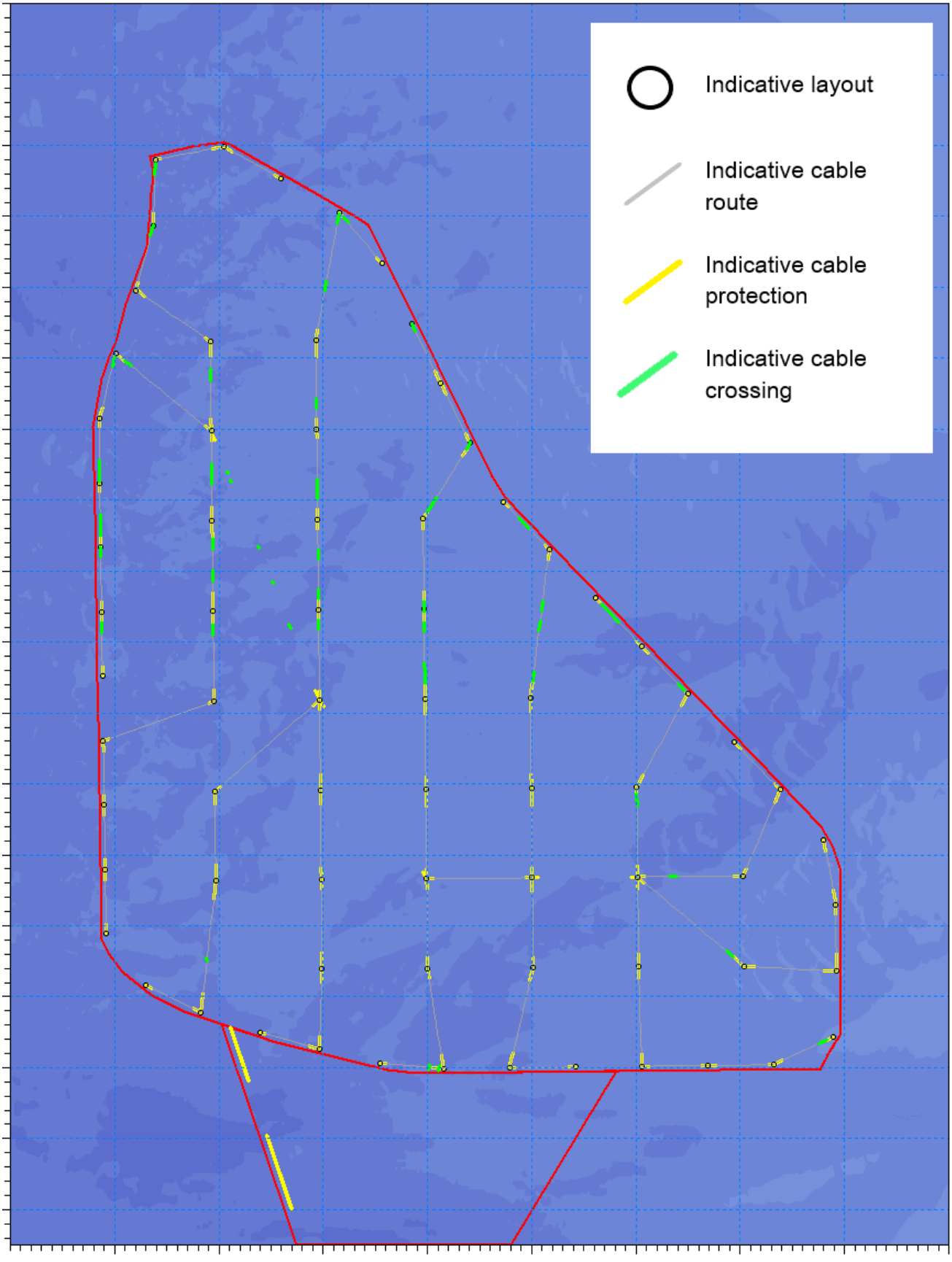

Figure 1.65: Modelled array and trenching route indicative layout for PEIR.

Post-construction hydrography

Tidal flow

1.3.6.5 The hydrodynamic simulations were repeated with the addition the infrastructure as outlined in the previous section. The bathymetry was also amended to take account of scour and cable protection. The following figures show the same mid flood and mid ebb steps from the simulation as were presented in Figure 1.31 and Figure 1.32 respectively, but with the Mona Offshore Wind Project foundation and structures as defined in the PEIR in place. Where appropriate, the Mona PEIR Offshore Cable Corridor has been indicated on the figures along with the Mona PEIR Array Area, to indicate the locality of the works without obscuring the model results. Additionally, for reference, the designated areas associated with physical processes is outlined in pink on each figure. Due to the limited magnitude of the changes, difference plots have also been provided. These are the proposed minus the baseline condition, therefore increases in current speed will be positive. The same procedure for calculating differences and plotting figures has been implemented throughout this report.

1.3.6.6 Figure 1.66 shows the post-construction flood tide flow patterns with Figure 1.67 showing the changes and as the changes are limited to the vicinity of the development a more focused plot is provided in Figure 1.68. In the difference figures a log scale has been introduced to accentuate the values for clarity. Similarly, Figure 1.69, Figure 1.70 and Figure 1.71 show the same information for the ebb tide. During peak current speed the flow is redirected in the immediate vicinity of the structures and cable protection. The variation is a maximum of 5 cm/s in the immediate vicinity of the structure which constitutes less than 5% of the peak flows. This reduces significantly with increased distance from each structure with changes being significantly smaller in the areas where cable protection is present within 200 m of the installation changes are <2 mm which would be indiscernible from baseline conditions.

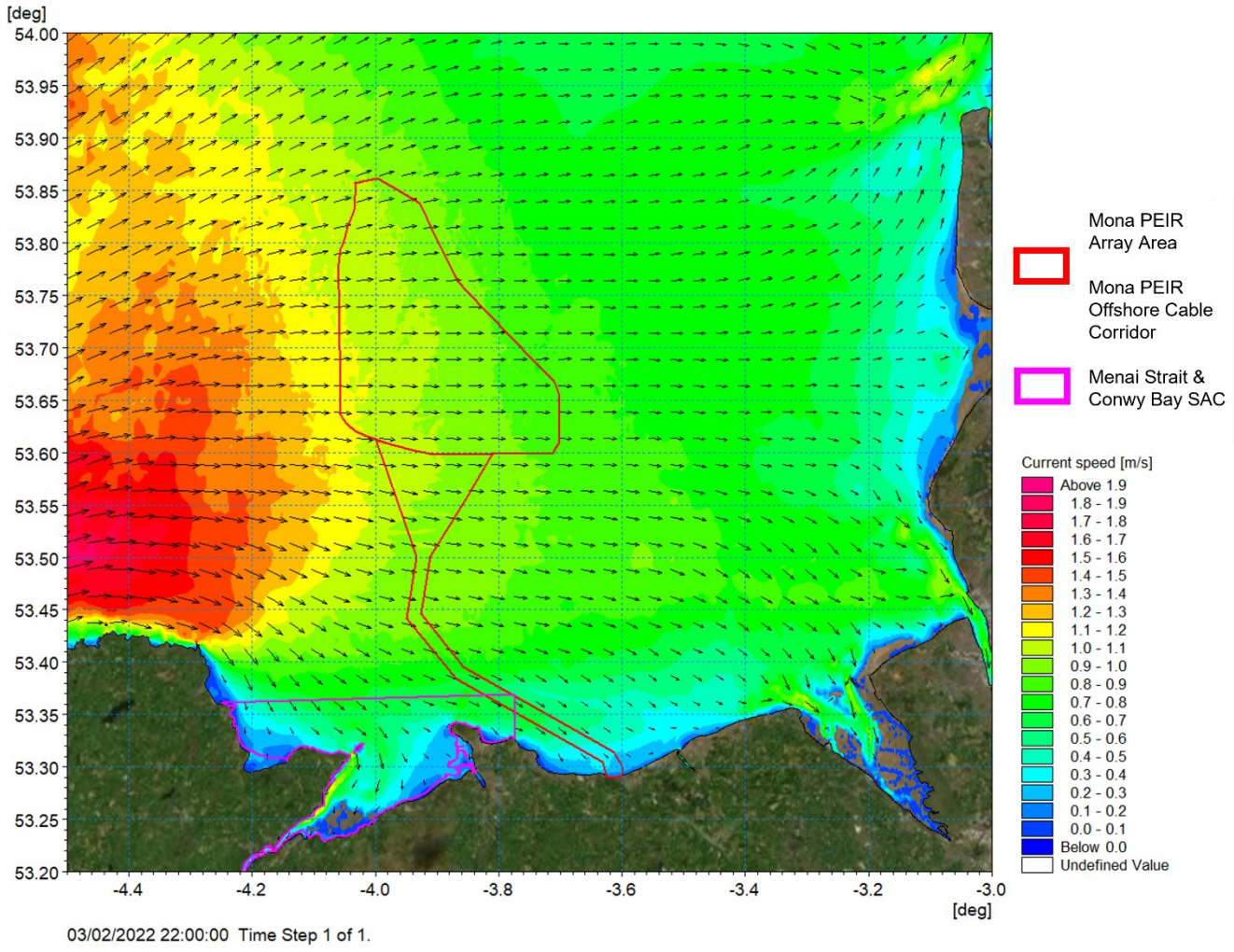

Figure 1.66: Post-construction tidal flow pattern – flood tide.

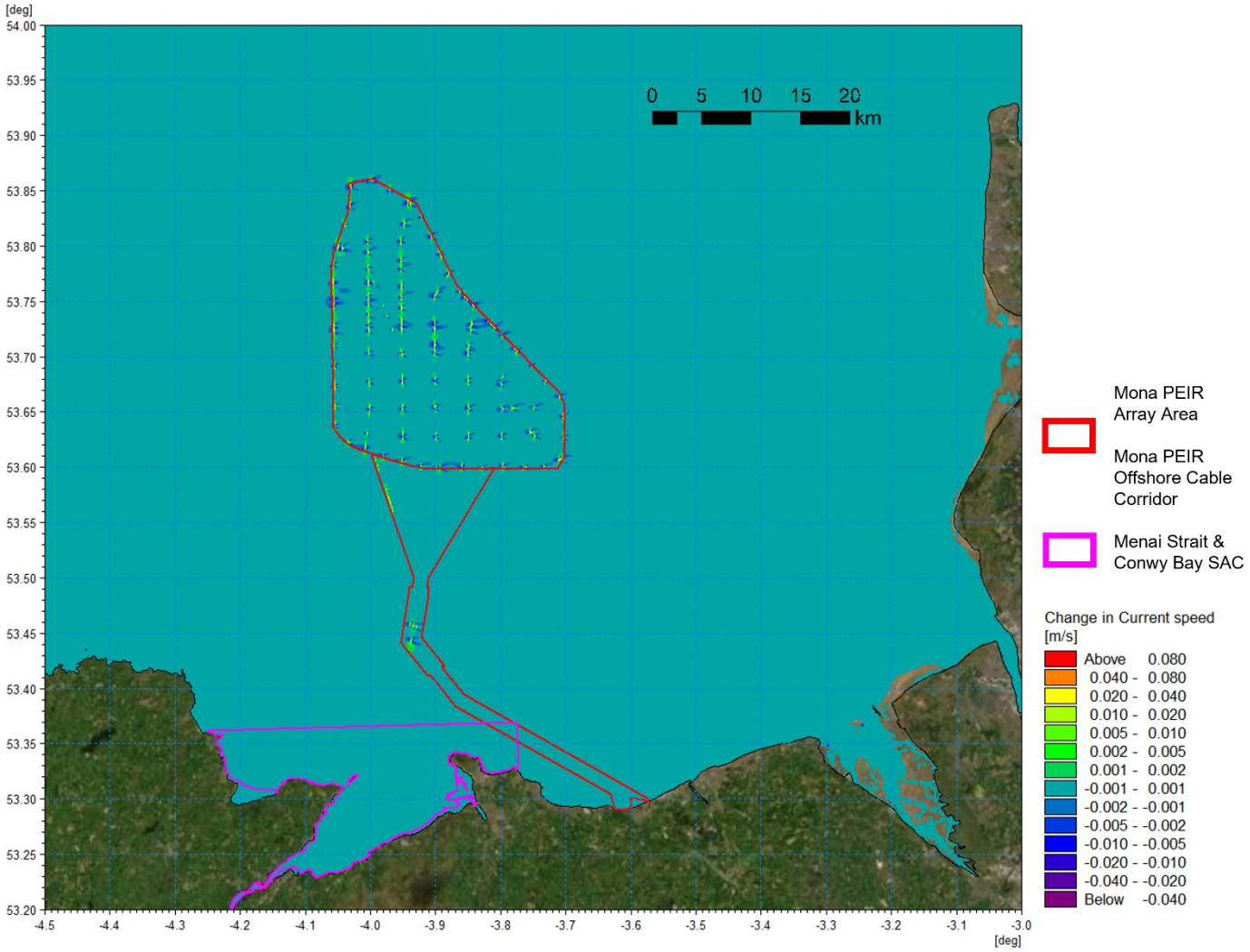

Figure 1.67: Change in tidal flow (post-construction minus baseline) – flood tide.

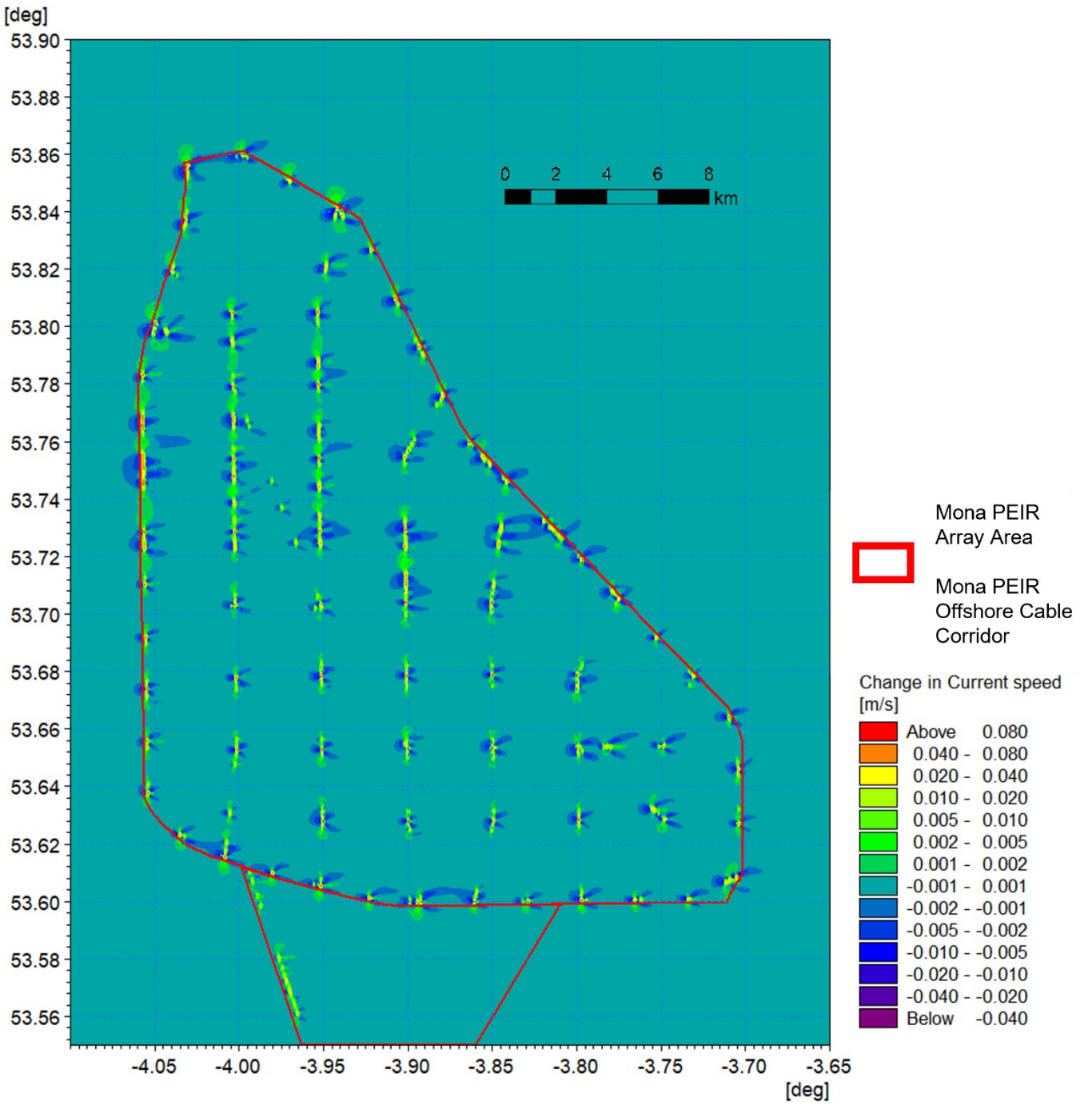

Figure 1.68: Change in tidal flow (post-construction minus baseline) PEIR Mona Array Area – flood tide detail view.

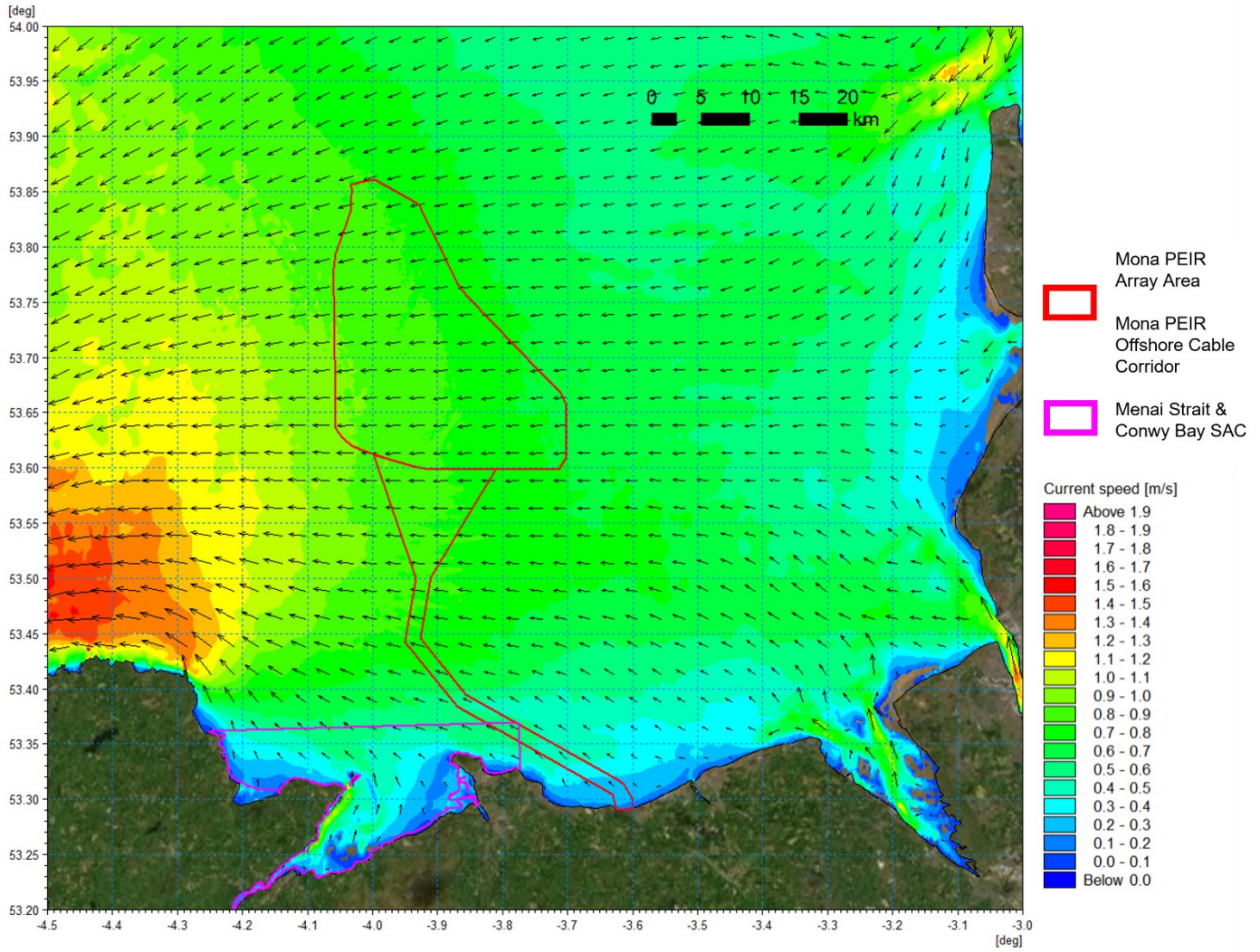

Figure 1.69: Post-construction tidal flow pattern – ebb tide.

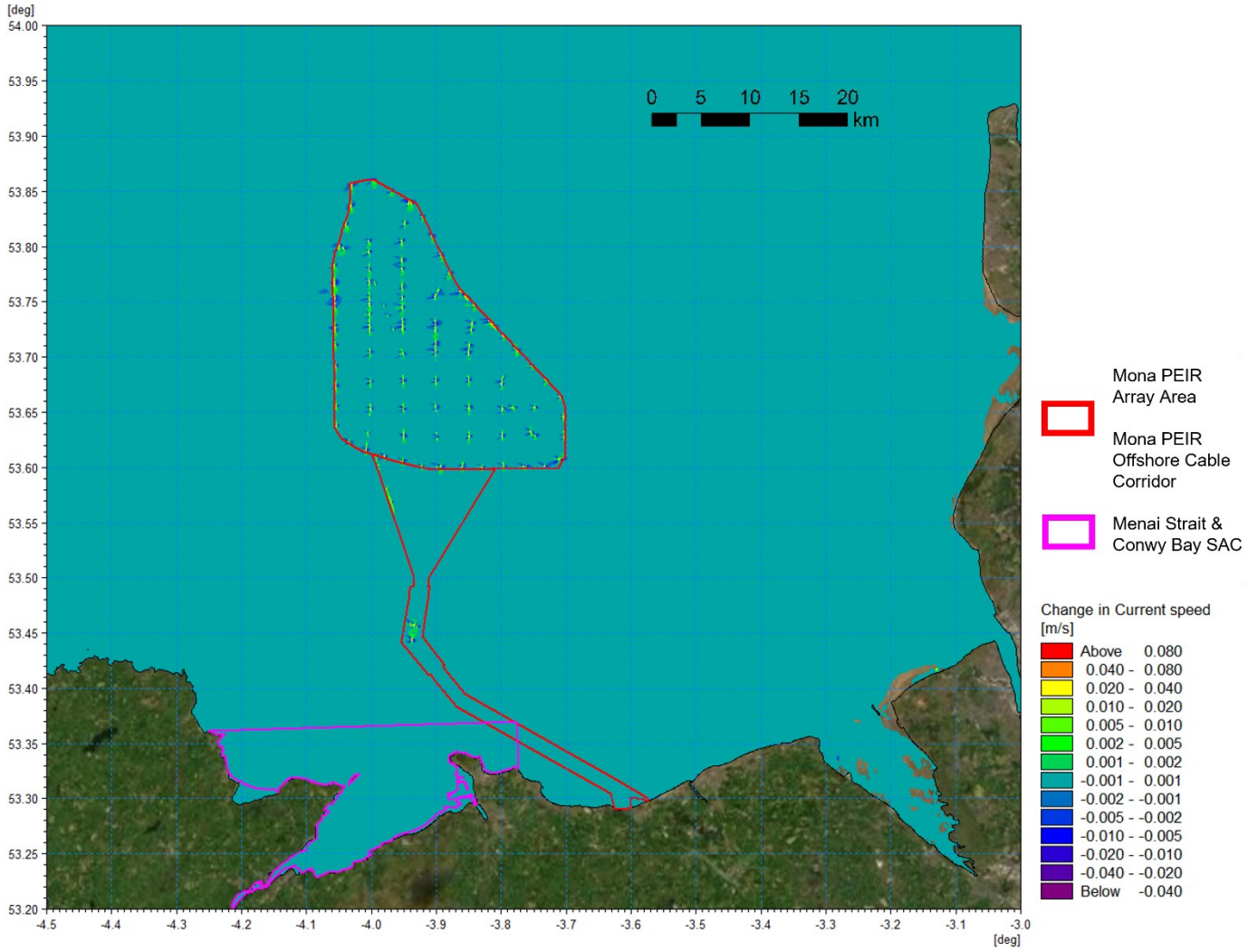

Figure 1.70: Change in tidal flow (post-construction minus baseline) – ebb tide.

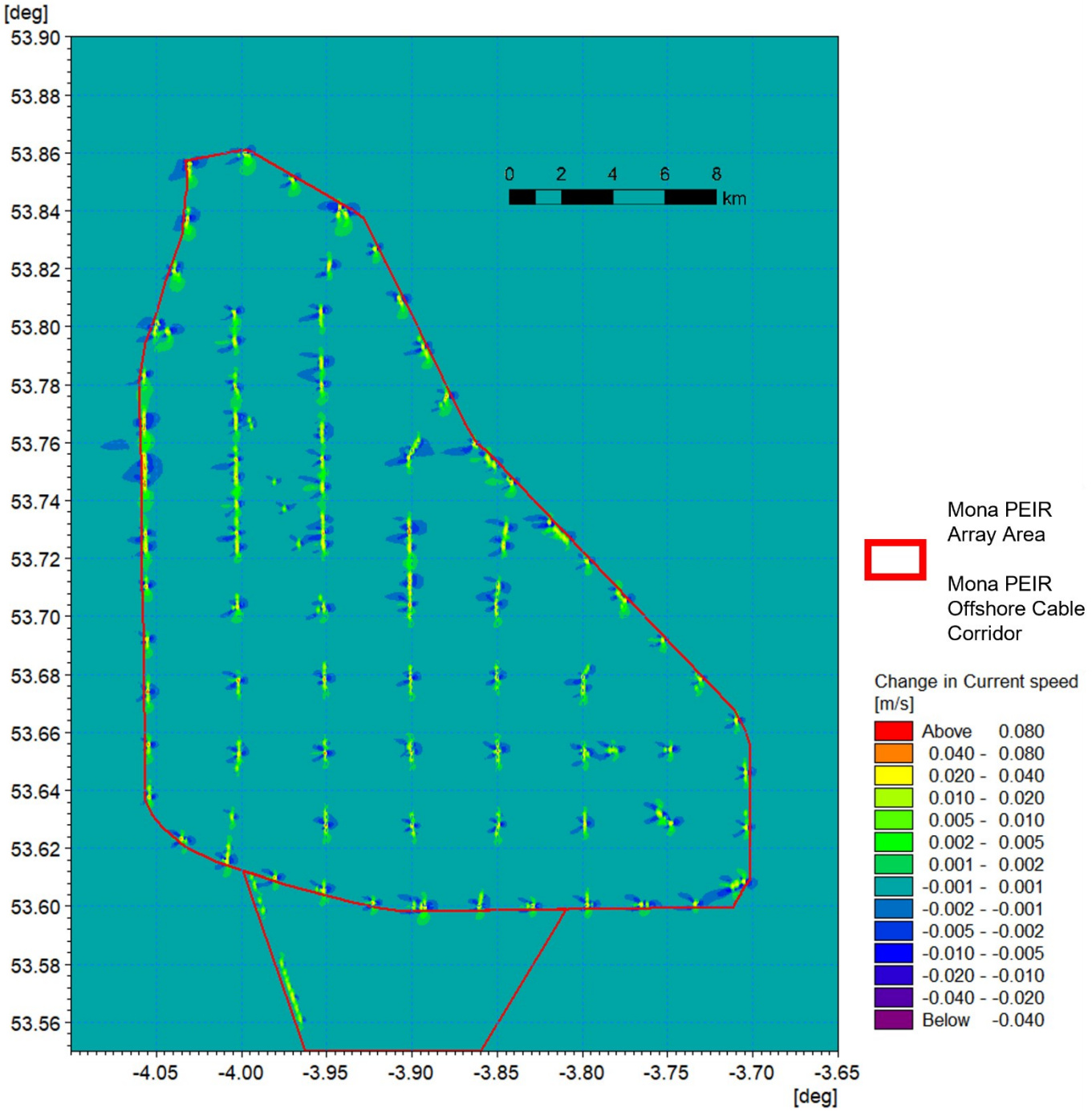

Figure 1.71: Change in tidal flow (post-construction minus baseline) PEIR Mona Array Area – ebb tide detailed view.

Wave climate

1.3.6.7 Using the same principle as for the tidal modelling, the wave climate modelling was repeated with the inclusion of the Mona Offshore Wind Project structures, foundations and cable protection as defined in the PEIR. Again, changes were found to be indiscernible from the baseline scenario by visual inspection therefore difference plots have been provided and using the same scale for all scenarios. The same principal directions are presented for the 1 in 1 year storm and 1 in 20 year storm as presented for the baseline in section 1.3.5.

1.3.6.8 The post construction phase 000° storm is presented for the 1 in 1 year in Figure 1.72 with the difference shown in Figure 1.73. Similarly, the 1 in 20 year storm from this direction is presented in Figure 1.74 and Figure 1.75. The changes are seen as reductions in the lee of the structures. The maximum changes are in the order of 3 cm for the annual event and 4.5 cm for the more extreme storm event which represents less than 1% of the baseline significant wave height. The wave shadow is typically less than one half of this value. These changes would be indiscernible from the baseline wave climate and would not impact on the shoreline or nearshore banks.

1.3.6.9 The potential change in wave climate relative to baseline conditions for annual and more extreme storms are of similar proportions so, for brevity, only the 1 in 20 year results are presented for the remain directions. Figure 1.76 depicts the 030° post construction scenario with Figure 1.77 showing the change from baseline conditions. The magnitude of the changes at the location of the structures is a reduction in wave height of 3 cm whilst, once again the shadow if typical less 2 cm which is less than 1% of the baseline condition.

1.3.6.10 For the westerly storms from 240° and 270° the incident wave heights are typically twice that of the fetch limited directions. For these scenarios the effect of the presence of the infrastructure is much smaller with changes in wave height typically less than 0.25% as presented in Figure 1.78 to Figure 1.81.

1.3.6.11 In summary, the presence of the Mona Offshore Wind Project as defined in the PEIR was seen to have the greatest influence when storms approached from the northerly sectors where baseline wave height were smallest. In all cases the changes in wave climate would be imperceptible and would not interact with the shoreline or nearshore banks and morphology.

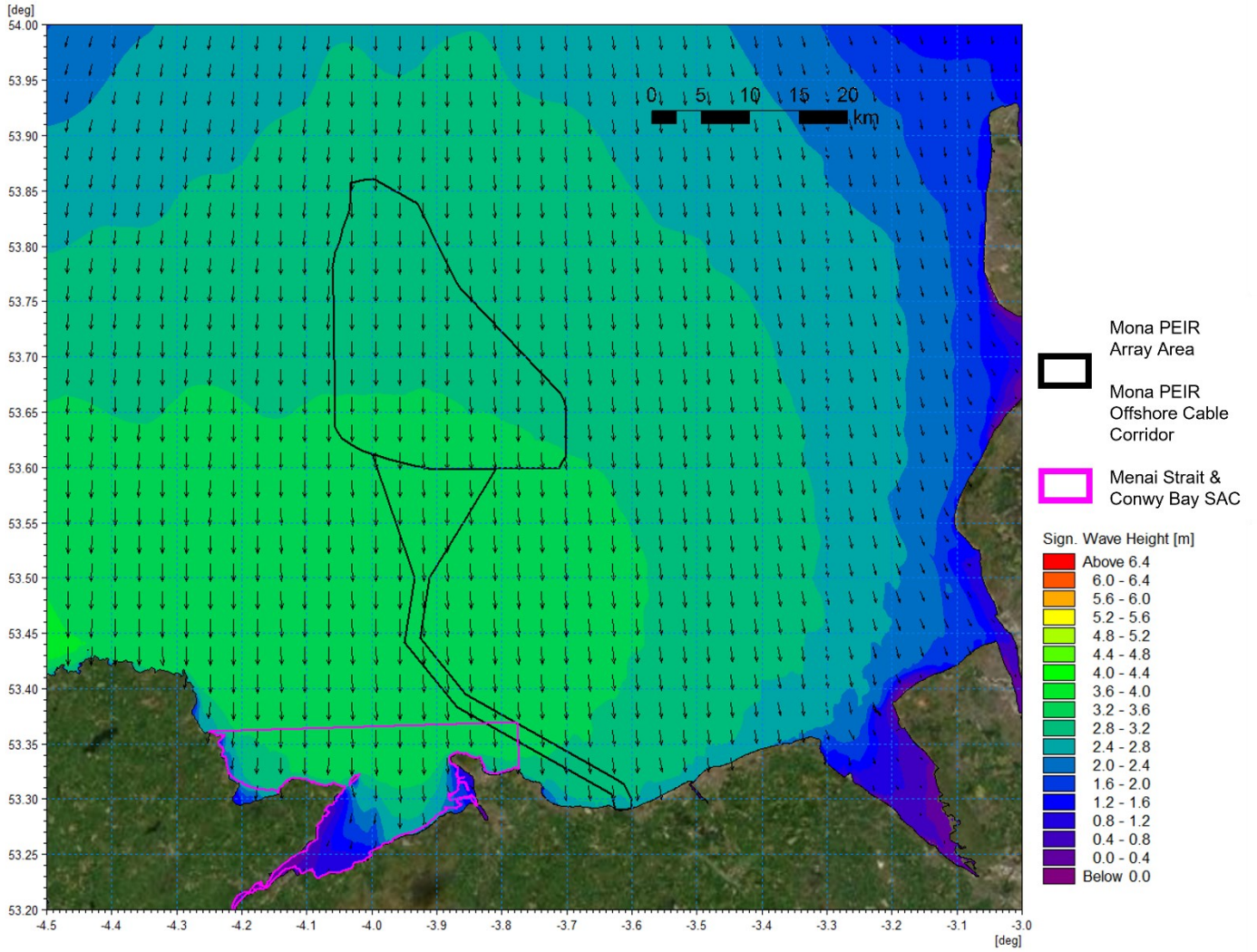

Figure 1.72: Post-construction wave climate 1 in 1 year storm 000° MHW.

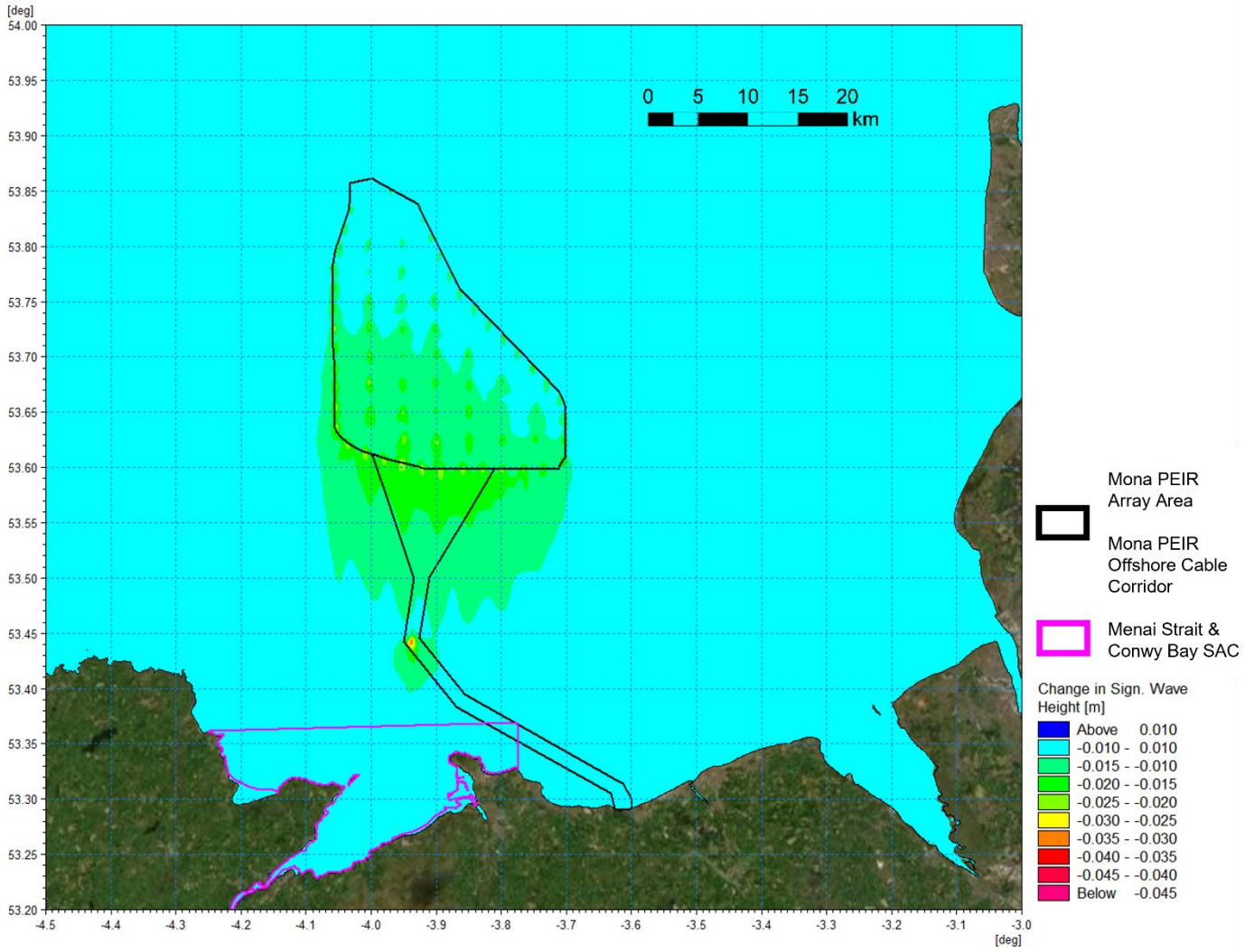

Figure 1.73: Change in wave climate 1 in 1 year storm 000° MHW (post-construction minus baseline).

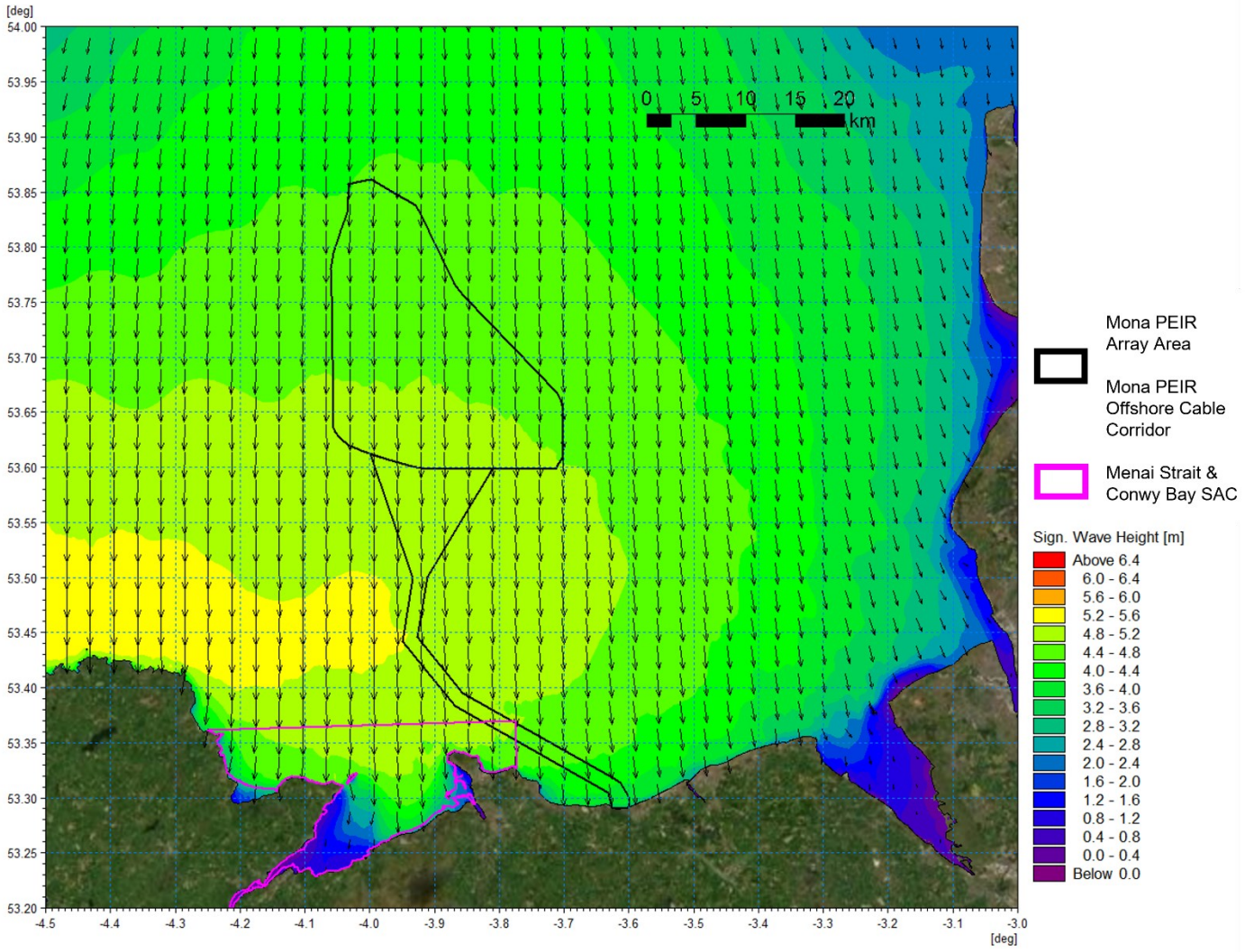

Figure 1.74: Post-construction wave climate 1 in 20 year storm 000° MHW.

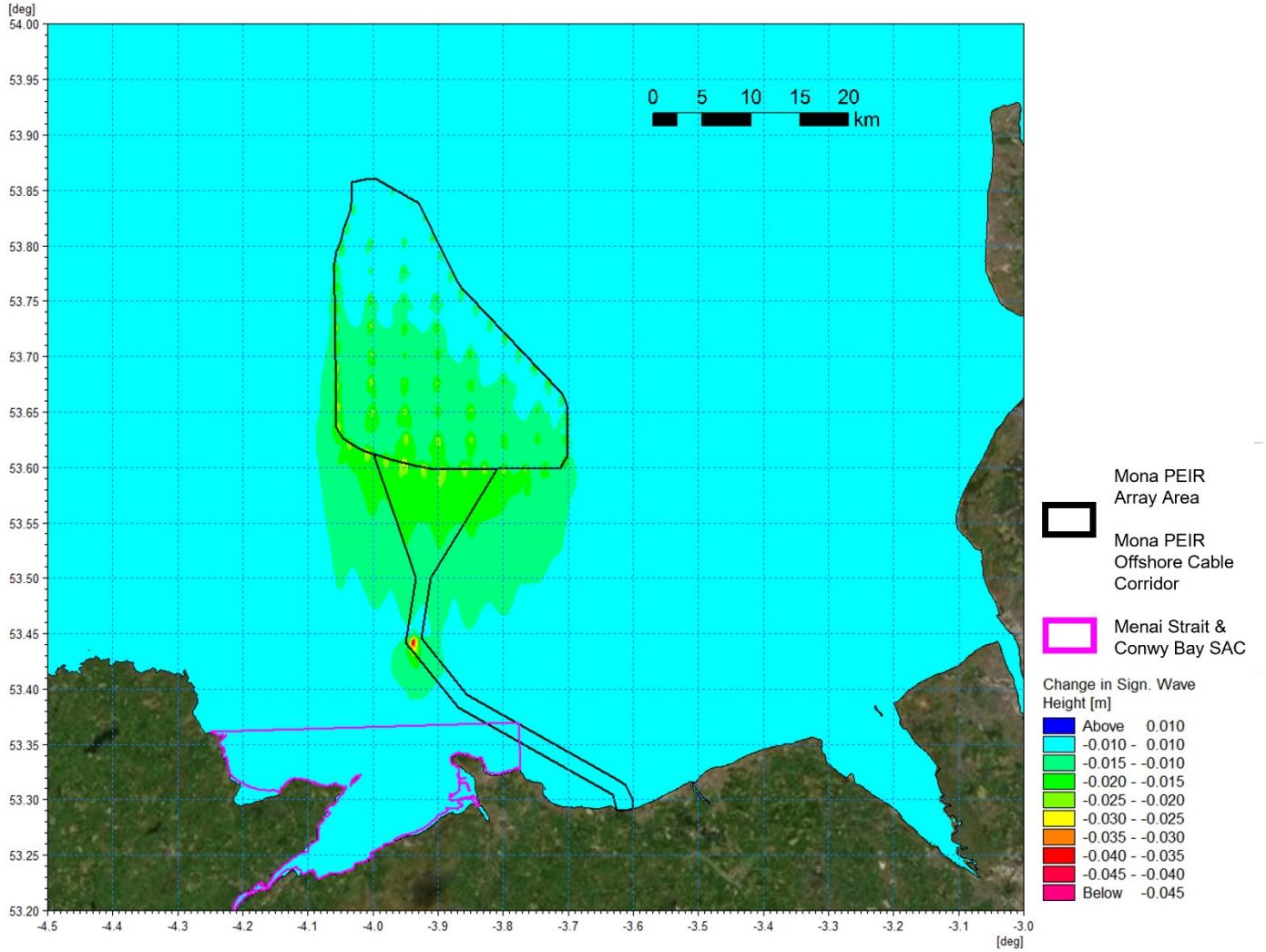

Figure 1.75: Change in wave climate 1 in 20 year storm 000° MHW (post-construction minus baseline).

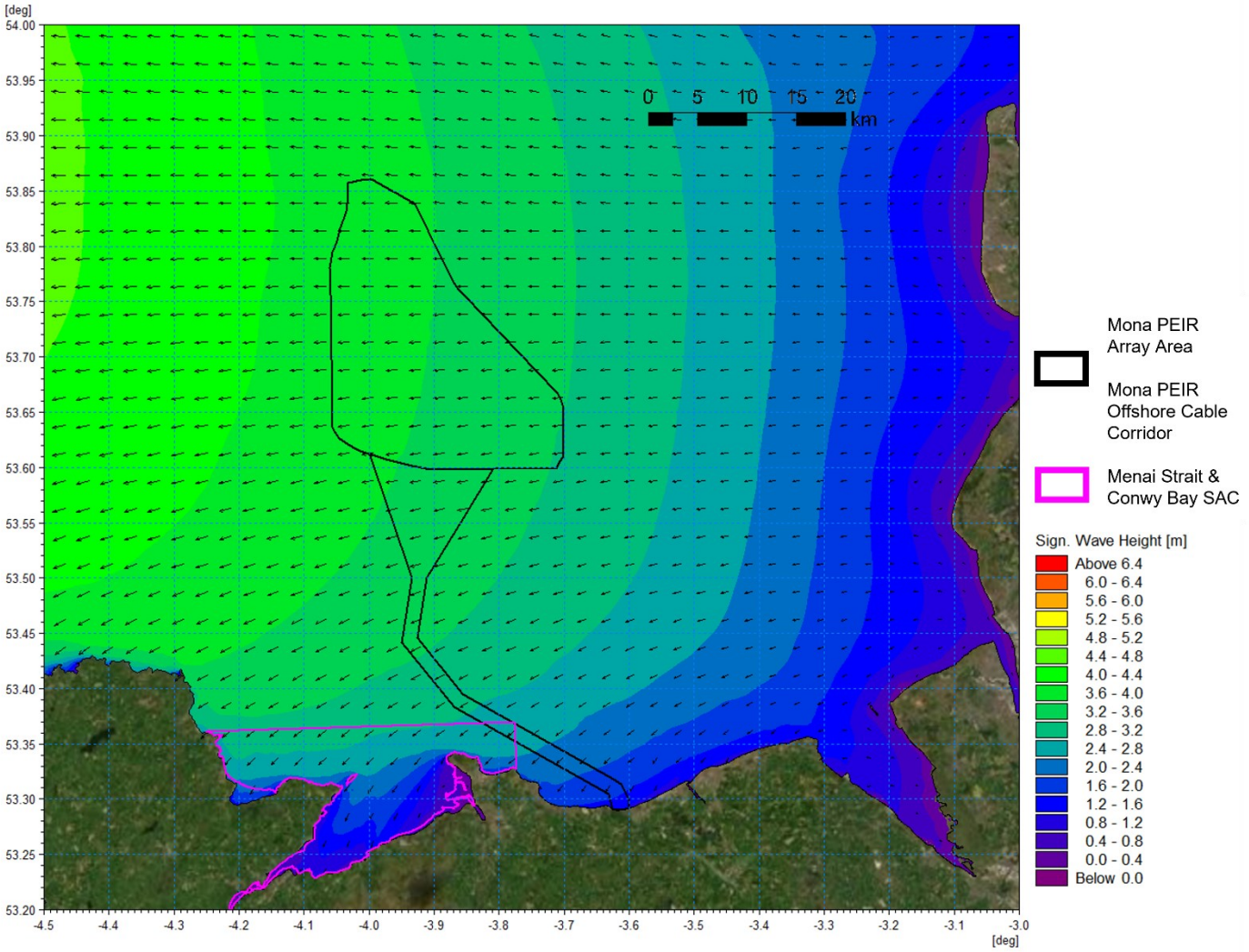

Figure 1.76: Post-construction wave climate 1 in 20 year storm 090° MHW.

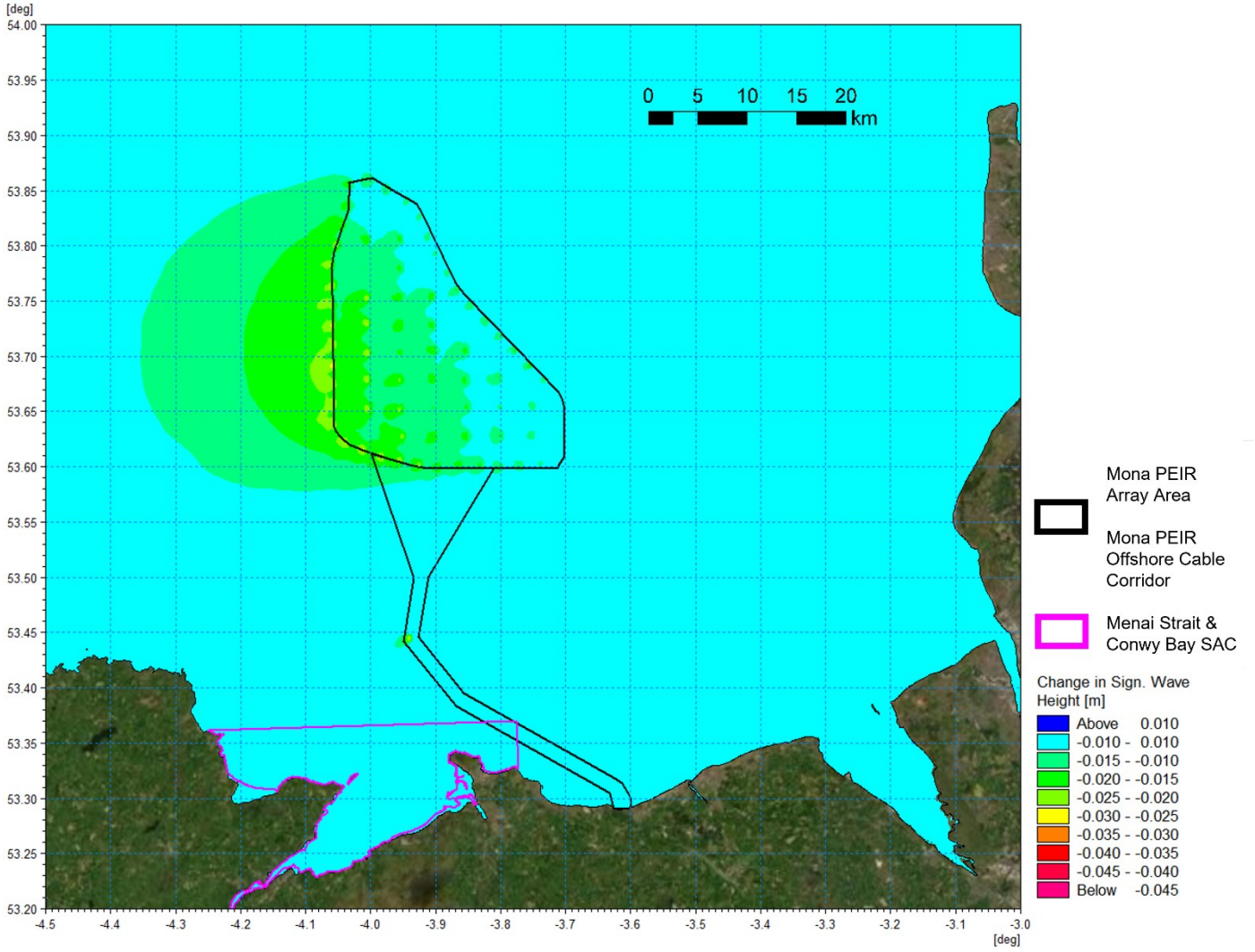

Figure 1.77: Change in wave climate 1 in 20 year storm 090° MHW (post-construction minus baseline).

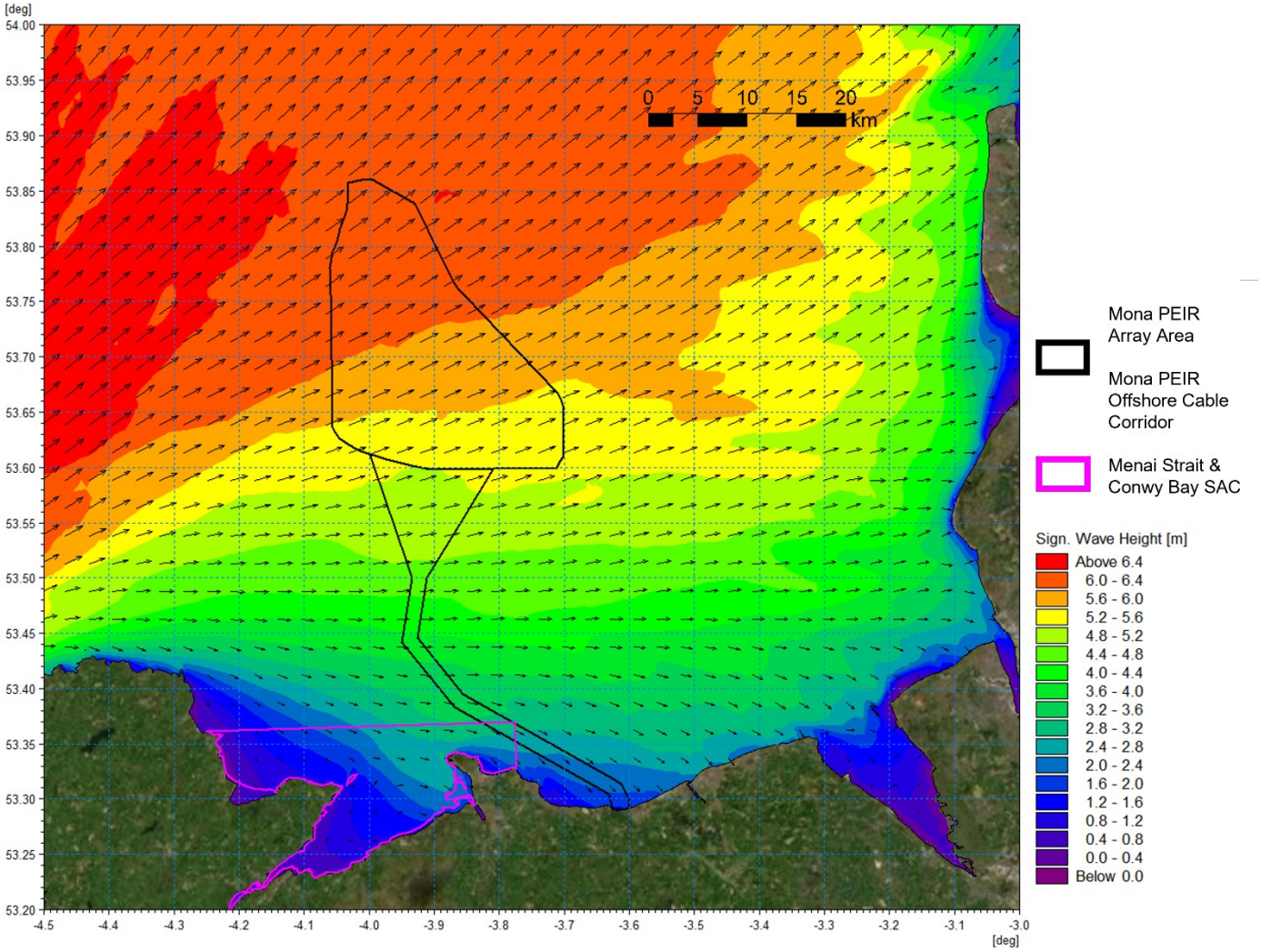

Figure 1.78: Post-construction wave climate 1 in 20 year storm 240° MHW.

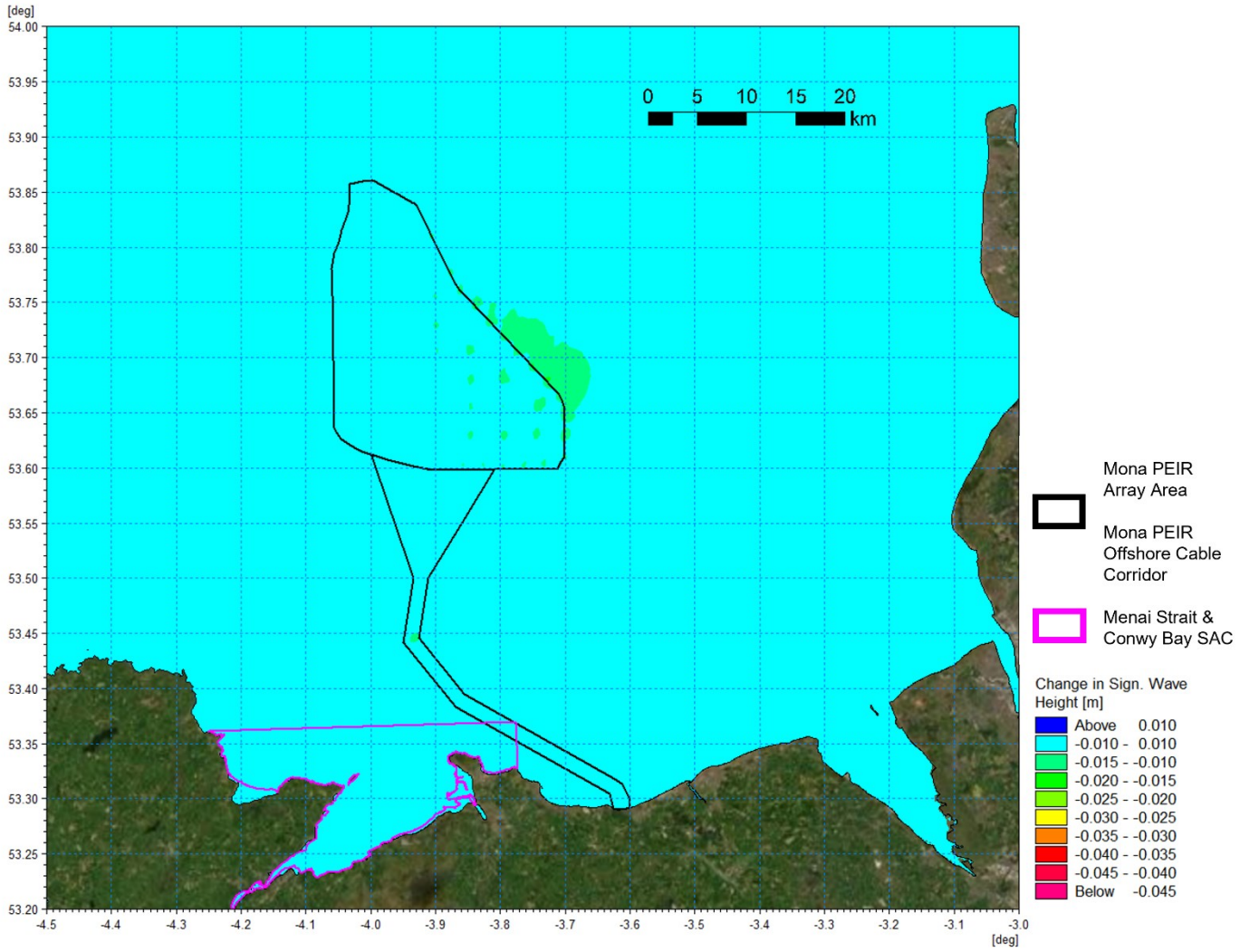

Figure 1.79: Change in wave climate 1 in 20 year storm 240° MHW (post-construction minus baseline).

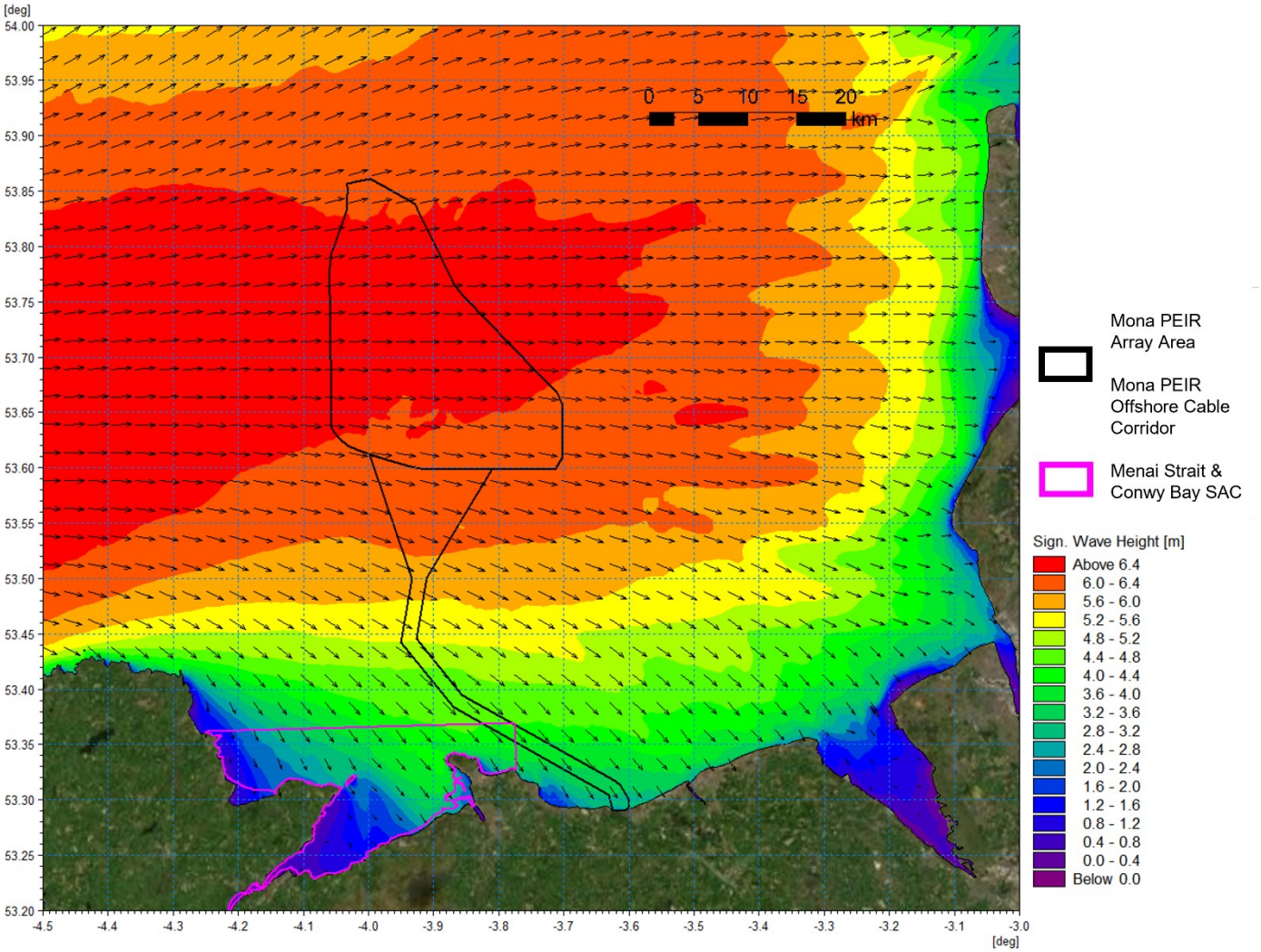

Figure 1.80: Post-construction wave climate 1 in 20 year storm 270° MHW.

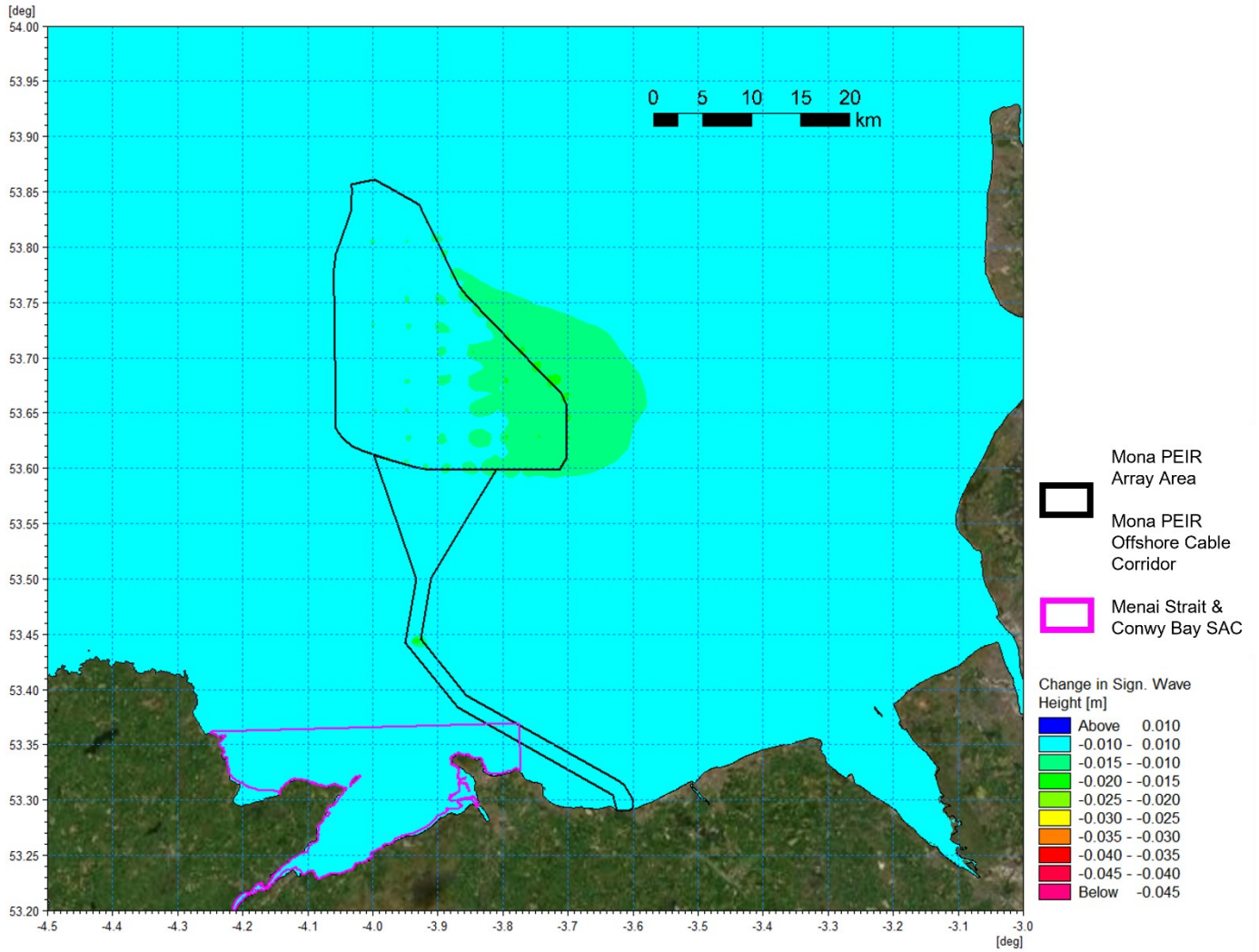

Figure 1.81: Change in wave climate 1 in 20 year storm 270° MHW (post-construction minus baseline).

Littoral currents

1.3.6.12 The previous sections established the magnitude of the changes in tidal currents and wave conditions individually, however sediment transport regimes are driven by a combination of these factors. Although the modelling has demonstrated that the Mona Offshore Wind Project as defined in the PEIR results in minor localised changes for each aspect, for the sake of completeness, the influence on littoral currents was examined.

1.3.6.13 The modelling was extended to include the post-construction scenario for the 1 in 1 year storm from 270°. The baseline littoral currents for mid ebb and mid flood were presented in Figure 1.54 and Figure 1.55 respectively. The corresponding post-construction littoral currents are shown in Figure 1.82 and Figure 1.85 for the ebb and flood tides.

1.3.6.14 As with the previous difference in current speed post construction, a log plotting scale was necessary to present the changes due to their localised nature. The changes for the flood tide are presented in Figure 1.83 a more detailed plot in Figure 1.84 whilst for the ebb tide Figure 1.86 and Figure 1.87 show the corresponding information.

1.3.6.15 During the flood tide the influence of the wave climate is in concert with the tidal current and during the ebb tide, the tidal flow is in opposition to the wave climate and the resultant littoral current is reduced in magnitude. The presence of the structures was seen to have a limited influence on the wave climate and there is little difference between changes in littoral current magnitude and the tidal flows alone due to the installation during the flood tide. The extent of the changes is larger for the ebb tide condition particularly at the south of the Mona PEIR Array Area, although it should be noted that these are still <1% of baseline tidal flow. Overall, the magnitude of these changes remains limited to ±5% of the baseline currents at 200 m and reduces significantly with increased distance from each structure.

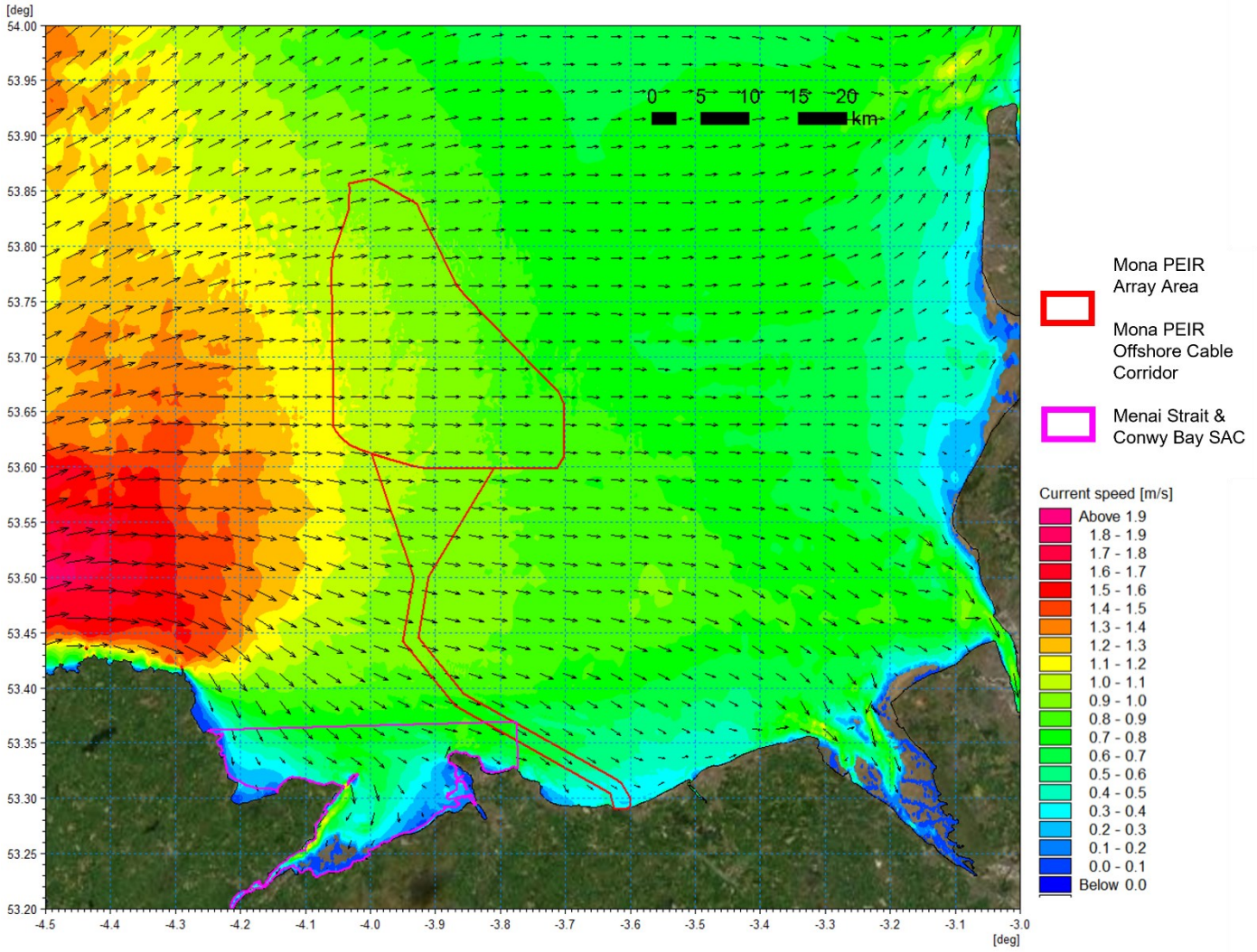

Figure 1.82: Post-construction littoral current 1 in 1 year storm from 270° - Flood Tide.

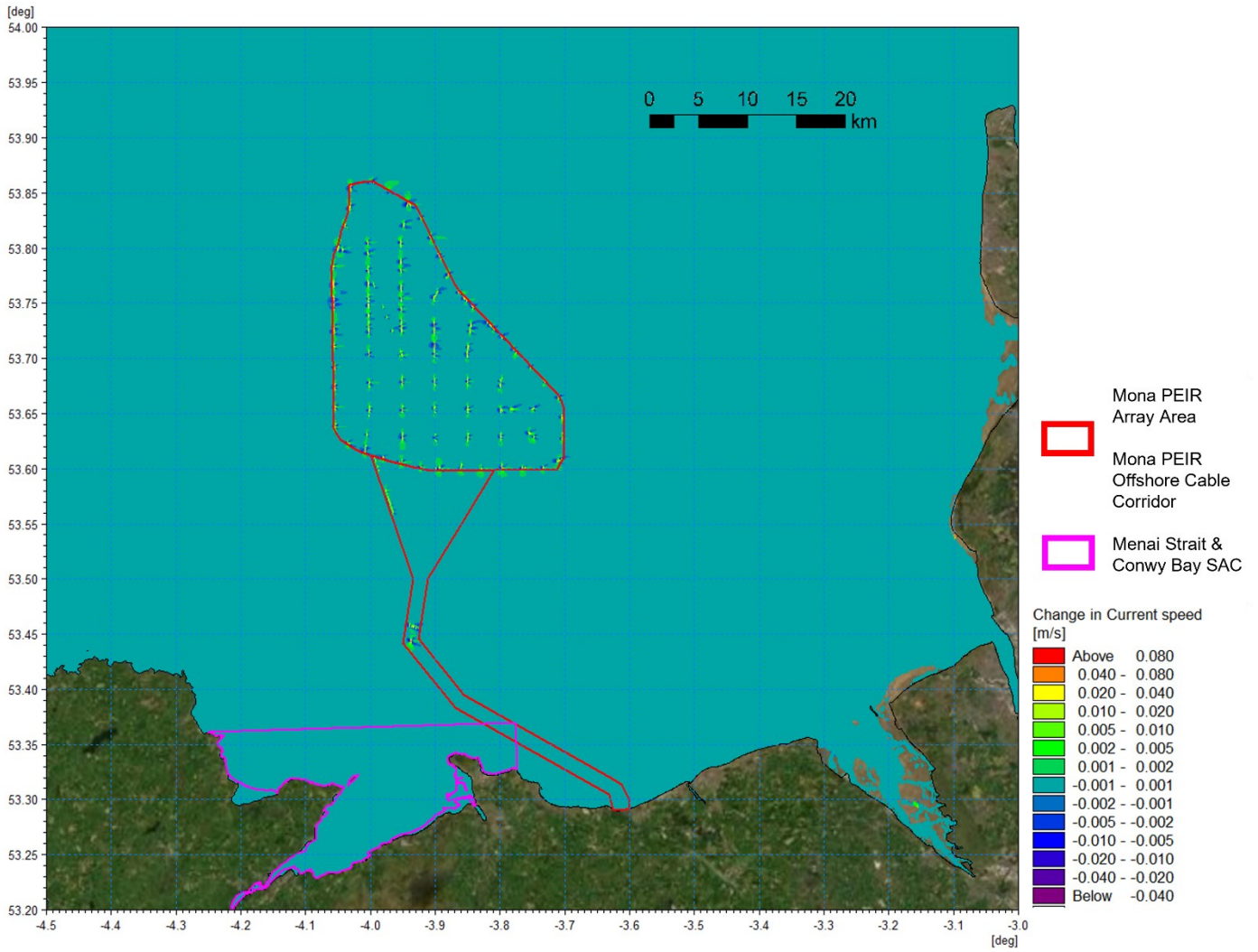

Figure 1.83: Change in littoral current 1 in 1 year storm from 270° - flood tide (post-construction minus baseline).

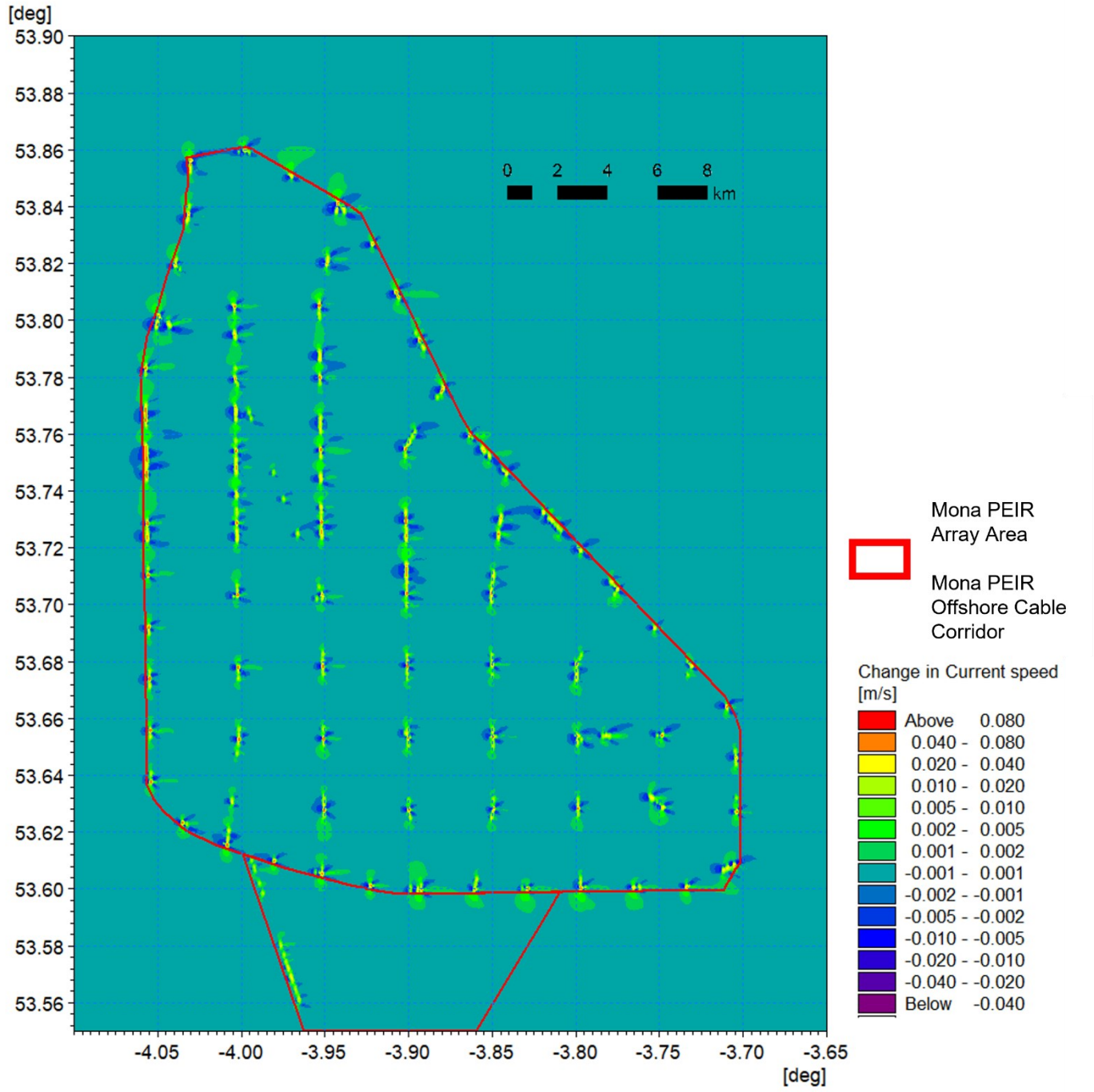

Figure 1.84: Change in littoral current 1 in 1 year storm from 270° - flood tide (post-construction minus baseline) detailed view.

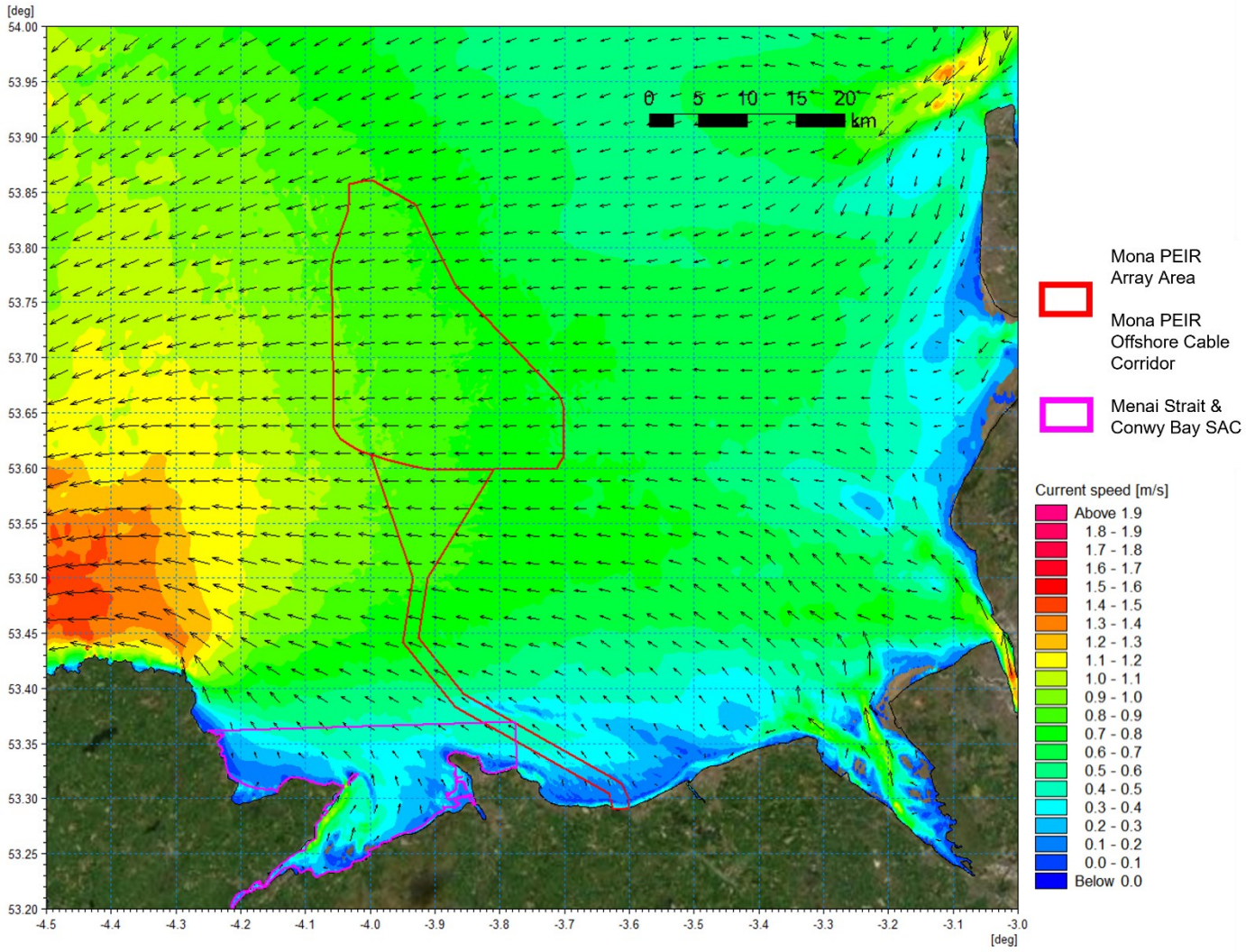

Figure 1.85: Post-construction littoral current 1 in 1 year storm from 270° - ebb tide.

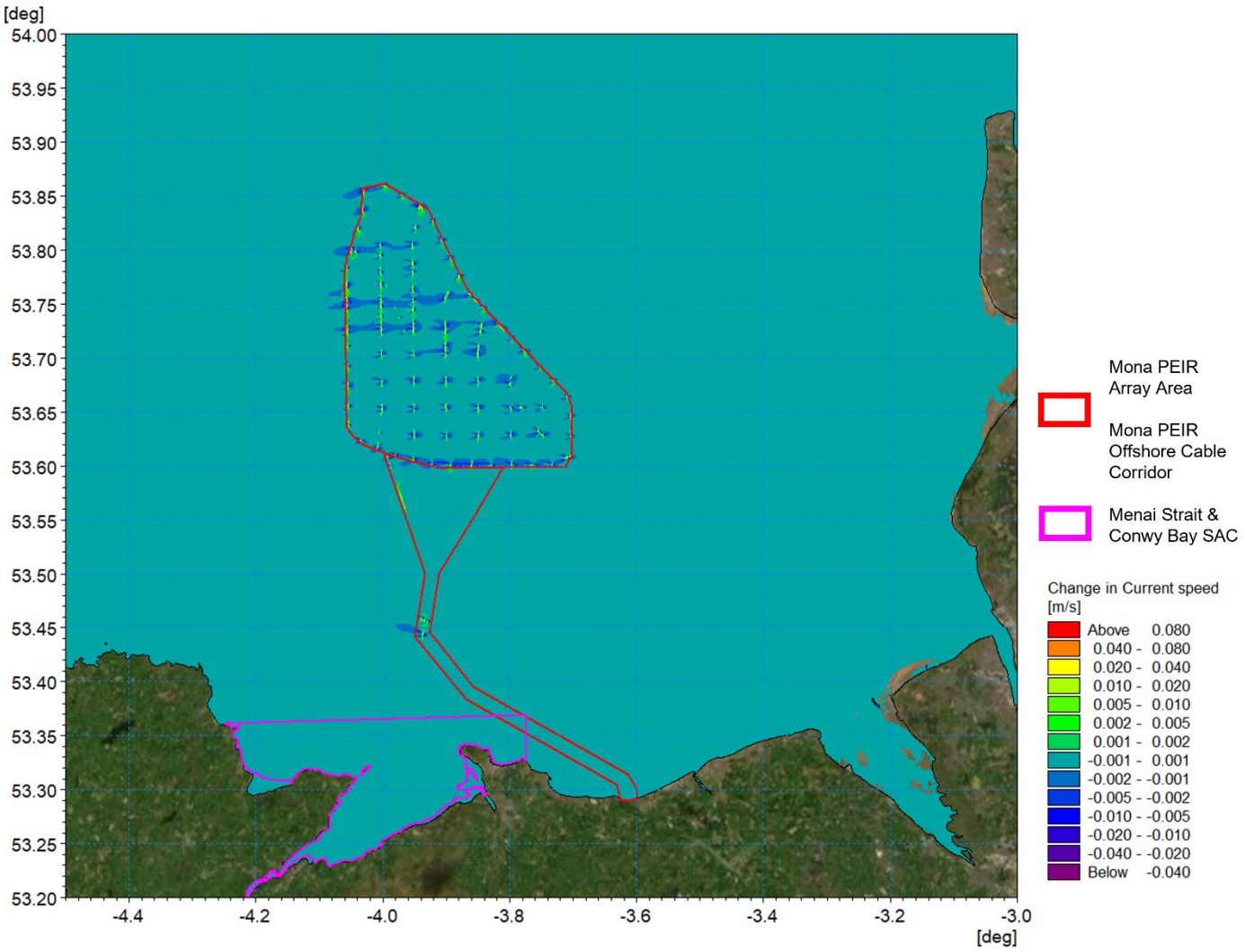

Figure 1.86: Change in littoral current 1 in 1 year storm from 270° - ebb tide (post-construction minus baseline).

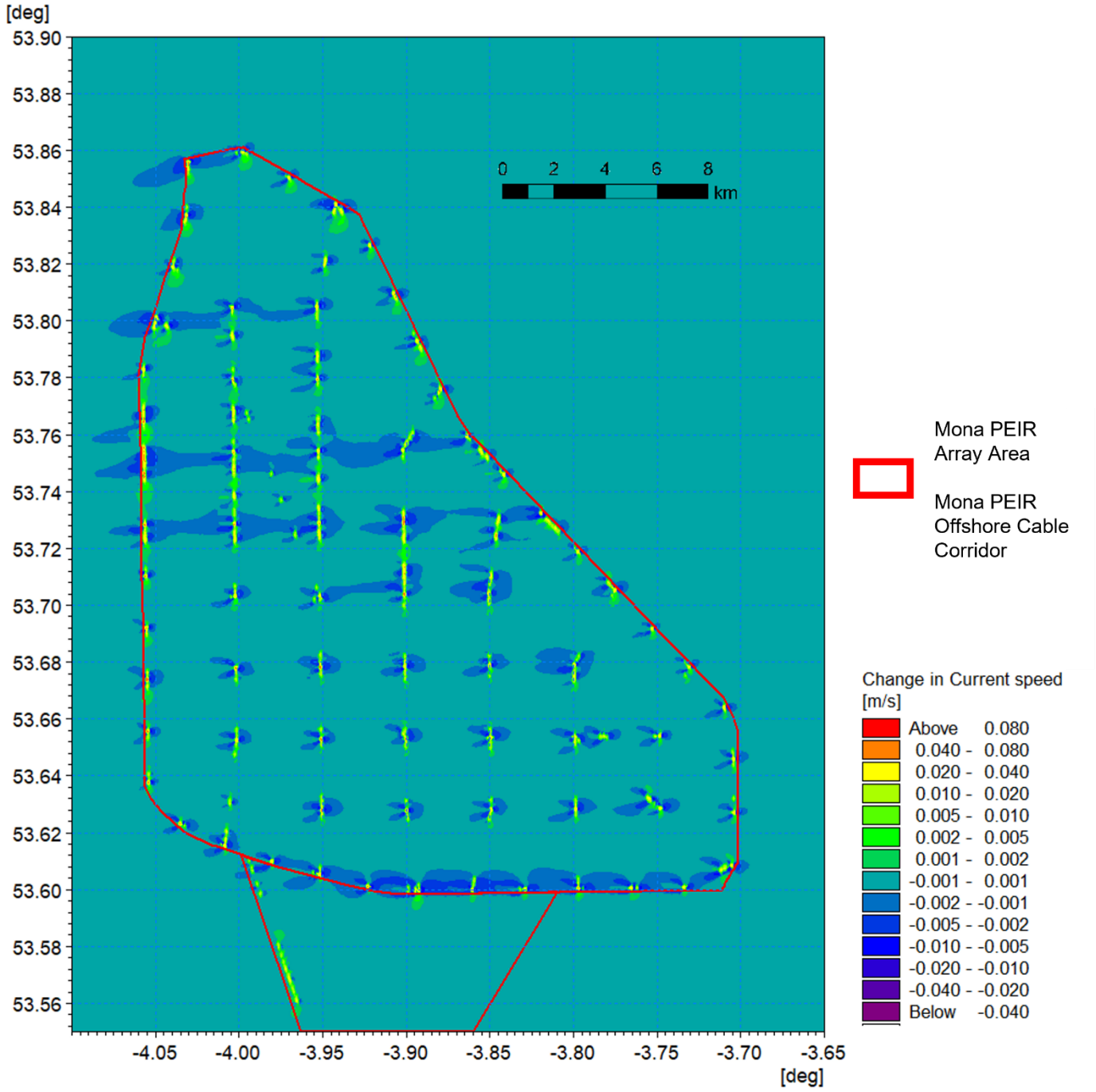

Figure 1.87: Change in littoral current 1 in 1 year storm from 270° - ebb tide (post-construction minus baseline) detailed view.

Post-construction sedimentology

Sediment transport

1.3.6.16 The numerical modelling methodology for sediment transport was described in section 1.6.6, which indicated how the baseline information was discretised to form the basis of the modelled scenarios. For the post-construction scenario, in addition to the Mona PEIR Offshore Wind Project structures being included in the tide and wave models, the bed material map was edited to represent the areas of scour protection where sediment supply is restricted. In each case an area of fixed bed was applied overlain

with a thin layer of sand to initialise the model and avoid instabilities. The scour protection was defined as 56 m diameter for each turbine structure leg and 49 m diameter for each OSP leg. Cable protection was modelled at locations where trenched cables would surface to connect with wind turbine infrastructure, and also in areas where the sufficient trenching depths may potentially not be achieved. This included two consecutive sections of cable protection set perpendicular to the predominant sediment transport direction located on the northern section of the export cable (Figure 1.65), where coarser moraine features comprised of glacial till (or rocky material as defined by EMODnet) was identified (noting that no cable protection will be installed over Constable Bank – see paragraph 1.3.7.11). The models were then re-run for a spring tide under calm conditions.

1.3.6.17 There are a number of approaches for quantifying potential sediment transport, given that transport rates vary both across the area and due to tidal state and climate conditions. For this analysis, the residual current was calculated over the course of two tidal cycles (one day) with the structures in place and compared with that for the baseline (Figure 1.58) for the calm condition as this is effectively the driver for sediment transport. The post-construction residual current and changes are shown in Figure 1.88 and Figure 1.89 respectively. As with previous results a more detailed plot is presented in Figure 1.90.

1.3.6.18 The corresponding sediment transport was simulated over the course of one day where the equivalent baseline daily sediment transport rate was shown in Figure 1.59. The post-construction daily sediment transport rate and differences are shown in Figure 1.91 and Figure 1.92 respectively. It should be noted that both the sediment transport and difference plots use a log palette as there is a large range in sediment transport potential across the domain.

1.3.6.19 This analysis shows that although there are changes as a result of the installation of the Mona PEIR Offshore Wind Project structures and associated scour and cable protection, the extent and magnitude is limited. As anticipated, in areas of reduced residual current in the lee of structures the sediment transport rate is also reduced and vice versa. Within the context of this comparative study there is a maximum change in residual current and sediment transport of circa ±10% which is largely sited within close proximity to the turbine foundation structures (less than 250 m elongated in the direction of principle tidal currents). It is noted that areas of reduced residual current and sediment transport are often accompanied by a similar increase in close proximity. This indicates that the residual current and resulting sediment transport paths are adjusted to accommodate the structures rather than transport pathways being cut off.

1.3.6.20 This process was repeated for the 1 in 1 year storm. The baseline residual current (Figure 1.62) was compared with the equivalent post-construction residual current pattern as shown in Figure 1.93; with the difference in Figure 1.94 and in more detail in Figure 1.95. The pattern of changes is similar to the previous scenario but with a wider area of influence. It should however be noted that although the absolute values of these changes are increased from the purely tidal condition the underlying baseline residual currents are of greater magnitude under storm conditions and are proportionately smaller than those exhibited under calm conditions.

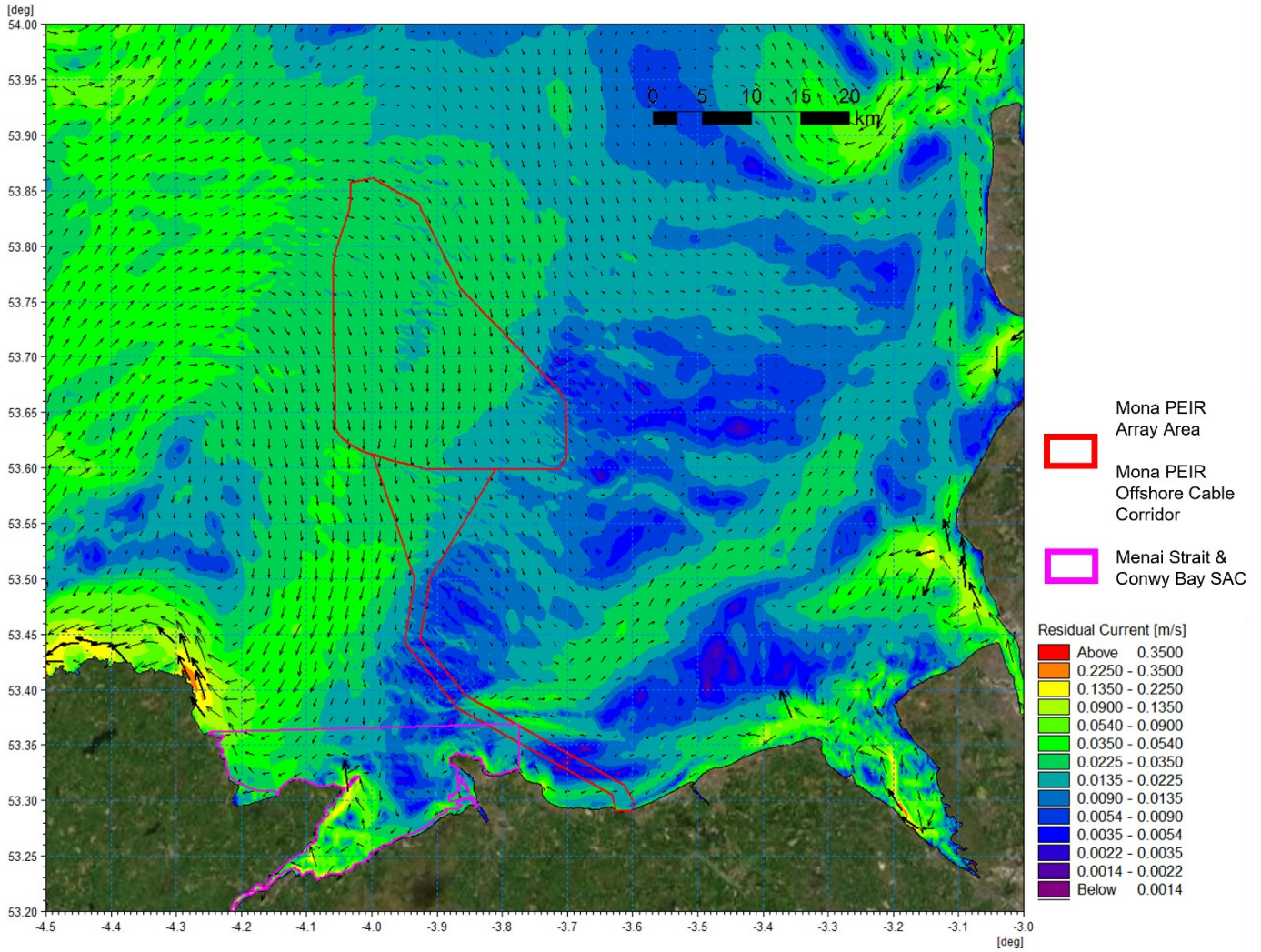

Figure 1.88: Post-construction residual current spring tide.

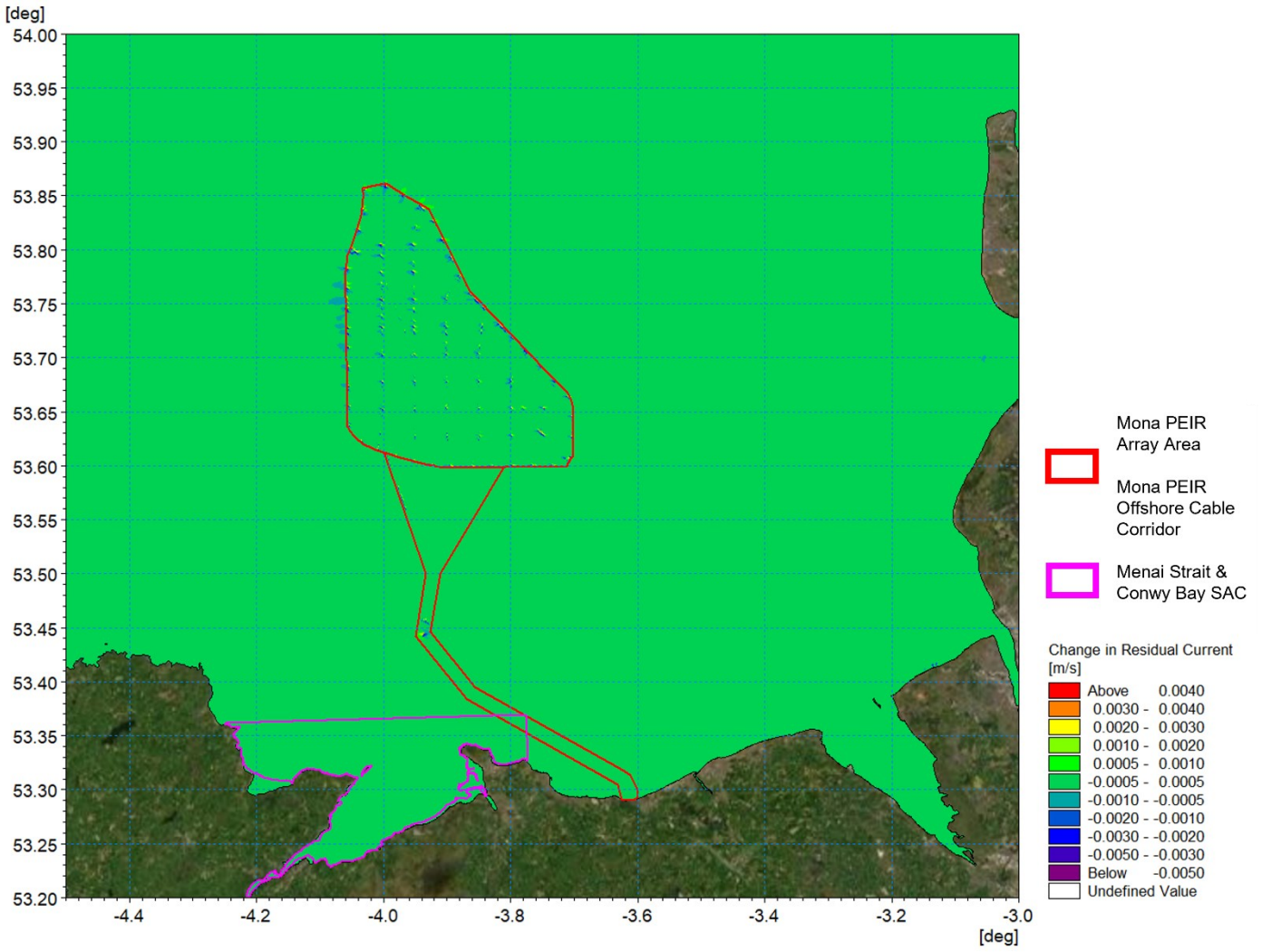

Figure 1.89: Change in residual current spring tide (post-construction minus baseline).

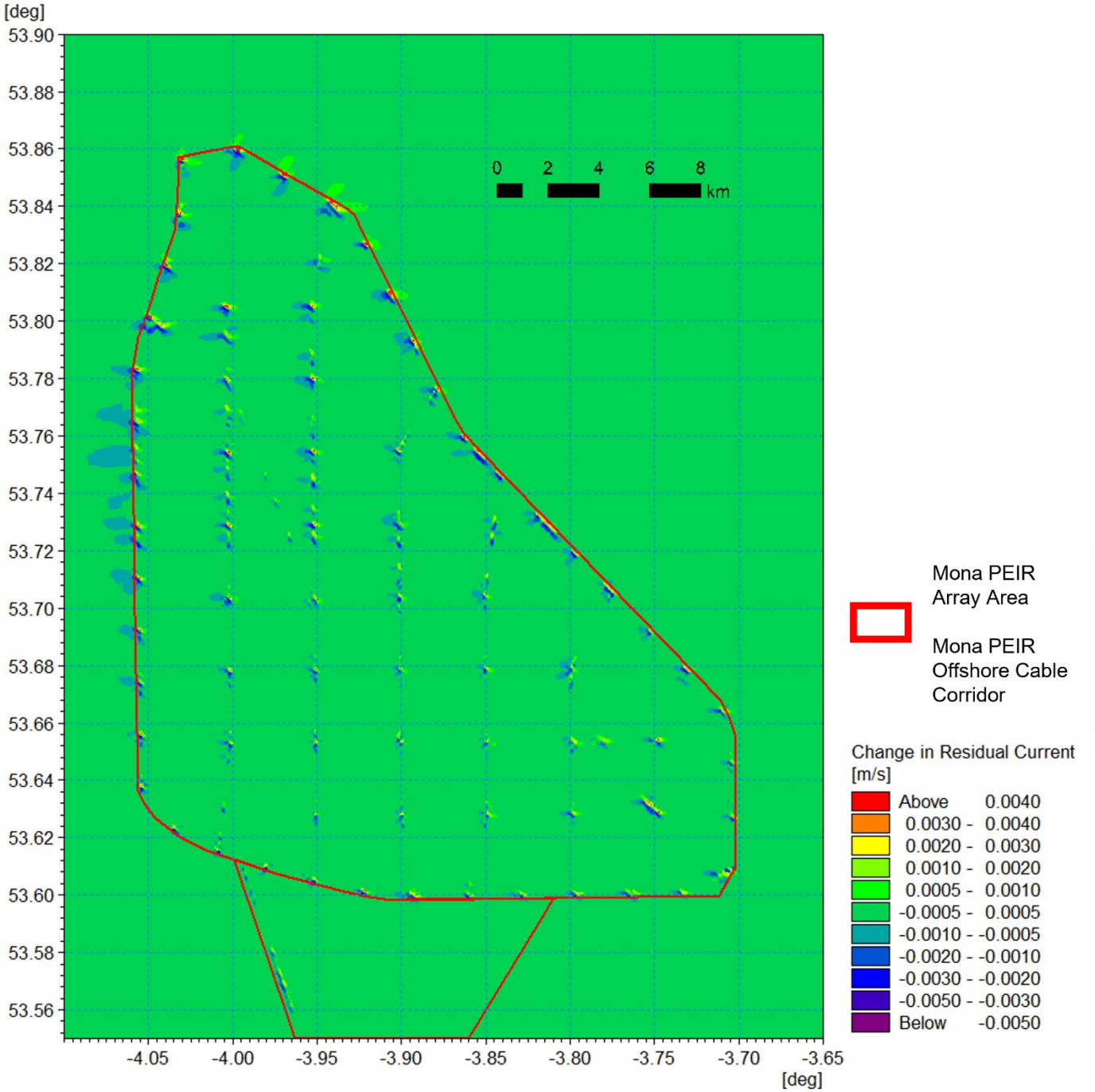

Figure 1.90: Change in residual current spring tide (post-construction minus baseline) Mona Offshore Wind Project PEIR detailed view.

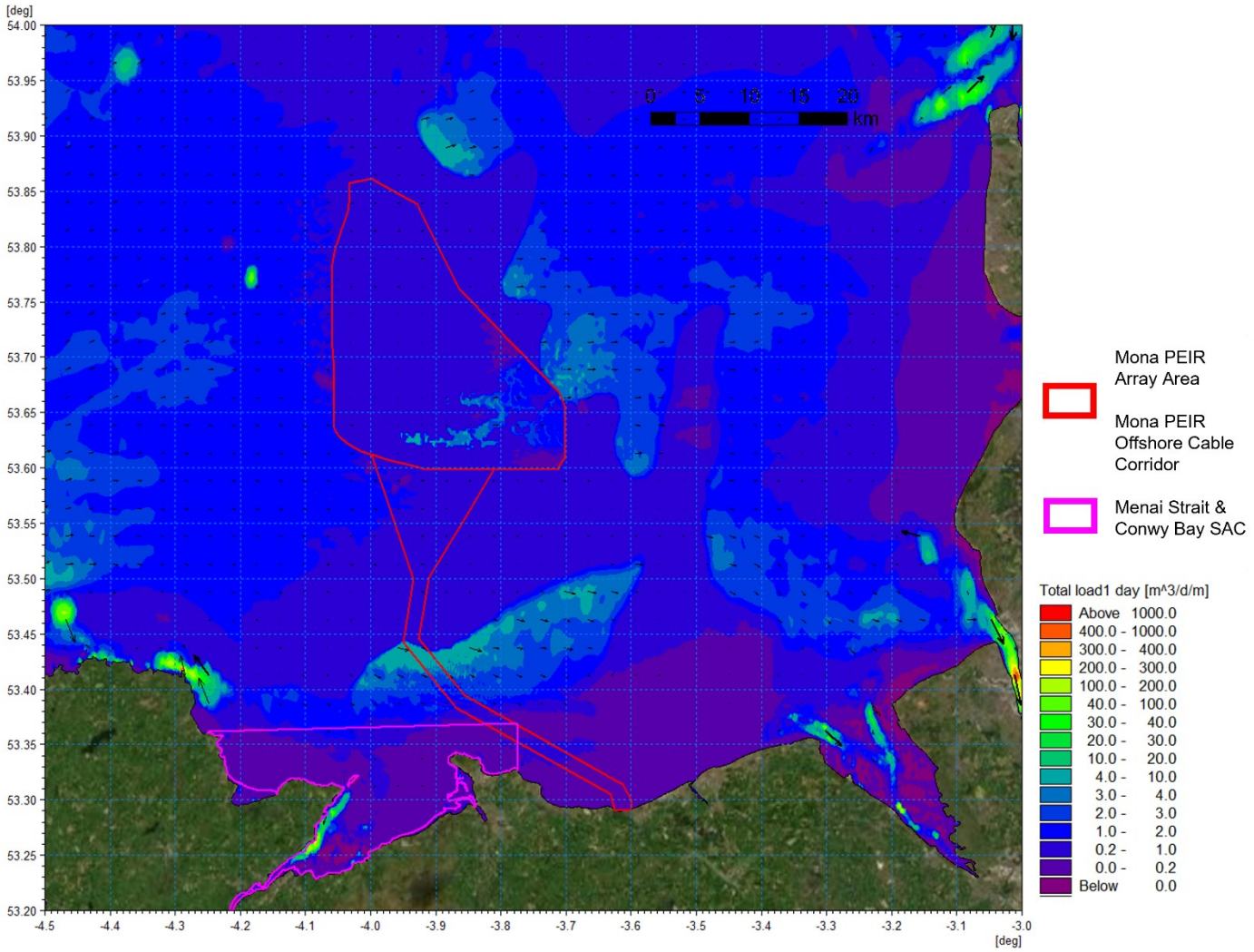

Figure 1.91: Post-construction potential sediment over the course of 1 day (two tide cycles).

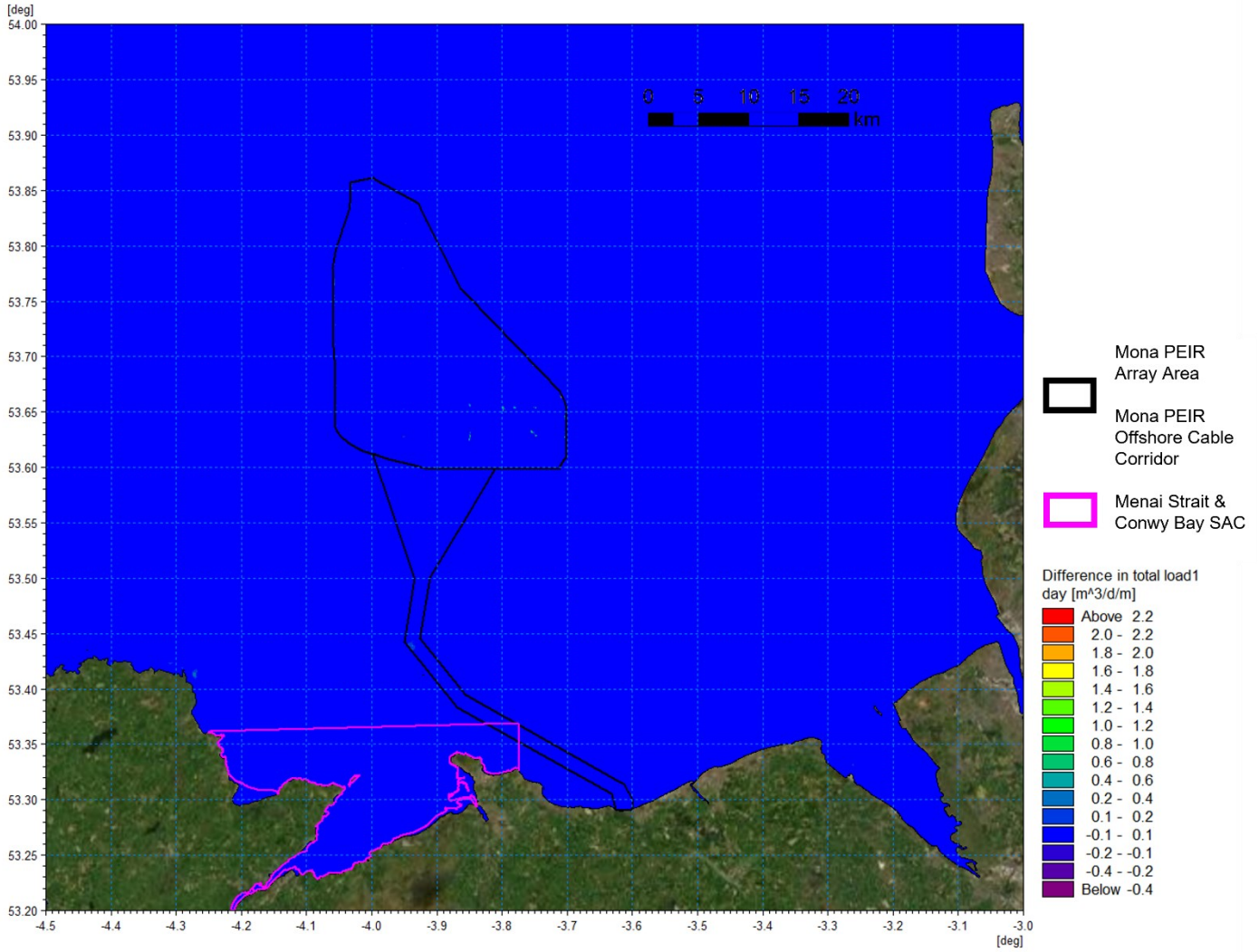

Figure 1.92: Difference in potential sediment transport over the course of 1 day (post-construction minus baseline).

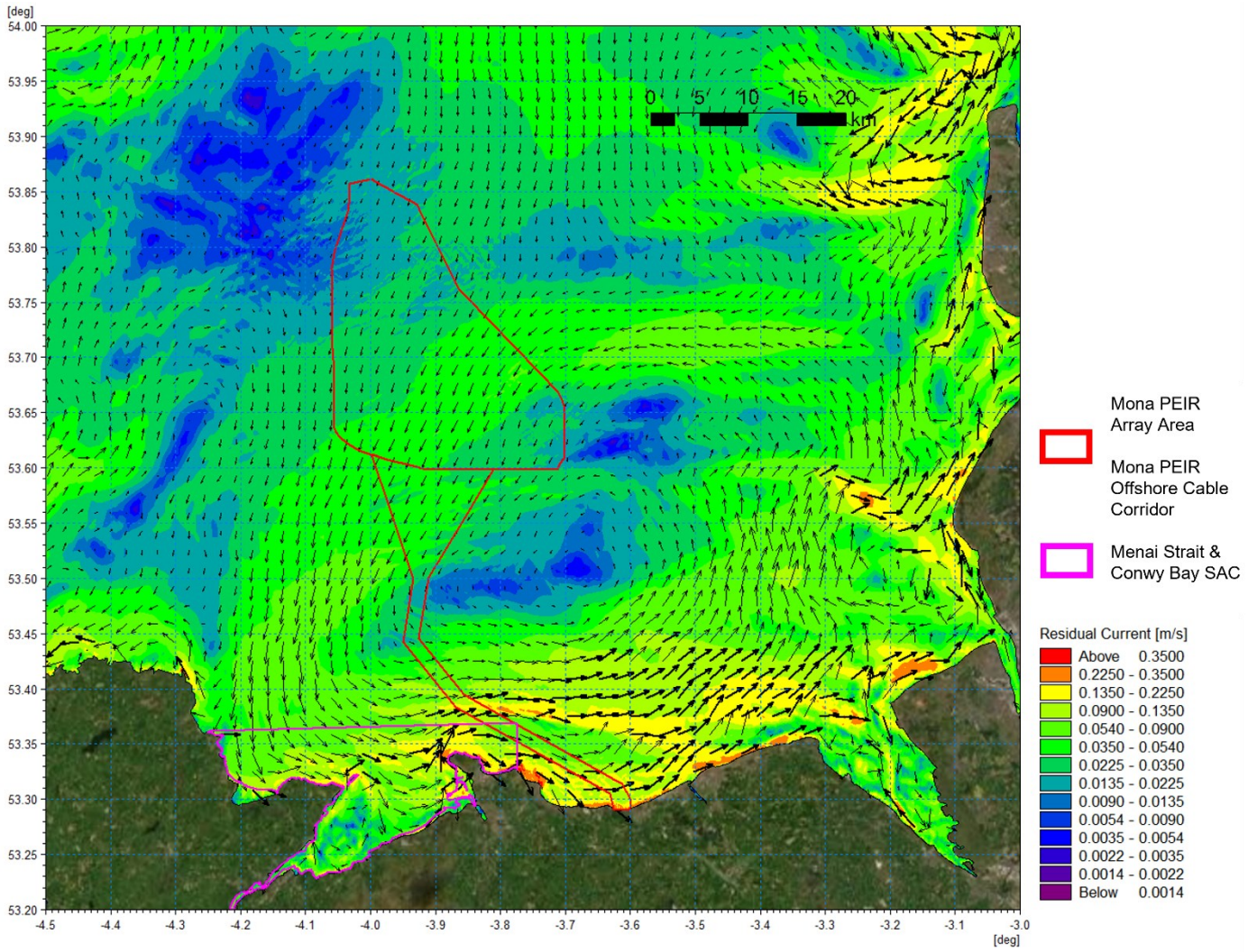

Figure 1.93: Post-construction residual current 1 in 1 year storm from 270° spring tide.

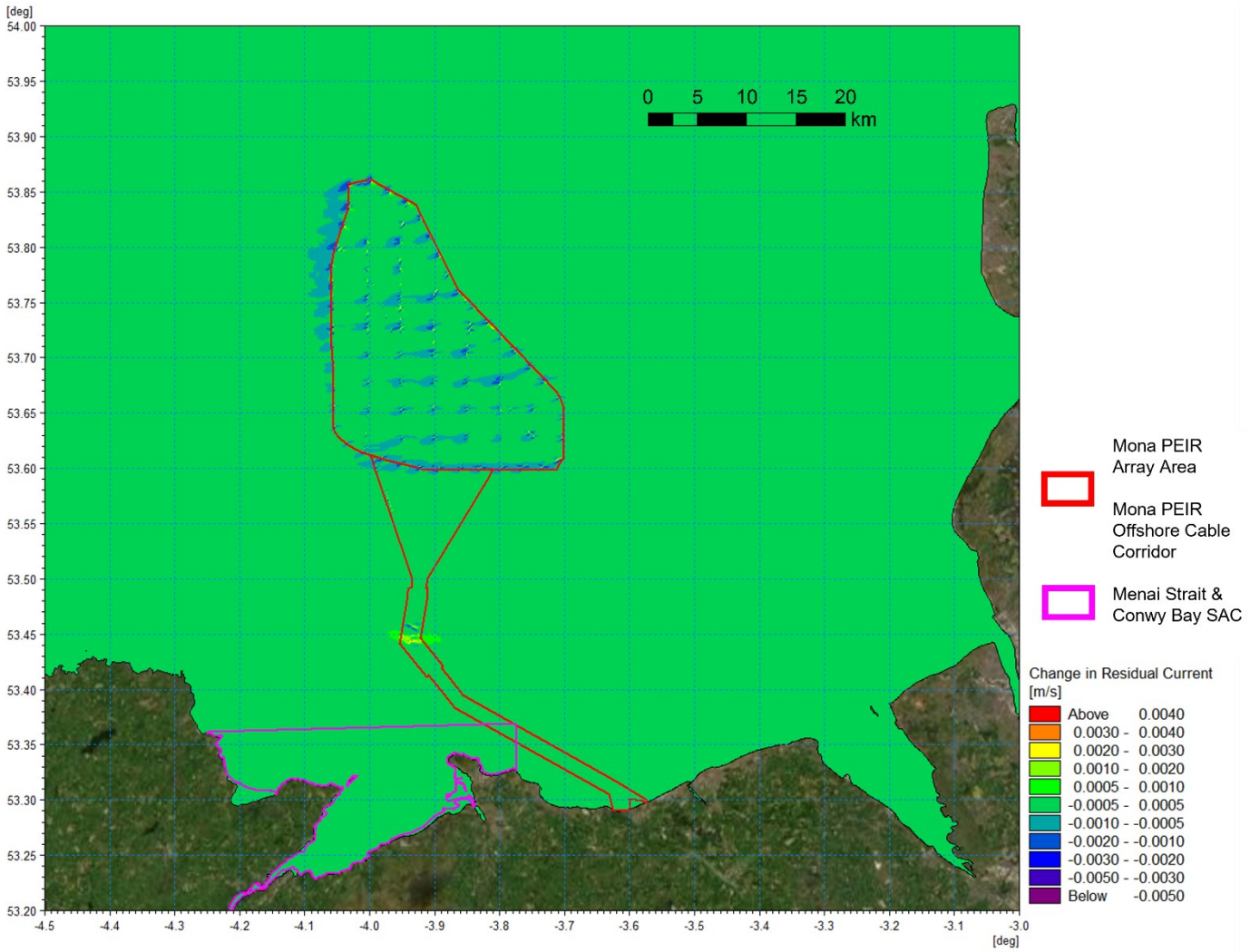

Figure 1.94: Change in residual current 1 in 1 year storm from 270° spring tide (post-construction minus baseline).

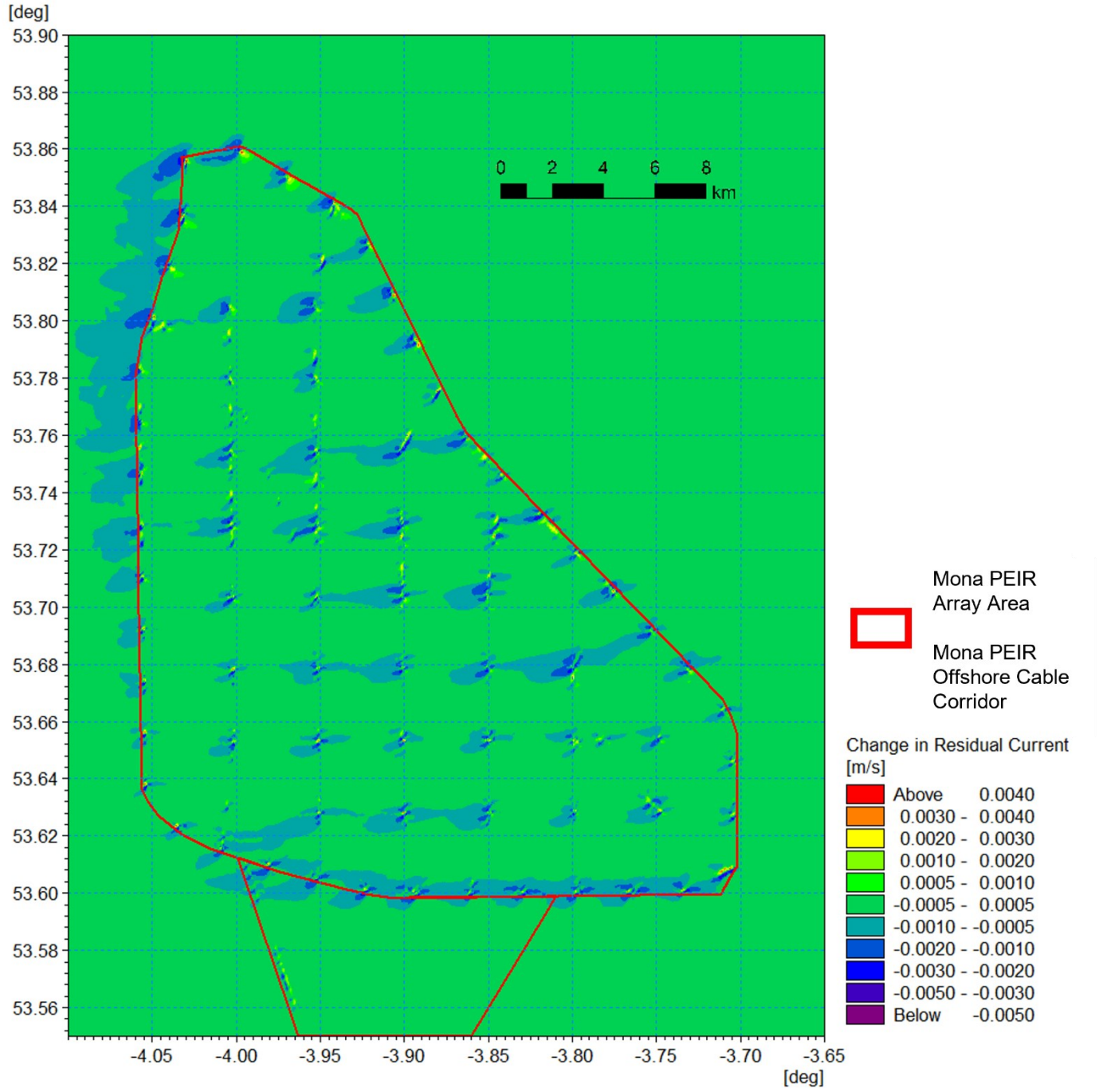

Figure 1.95: Change in residual current 1 in 1 year storm from 270° spring tide (post-construction minus baseline) Mona Offshore Wind Project PEIR detailed view.

1.3.7 Potential changes during construction (as presented in the PEIR)

1.3.7.1 In addition to the changes in physical process resulting from the presence of the Mona Offshore Wind Project as defined in the PEIR, the construction phase influences were quantified. The principal construction elements relate to the transport and fate of sediment brought into suspension due to seabed preparation, the installation of the foundation structures and the laying of inter-array/interconnector cables between the wind turbines/OSPs and the Mona PEIR Offshore Cable Corridor to shore. An overview of the modelling techniques implemented is provide in Table 1.1.

1.3.7.2 As with the post-construction aspects, the approach was to examine the construction technique which represents the MDS in terms of coastal processes. In practice, these changes are therefore likely to be of lesser magnitude. In each scenario the modelling examined excess SSC arising from the proposed activities (i.e. ambient SSC were not included). Baseline studies outlined in section 1.6.7 indicate that turbidity levels vary greatly across the domain and throughout the year, being relatively low in deep water areas compared with active sediment transport mechanisms within the estuaries. Therefore, the excess SCC data presented would be applicable independent of the season in which the operations are undertaken.

1.3.7.3 The baseline residual currents and sediment transport modelling has corroborated the knowledge that the east Irish Sea is a sediment sink with active sediment transport processes. Sedimented material arising from the construction phase activities would therefore be amalgamated into the sediment transport regime. The numerical modelling provides depth averaged suspended sediment concentration values and do not therefore differentiate between bed load and water column suspended sediment.

1.3.7.4 During each phase of the assessment the transport of suspended sediment was modelled by undertaking simulations which released sediment at a rate and location appropriate to each type of construction. It is recognised that the dispersion and subsequent deposition may be affected by a range of factors including tidal phase and meteorological conditions. Significant wind and/or wave driven currents have the potential to increase the size of a sediment plume produced by seabed preparation or installation operations. However, these conditions would also inherently decrease SSC and deposition levels as a direct consequence of increased dispersion. It is noted that during adverse weather background turbidity levels would be increased and it is also unlikely that marine based works would be undertaken for operational safety reasons. The modelling of sediment release was therefore undertaken under tide only conditions using a variety of tidal ranges to provide an indication of potential SSC and deposition levels. The sediment released was defined according to the characteristics derived from the BGS data at each specific location. Where a number of locations were encountered, such as a dredging path, then a representative grading was used. The sediment sample locations are presented in Figure 1.56.

Seabed preparation

1.3.7.5 Due to the nature of the seabed in the Mona PEIR Array Area and Mona PEIR Offshore Cable Corridor, the cable installation will require seabed preparation in the form of seabed features clearance. The project description for PEIR indicated that sand waves may be cleared for the offshore, inter-array and interconnector cabling along up to a 104 m wide corridor. Clearance activities may extend along circa 70% of the Mona PEIR Offshore Cable Corridor with an average clearance depth of up to 5.1 m and 50% of the inter-array cable route with an average clearance depth up to 5.1 m. It was noted that these are the upper bounds of parameters and not likely to represent ‘typical’ clearance operations with any necessary clearance within designated areas being reduced to a minimum.

1.3.7.6 The modelling undertaken to quantify the potential increases in suspended sediment concentration and sedimentation simulated the use of a suction hopper dredger to undertake sandwave clearance. Material from sandwave crests would be side-cast and therefore be available for sandwave reformation and to provide additional coverage for cables in trough areas following redistribution of the mobilised material. In practice plough dredging may be undertaken however this type of operation would have less impact in terms of both suspended sediment concentrations and

sedimentation footprint as material is moved across the seabed rather than bringing it fully into suspension.

1.3.7.7 Two representative clearance operations were assessed, one relating to the offshore export cabling (located immediately adjacent to Constable Bank) and a second for the inter-array cables, which has the same characteristics as clearance for the inter-connector cables. The geophysical survey data was used to identify areas of sandwaves where the operations are most likely to be required. Figure 1.96 indicates the clearance routes modelled for the inter-array and offshore export cable for the PEIR. In each case the clearance was undertaken in a southwest direction with a dredging rate of 10,000 m^3/h with a spill of 3%.

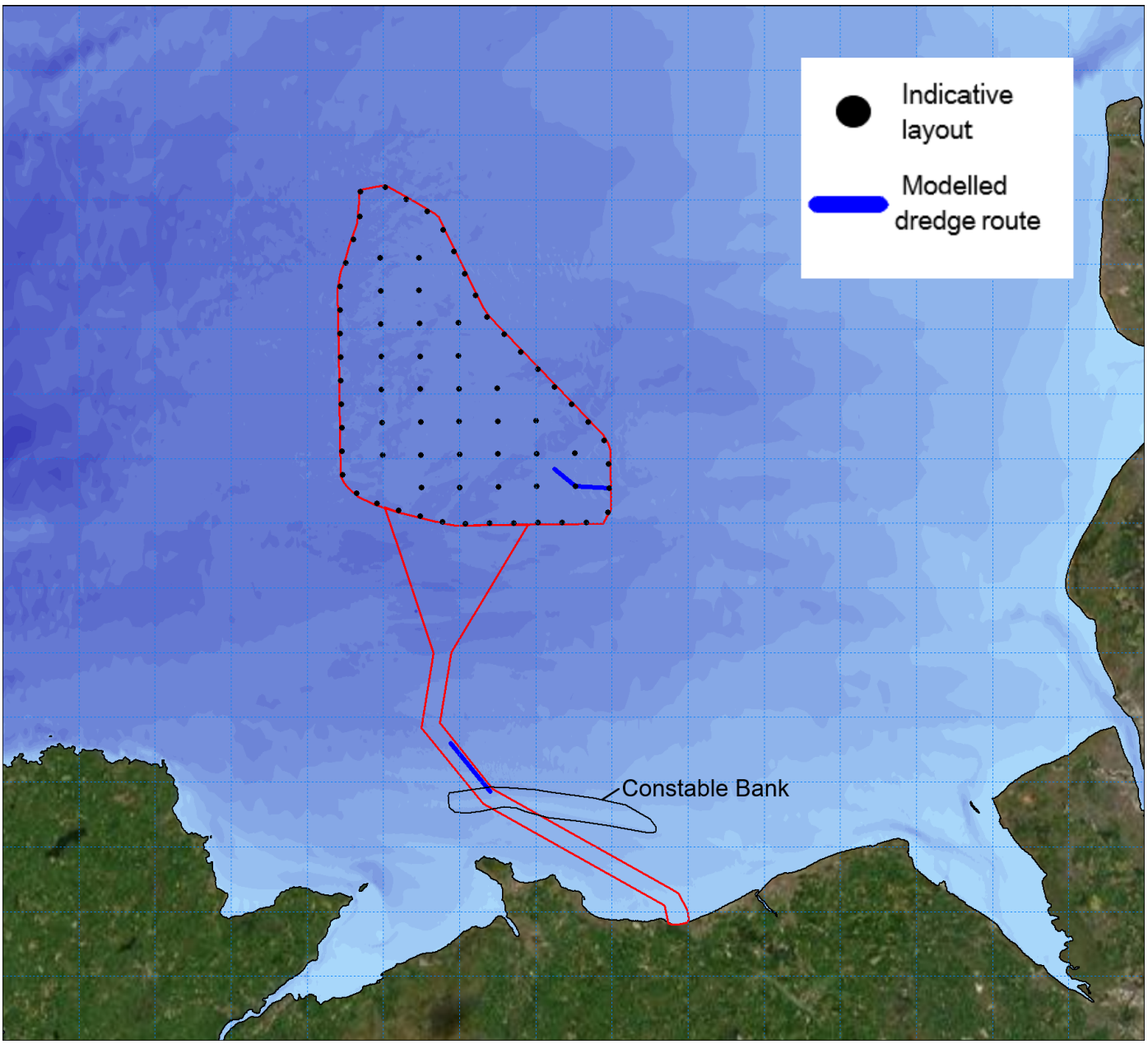

Figure 1.96: Sand wave clearance paths modelled for PEIR.

Offshore export cable sandwave clearance

1.3.7.8 The offshore export cable route was cleared at 100 m/h along the 104 m wide route for a period of four hours, in line with dredging rate and plant required to carry out the operation. The material was then deposited over a 45 minute period from the hopper with the modelled route of 5 km taking two days to prepare. The selected location was immediately to the north of Constable Bank as a series of sandwaves are present at this location and dredging operations within the Bank will be minimised. The redistributed material was classified using the properties identified from the sampling undertaken along the route simulated.

- Very coarse sand/gravel: 8%
- Coarse sand: 23%
- Medium sand: 48%
- Fine sand: 10%
- Very fine sand/mud: 11%.

1.3.7.9 The suspended sediment concentrations vary greatly during the course of the operation. During the dredging phase, when 3% of the material is spilled at the seabed, the sediment plumes exhibit much lower concentrations. These are typically <50 mg/l along the clearance route as shown in Figure 1.98. During the dumping phase the plume is slightly larger (Figure 1.99) with concentrations reaching 1000 mg/l at the release site. However, the most extensive increases are seen as the deposited material is redistributed on the successive tides, where sedimentation occurs on the slack tide reducing the SSC completely and resuspension and transport occurs when the tidal currents increase. Under these circumstance concentrations of 300 mg/l to 500 mg/l are seen as illustrated in Figure 1.100 which shows SSC arising at peak current speed. The average suspended sediment concentration during the course of the operation is presented in Figure 1.101 with values <300 mg/l with a plume envelope width of circa 20 km which corresponds with the tidal excursion.

1.3.7.10 The average sedimentation depth is shown in Figure 1.102, with a detailed view shown in Figure 1.103 and illustrates how the deposited material is focussed within 100 m of the site of release with a maximum depth 0.5 m to 1 m whilst the finer sediment fractions are distributed in the vicinity at much smaller depths circa 5 mm to 10 mm. The dispersion of the released material would continue on successive tides. The sedimentation one day following the cessation of the clearance operation is presented in Figure 1.104, with a detailed plot shown in Figure 1.105 and is consistent with this mechanism with the production of sandwaves visible.

Constable Bank

1.3.7.11 Overlapping with the Mona PEIR Offshore Cable Corridor is the sandbank known as Constable Bank. This sandbank meets the requirements for an Annex 1 habitat under Annex 1 of the EC Habitats outside of a designated site.

1.3.7.12 Figure 1.97 shows the location of the Mona Offshore Cable Corridor with respect to the Constable Bank. For information the extent of Constable Bank has been overlaid as a black outline on the modelling output.

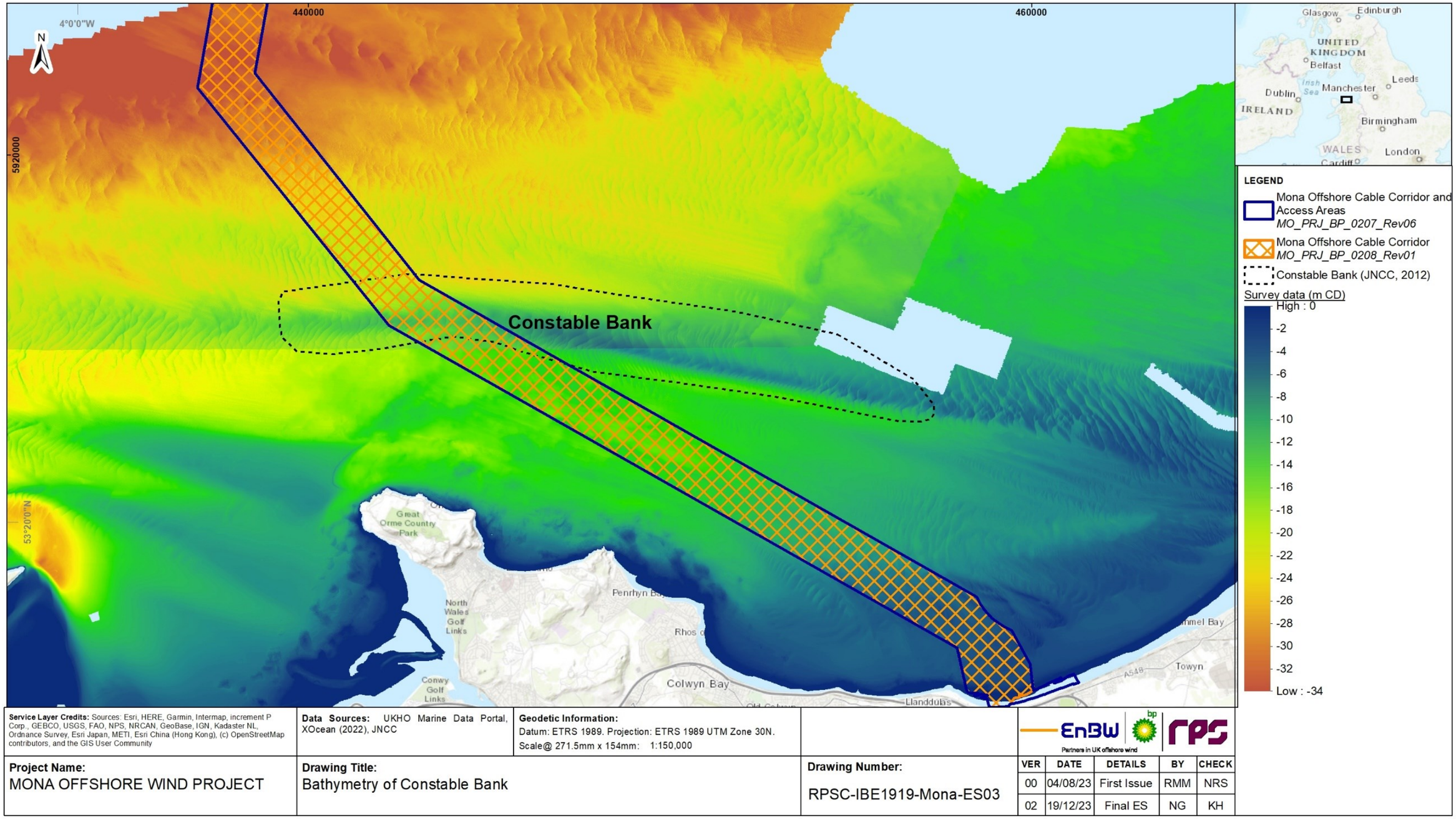

Service Layer Credits: Sources: Esri, HERE, Garmin, Intermap, increment P Corp., GEBCO, USGS, FAO, NPS, NRCAN, GeoBase, IGN, Kadaster NL, Ordnance Survey, Esri Japan, METI, Esri China (Hong Kong), (c) OpenStreetMap contributors, and the GIS User Community	**Data Sources:** UKHO Marine Data Portal, XOcean (2022), JNCC	**Geodetic Information:** Datum: ETRS 1989. Projection: ETRS 1989 UTM Zone 30N. Scale@ 271.5mm x 154mm: 1:150,000		
Project Name: MONA OFFSHORE WIND PROJECT	**Drawing Title:** Bathymetry of Constable Bank		**Drawing Number:** RPSC-IBE1919-Mona-ES03	

VER	DATE	DETAILS	BY	CHECK
00	04/08/23	First Issue	RMM	NRS
02	19/12/23	Final ES	NG	KH

Figure 1.97: Location of Constable Bank in relation to the Mona Offshore Cable Corridor.

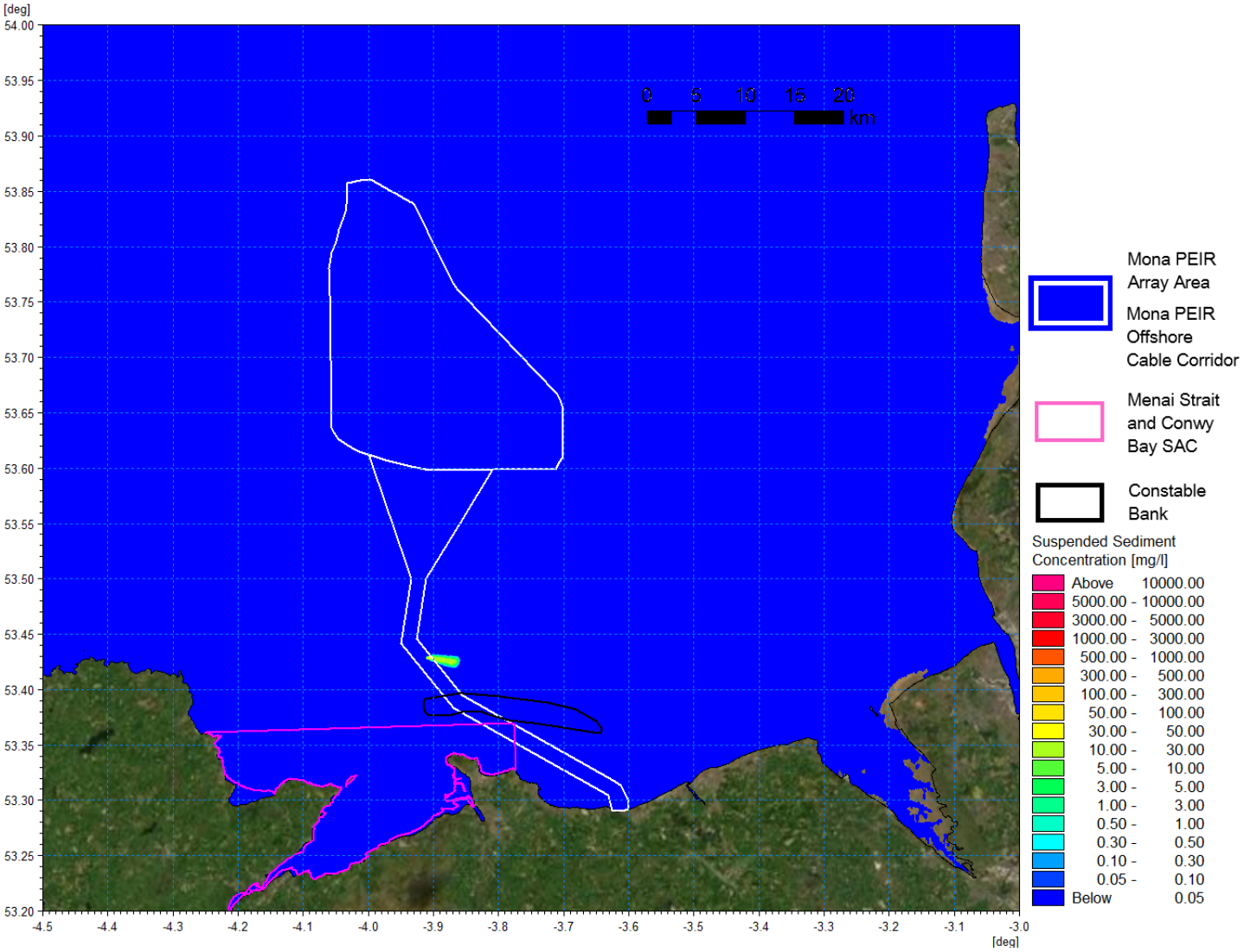

Figure 1.98: Suspended sediment concentration during dredging phase – offshore export cable path. [1]

[1] Modelled output does not illustrate intertidal access areas.

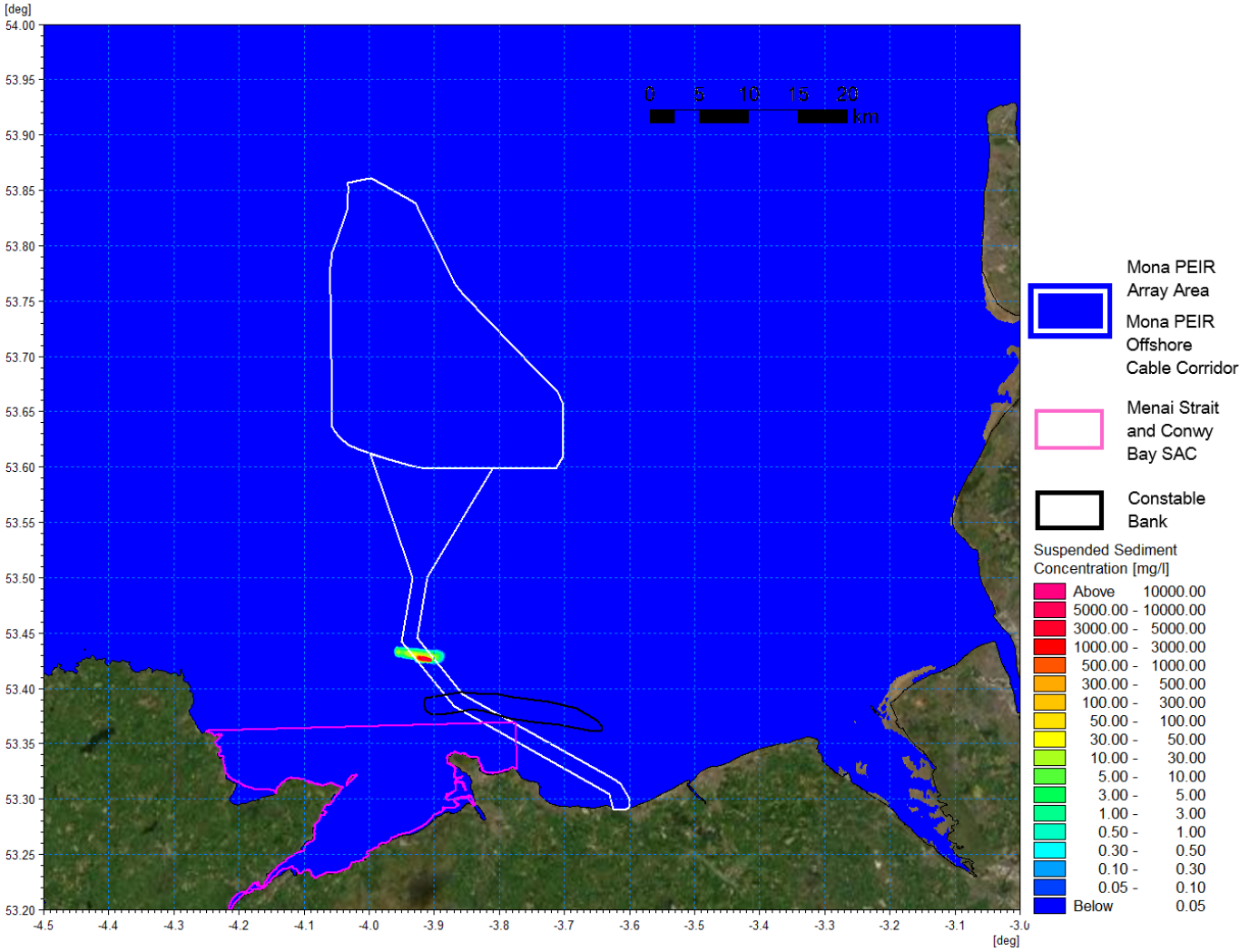

Figure 1.99: Suspended sediment concentration during dumping phase – offshore export cable path.

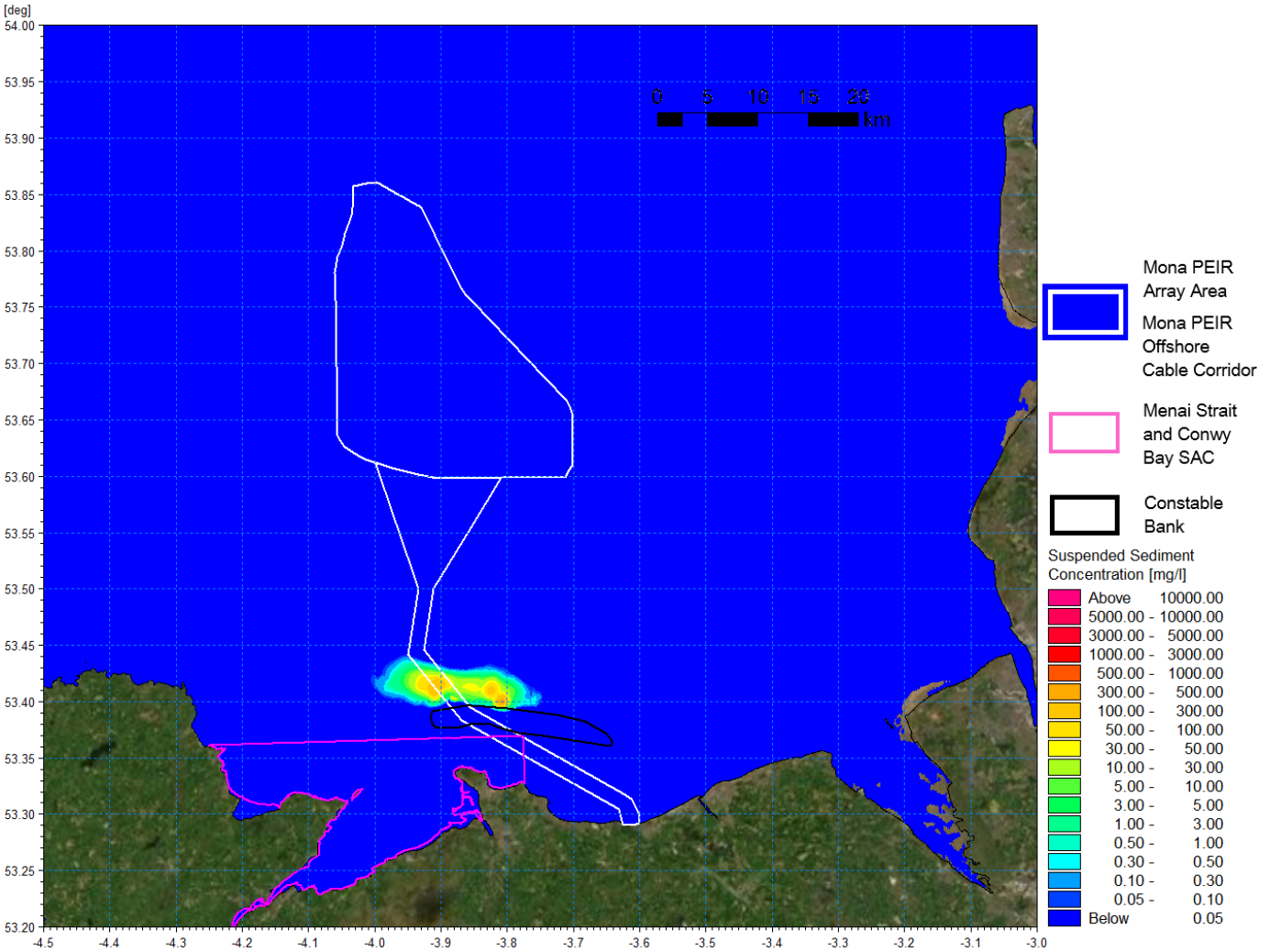

Figure 1.100: Suspended sediment concentration with sediment re-mobilisation – offshore export cable path.

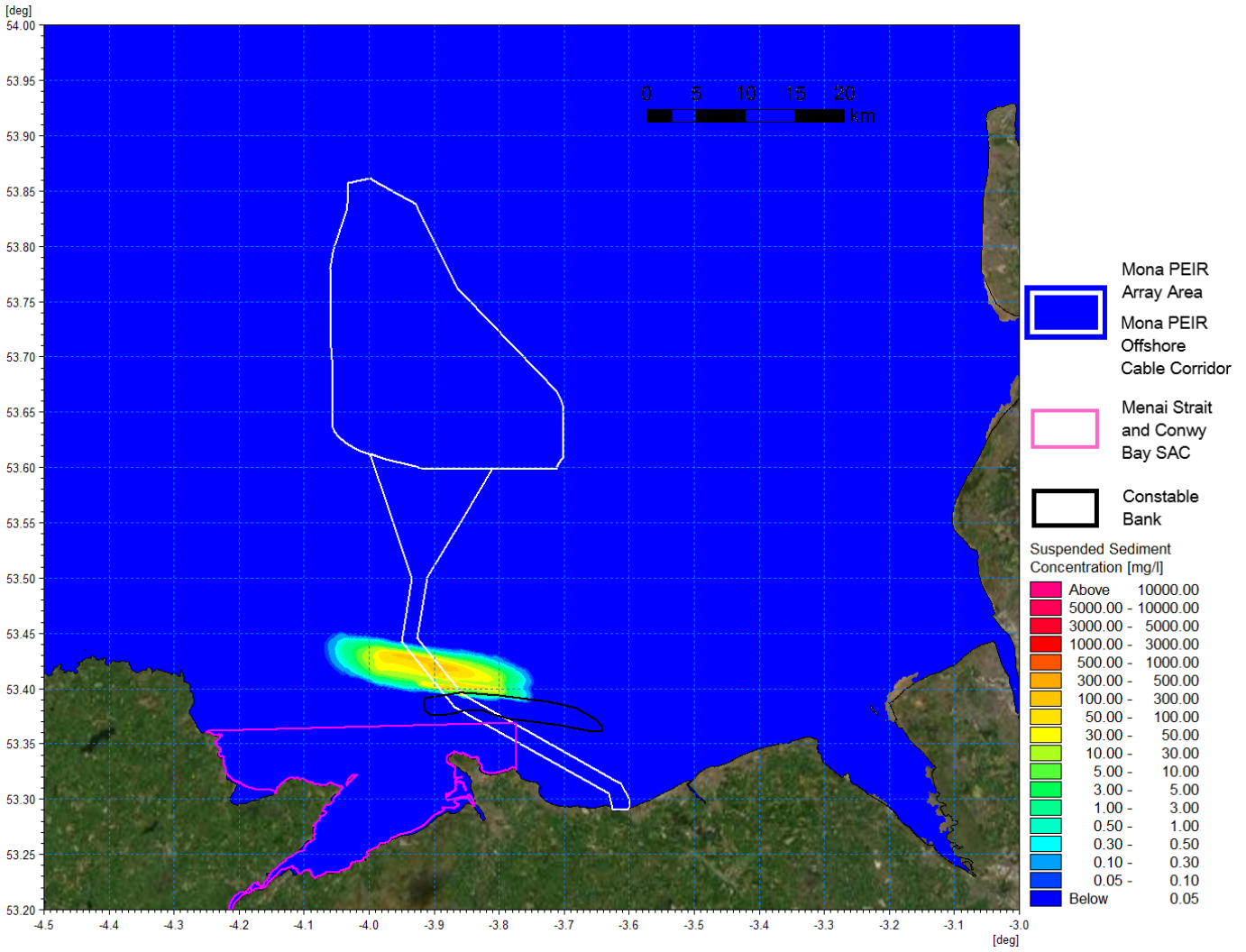

Figure 1.101: Average suspended sediment concentration during operation – offshore export cable path.

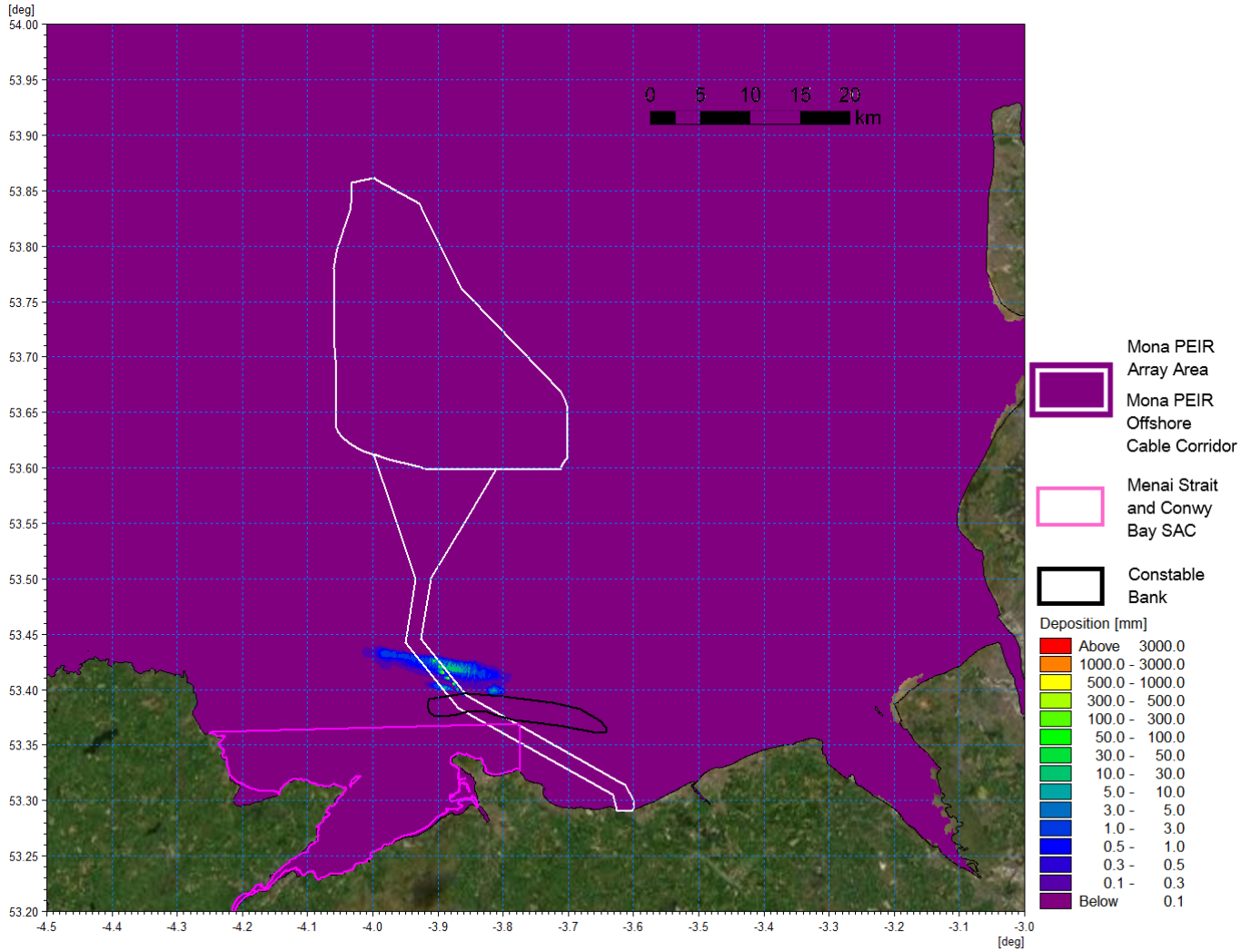

Figure 1.102: Average sedimentation during operation – offshore export cable path.

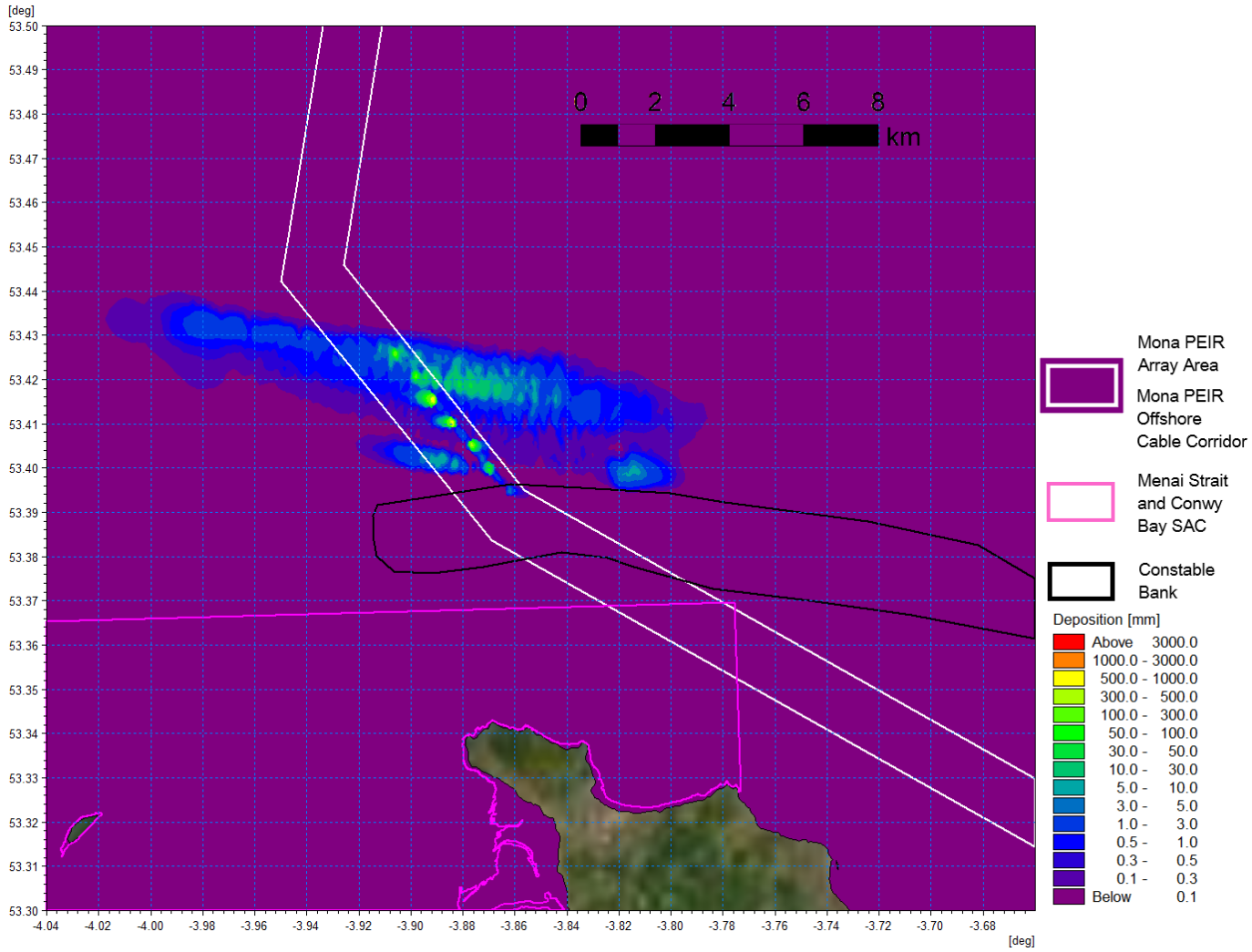

Figure 1.103: Average sedimentation during operation – offshore export cable path detailed view.

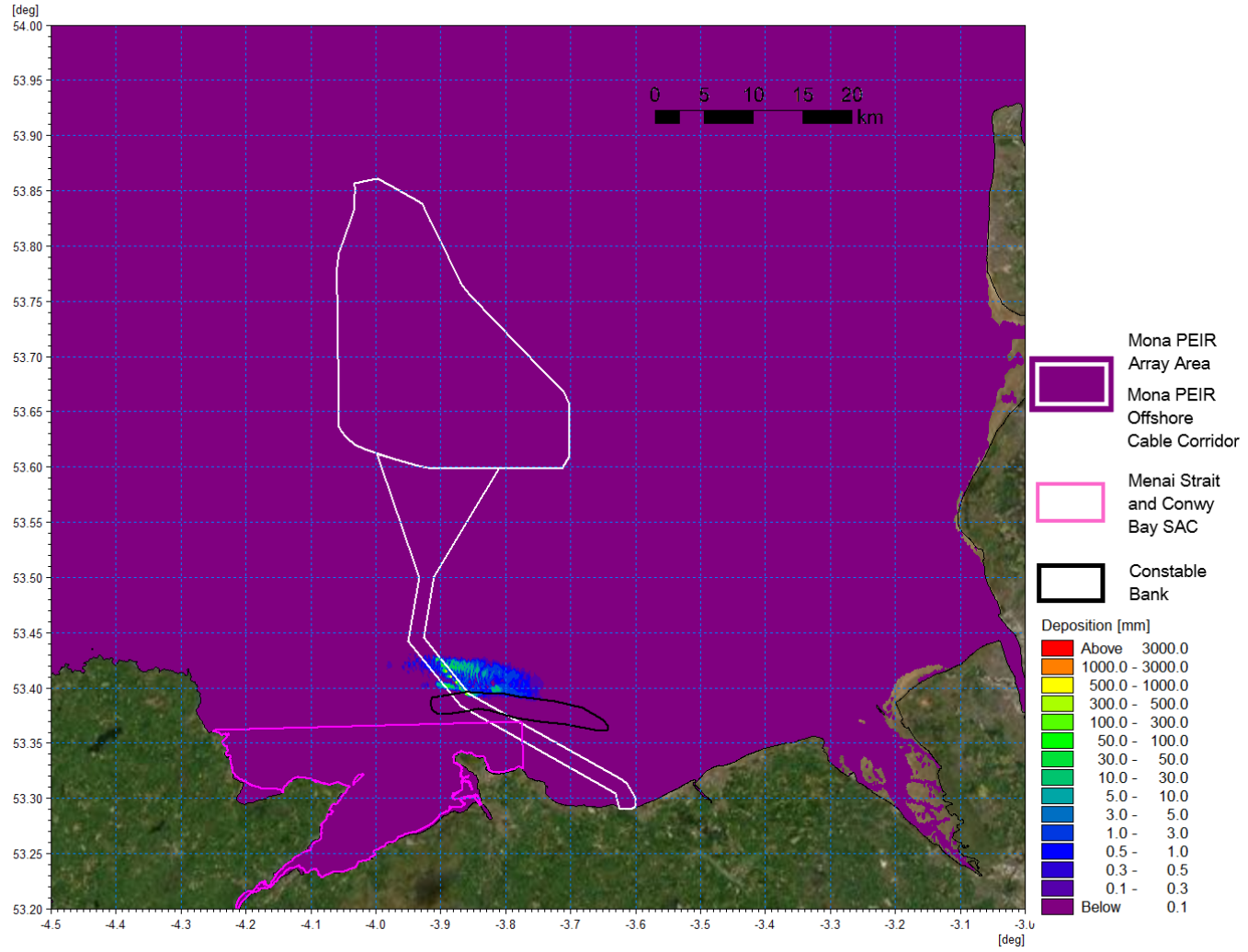

Figure 1.104: Sedimentation 1 day following cessation of operation – offshore export cable path.

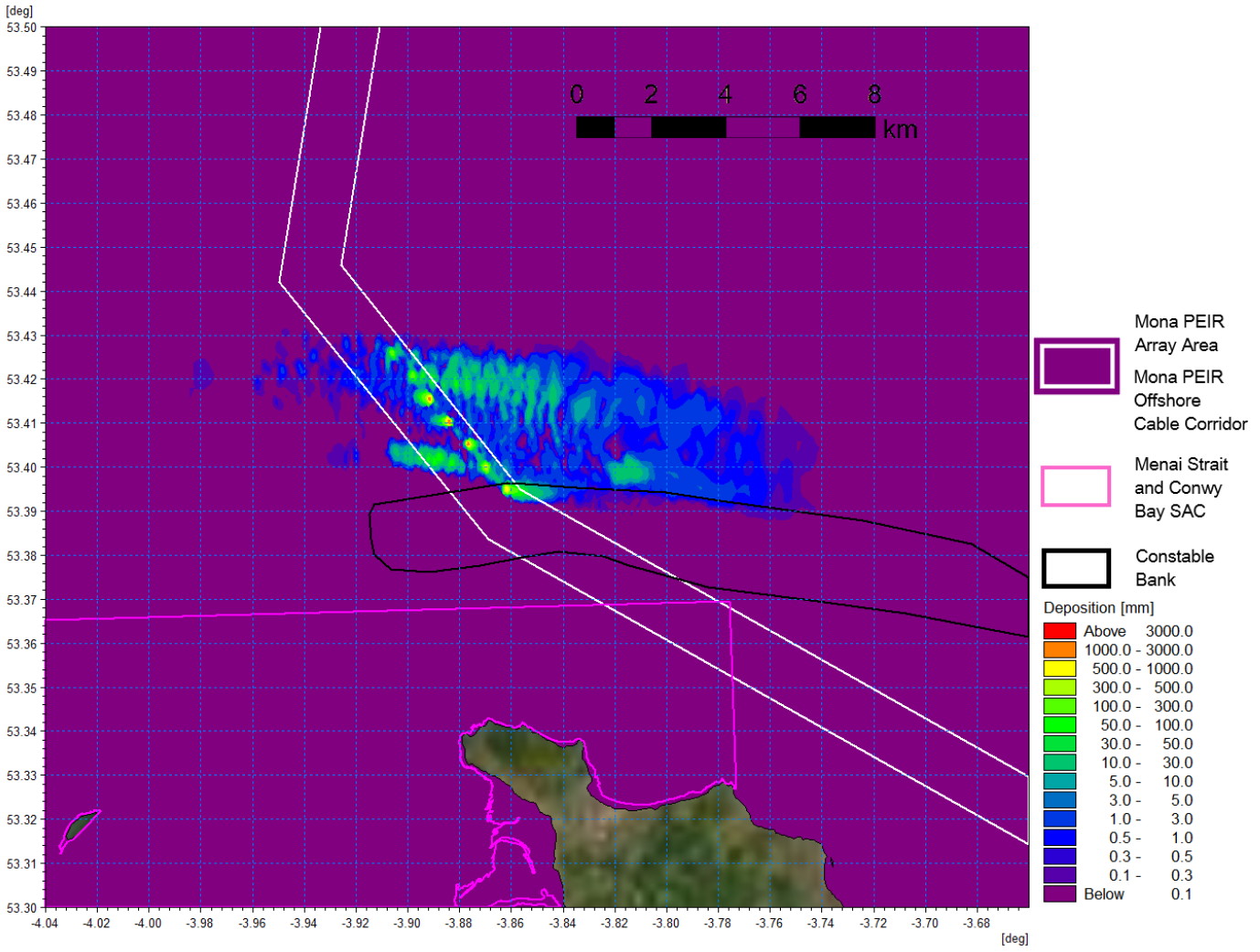

Figure 1.105: Sedimentation 1 day following cessation of operation – offshore export cable path detailed view.

Inter-array cable sandwave clearance

1.3.7.13 The inter-array cable route was cleared at 100 m/h along the 104 m wide route for a period of four hours, in line with the dredging rate and removal depth. The material was then deposited over a 45 minute period from the hopper with the 5 km modelled route taking two days to prepare. As previously, the redistributed material was classified using the properties identified from the sampling undertaken along the route simulated.

- Very coarse sand/gravel: 8%
- Coarse sand: 23%
- Medium sand: 48%
- Fine sand: 10%
- Very fine sand/mud: 11%.

1.3.7.14 The resulting suspended sediment concentrations showed similar characteristics to the offshore cable clearance. The dredging phase plumes were smaller than the dumping as 3% spill of the material is released along the route and again

concentrations are <50 mg/l as shown in Figure 1.106. Similarly, the release phase plume is slightly larger than the dredging plume with concentrations reaching 3000 mg/l at the dump site, Figure 1.107. At this site the greatest area of increased suspended sediment concentration, extending a tidal excursion circa 20 km from the site, is also associated with re-mobilisation of the deposited material on subsequent tides with concentrations of 500 mg/l to 1000 mg/l whilst average levels <500 mg/l as illustrated in Figure 1.108 and Figure 1.109 respectively.

1.3.7.15 The average sedimentation depth, shown in Figure 1.110 and in detail in Figure 1.111, is similar in form to that of the Mona PEIR Offshore Cable Corridor works. The sedimentation one day following the cessation of the clearance operation is presented in Figure 1.112 and Figure 1.113 and shows deposited material at the site of release with depth 1 m whilst in the locality lower depths, typically <30 mm, are present at circa 100 m distance from the release with the formation of sandwaves being visible.

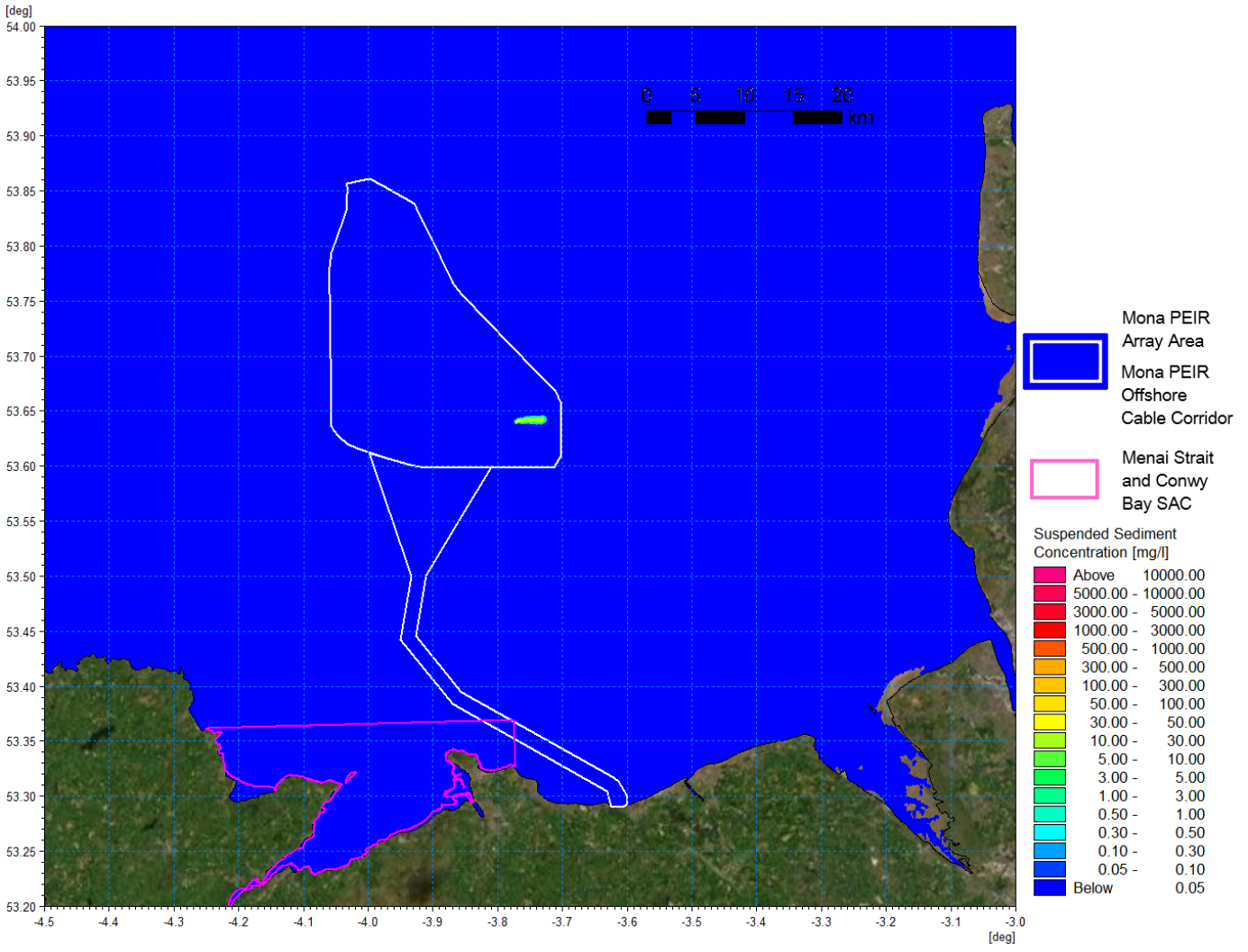

Figure 1.106: Suspended sediment concentration during dredging phase – inter-array cable path.

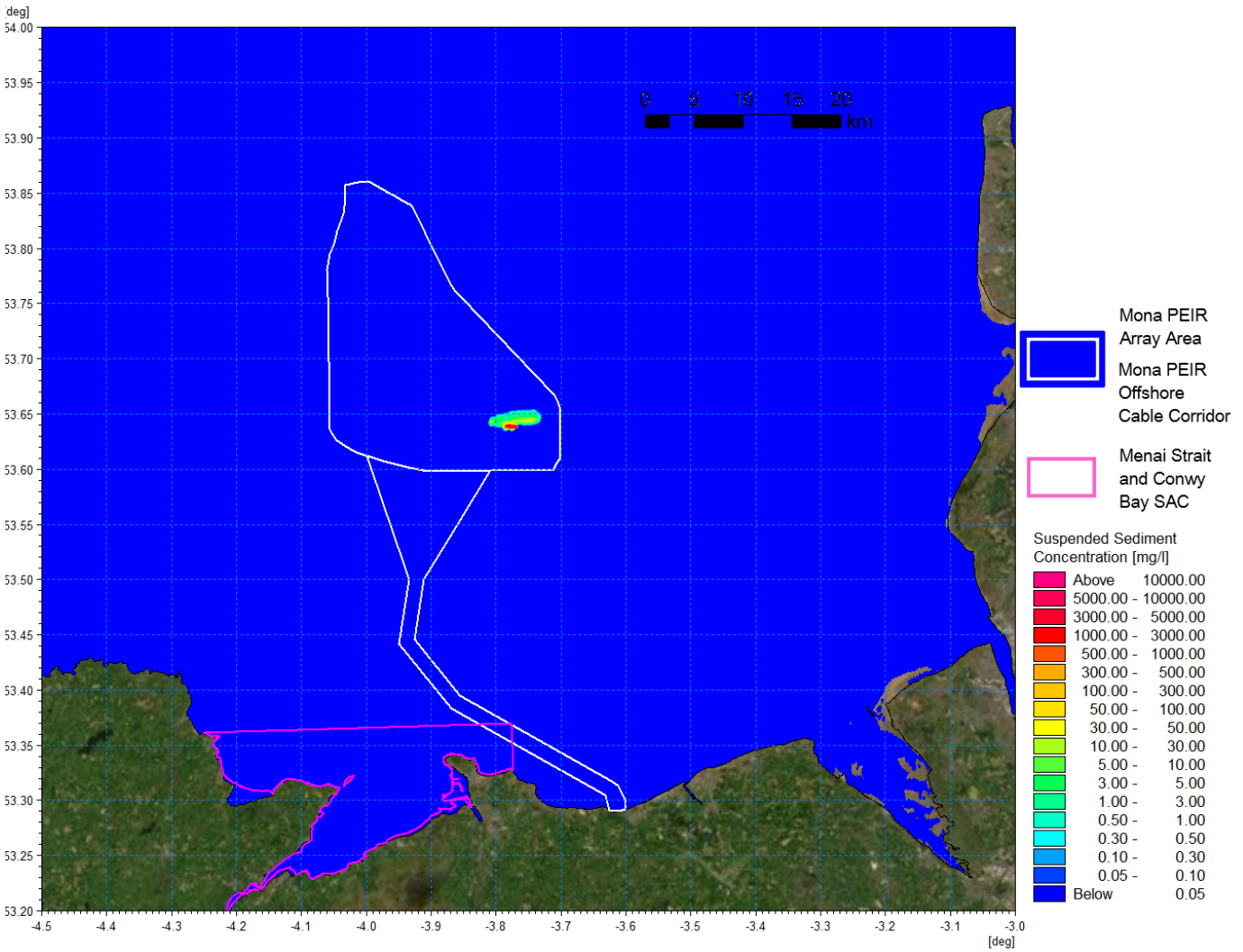

Figure 1.107: Suspended sediment concentration during dumping phase – inter-array cable path.

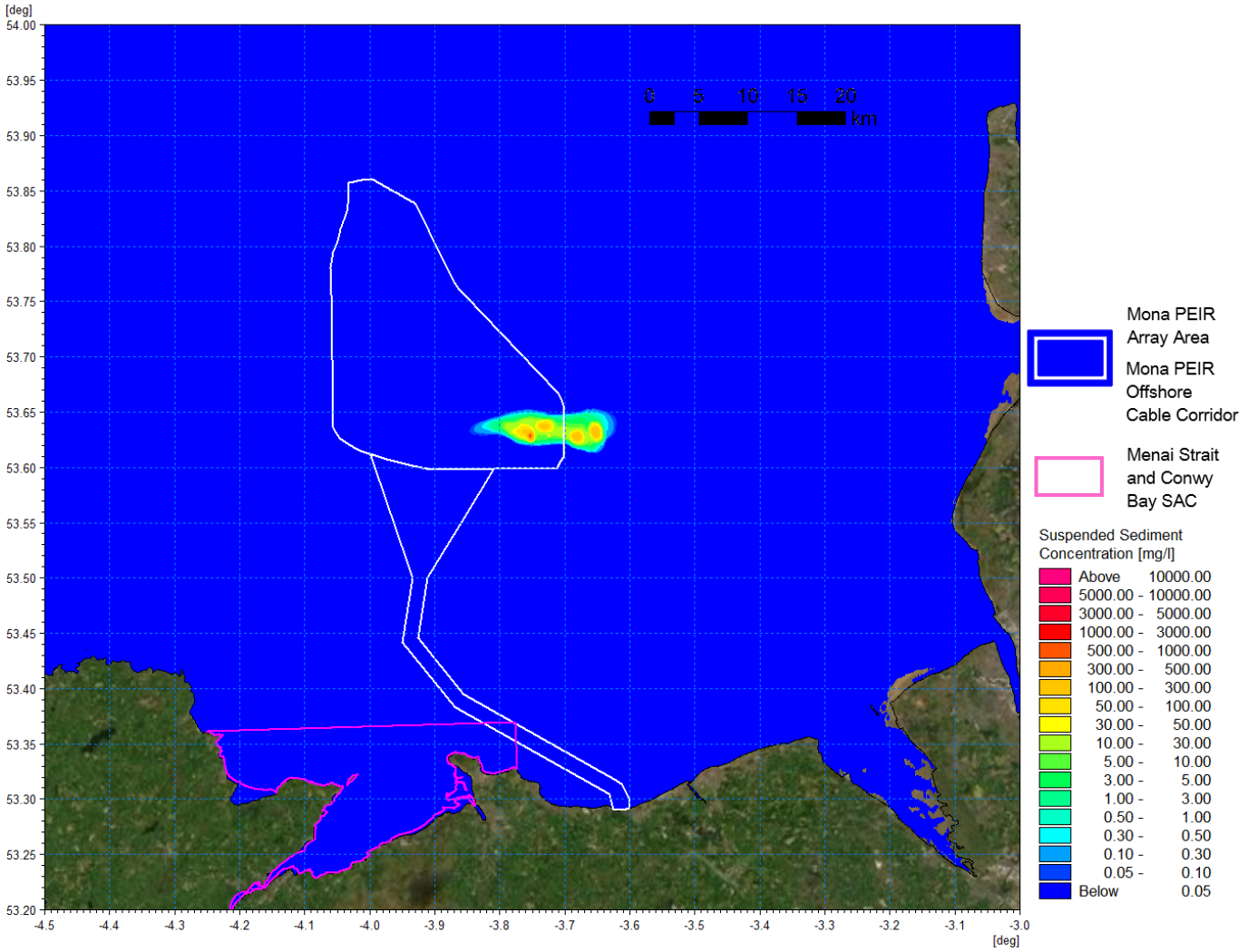

Figure 1.108: Suspended sediment concentration with sediment re-mobilisation – inter-array cable path.

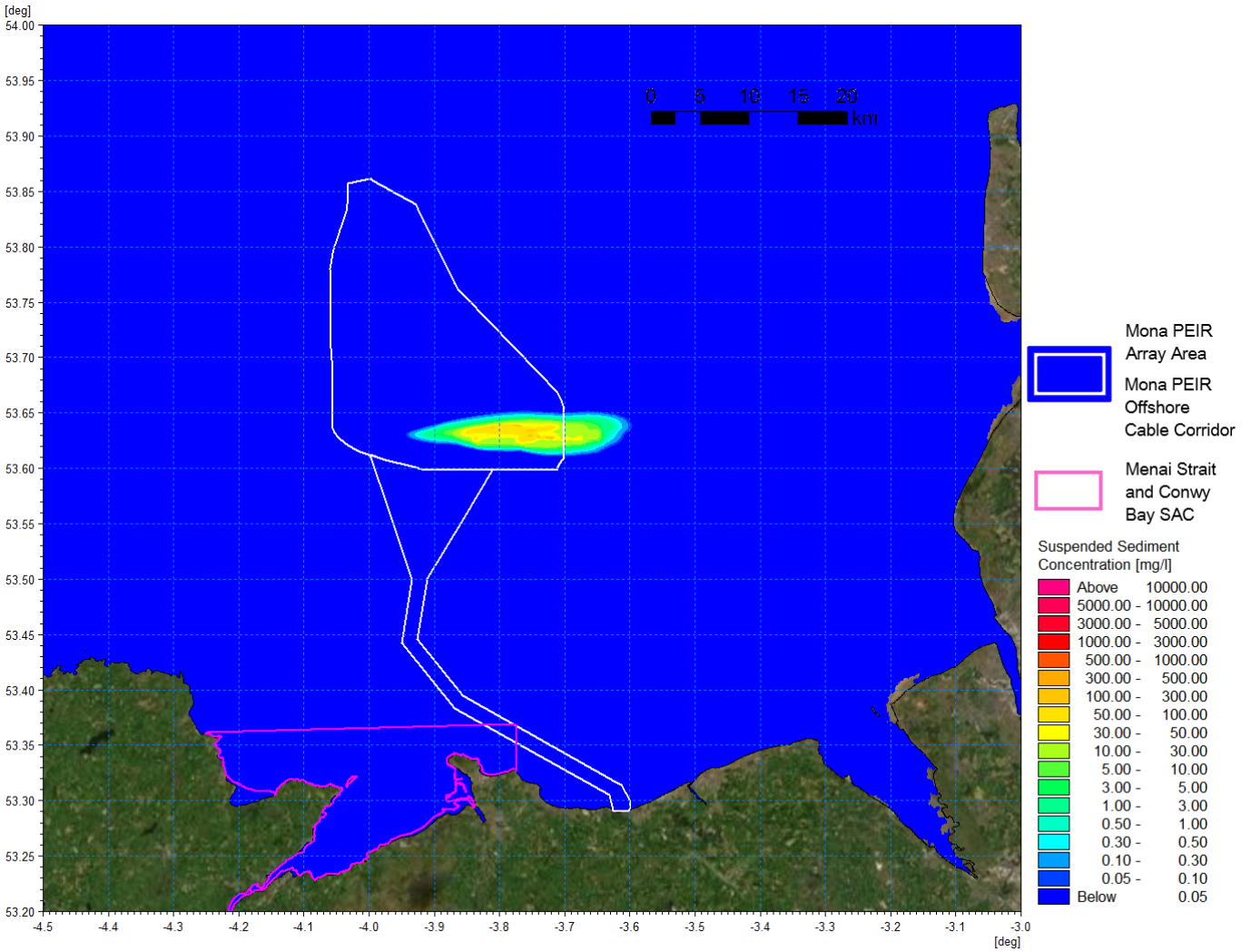

Figure 1.109: Average suspended sediment concentration during operation – inter-array cable path.

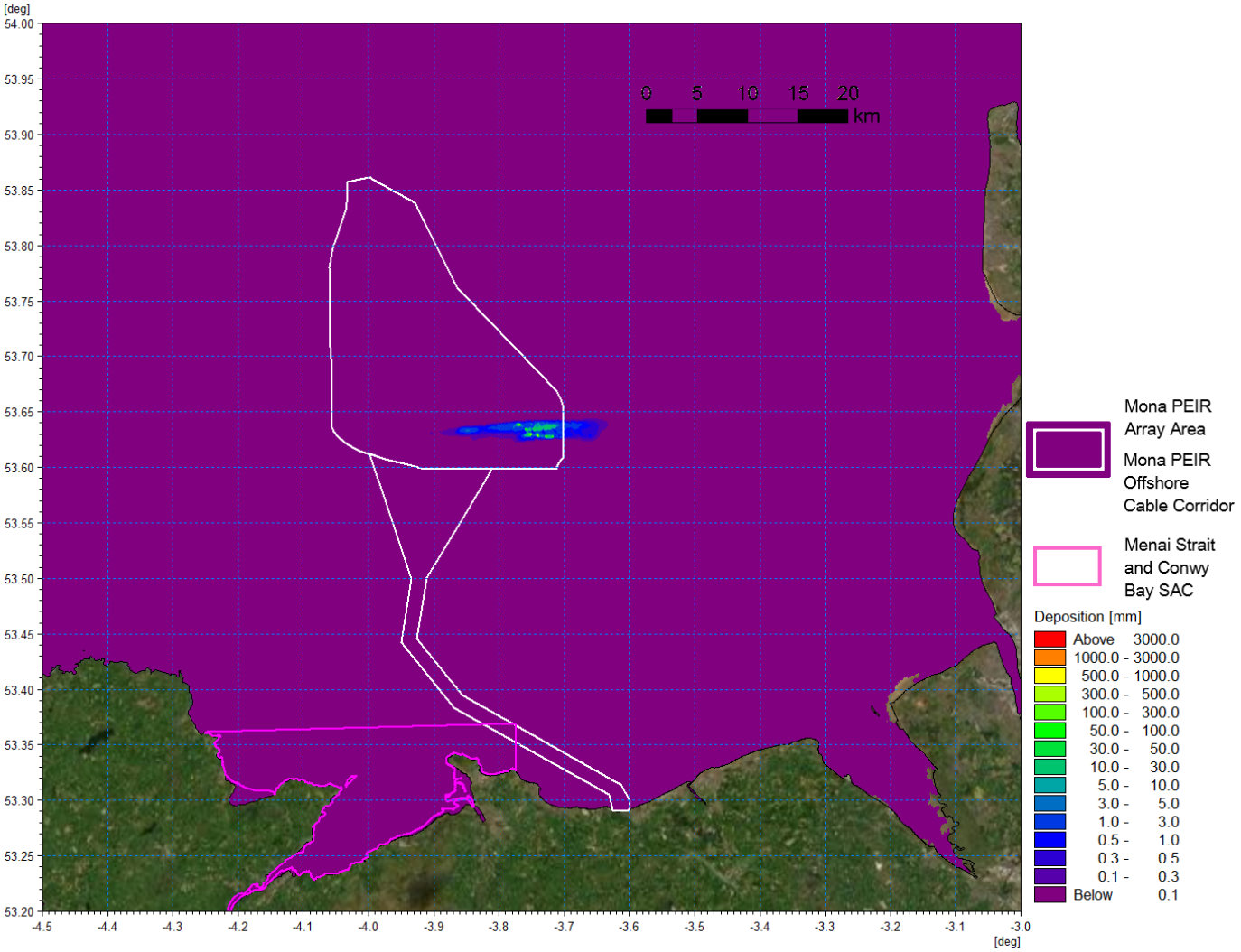

Figure 1.110: Average sedimentation during operation – inter-array cable path.

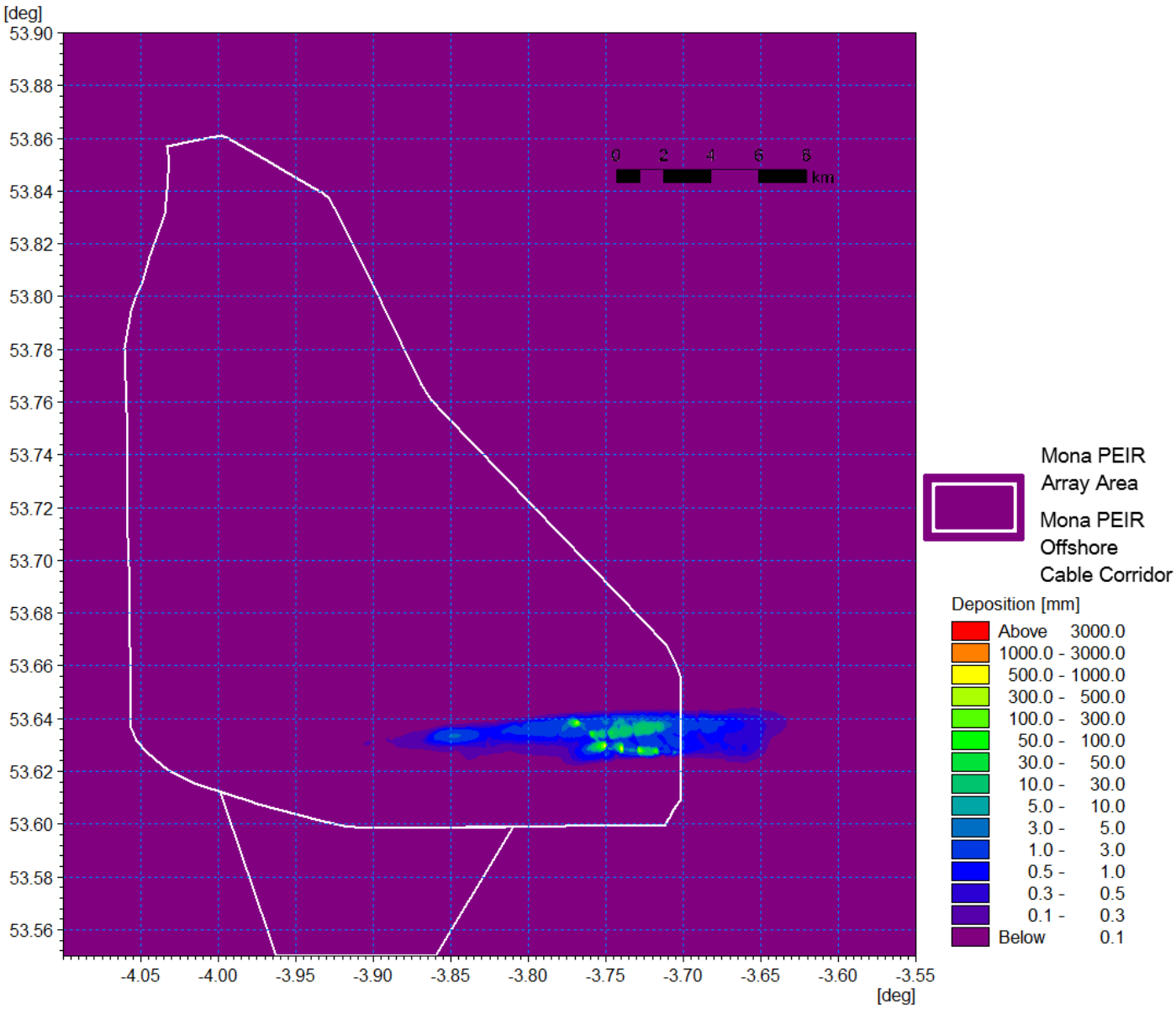

Figure 1.111: Average sedimentation during operation – inter-array cable path detailed view.

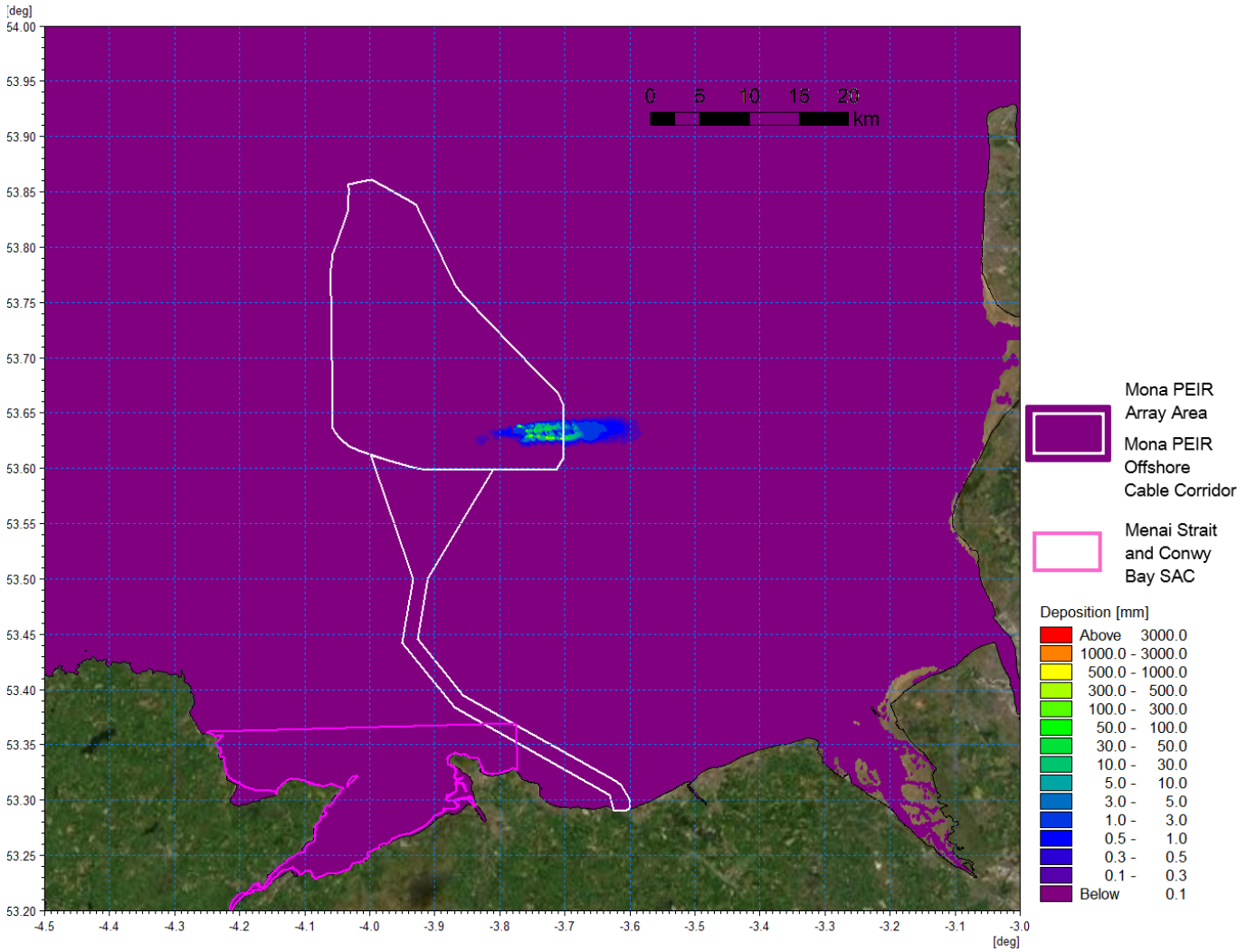

Figure 1.112: Sedimentation 1 day following cessation of operation – inter-array cable path.

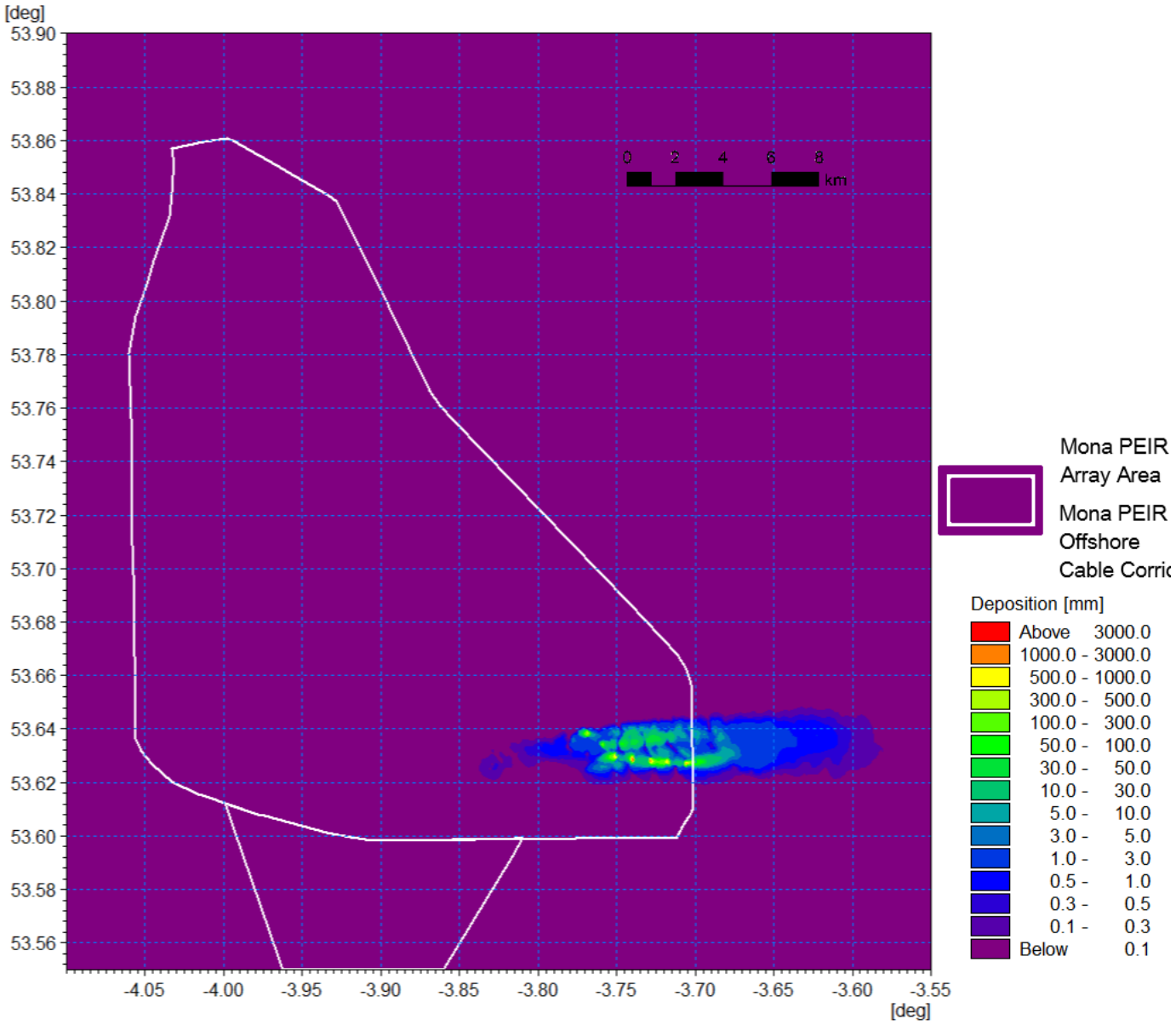

Figure 1.113: Sedimentation 1 day following cessation of operation – inter-array cable path detail view.

Foundation installation

1.3.7.16 The PDE (Project Design Envelope) for the PEIR included a number of potential foundation types including piled and suction caissons foundations. The caissons were applied in the hydrographic assessments as they created the largest potential obstruction to tidal flow and sediment transport however the installation produces much less seabed disturbance than installation of piled foundations. Therefore, the piled structures were assessed in terms of potential increases in suspended sediment concentrations. The PDE presented in the PEIR included monopile foundations, however these have since been removed from the project description (see Volume 1, Chapter 3: Project description of the Environmental Statement). As monopiles formed the maximum design scenario for the modelling of increases in suspended sediment concentrations undertaken and presented in the PEIR, the results of this modelling is presented below to inform the conclusions made in the Environmental Statement.

1.3.7.17 The largest potential release would be from augured (drilled) piles, where the material would be jetted and released to the water column as a plume. It was anticipated that all piles across the site may require drilling up to the full pile depth. The modelling assumed that at each site the material which is released has a similar composition to the sampled sediment. In reality, to require drilling (rather than driving) the sediments are generally less granular and augured material would be less easily brought into suspension therefore the modelled scenario provides a conservative assessment in terms of suspended sediment concentration.

1.3.7.18 A sample of four representative pile installation scenarios were simulated to cover the range of conditions in terms of water depth, tidal currents and sediment grading. It also took account of the proximity of piling where two concurrent events may take place. The modelling was undertaken using the MIKE MT module which allows the modelling of erosion, transport and deposition of cohesive and non-cohesive/granular sediments. This model is suited to sediment releases in the water column and allows sediment sources which may vary spatially and temporally. In this case, the cohesive functions were not utilised as the material released comprised sand. The sediment grading was defined for each location and assumed two concurrent drilling operations located at adjacent wind turbine or offshore platform locations to provide the largest augmented sediment plume concentration.

1.3.7.19 At each location it was assumed that the auguring was required to the 60 m pile depth for an assumed 16 m diameter pile with 0.9 m casing as a worst-case scenario (i.e. 13,460 m^3 per pile). The drilling rate was taken as 0.89 m/h which was both prescribed in the project description for PEIR and also allowed the release to cover the full range of tidal conditions. The auguring was undertaken continuously over a 67 hour period with material released throughout the water column.

1.3.7.20 For each location a set of results are presented. Firstly, the average suspended sediment plume during the course of the installation is shown. Due to the variation in suspended sediment levels, instantaneous plots of the sediment plumes are also presented during peak flood and ebb tides on two installation days. It should be noted that all the plots require the use of a log scale to cover this range of values whilst providing clarity and during slack water suspended sediment concentrations decrease significantly to values in the order of background levels.

1.3.7.21 The final set of plots relates to sedimentation. Due to the fine sandy nature of the material, it is clear that the sediment will be dispersed. It will be transported mid-tide, settle on slack water and be re-suspended and further dispersed on the resumption of tidal flow. For all simulations, sediment levels after the cessation of construction are presented. The piling activities do not remove any material from the immediate vicinity of the site and the released material returns the native sediment back into the existing sediment transport regime.

Piling scenario A

1.3.7.22 The two piles locations were sited at the locations shown in Figure 1.114. The sediment release was modelled over successive neap tidal cycles and at the location coarser material is present with the following composition being implemented within the simulation.

- Very coarse sand/gravel: 20%
- Coarse sand: 22%
- Medium sand: 46%

- Fine sand: 9%
- Very fine sand/mud: 3%.

1.3.7.23 This location exhibits slightly coarser graded material than at other locations and current speeds are lower during neap tides therefore this presents a scenario with a reduced plume envelope and higher SCC for the range of potential operations. The average suspended sediment plot shown in Figure 1.115, illustrates the effect of the dominant flood tide with the plume envelope extending further to the east. Average concentrations are typically <10 mg/l at the sites and reduce rapidly with distance from the two discharge locations. Where the plumes converge concentrations are <1 mg/l.

1.3.7.24 Figure 1.116 and Figure 1.117 illustrate the instantaneous concentrations on the flood and ebb tide of the first day of the drilling whilst Figure 1.118 and Figure 1.119 correspond with the same information for the third day. Areas of increased suspended sediment are evident on the latter plots where material has been deposited on slack tide and subsequently re-suspended. Typically, the plume concentration is <10 mg/l, and reduces with the distance from the site as the sediment is dispersed.

1.3.7.25 Figure 1.120 and Figure 1.121 show the average sedimentation, with the latter providing a more detailed view. It is evident that the greatest sedimentation depths occur at the drilling site itself with very localised values circa 300 mm. This corresponds with the immediate settlement of coarser material fractions, the lower neap current speed and also for the portion of work undertaken on slack tide. Figure 1.122 and Figure 1.123 present sedimentation one day following cessation of the drilling operation. The coarser material is seen to remain at the drill site whilst the finer sand fraction migrates to the east on the residual current albeit with deposition depths <1 mm due to the limited volume of material released.

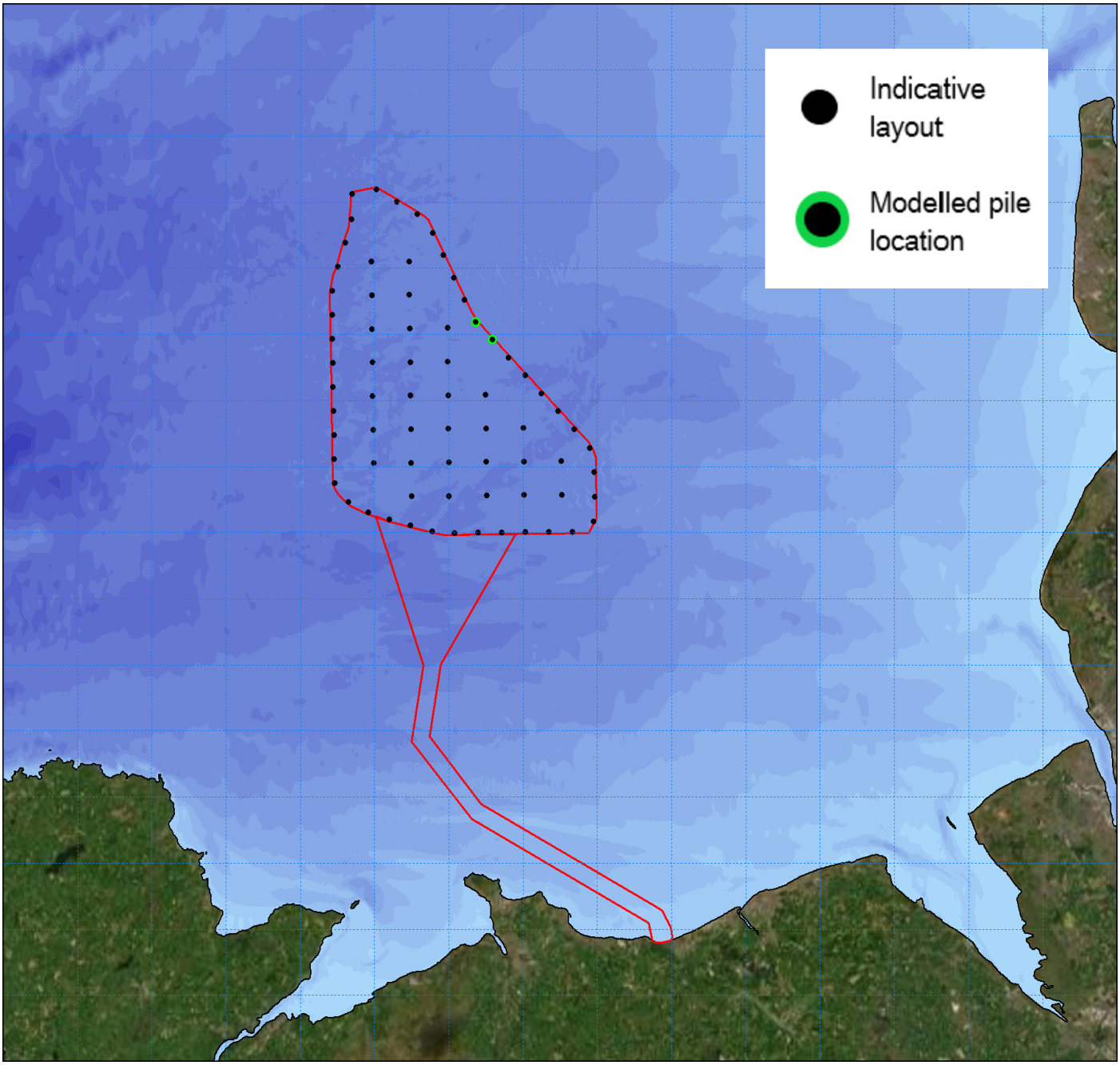

Figure 1.114: Location of modelled piled installation for piling – PEIR scenario A.

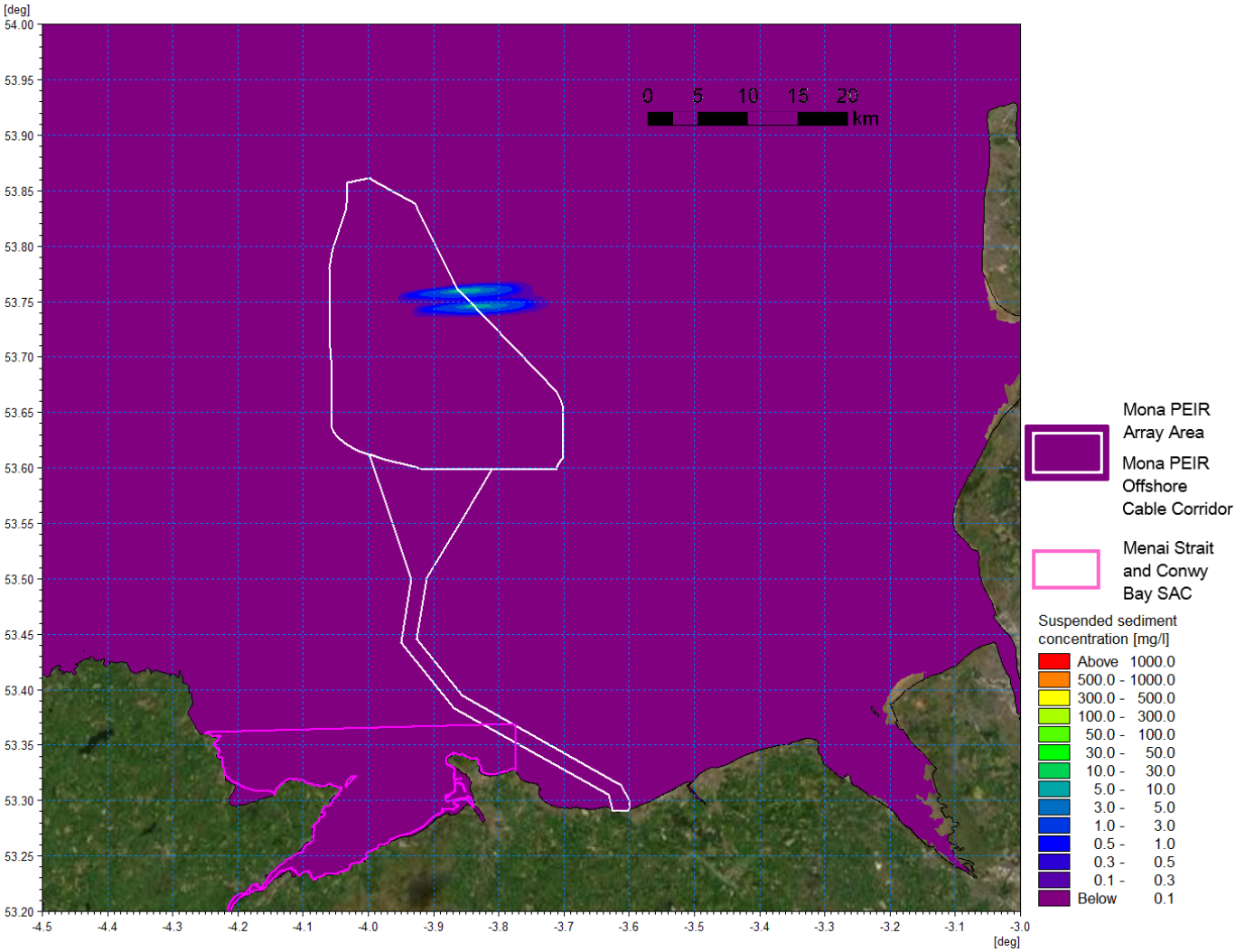

Figure 1.115: Average suspended sediment concentration – pile installation scenario A.

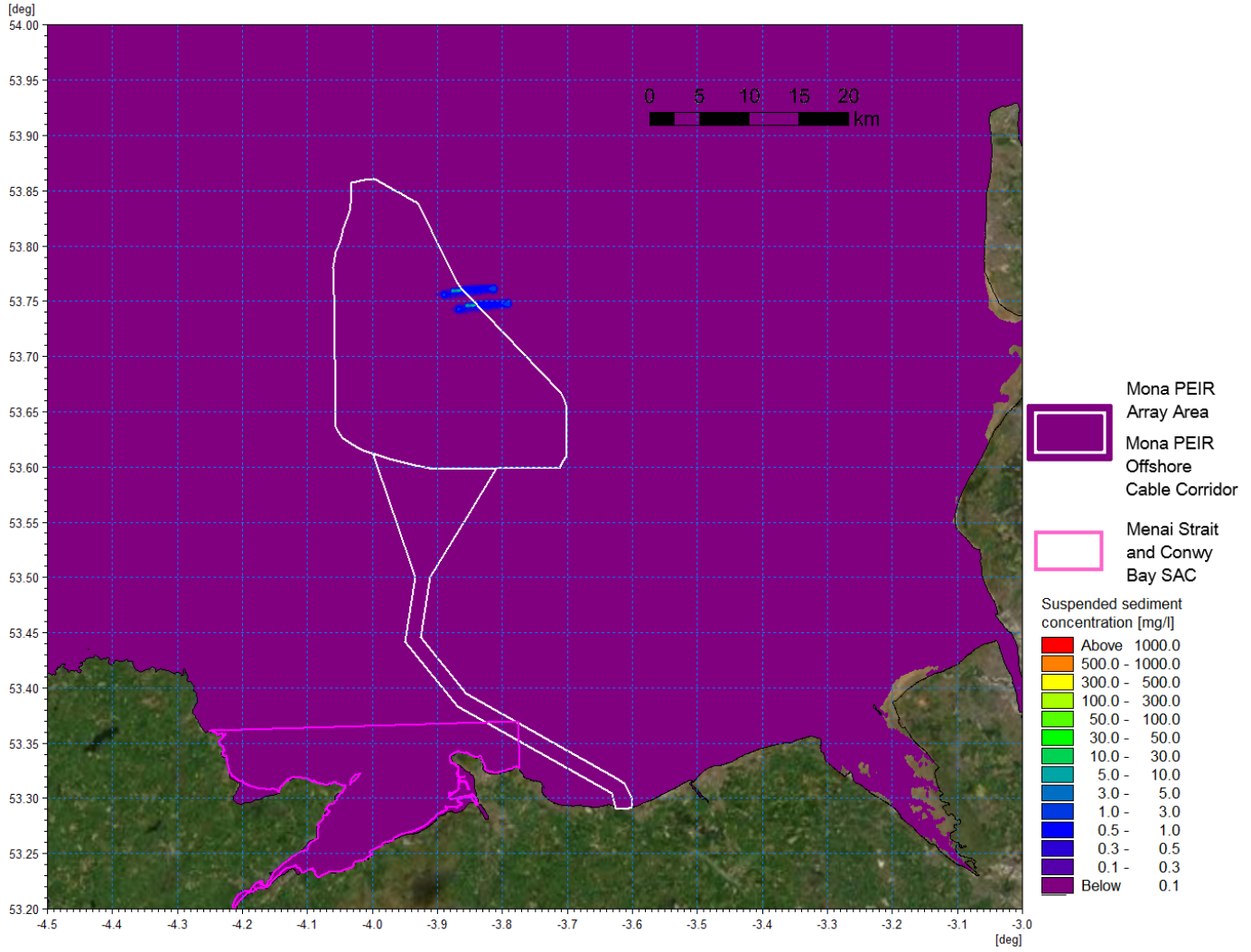

Figure 1.116: Suspended sediment concentration day 1 flood – pile installation scenario A.

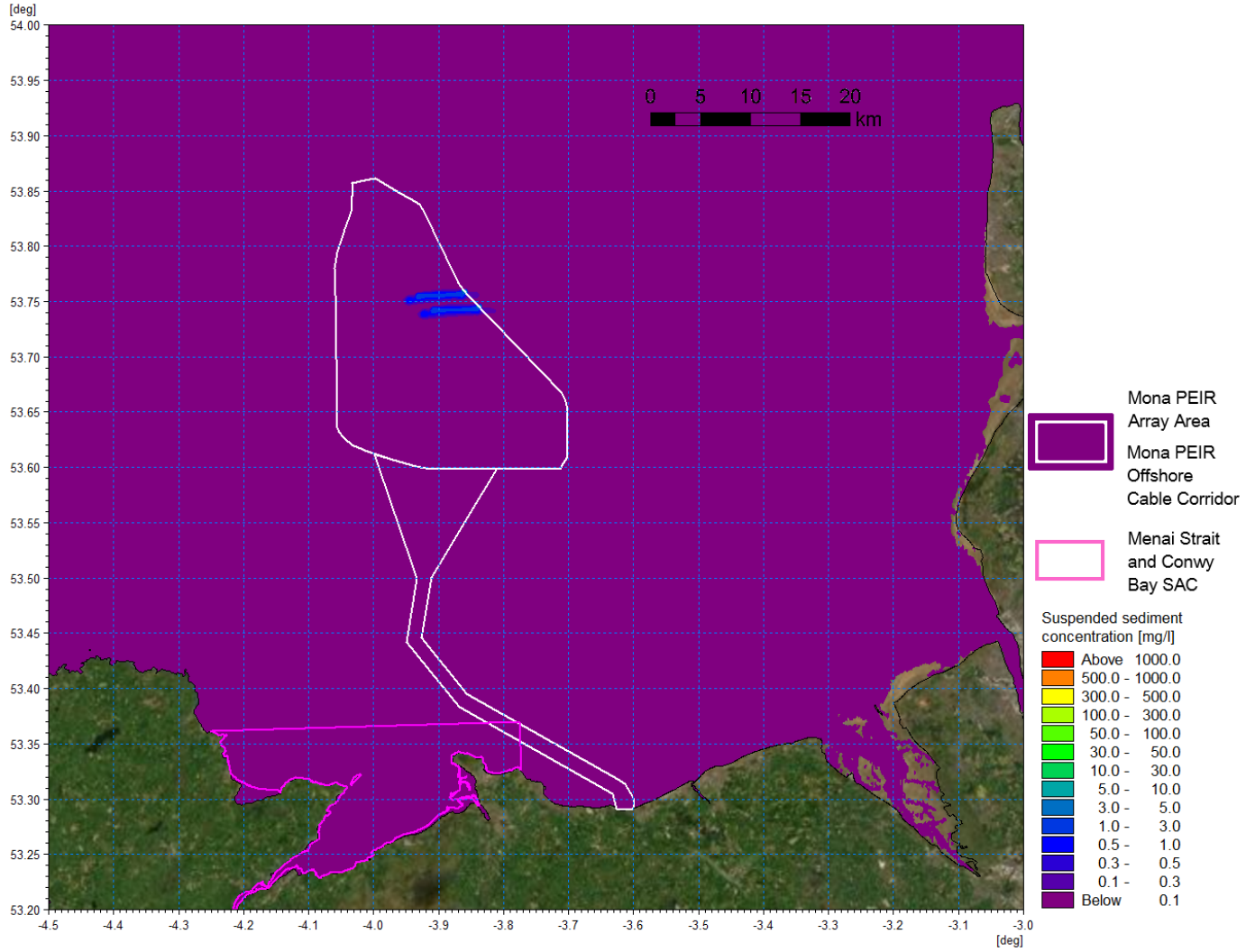

Figure 1.117: Suspended sediment concentration day 1 ebb – pile installation scenario A.

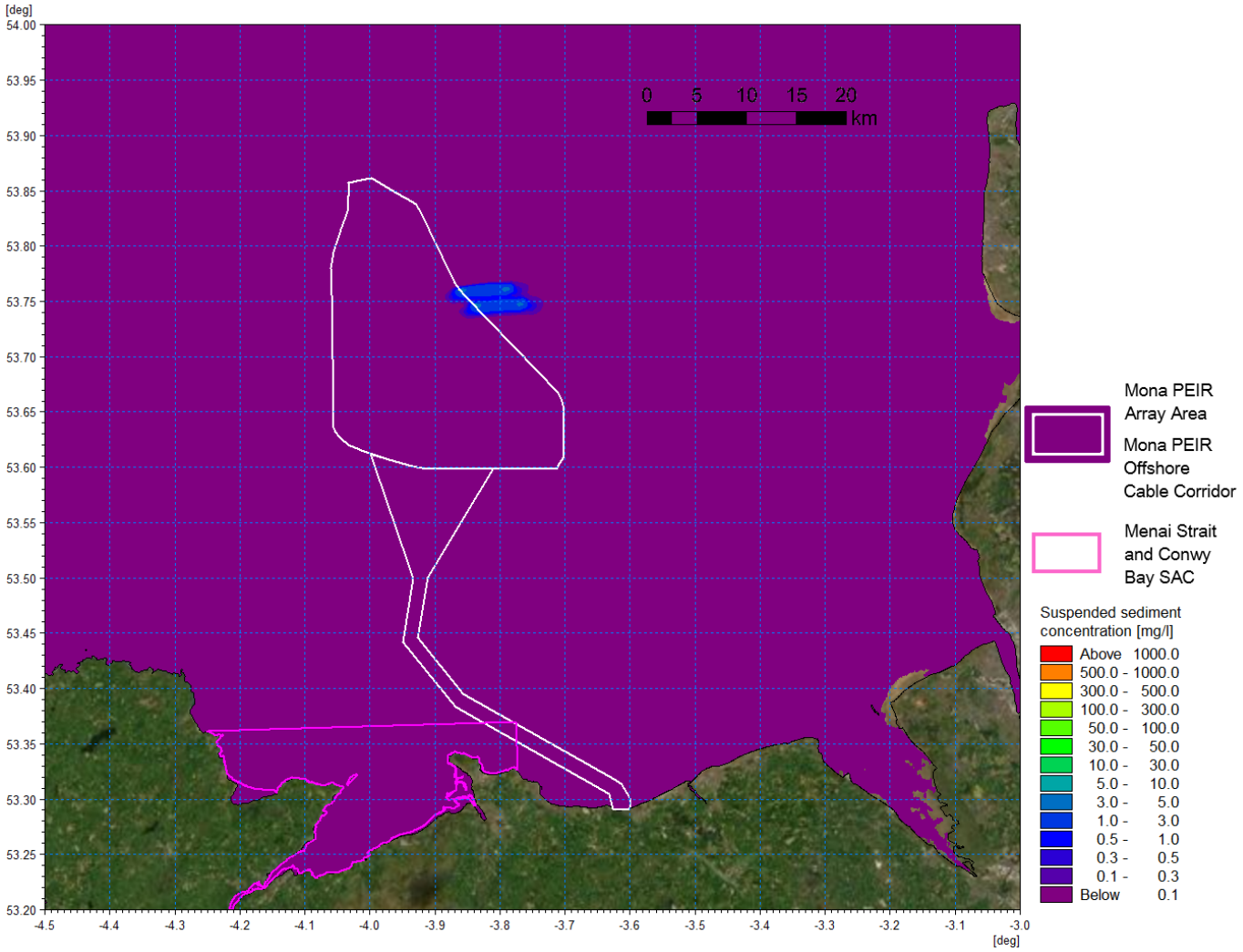

Figure 1.118: Suspended sediment concentration day 3 flood – pile installation scenario A.

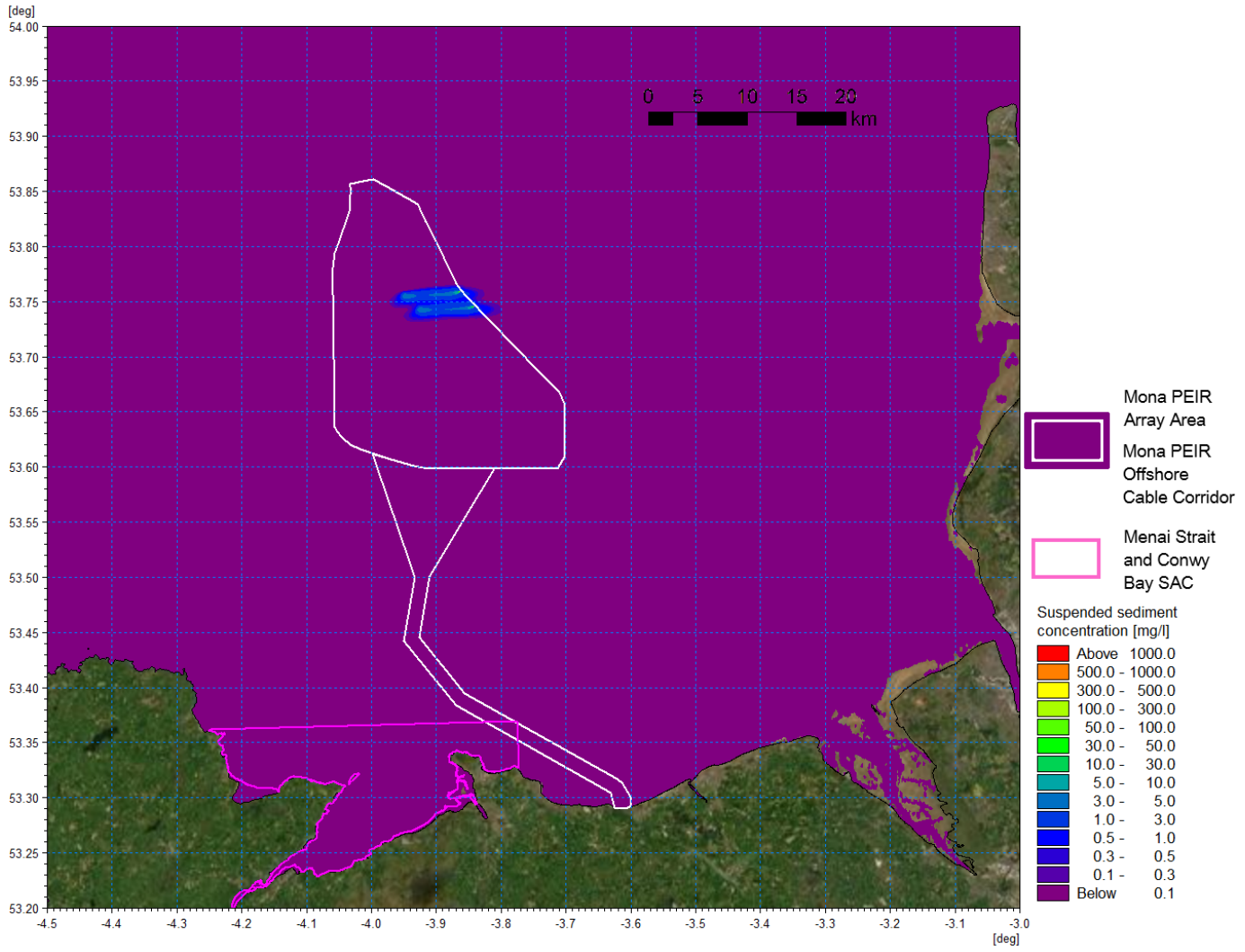

Figure 1.119: Suspended sediment concentration day 3 ebb – pile installation scenario A.

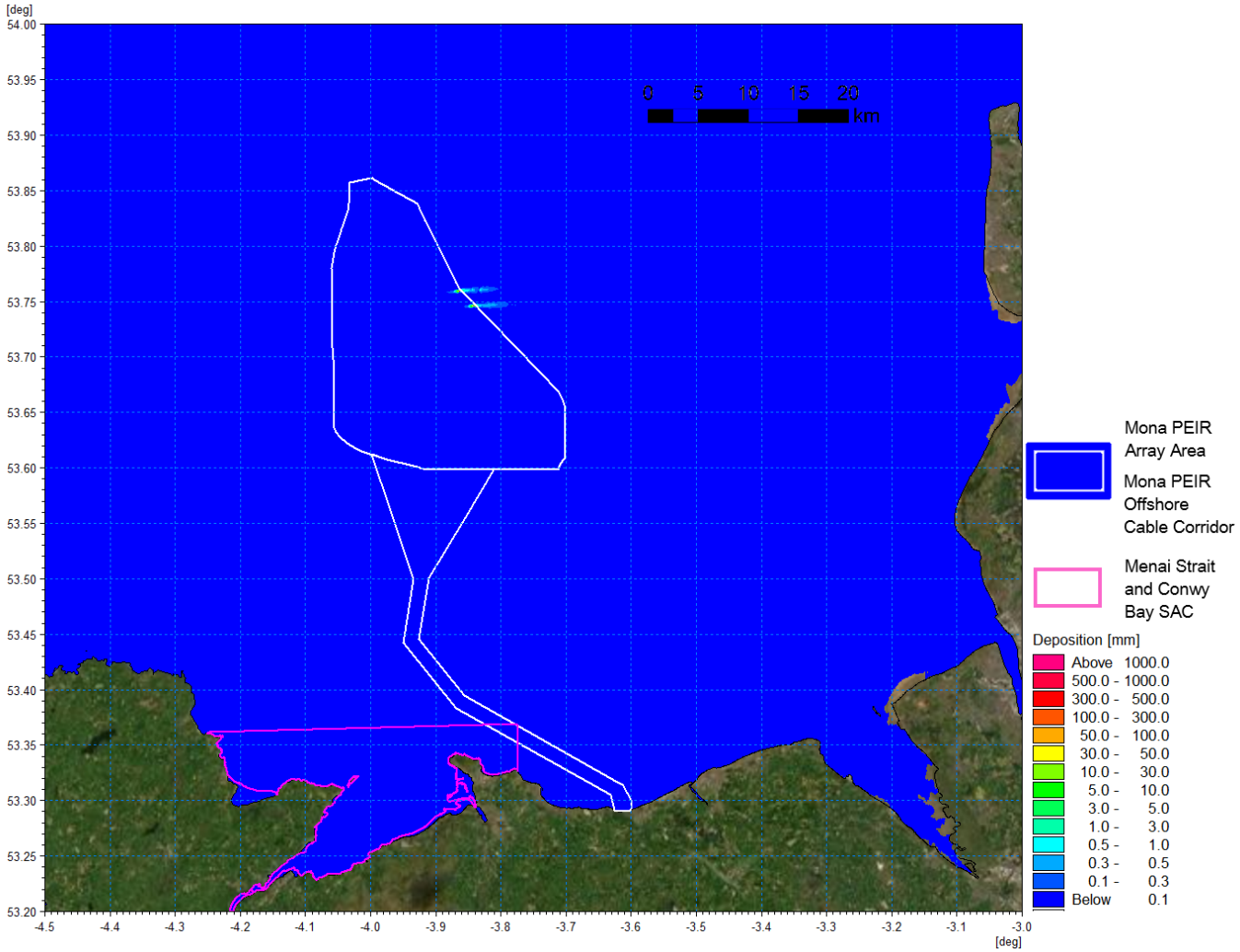

Figure 1.120: Average sedimentation during pile installation – scenario A.

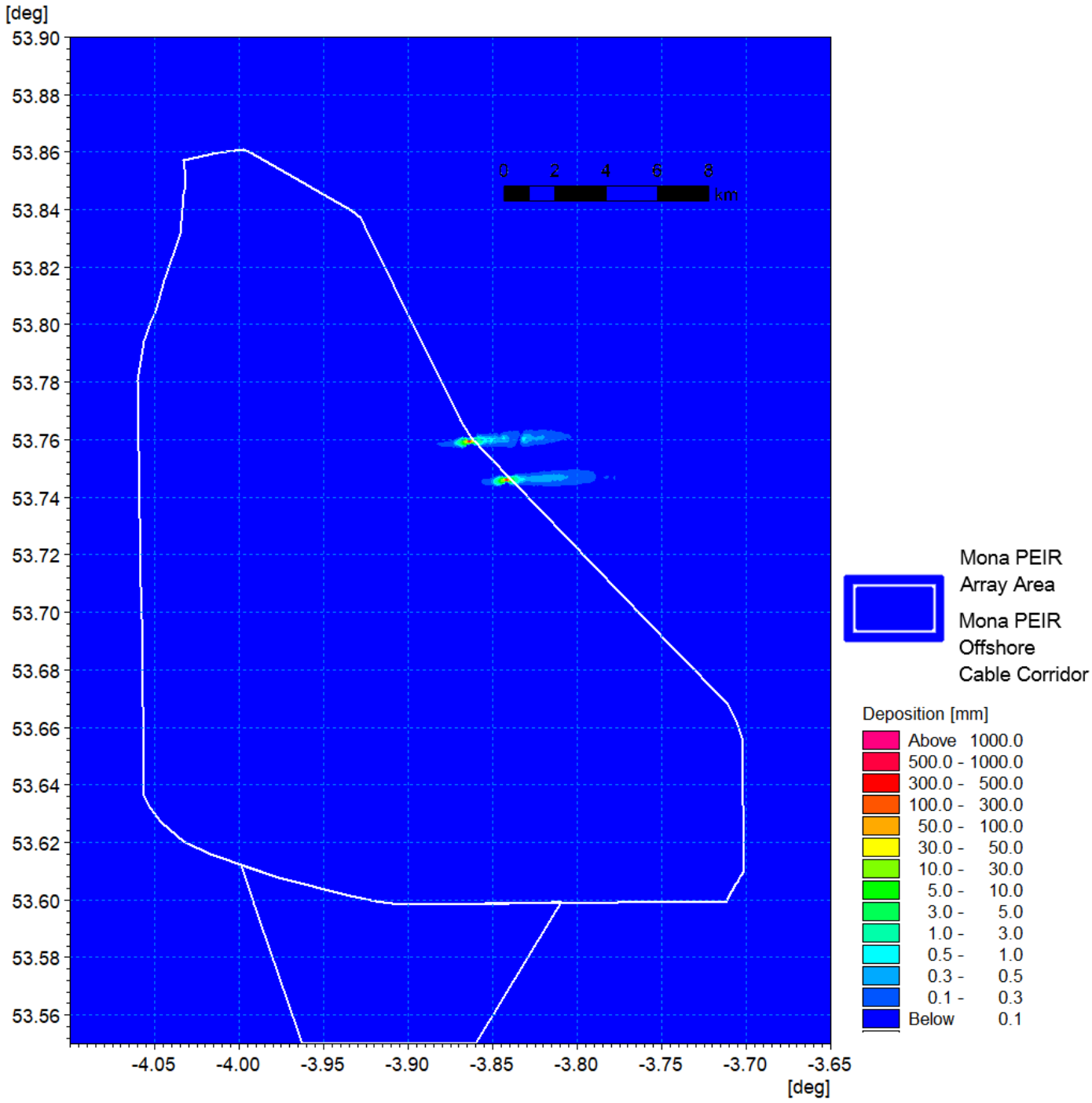

Figure 1.121: Average sedimentation during pile installation – scenario A detail view.

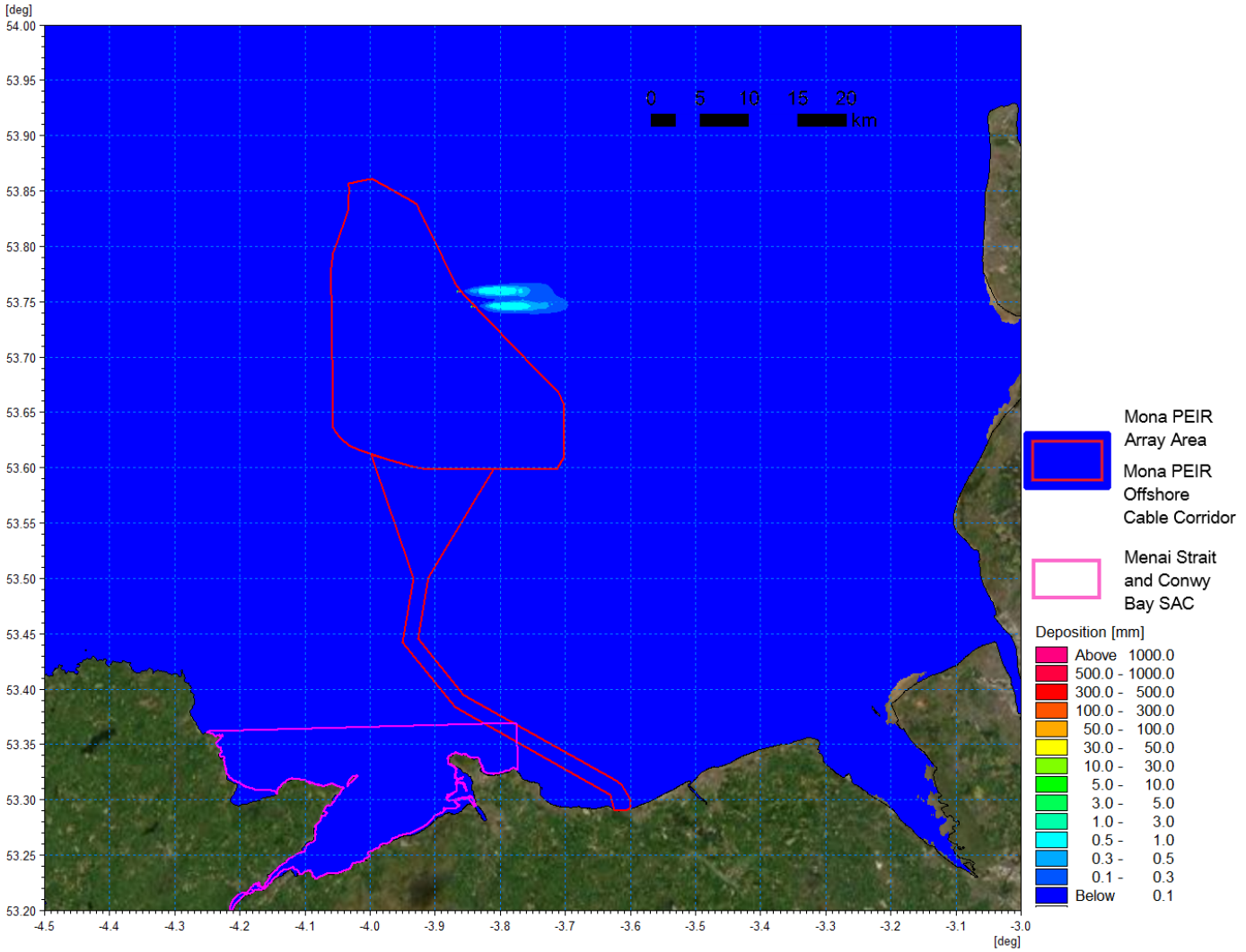

Figure 1.122: Sedimentation 1 day following cessation of pile installation – Pile scenario A.

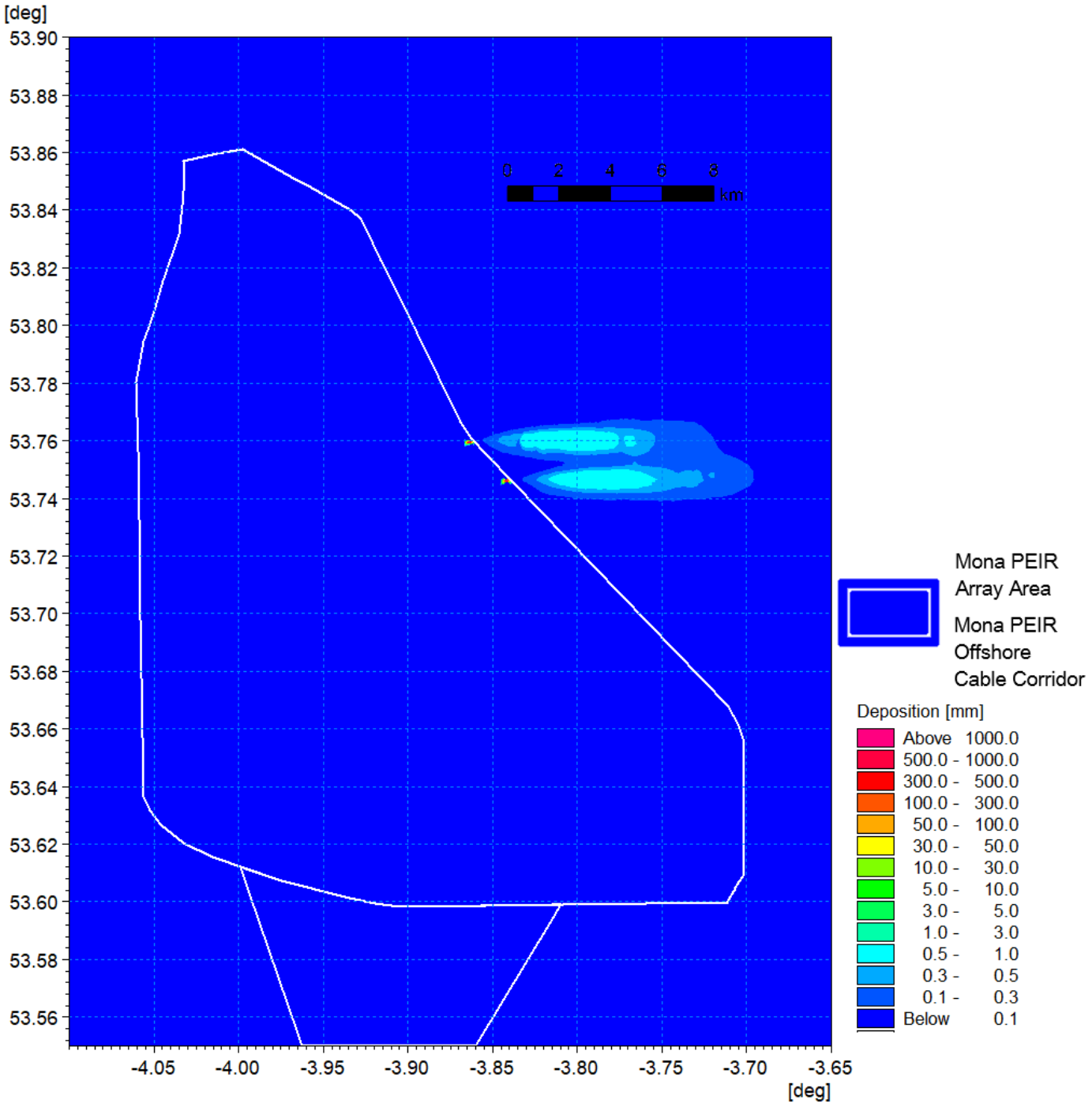

Figure 1.123: Sedimentation 1 day following cessation of pile installation – Pile scenario A detail view.

Piling scenario B

1.3.7.26 The piling locations are sited to the east of the Mona PEIR Array Area as shown in Figure 1.124. The simulation was undertaken for successive spring tides and at this location finer sediment and sandwaves are present. The following composition was implemented within the modelling.

- Very coarse sand/gravel: 8%
- Coarse sand: 23%

- Medium sand: 48%
- Fine sand: 10%
- Very fine sand/mud: 11%.

1.3.7.27 The average suspended sediment plume envelope is shown in Figure 1.125. As anticipated the extent of the envelope is greater than that for the previous scenario as it was undertaken during spring tides when peak currents are typically double that of neap tides. It may be expected that the subsequent concentrations would be lower as the water depths are similar at the two locations however the stronger currents and finer material means that a greater proportion of the material is in suspension. The instantaneous figures for day one and three, ebb and flood tides are presented in Figure 1.126 to Figure 1.129, where peak concentrations are circa 50 mg/l and average values are typically less than one fifth of this magnitude. At this location the transport cycle is also evident with material settling out on slack tides and becoming re-suspended with increasing current speeds.

1.3.7.28 The highly dispersive nature of spring tidal currents coupled with the finer material located at this site is evident in the sedimentation plots. The average sedimentation shown in Figure 1.130 and Figure 1.131 indicates this transport cycle with the material being dispersed to the east further following the end of the operation as illustrated in Figure 1.132 and Figure 1.133. The resulting sedimentation depths are typically <0.1 mm from the two drilling operations and demonstrates that this settlement would be imperceptible from the background sediment transport activity.

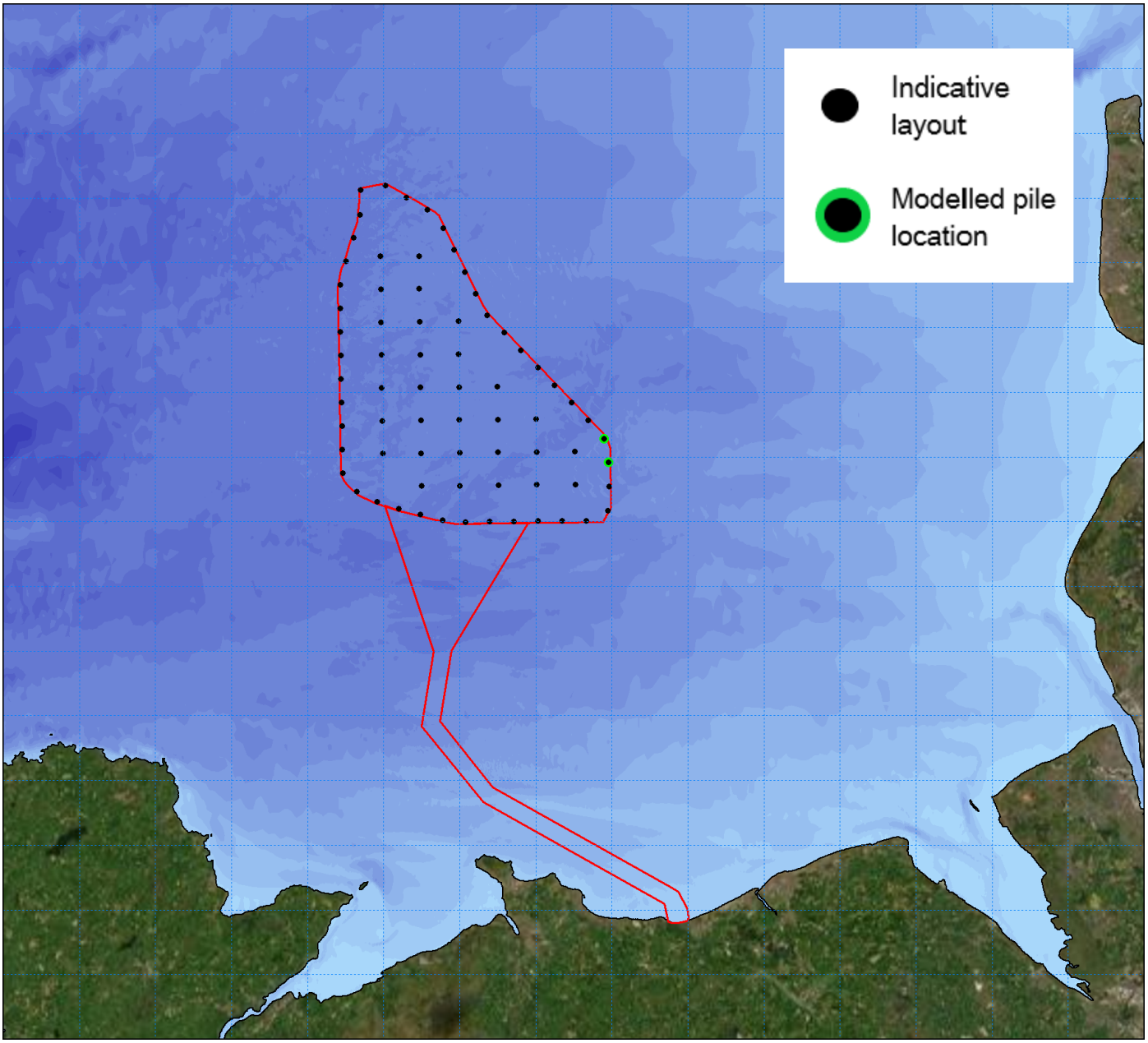

Figure 1.124: Location of modelled piled installation for piling – PEIR scenario B.

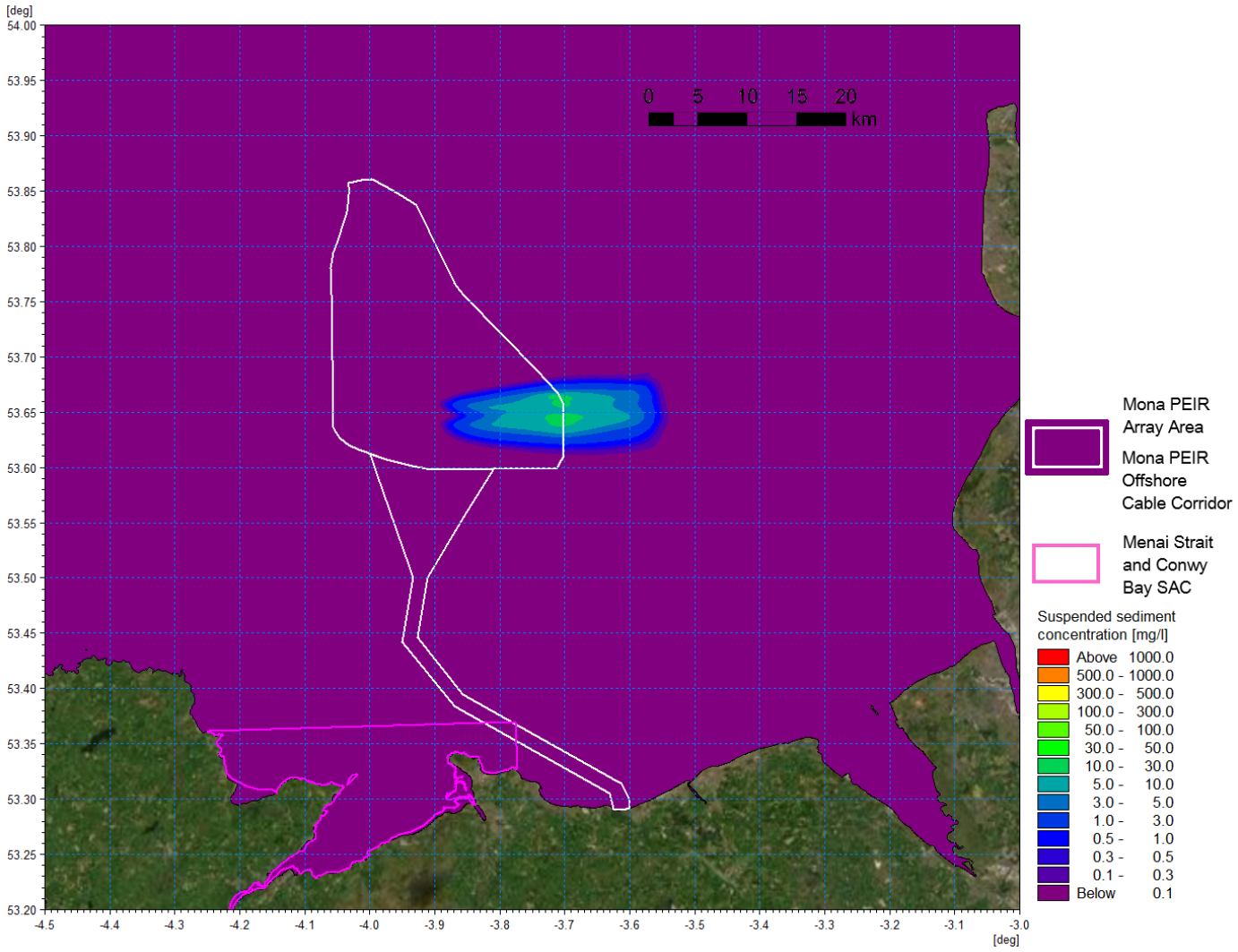

Figure 1.125: Average suspended sediment concentration – pile installation scenario B.

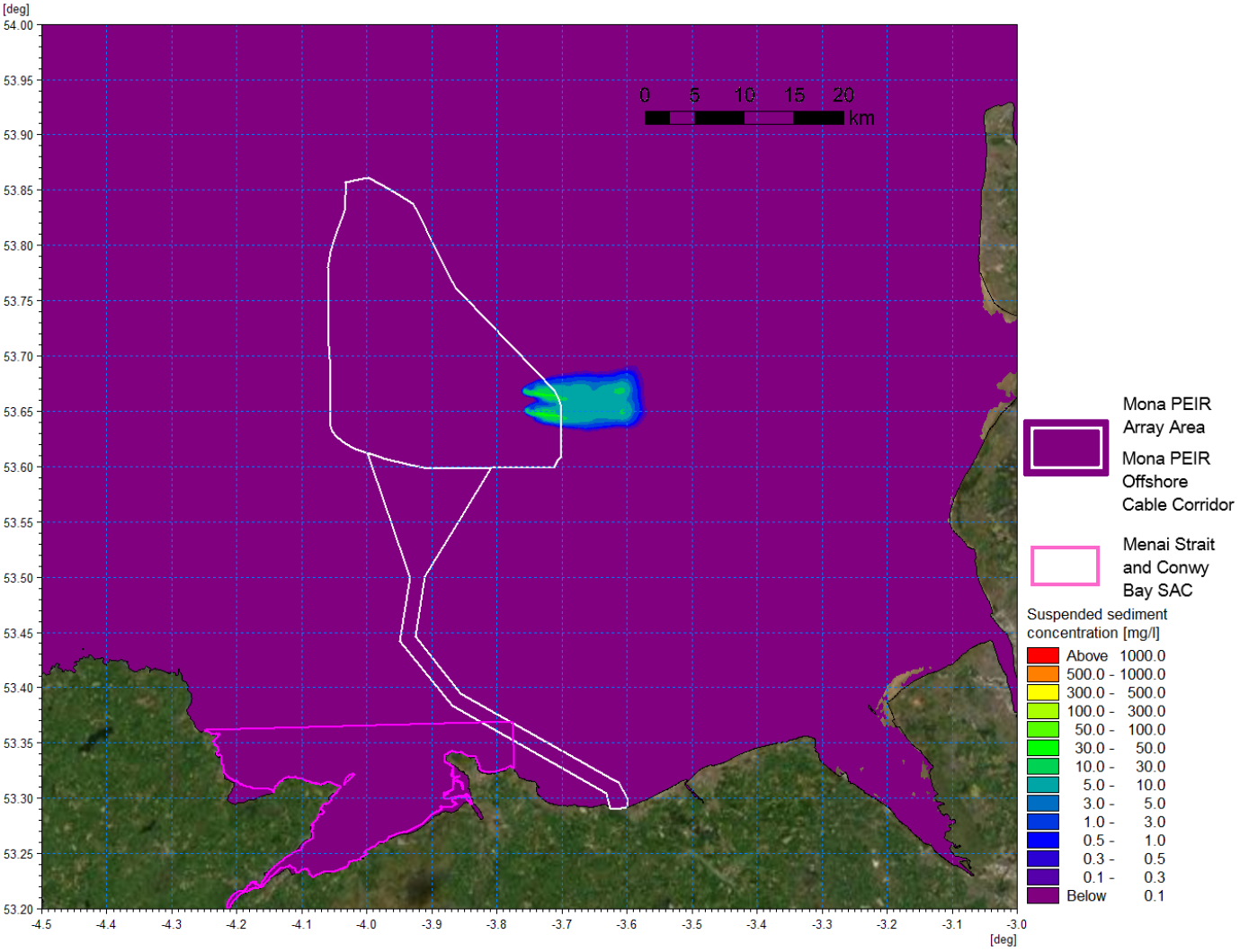

Figure 1.126: Suspended sediment concentration day 1 flood – pile installation scenario B.

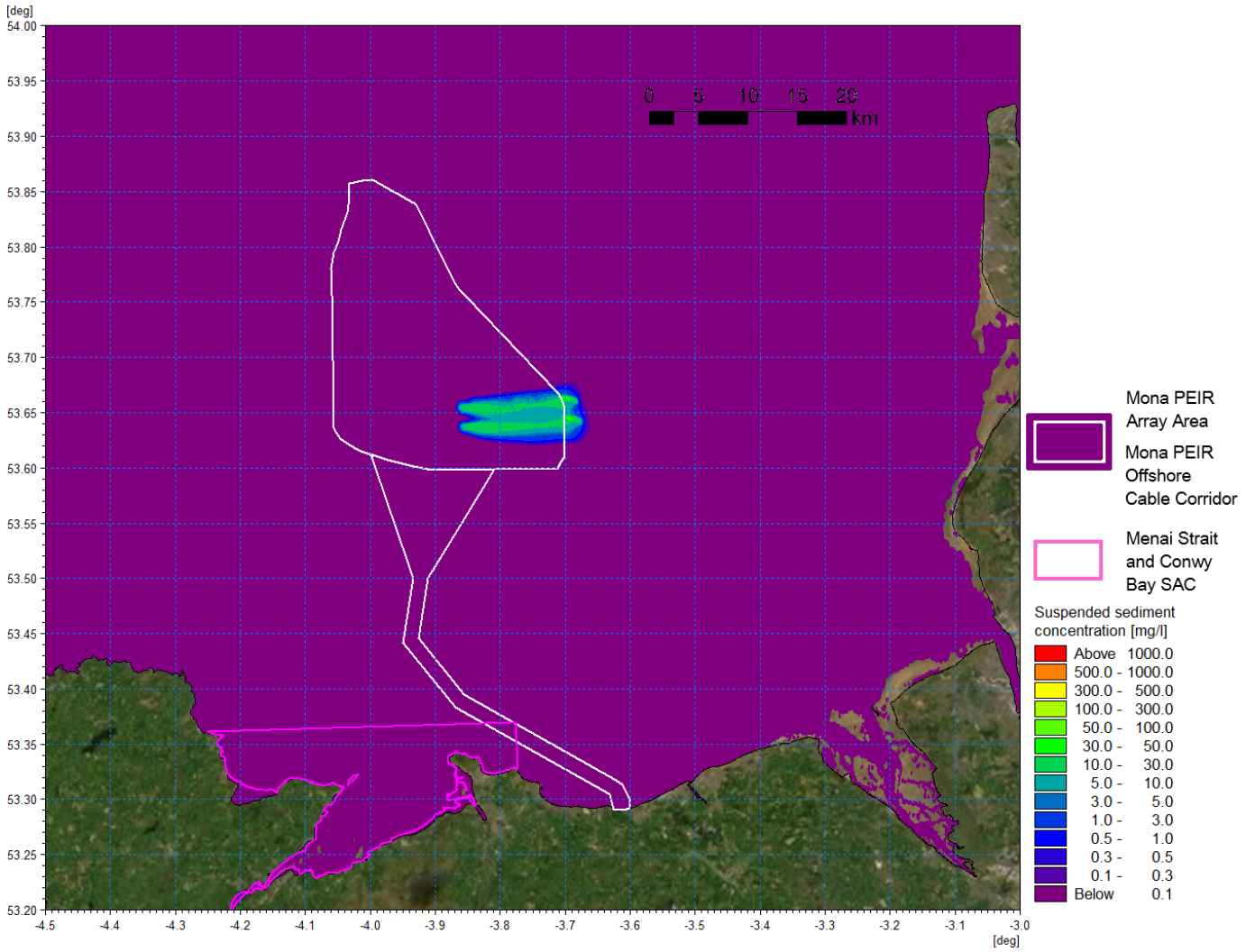

Figure 1.127: Suspended sediment concentration day 1 ebb – pile installation scenario B.

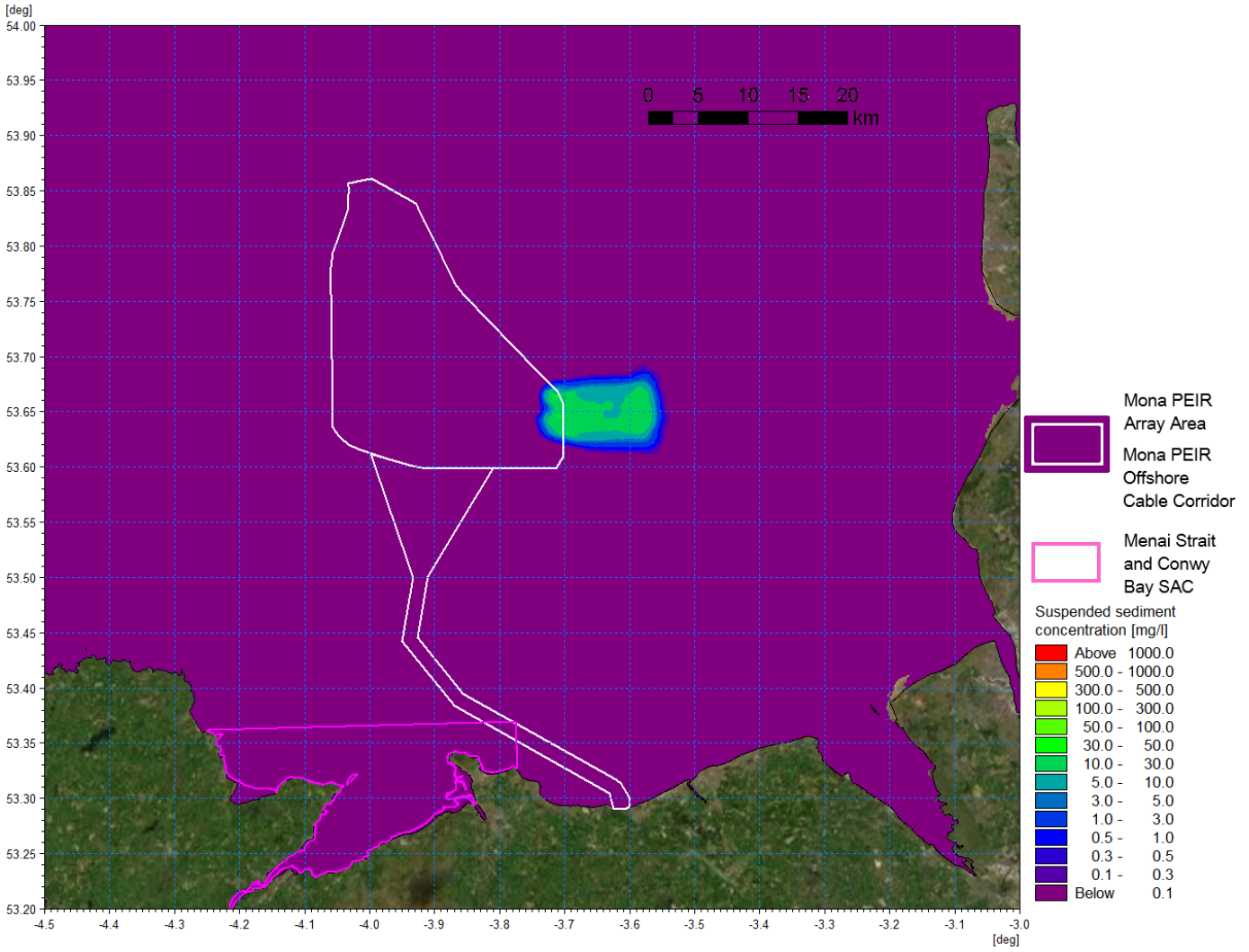

Figure 1.128: Suspended sediment concentration day 3 flood – pile installation scenario B.

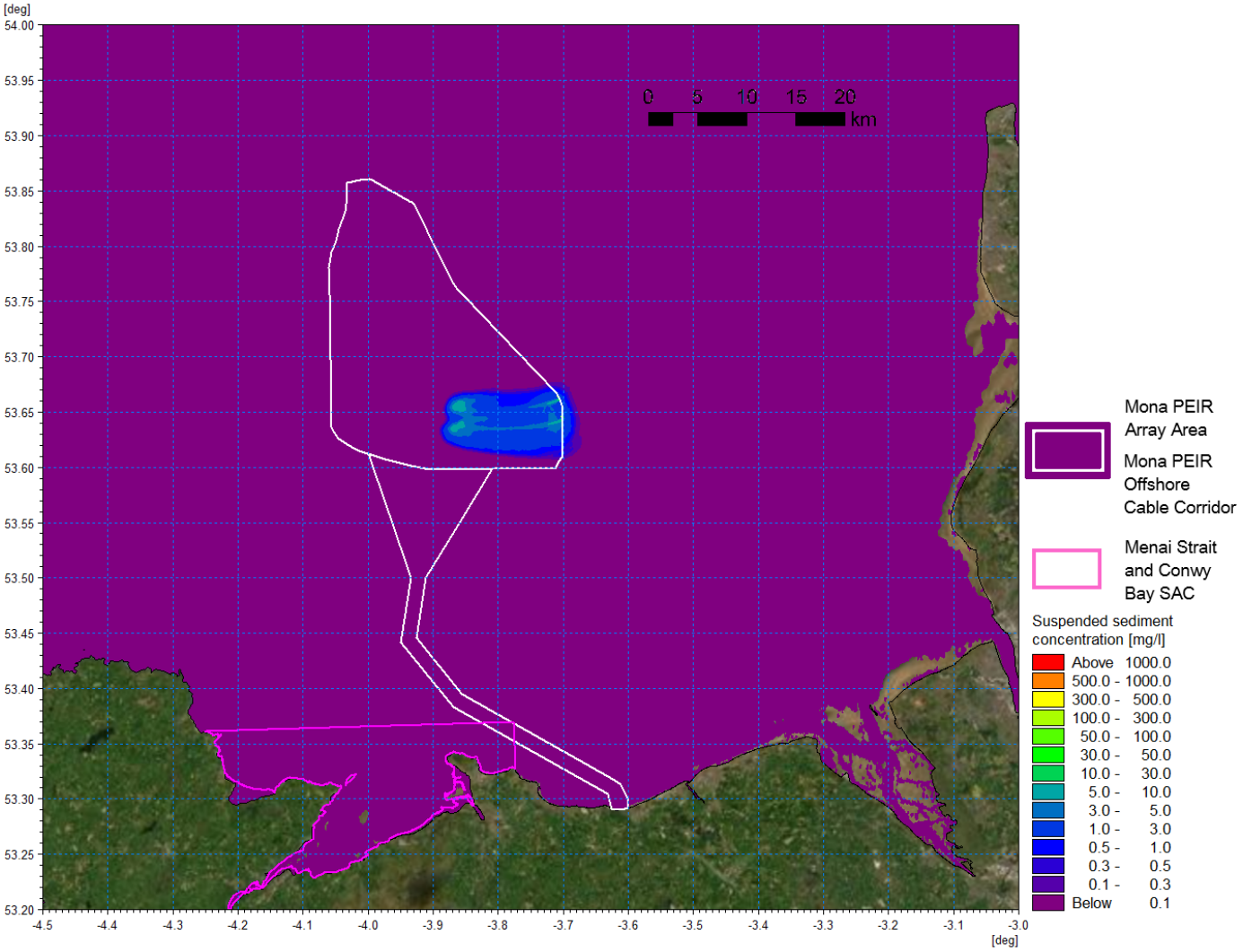

Figure 1.129: Suspended sediment concentration day 3 ebb – pile installation scenario B.

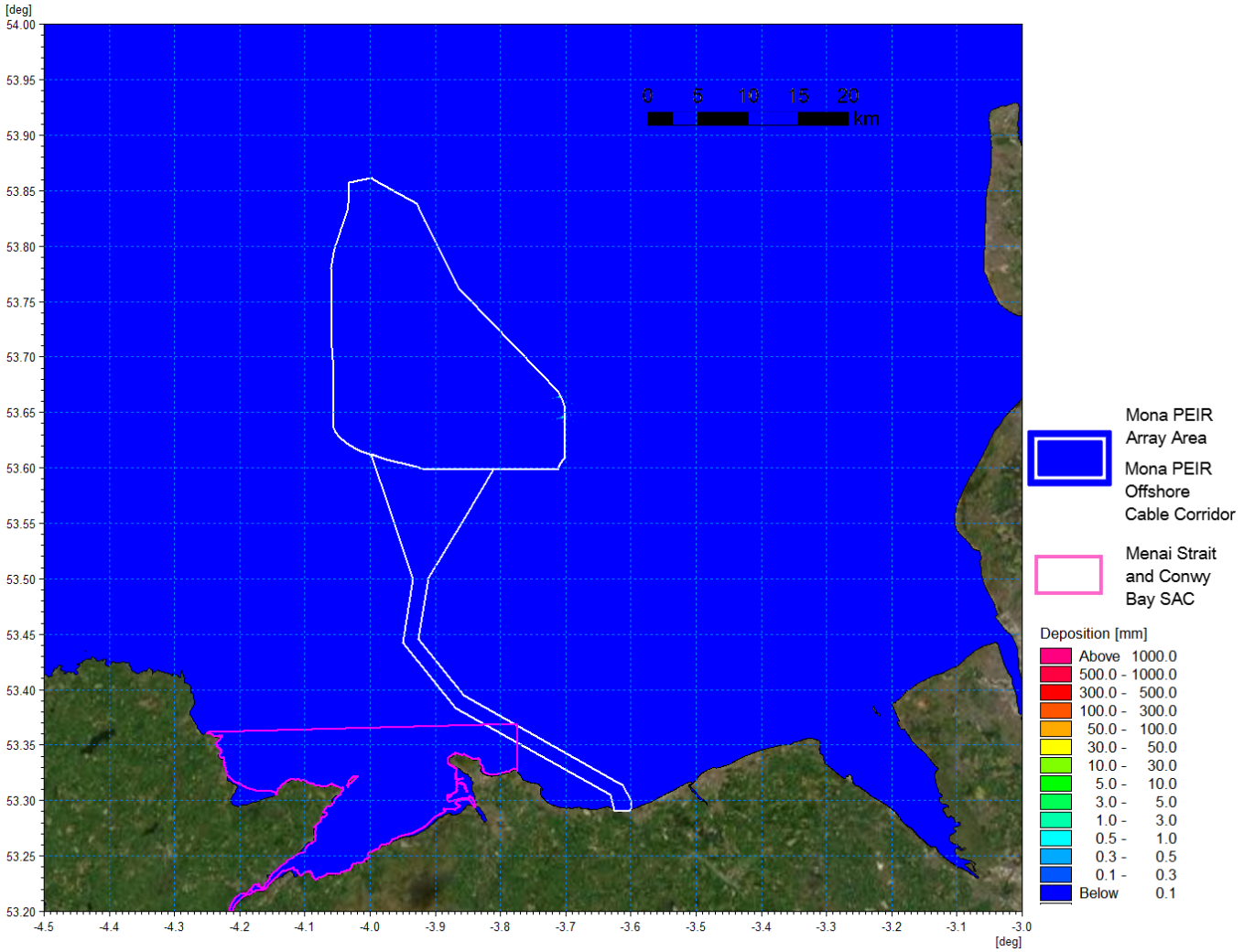

Figure 1.130: Average sedimentation during pile installation – scenario B.

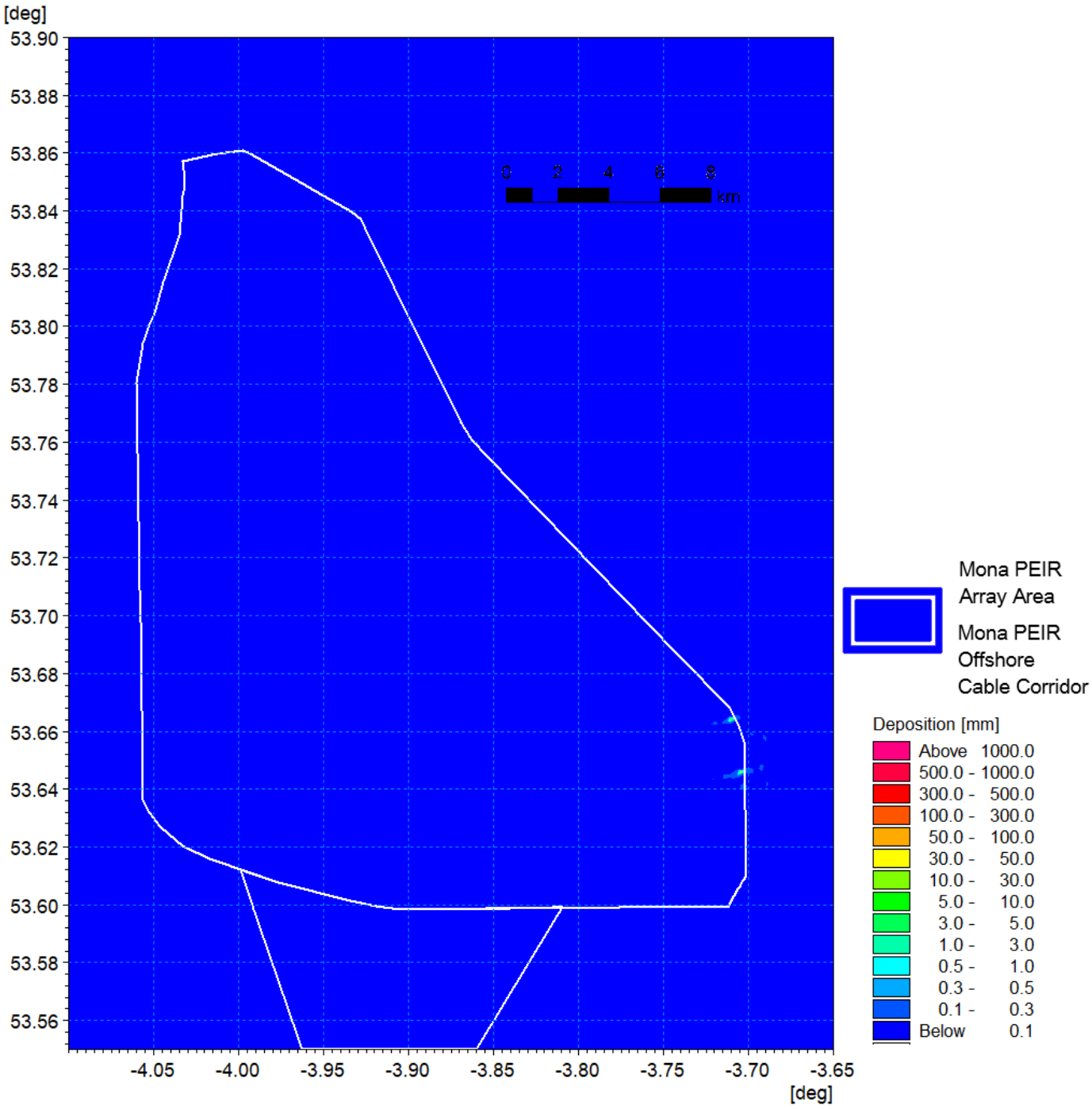

Figure 1.131: Average sedimentation during pile installation – scenario B detail view.

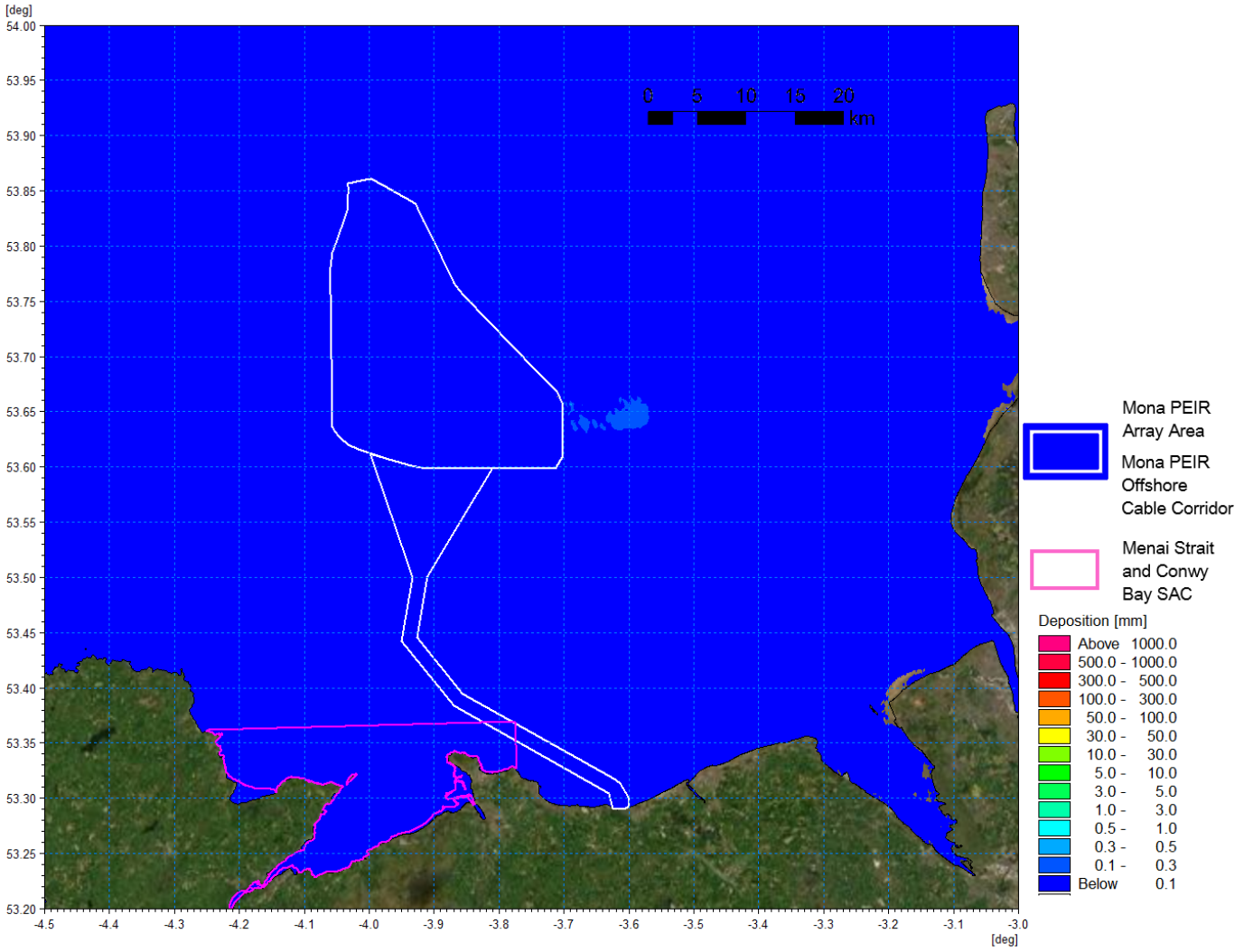

Figure 1.132: Sedimentation 1 day following cessation of pile installation – Pile scenario B.

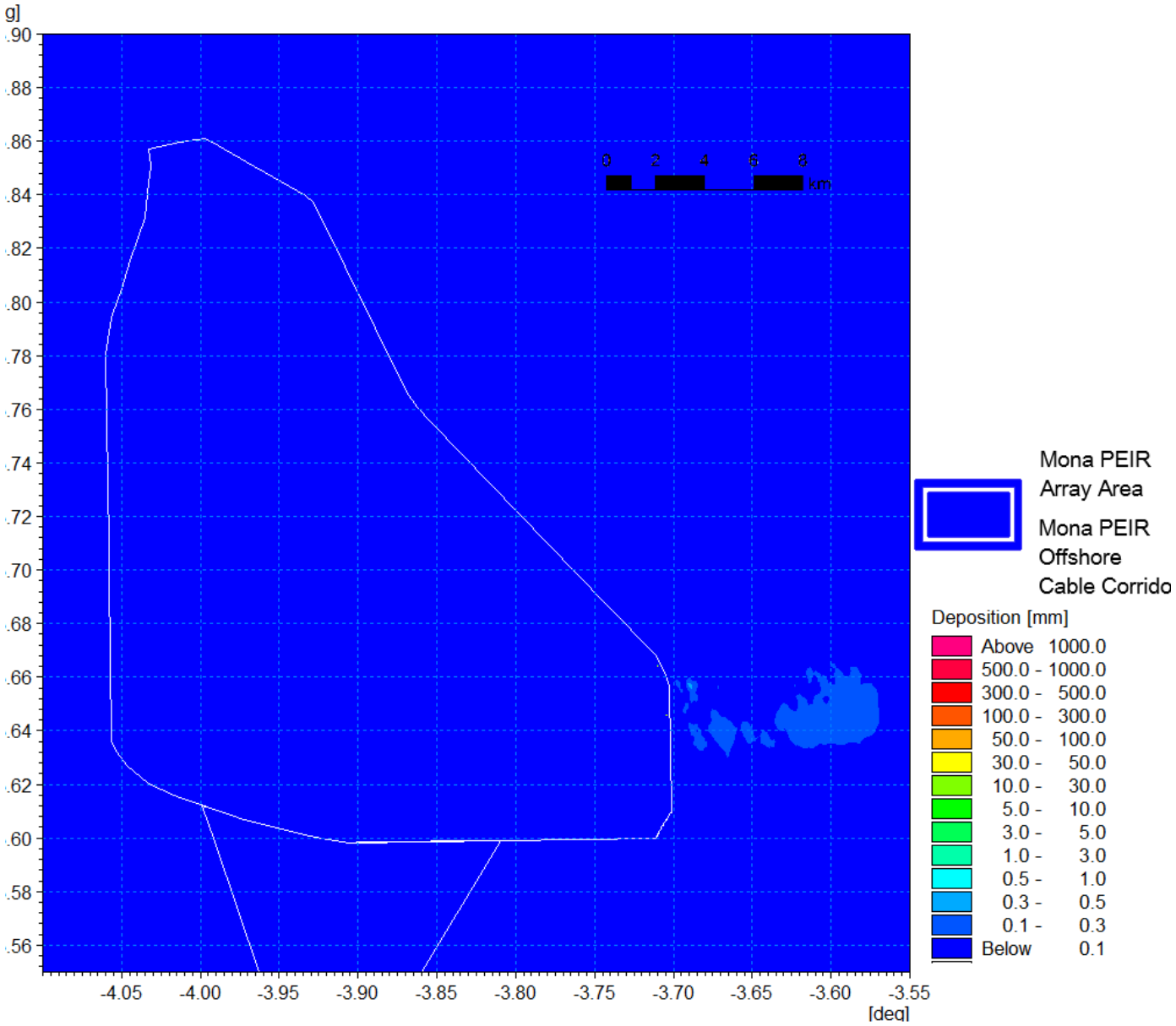

Figure 1.133: Sedimentation 1 day following cessation of pile installation – Pile scenario B detail view.

Piling scenario C

1.3.7.29 The piling locations are illustrated in Figure 1.134 and they are orientated normal to the tidal current to provide an augmented plume scenario under mean tidal currents. The sediment composition at this location comprised mixed sediments similar to those at scenario A as follows.

- Very coarse sand/gravel: 19%
- Coarse sand: 22%
- Medium sand: 46%
- Fine sand: 9%
- Very fine sand/mud: 4%.

1.3.7.30 The average plume envelope shown in Figure 1.135 has a similar extent to the circa 25 km shown in the spring tide scenario B; this is accounted for by the average tidal range coupled with the orientation of the releases. Average concentrations of circa 50 mg/l are evident where the plumes coalesce. This is similar to the unmerged values as the plumes are travelling in concert with the tide (and not towards one another) and at the point that the plume reaches the adjacent discharge it is highly dispersed.

1.3.7.31 The suspended sediments for peak flood and ebb tides on the first day are shown in Figure 1.136 and Figure 1.137 respectively. At the centre of the plume envelope peak values are circa 50 mg/l. The plots for day three tides (Figure 1.138 and Figure 1.139) have been selected to illustrate the settlement and mobilisation patterns. With decreased current speed, sediment concentrations reduce as material settles and, as current speed increase through the tidal cycle, settled material is mobilised and concentration increase once again. Under these circumstances peak concentrations are <30 mg/l and average values are typically one tenth of this value, with the peaks centred on areas of remobilised material.

1.3.7.32 The accumulated deposition from the two operations is evident in the sedimentation plots Figure 1.140 to Figure 1.143. As with scenario A, the coarser material is retained at the site of the operation with a similar maximum depth of 300 mm. However, the material carried to the east on the residual current is circa twice the depth at 3 mm. Once again, the formulation of sand ripples is evident. As noted previously, this is native material from the sediment cells and would be entrained into the baseline sediment transport patterns.

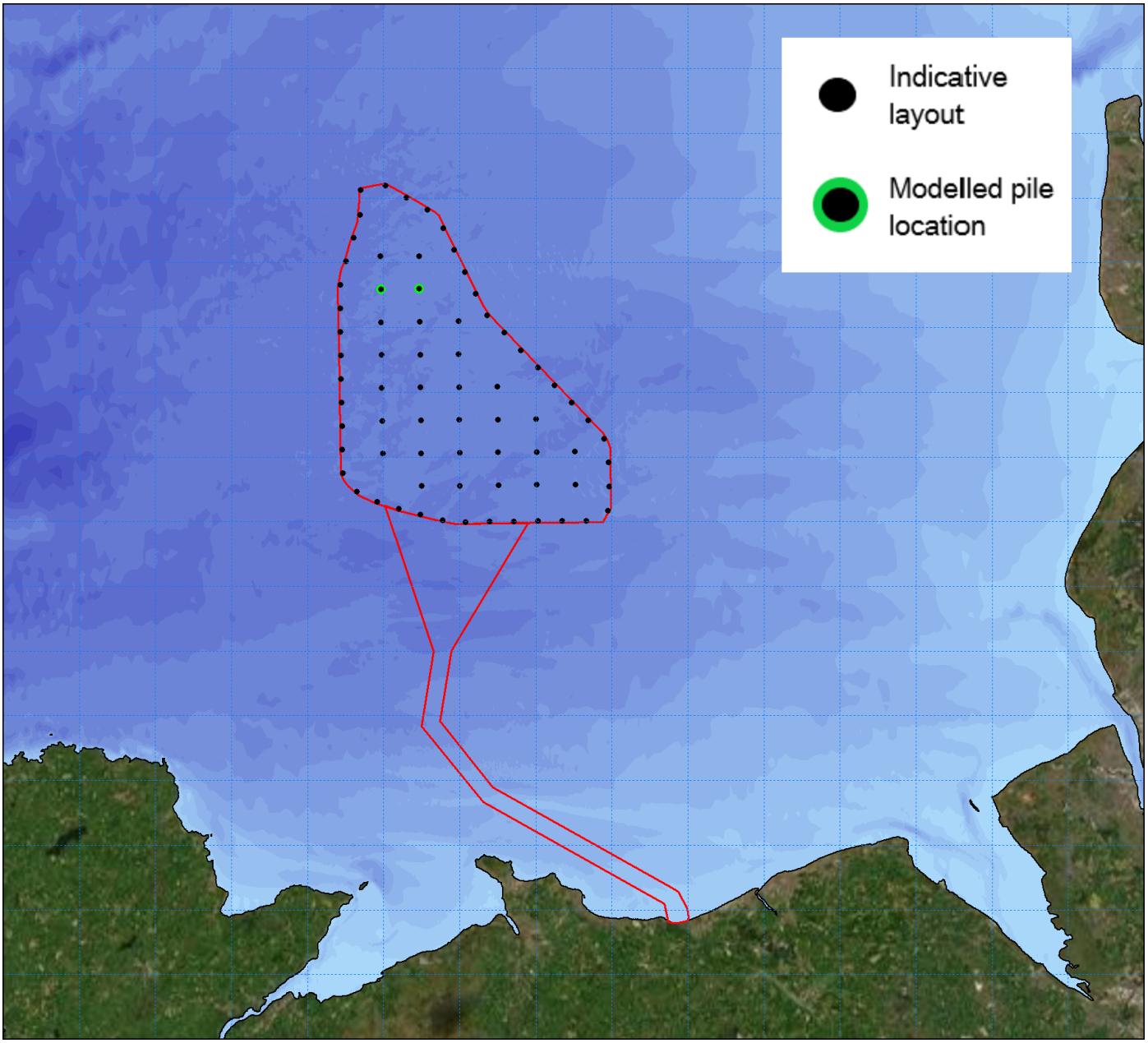

Figure 1.134: Location of modelled piled installation for piling – PEIR scenario C.

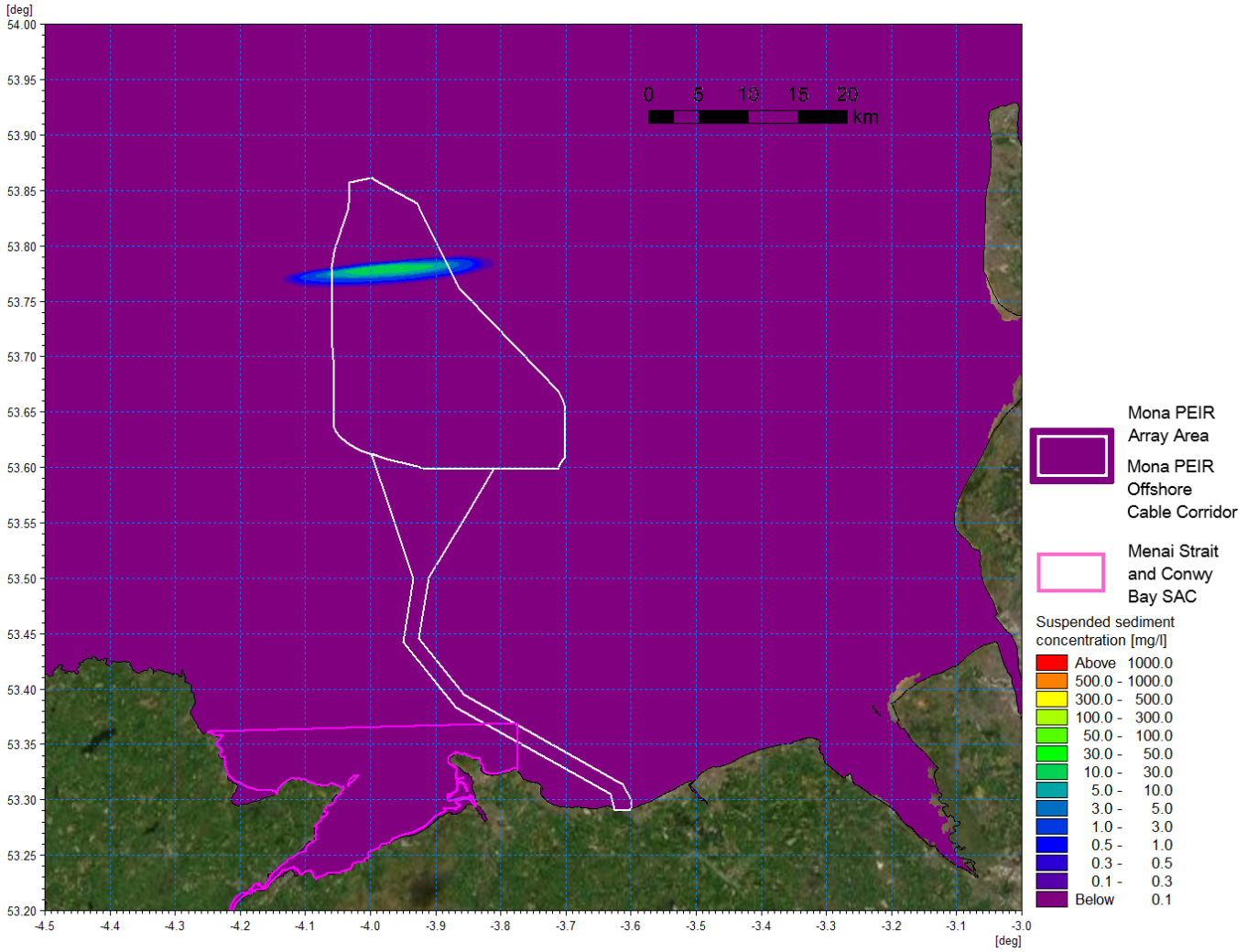

Figure 1.135: Average suspended sediment concentration – pile installation scenario C.

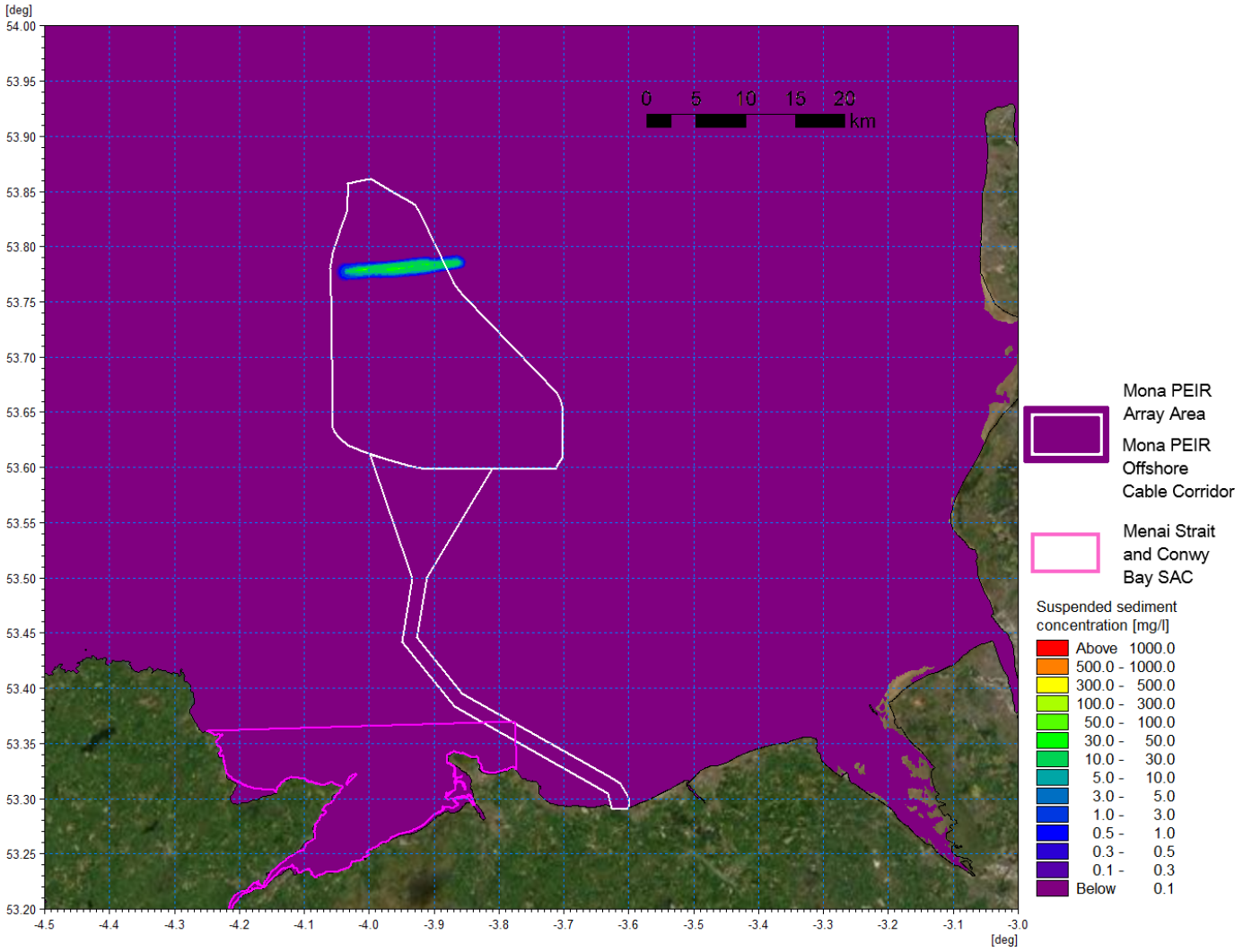

Figure 1.136: Suspended sediment concentration day 1 flood – Pile Installation scenario C.

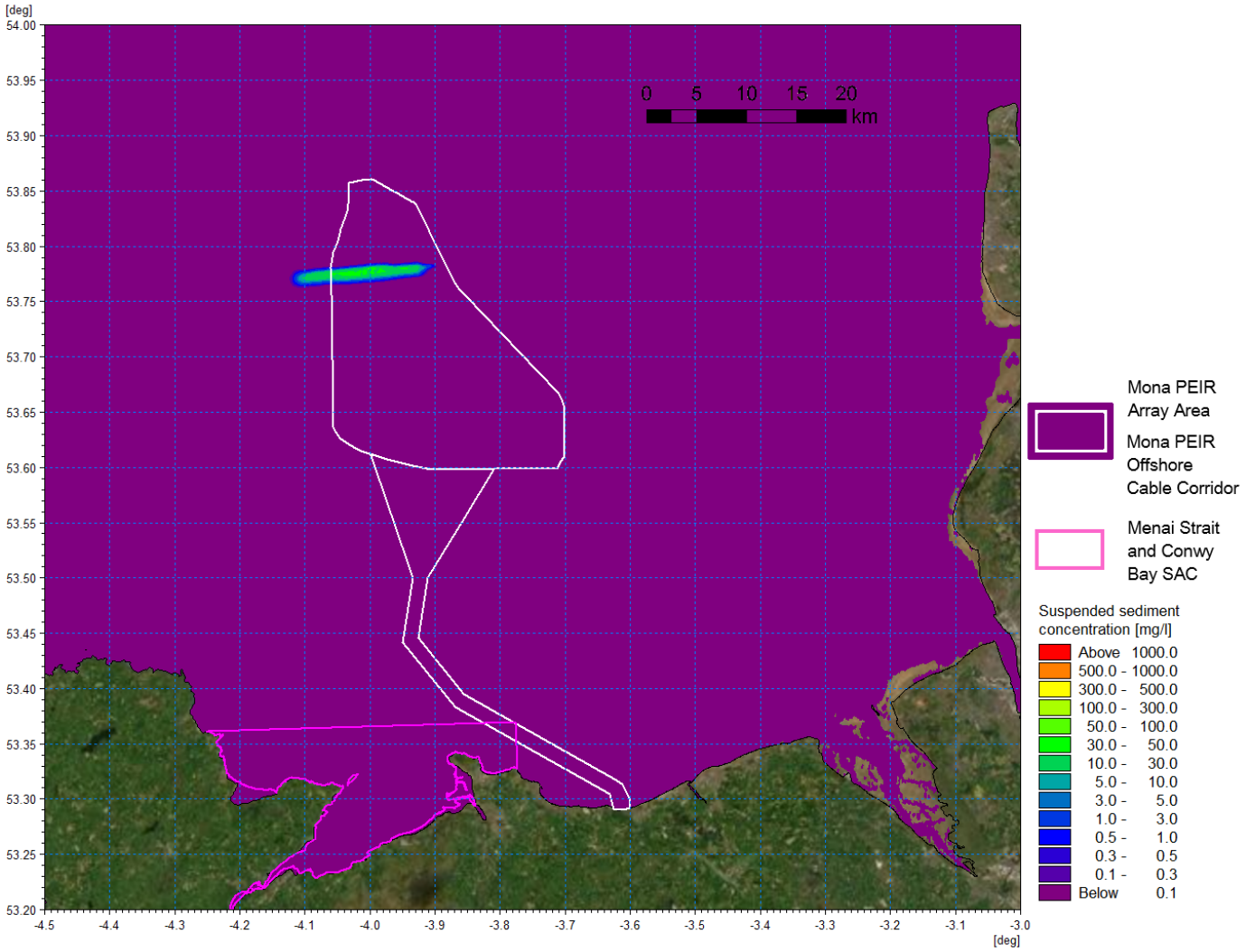

Figure 1.137: Suspended sediment concentration day 1 ebb – pile installation scenario C.

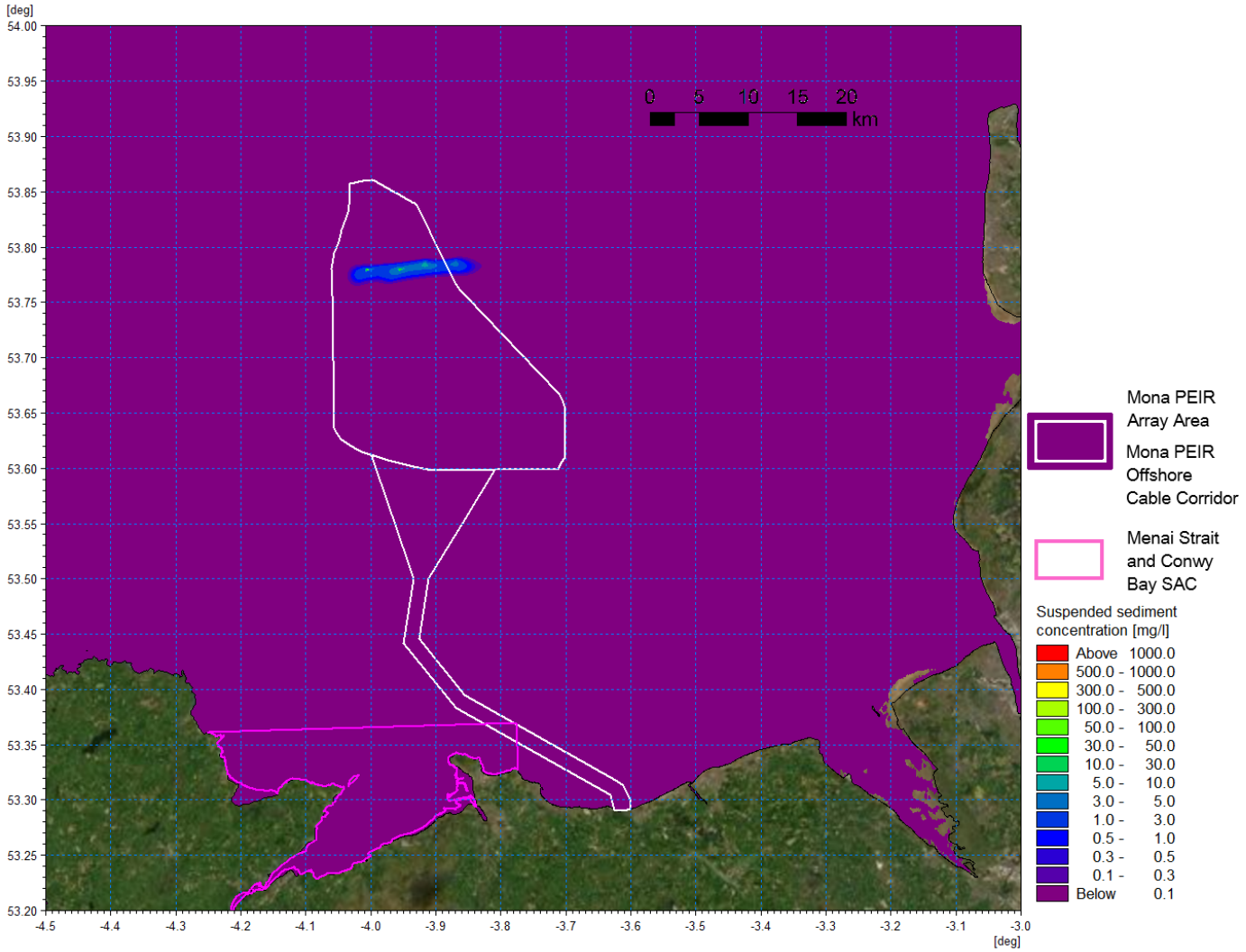

Figure 1.138: Suspended sediment concentration day 3 flood – pile installation scenario C.

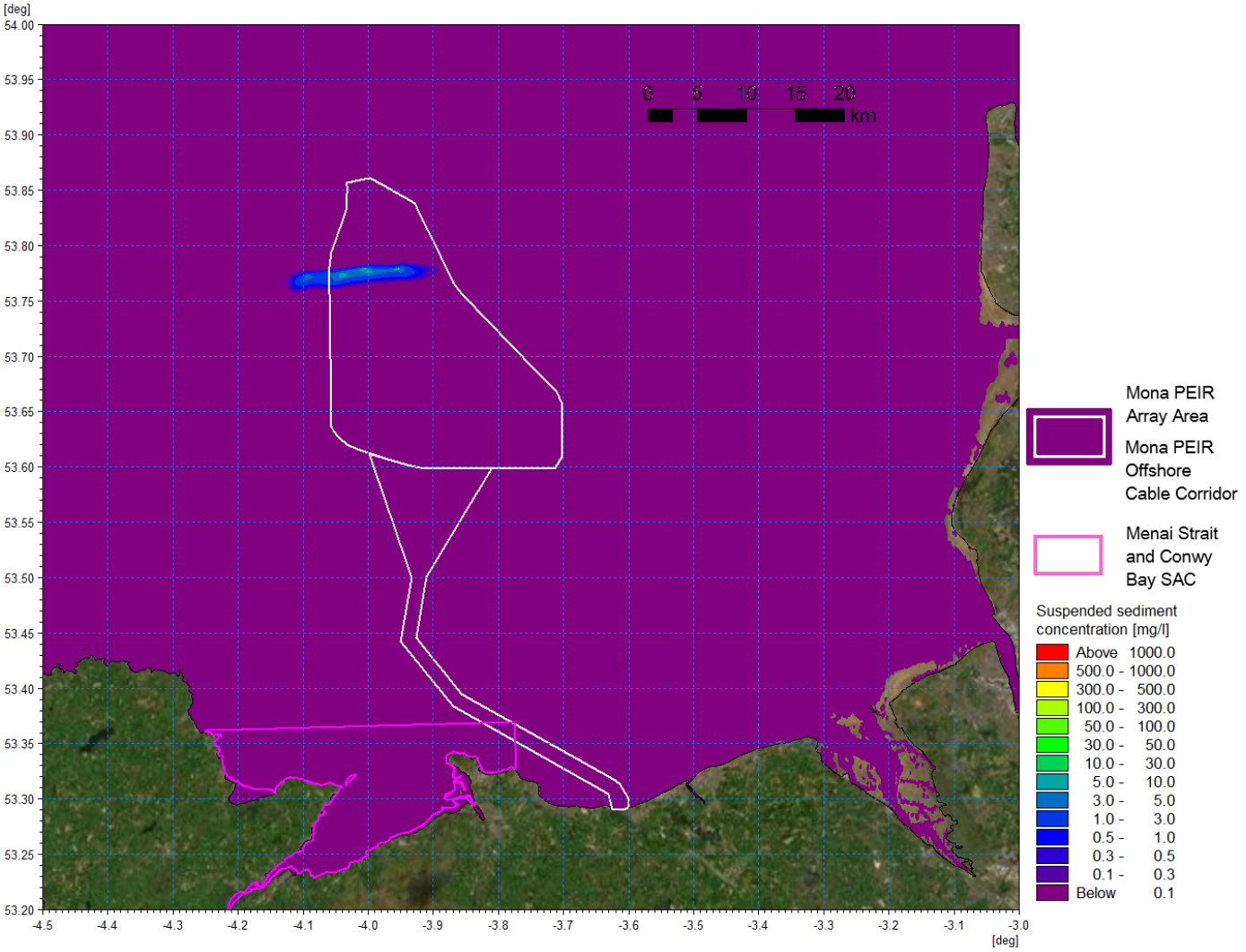

Figure 1.139: Suspended sediment concentration day 3 ebb – pile installation scenario C.

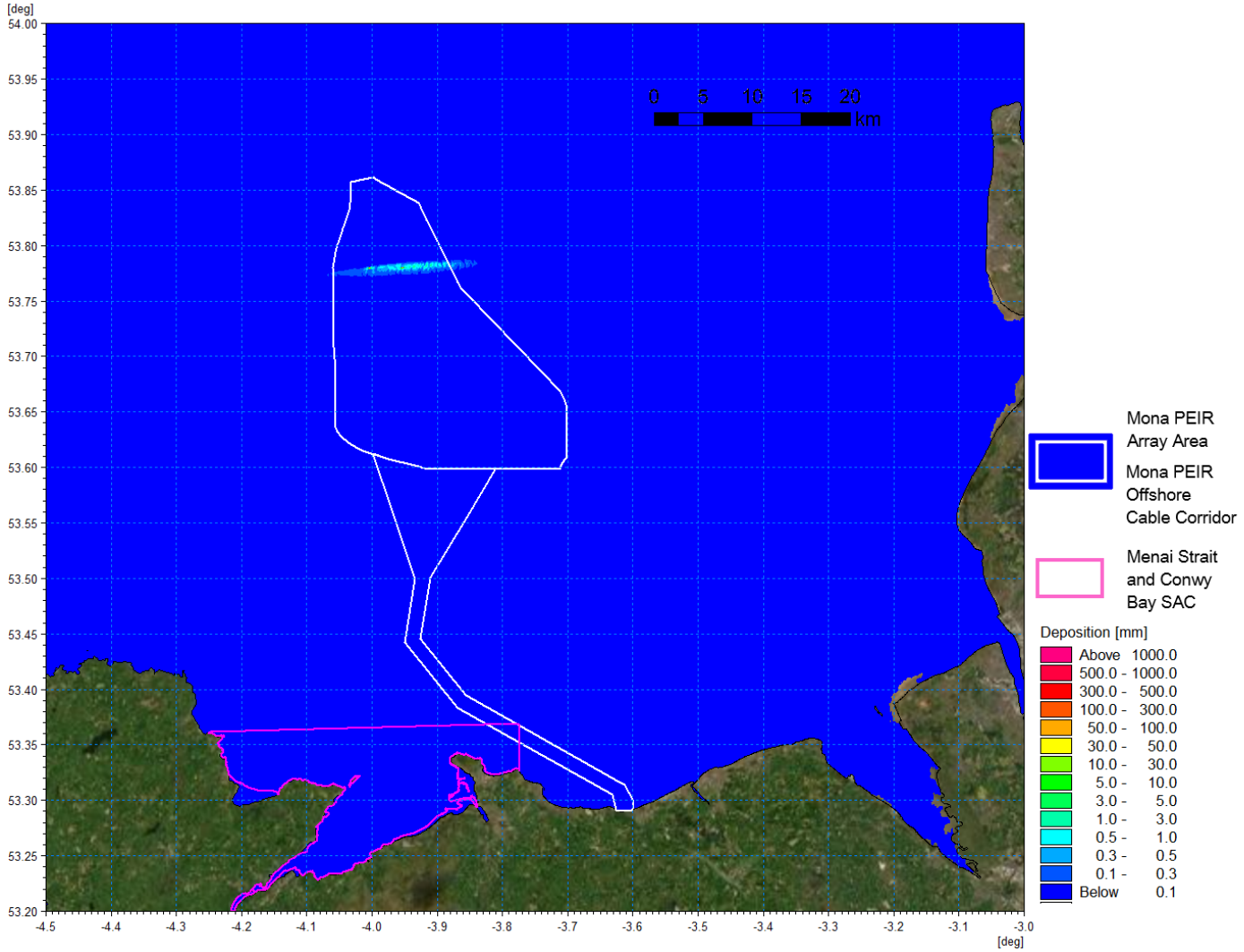

Figure 1.140: Average sedimentation during pile installation – scenario C.

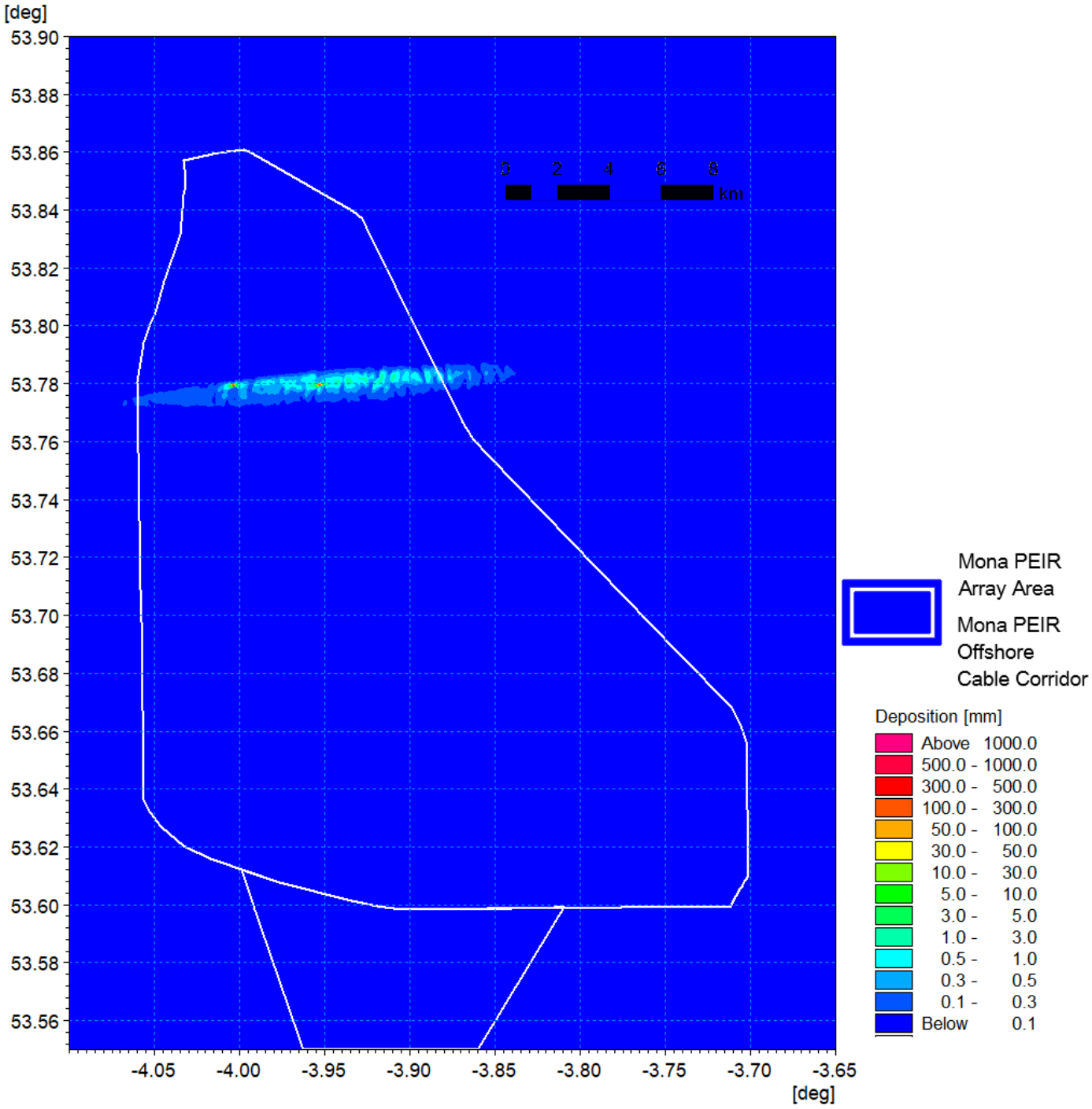

Figure 1.141: Average sedimentation during pile installation – scenario C detail view.

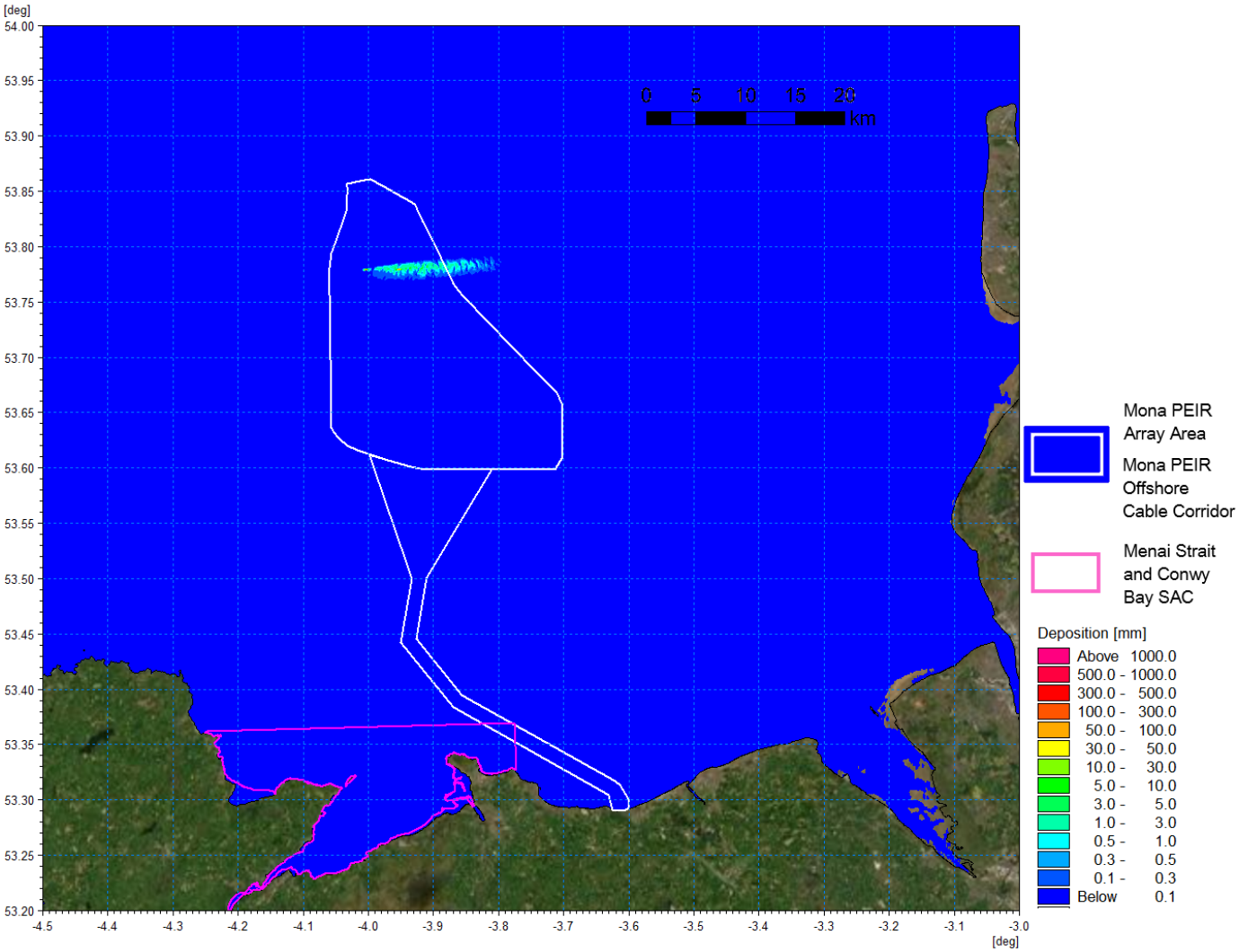

Figure 1.142: Sedimentation 1 day following cessation of pile installation – Pile scenario C.

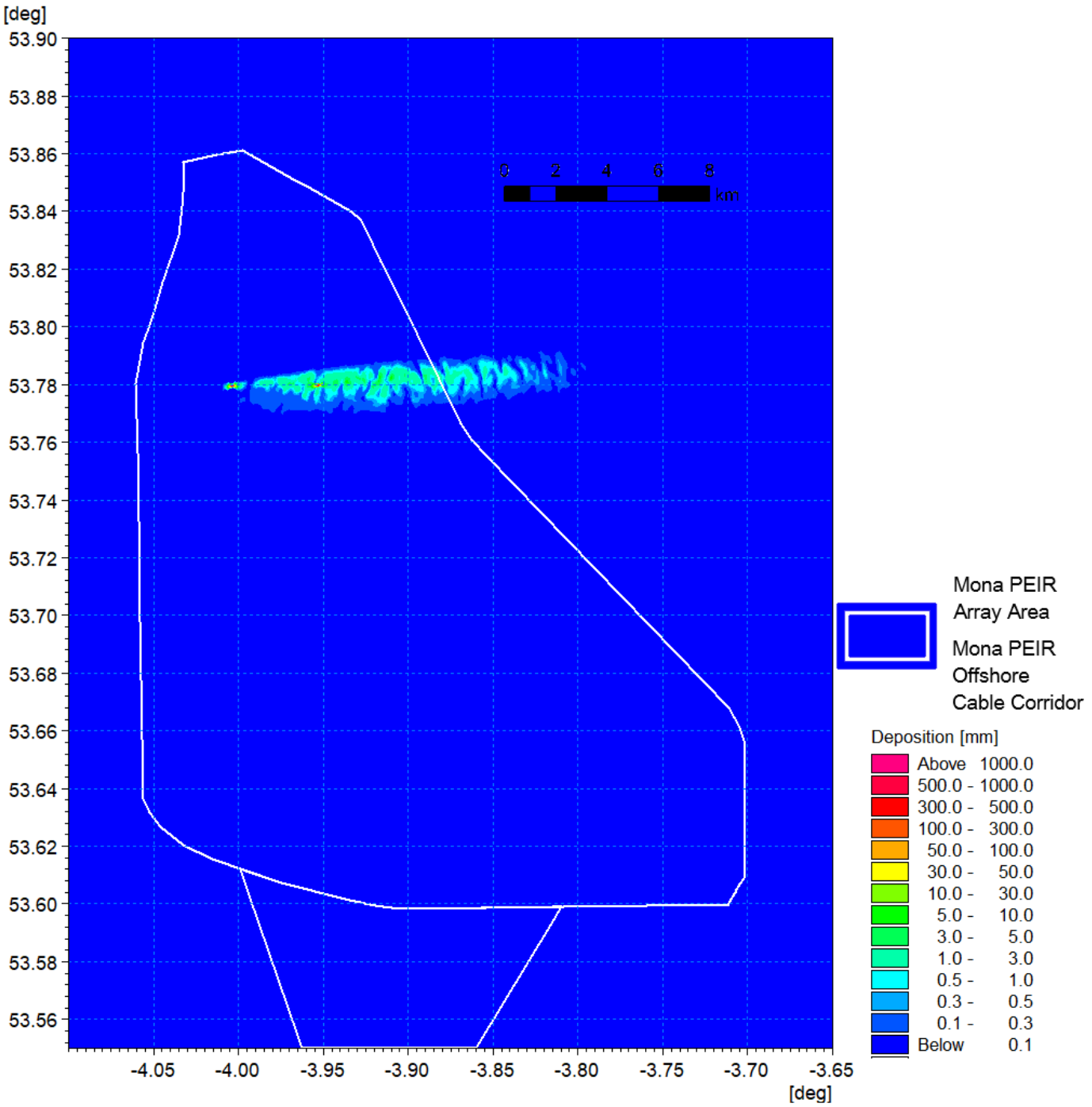

Figure 1.143: Sedimentation 1 day following cessation of pile installation – Pile scenario C detail view.

Cable installation

1.3.7.33 The third aspect of the construction phase is cable installation, including the inter-array cables, interconnector cables and export cables to shore. For the MDS in terms of release of sediment into the water column, cables were assumed to be trenched. A number of trenching techniques may be suited to the ground conditions; however it was assumed within the modelling that a trench of material of the maximum depth of 3 m as presented in the project description for the Mona Offshore Wind Project PEIR was mobilised into the lower water column as a result of the burial process, in line with

the Business Enterprise and Regulatory Reform (BERR) guidelines (BERR, 2008). In reality the final installation technique may result in less sediment being mobilised and the maximum depth may not always be achieved with a corresponding reduction in the amount of material disturbed.

1.3.7.34 Similar to the pile installation, the model simulations used the sediment grading determined from BGS sediment sampling data. However, the modelling was undertaken using the MIKE PT module. This module was implemented as it had the advantage that it could be used to describe the transport of material released in a specific part of the water column. In this way, the dispersion would not be over-estimated or the corresponding sedimentation under-estimated by the application of a current profile through the water column.

1.3.7.35 Trenching rates can vary widely depending on the bed material and equipment used; typically, rates are between 25 m/h and 780 m/h. For the simulation, a relatively high rate of 450 m/h was used over an extensive sample route ensuring that material was released at all tidal states over a number of tides and ensuring initial concentrations were not underestimated.

Inter-array/interconnector cables

1.3.7.36 Inter-array and interconnector cable installation will be undertaken along a number of paths which connect groups of turbines to a local hub (i.e. the OSP) or which connect two OSPs to each other. Each route would be undertaken as a separate operation and thus a single example has been selected to quantify the potential suspended sediment levels during the installation. Figure 1.144 shows an indicative wind turbine layout for the Mona PEIR Array Area with the modelled inter-array cable route shown in green. This route was run from the north of the site, perpendicular to the tidal flow, then in line with tidal flows in an easterly direction. This ensured that the full extent of the site and tidal conditions were incorporated into the simulation.

1.3.7.37 The inter-array cabling was undertaken along the indicated route with a trench 3 m wide at the bed and 3 m in depth with a triangular cross-section in accordance with a trenching plough. Thus circa 220,500 m^3 of material was mobilised during the 4 day simulation along the 49 km route. The sediment grading characteristics were derived from sediment sampling along the route and defined by the following sand fractions.

- Very coarse sand/gravel: 24%
- Coarse sand: 20%
- Medium sand: 35%
- Fine sand: 9%
- Very fine sand/mud: 12%.

1.3.7.38 The model results presented follow the same format as those for the piled foundation installation described in the previous section. Figure 1.145 shows the average suspended sediment concentration over the course of the trenching phase. It is clear that the sediment is dispersed on subsequent tides as the plume envelope illustrates the flood and ebb tidal excursions with peak values of 100 mg/l to 300 mg/l.

1.3.7.39 Figure 1.146 to Figure 1.151 shows the suspended sediment patterns over the course of this operation, day two, three and four mid flood and ebb tides respectively. The volume of material mobilised is relatively large, and elevated tidal currents disperse the material giving rise to concentrations of up to 500 mg/l. As was evident in the previous operations, the material settles during slack water and then is re-suspended

to form a secondary plume which becomes amalgamated. This is further illustrated in Figure 1.152 and Figure 1.153 which show the average sedimentation and the sedimentation one day following cessation at slack water. The sedimentation is greatest at the location of the trenching and may be up to 30 mm in depth where the coarser material has settled within close proximity, circa 100 m. The depths reduce significantly with distance to <0.5 mm which is indicated by the use of a log scale in all figures. Although the material is dispersed, it remains within the sediment cell and is therefore retained within the transport system.

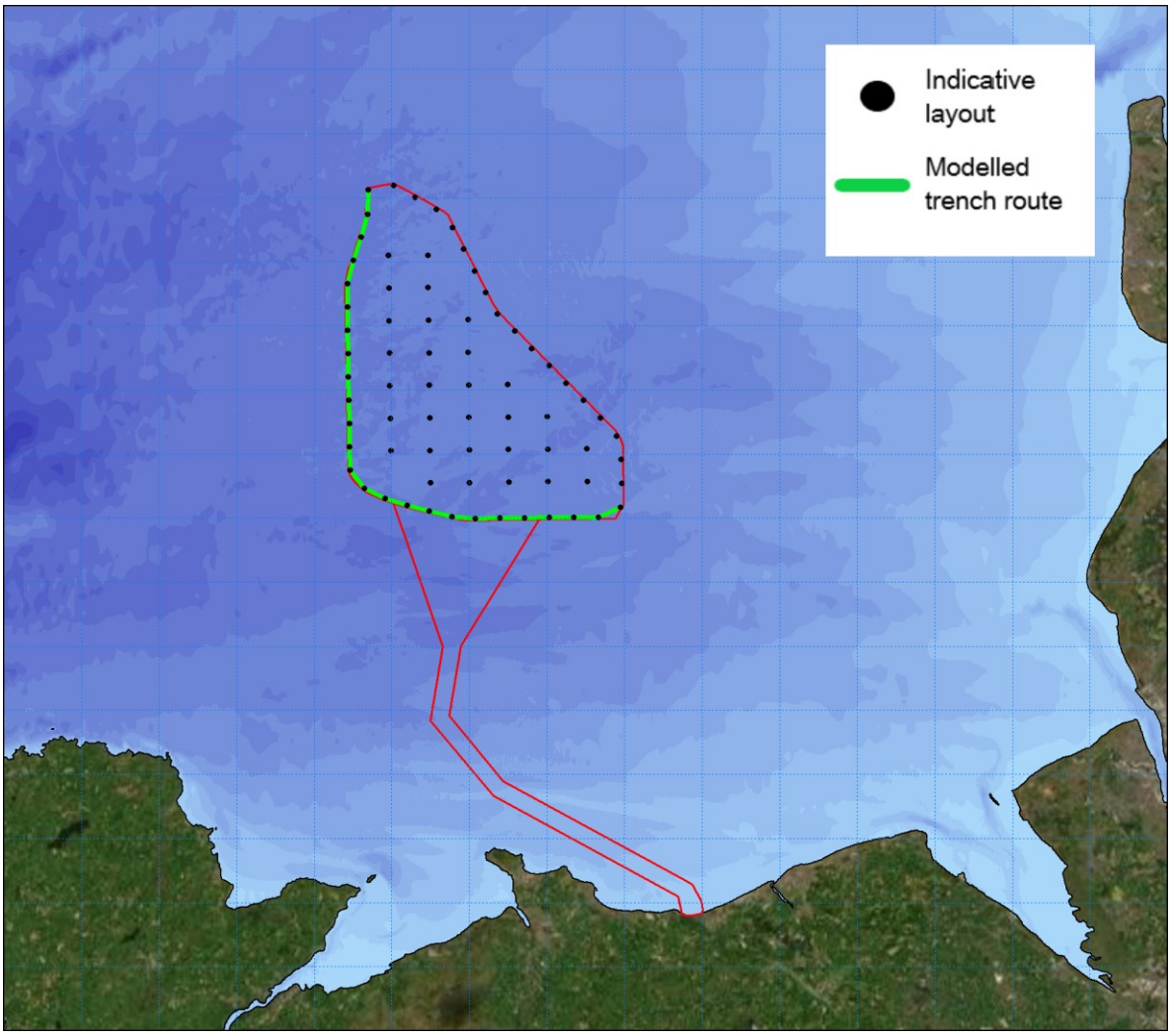

Figure 1.144: Modelled inter-array cable route for PEIR.

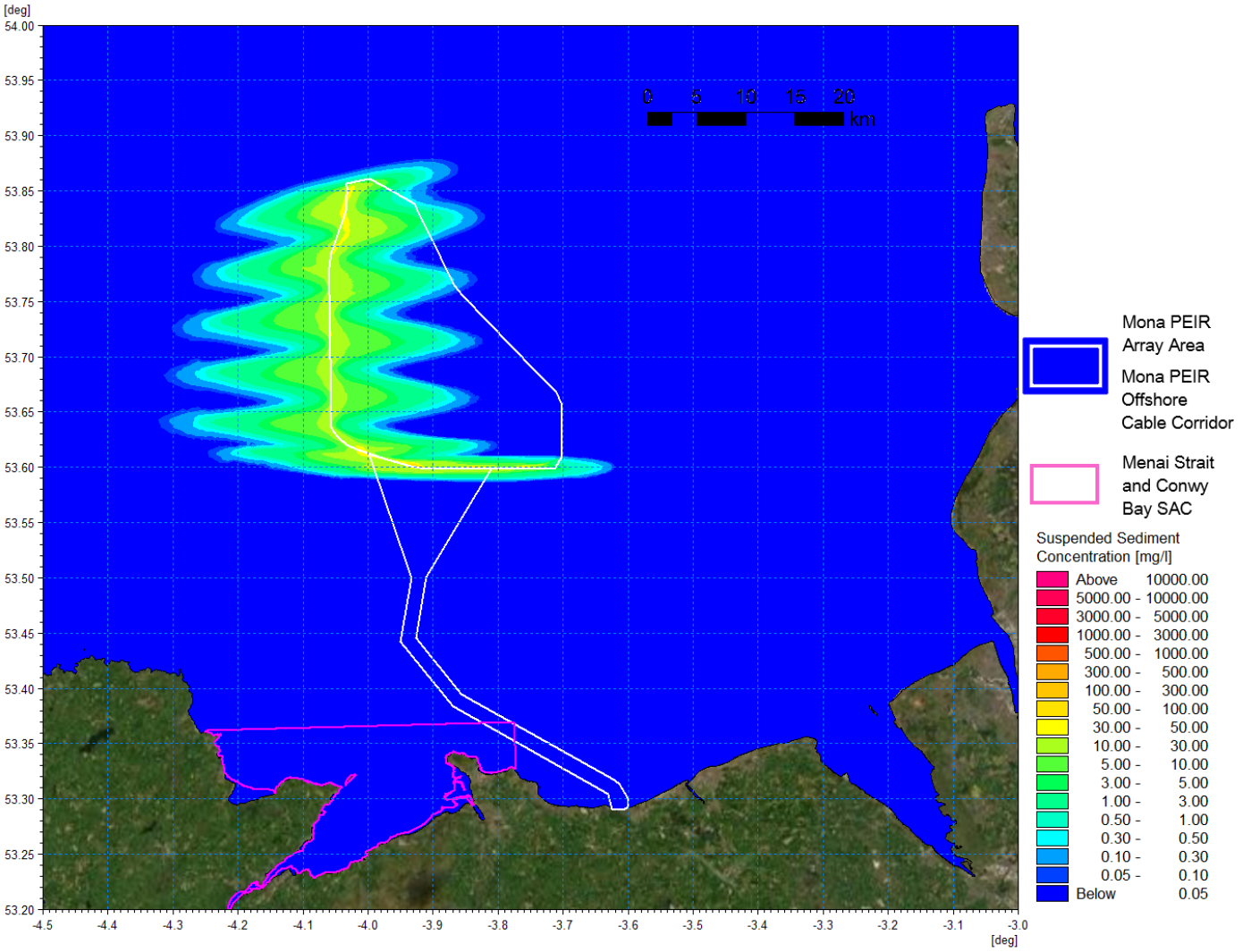

Figure 1.145: Average suspended sediment concentration during inter-array cable trenching.

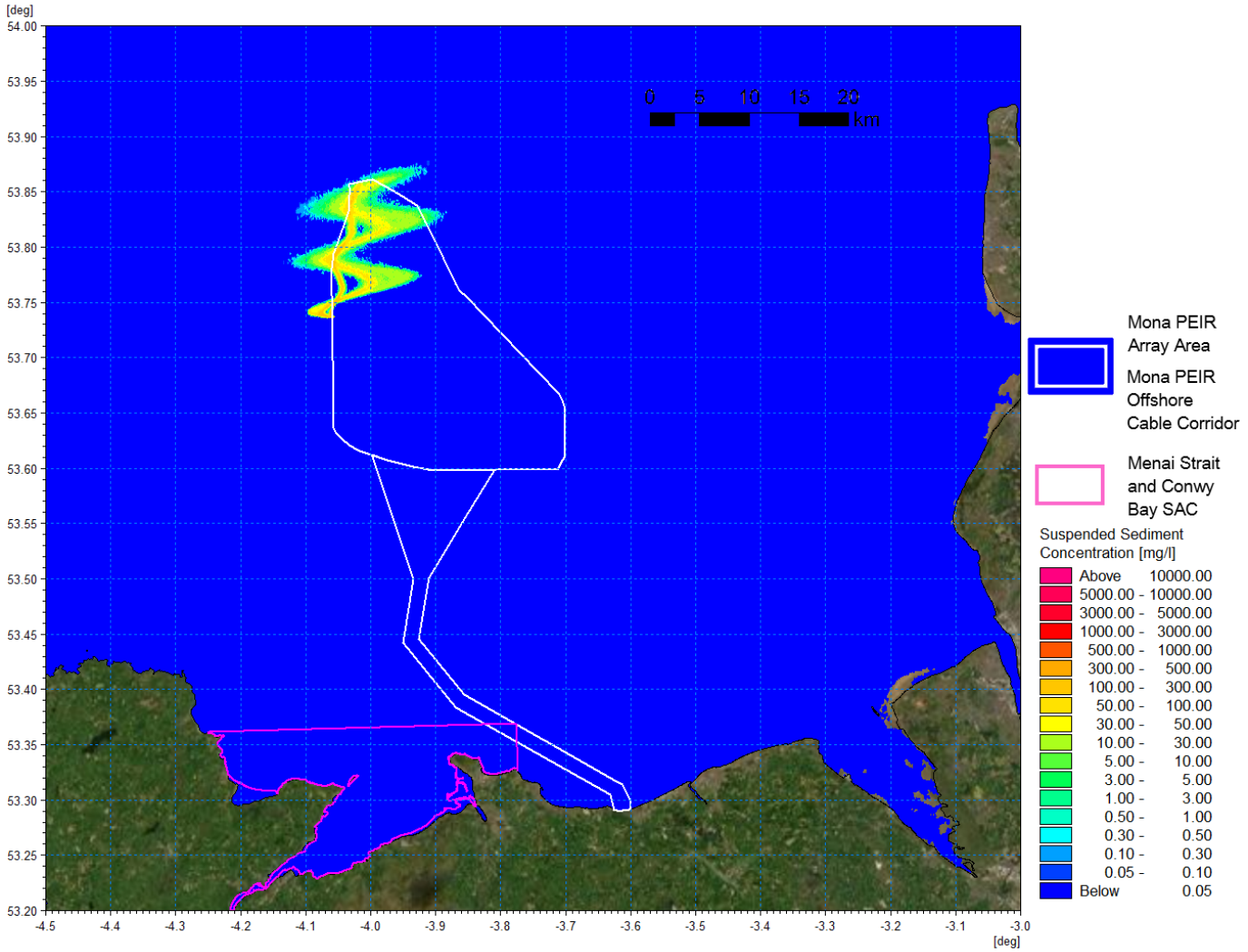

Figure 1.146: Suspended sediment concentration day 2 flood – inter-array cable installation.

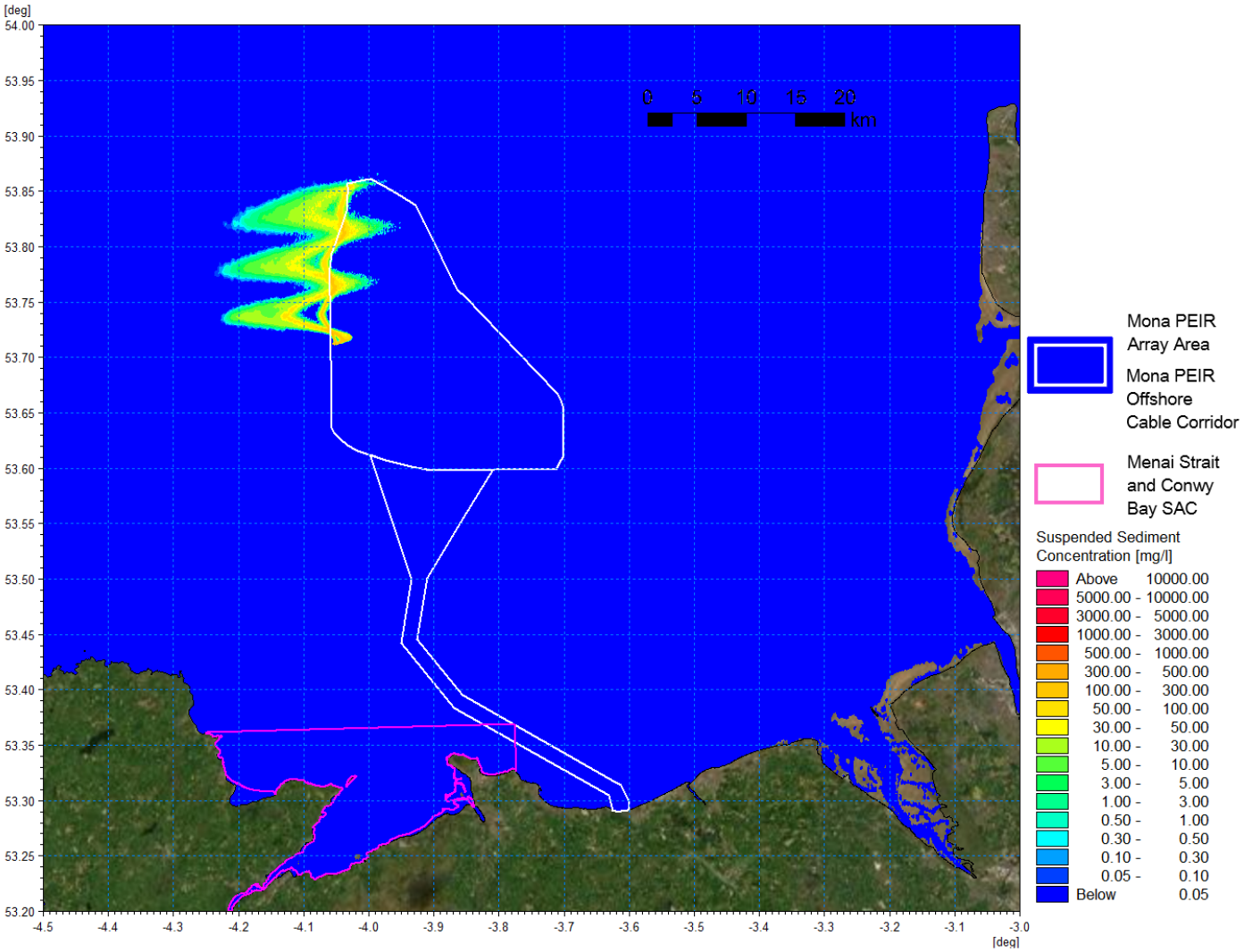

Figure 1.147: Suspended sediment concentration day 2 ebb – inter-array cable installation.

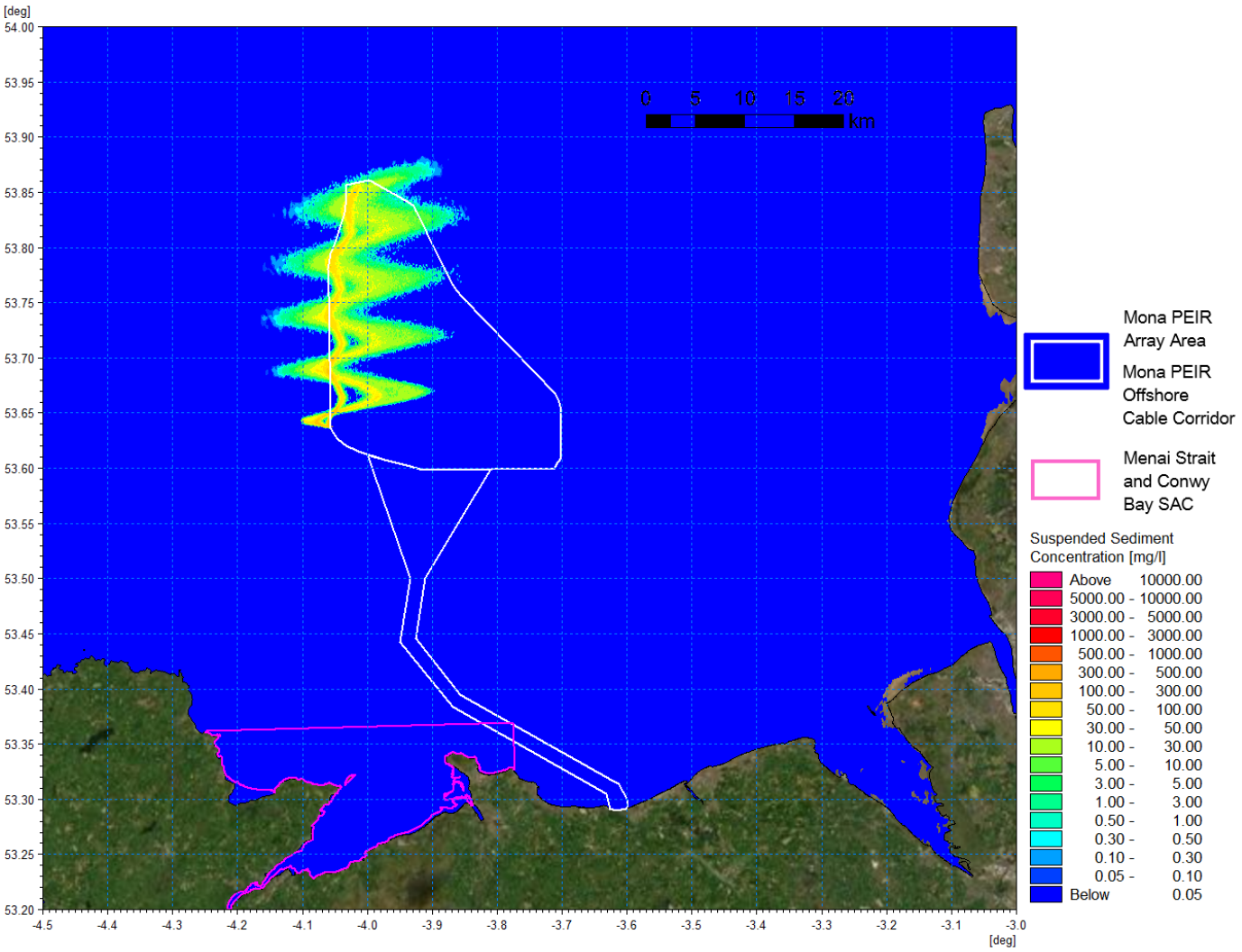

Figure 1.148: Suspended sediment concentration day 3 flood – inter-array cable installation.

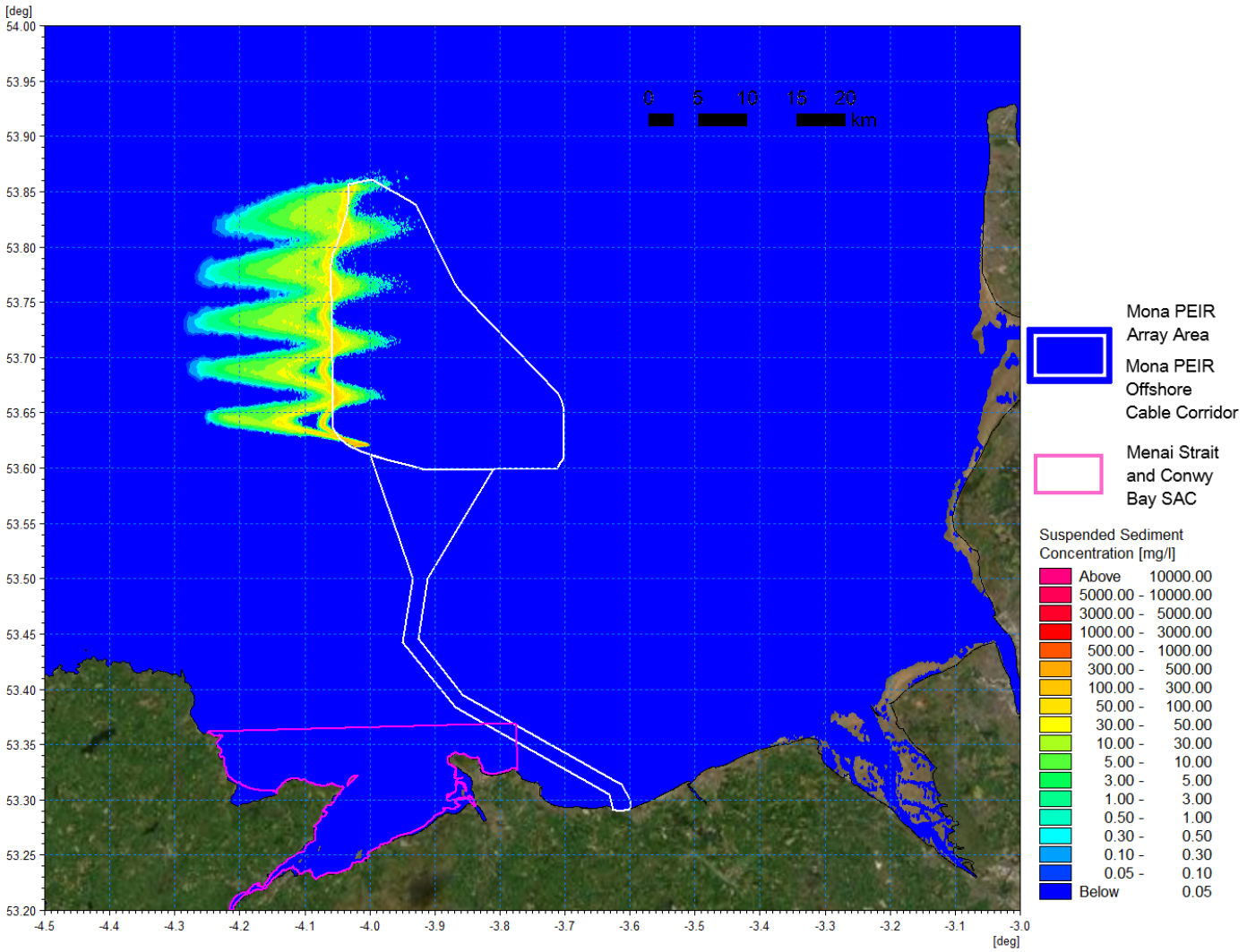

Figure 1.149: Suspended sediment concentration day 3 ebb – inter-array cable installation.

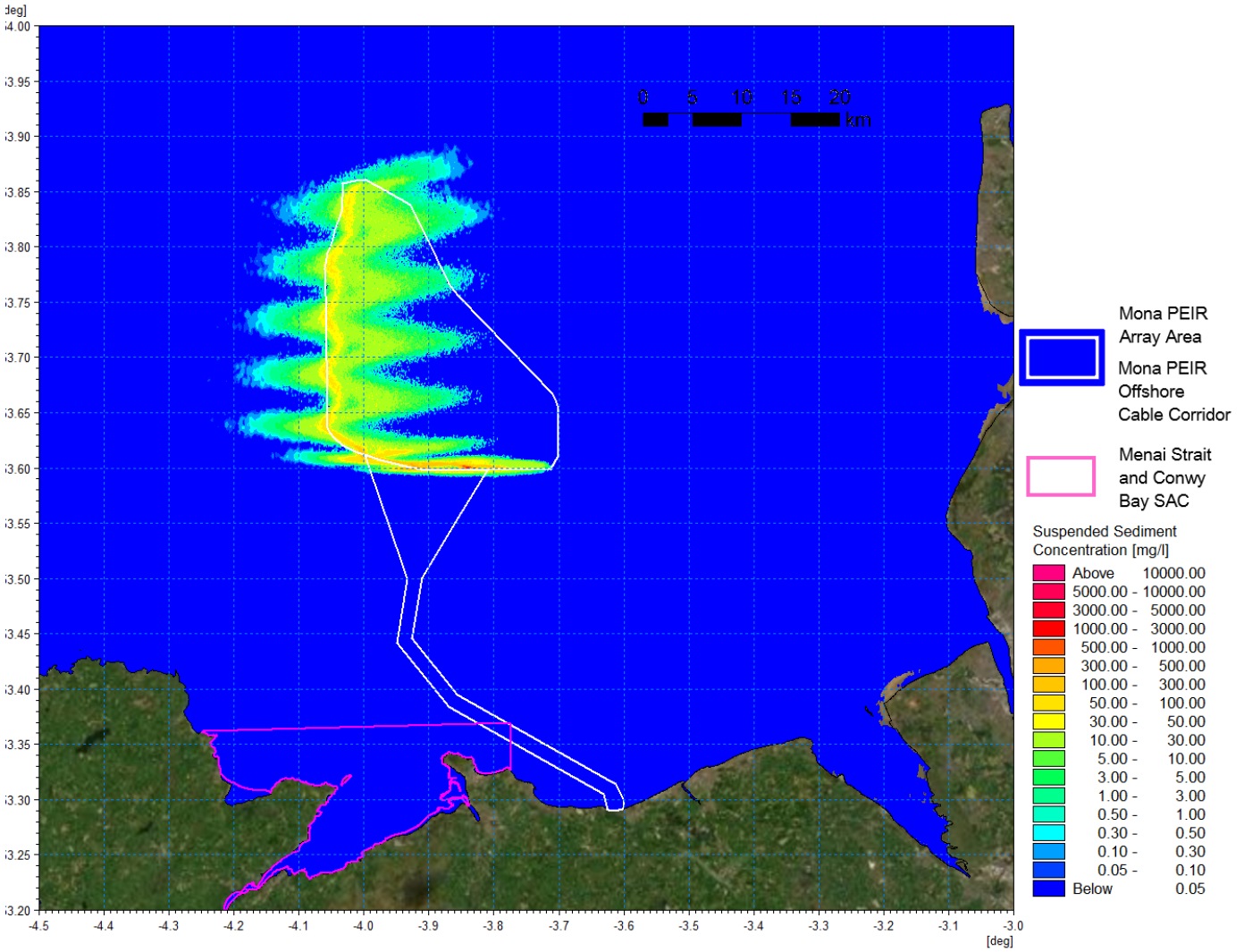

Figure 1.150: Suspended sediment concentration day 4 flood – inter-array cable installation.

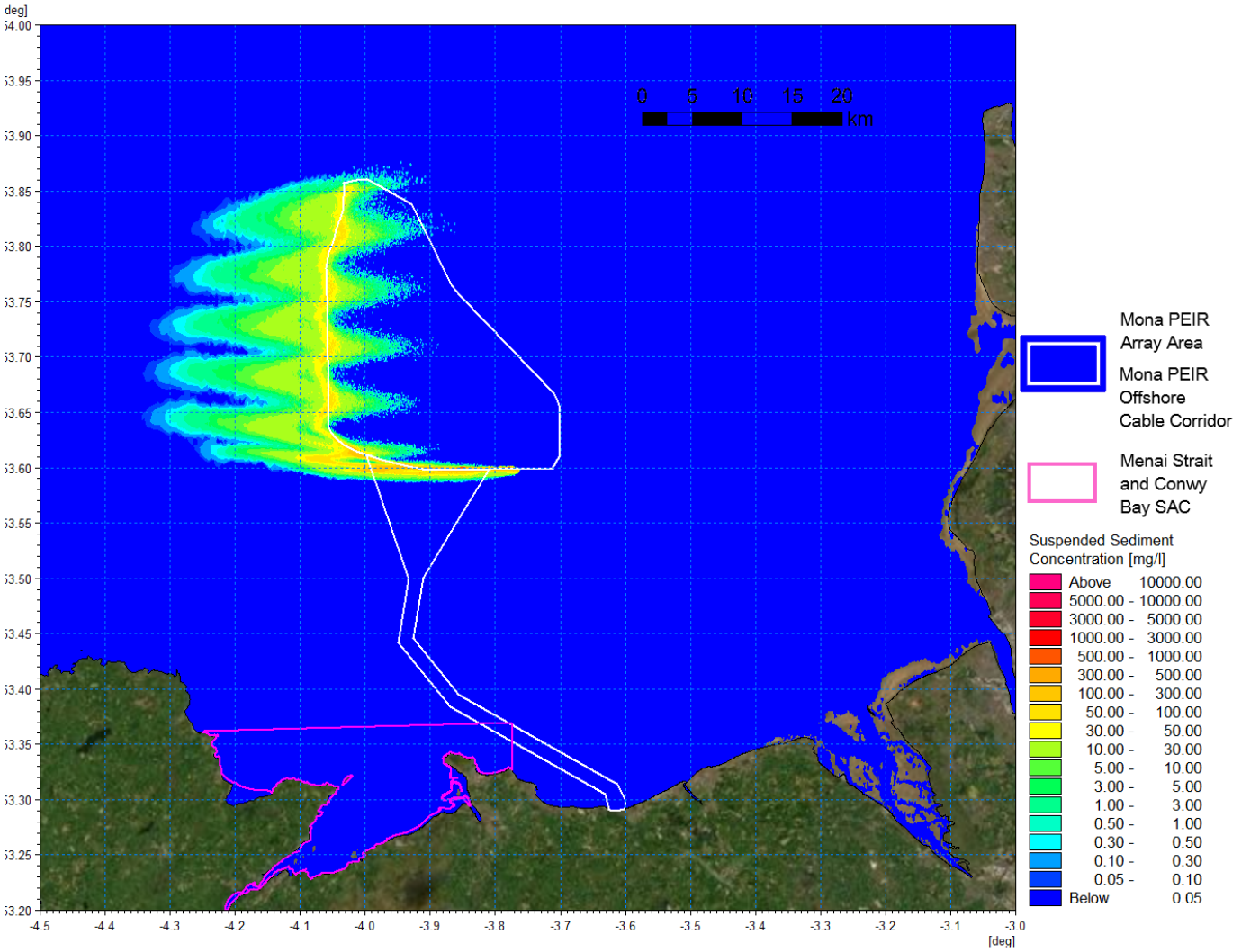

Figure 1.151: Suspended sediment concentration day 4 ebb – inter-array cable installation.

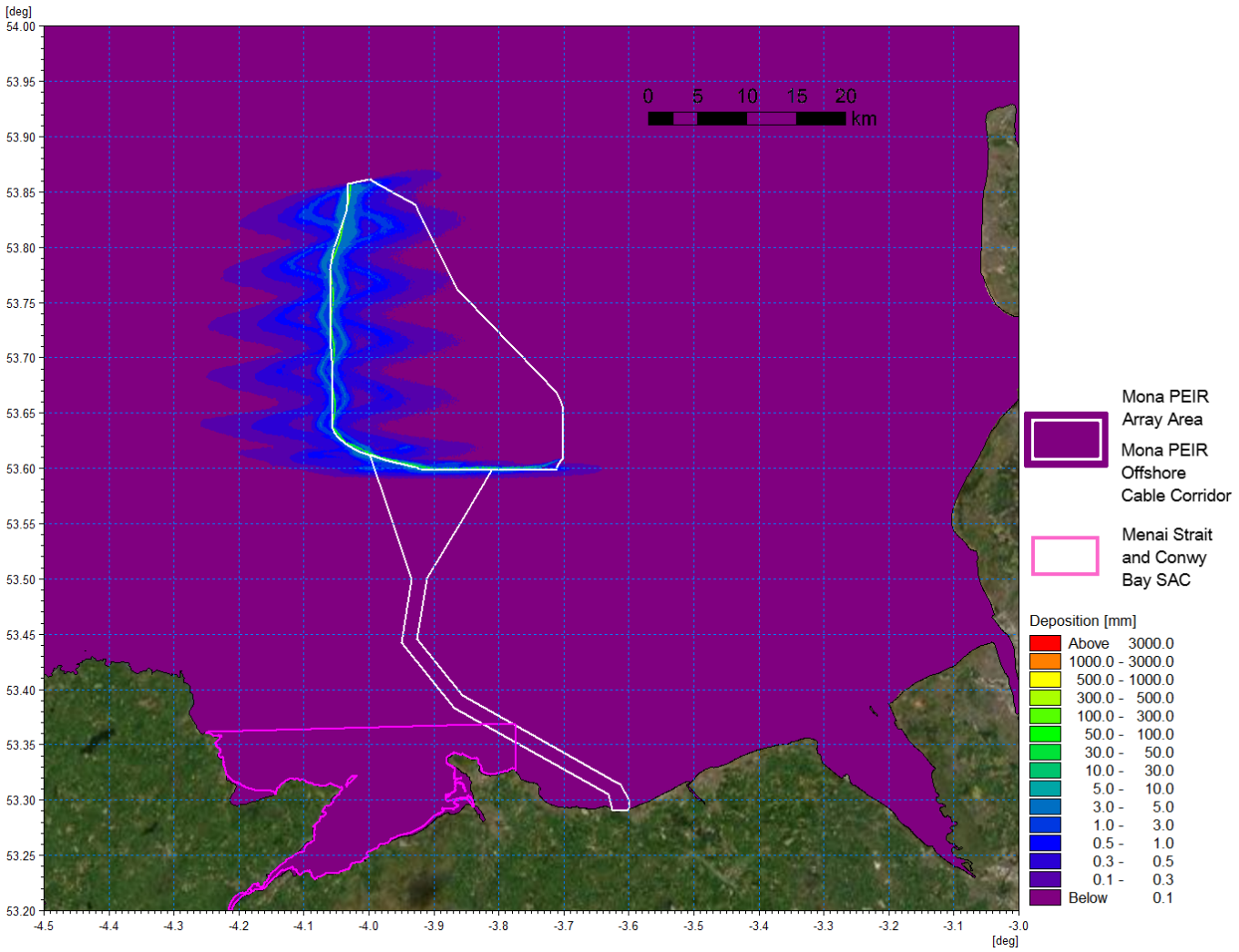

Figure 1.152: Average sedimentation during inter-array cable installation.

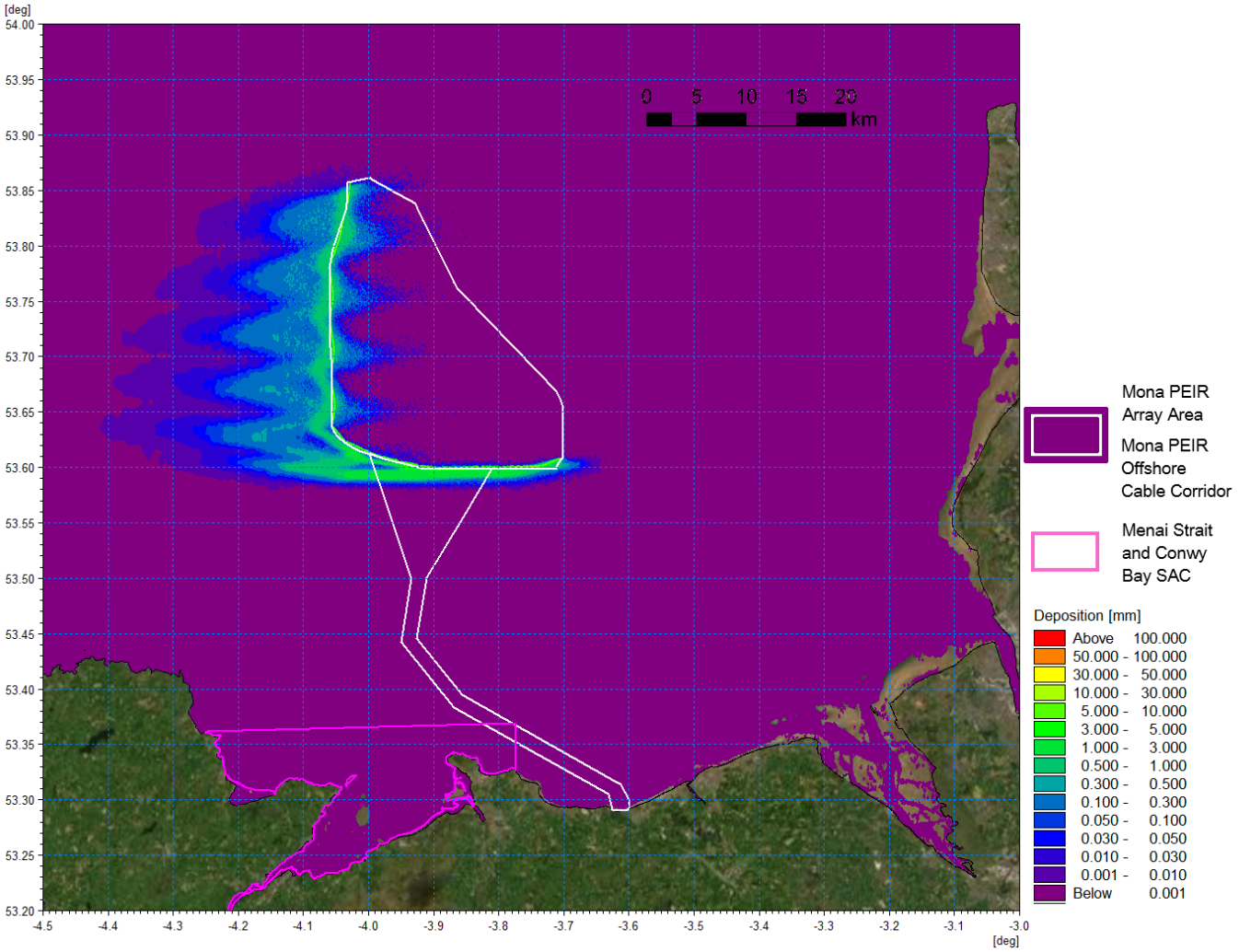

Figure 1.153: Sedimentation 1 day following cessation of inter-array cable installation.

Offshore export cables

1.3.7.40 The Mona PEIR Offshore Cable Corridor and Access Areas were examined using numerical modelling. The simulation assumed the same trenching rate as with the inter-array cables, (i.e. 450 m/h), and that installation began from offshore and continued to the nearshore region of a trenchless landfall. Each trench was 3 m at the surface extending to a depth of 3 m, (i.e. the greatest burial depth proposed), with a triangular profile. The operation took approximately 4 days to complete encompassing a range of tidal conditions and mobilised 206,550 m^3 of material. The composition was determined from the sampling data and was of generally slightly more finely graded material than the inter-array route material.

- Very coarse sand/gravel: 20%
- Coarse sand: 10%
- Medium sand: 35%
- Fine sand: 30%
- Very fine sand/mud: 5%.

1.3.7.41 The trenching route modelled is illustrated by the green trace in Figure 1.154 and the average suspended sediment plume during the course of the operation is shown in Figure 1.155. The figure shows how the plume travels east and west on the tide as the release progresses along the route perpendicular to the tidal flow. This gives rise to average suspended sediment concentrations <50 mg/l offshore rising to 300 mg/l nearshore as the water depth decreases. The extent of Constable Bank has been overlaid in black to provide context.

1.3.7.42 The instantaneous suspended sediment concentrations for mid flood and ebb tides are presented for day two, day three and day four in Figure 1.156 to Figure 1.161 respectively. They show increases where sediment is released at the cable location but also at the extent of each tidal cycle as material is re-suspended. The plume travels east and west on the tide as the release progresses along the route perpendicular to the tidal flow and sediment concentrations reduce to background levels on slack tides. Suspended sediment concentrations along the route range between 50 mg/l and 1,000 mg/l where the greatest levels are located at the source of the sediment release in the shallowest water.

1.3.7.43 Finally, Figure 1.162 shows the average sedimentation whilst Figure 1.163 illustrates sedimentation levels one day following cessation of the sediment release. Tidal patterns indicate that although the released material migrates both east and west by settling and being re-suspended on successive tides, the sedimentation level is small typically <0.5 mm and the greatest levels of deposition occur along the trenching route as coarser material settles. Although the material is widely dispersed, sediment remains within the cell and would be drawn into the baseline transport regime with small increases in bed sediment levels. It is noted that due to the nature of the tidal flow mobilised sediment is carried offshore and does not accumulate along the coastline.

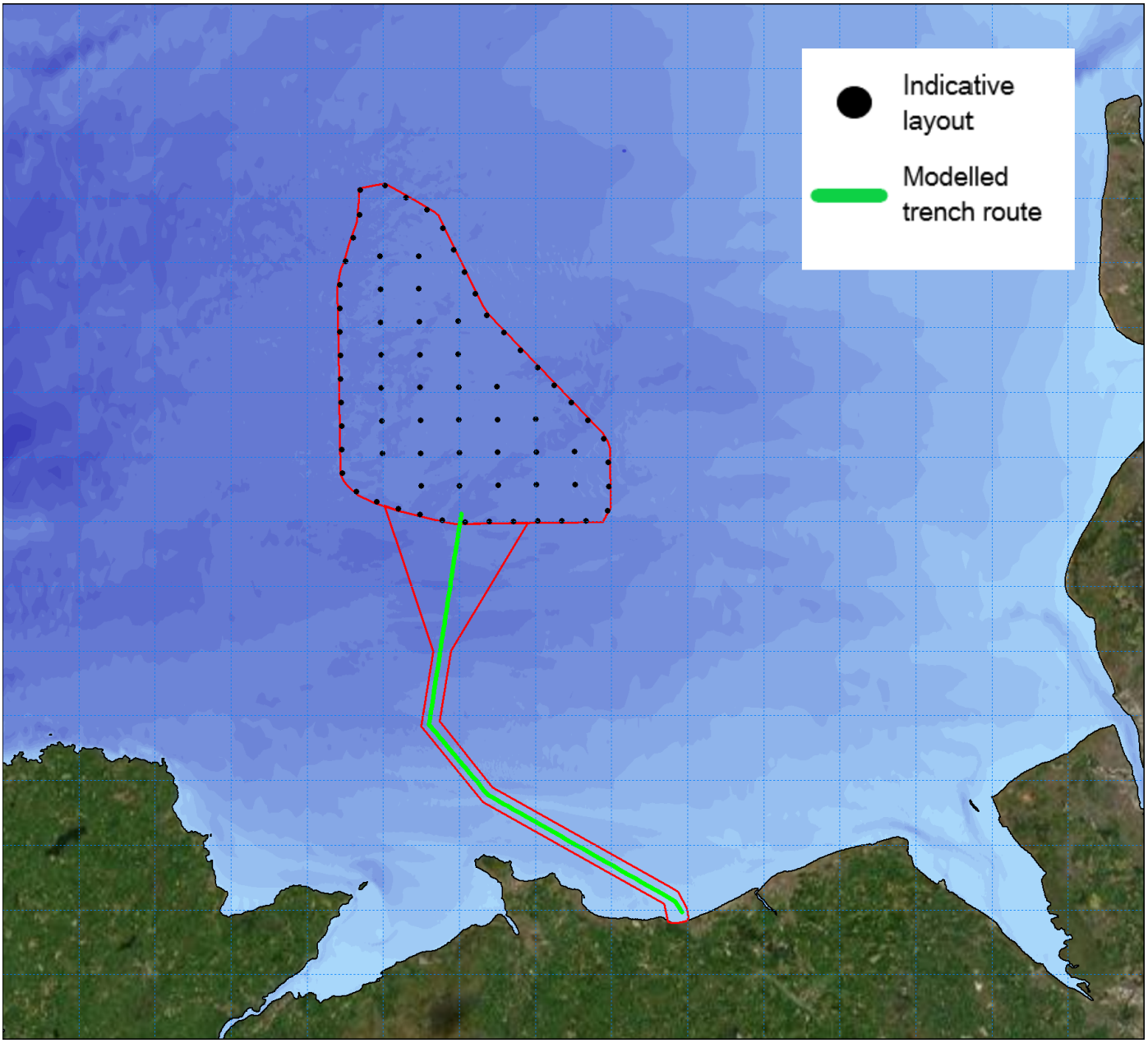

Figure 1.154: Modelled export cable route for PEIR.

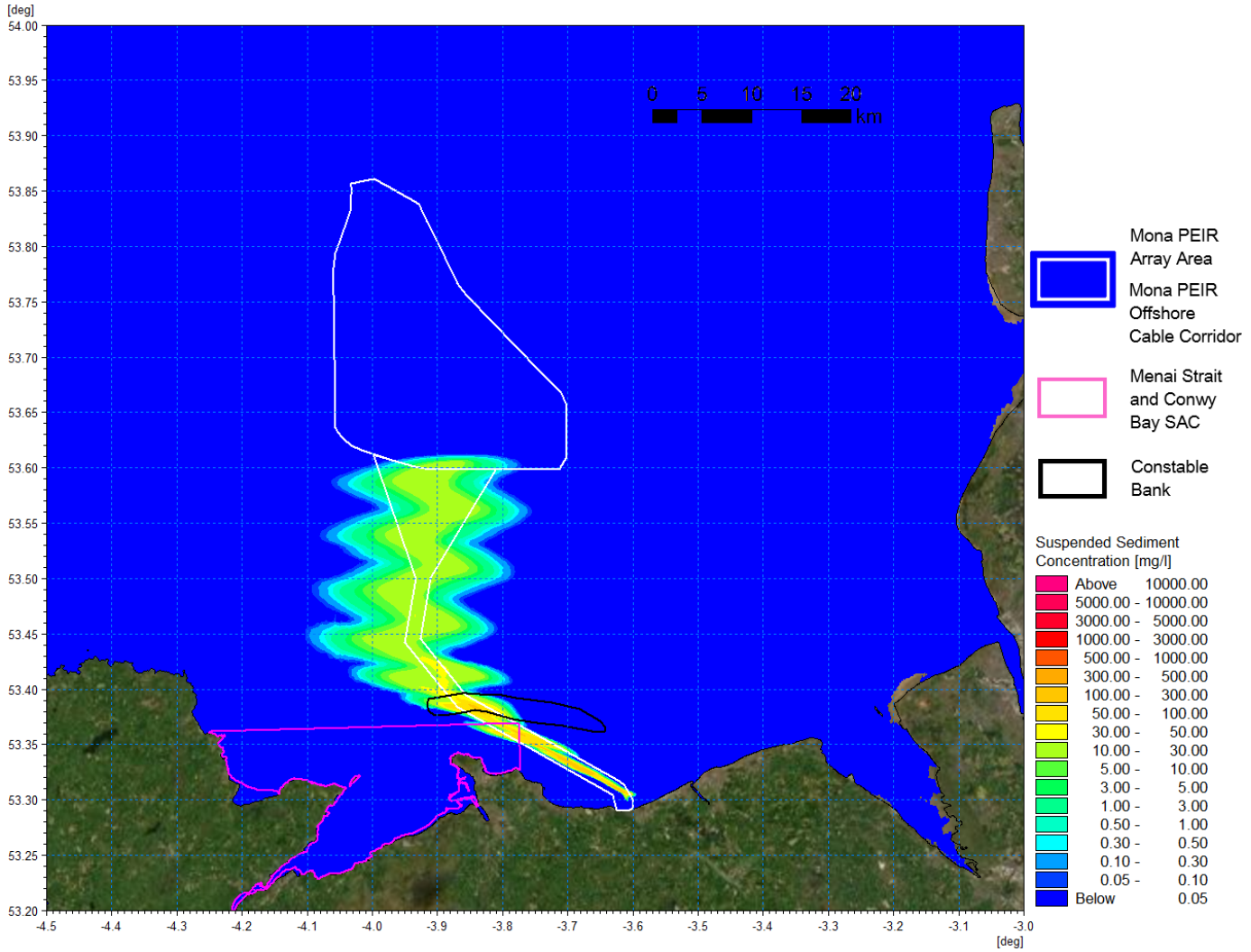

Figure 1.155: Average suspended sediment concentration during offshore export cable trenching.

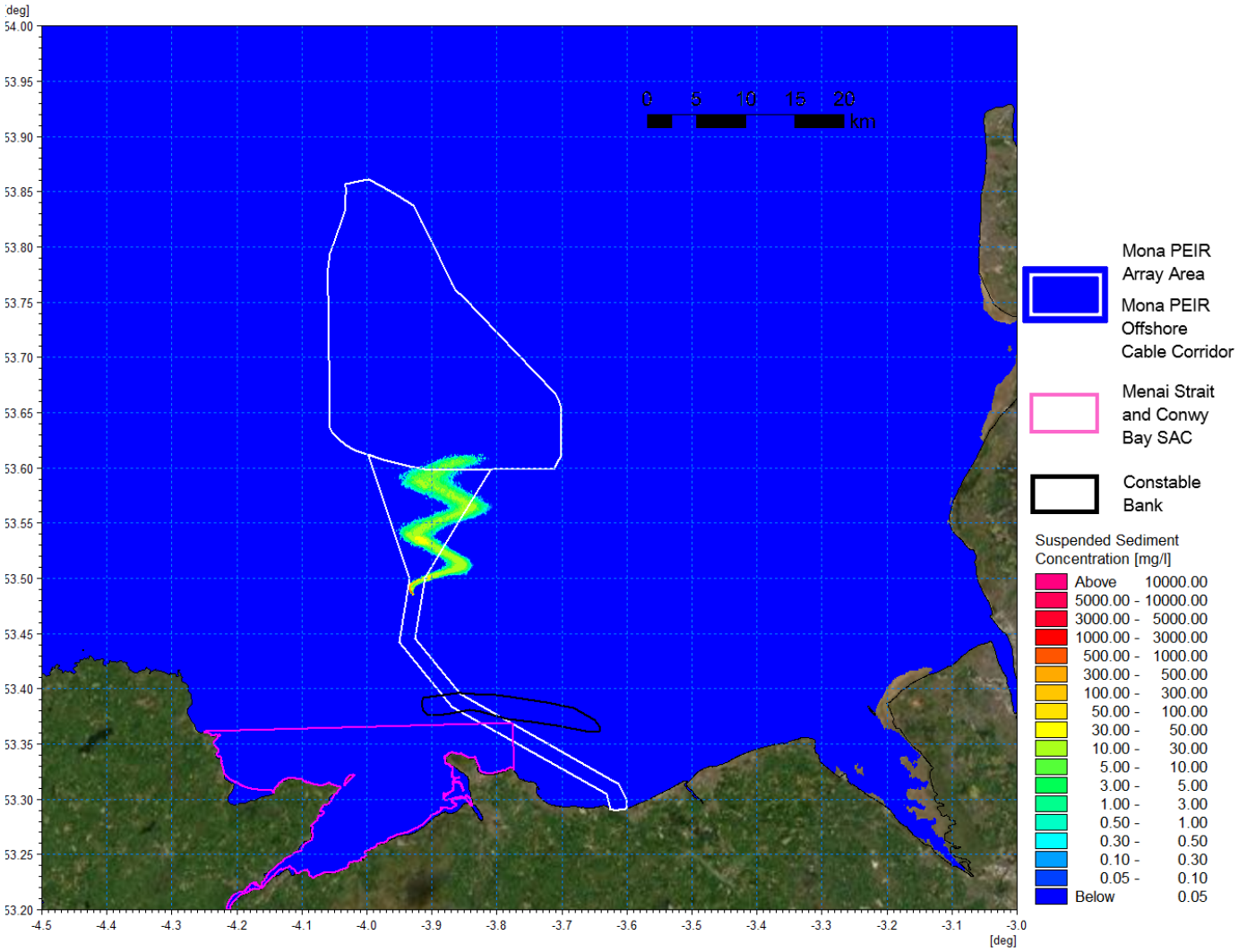

Figure 1.156: Suspended sediment concentration day 2 peak flood – offshore export cable installation.

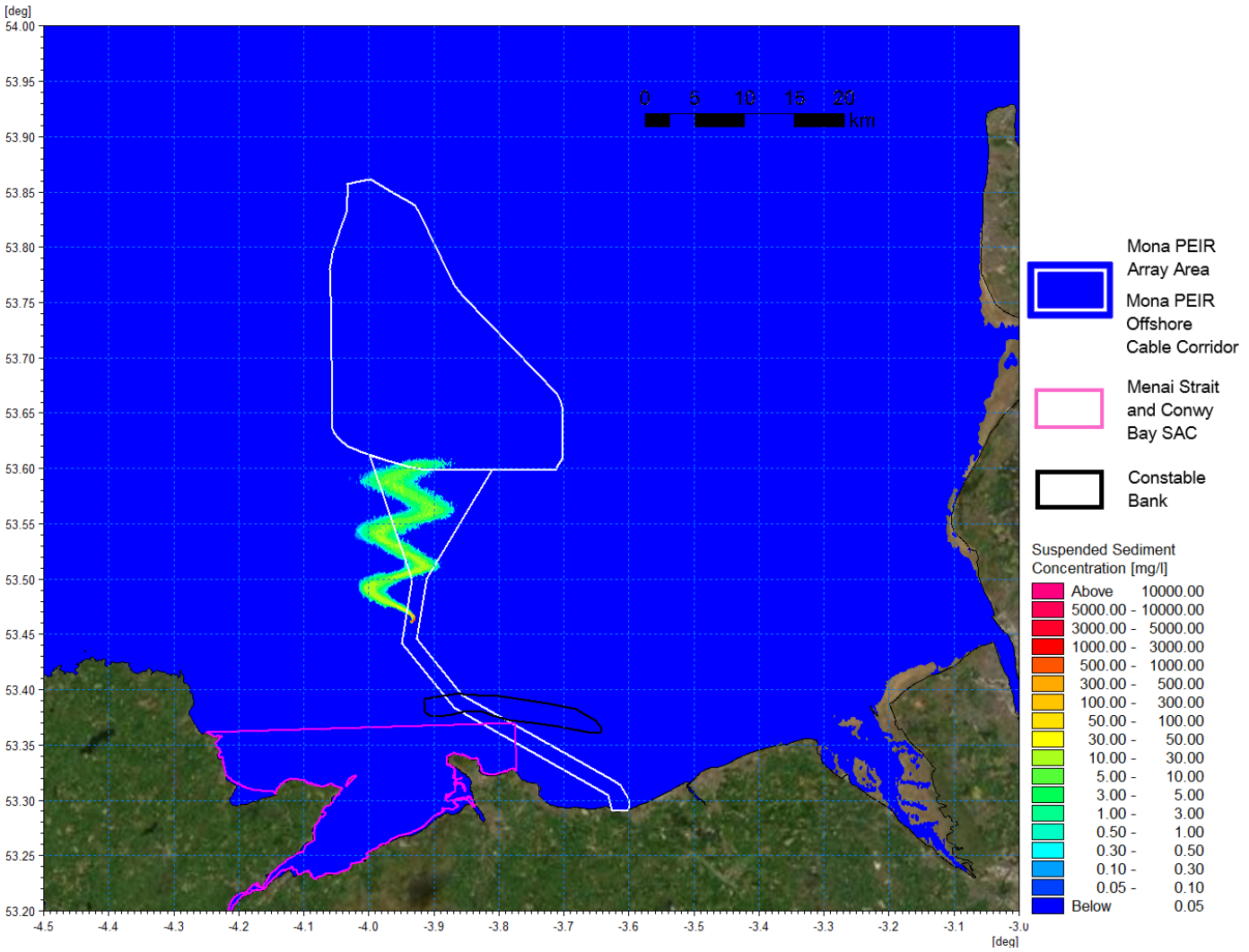

Figure 1.157: Suspended sediment concentration day 2 peak ebb – offshore export cable installation.

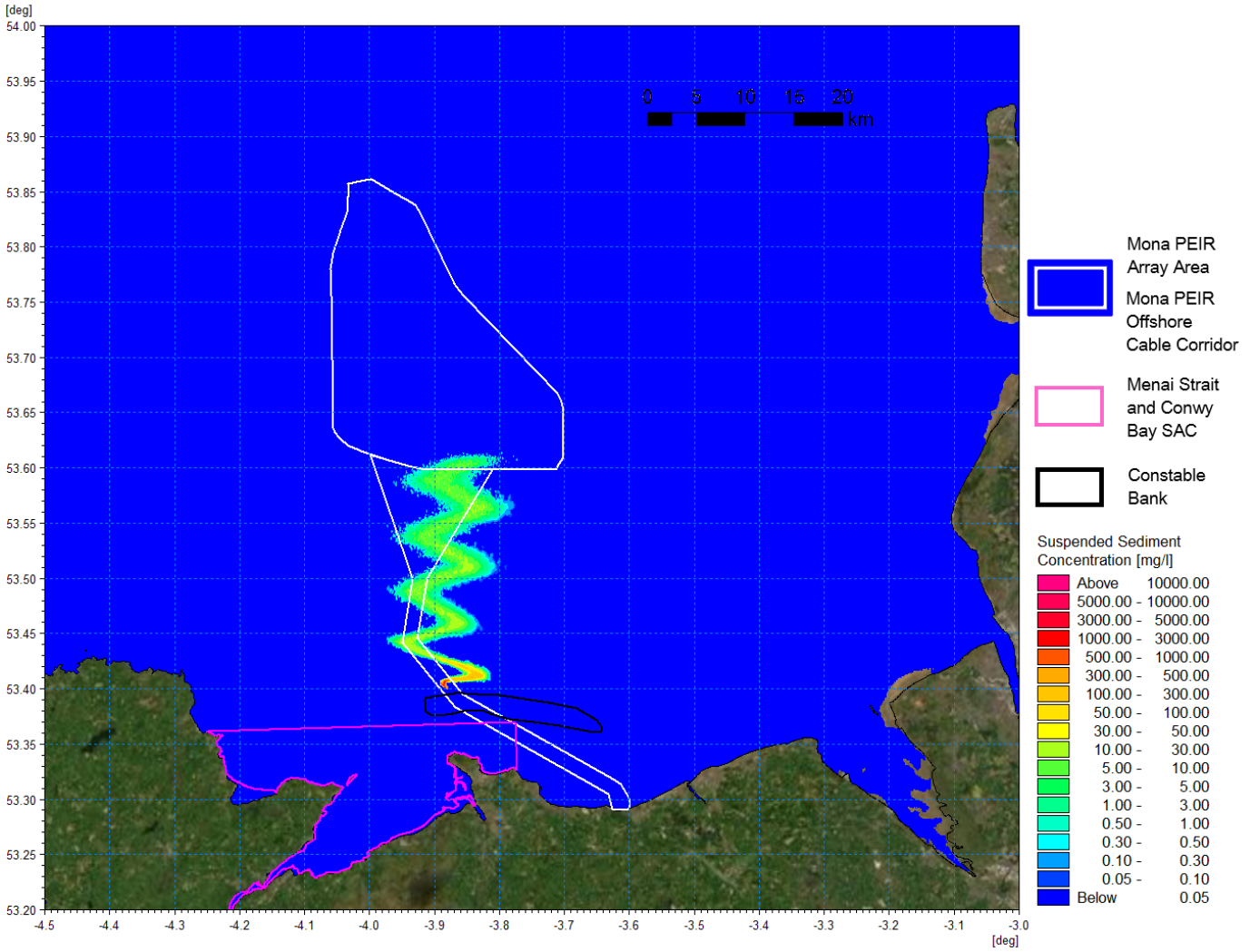

Figure 1.158: Suspended sediment concentration day 3 peak flood – offshore export cable installation.

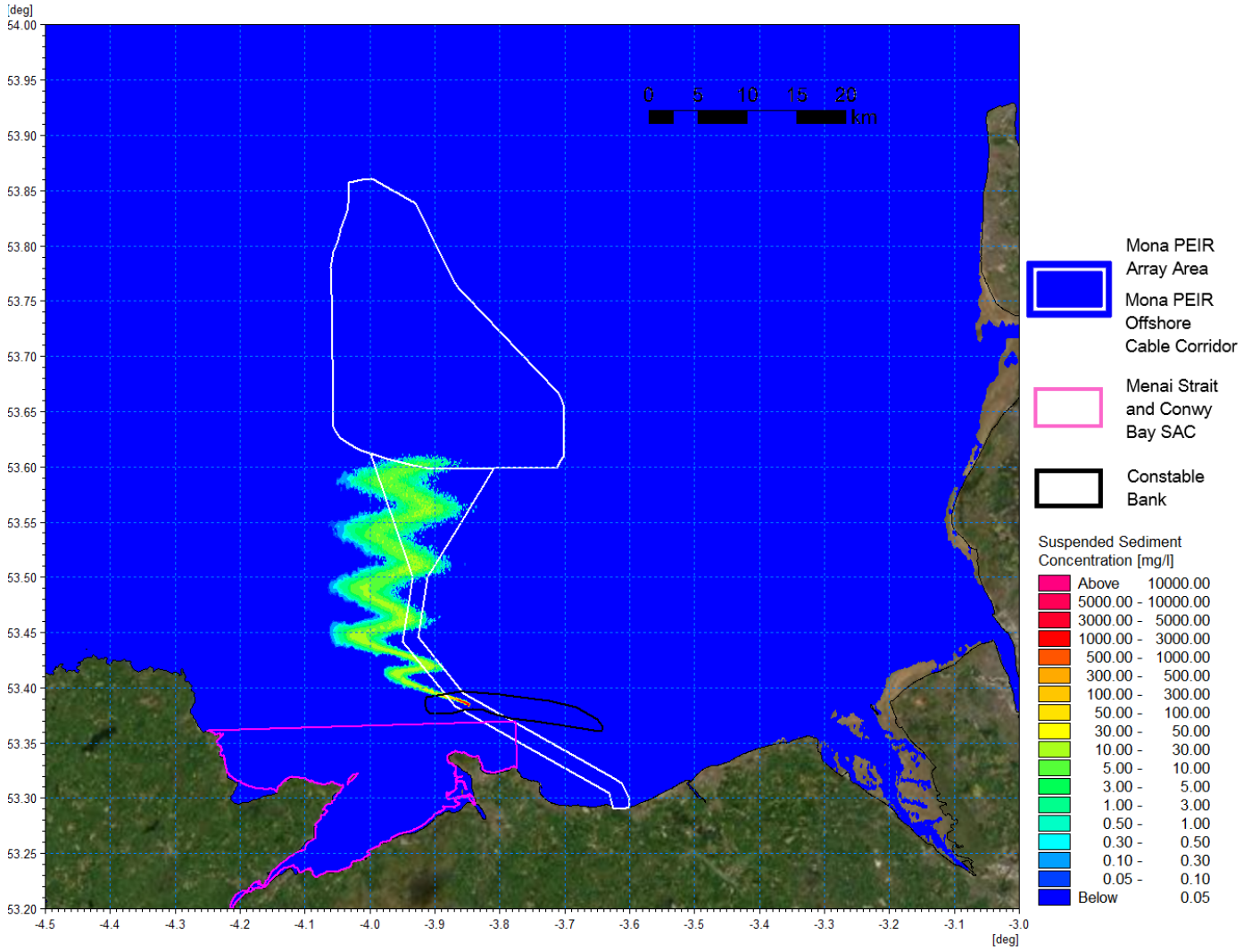

Figure 1.159: Suspended sediment concentration day 3 peak ebb – offshore export cable installation.

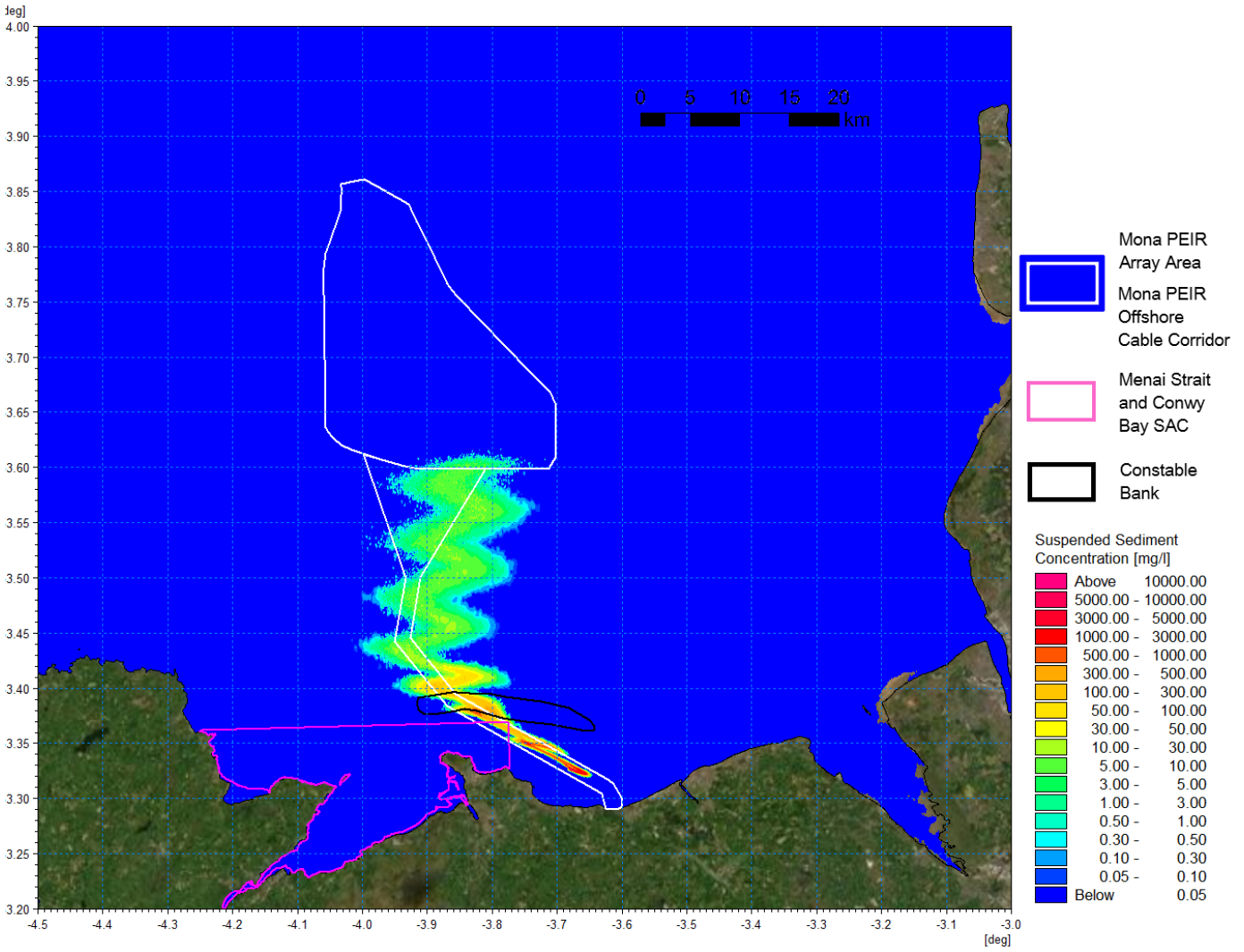

Figure 1.160: Suspended sediment concentration day 4 peak flood – offshore export cable installation.

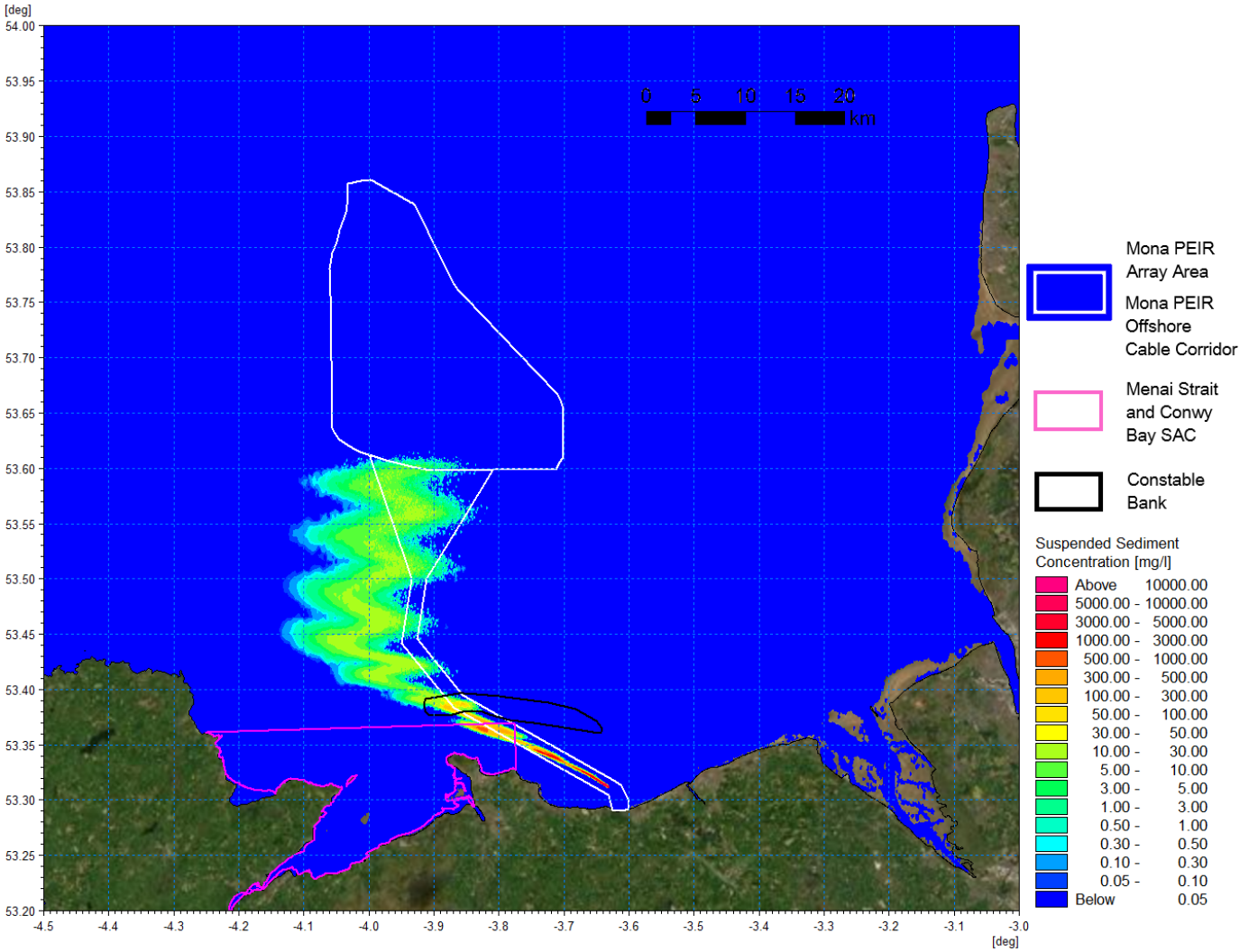

Figure 1.161: Suspended sediment concentration day 4 peak ebb – offshore export cable installation.

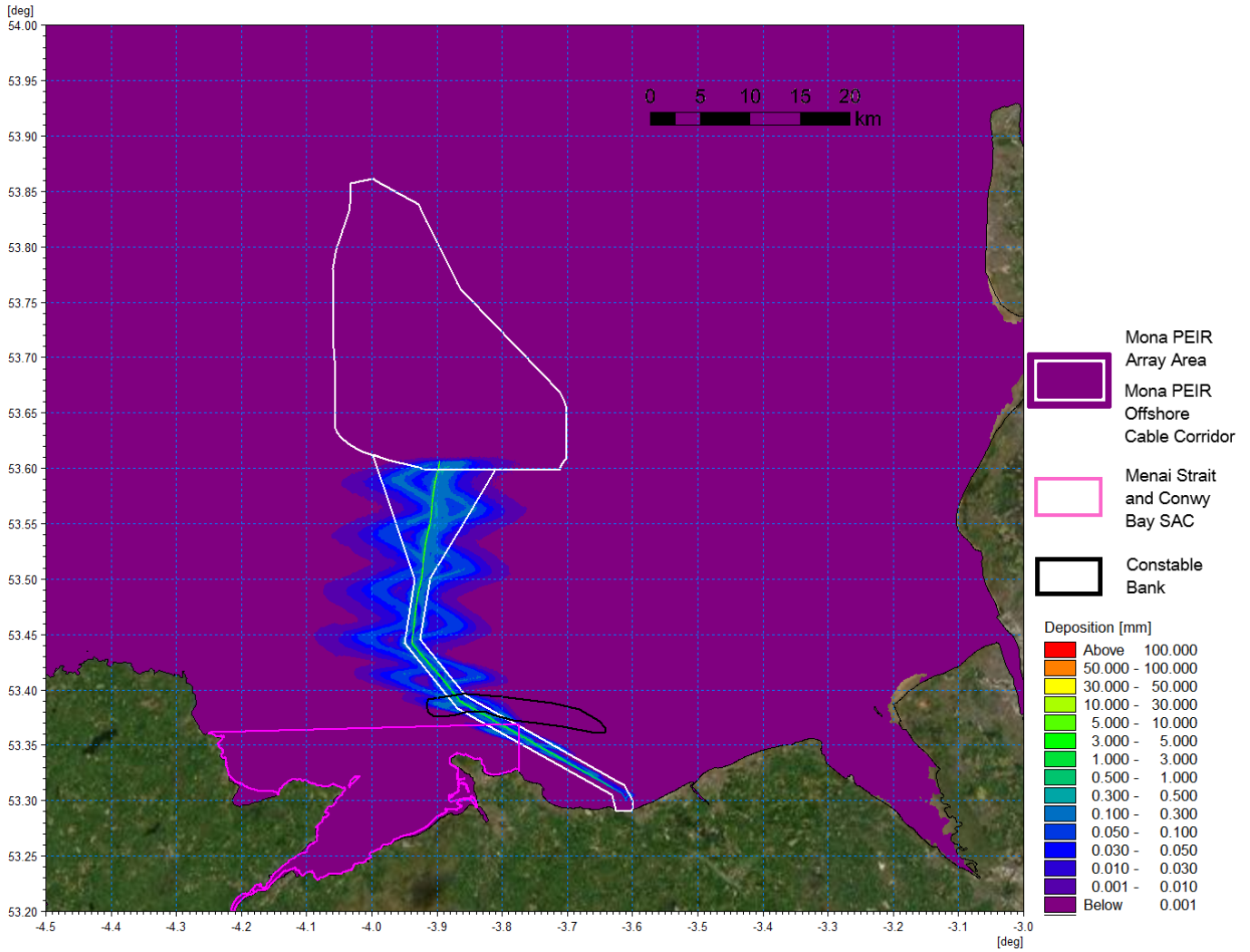

Figure 1.162: Average sedimentation during offshore export cable installation.

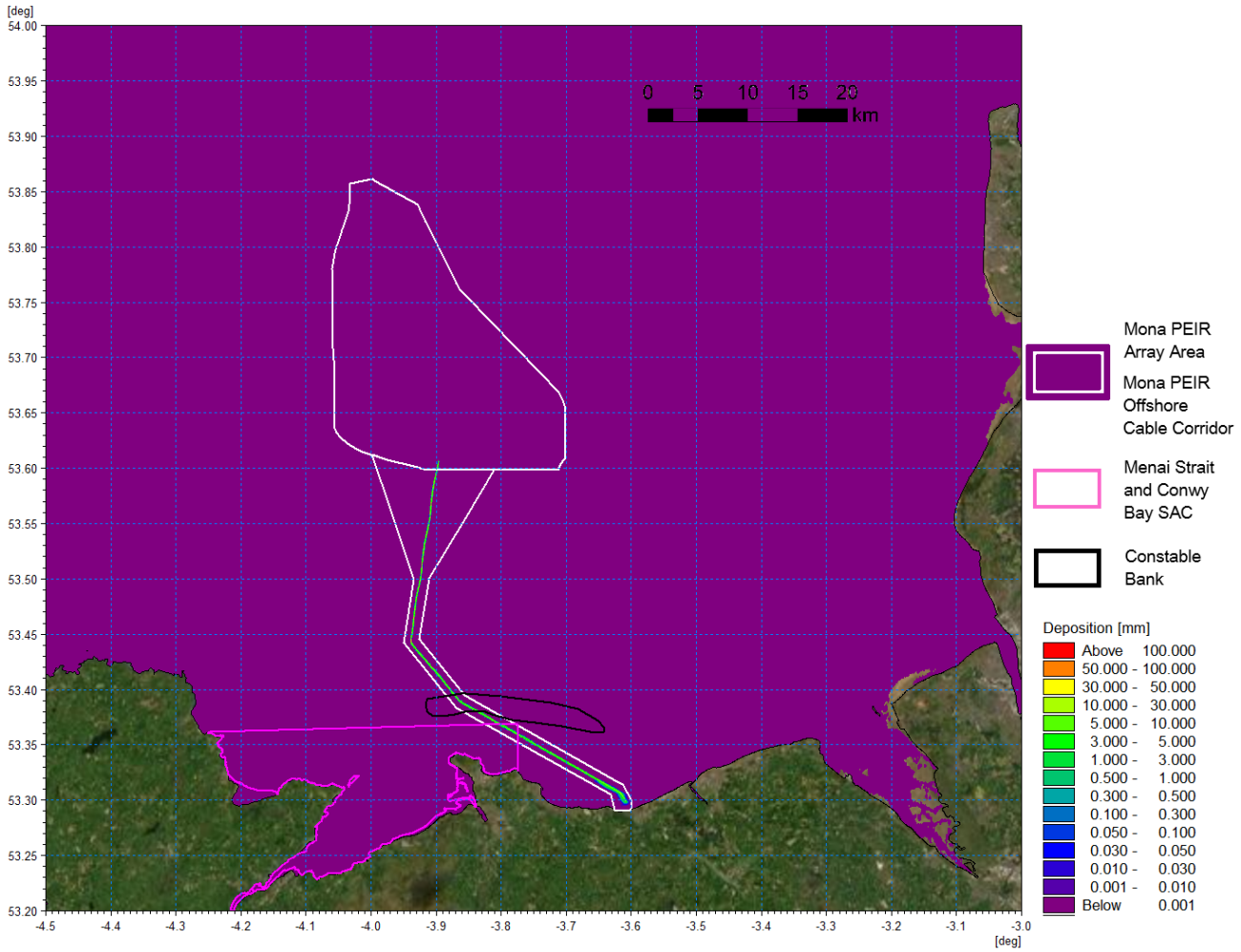

Figure 1.163: Sedimentation 1 day following cessation of offshore export cable installation.

Offshore export cables in the intertidal area

1.3.7.44 The final cable installation scenario examined using numerical modelling related to trenching of offshore export cables in the intertidal area as defined by Mona Offshore Wind Project PEIR. The simulation assumed a lower trenching rate of 100 m/h and was undertaken over an 8 hour period. The installation began from offshore and continued 800 m to the high water mark (HWM). The trench was 1 m at the surface extending to a depth of 3 m (i.e. the greatest burial depth proposed), mobilising 2,400 m^3 of material. The composition was determined from the sampling data and comprised mainly fine sand:

- Very coarse sand/gravel: 0.5%
- Coarse sand: 0.5%
- Medium sand: 6%
- Fine sand: 55%
- Very fine sand/mud: 38%.

1.3.7.45 The trenching route modelled is illustrated by the green trace in Figure 1.164 and the average suspended sediment plume during the course of the operation is shown in

Figure 1.165, with a detailed view in Figure 1.166, each with designated Site of Special Scientific Interest (SSSI) overlaid in light blue and Special Area of Conservation (SAC) shown in pink. The figures show how the plume is strongly dependant on the prevailing tidal conditions at the time of sediment release; in this case the first half of the operation occurs during flood tide and the latter portion during ebb. This gives rise to average suspended sediment concentrations 500 mg/l to 1,000 mg/l due to the limited water depth however the plume extent is restricted.

1.3.7.46 The instantaneous suspended sediment concentrations for mid flood and ebb tides are presented in Figure 1.167 and Figure 1.168 respectively. They show increases where sediment is released at the cable location but also at the extent of each tidal cycle as material is re-suspended. Suspended sediment concentrations are seen to exceed 1,000 mg/l where the greatest levels are located at the source of the sediment release in the shallowest water, however the plume excursion is circa 5 km.

1.3.7.47 Finally, Figure 1.169 and Figure 1.170 show the average sedimentation whilst Figure 1.171 and Figure 1.172 illustrates sedimentation levels one day following cessation of the sediment release. Tidal patterns indicate that although the released material migrates both east and west by settling and being re-suspended on successive tides, some sediment is deposited on the shoreline with a maximum depth of around 10 mm. As the trenching closest to the shoreline was modelled on an ebb tide, the predominant deposition is to the west of the trenching. It should however be noted that under all tidal states this is native material, originating from less than 1 km from the shoreline and would therefore remain within the existing shoreline transport cell.

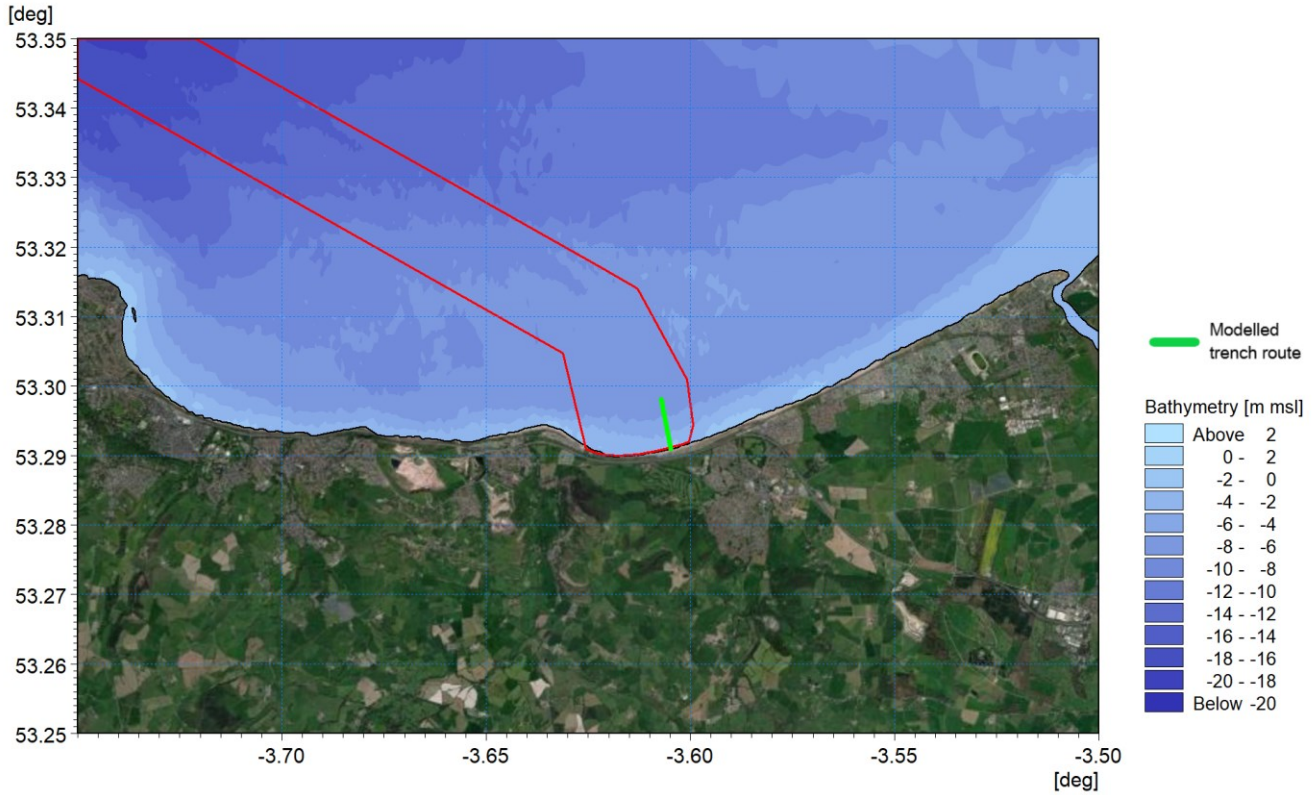

Figure 1.164: Modelled offshore export cables in the intertidal area for PEIR.

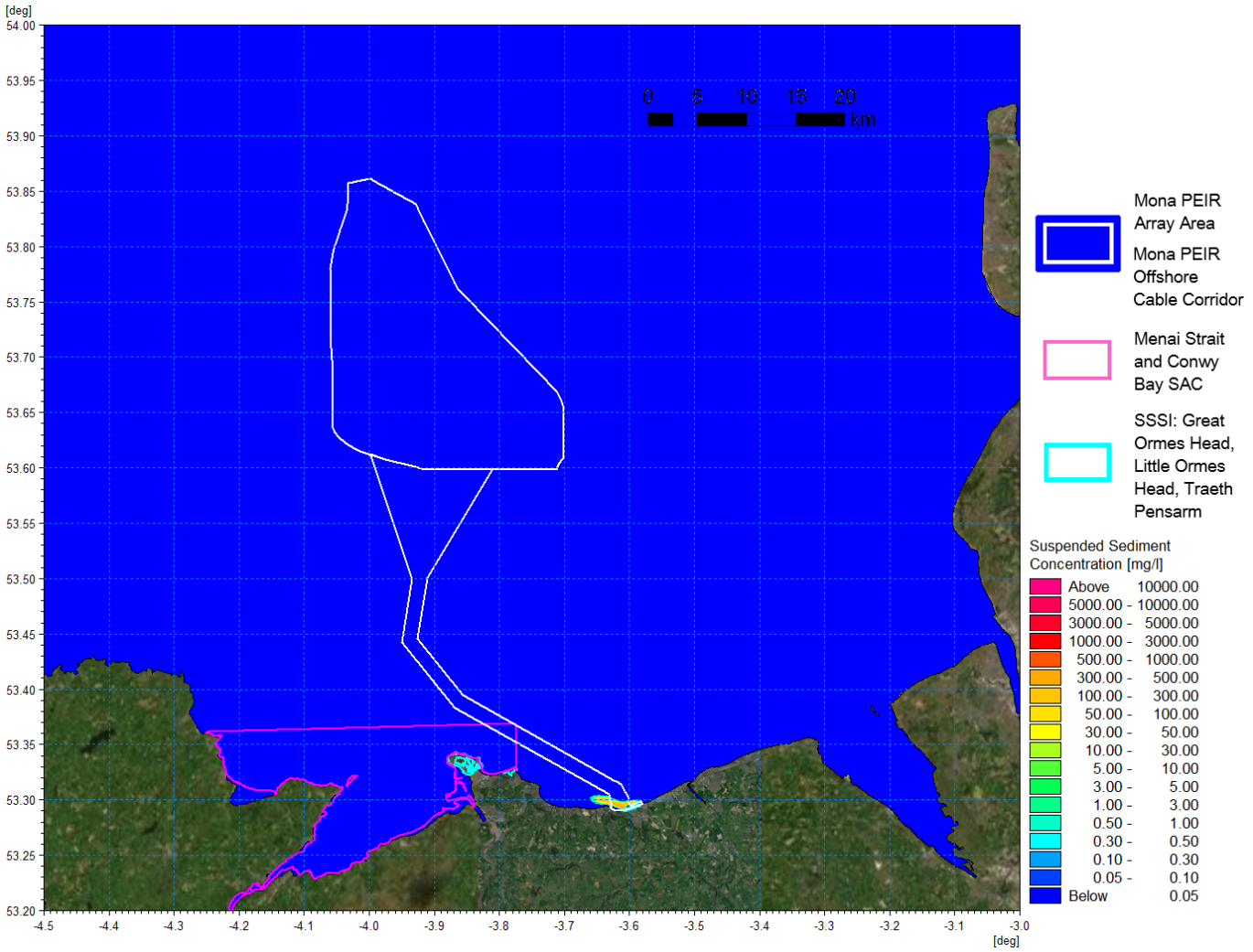

Figure 1.165: Average suspended sediment concentration during offshore export cables in the intertidal area trenching (SSSI – light blue, SAC – pink).

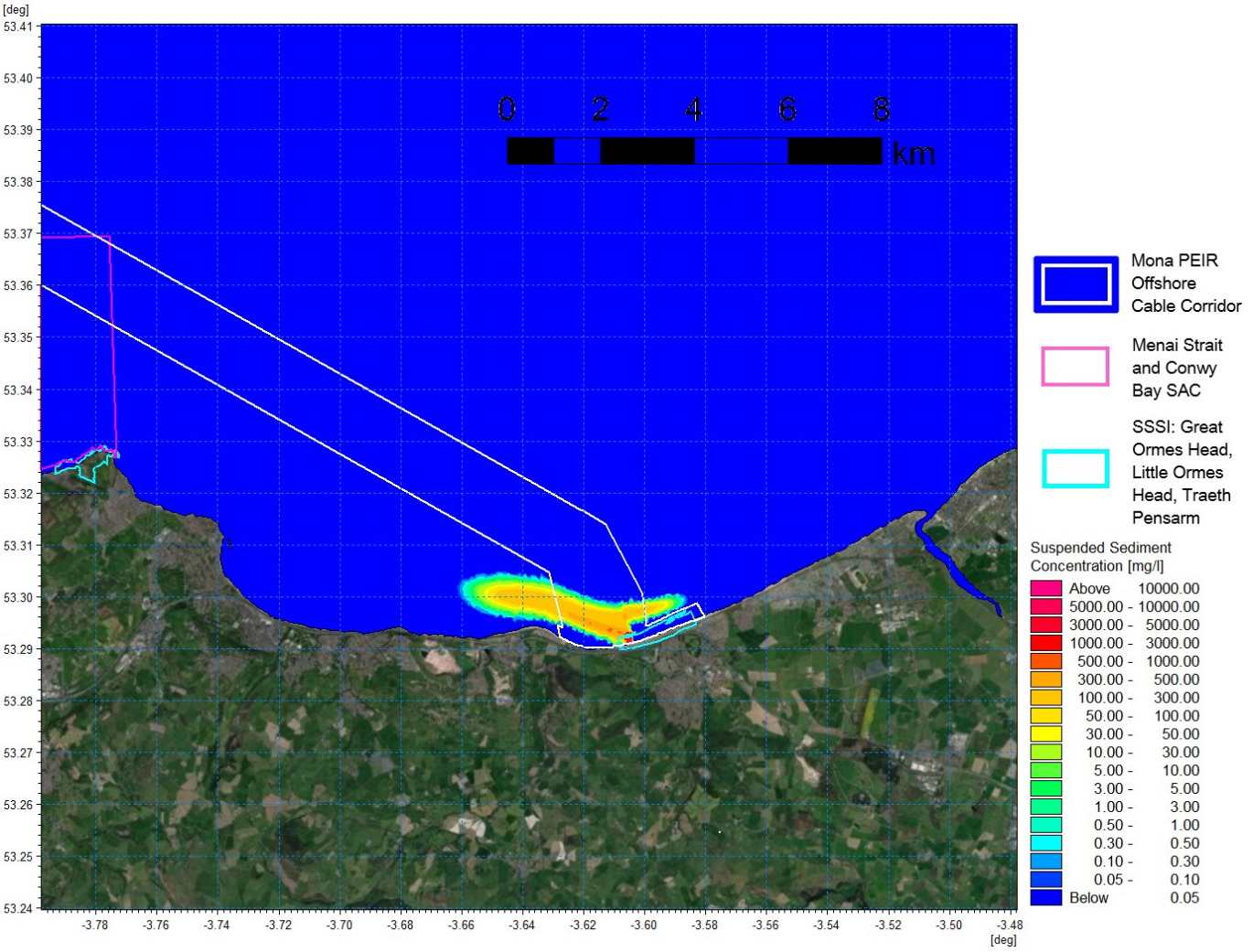

Figure 1.166: Average suspended sediment concentration during offshore export cables in the intertidal area trenching detailed view (SSSI – light blue, SAC – pink).

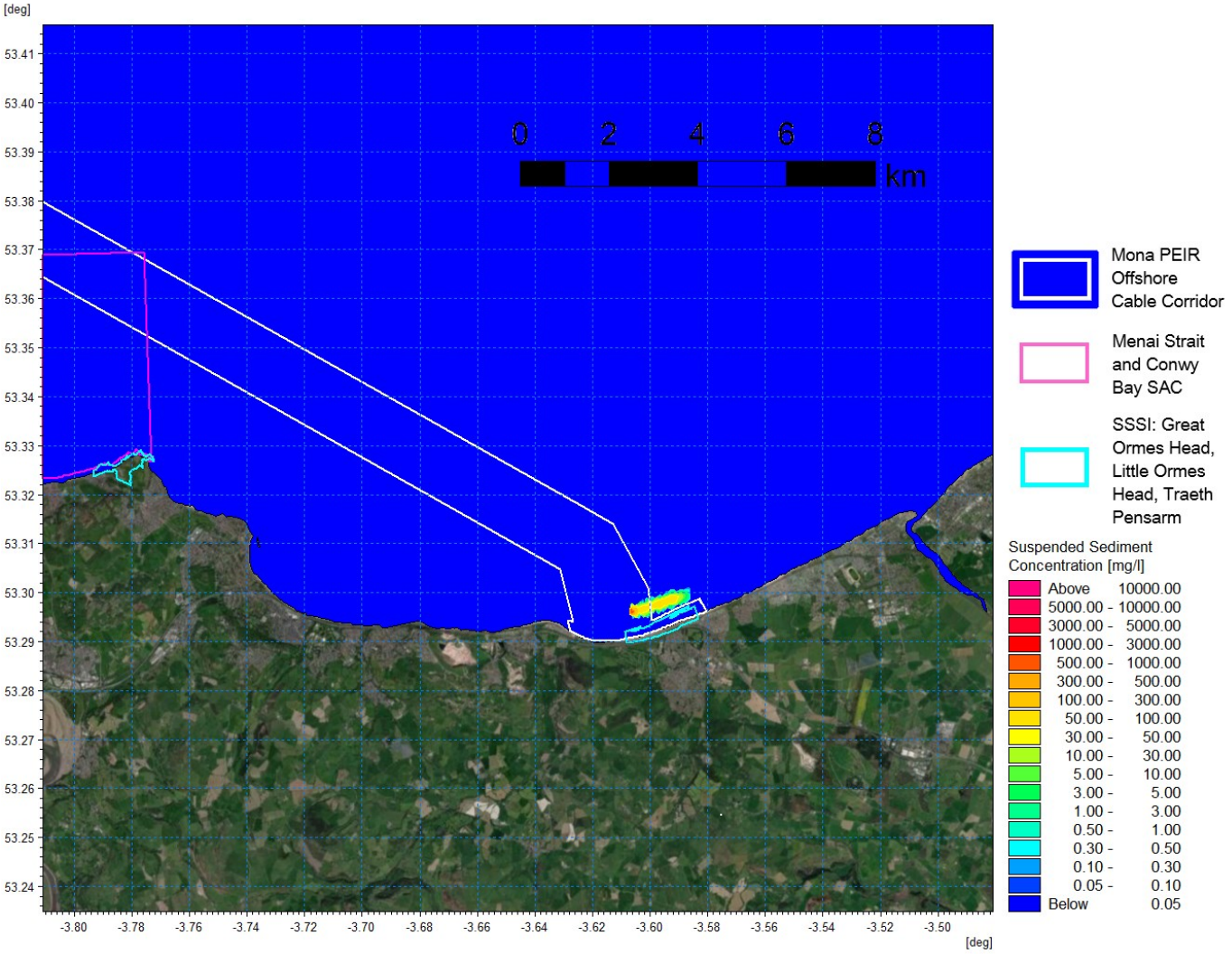

Figure 1.167: Suspended sediment concentration flood – offshore export cables in the intertidal area installation (SSSI – light blue, SAC – pink).

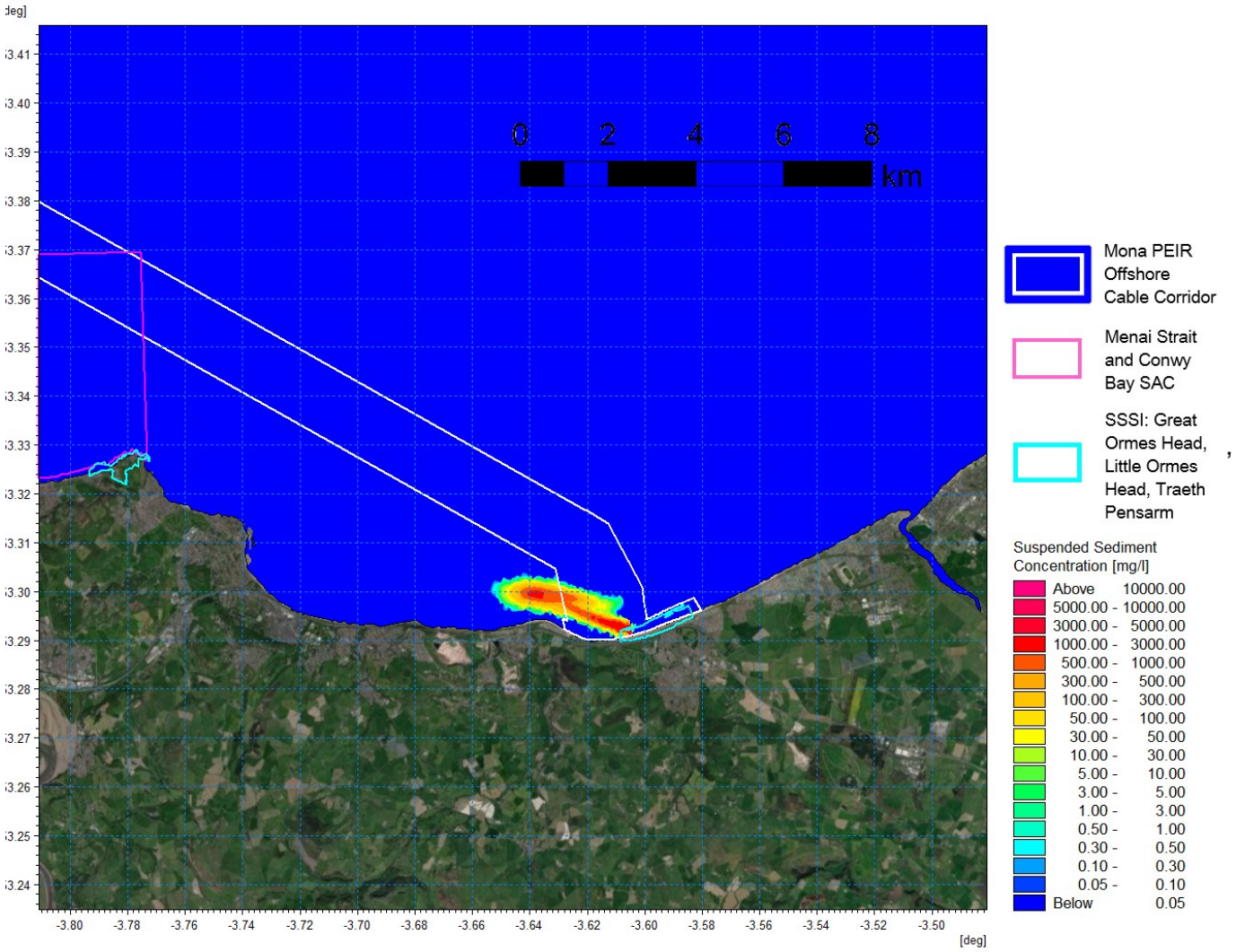

Figure 1.168: Suspended sediment concentration ebb – offshore export cables in the intertidal area installation (SSSI – light blue, SAC – pink).

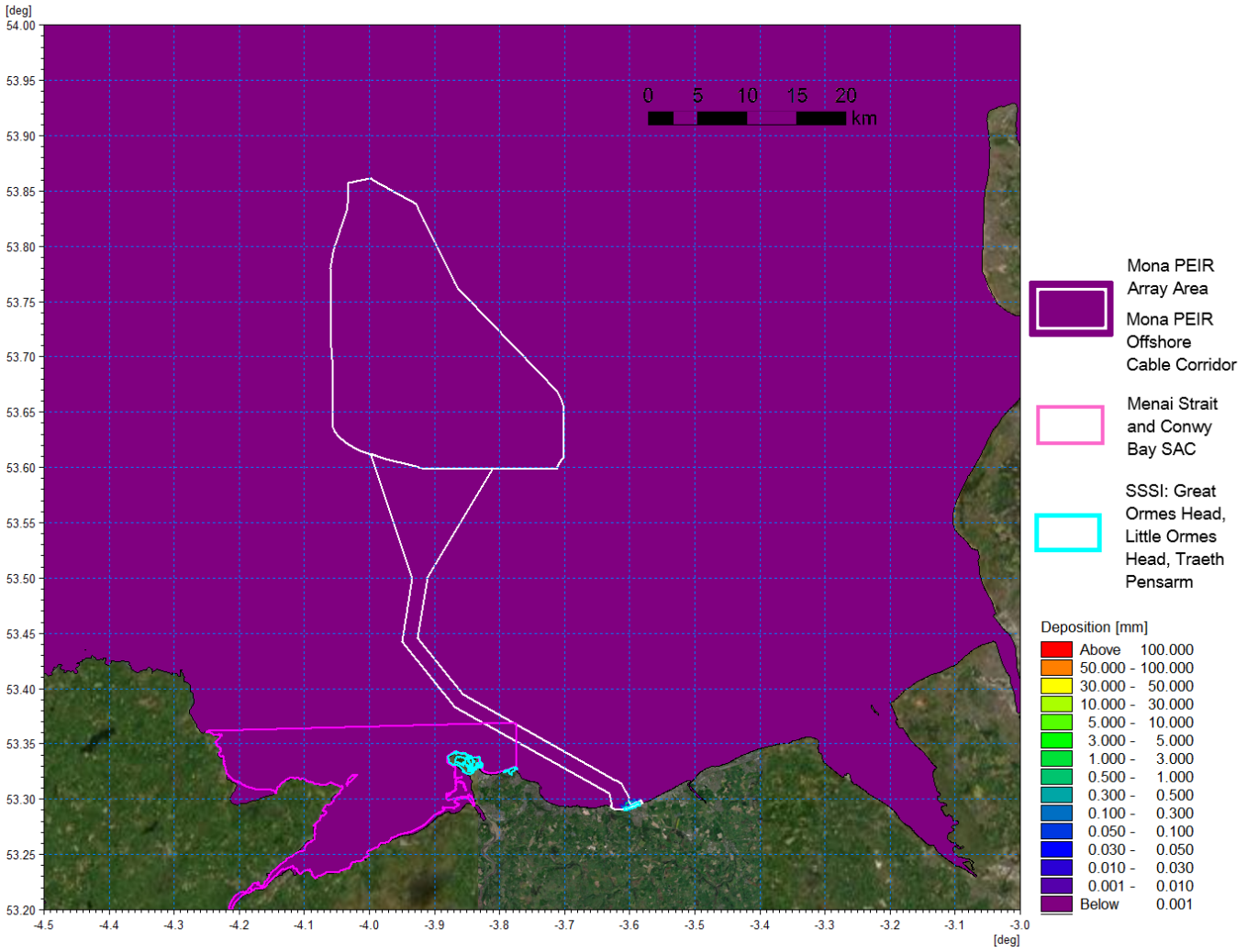

Figure 1.169: Average sedimentation during offshore export cables in the intertidal area installation (SSSI – light blue, SAC – pink).

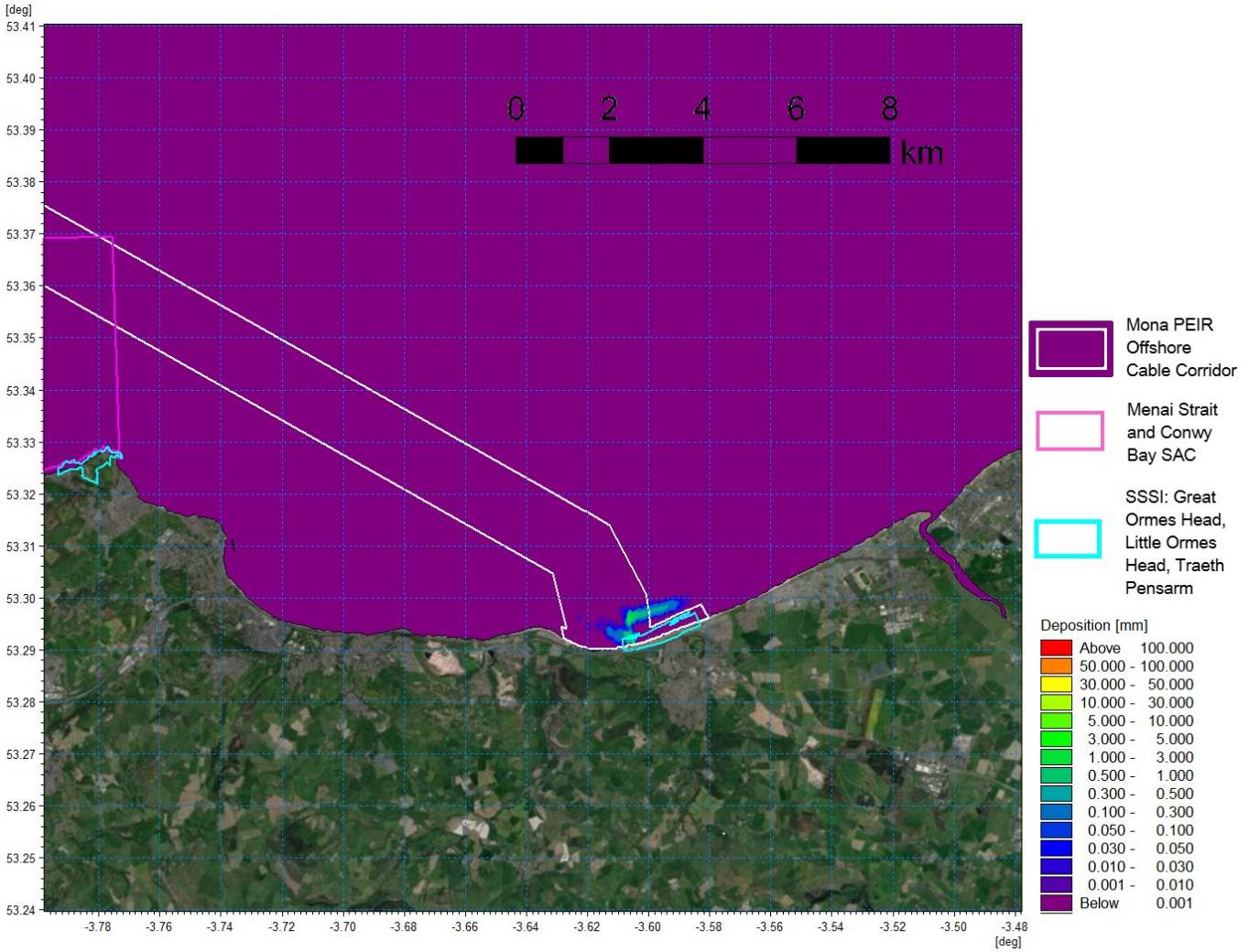

Figure 1.170: Average sedimentation during offshore export cables in the intertidal area installation detail view (SSSI – light blue, SAC – pink).

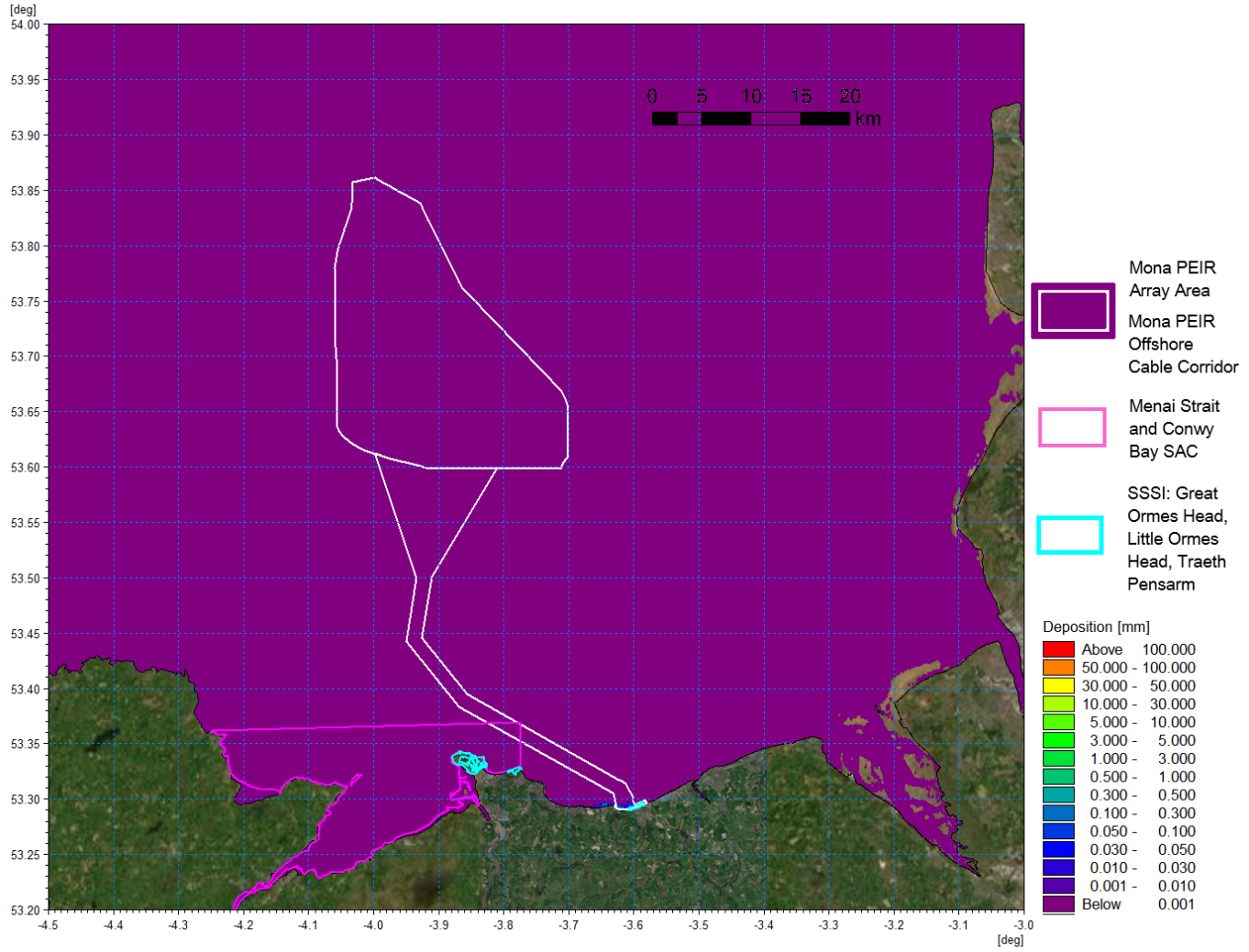

Figure 1.171: Sedimentation 1 day following cessation of offshore export cables in the intertidal area installation (SSSI – light blue, SAC – pink).

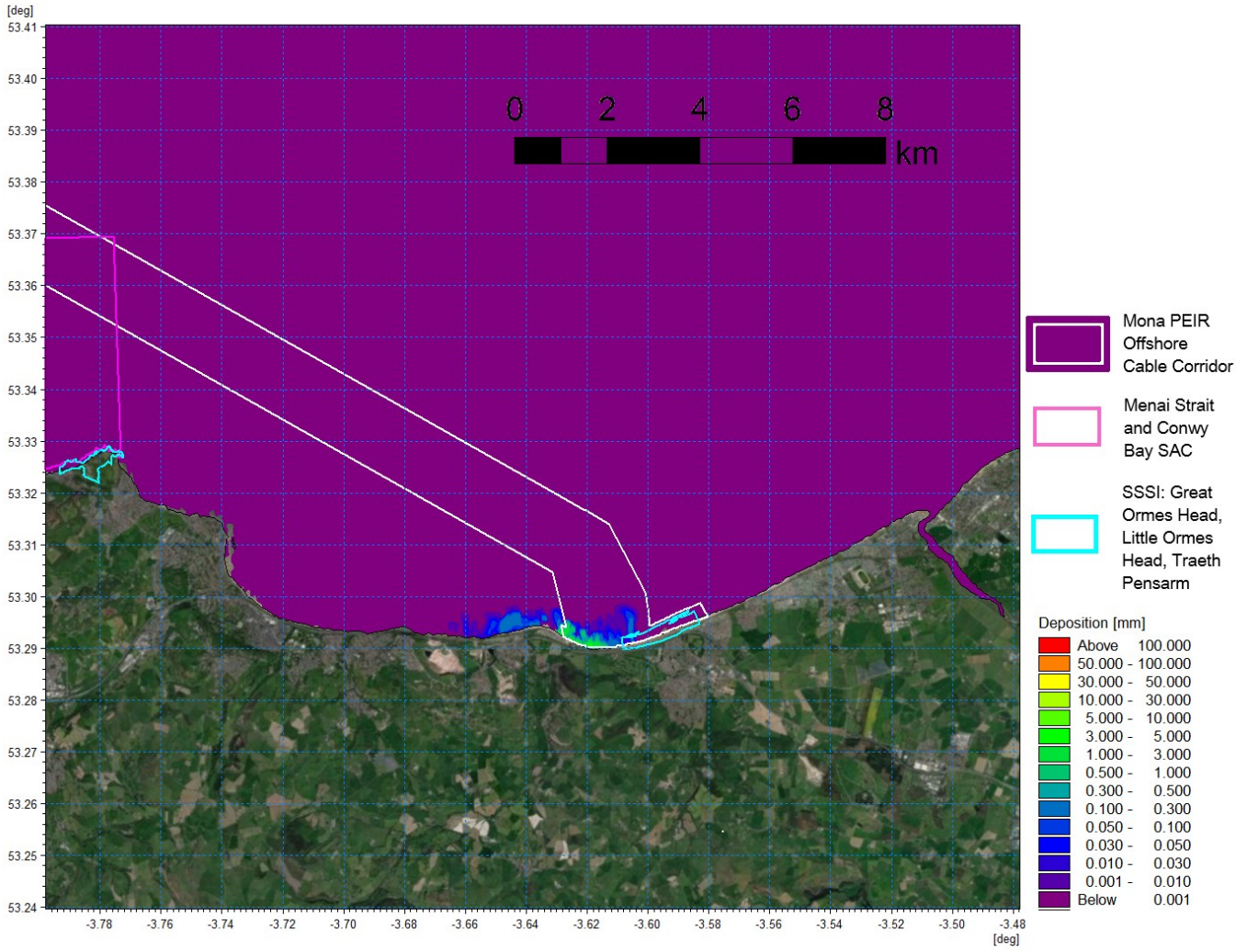

Figure 1.172: Sedimentation 1 day following cessation of offshore export cables in the intertidal area installation detail view (SSSI – light blue, SAC – pink).

1.4 Modelling to support the Environmental Statement

1.4.1 Overview

1.4.1.1 As described in sections 1.1 and 1.3, the application process is a live process and design parameters may be revised between the publication of the Mona Offshore Wind Project PEIR and Environmental Statement. Updates have been made to both the Mona PEIR Array Area and associated revisions to the project parameters since the publication of the PEIR (Mona Offshore Wind Limited, 2023), and as such it was deemed appropriate that additional sensitivity modelling should be undertaken in line with these changes. This would not only provide additional information to support the environmental assessment but also to investigate the assumptions taken in the selection of scenarios modelled in the context of the PEIR study.

1.4.1.2 The modelling study undertaken for the PEIR and presented in the preceding sections of this document was based on a holistic approach to developing a MDS from the PDE. The aim was to provide supporting information for a balanced assessment for physical processes which comprise a number of integrated parameters, each of which may be influenced differently from a range of design aspects. For example, suction bucket foundations may provide the greatest impediment at both the surface (influencing

waves) and at the seabed (influencing sediment transport pathways), but a gravity base foundation may present a greater water column blockage (influencing tides). Physical processes parameters do not occur in isolation, for example, sediment transport is influenced by littoral currents (both tides and waves) along with available transport pathways. Therefore, for the additional modelling to support the Environmental Statement, it was prudent to undertake sensitivity testing for different foundation types.

1.4.1.3 Three types of single unit installations located at the centre of the Mona Array Area were examined, the site of which is displayed in green in Figure 1.173. The model mesh was adapted to enable all sensitivity tests to be undertaken with the same cell arrangement, with bed levels adjusted to represent the scour protection associated with each foundation type.

1.4.1.4 The three selected foundation types and scales were selected to be representative of the range of installations proposed within the context of the Environmental Statement, as outlined in Table 1.6. The suction bucket foundation scenario echoed that used in the array modelling presented in the Mona Offshore Wind Project PEIR (applying the holistic approach). The conical gravity base is that of the largest wind turbine units proposed and a typical size relating to OSP foundations. Finally, the rectangular gravity base relates to the much larger single semi-submersible OSP structure.

1.4.1.5 As with the modelling presented in the Mona Offshore Wind Project PEIR, any deviation from the additional modelled scenarios for the Environmental Statement will be noted in the context of the assessment.

Table 1.6: Summary of Modelled Environmental Variation Scenarios for the Environmental Statement.

Variation/ operation	Description	Parameter modelled
Sensitivity testing	Models updated to examine the effect of a single installation to quantify: • Changes to tidal currents • Changes to wave climate.	Four-legged suction bucket foundation • Each jacket leg with a diameter of 5 m, spaced 48 m apart, and each bucket with a diameter of 16 m • Scour protection to a height of 2.5 m extending 20 m from the bucket. Conical gravity base foundation • Caisson diameter of 37 m and 15 m diameter at sea surface • Scour protection average depth of 2.6 m extending 24 m from the foundation. Rectangular gravity base foundation • 60 m by 80 m dimension at the surface, a slab base diameter dimension of 80 m by 100 m • Scour protection to a height of 2.6 m extending 25 m from the slab.

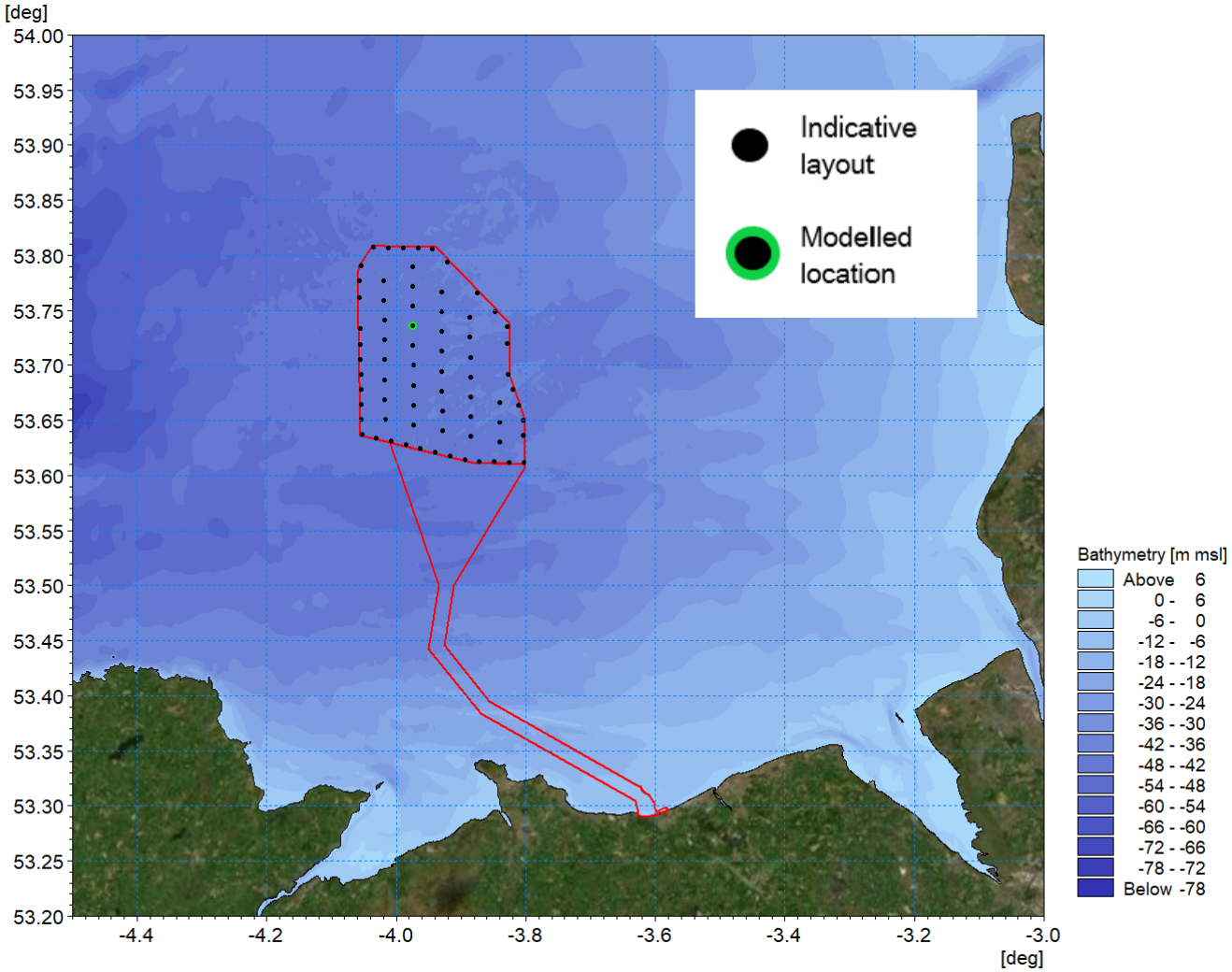

Figure 1.173: Location of foundation used for sensitivity modelling within the Mona Offshore Wind Project Environmental Statement Boundary.

1.4.2 Suction bucket foundations

1.4.2.1 The suction bucket foundation scenario echoed that used in the array modelling presented in the Mona Offshore Wind Project PEIR, applying the holistic approach. This was applied to select the foundation with the greatest overall influence on physical processes to be used for turbine foundations (i.e. greatest seabed footprint and water column obstruction for each unit). The suction bucket scenario comprised the following:

- Four-legged suction bucket foundations
- Each jacket leg with a diameter of 5 m, spaced 48 m apart
- Each bucket with a diameter of 16 m
- Scour protection to a height of 2.5 m extending 20 m from the bucket.

Tidal flow

1.4.2.2 A sensitivity test was performed by repeating the hydrodynamic simulations used to describe the baseline, with the addition of one four-legged suction bucket foundation.

The suction bucket foundation was included in the sensitivity modelling based on a holistic selection process as used before in section 1.3. The bathymetry was also amended to take account of scour protection. The following figures show the same reference mid flood and mid ebb steps from the simulation as were presented previously. Due to the limited magnitude of the changes, difference plots have been provided. These are the proposed minus the baseline condition, therefore increases in current speed will be positive. The same procedure for calculating differences and plotting figures has been implemented throughout this report. For context, an indicative wind turbine layout is shown on each plot indicating the proximity of the nearest installation (black circles).

1.4.2.3 Figure 1.174 presents the baseline flood tide flow patterns with Figure 1.175 showing a focussed plot of the post-construction changes which are limited to the vicinity of the foundation. In the difference figures a log scale has been introduced to accentuate the values for clarity. Similarly, Figure 1.176 and Figure 1.177 show the same information for the ebb tide. During peak current speed the flow is redirected in the immediate vicinity of the structure. The variation is a maximum of 2 cm/s in the immediate vicinity (50 m) of the structure which constitutes less than 2% of the peak flows. This reduces significantly with increased distance from each structure falling to a maximum of 1 cm/s, just 100 m from the structure.

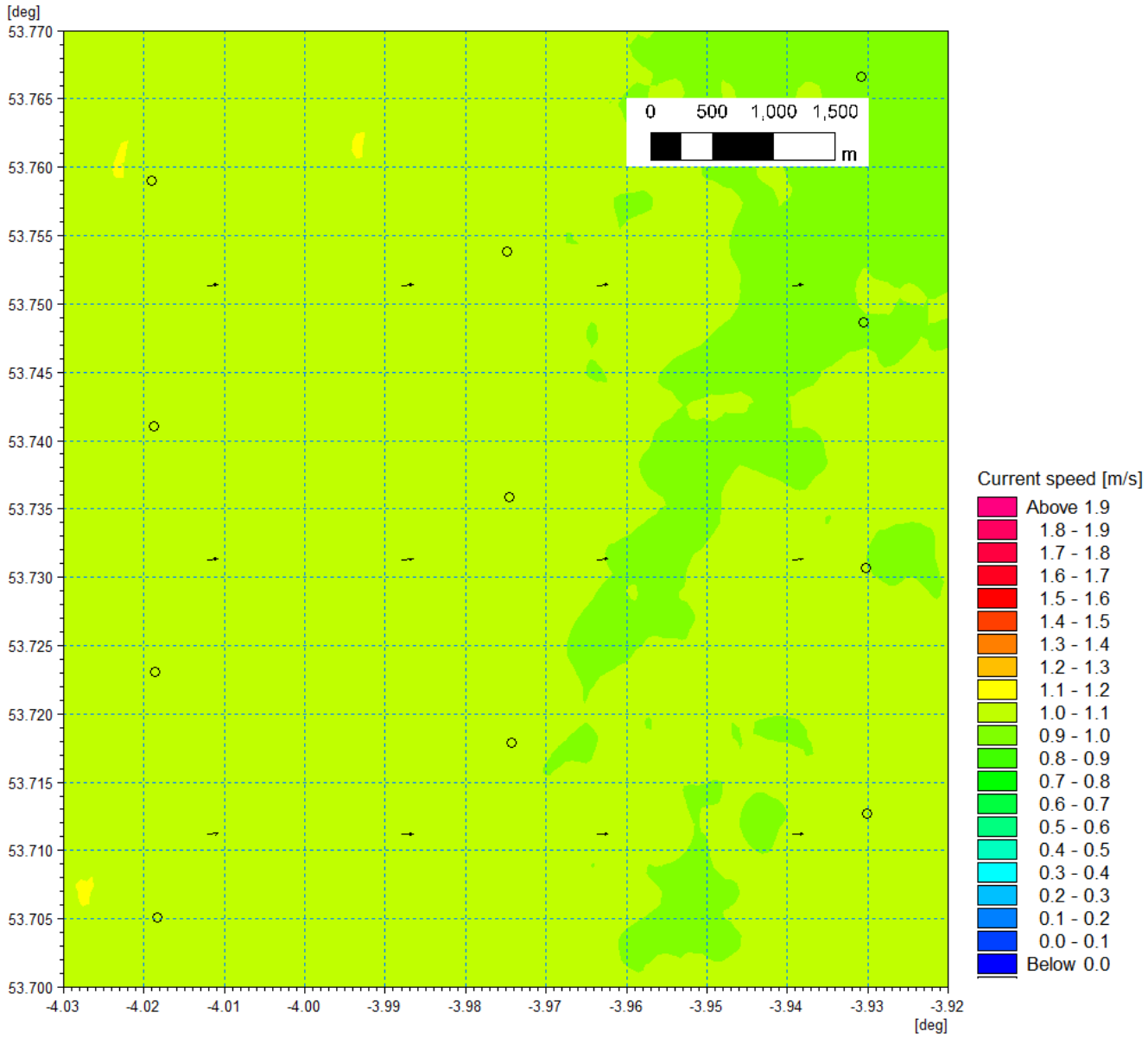

Figure 1.174: Baseline tidal flow pattern – flood tide.

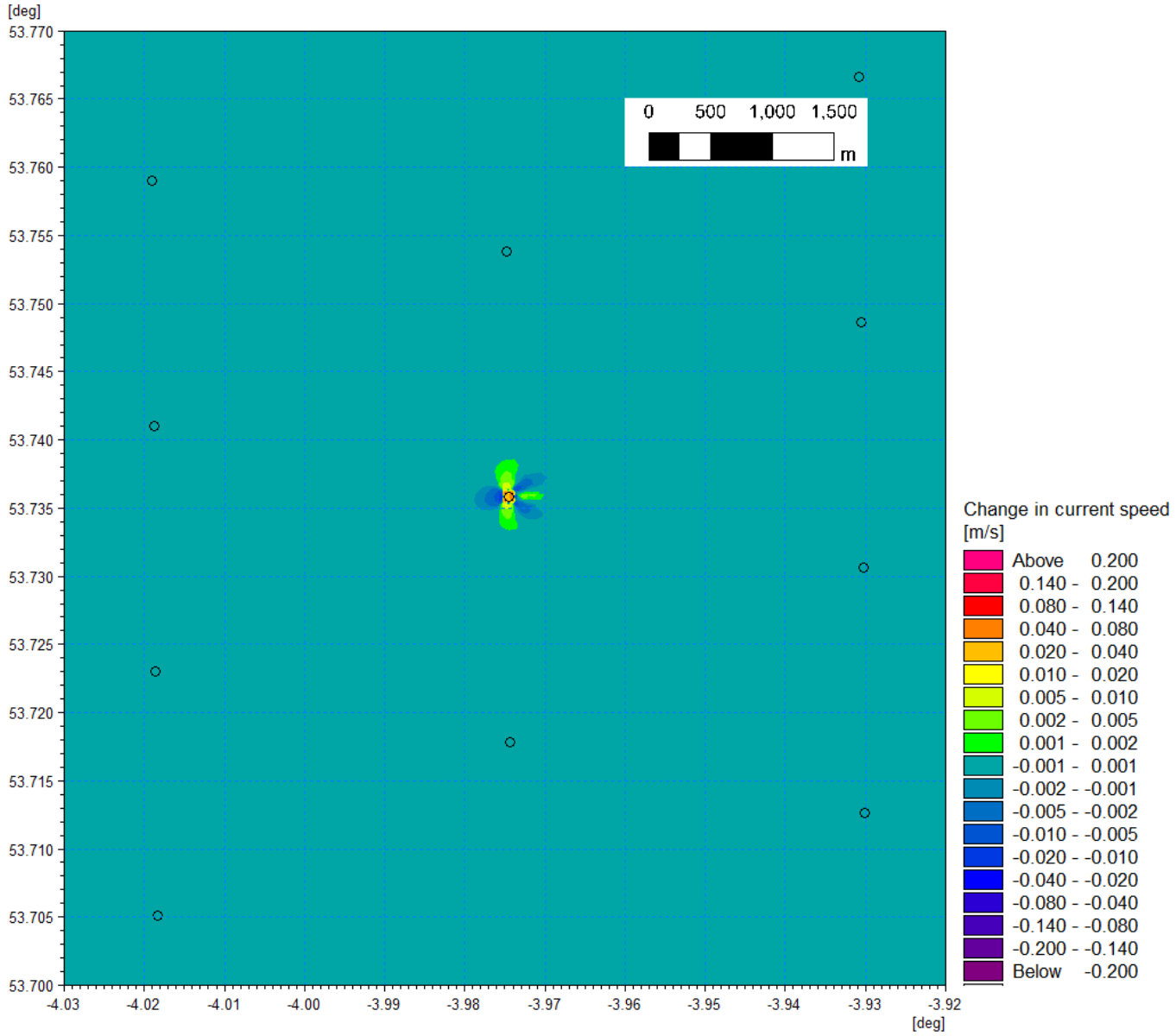

Figure 1.175: Change in tidal flow (post-construction minus baseline) suction bucket foundation – flood tide.

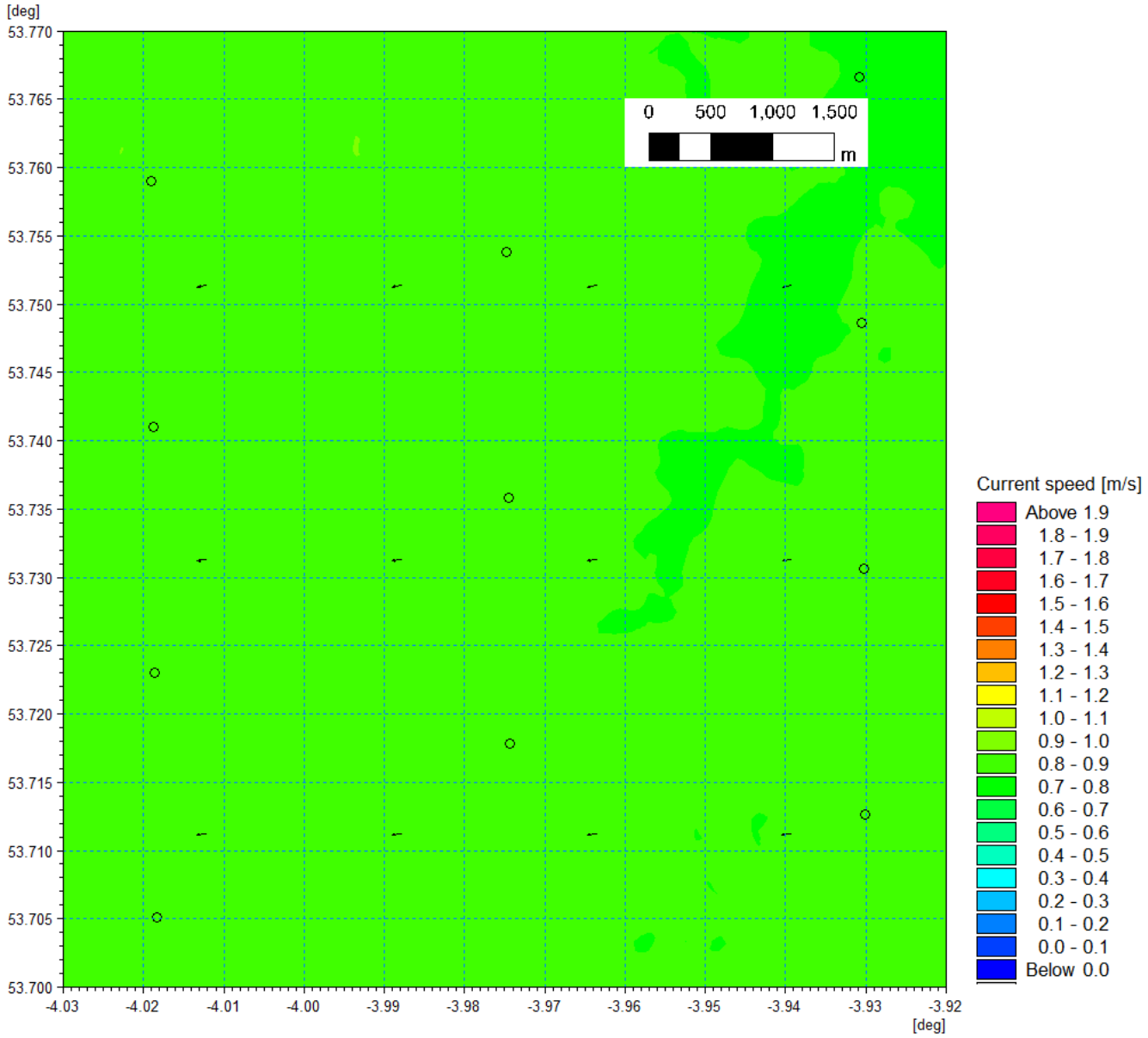

Figure 1.176: Baseline tidal flow pattern – ebb tide.

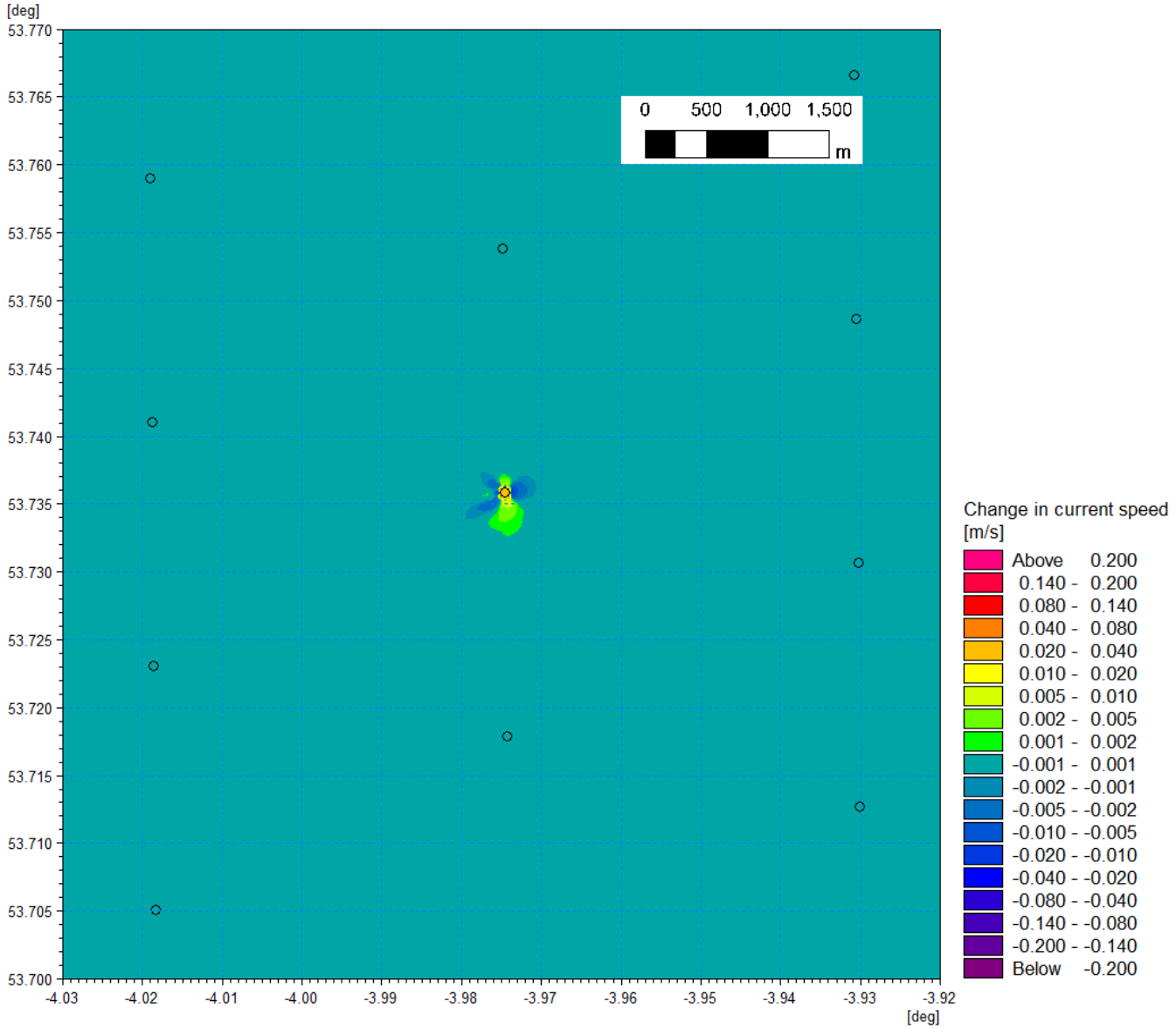

Figure 1.177: Change in tidal flow (post-construction minus baseline) suction bucket foundation – ebb tide.

Wave climate

1.4.2.4 Using the same principle as the tidal modelling, the wave climate modelling was repeated with the inclusion of the suction bucket foundations and scour protection. Again, changes were found to be indiscernible from the baseline scenario by visual inspection therefore difference plots have been provided using the same scale for all scenarios.

1.4.2.5 The baseline 000° storm is presented for the 1 in 1 year in Figure 1.178 with the difference shown in Figure 1.179. Similarly, the 1 in 20 year storm from this direction is presented in Figure 1.186 and Figure 1.187. The changes are seen as reductions in the lee of the foundation. The maximum changes observed in the immediate vicinity (50 m) were limited to a maximum of 6 cm which represents *c.* 1.25% of the baseline significant wave height (4.8 m). The wave shadow is typically less than one half of this value. These changes would be indiscernible from the baseline wave climate.

1.4.2.6 The changes to waves originating from 090° sector are shown in Figure 1.180 and Figure 1.189, both 1 in 1 and 1 in 20 year storm waves are of similar magnitudes to those experienced from the seen from 000° sector, limited to *c.* 2% of the baseline wave height (3.8 m) within 50 m of the structure. These changes fall to around half of this value 100 m from the foundation.

1.4.2.7 For the westerly storms from 240° and 270° the incident wave heights are typically twice that of the fetch limited directions. For these scenarios the effect of the presence of the infrastructure is much smaller with changes in wave height typically less than 1% (6 cm) during the more onerous 1 in 20 year storms, as presented in Figure 1.191 and Figure 1.193. Positive changes to wave height are also observed within the wave shadow with a similar magnitude as the increases described above. Both positive and negative changes to wave height fall below 0.5% within 100 m of the foundation, and to indiscernible levels of change within 200 m.

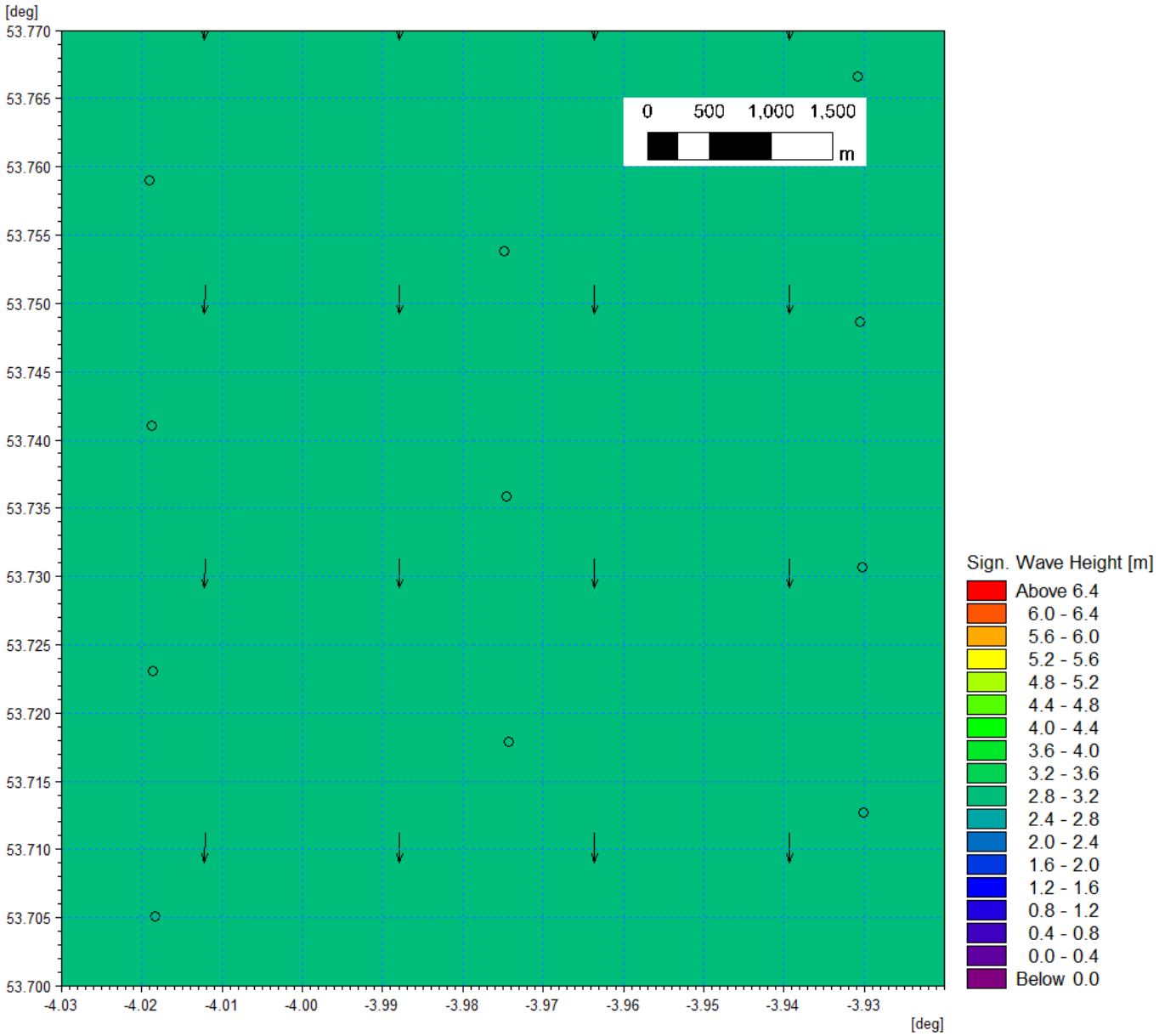

Figure 1.178: Baseline wave climate 1 in 1 year storm 000° MHW.

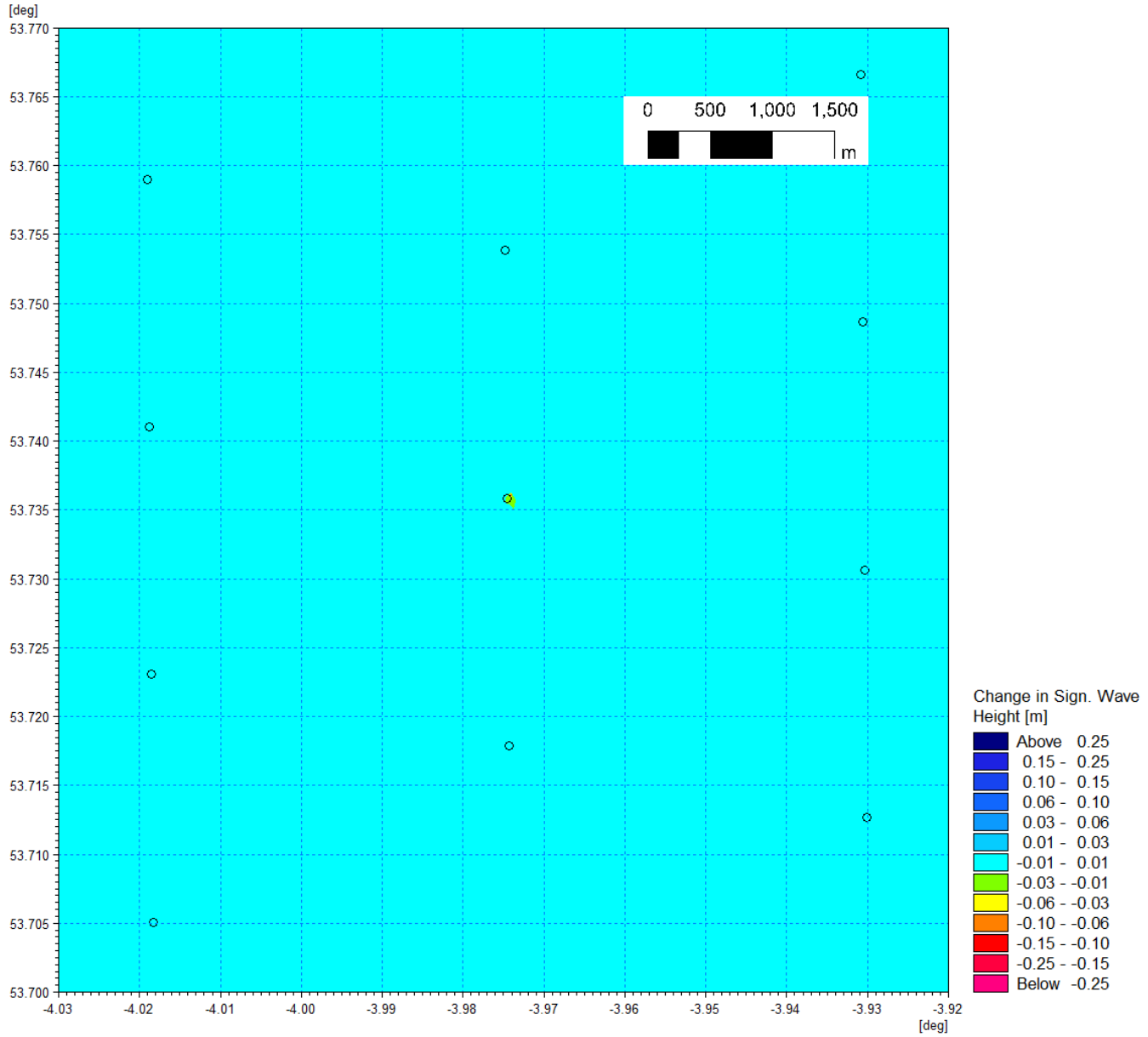

Figure 1.179: Change in wave climate 1 in 1 year storm 000° MHW (post-construction minus baseline) – suction bucket foundation.

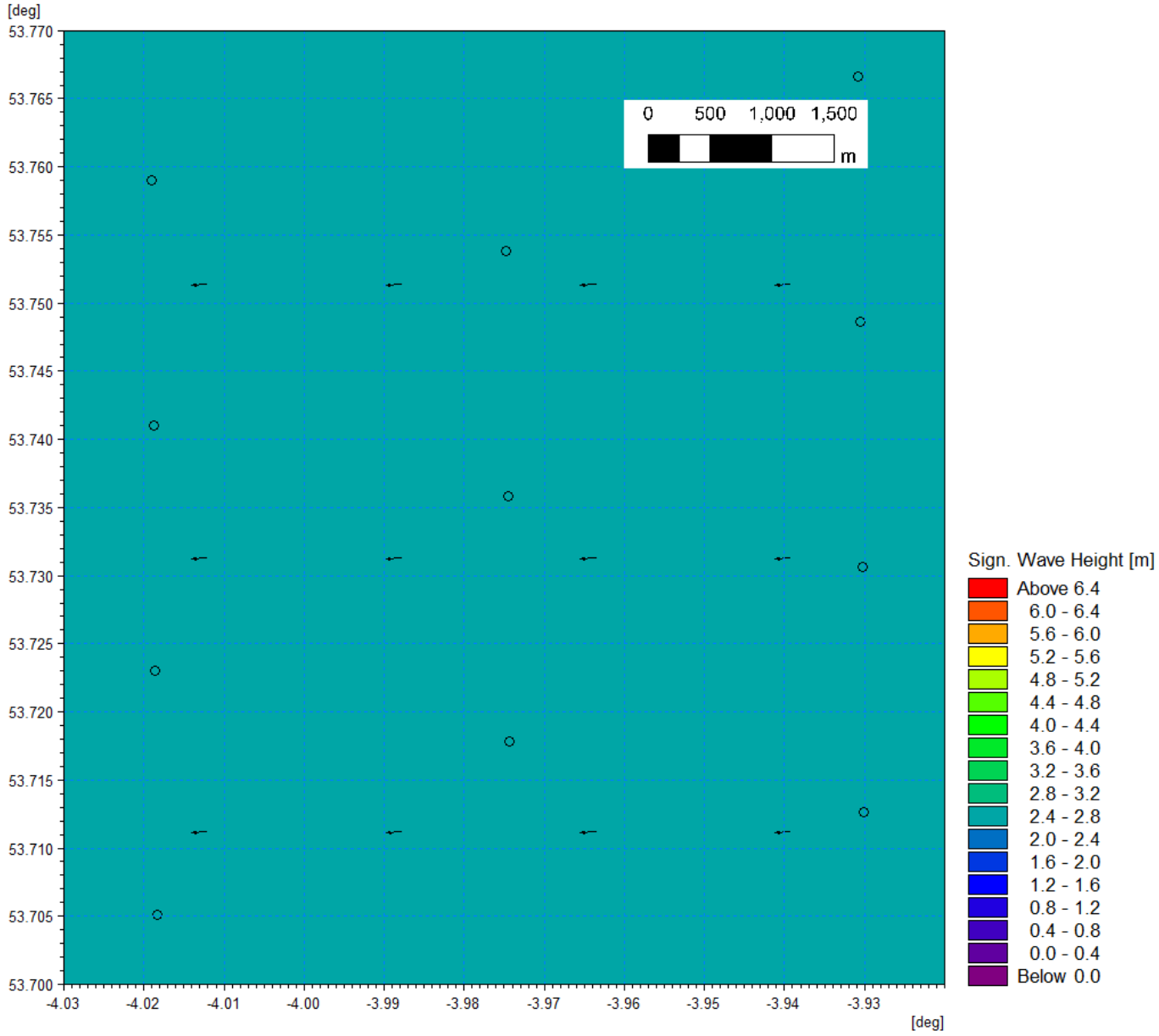

Figure 1.180: Baseline wave climate 1 in 1 year storm 090° MHW.

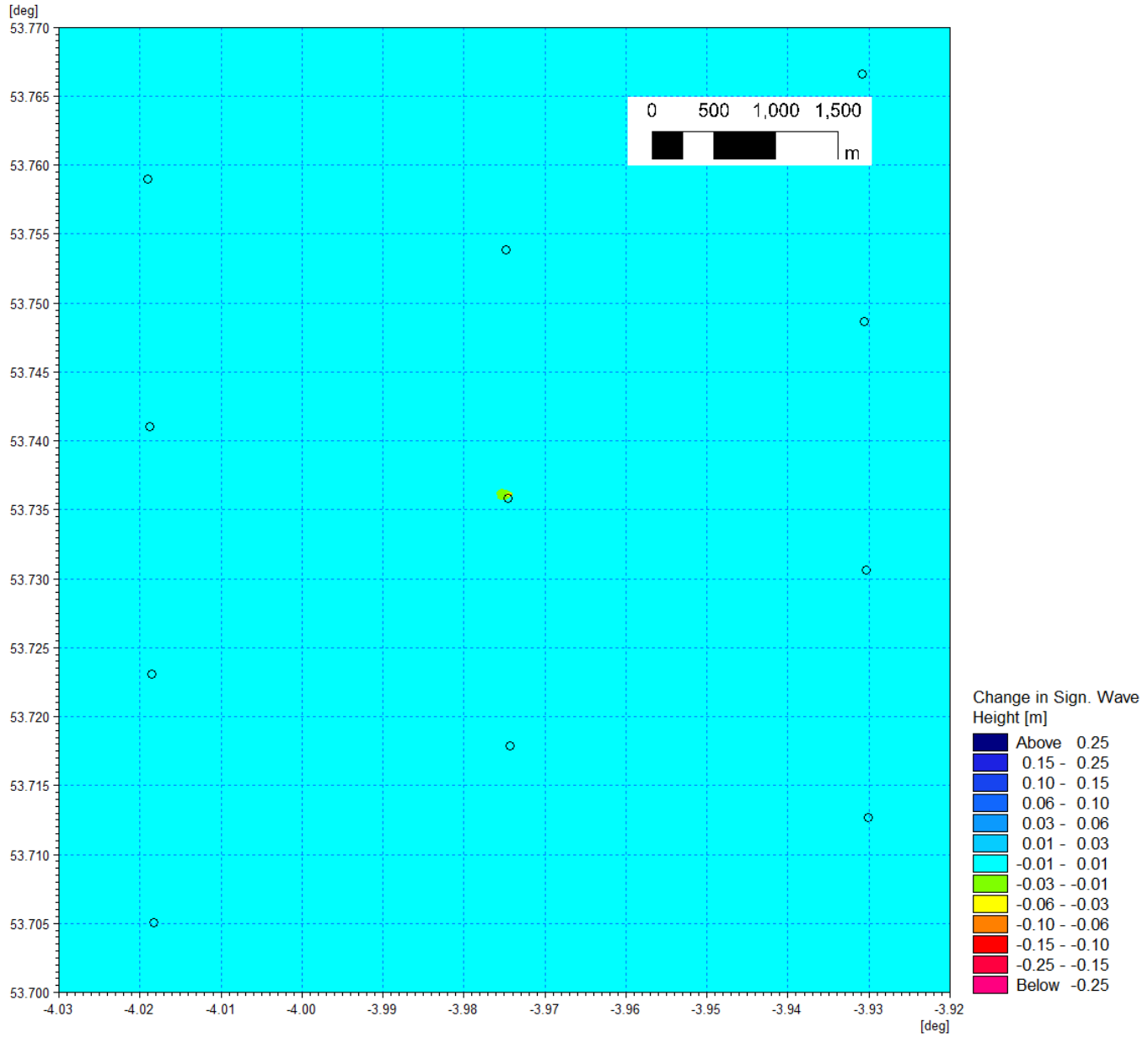

Figure 1.181: Change in wave climate 1 in 1 year storm 090° MHW (post-construction minus baseline) – suction bucket foundation.

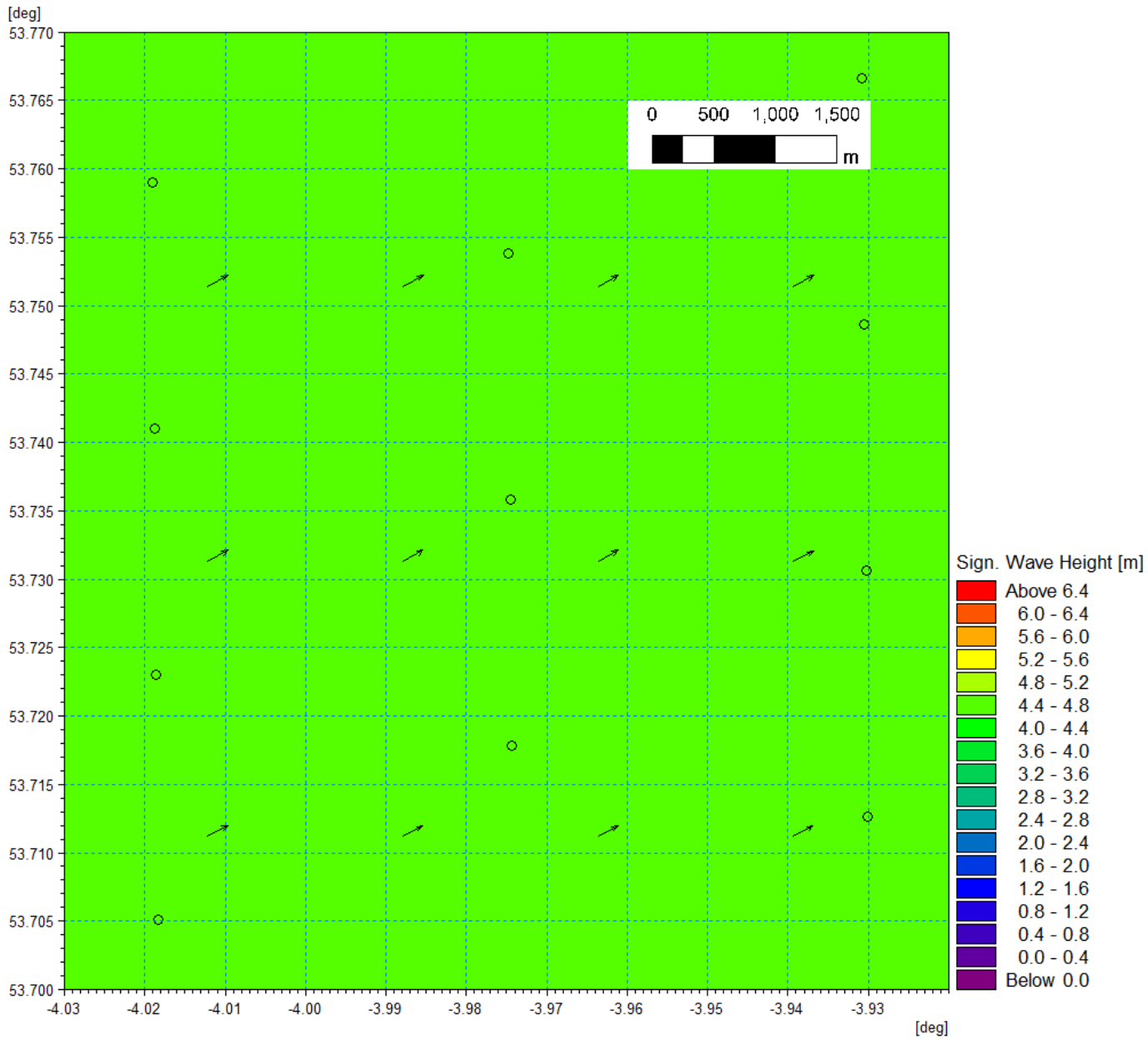

Figure 1.182: Baseline wave climate 1 in 1 year storm 240° MHW.

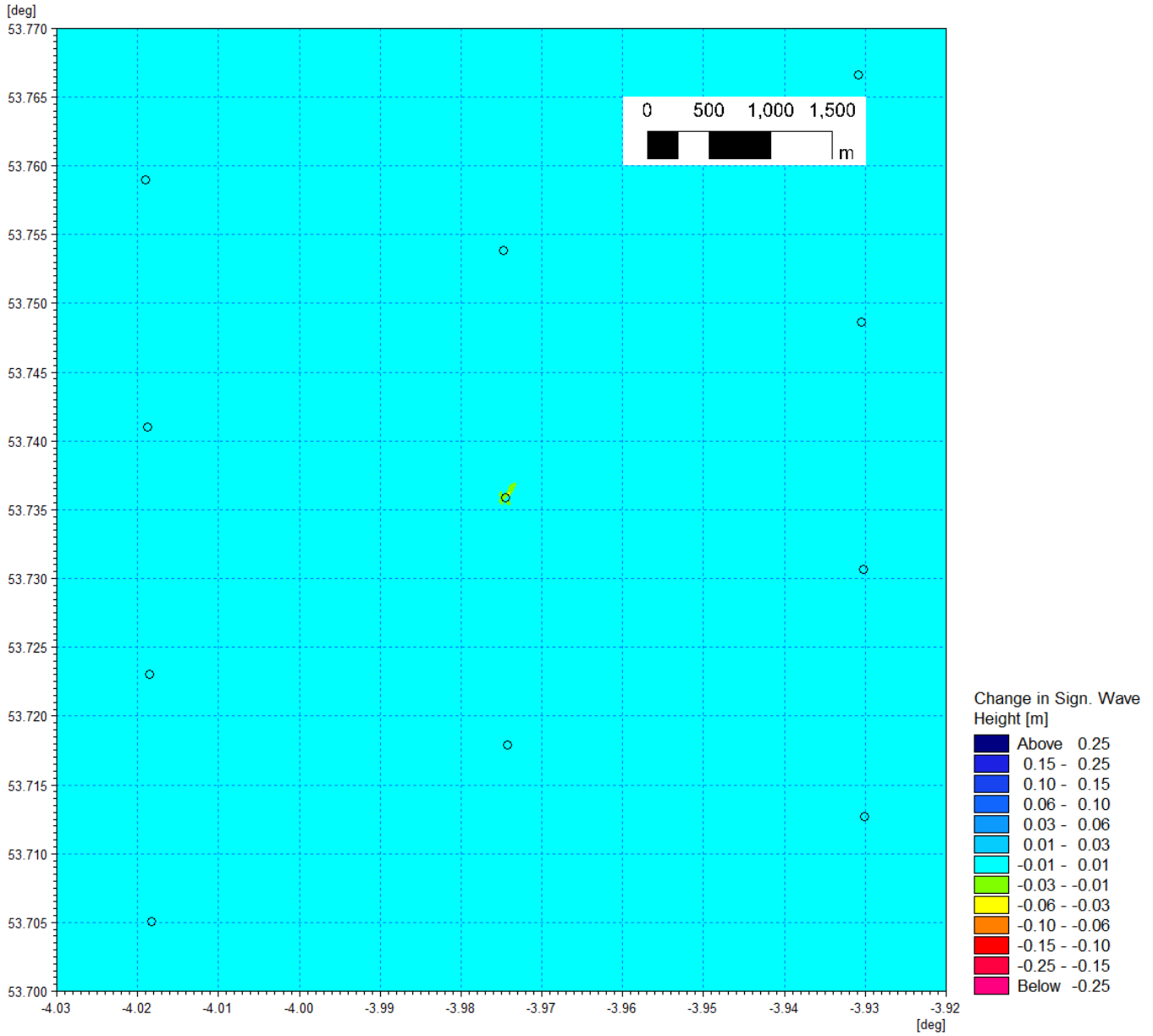

Figure 1.183: Change in wave climate 1 in 1 year storm 240° MHW (post-construction minus baseline) – suction bucket foundation.

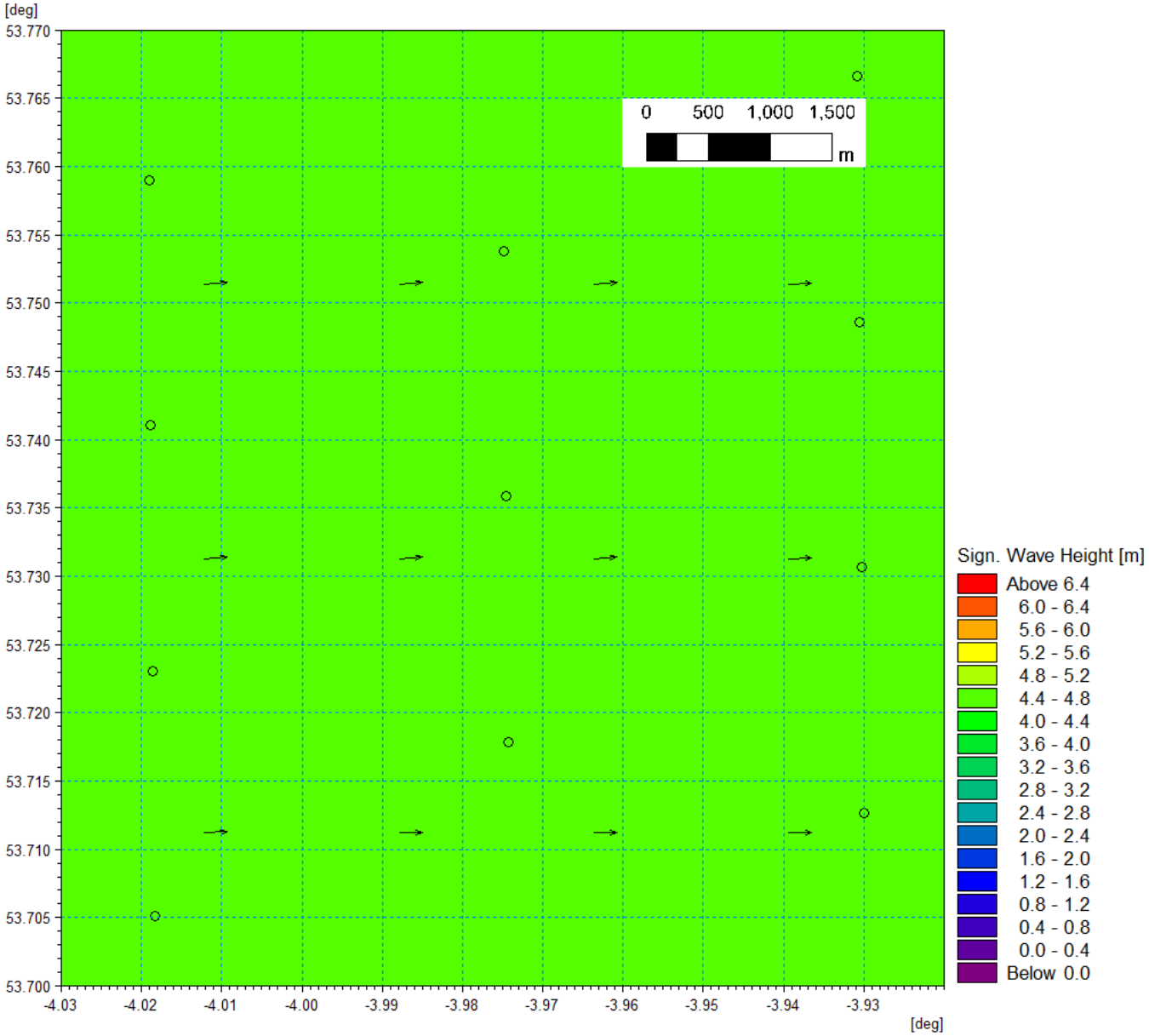

Figure 1.184: Baseline wave climate 1 in 1 year storm 270° MHW.

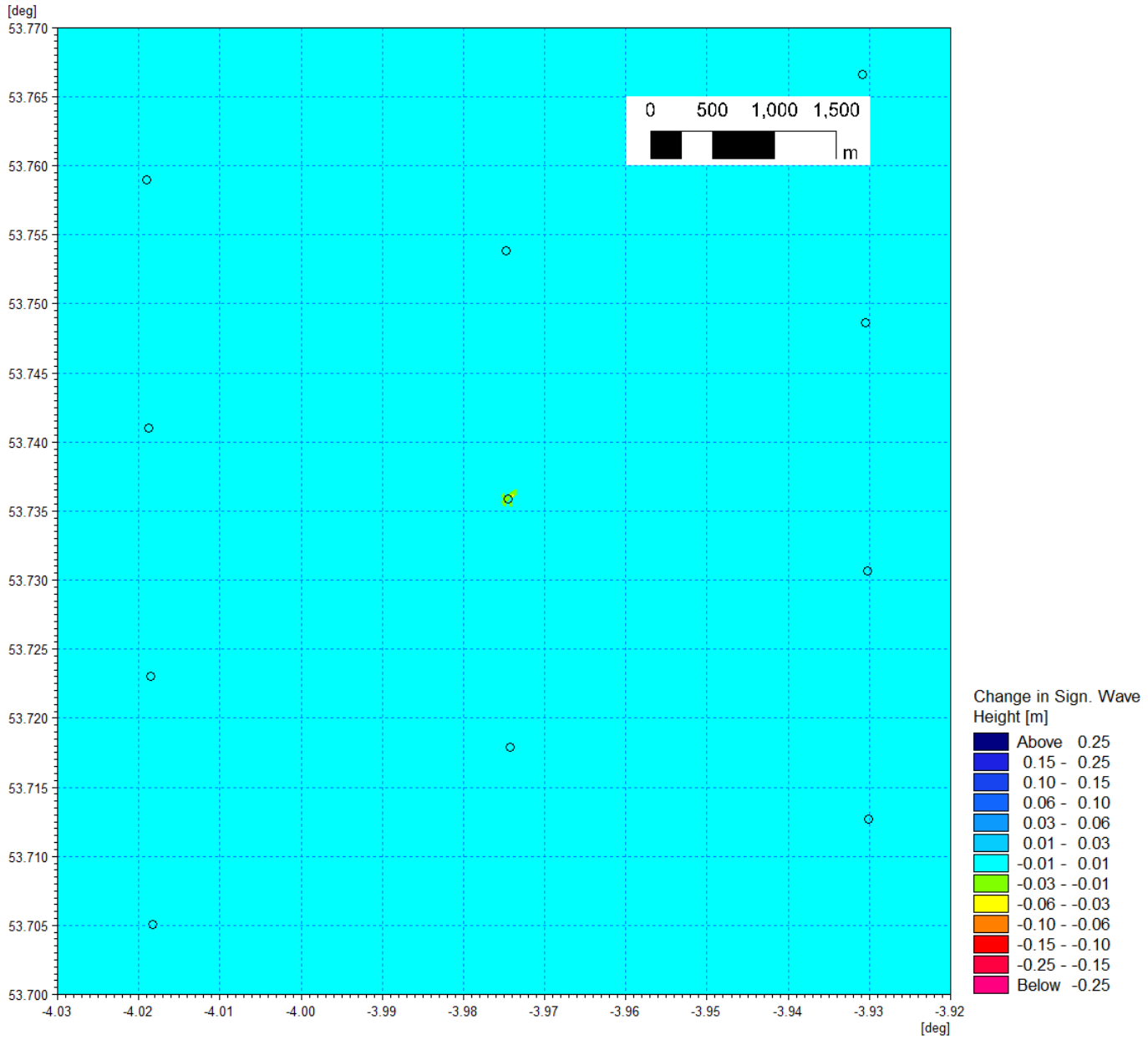

Figure 1.185: Change in wave climate 1 in 1 year storm 270° MHW (post-construction minus baseline) – suction bucket foundation.

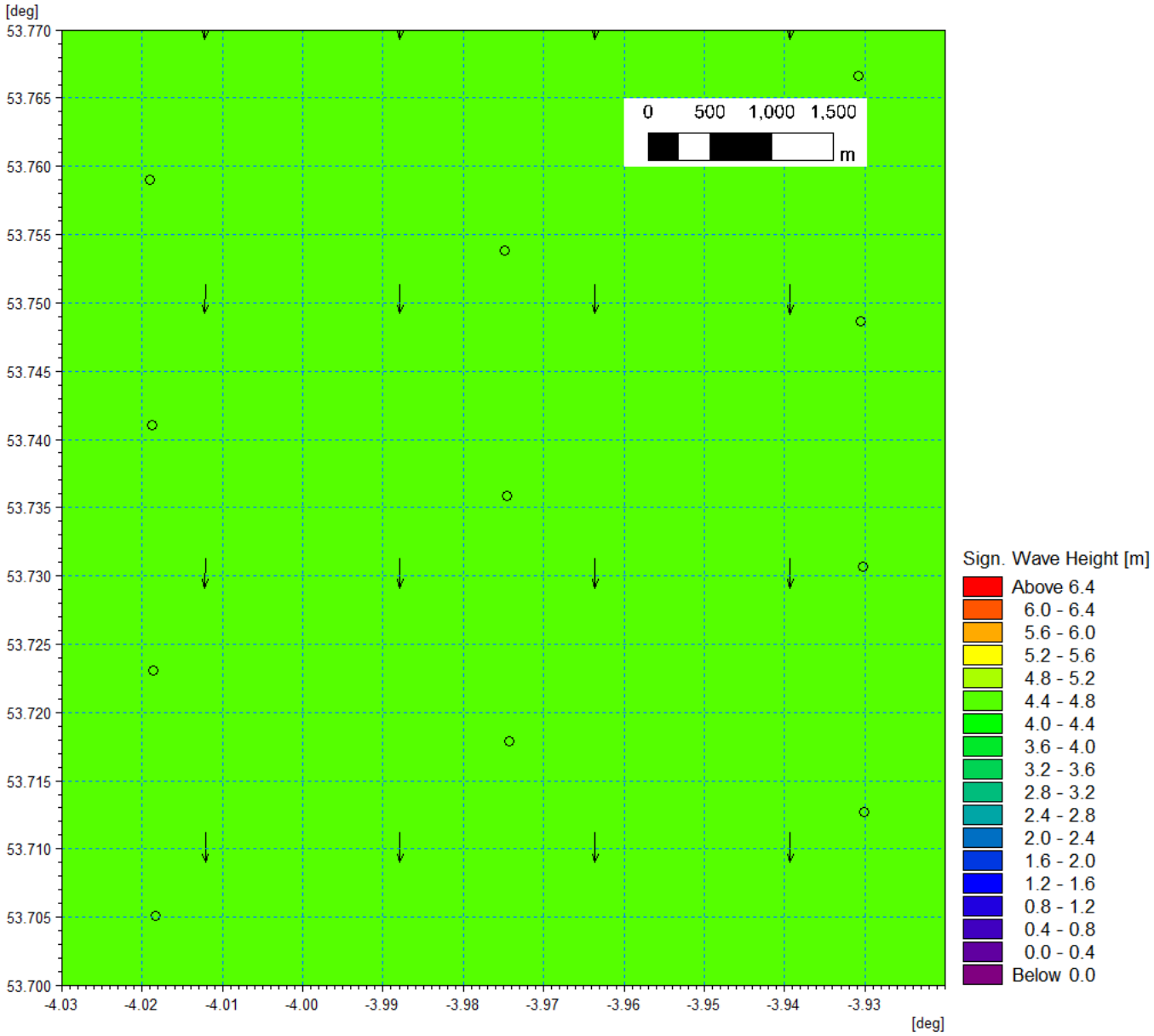

Figure 1.186: Baseline wave climate 1 in 20 year storm 000° MHW.

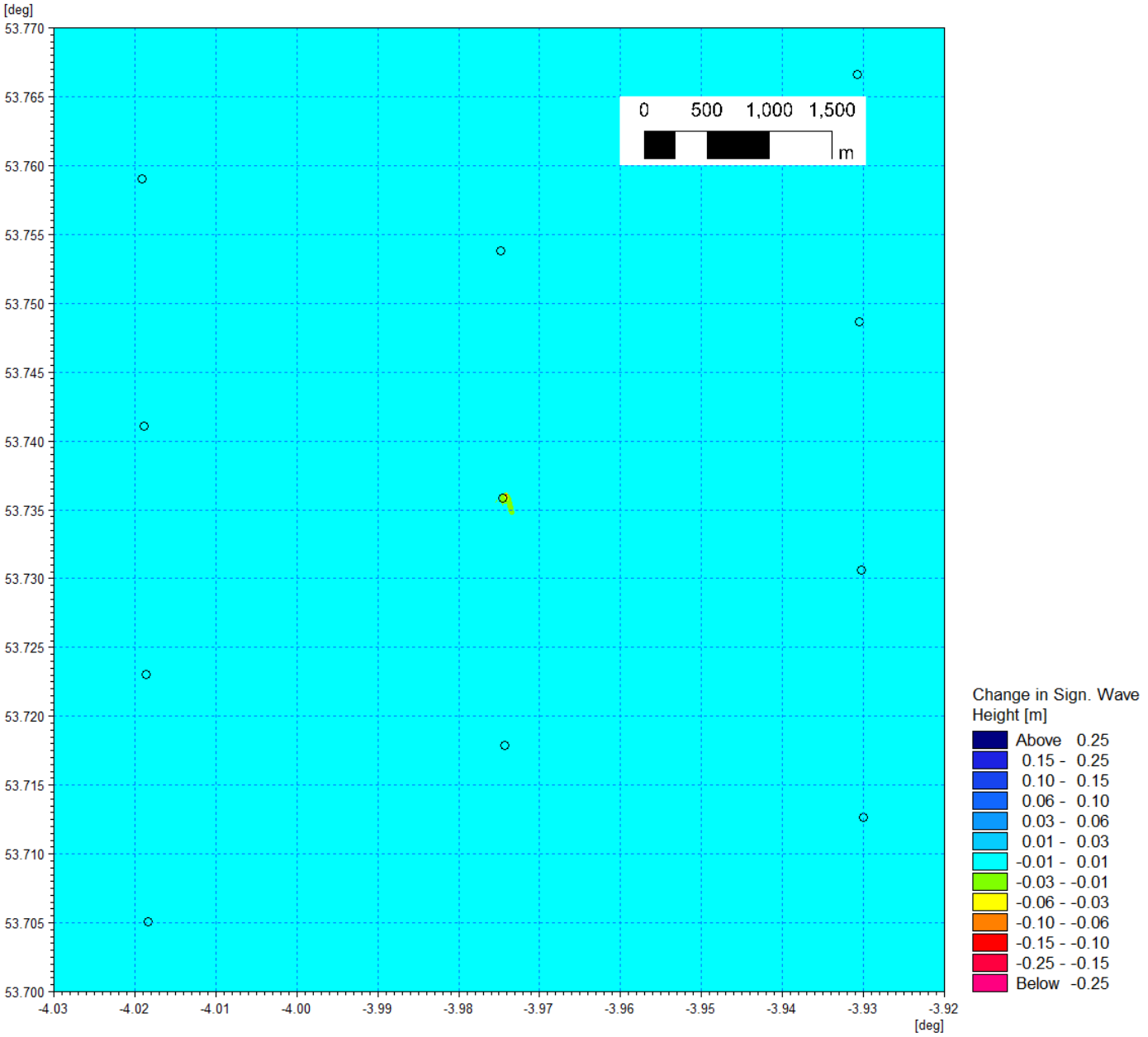

Figure 1.187: Change in wave climate 1 in 20 year storm 000° MHW (post-construction minus baseline) – suction bucket foundation.

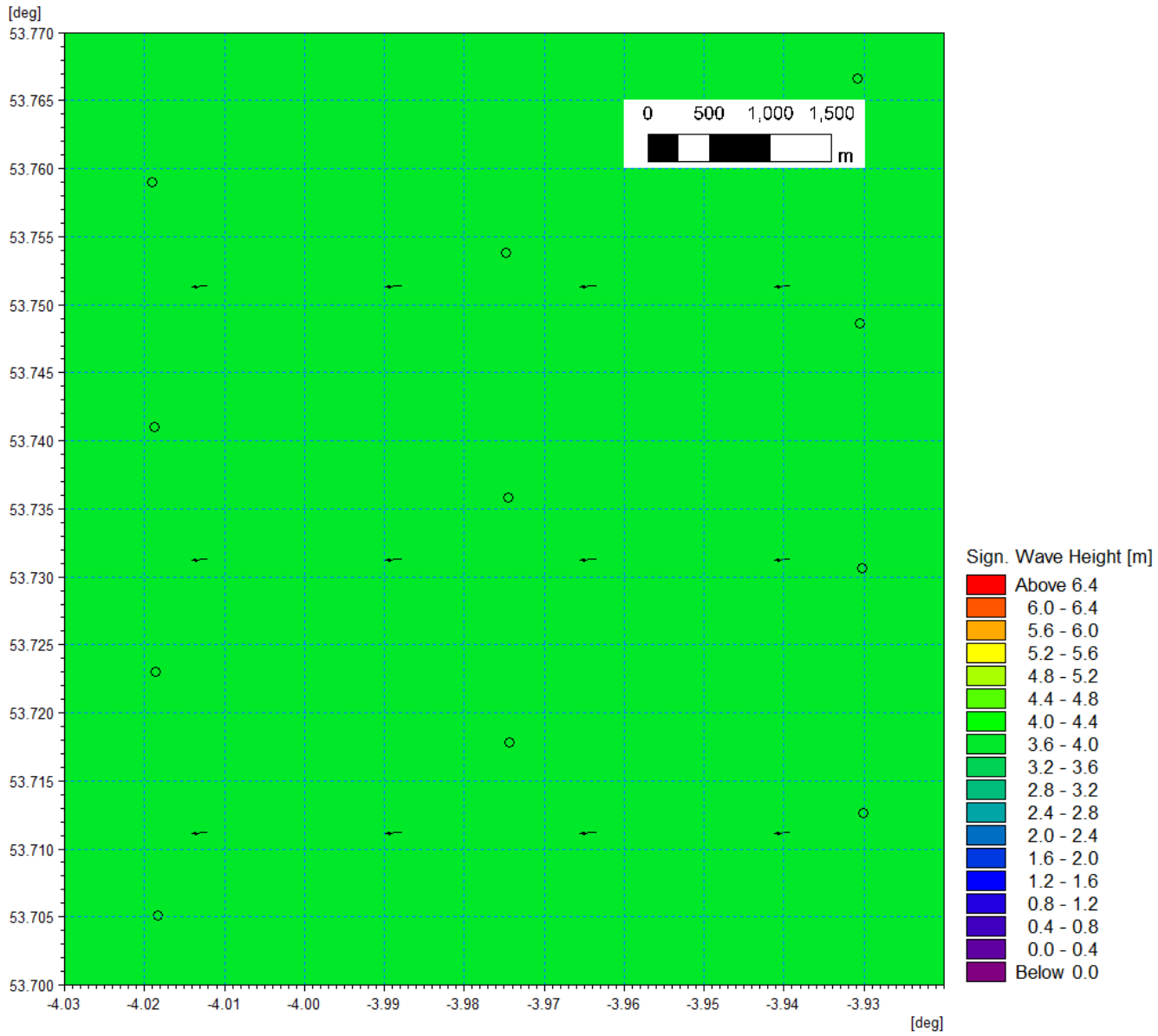

Figure 1.188: Baseline wave climate 1 in 20 year storm 090° MHW.

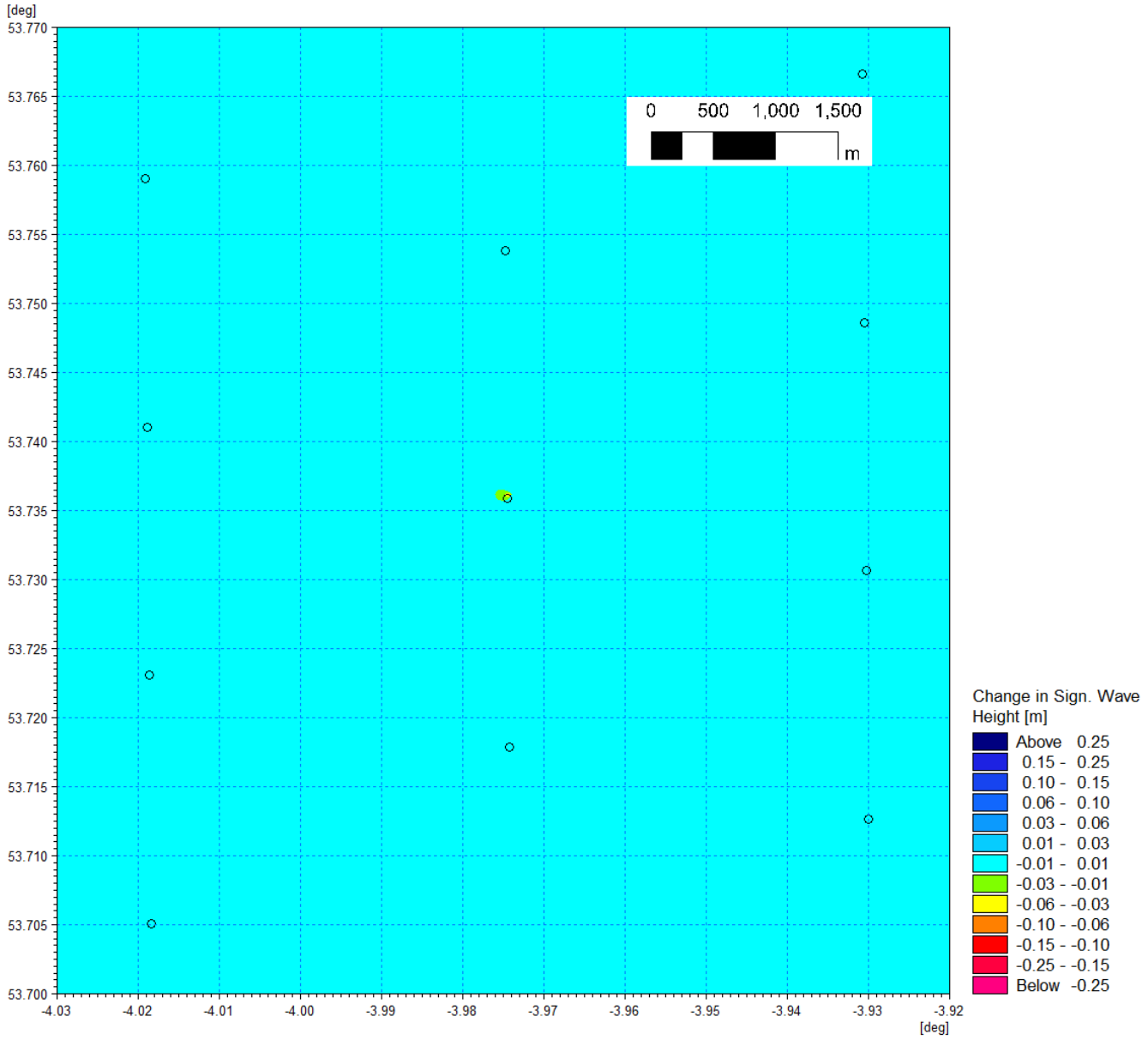

Figure 1.189: Change in wave climate 1 in 20 year storm 090° MHW (post-construction minus baseline) – suction bucket foundation.

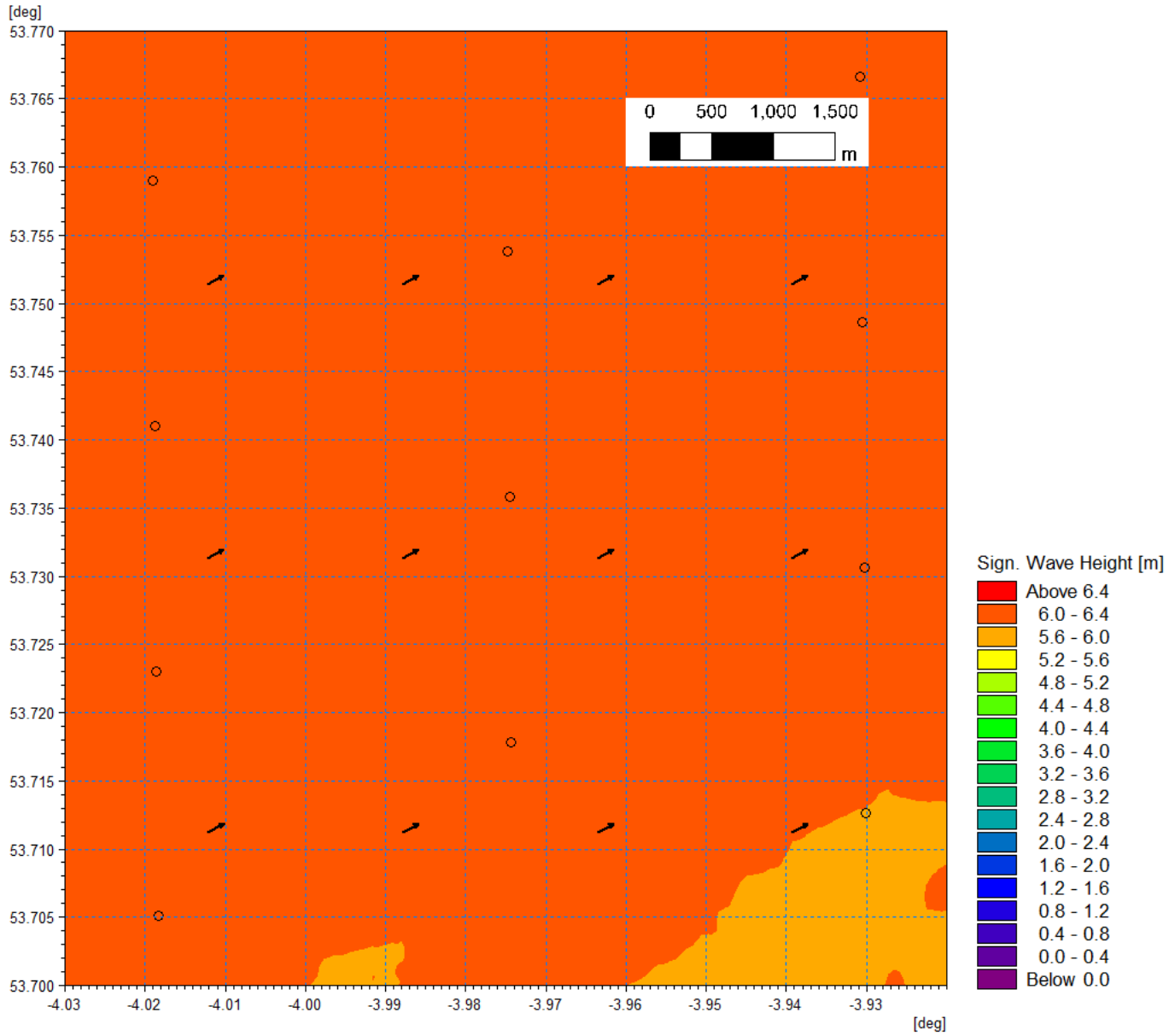

Figure 1.190: Baseline wave climate 1 in 20 year storm 240° MHW.

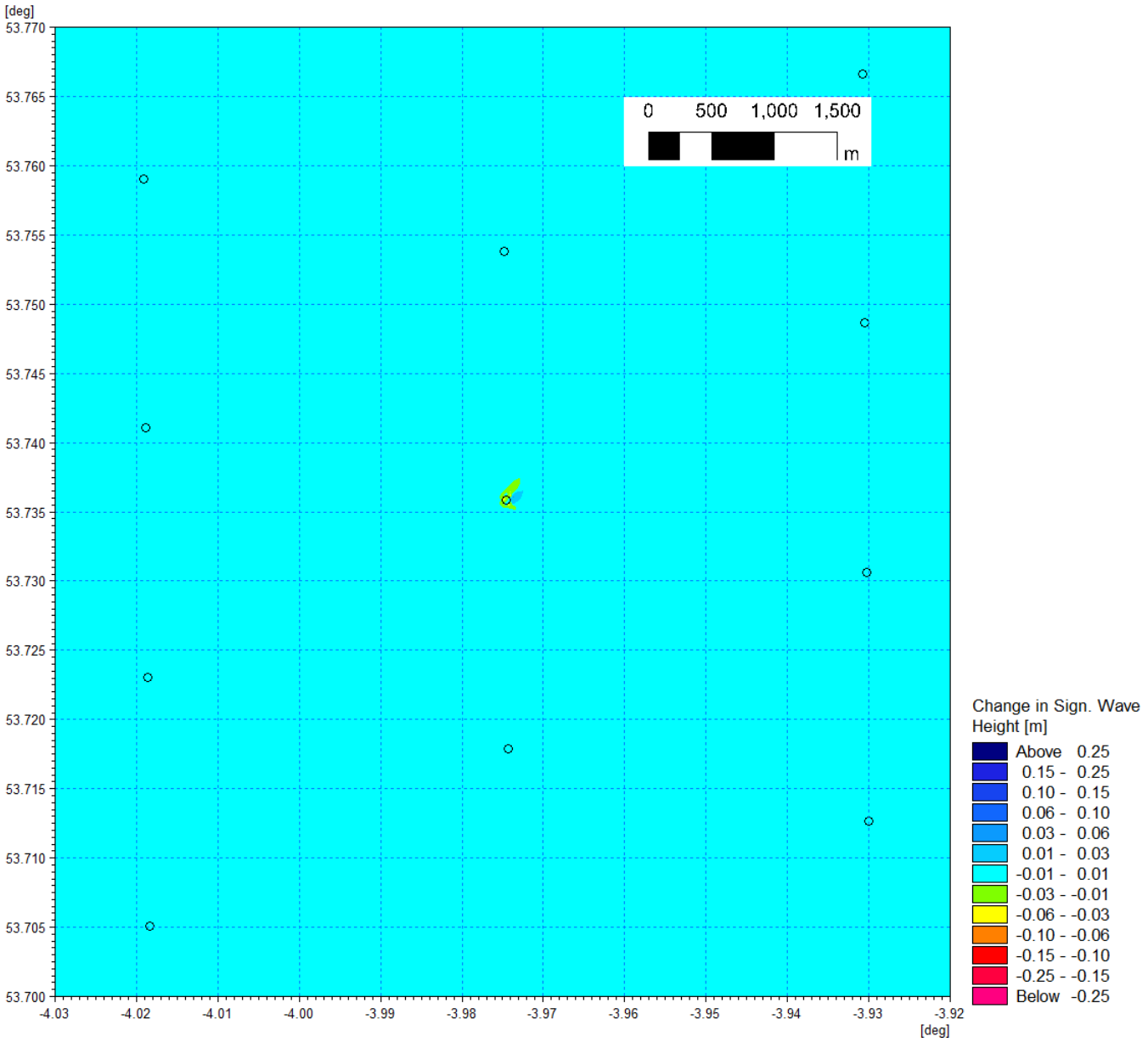

Figure 1.191: Change in wave climate 1 in 20 year storm 240° MHW (post-construction minus baseline) – suction bucket foundation.

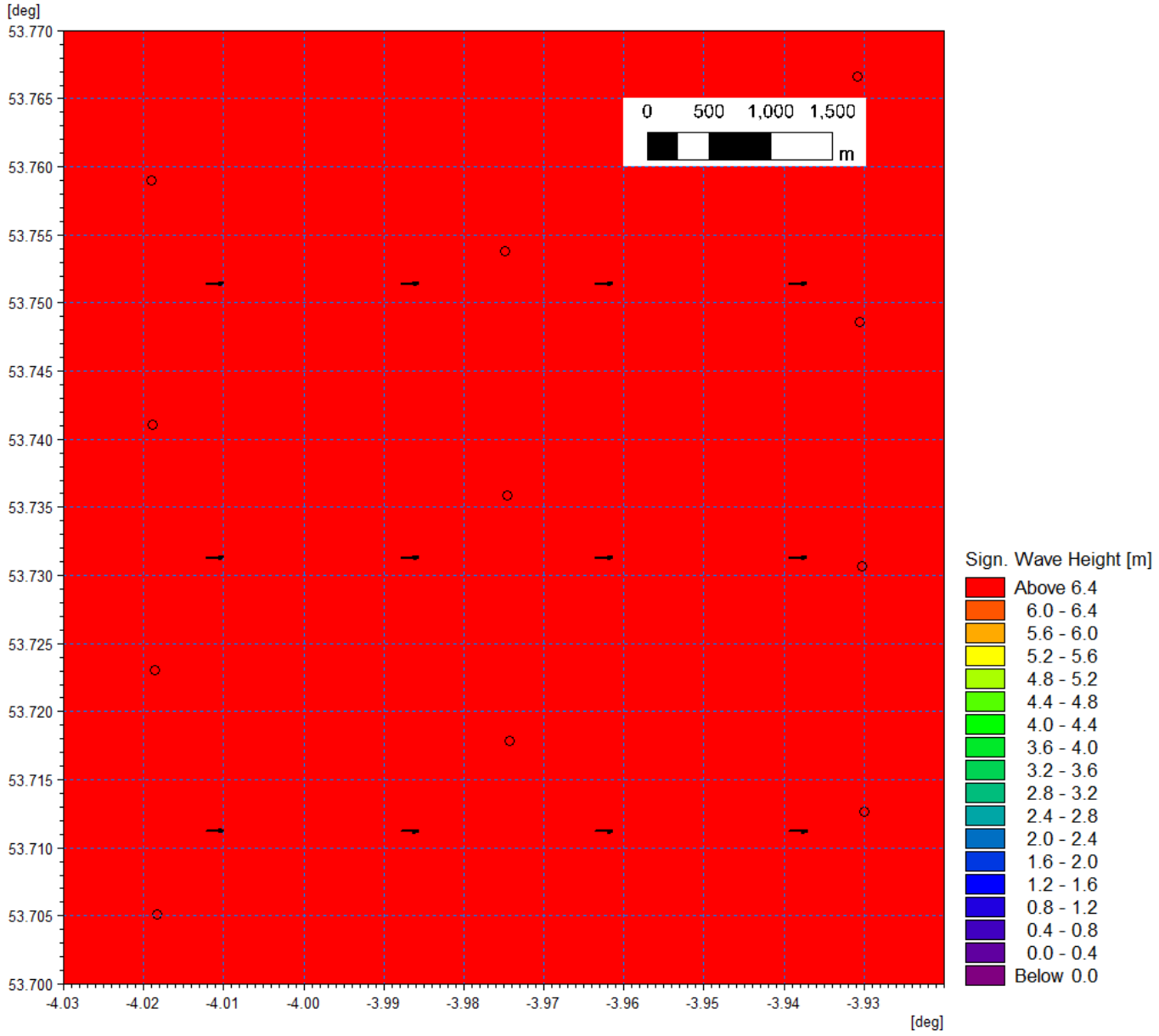

Figure 1.192: Baseline wave climate 1 in 20 year storm 270° MHW.

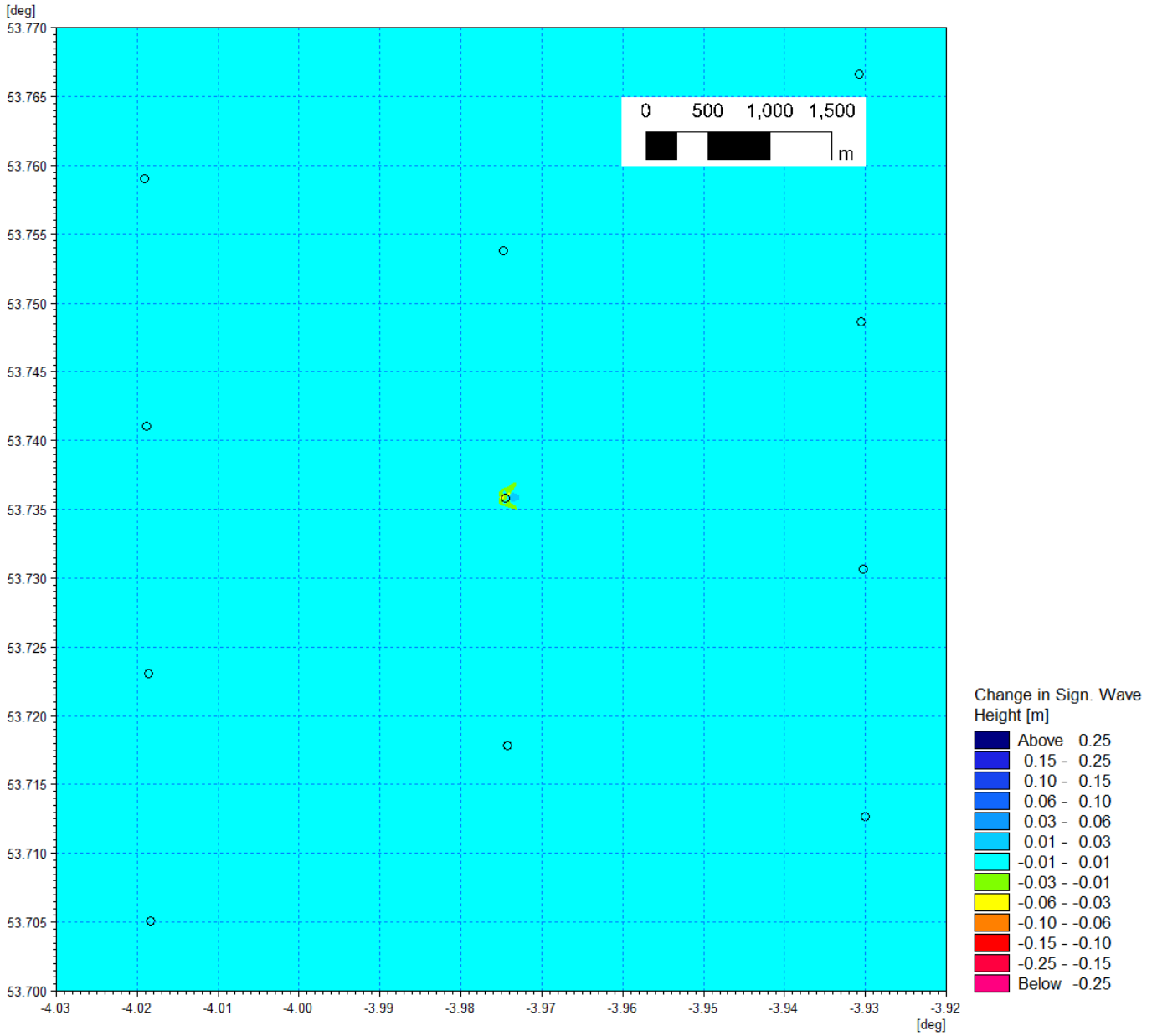

Figure 1.193: Change in wave climate 1 in 20 year storm 270° MHW (post-construction minus baseline) – suction bucket foundation.

1.4.3 Conical gravity base foundations

1.4.3.1 The WTG scenario modelled is the largest conical foundation and is cited in the assessment. The rectangular base provides the MDS for OSP's and is modelled in the final scenario in section 1.4.4. The conical gravity base comprised the following:

- Caisson diameter of 37 m and 15 m diameter at sea surface
- Scour protection average height of 2.6 m extending 24 m from the foundation.

Tidal flow

1.4.3.2 Again, sensitivity testing was performed by repeating the hydrodynamic simulations used to describe the baseline, with the addition of one conical gravity base foundation.

The conical gravity base foundation was included in the sensitivity modelling as it represents the largest potential wind turbine foundation and a typical OSP foundation. The bathymetry was also amended to take account of scour protection. The following figures show the mid flood and mid ebb steps from the simulation respectively, but with one conical gravity base foundation in place.

1.4.3.3 Figure 1.194 shows the baseline flood tide flow patterns with Figure 1.195 showing a focussed plot of the post-construction changes which are limited to the vicinity of the development. In the difference figures a log scale has been introduced to accentuate the values for clarity. Similarly, Figure 1.196 and Figure 1.197 show the same information for the ebb tide. During peak current speed the flow is redirected in the immediate vicinity of the structure. The variation is a maximum of 4 cm/s (decrease in current speed) in the immediate vicinity (50 m) of the structure which constitutes 4% of flows on the flood and *c.* 4.7% on the ebb tide. This reduces significantly with increased distance from each structure falling to a maximum of 2 cm/s, just 100 m from the structure.

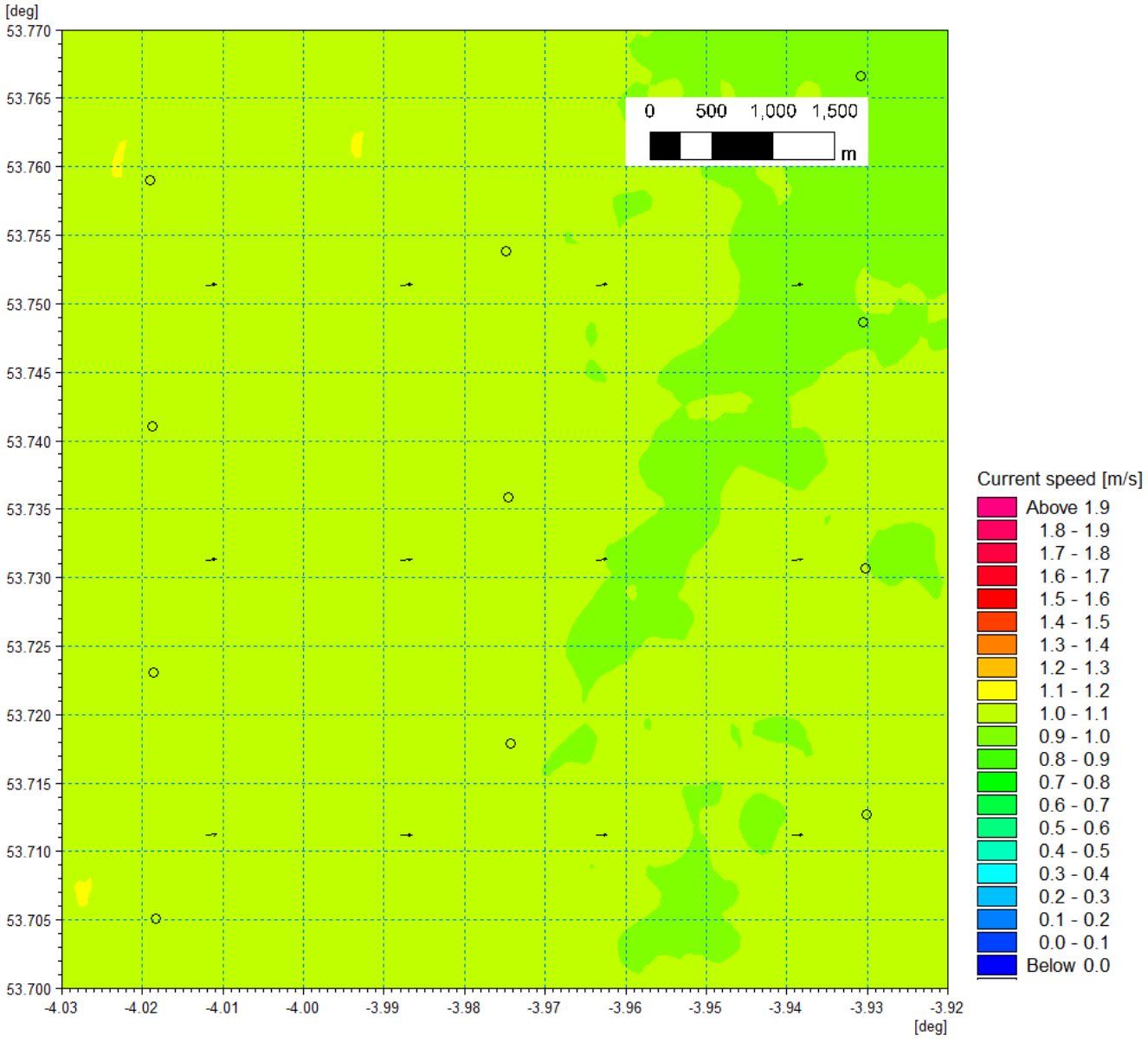

Figure 1.194: Baseline tidal flow pattern – flood tide.

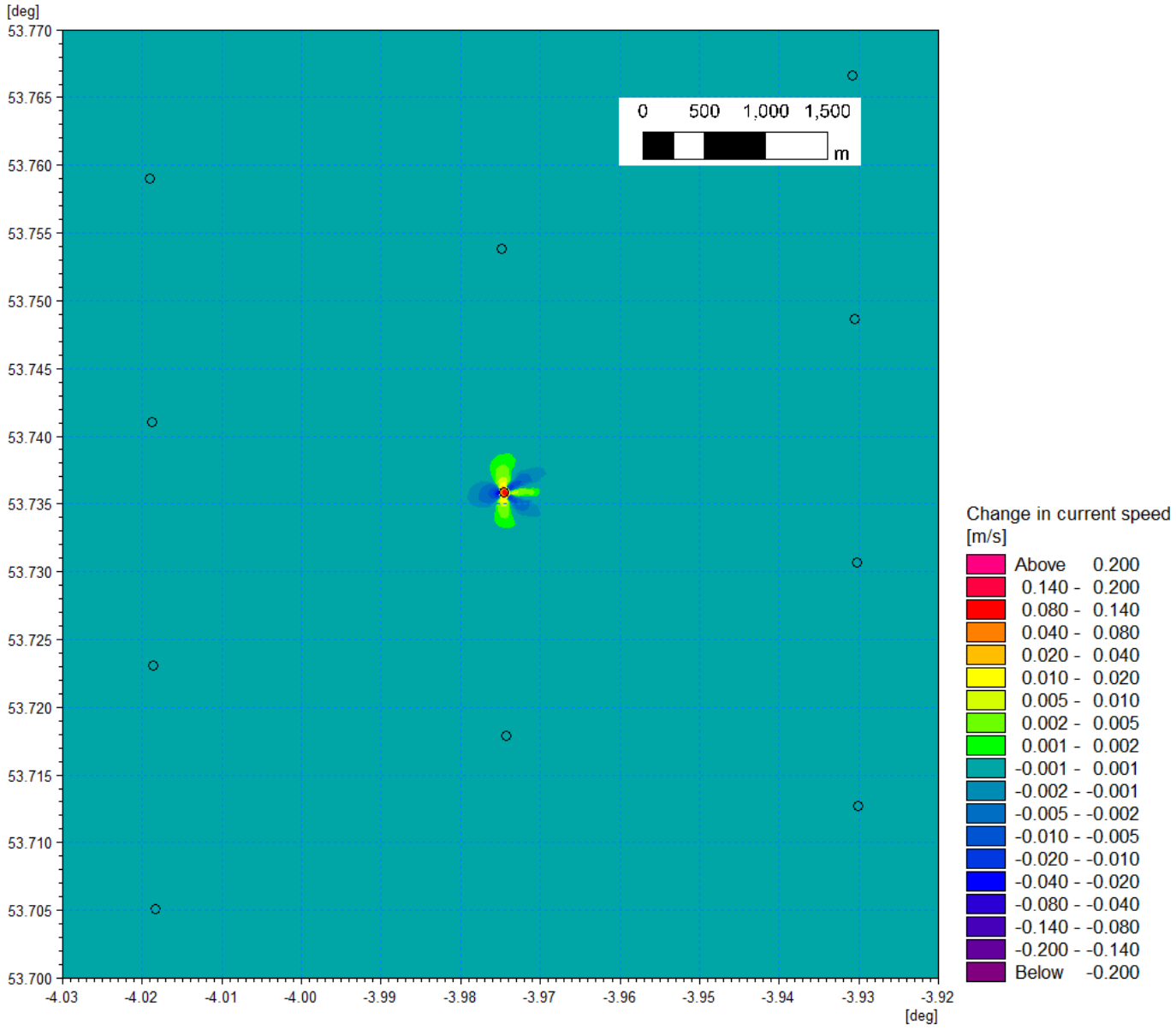

Figure 1.195: Change in tidal flow (post-construction minus baseline) conical gravity base foundation – flood tide.

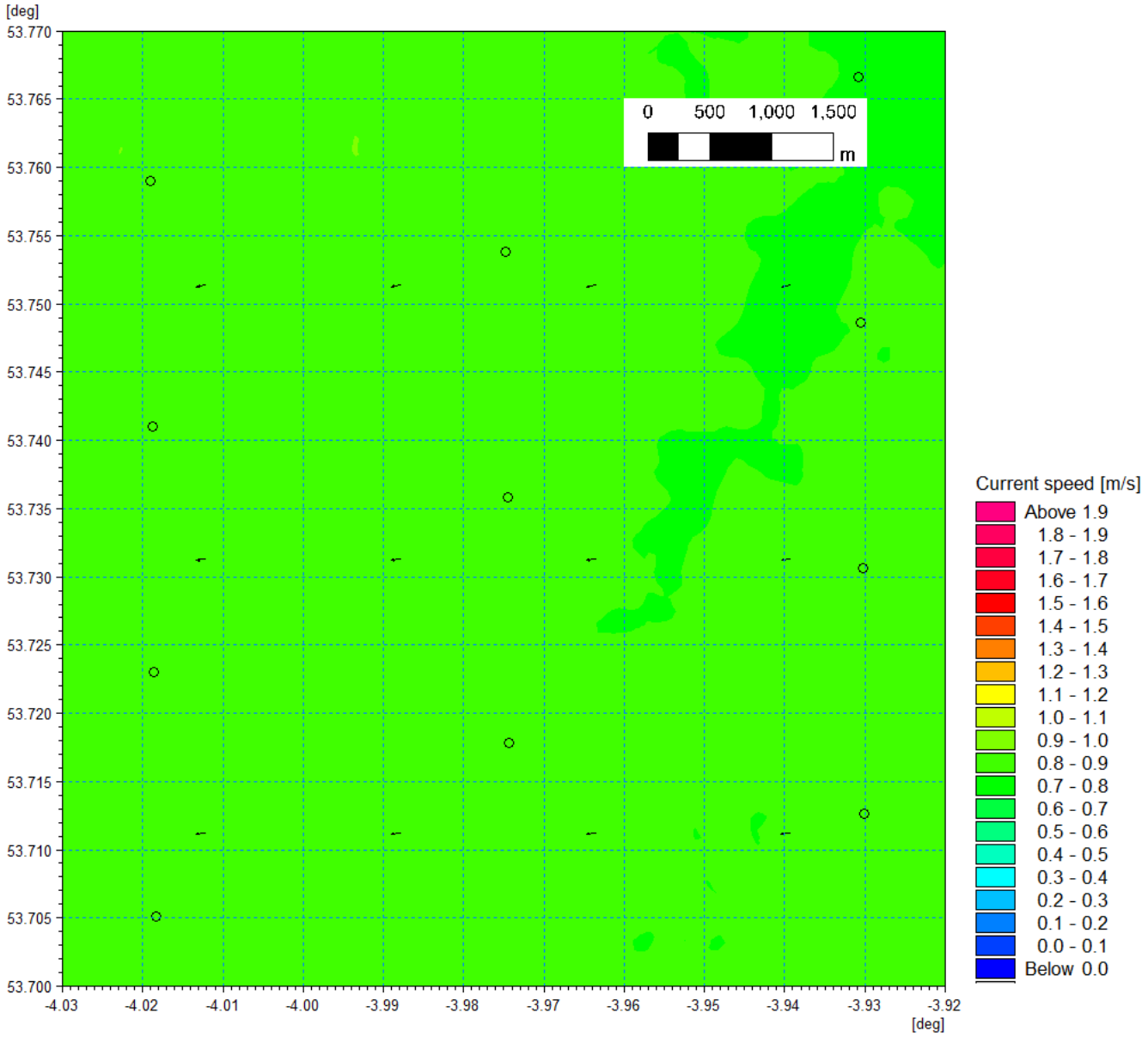

Figure 1.196: Baseline tidal flow pattern – ebb tide.

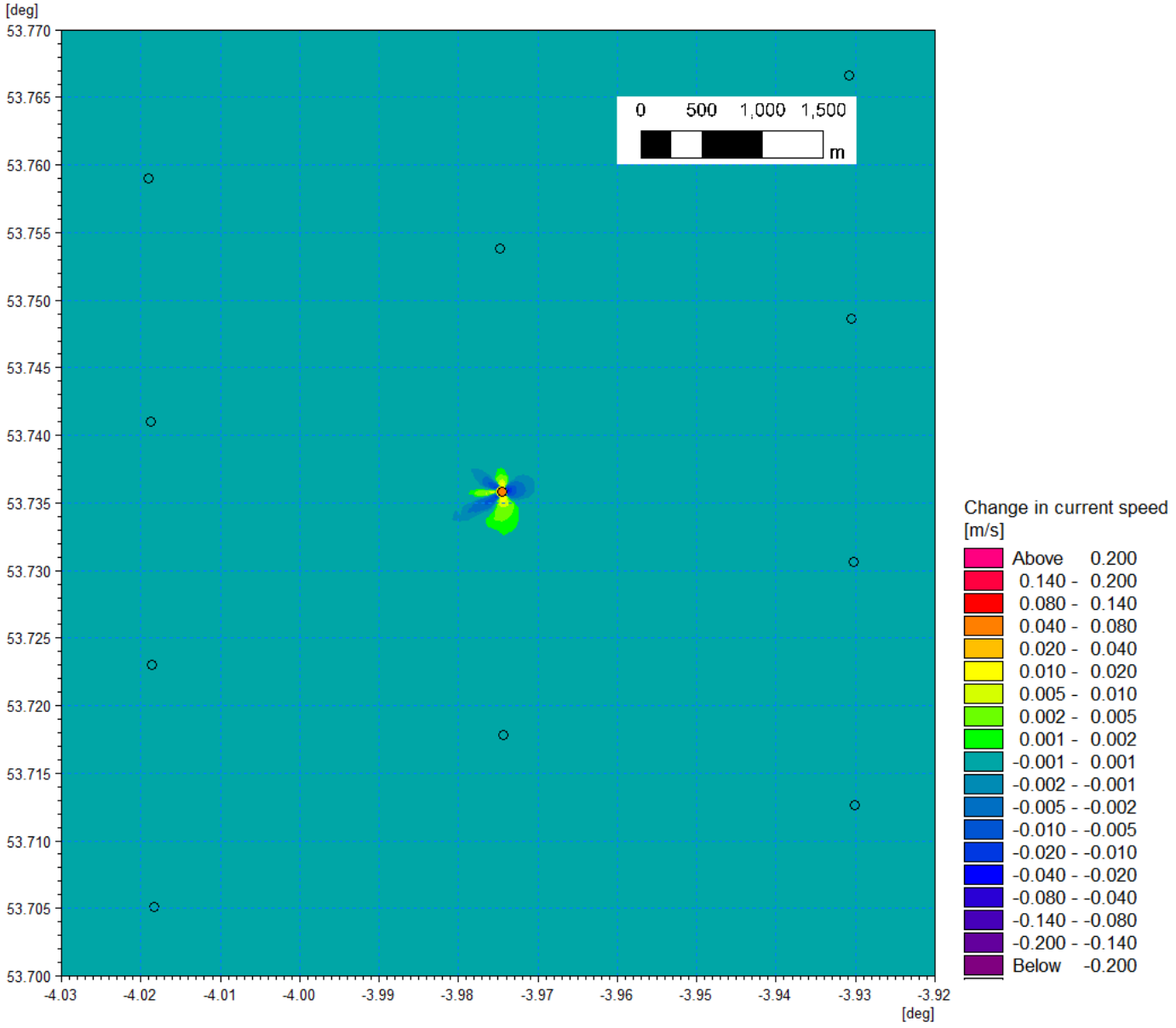

Figure 1.197: Change in tidal flow (post-construction minus baseline) conical gravity base foundation – ebb tide.

Wave climate

1.4.3.4 The baseline phase 000° storm is presented for the 1 in 1 year in Figure 1.198 with the difference shown in Figure 1.199. Similarly, the 1 in 20 year storm from this direction is presented in Figure 1.200 and Figure 1.207. The changes are seen as reductions in the lee of the conical gravity base foundation. The maximum changes observed in the immediate vicinity (50 m) were limited to a maximum of 10 cm which represents *c.* 2% of the baseline significant wave height (4.8 m). The wave shadow is typically less than one half of this value. These changes would be indiscernible from the baseline wave climate.

1.4.3.5 The changes to waves originating from 090° sector are shown in Figure 1.201 and Figure 1.209, both 1 in 1 and 1 in 20 year storm waves are of similar magnitudes to those experienced from the seen from 000° sector, falling within *c.* 2.5% of the baseline wave height (3.8 m) within 50 m of the structure. These changes reduce in magnitude

with distance from the structure, 100 m and 200m from the foundation changes are limited to 6 cm (*c.* 1.5%) and 3 cm (*c.* 1%) respectively.

1.4.3.6 Storm waves originating from 240° and 270° are of a greater magnitude than those discussed above, with significant wave heights in excess of. 6.2 m in the vicinity of the modelled foundation. During a 1 in 20 year storm post construction waves may experience a change up to a maximum of 25 cm or *c.* 4% in the immediate vicinity of the conical gravity base foundation. These changes reduce in magnitude with distance from the structure, 200m from the foundation changes are limited to 6 cm (<1%).

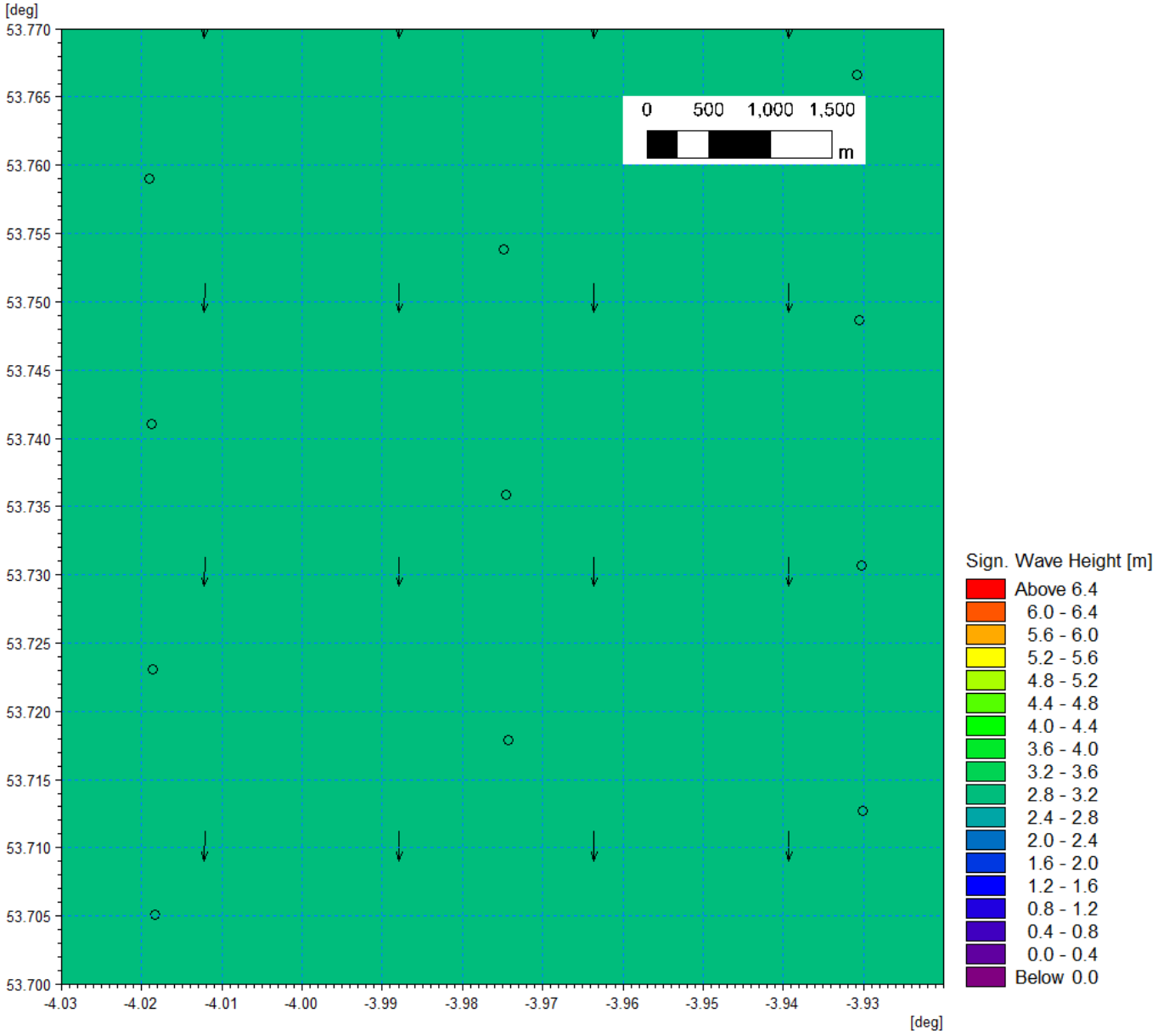

Figure 1.198: Baseline wave climate 1 in 1 year storm 000° MHW.

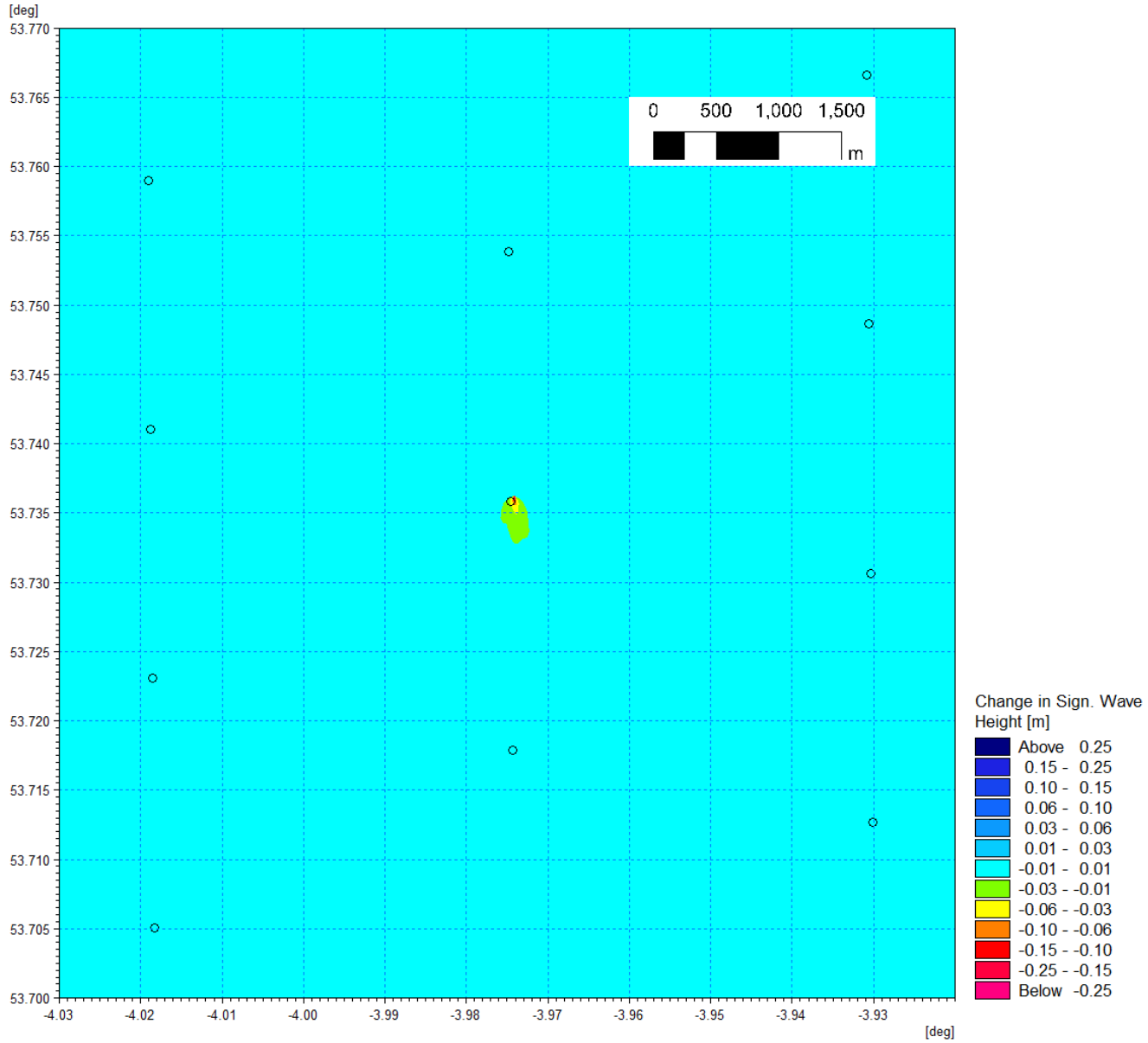

Figure 1.199: Change in wave climate 1 in 1 year storm 000° MHW (post-construction minus baseline) – conical gravity base foundation.

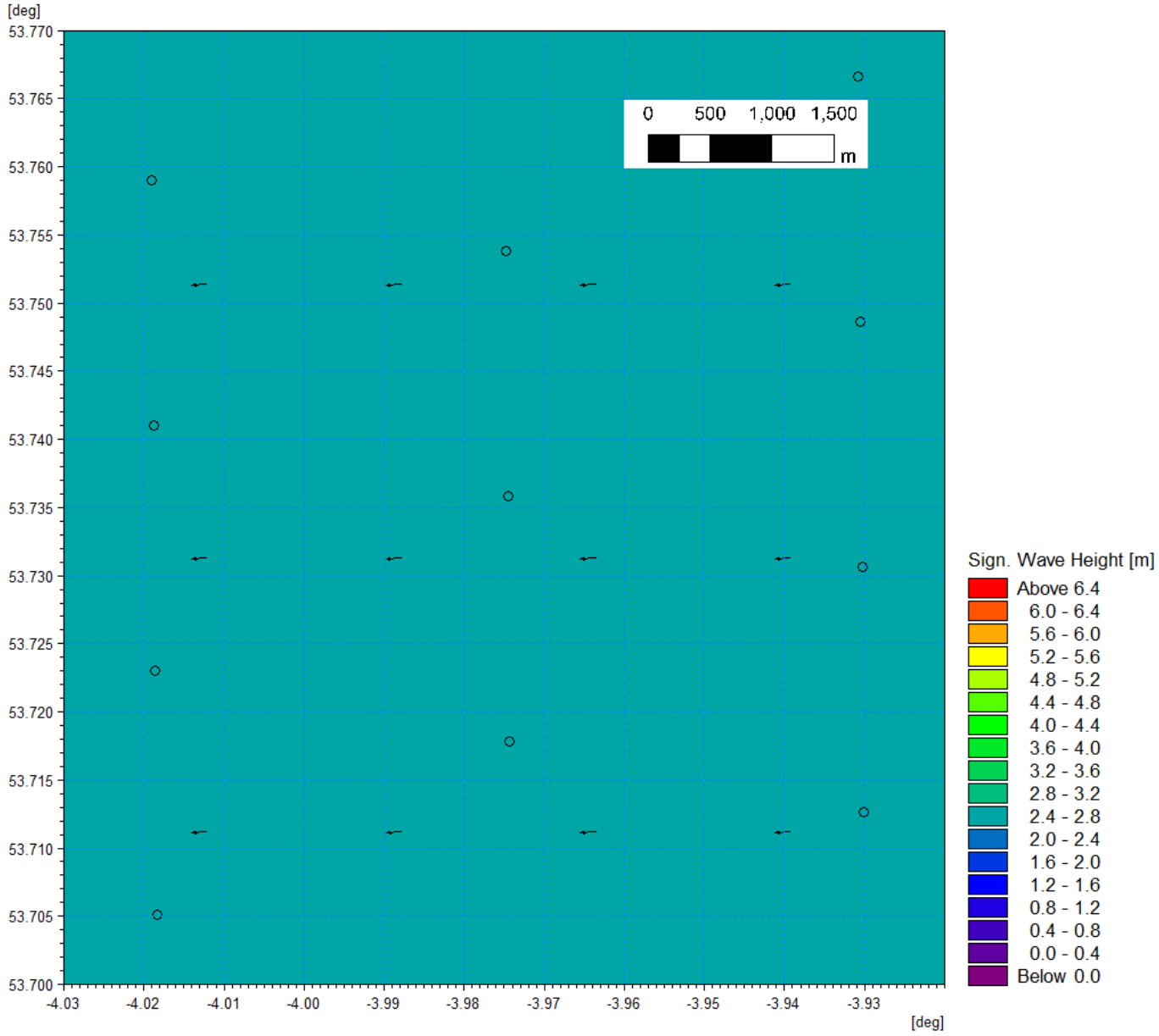

Figure 1.200: Baseline wave climate 1 in 1 year storm 090° MHW.

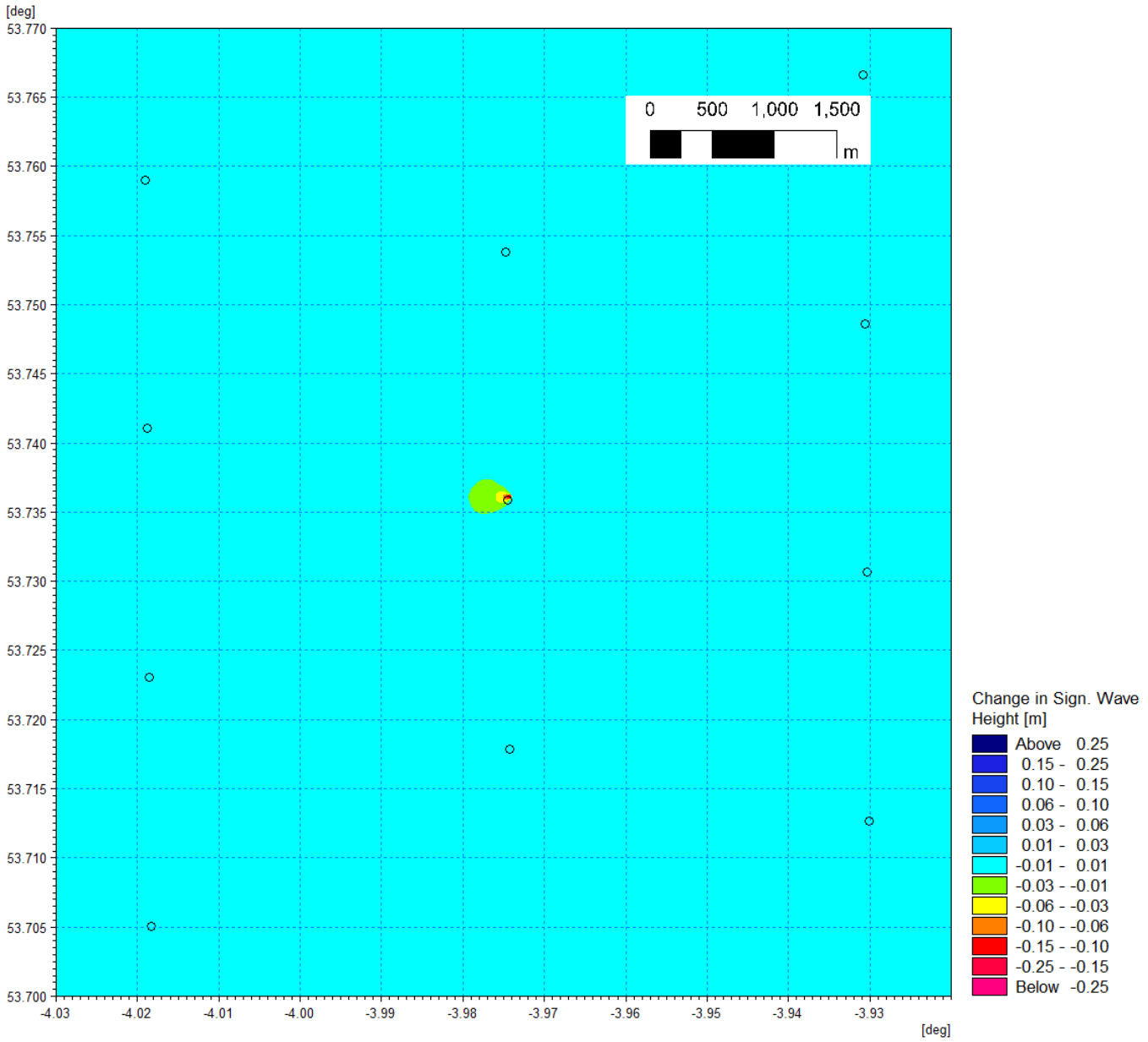

Figure 1.201: Change in wave climate 1 in 1 year storm 090° MHW (post-construction minus baseline) – conical gravity base foundation.

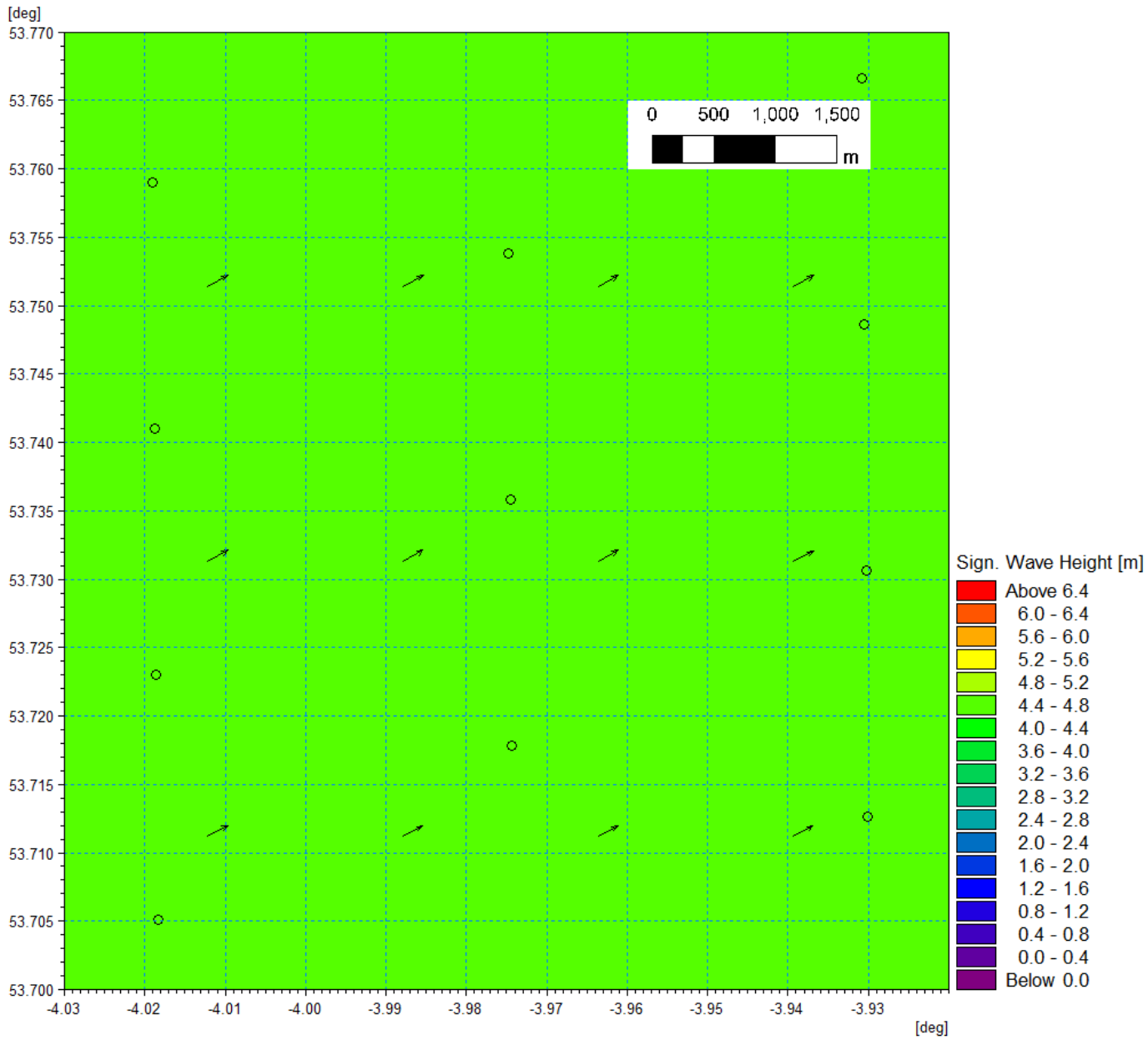

Figure 1.202: Baseline wave climate 1 in 1 year storm 240° MHW.

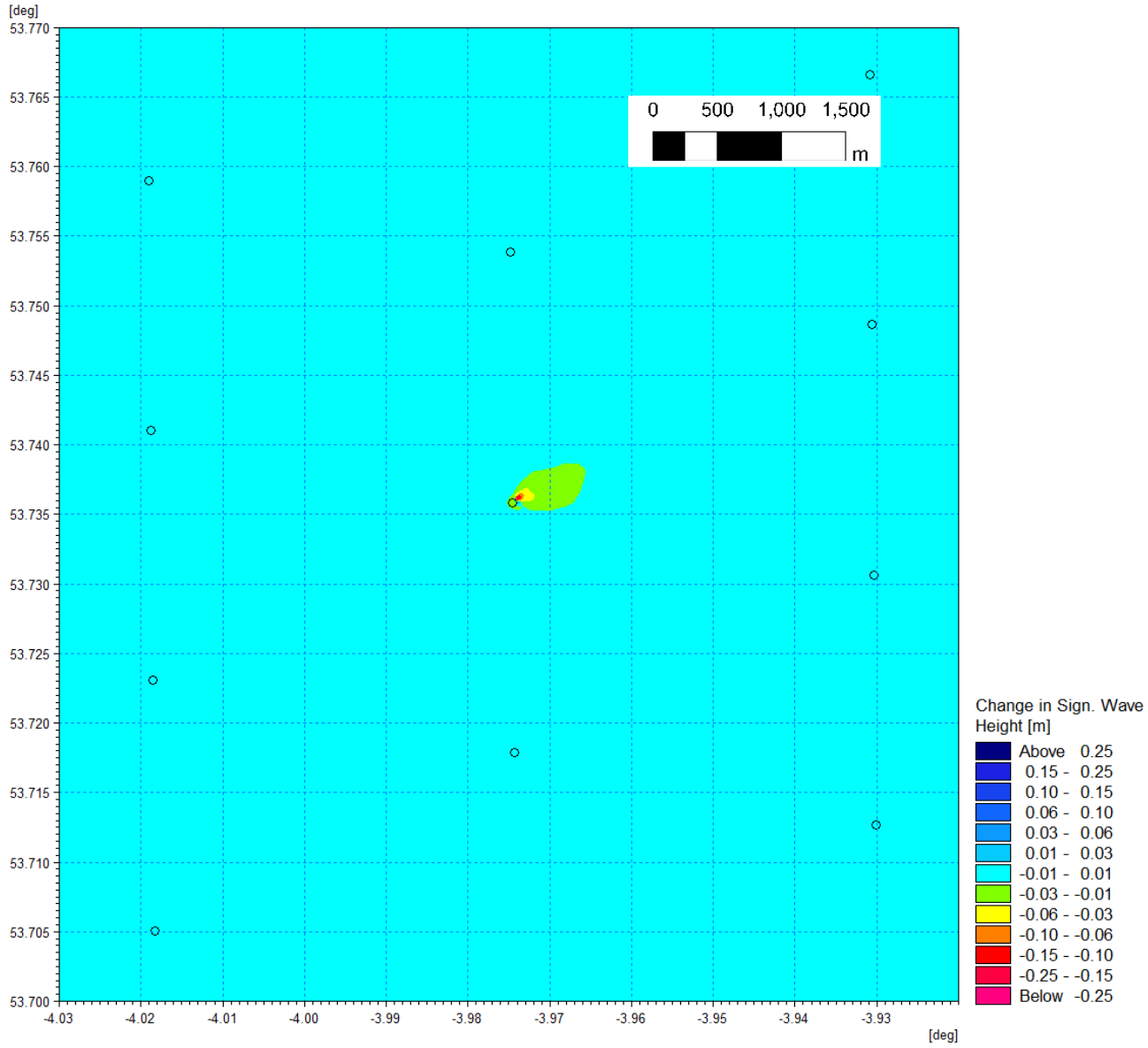

Figure 1.203: Change in wave climate 1 in 1 year storm 240° MHW (post-construction minus baseline) – conical gravity base foundation.

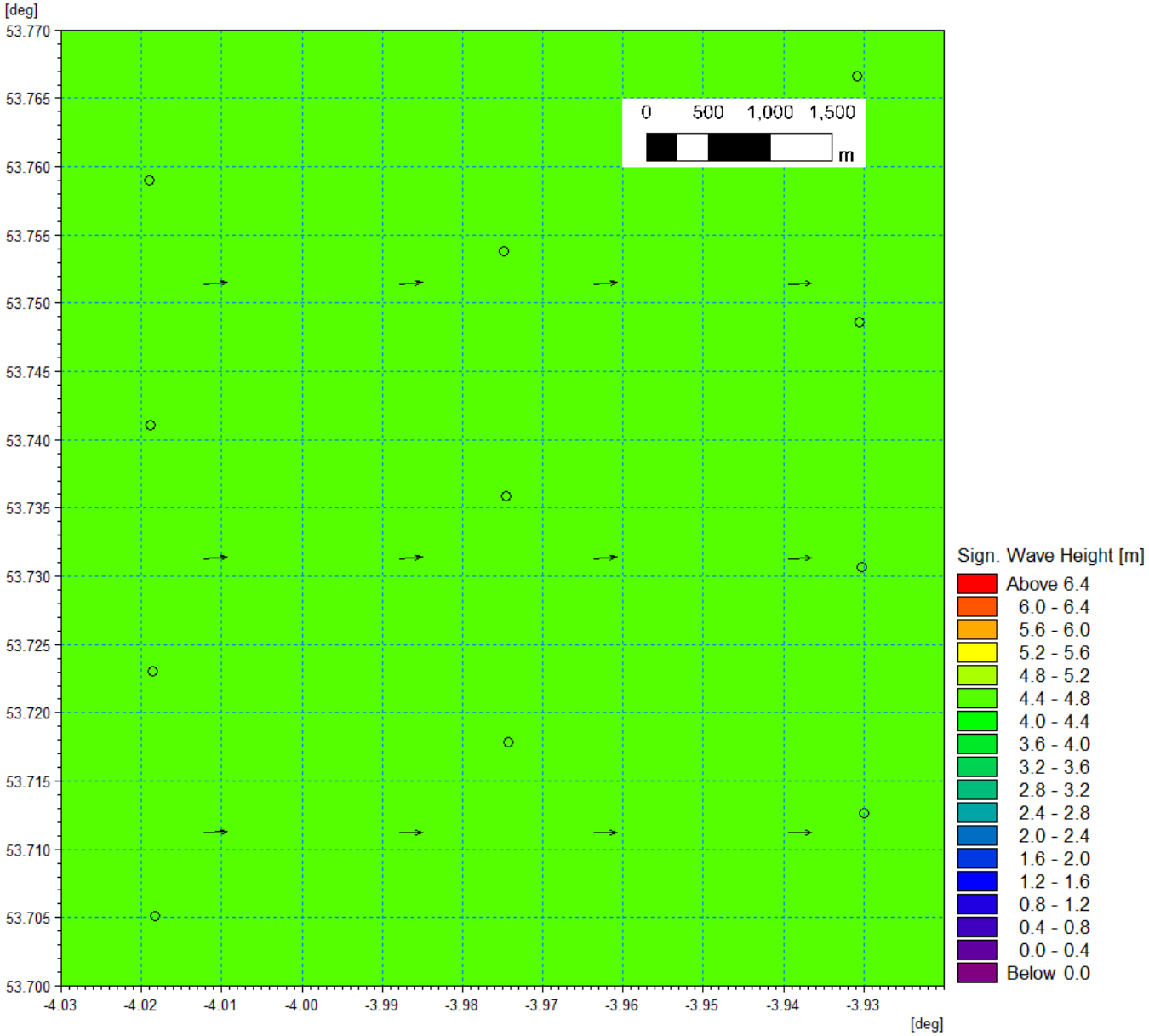

Figure 1.204: Baseline wave climate 1 in 1 year storm 270° MHW.

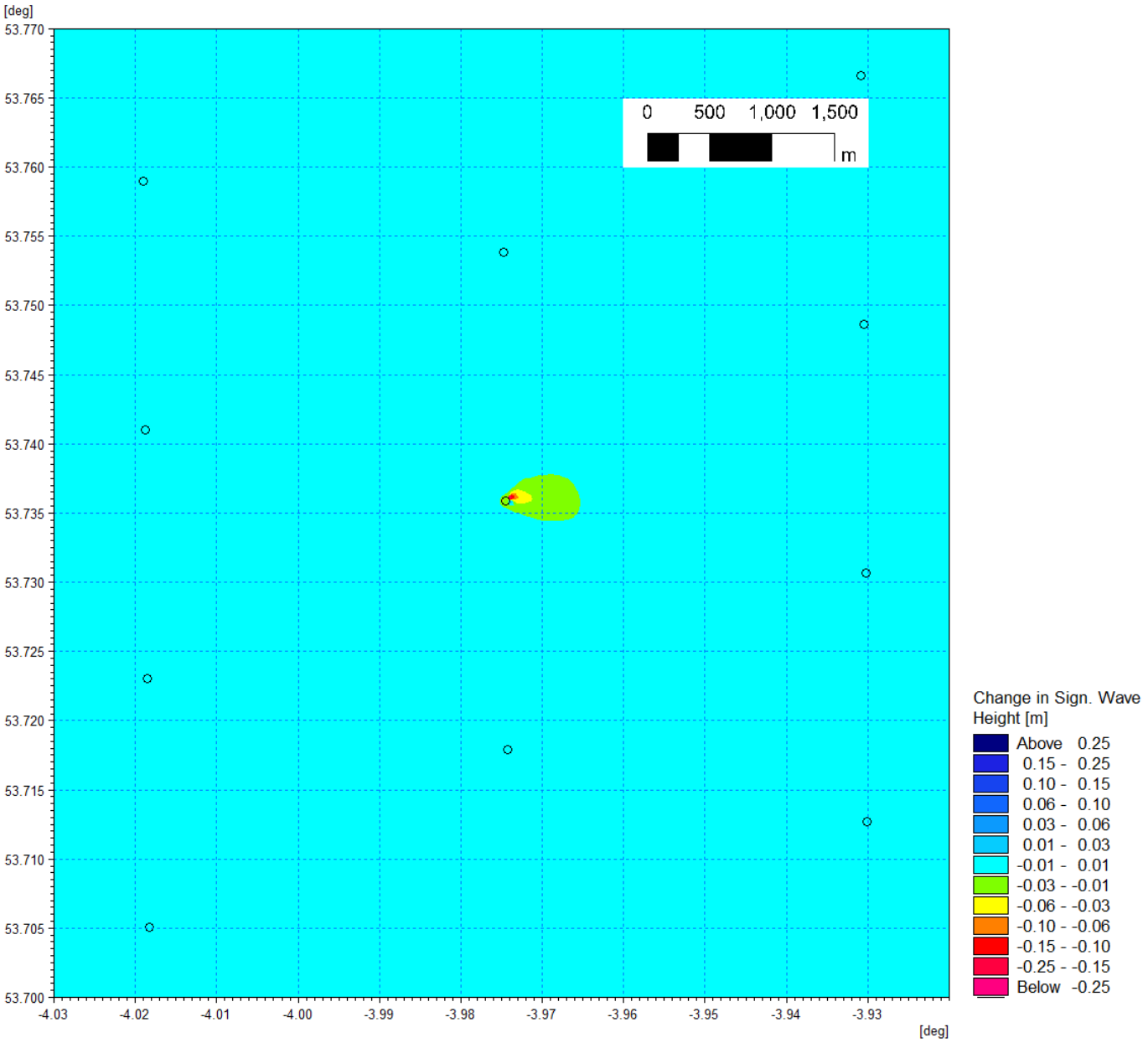

Figure 1.205: Change in wave climate 1 in 1 year storm 270° MHW (post-construction minus baseline) – conical gravity base foundation.

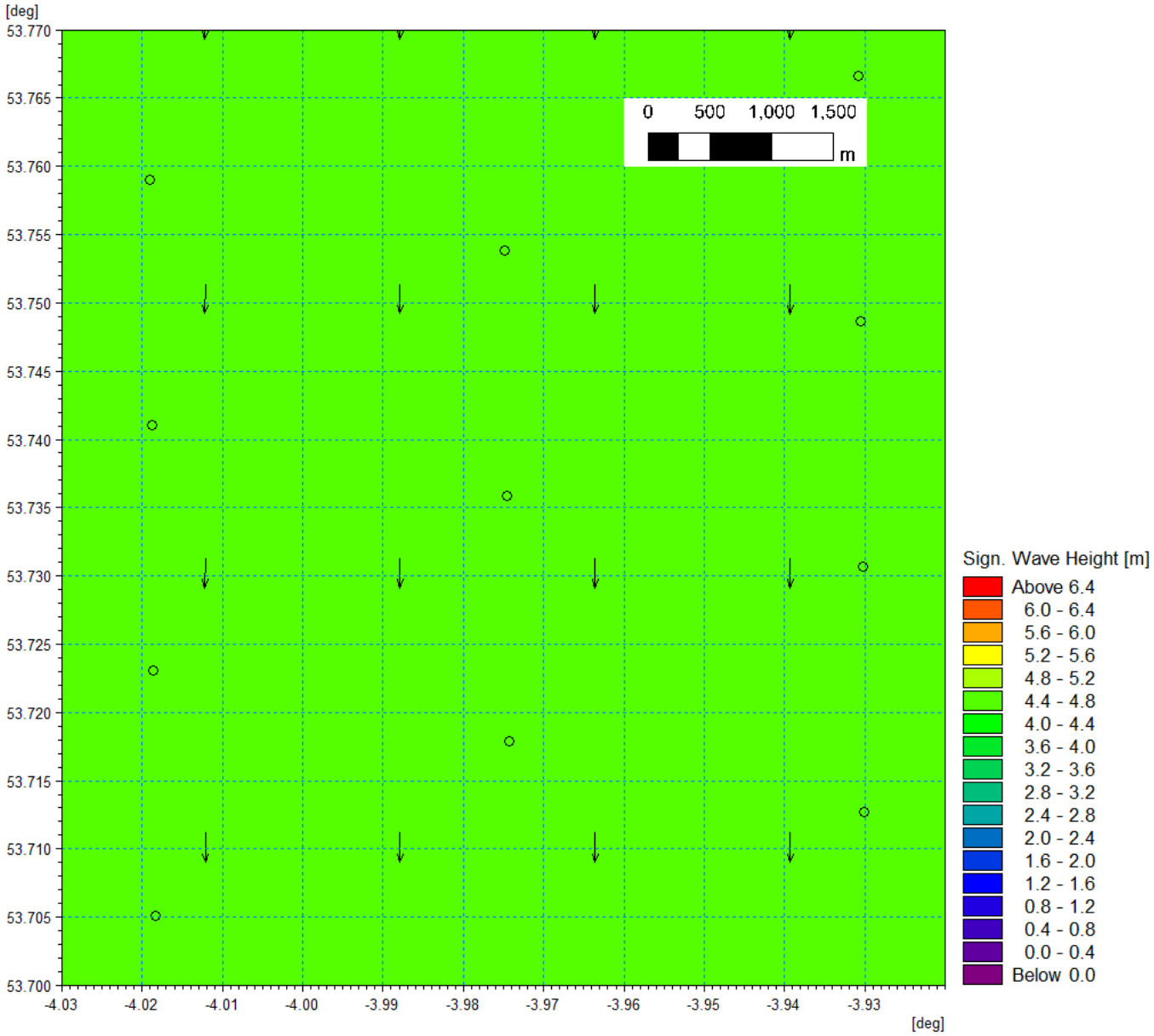

Figure 1.206: Baseline wave climate 1 in 20 year storm 000° MHW.

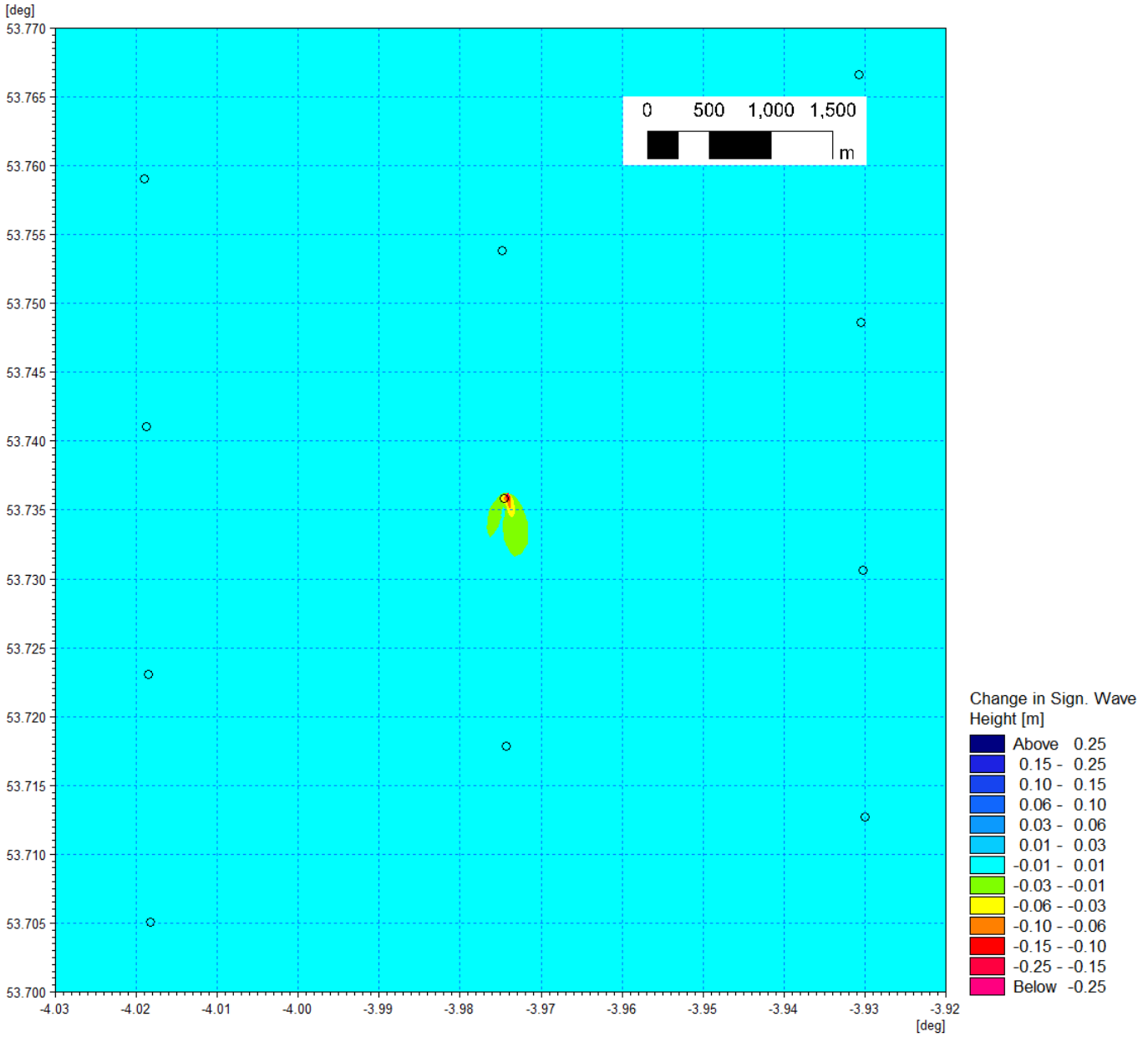

Figure 1.207: Change in wave climate 1 in 20 year storm 000° MHW (post-construction minus baseline) – conical gravity base foundation.

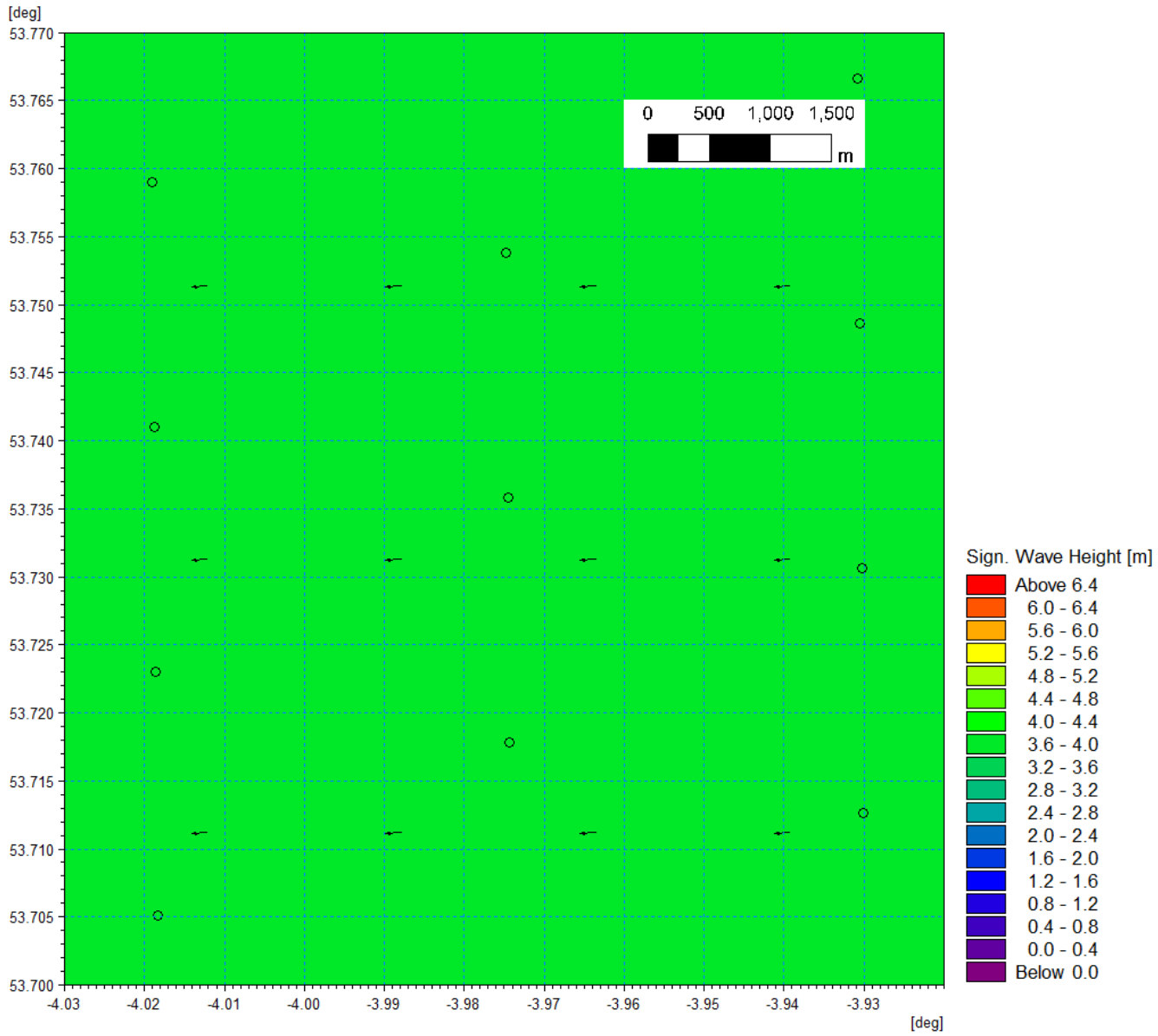

Figure 1.208: Baseline wave climate 1 in 20 year storm 090° MHW.

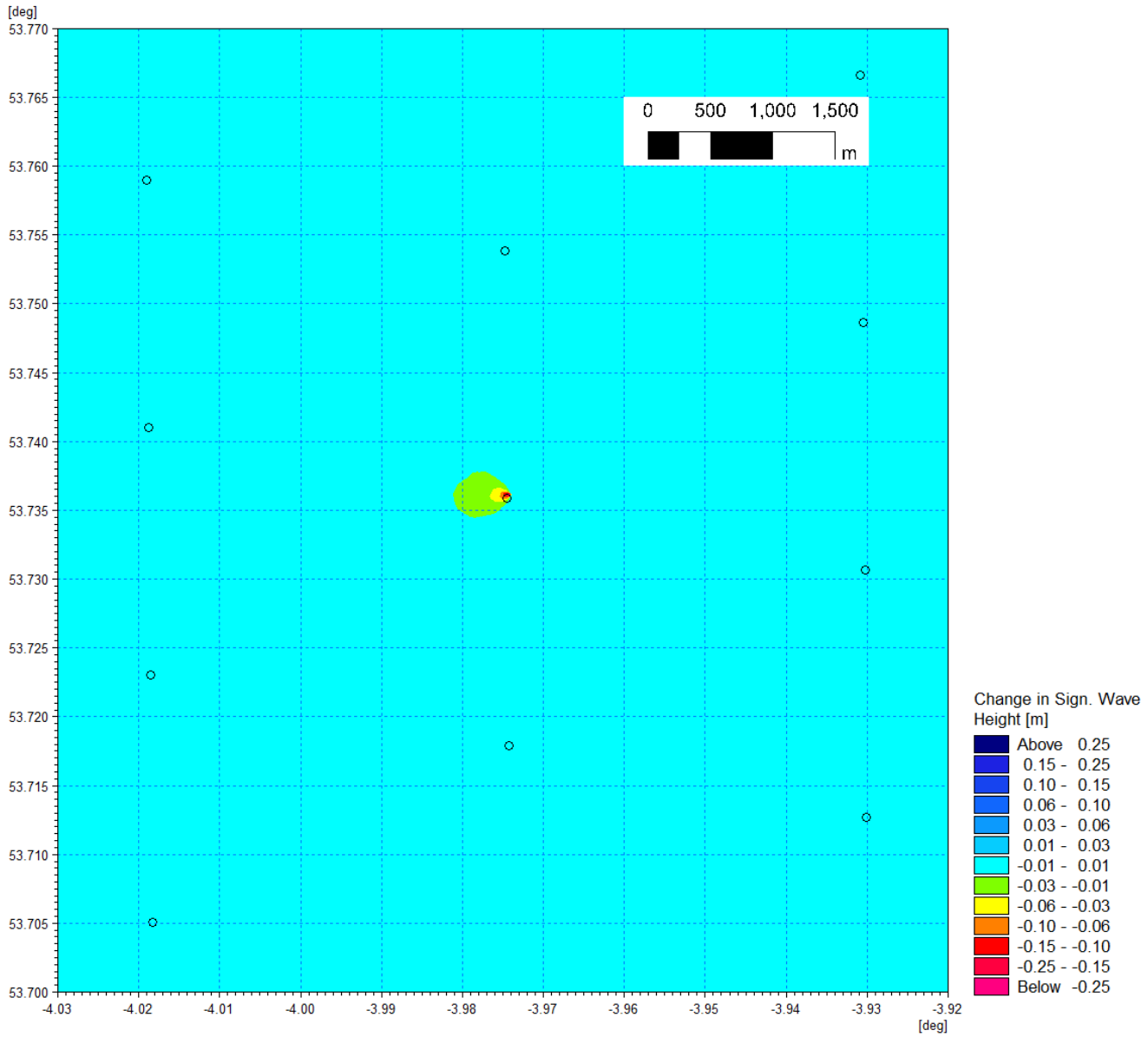

Figure 1.209: Change in wave climate 1 in 20 year storm 090° MHW (post-construction minus baseline) – conical gravity base foundation.

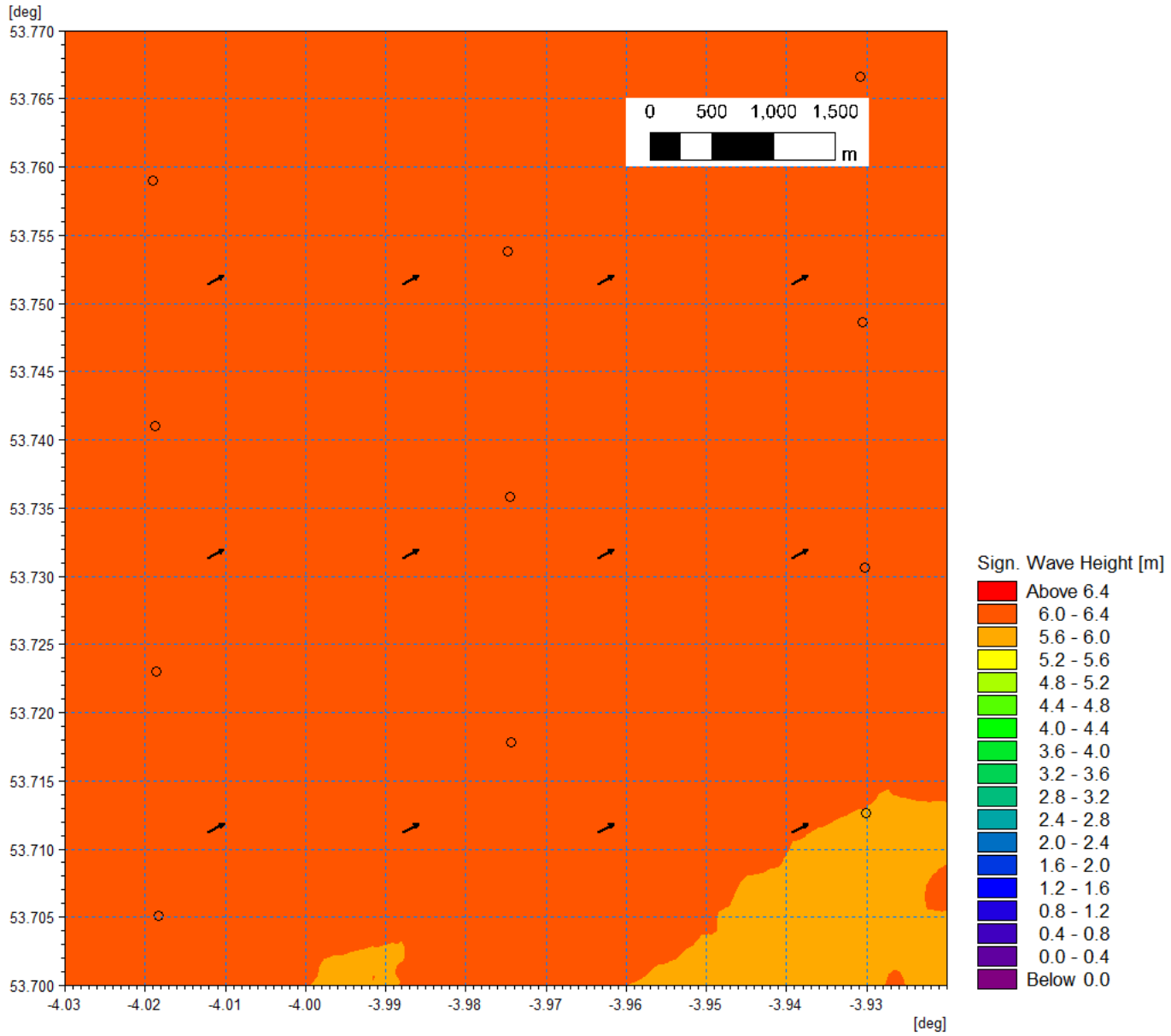

Figure 1.210: Baseline wave climate 1 in 20 year storm 240° MHW.

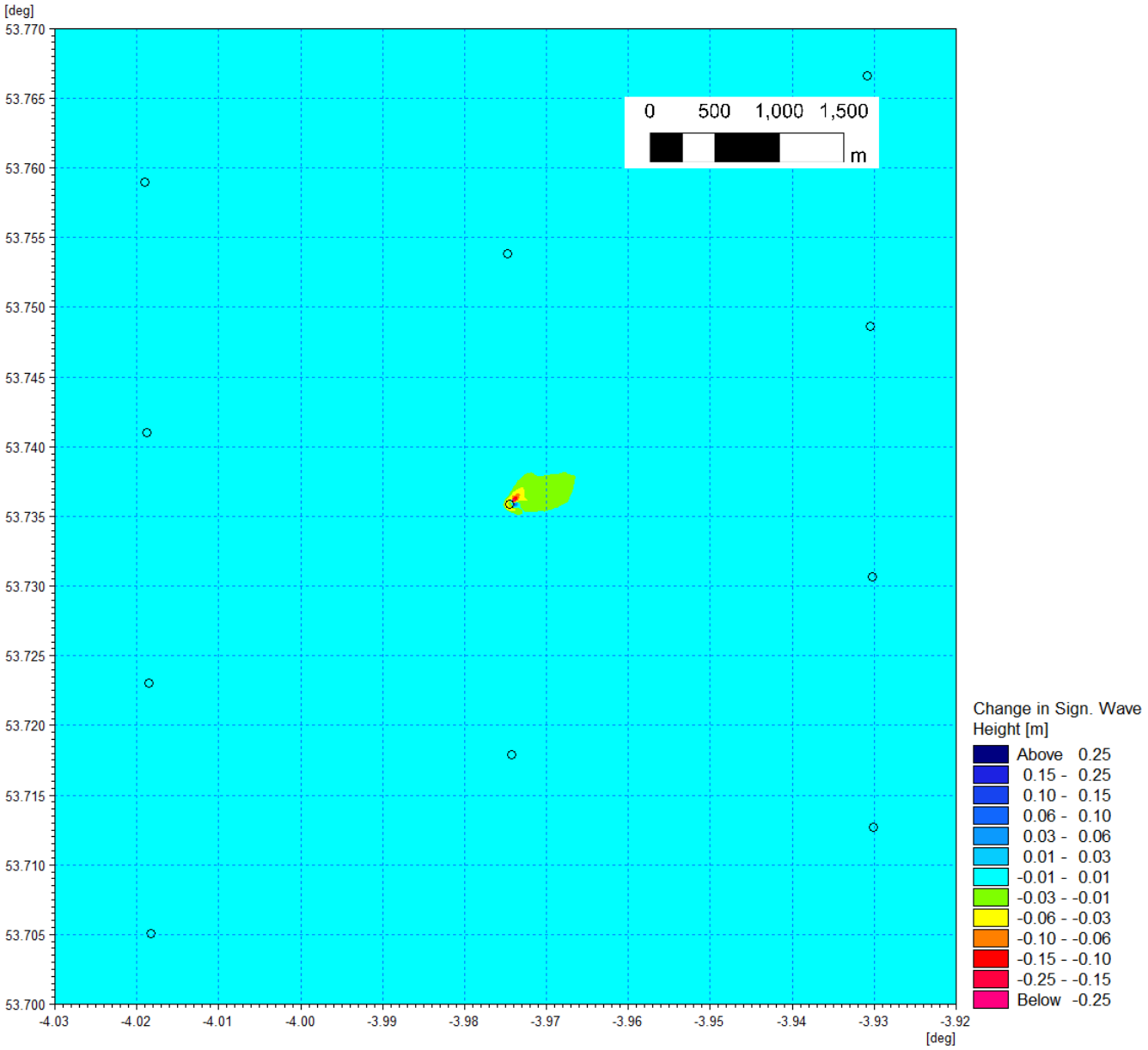

Figure 1.211: Change in wave climate 1 in 20 year storm 240° MHW (post-construction minus baseline) – conical gravity base foundation.

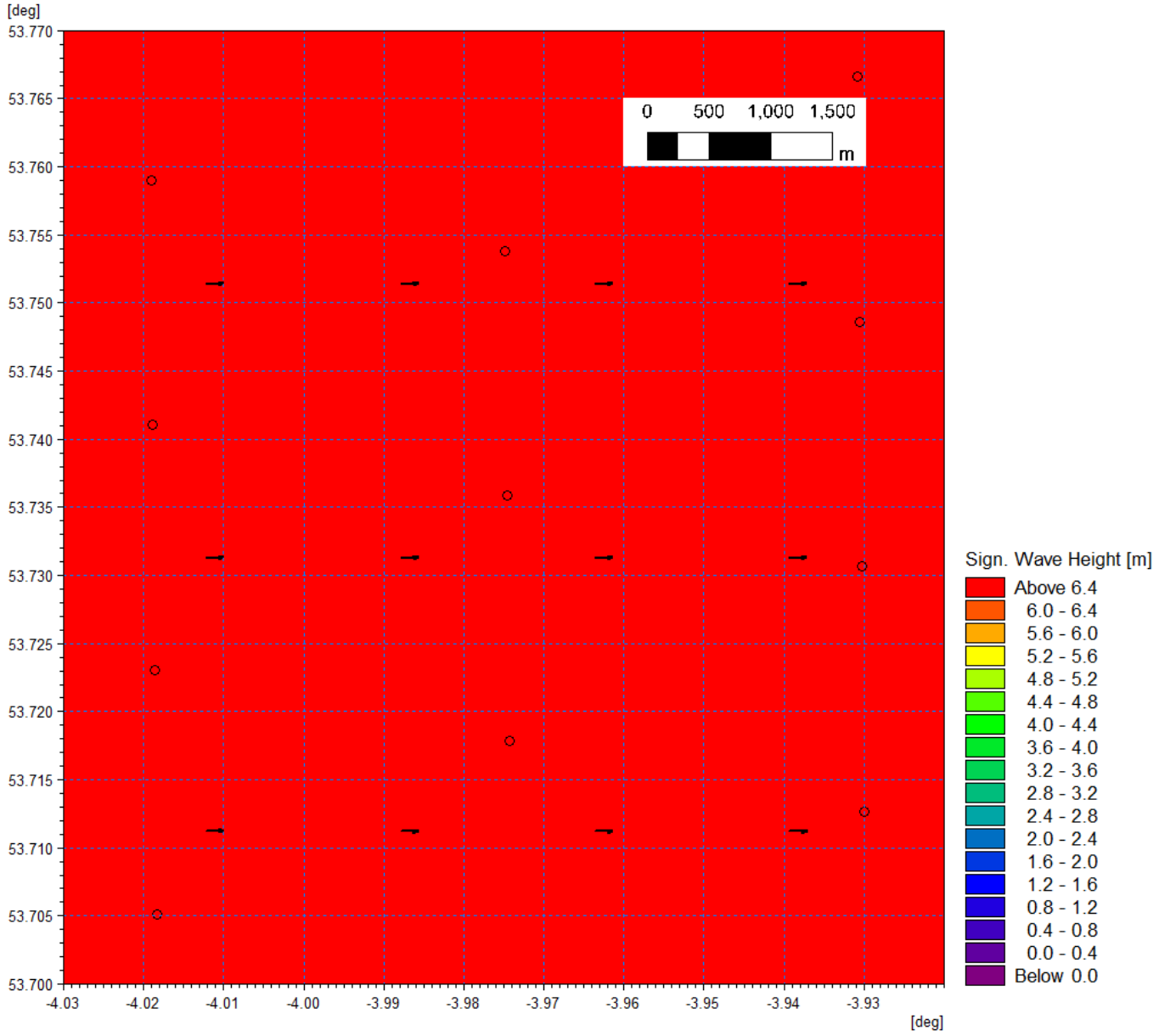

Figure 1.212: Baseline wave climate 1 in 20 year storm 270° MHW.

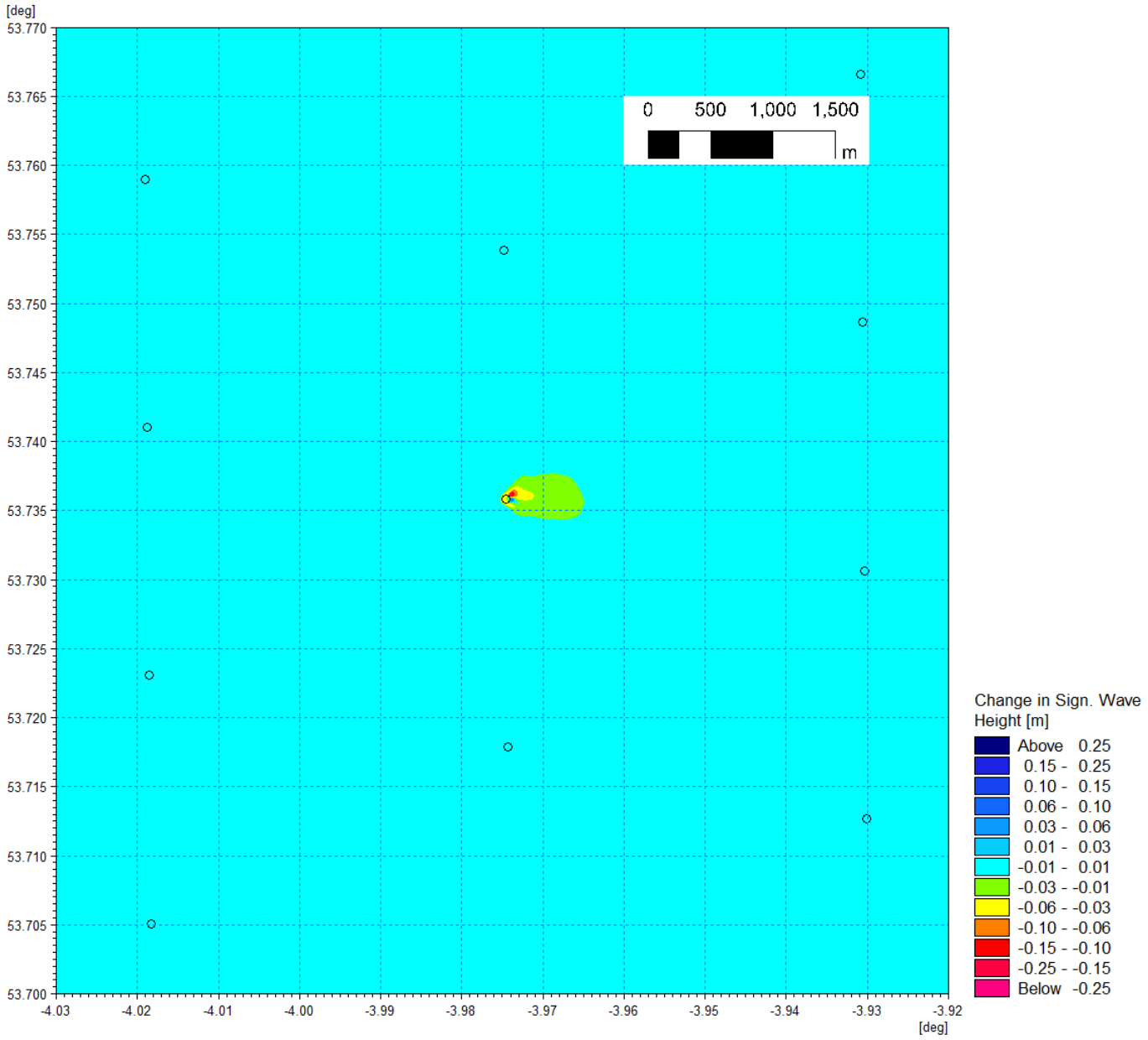

Figure 1.213: Change in wave climate 1 in 20 year storm 270° MHW (post-construction minus baseline) – conical gravity base foundation.

1.4.4 Rectangular gravity base foundations

1.4.4.1 Finally, the rectangular gravity base relates to the much larger single semi-submersible OSP structure. The rectangular gravity base modelled reflects a typical design and is comprised of the following:

- Surface dimension 80 m by 60 m
- Slab base 100 m by 80 m
- Six rectangular legs circa 15 m diameter
- Scour protection to a height of average 2.6 m extending 25 m from the slab.

Tidal flow

1.4.4.2 Sensitivity testing was undertaken by repeating the hydrodynamic simulations used to describe the baseline, with the addition of one rectangular gravity base foundation. This represents the largest possible installation for an OSP foundation. The bathymetry was also amended to take account of scour protection. The following figures show the mid flood and mid ebb steps from the simulation respectively, but with one rectangular gravity base foundation in place.

1.4.4.3 Figure 1.174 shows the baseline flood tide flow patterns with Figure 1.175 showing a focussed plot of the post-construction changes which are limited to the vicinity of the foundation. Similarly, Figure 1.176 and Figure 1.177 show the same information for the ebb tide. During peak current speed the flow is redirected in the immediate vicinity of the structure. Currents accelerate at the exposed face of structure and along the sides, whilst decreasing on the sheltered lee side. The variation is a maximum of 20 cm/s (decrease in current speed) in the immediate vicinity (50 m) of the structure's lee side which constitutes 20% of flows on the flood and *c*. 29% on the ebb tide. Due to the size of the structure, a decrease of 14 cm/s to 20 cm/s may extend 100 m from the structure and a decrease of 8 cm/s to 14 cm/s at a distance of 200 m from the base. Positive increases in current are of a lower magnitude, the largest occurring in the region of 2 cm/s to 4 cm/s, representing 2% to 4% of the baseline current speed. This is a much larger unit than the previous foundation types considered, however, it would be implemented as a single OSP structure to serve the entire wind project, with other adjacent wind turbines comprised of the smaller foundation types.

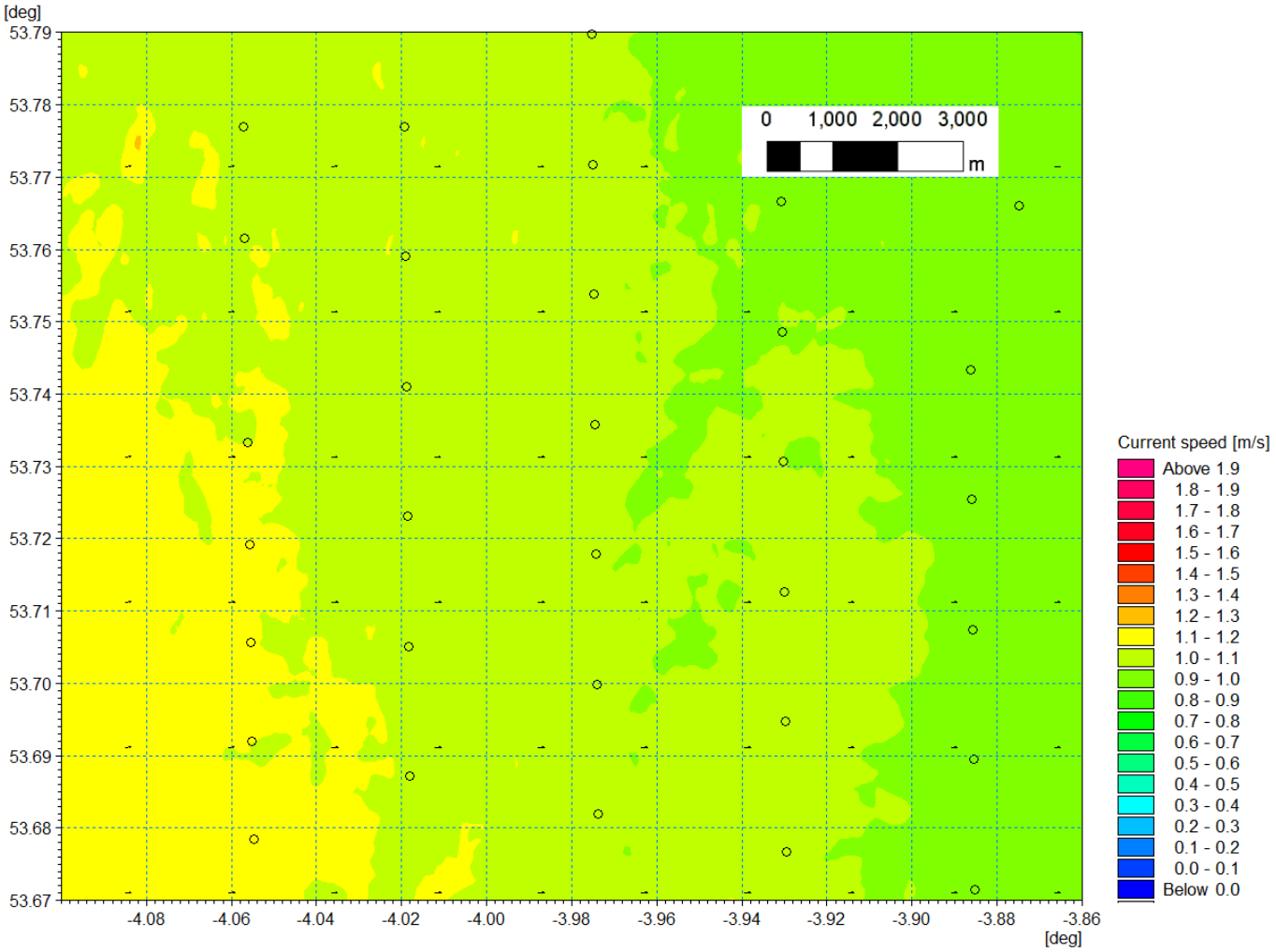

Figure 1.214: Baseline tidal flow pattern – flood tide.

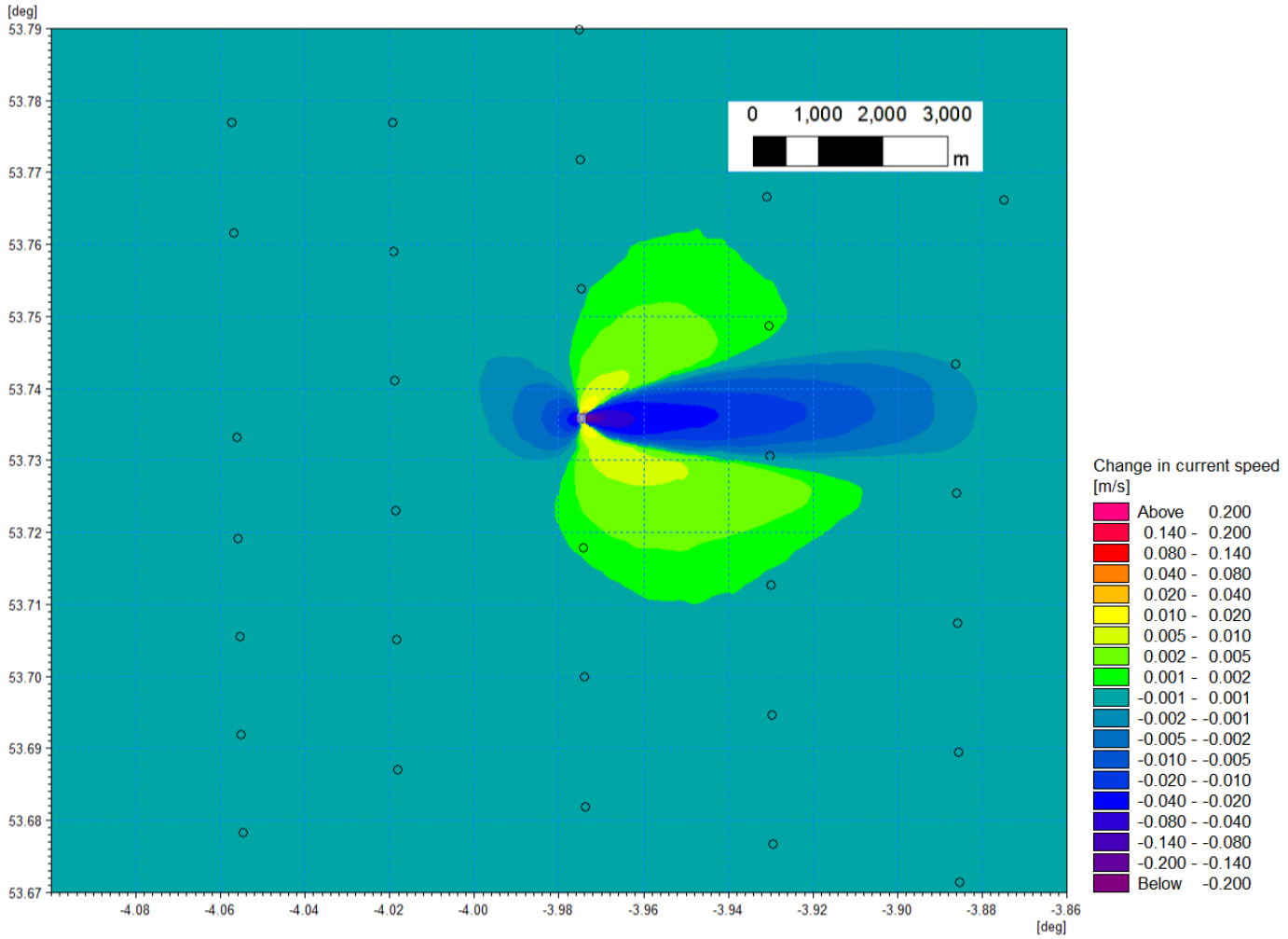

Figure 1.215: Change in tidal flow (post-construction minus baseline) rectangular gravity base foundation – flood tide.

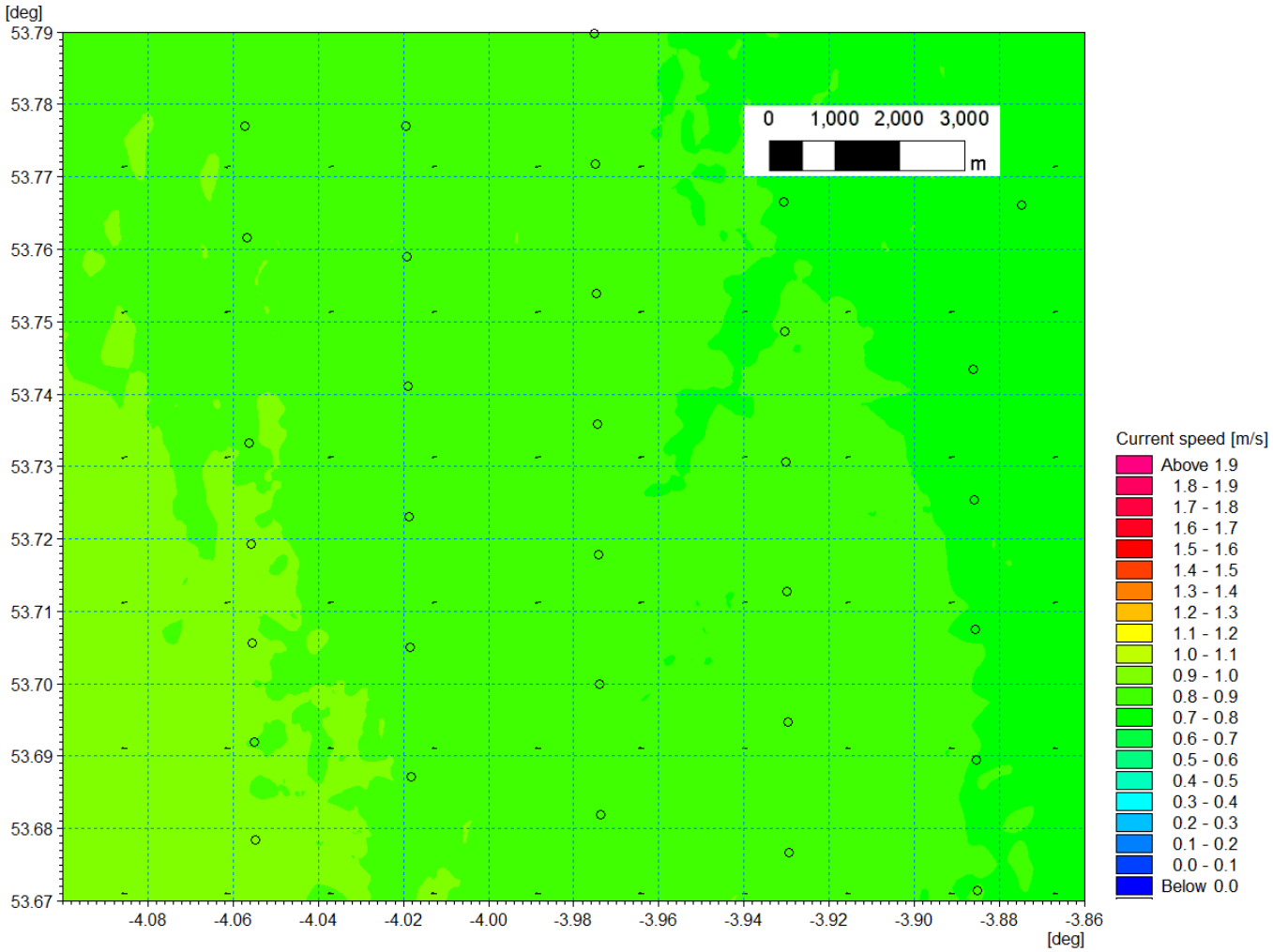

Figure 1.216: Baseline tidal flow pattern – ebb tide.

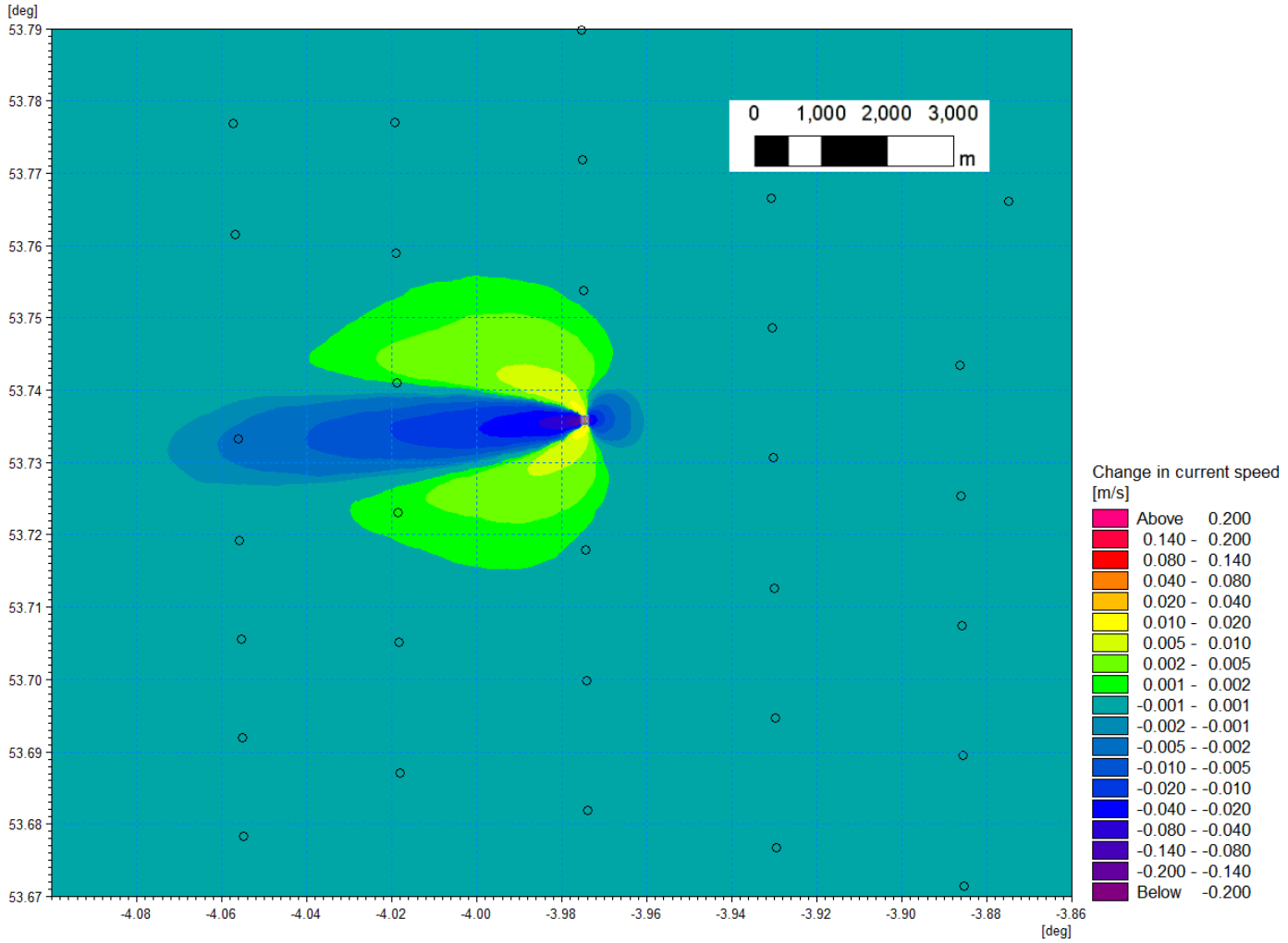

Figure 1.217: Change in tidal flow (post-construction minus baseline) rectangular gravity base foundation – ebb tide.

Wave climate

1.4.4.4 The baseline 000° storm is presented for the 1 in 1 year in Figure 1.178 with the difference shown in Figure 1.219. Similarly, the 1 in 20 year baseline and changes from this direction are presented in Figure 1.226 and Figure 1.227. The changes are seen as reductions in the lee of the rectangular gravity base foundation. The maximum changes observed in the immediate vicinity (50 m) were limited to a maximum of 25 cm during the 1 in 20 year scenario, which represents less than *c.* 5% of the baseline significant wave height of *c.* 4.8 m. 100 to 200 m from the structure these changes fall to <15 cm (*c.* 3%).

1.4.4.5 The changes to waves originating from 090° sector are shown in Figure 1.221 and Figure 1.228, both 1 in 1 and 1 in 20 year storm waves are of slightly greater than those experienced from the 000° sector due to a lower significant wave height. Whilst still limited to a 25 cm change in significant wave height, this would represent *c.* 6.5% of the baseline wave height (3.8 m) within 50 m of the structure. This level of change may persist up to 100 m from the offshore platform, after which they would reduce to <15 cm.

1.4.4.6 Storm waves originating from 240° and 270° are of a greater magnitude than those discussed above, with significant wave heights in excess of. 6.2 m in the vicinity of the modelled foundation. During a 1 in 20 year storm post construction waves may experience a change up to a maximum of 25 cm or *c.* 4% in the immediate vicinity of the rectangular gravity base foundation. These changes reduce in magnitude with distance from the structure, 100 to 200 m from the structure these changes fall to <15 cm (*c.* 2.5%).

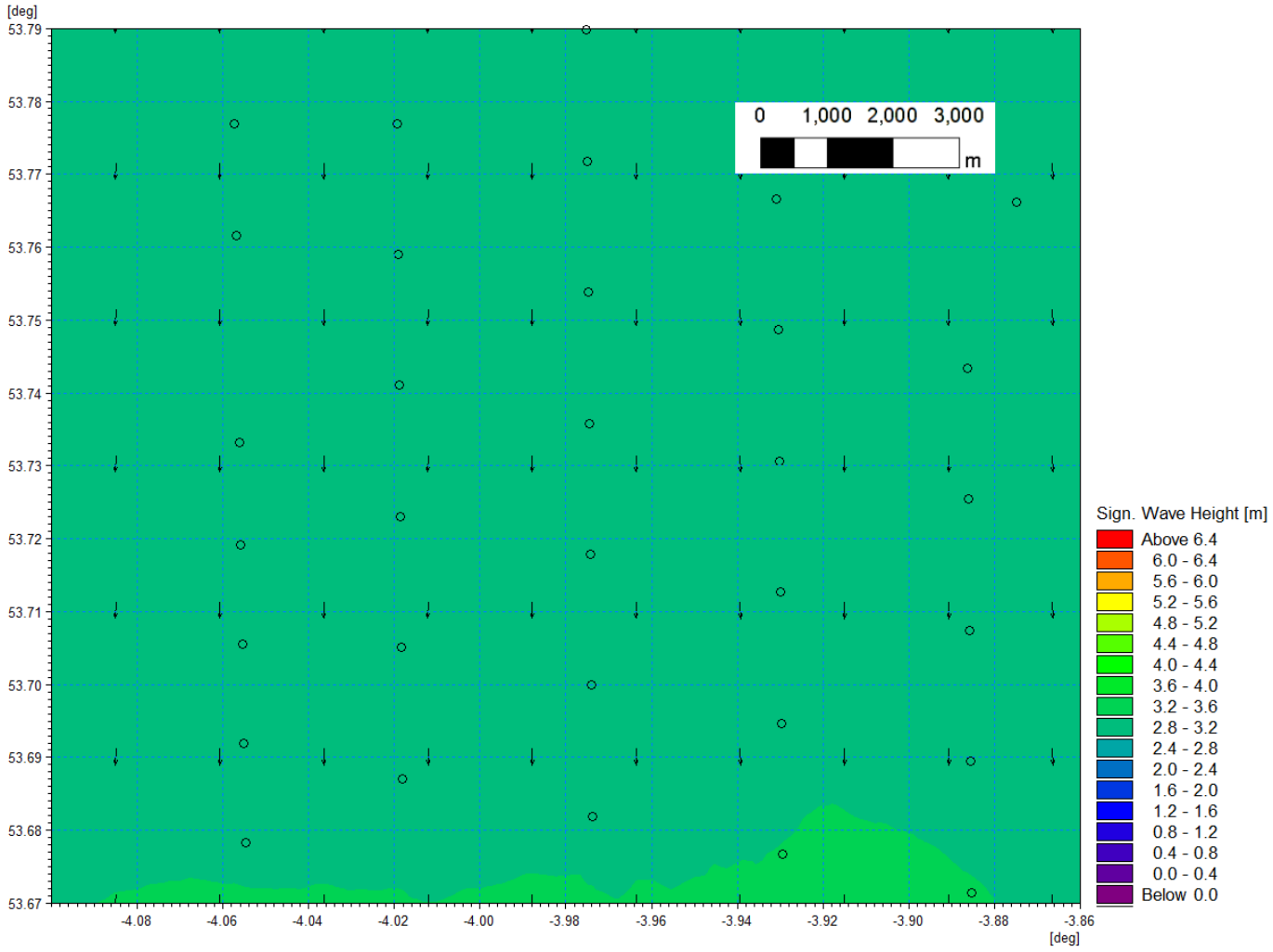

Figure 1.218: Baseline wave climate 1 in 1 year storm 000° MHW.

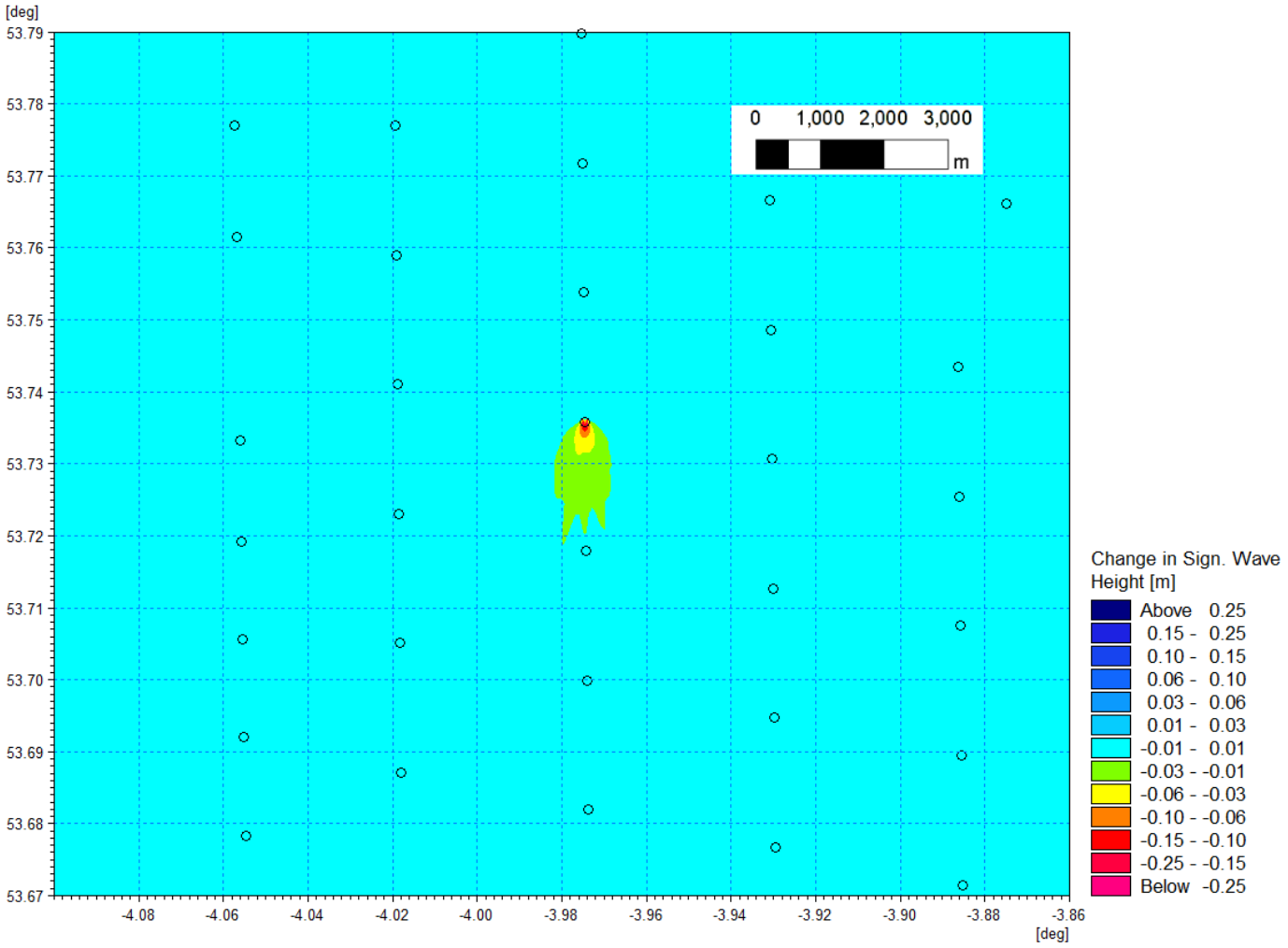

Figure 1.219: Change in wave climate 1 in 1 year storm 000° MHW (post-construction minus baseline) - rectangular gravity base foundation.

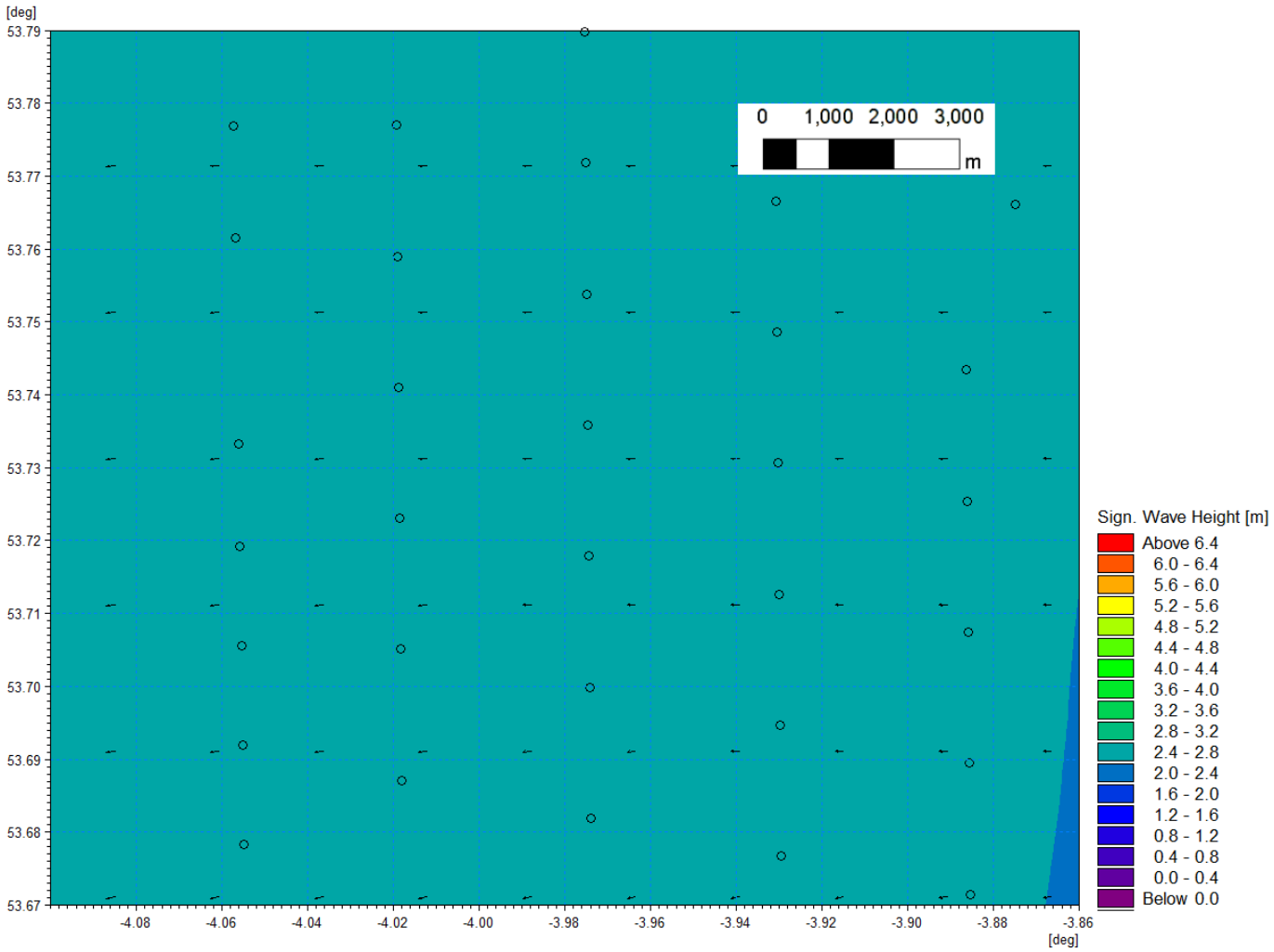

Figure 1.220: Baseline wave climate 1 in 1 year storm 090° MHW.

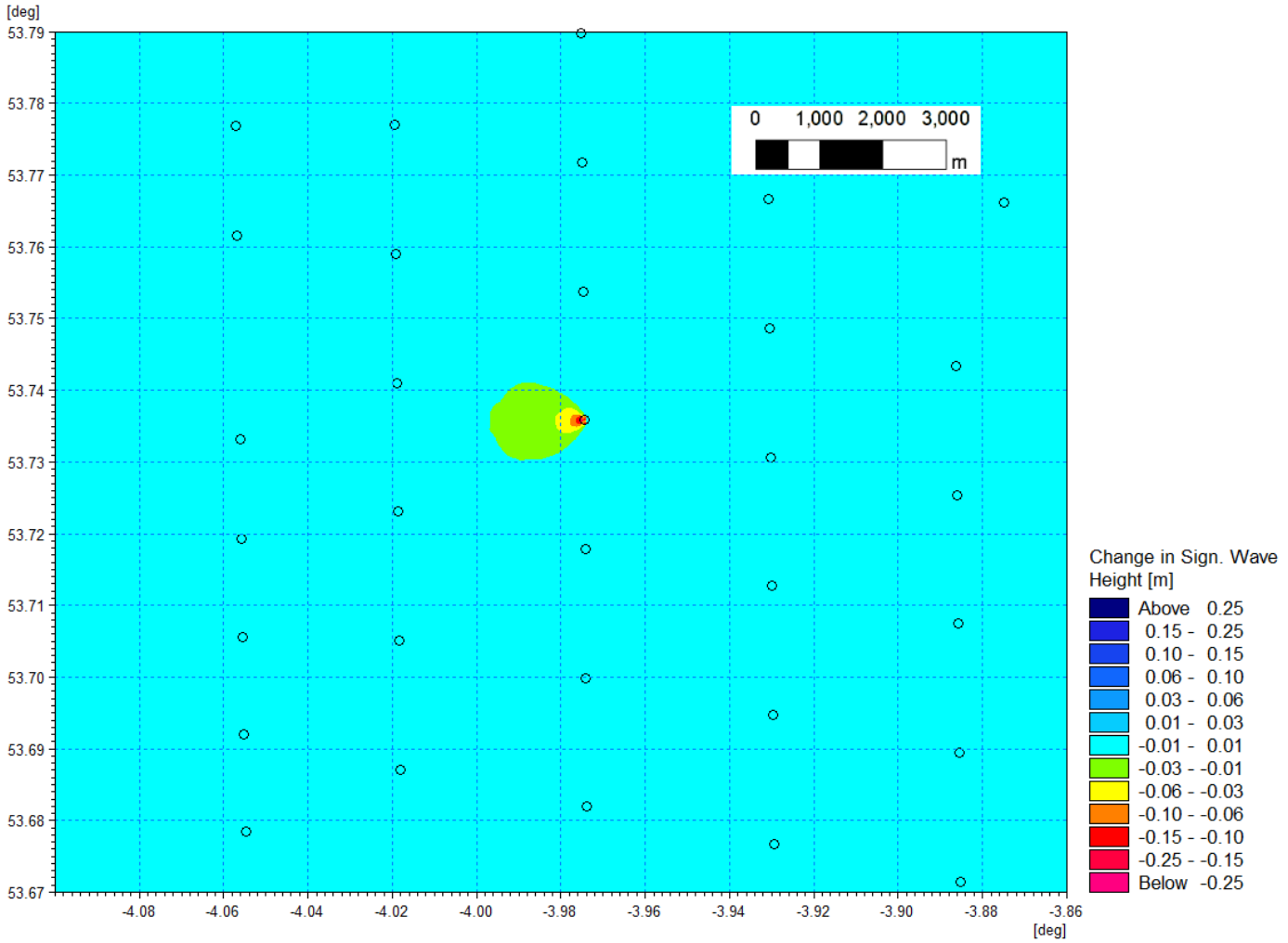

Figure 1.221: Change in wave climate 1 in 1 year storm 090° MHW (post-construction minus baseline) - rectangular gravity base foundation.

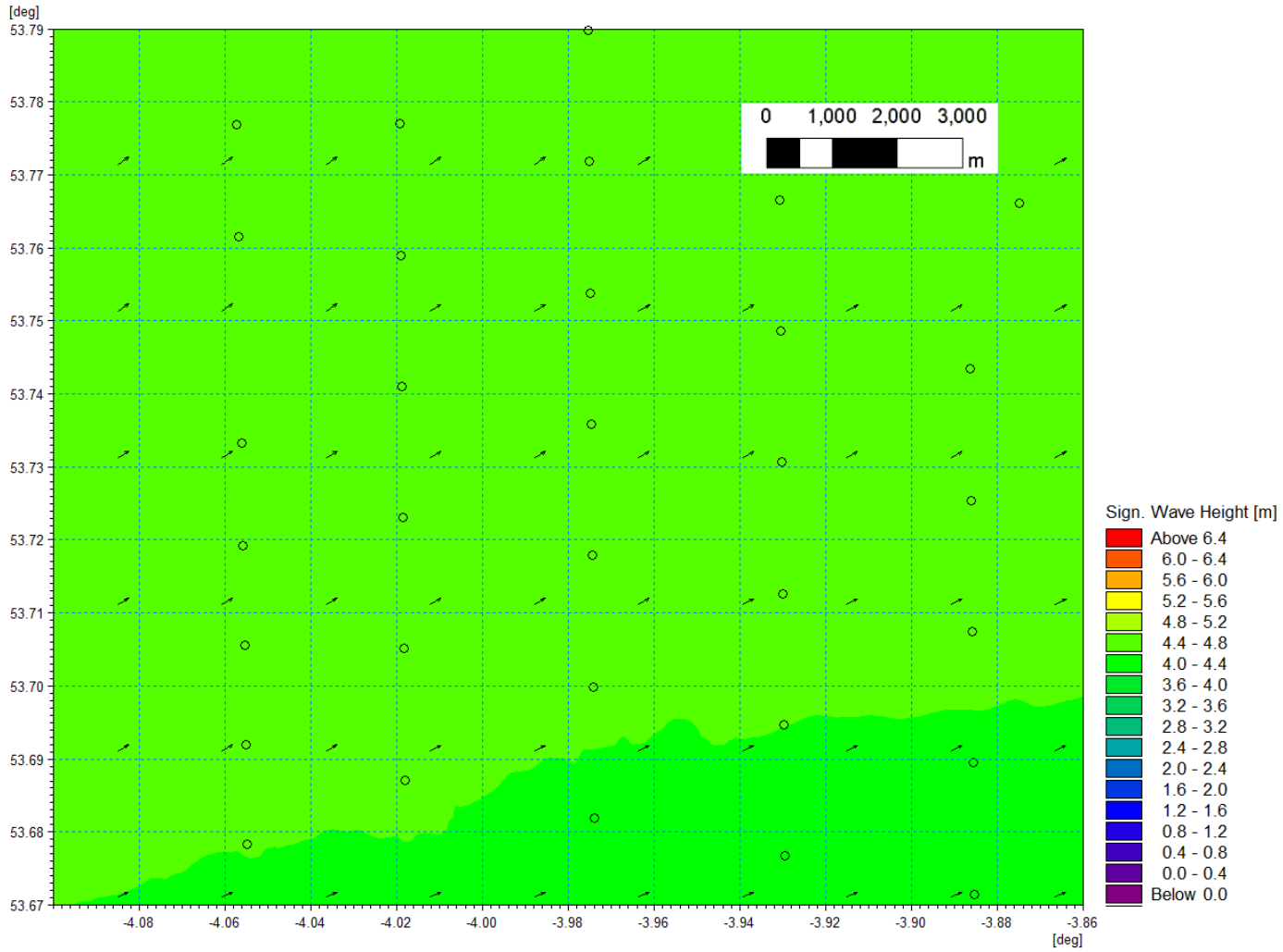

Figure 1.222: Baseline wave climate 1 in 1 year storm 240° MHW.

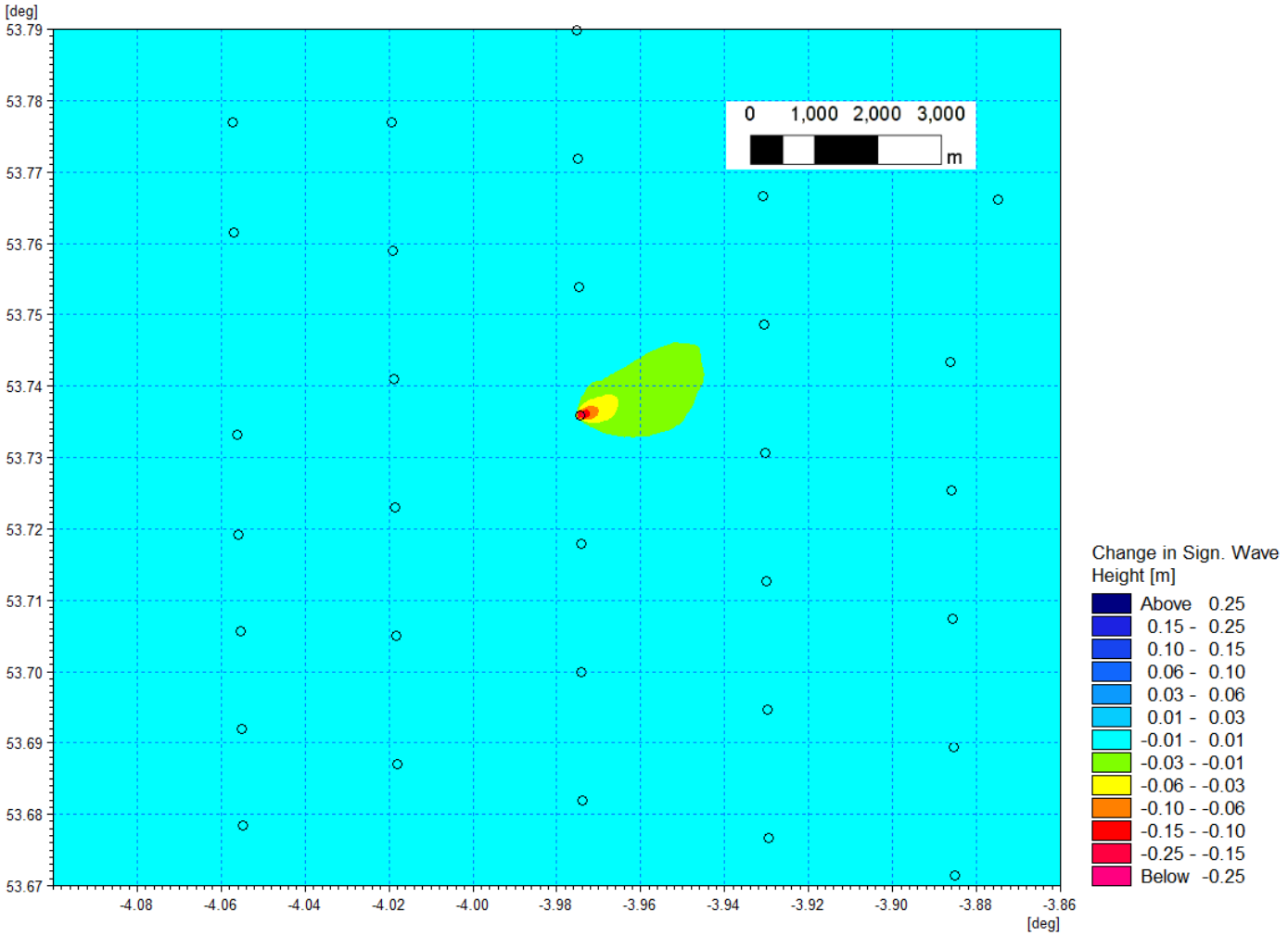

Figure 1.223: Change in wave climate 1 in 1 year storm 240° MHW (post-construction minus baseline) - rectangular gravity base foundation.

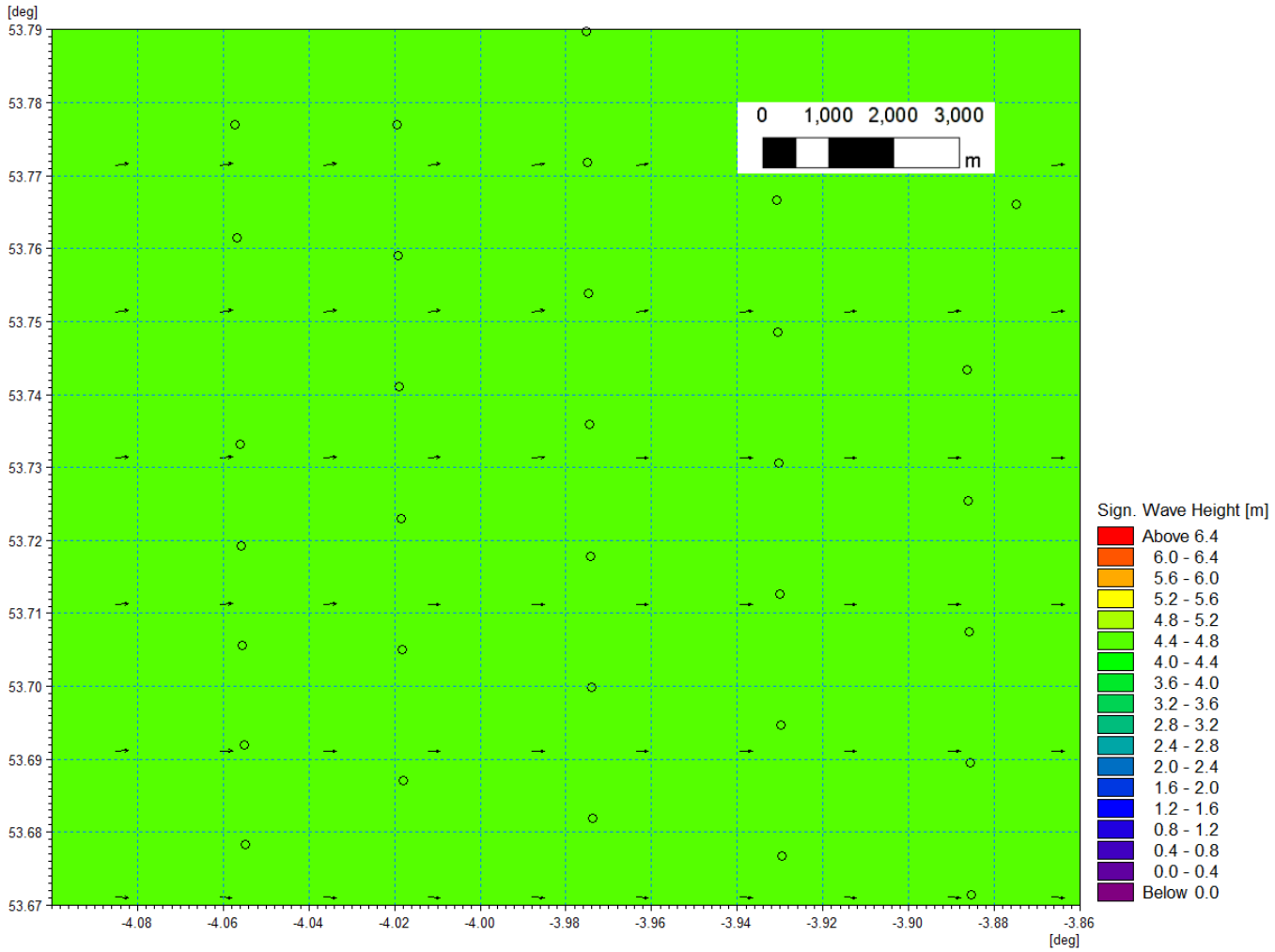

Figure 1.224: Baseline wave climate 1 in 1 year storm 270° MHW.

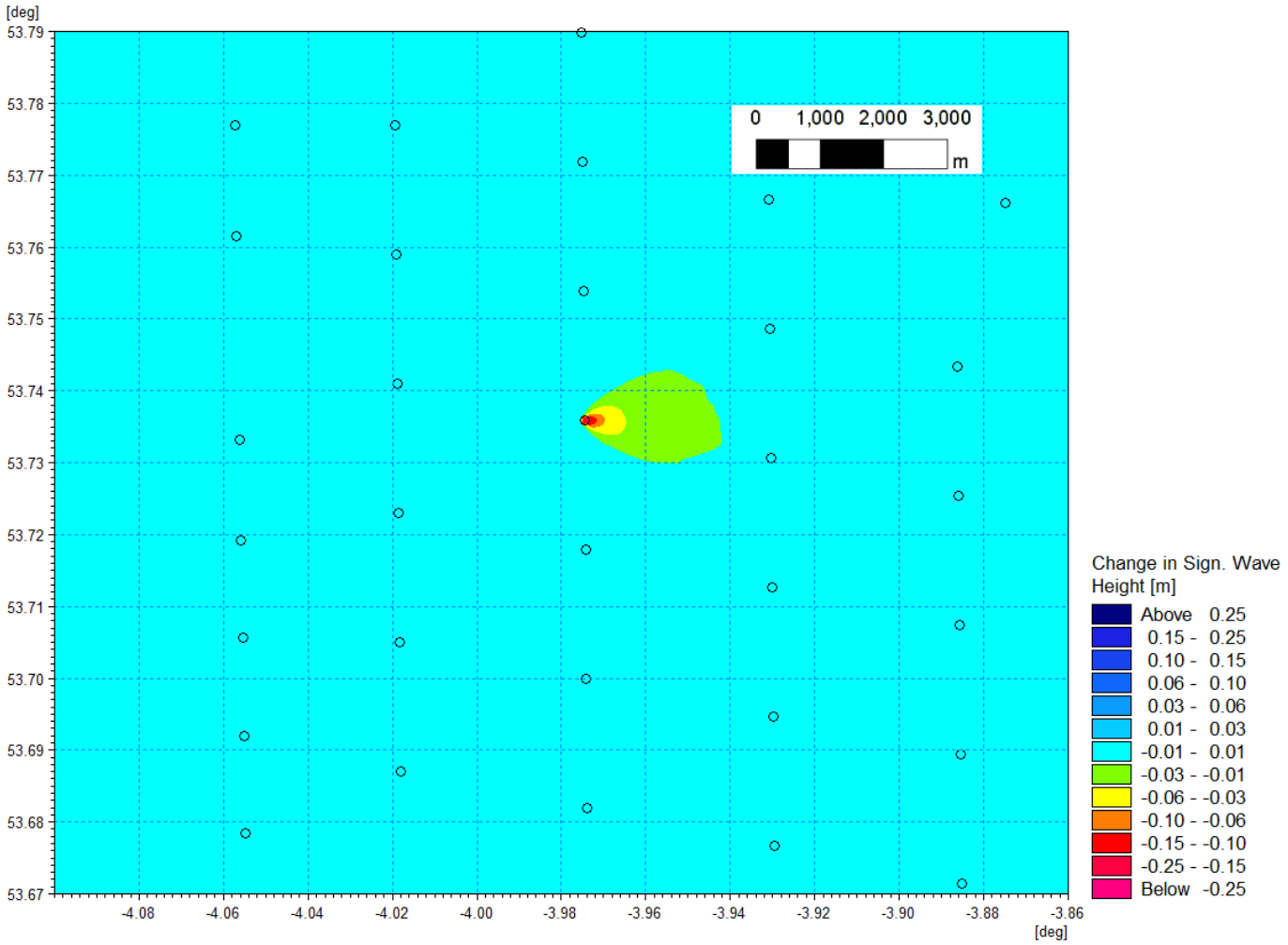

Figure 1.225: Change in wave climate 1 in 1 year storm 270° MHW (post-construction minus baseline) - rectangular gravity base foundation.

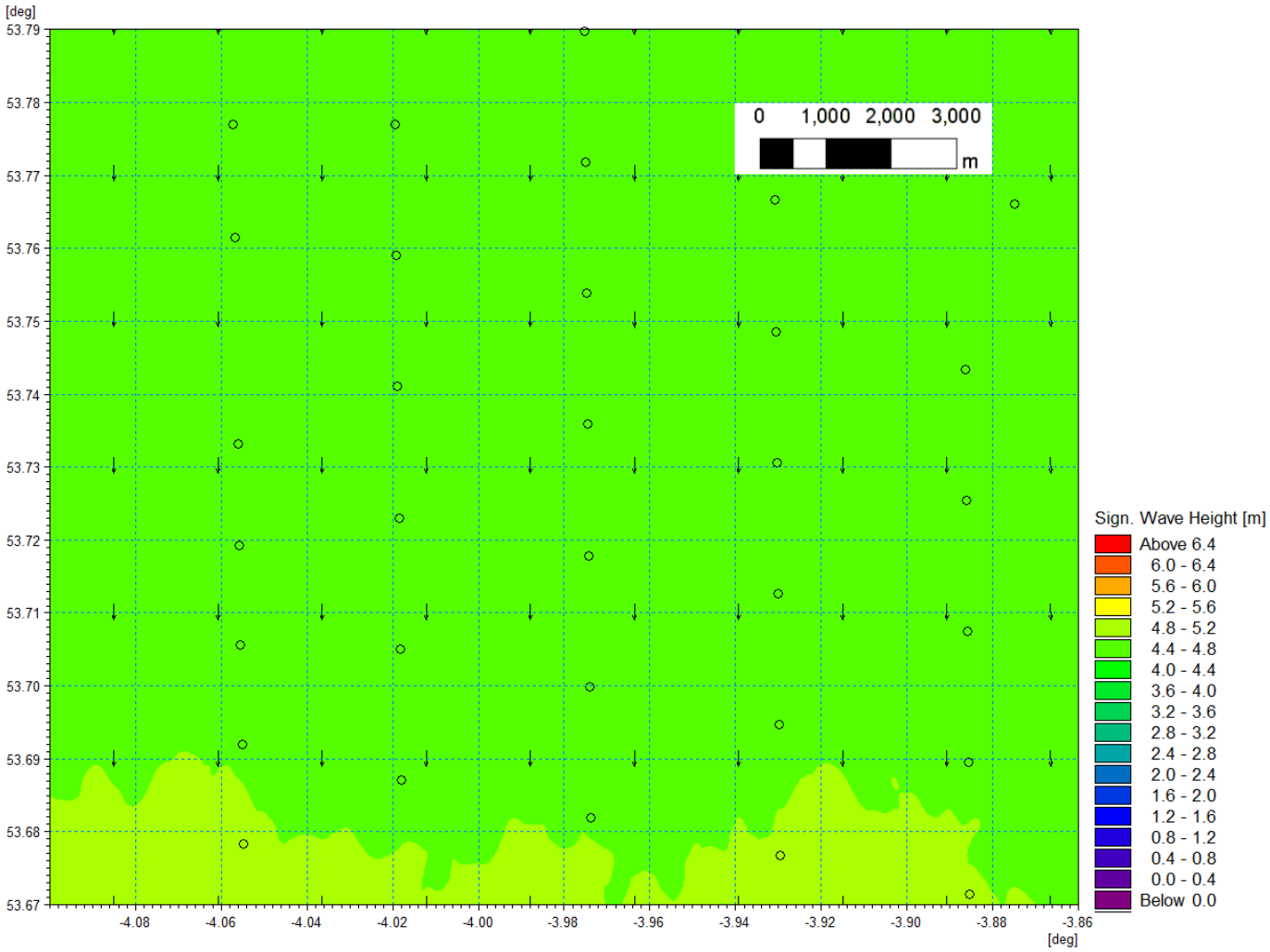

Figure 1.226: Baseline wave climate 1 in 20 year storm 000° MHW.

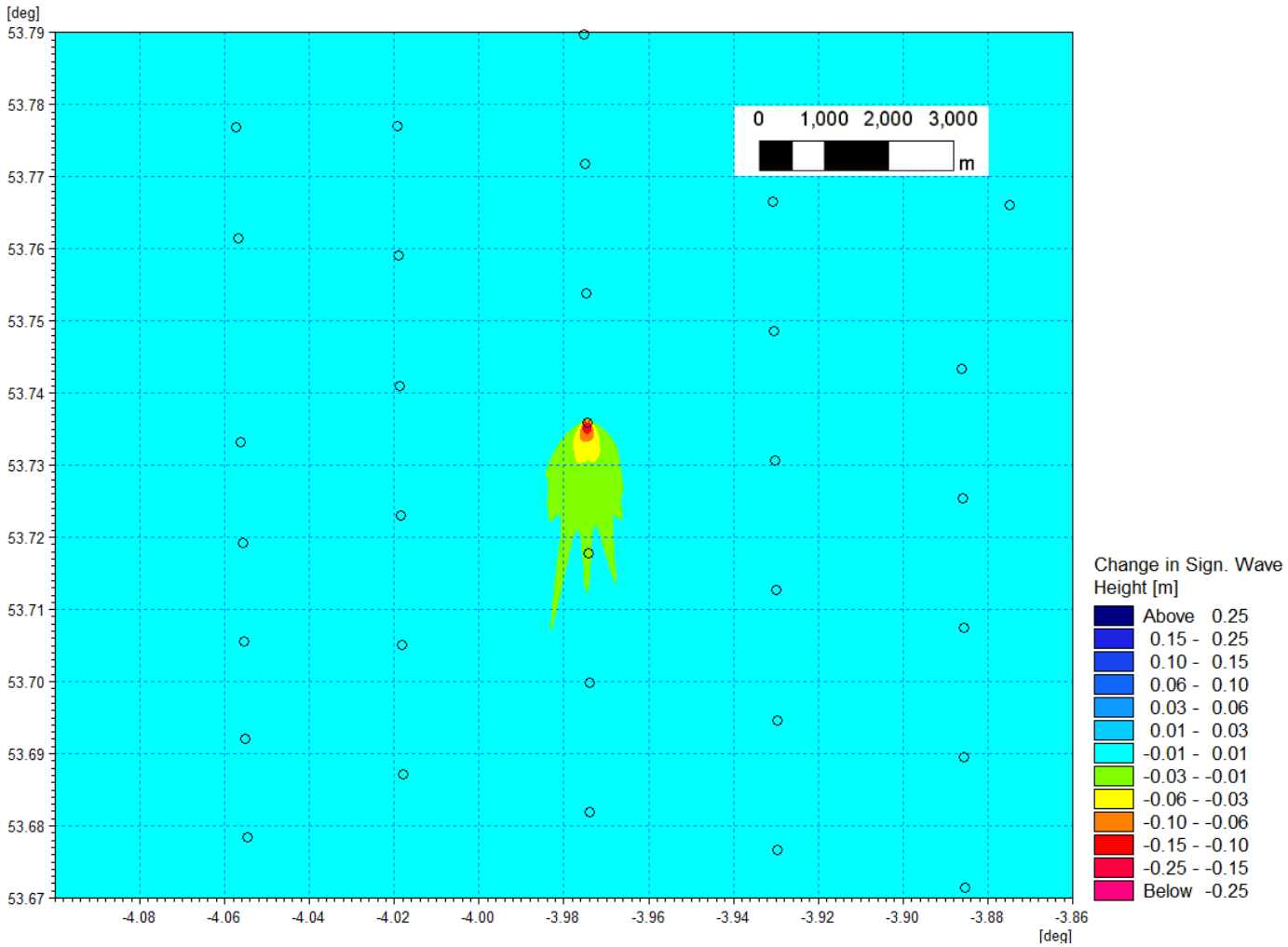

Figure 1.227: Change in wave climate 1 in 20 year storm 000° MHW (post-construction minus baseline) - rectangular gravity base foundation.

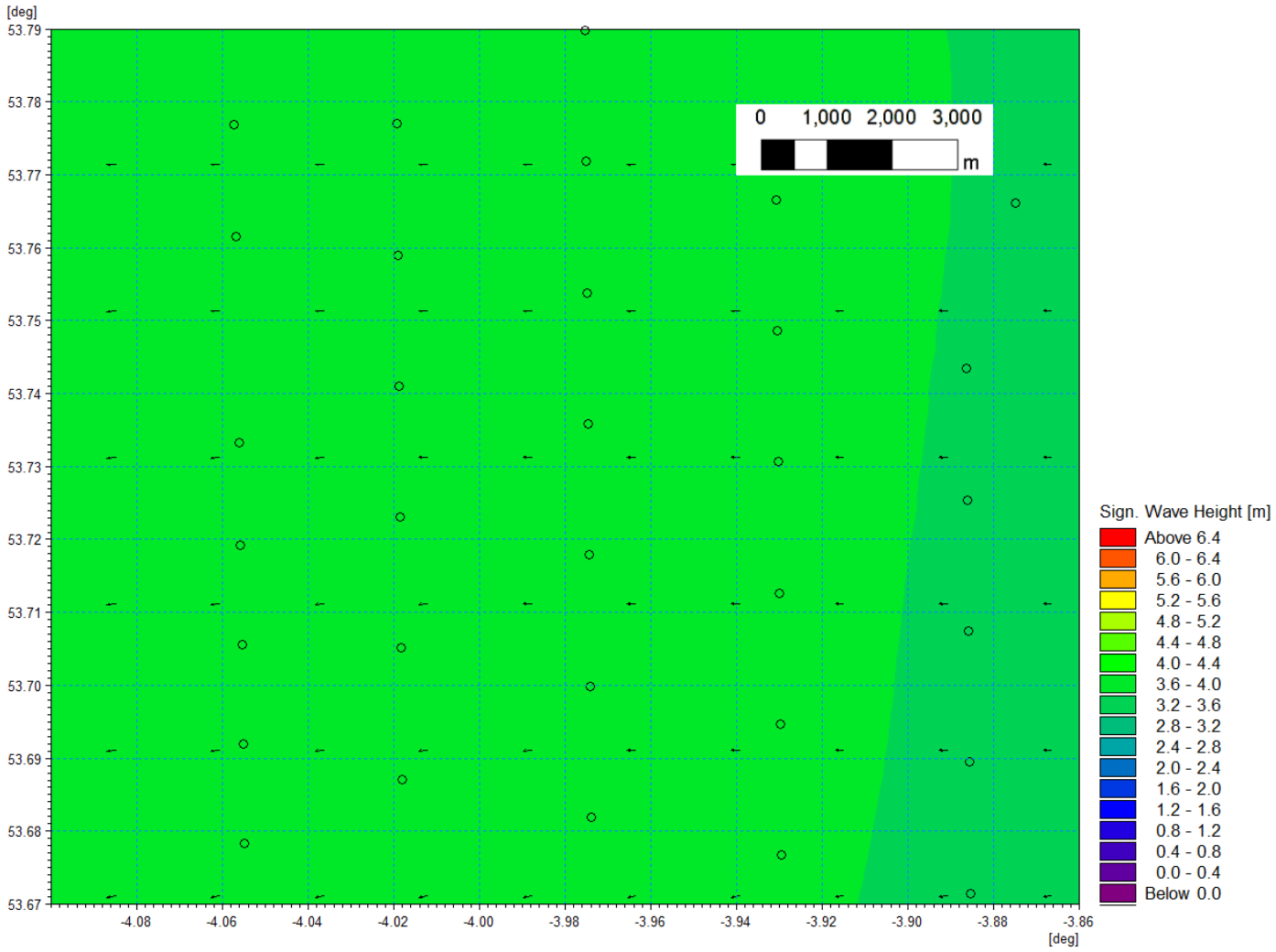

Figure 1.228: Baseline wave climate 1 in 20 year storm 090° MHW.

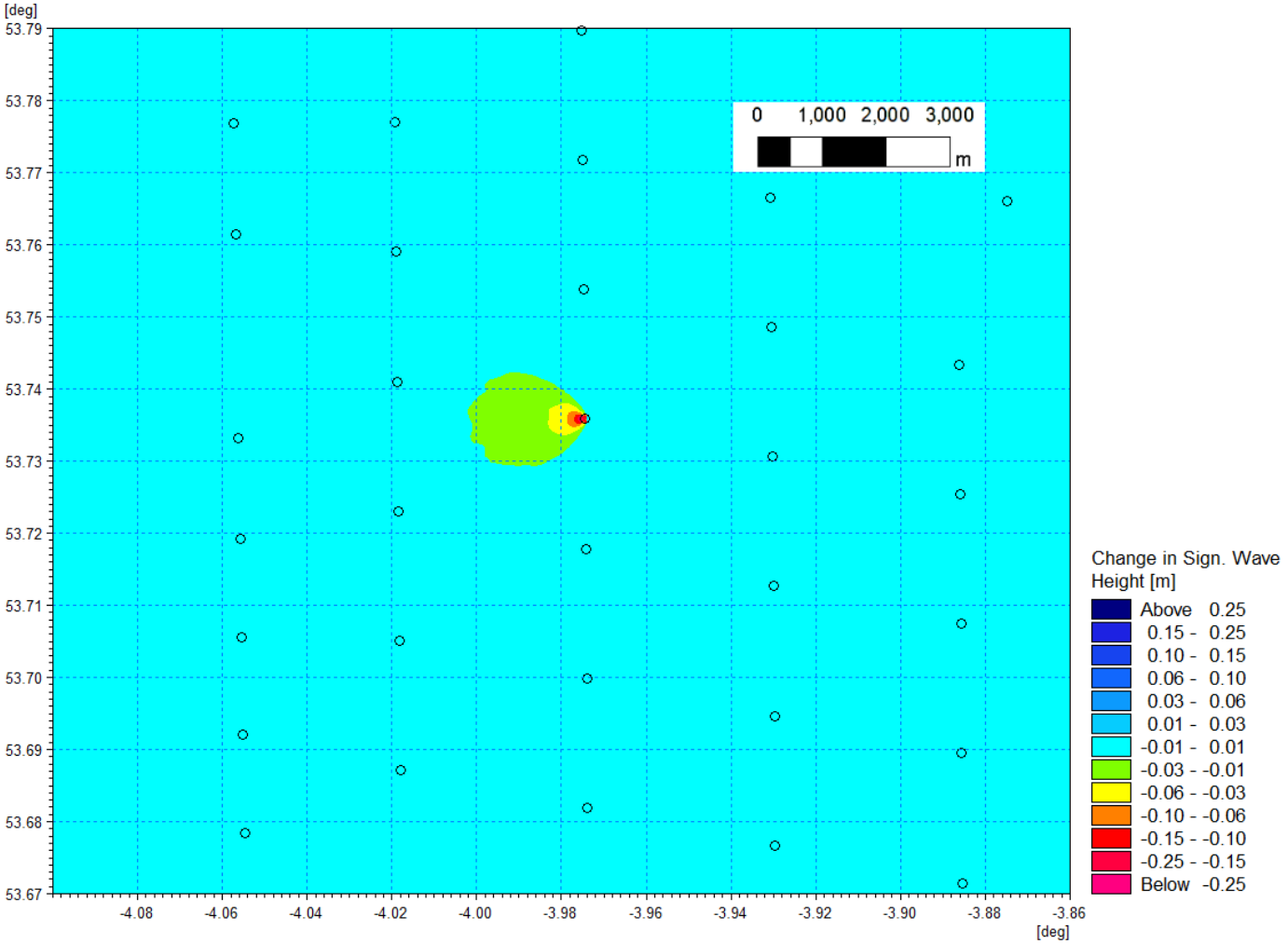

Figure 1.229: Change in wave climate 1 in 20 year storm 090° MHW (post-construction minus baseline) - rectangular gravity base foundation.

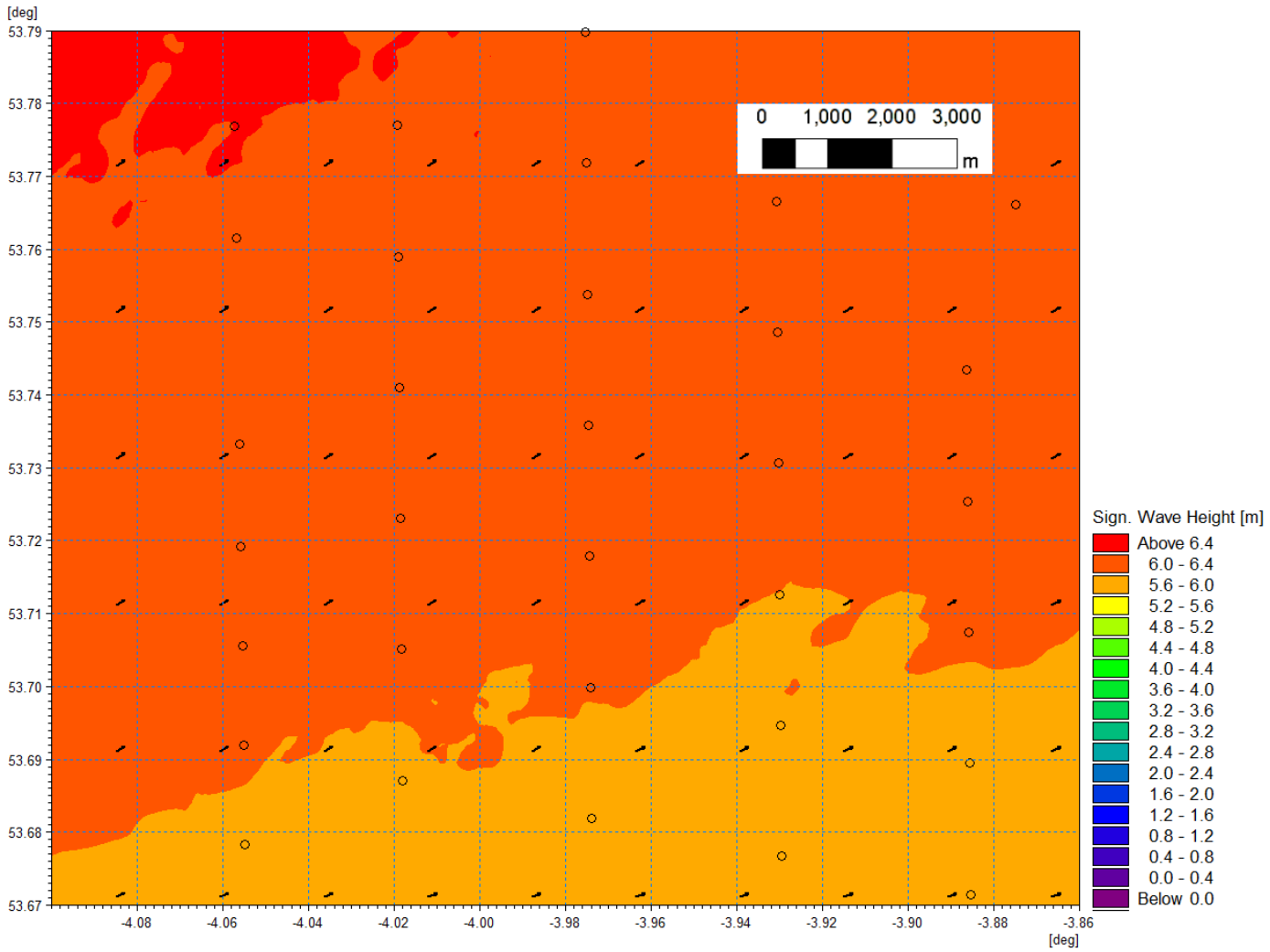

Figure 1.230: Baseline wave climate 1 in 20 year storm 240° MHW.

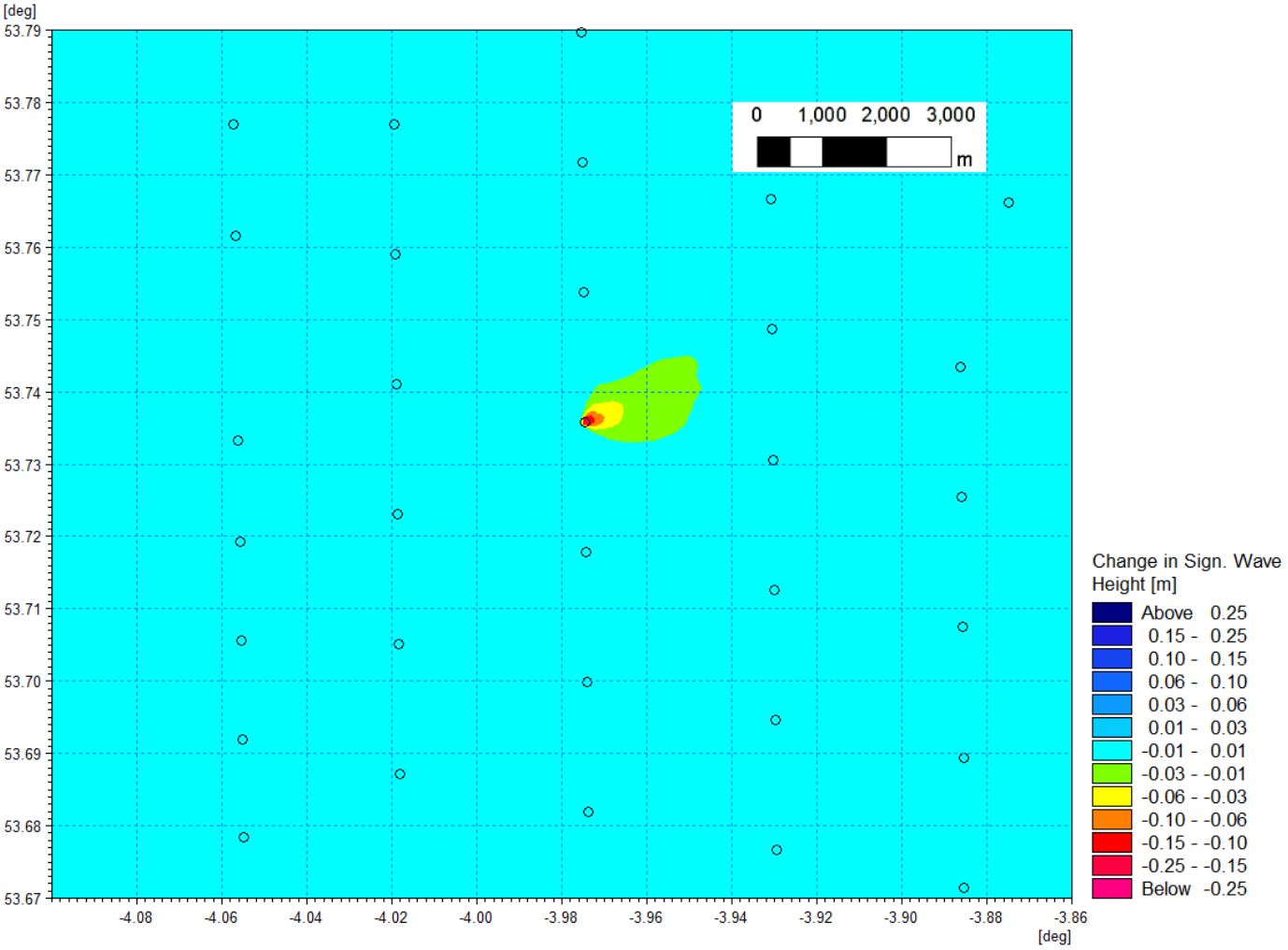

Figure 1.231: Change in wave climate 1 in 20 year storm 240° MHW (post-construction minus baseline) - rectangular gravity base foundation.

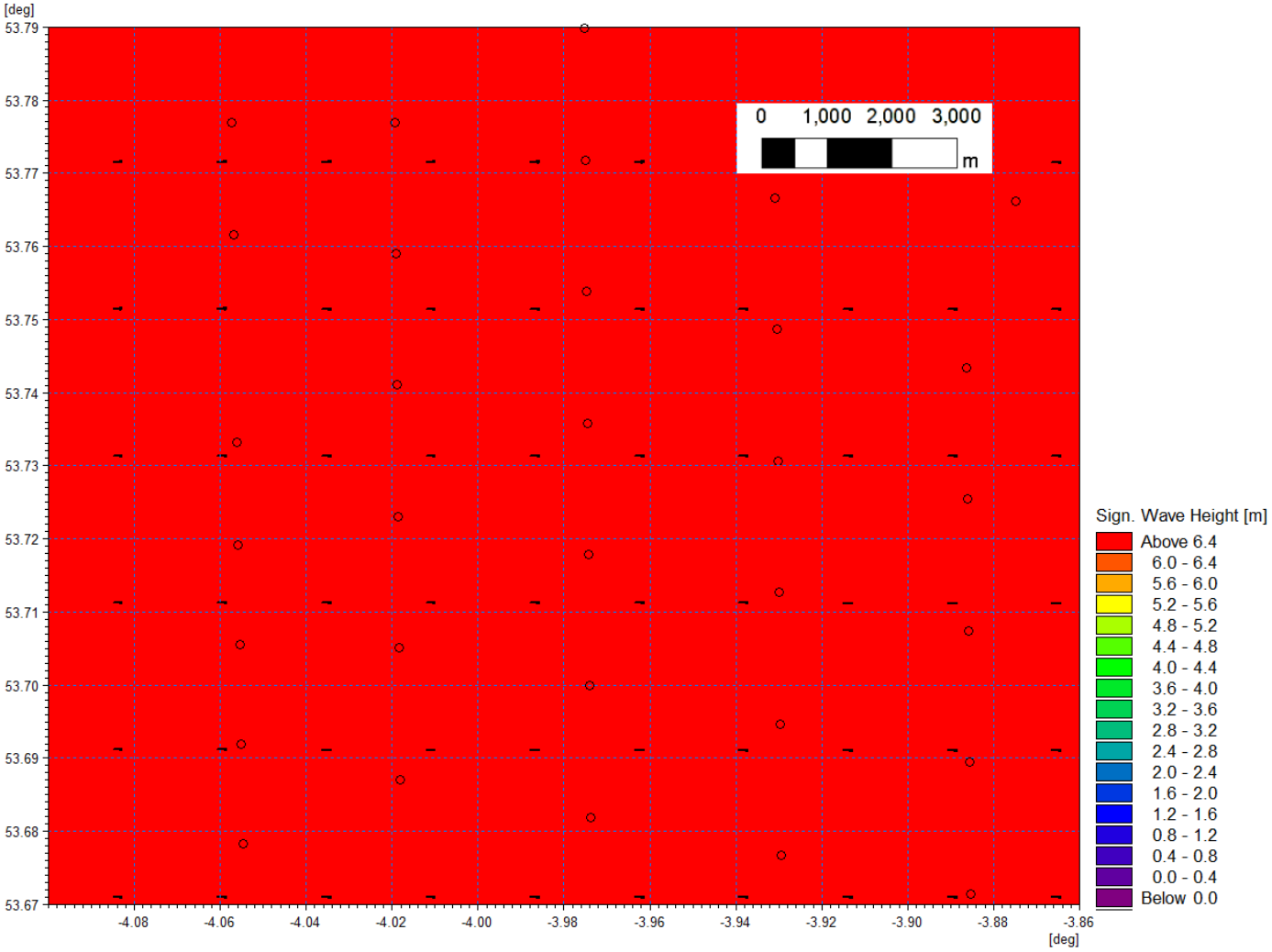

Figure 1.232: Baseline wave climate 1 in 20 year storm 270° MHW.

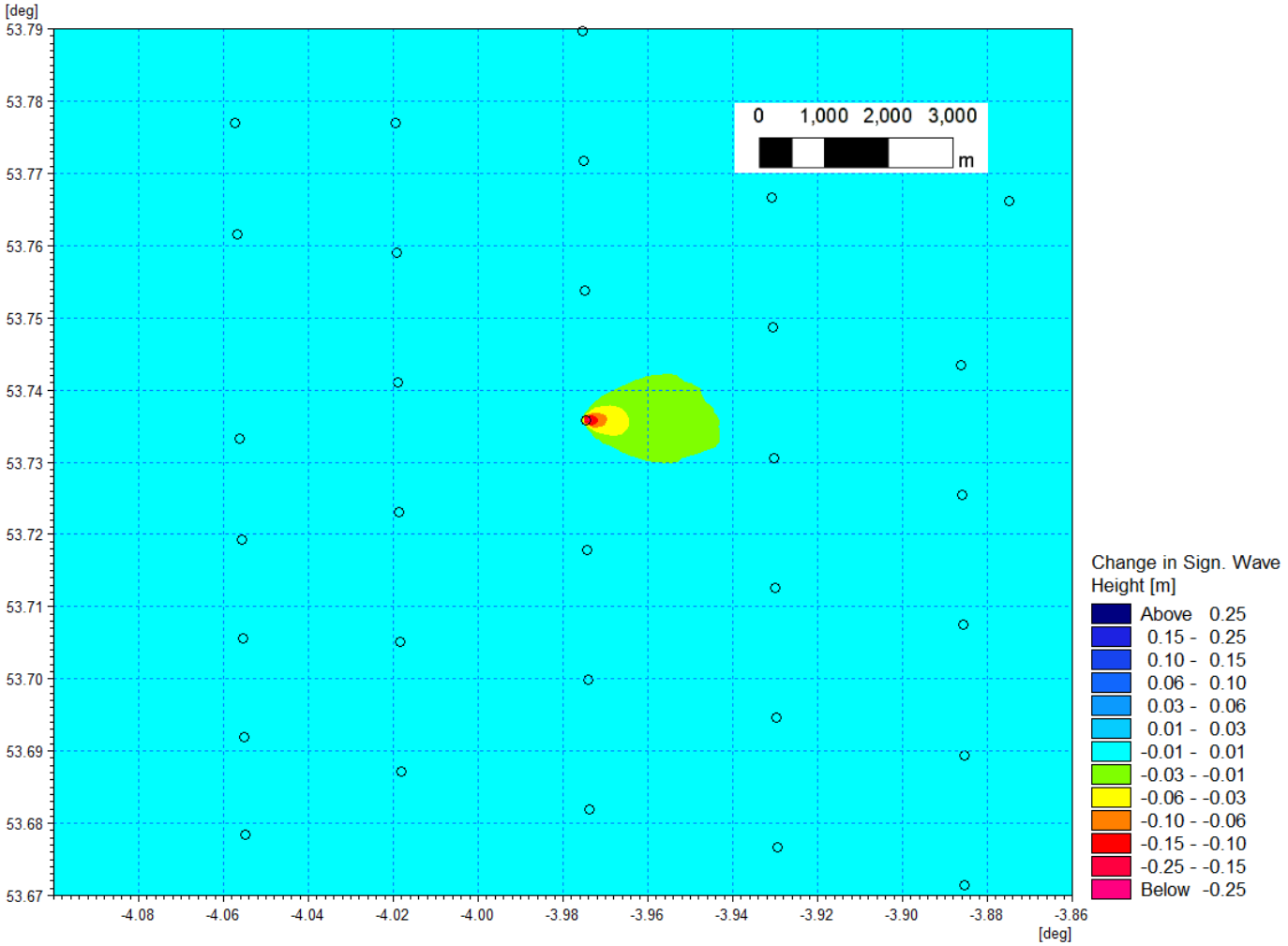

Figure 1.233: Change in wave climate 1 in 20 year storm 270° MHW (post-construction minus baseline) - rectangular gravity base foundation.

1.5 Summary

1.5.1.1 A numerical modelling study was undertaken to inform and quantify the potential impacts of the Mona Offshore Wind Project on physical processes. This report contains modelling undertaken for the PEIR stage of the application, which is considered to provide suitable supporting information for the assessment given the limited changes to the Mona Offshore Wind Project Boundary presented in the project description in the Environmental Statement. Additionally, sensitivity modelling carried out to review alternative foundation types in support of the Environmental Statement is also presented. Thus the report is formed of two main sections, the first of which utilises boundaries and parameters presented within the PEIR and the second which is based on the project description provided in the Environmental Statement.

1.5.1.2 This report has outlined the baseline characteristics of the region in terms of physical processes. This includes tidal current, wave climate and sediment transport under both calm and storm conditions. Numerical modelling has been used to quantify the changes in physical processes due to the installation of the Mona PEIR Offshore Wind Project. The presence of the wind turbine foundations redirects both waves and tidal flow and although some changes in sediment transport were revealed, these were limited in magnitude and represented an adjustment in the transport path alignment.

1.5.1.3 The installation of the Mona PEIR Offshore Wind Project was seen to marginally reduce wave heights in the lee of the structures whilst a marginal increase was noted at the periphery, however during larger storm events these effects were less marked. Any significant changes in tidal currents and wave climate would not extend to the coastline and there would be no change in coastal processes in this area.

1.5.1.4 Suspended sediment plumes for construction activities were quantified. In all cases, the material released was native to the bed sediments and, although there are periods of increased turbidity, the material was retained in the sediment cell and would be subsequently assimilated into the existing sediment transport regime.

1.5.1.5 Finally, sensitivity modelling was undertaken to compare the influence of foundation type on tidal flow and wave climate, in line with the project description presented in Volume 1, Chapter 3: Project description of the Environmental Statement. Both suction bucket and conical gravity base foundations were found to have little influence on baseline tides and wave patterns. The much larger single OSP with a rectangular gravity base was seen to induce the greatest change in baseline conditions, however, even these were confined within the Mona Array Area, extending, at the furthest, to adjacent wind turbine structures.

1.6 References

ABPmer (2008) WebVision Atlas of UK Marine Renewable Energy Resources. Available: https://www.renewables-atlas.info/explore-the-atlas/. Accessed: June 2022.

ABPmer (2018) Data Explorer. Available: https://www.seastates.net/explore-data/. Accessed: June 2022.

BERR (2008). Review of Cabling Techniques and Environmental Effects applicable to the Offshore Windfarm Industry. Technical Report, Department for Business Enterprise and Regulatory Reform (BERR), in association with Defra, 164pp.

Bp (2023) Geological Ground Model Mona Windfarm Development Irish Sea

British Geological Survey (2022) Sediment sample data. Available: https://www.bgs.ac.uk/information-hub/bgs-maps-portal/. Accessed: May 2022.

British Oceanographic Data Centre (BODC) (2021). UK tide gauge network. Available at: https://www.bodc.ac.uk/data/hosted_data_systems/sea_level/uk_tide_gauge_network/. Accessed on: 24 June 2022.

Centre for Environment, Fisheries and Aquaculture Science (Cefas) (2016) Suspended Sediment Climatologies around the UK, CEFAS.

Centre for Environment, Fisheries and Aquaculture Science (Cefas) (2022). Wave data. Available at https://wavenet.cefas.co.uk/map. Accessed June 2022.

Department for Environment Food and Rural Affairs (2022). Bathymetry and SSSI information. Available at https://environment.data.gov.uk/DefraDataDownload. Accessed on: 15 June 2022.

European Centre for Medium-range Weather Forecast (ECMWF) (2022), Long term wind and wave datasets. https://www.ecmwf.int/en/forecasts/datasets.

EMODnet (2020) Bathymetry. Available: https://www.emodnet-bathymetry.eu/. Accessed May 2022.

EMODnet (2022b). EODnet Geology. Available at: https://www.emodnet-geology.eu/. Accessed on: 10 June 2022.

EMODnet (2022c). EODnet Geology. Available at: https://www.emodnet-physics.eu/. Accessed on: 28 June 2022.

EMU (2013) Irish Sea Zone, Hydrodynamic measurement campaign October 2010- October 2012. Report issued to Centrica Energy Renewable Investments.

Fugro (2022) Metocean Data Report, Morgan and Mona Offshore Wind Projects. Ref: 210674_190291-MDR-01 02

Gardline Ltd (2022) Integrated Offshore Wind Farm Site Survey. Document number: 11602.

Gardline Ltd (2023) Mona Geophysics Interpretation Report. Document number: 11781.

GEMS (2011) Metocean data collection, Ormonde wind farm project. Report prepared for: Offshore Design Engineering Ltd Document number: GSL10108-FIN-001-01.

Howarth M.J. (2005) Hydrography of the Irish Sea, SEA6 Technical Report, POL Internal document 174.

Integrated Mapping for the Sustainable Developments of Ireland's Marine Resource (INFOMAR) (2022), Seabed mapping data Geological Survey Ireland (GSI) and Marine Institute. Available at http://www.infomar.ie/. Accessed Feb 2022.

Kennington, K. and Hiscott, A. (2018). Hydrology, weather and climate, climatology. Manx Marine Environmental Assessment (2nd Ed.). Isle of Man Government. 45 pp.

Marine Environmental Data Information Network (MEDIN) (2021). Bathymetry data. Available at: https://data.admiralty.co.uk/portal/apps/sites/#/marine-data-portal. Accessed on: March 2021.

Mellett, C, Long, D, Carter, G, Chiverell, R and Van Landeghem, K. (2015) Geology of the seabed and shallow subsurface: The Irish Sea. British Geological Survey Commissioned Report, CR/15/057 52pp.

Mona Offshore Wind Limited (2023) Mona Offshore Wind Project. PEIR. Available at https://www.morganandmona.com/en/. Accessed August 2023.

National Network of Regional Coastal Monitoring Programmes (2022). Metocean data. Available at https://coastalmonitoring.org/cco/. Accessed June 2022.

National Oceanic and Atmospheric Administration (NOAA) (2022). Metocean data. Available at https://www.dhigroup.com/data-portals/metocean-data-portal. Accessed April 2022.

Ocean Ecology (2023) 11781 bp Mona Environmental Data.xlsx

The Environment Agency National LiDAR Programme (2022). LiDAR data. Available at Find open data - data.gov.uk. Accessed May 2022.

Whitehouse, R.J.S., Sutherland, J. and O'Brien, D. (2006) Seabed scour assessment for offshore windfarm. Proceedings Third International Conference on Scour and Erosion, November 1-3, CURNET, Gouda, The Netherland.

RPS (2018) Tide and Storm Surge Forecast (TSSF) model of Irish coastal waters.

UKHO (2022), Admiralty Tide Tables – Volume 1B.

XOCEAN Ltd (2022) 00275-BPX-UKX-WIND bp Elizabeth Project Processing Report.